JUNE 27–29, 2022
ISEP · PORTO, PORTUGAL

INTERNATIONAL CONFERENCE Mathematical Analysis and Applications in Science and Engineering

Book of Extended Abstracts

isep Instituto Superior de Engenharia do Porto · P.PORTO · U.PORTO
UNIVERSIDAD COMPLUTENSE MADRID · 1 DECEMBRIE 1918 UNIVERSITY OF ALBA IULIA · جامعة 8 ماي 1945 قالمة · espol Escuela Superior Politécnica del Litoral

INTERNATIONAL CONFERENCE on Mathematical Analysis and Applications in Science and Engineering ICMA^{2}SC'22

BOOK OF EXTENDED ABSTRACTS

Bibliographic Information

Book Title

International Conference on Mathematical Analysis and Applications in Science and Engineering – Book of Extended Abstracts

Series Editors

Carla M.A. Pinto, School of Engineering, Polytechnic of Porto and Centre for Mathematics, University of Porto

Jorge Mendonça, School of Engineering, Polytechnic of Porto

Lurdes Babo, Porto Accounting and Business School

Dumitru Baleanu, Cankaya University

Publication Year: 2022

Publisher

ISEP | P.PORTO

Book ISBN & DOI

978-989-53496-3-0

https://doi.org/10.34630/20734

Conference Name

ICMA²SC'2022

Dates & Location

June 27th-29th 2022, School of Engineering, Polytechnic of Porto, Porto, Portugal

Copyright Information

Information about the Editors

Dr. Carla M.A. Pinto is a Coordinating Professor in the School of Engineering, Polytechnic of Porto, Portugal. Her main research topic is epidemiology, in particular Mathematical Epidemiology. She is interested in mathematical challenges and their role in providing advice on public health policies. Mrs Pinto is trained in Nonlinear Dynamics, Bifurcation Theory. Previous research included the analysis of Central Pattern Generators for Animal and Robot Locomotion, coupled cell networks, neuron-like equations (Hodgkin-Huxley equations, Fitz-Hugh Nagumo, Morris-Lecar).

Dr. Jorge Mendonça is Adjunct Professor in the School of Engineering, Polytechnic of Porto, Portugal. He holds a PhD degree in Statistics and Operational Research from the University of Vigo, a Master's degree in Statistics and Probability from the Faculty of Sciences of the University of Lisbon. Survival analysis is his main interest particularly applications of the missing censoring indicator model. Other interests are innovative methodologies in Engineering education, interactive learning and survey analysis.

Dr. Lurdes Babo is senior lecturer at ISCAP, the Porto Accounting and Business School from the Polytechnic of Porto, Portugal, and researcher at CEOS.PP. She has experience in lecturing mathematics and statistics. She holds a PhD in Applied Mathematics, University of Porto, Portugal. Her research interests include ICT, Finance, Time Series Analysis, Simulation and QMC methods.

Professor Dumitru Baleanu is a Professor at the Institute of Space Sciences, Magurele-Bucharest, Romania and a visiting staff member at the Department of Mathematics,Cankaya University, Ankara, Turkey. Dumitru Baleanu got his PhD from the Institute of Atomic Physics in 1996. His fields of interest include the fractional dynamics and its applications, fractional differential equations and their applications, discrete mathematics, image processing, bio-informatics, mathematical biology, mathematical physics, soliton theory, Lie symmetry, dynamic systems on time scales, computational complexity, the wavelet method and its applications, quantization of systems with constraints, the Hamilton-Jacobi formalism, geometries admitting generic and non-generic symmetries. Dumitru Baleanu is one of the pioneers of the fractional variational principles and their applications in control theory.

Dedication

In memoriam of Professor J.A. Tenreiro Machado (1957 - 2021), an enthusiastic scientist, respected colleague, generous person, and trustworthy friend. More information here.

Professor J.A. Tenreiro Machado (1957 - 2021)

Preface

The present volume on Mathematical Analysis and Applications in Science and Engineering - Book of Extended Abstracts of the ICMASC'2022 collects the extended abstracts of the talks presented at the International Conference on Mathematical Analysis and Applications in Science and Engineering – ICMA2SC'22 that took place at the beautiful city of Porto, Portugal, in June 27th-June 29th 2022 (3 days).

Its aim was to bring together researchers in every discipline of applied mathematics, science, engineering, industry, and technology, to discuss the development of new mathematical models, theories, and applications that contribute to the advancement of scientific knowledge and practice. Authors proposed research in topics including partial and ordinary differential equations, integer and fractional order equations, linear algebra, numerical analysis, operations research, discrete mathematics, optimization, control, probability, computational mathematics, amongst others.

The conference was designed to maximize the involvement of all participants and will present the state-of-the-art research and the latest achievements.

Main topics included:

- Ordinary and Partial Differential Equations: Theory and Applications
- Mathematical Modelling involving time fractional ODEs and PDEs
- Integral Equations and Integral Transforms
- Uncertainty Quantification in Mathematical Modelling
- Control Theory, Optimization and their Applications
- Probability, Statistics and Numerical Analysis
- Inverse Problems: Modelling and Simulation
- Computational Methods in Sciences and Engineering
- Fractional Dynamic Systems and Applications
- Fractional Signals and Systems
- Singularities Analysis and Integral Representations for Fractional Differential Systems
- Special Functions Related to Fractional Calculus
- Applications in Biological Systems and Cancer Dynamics.
- Applications to Electrical Engineering, Electronics, Electromagnetism, Electrochemistry, Finance and Economics, Fractional Earth Science, Image Processing, Robotics, Automatic Control, Mechanics, Viscoelasticity, Thermal Engineering
- History of Fractional Calculus
- Mathematics Education

The volume is dedicated to the memory of our colleague J.A. Tenreiro Machado (1957–2021), a visionary scientist, respected colleague, generous mentor. Professor Tenreiro Machado was a Portuguese scientist. He authored more than 1100 publications, including 11 books, 575 journal papers, 118 book chapters. He was member of the editorial boards and associate editor in several scientific journals and editor-in-chief of three of them. He was a Highly Cited Researcher in the category Cross-Field of Clarivate Analytics. His scientific legacy spreads in different topics namely Control & Robotics, Complex Systems and Fractional Calculus. J.A. Tenreiro Machado was a notable scientist, with a strong wisdom, passion for research, diligence, and integrity. The nonlinear dynamics, complexity science, and fractional communities were all transformed by his presence and legacy.

The collection of works in this edited volume opens with the contribution of Professor Candace Kent, and coworkers on the analysis of a model for epilepsy. This is followed by more than 160 papers on mathematical models in epidemiology, fractional order models, and applications in Engineering.

We hope that the whole scientific community will benefit from this edited volume.

July 2022, Porto, Portugal

The Editors

Carla M.A. Pinto

Jorge Mendonça

Lurdes Babo

Dumitru Baleanu

SCIENTIFIC COMMITTEE

CHAIRS OF THE SCIENTIFIC COMMITTEE

Dumitru Baleanu, Romania

Juan J. Nieto, Spain

Ruy M. Ribeiro, Los Alamos, USA

MEMBERS

Om P. Agarwal, USA

Praveen Agarwal, India

Obaid Algahtani, Saudi Arabia

Iván Area, Spain

José Ferreira Alves, Portugal

Omar Abu Arqub, Jordan

Lurdes Babo, Portugal

Jose Manoel Balthazar, Brazil

Jorge Buescu, Portugal

Hasan Bulut, Turkey

Raul Campilho, Portugal

Carlo Cattani, Italy

Chinmay Chakraborty, India

YangQuan Chen, USA

Dana Copot, Belgium

Michael Dellnitz, Germany

Flávio Ferreira, Portugal

Jorge M. Freitas, Portugal

Stefano Galatolo, Italy

Alexandra Galhano, Portugal

Sílvio Gama, Portugal

Alireza K. Golmankhaneh, Iran

Tomas Götz, Germany

Carlos Herdeiro, Portugal

R. Hilfer, Germany

Maaita Jamal-Odysseas. Greece

Devendra Kumar, India

Daniel Cao Labora, Spain

Walter Lacarbonara, Italy

Stefano Lenci, Italy

Changpin Li, China

António M. Lopes, Portugal

Rosana Rodriguez Lopez, Spain

Albert Luo, USA

Nedra Moalla, Tunisia

Shaher Momani, Jordania

Cristina Muresan, Romania

Manuel Ortigueira, Portugal

Necati Ozdemir, Turkey

Marcello Pellicciari, Italy

Luís Miguel Pinho, Portugal

Alberto Adrego Pinto, Portugal

Carlos Ramos, Portugal

Julio C. Rebelo, France

Magda Rebelo, Portugal

Helena Reis, Portugal

Shahram Rezapour, Taiwan

Diogo Rodrigo Ribeiro, Portugal

José C. Sá, Portugal

Gilberto Santos, Portugal

António Sartal, Spain

Stefan Siegmund, Germany

Francisco Silva, Portugal

Jaime Silva, Portugal

A. Augusto Sousa, Portugal

Hari M. Srivastava, Canada

Ivanka Stamova, USA

Nasser Sweilam, Egypt

Hong Guan Sun, China

Stefania Tomasiello, Estonia

Delfim F.M. Torres, Portugal

Juan Trujillo, Spain

Duarte Valério, Portugal

Dimitri Volchenkov, USA

Xiao-Jun Yang, China

Dia Zeidan, Jordan

ORGANIZING COMMITTEE

CHAIRS OF THE ORGANIZING COMMITTEE

António Vega Y De La Fuente, Portugal

Maria João Viamonte, Portugal

CO-CHAIRS OF THE ORGANIZING COMMITTEE

Amar Debbouche, Algeria

Angel Ramos del Olmo, Spain

Vladimir Vasyliev, Russia

MEMBERS

Sandra Aires, Portugal

Luís Afonso, Portugal

Valerii Antonov, Russia

Vítor Cardoso, Portugal

Fernando Carvalho, Portugal

Joseph Páez Chávez, Ecuador

Vítor Cunha, Portugal

Luís Pinto Ferreira, Portugal

Maria Hermínia Ferreira, Portugal

Nuno Miguel Ferreira, Portugal

Isabel Figueiredo, Portugal

Alexandra Gavina, Portugal

Maria da Graça Marcos, Portugal

João Matos, Portugal

Ana Cristina Meira, Portugal

Jorge Mendonça, Portugal

Marisa Oliveira, Portugal

Arnaldo Pinto, Portugal

Isabel Pinto, Portugal

Ioan-Lucian Popa, Romania

Gisela Ramadas, Portugal

Pedro Reis, Portugal

Rui Rocha, Portugal

Marcelo Zannin da Rosa, Brazil

António Varejão, Portugal

SECRETARY

Ana Costa, Portugal

ORGANIZATIONS

The conference is a joint organization by:

SPONSORS

LIST OF PLENARY SPEAKERS

Ravi P. Agarwal

Texas A&W University

Kingsville, USA

An Integral equation related to infectious disease

A nonlinear integral equation related to infectious disease is investigated. Using a fixed-point theorem for convex-concave and nondecreasing operators defined in a Banach space with a normal solid cone, we derive some existence and uniqueness results of positive solutions to the considered equation. Moreover, an iterative algorithm that converges to the unique solution is provided. Our results are supported by examples.

Short bio

Ravi P. Agarwal was born in Moradabad (India) on July 10, 1947. He earned his Master's degree from Agra University in 1969, ranking 2nd among over 500 in that year. In 1973, he earned his Ph. D. (Mathematics) at the Indian Institute of Technology in Madras, India, which is one of the highest ranking universities in India. Since then, for the last 50 years, Dr. Agarwal has been actively involved in research and pedagogical activities. He has made significant contributions in various research fields, including Numerical Analysis, Differential and Difference Equations, Inequalities, and Fixed Point Theorems. He is an excellent scholar, a dedicated teacher, and a prolific researcher. He has published 50 research monographs, and more than 1,700 publications (with almost 680 mathematicians all over the world) in prestigious national and international mathematics journals.

According to Google Scholar, Dr. Agarwal has been cited more than 46,783 times. On MathSciNet, his work has been cited more than 16,800 times by 6,800 scientists. Dr. Agarwal is the recipient of several notable honors and awards, including Doctor Honoris Causa (2015 by University of Constanta, Romania), Professor Honoris Causa (2015 by University of Cluj, Romania), Honorary Doctorate (2017 by University of Nis, Serbia), Doctor Honoris Causa (2017 by Plovdiv University, Bulgaria), Doctor Honoris Causa (2017 by Constantin Brancusi, University of Targu-Jiu, Romania), Doctor Honoris Causa (2017 by University of Oradea, Romania, 2017), Doctor Honoris Causa (by 1 December 1918, University of Alba Lulia, Romania), Honorary Doctorate (2019 by Istanbul Gelisim University, Turkey), and Doctor Honoris Causa (2019 by Transilvania University of Brasov, Romania). He was also nominated as a possible candidate for the Banco Bilbao Vizcaya

Argentaria (BBVA) Foundation Frontiers of Knowledge Award, an international award scheme recognizing significant contributions in the areas of scientific research and cultural creation. Many BBVA award winners are Nobel laureates, including Stephen Hawkings. Florida Institute of Technology (USA) and King Abdulaziz University have recently offered him Distinguished University Professorship of Mathematics.

Praveen Agarwal

Anand International College of Engineering, Jaipur

India

Some Properties and Applications of Extended Hypergeometric Function and Applications

Euler's beta, gamma functions (hypergeometric functions) are of the important members of the family of special functions and it plays a vital role in the whole theory of special functions. These hypergeometric functions together with their extension have many applications in research fields such as engineering, chemical, statistics, fractional calculus, and physical problems. In this Symposium, our discuses have been focus on the extended Euler's beta function, which is developed by using the 2-parameter Mittag-Leffler function as the kernel. We discuss various basic properties and formulas of the extended Euler's beta function such as integral representations, transformation formulas, and summation formulas. We also introduce the logarithmicconvexity and some important inequalities for this extended Euler's beta function. Then by using this extended Euler's beta function as kernel, we have generalized hypergeometric functions and study various properties of these extended hypergeometric functions. For application point of view, we have also derived some relations between this extended Euler's beta function and extended fractional derivative operators such as Caputo fractional derivative operator and Riemann-Liouville fractional operators.

Keywords: Beta function, Gamma function, fractional calculus

Short bio

Dr. P. Agarwal was born in Jaipur (India) on August 18, 1979. After completing his schooling, he earned his Master's degree from Rajasthan University in 2000. In 2006, he earned his Ph. D. (Mathematics) at the Malviya National Institute of Technology (MNIT) in Jaipur, India, one of the highest ranking universities in India. **Recently, Prof. Agarwal is listed as the World's Top 2% Scientist 2020 and 21, Released by Stanford University**

Dr. Agarwal has been actively involved in research as well as pedagogical activities for the last 20 years. His major research interests include Special Functions, Fractional Calculus, Numerical Analysis, Differential and Difference Equations, Inequalities, and Fixed Point Theorems. He is an excellent scholar, dedicated teacher, and prolific researcher. He has published 9 research monographs and edited volumes and more than 250 publications (with almost 100 mathematicians all over the world) in prestigious national and international mathematics journals. Dr. Agarwal worked previously either as a regular faculty or as a visiting professor and scientist in universities in several countries, including India, Germany, Turkey, South Korea, UK, Russia, Malaysia andThailand. He has held several positions including Visiting Professor, Visiting Scientist, and Professor at various universities in different parts of the world. Specially, he was awarded most respected International Centre for Mathematical Sciences (ICMS) Group Research Fellowship to work with Prof. Dr. Michael Ruzhansky-Imperial College Londonat ICMS Centre, Scotland, UK, and during 2017-18, he was awarded most respected TUBITAK Visiting Scientist Fellowship to work with Prof. Dr. Onur at AhiEvran University, Turkey. He has been awarded by Most Outstanding Researcher-2018 (Award for contribution to Mathematics) by the Union Minister of Human Resource Development of India, Mr. Prakash Javadekar in 2018. According to Google Scholar, Dr. Agarwal is cited more than 4, 580 times, and on Scopus his work is cited more than 2,689 times. Dr. Agarwal is the recipient of several notable honors and awards.

Dr. Agarwal provided significant service to Anand International College of Engineering, Jaipur. Under his leadership during 2010-20, Anand-ICEconsistently progressed in education and preparation of students, and in the new direction of academics, research and development. His overall impact to the institute is considerable. Many scholars from different nations,including China, Uzbekistan, Thailand and African Countriescameto work under his guidance. The majority of these visiting post-doctoral scholars weresent to work under Dr. Agarwal by their employing institutions for at least one month.

Dr. Agarwal regularly disseminates his research at invited talks/colloquiums (over 25 Institutions all over the world).He has been invited to give plenary/keynote lectures at international conferences in the USA, Russia, India, Turkey, China, Korea, Malaysia, Thailand, Saudi Arabia, Germany, UK, Turkey, and Japan.

He has served over 50 Journals in the capacity of an Editor/Honorary Editor, or Associate Editor, and published 9 books as an editor. Dr. Agarwal has also organized International Conferences/ workshops'/seminars/summer schools.

In summary of these few inadequate paragraphs, Dr. P. Agarwal is a visionary scientist, educator, and administrator who have contributed to the world through his long service, dedication, and tireless efforts.

Maíra Aguiar

University of Trento, Italy

BCAM, Spain

ON THE ORIGIN OF COMPLEX DYNAMICS IN MULTI-STRAIN DENGUE MODELS

Dengue fever epidemiological dynamics shows large fluctuations in disease incidence, and several mathematical models describing the transmission of dengue viruses have been proposed to explain the irregular behavior of dengue epidemics. Multi-strain dengue models are often modeled with SIR-type models where the SIR classes are labeled for the hosts that have seen the individual strains. The extended models show complex dynamics and qualitatively a very good result when comparing empirical data and model simulations. However, modeling insights for epidemiological scenarios characterized by chaotic dynamics, such as for dengue fever epidemiology, have been largely unexplored. The problem is mathematically difficult and to make the urgently needed progress in our understanding of such dynamics, concepts from various fields of mathematics as well the availability of good data for model evaluation are needed.
In this talk, I will present a set of models motivated by dengue fever epidemiology and compare different dynamical behaviors originated when increasing complexity into the model framework.

Short Bio

Dr. Maíra Aguiar is a mathematical epidemiologist working on infectious disease dynamics. With a multidisciplinary research profile, is trained in dynamical systems theory, stochastic processes, nonlinear dynamics, bifurcation analysis and biostatistics and her scientific interests addresses significant mathematical and fundamental questions in biology and medicine, with special focus on public health epidemiology modeling.

Dr. Aguiar is a former Marie Curie Fellow at Trento University, Italy and she is presently the founder and the leader of the MTB group (Mathematical and Theoretical Biology Group) at BCAM (the Basque Center for Applied Mathematics in the Basque Country), Spain. Dr. Aguiar is member of the Board of Directors of the European Society for Mathematical and Theoretical Biology (ESMTB), serving as Vice-President from 2018-2020. As a member of the Basque Modeling Task Force, Dr. Aguiar is currently assisting the Basque Health Managers and the Basque Government during the COVID-19 responses.

Dumitru Baleanu

Cankaya University

Turkey

Mathematical Biology: A Field Where the Fractional Calculus Operators Are Validated

The fractional calculus is a powerful tool to get new insights of complicated dynamics. Among various fields of science and engineering where the fractional calculus operators found substantial real-world applications, perhaps the mathematical biology is one of the most representative. In my talk I will present some of the main results reported so far within fractional mathematical biology models and I will discuss some open problems in this filed.

Short bio

Dumitru Baleanu is a Professor at the Institute of Space Sciences, Magurele-Bucharest, Romania and a visiting staff member at the Department of Mathematics,Cankaya University, Ankara, Turkey. Dumitru Baleanu got his PhD from the Institute of Atomic Physics in 1996. His fields of interest include the fractional dynamics and its applications, fractional differential equations and their applications, discrete mathematics, image processing, bio-informatics, mathematical biology, mathematical physics, soliton theory, Lie symmetry, dynamic systems on time scales, computational complexity, the wavelet method and its applications, quantization of systems with constraints, the Hamilton-Jacobi formalism, geometries admitting generic and non-generic symmetries. Dumitru Baleanu is one of the pioneers of the fractional variational principles and their applications in control theory. He is one of the co-authors of the seminal paper entitled "Anomalous diffusion expressed through fractional order differential operators in the Bloch-Torrey equation", published in Journal of Magnetic Resonance (2008),which now plays a fundamental role within diffusion weighted MRI. Besides, together with G.C. Wu, L.G. Zeng ,X.C. Shi and F. Wu, Dumitru Baleanu is the coauthor of a Chinese Patent No ZL 2014 1 0033835.7 regarding the chaotic maps and its important role in the information encryption. Dumitru Baleanu is co-author of 18 books published by Springer, Elsevier and World Scientific. His H index is 85 and he is highly cited researchers in Mathematics. Dumitru Baleanu won several awards:

- 2020 - Best Research Award, given by the ITSR Foundation Award 2020 (organized by Institute of Technical and Scientific Research, India) and presented online on September 13th, 2020.

- 2020 - Distinguished Researcher Award, Given by the Jaipur Mathematical Society and presented during the 3rd International Conference on Mathematical Modelling, Applied Analysis and Computation (ICMMAAC-20),7-9 August 2020 at JECRC University,Jaipur, India
- 2019 - Award for 20 years of successful scientific activity in the field of fractional calculus and its applications by Istanbul Gelisim University, Turkey
- 2019 - Obada Prize. The Obada-Prize recognizes and encourages innovative and interdisciplinary research that cuts across traditional boundaries and paradigms. It aims to foster universal values of excellence, creativity, justice, democracy, and progress and to promote the scientific, technological and humanistic achievements that advance and improve our world.
- 2018 - Award of Merit given by the Embassy of Romania to the Republic of Turkey for the contribution to the development of the Romanian-Turkish relationship in the field of Education
- 2018 - ICFDA2018 Award:Innovation in Fractional Calculus. This award is granted to inventors of new patents which address major problems and have a great perspective by use of fractional calculus in real world applications.

Dumitru Baleanu is the Editor in Chief of Progress in Fractional Differentiation and Applications and a Co-editor in Chief of Discontinuity, Nonlinearity and Complexity. Dumitru Baleanu is a member of several editorial boards of journals indexed in SCI.

Martin Bohner

Missouri University of Science and Technology

USA

Hyers-Ulam and Hyers-Ulam-Rassias Stability of First-Order Linear and Nonlinear Dynamic Equations

We present several new sufficient conditions for Hyers–Ulam and Hyers–Ulam-Rassias stability of first-order linear and nonlinear dynamic equations for functions defined on a time scale with values in a Banach space.

1. Maryam A. Alghamdi, Alaa Aljehani, Martin Bohner, and Alaa Hamza. Hyers–Ulam and Hyers–Ulam–Rassias stability of first-order linear dynamic equations. Publ. Inst. Math. (Beograd) (N.S.), 109(123):83–93, 2021.
2. Maryam A. Alghamdi, Mymonah Alharbi, Martin Bohner, and Alaa Hamza. Hyers–Ulam and Hyers–Ulam–Rassias stability of first-order nonlinear dynamic equations. Qual. Theory. Dyn. Syst., 20(2):14, Art. No. 45, 2021.

Short bio

Martin Bohner is the Curators' Distinguished Professor of Mathematics and Statistics at Missouri University of Science and Technology in Rolla, Missouri, USA. He received the BS (1989) and MS (1993) in Econo-mathematics and PhD (1995) from University Ulm, Germany, and MS (1992) in Applied Mathematics from San Diego State University. He was a Postdoc, sponsored by the Alexander von Humboldt-Foundation, at National University of Singapore (1997) and at San Diego State University (1998). Martin Bohner is a Past President of ISDE, the International Society of Difference Equations. His research interests center around differential, difference, and dynamic equations as well as their applications to economics, finance, biology, physics, and engineering. He is the author of six textbooks and more than 300 publications, Editor-in-Chief of six international journals, and Associate Editor for almost 100 international journals. His work has been cited more than 17000 times in the literature, including more than 5000 citations of his book "Dynamic Equations on Time Scales: An Introduction with Applications", co-authored with Professor Allan Peterson. His h-index is 58, and his i10-index is 216. Professor Bohner's honors at Missouri S&T include five Faculty Excellence Awards, one Faculty Research Award, and eight Teaching Awards.

Juan Carlos Cortés

Polytechnic University of Valencia

Spain

Quantifying uncertainties in differential equations with Jumps

Differential equations are powerful tools to model real-world problems. However, their deterministic formulation neglects epistemic and aleatoric uncertainties coming from the lack of knowledge of the phenomenon under modeling and possible unpredictable facts often inherent to the random nature of the studied problem. Apart from randomness, the dynamics of many phenomena are often subject to abrupt changes such as shocks, harvesting or natural disasters. These short-term perturbations on rapid changes can be mathematically treated as having acted instantaneously using discontinuities or impulses. Combining the rigorous treatment of these two elements, uncertainties and impulses in the setting of differential equations is a significant challenge that is currently attracting the scientific community's attention. However, more progress has been made using stochastic differential equations where randomness is driven by a specific stochastic process, typically white noise and the Poisson process. This talk will present some recent results about Uncertainty Quantification for differential equations with discontinuities and jumps using the so-called Random Differential Equations (RDEs) approach. In this setting, uncertainties can be directly assumed in all the terms (initial conditions, source term and coefficients) of the RDE using arbitrary distributions. Moreover, we will present a method to calculate the probability density function of the solution, which is a stochastic process, rather than obtaining only the first moments. The theoretical findings

will be illustrated using simulations and real-world examples where inverse Uncertainty Quantification techniques will be applied to reasonably fix the distributions of the model parameters from real data.

Short bio

Juan Carlos Cortés López (http://www.upv.es/ficha-personal/jccortes), is a full professor in the Department of Applied Mathematics at the Universitat Politècncia de Valéncia (UPV), Spain. Since 2009, he is the deputy director of the University Institute of Multidisciplinary Mathematics of the UPV, developing his research in the MUNQU group (Modeling and Uncertainty Quantification) https://munqu.webs.upv.es/. His research is oriented to the extension of the classical theory of differential equations (in a broad sense; ODEs, PDEs, equations with delay, fractional ODEs, etc.) to the random scenario under the approach of the so-called Random Differential Equations (RDEs) and their application in modeling with real data, paying attention to the development of inverse techniques for the estimation of the probability distributions of the parameters that appear in the RDEs so that they capture the uncertainty of the phenomenon being modeled.

Walter Lacarbonara

Sapienza University of Rome

Italy

E-mail: walter.lacarbonara@uniroma1.it

A multi-band gap metamaterial with multi-frequency resonators

The main focus of this talk is on high-performance 1D and 2D metamaterials featuring a periodic distribution of highly tunable infinite-dimensional resonators. The embedded resonators are first treated as linear systems exhibiting eigenspectra with distinct features while the dispersion curves of the metamaterials show single or multiple band gaps across which no wave propagation occurs. The stop-bands sensitivity with respect to the design parameters is discussed. These resonators are then enriched by nonlinearities. The nonlinear wavefrequencies and waveforms away from internal resonances obtained via a perturbation approach are shown to exhibit a high nonlinear tunability which is a key for advanced applications. Various 3D printed metamaterial samples are tested experimentally using a 3D laser scanning vibrometer system to show very interesting wave propagation properties.

Short bio

Walter Lacarbonara is a Professor of Nonlinear Dynamics at Sapienza University and Director of the Sapienza Center for Dynamics. During his graduate education he was awarded a MS in Structural Engineering (Sapienza University) and a MS in Engineering Mechanics (Virginia Tech, USA), and a PhD in Structural Engineering (Sapienza/Virginia Tech). His research interests cover nonlinear structural dynamics; dissipation in carbon nanotube/polymer nanocomposites; asymptotic techniques; nonlinear control of vibrations; experimental nonlinear dynamics; dynamic stability of structures. He is Editor in Chief of Nonlinear Dynamics, former Associate Editor for ASME Journal of Applied Mechanics, Journal of Vibration and Acoustics, Journal of Sound and Vibration. He served as Chair of the ASME Technical Committee on Multibody System and Nonlinear Dynamics, General co-Chair and technical program co-Chair of the ASME 2015 (Boston, USA) and 2013 (Portland, USA) IDETC Conferences. He has organized over 10 international symposia/conference sessions and, very recently, the First, Second, and Third International Nonlinear Dynamics Conferences (NODYCON, www.nodycon.org/2019, www.nodycon.org/2021, www.nodycon.org/2023). His research is supported by national and international sources (EOARD/AFOSR, NSF, European Commission, Italian Ministry of Science and Education). He has published over 250 papers and conference proceedings, 4 international patents (EU/USA/China), 24 book chapters, 6 co-edited Springer books and a single-authored book (Nonlinear Structural Mechanics, Springer, NY, https://link.springer.com/book/10.1007/978-1-4419-1276-3) for which he received the 2013 Texty Award nomination by Springer US.

Agnieszka Malinowska

Bialystok University of Technology

Poland

Email: a.malinowska@pb.edu.pl

Stability of multi-agents systems under DoS attacks

We investigate multi-agent systems under Denial-of-Service (DoS) attacks. In the presence of DoS attacks, information can neither be received nor sent between the attacked nodes, and adversaries can attack partial or all channels at any time. Therefore, in multi-agent systems, these attacks may lead to a loss of stability. Our goal is to provide sufficient conditions for the stability of multi-agent systems under DoS attacks. Two types of systems are considered: (i) systems with memory, and (ii) systems defined on hybrid time domains.

Short bio

Agnieszka B. Malinowska is the Associate Professor and Director of the Institute of Information and Communication Technology of the Faculty of Computer Science in the Bialystok University

of Technology, Bialystok, Poland. She received the MS (1995) in mathematics from the Warsaw University (Bialystok Branch), PhD (2002) and habilitation (2014) in technical sciences on control engineering and robotics from the Systems Research Institute of the Polish Academy of Sciences. She was a Postdoc at the University of Aveiro, sponsored by the Ministry of Science and Higher Education, Republic of Poland, and at the University of Texas within the project Portugal - Austin UTAustin/MAT/0057/2008. Agnieszka B. Malinowska is the author and co-author of three monographs and more than 100 publications, an editorial board member of six international journals. Her scientific interests lie in the area of fractional calculus and time scales theory as well as their applications to optimal control and multi-agent systems.

ORCID ID: https://orcid.org/0000-0002-1309-8583

Irina Perfilieva

University of Ostrava

Czech Republic

Email: irina.perfilieva@osu.cz

Laplace Operators in Hilbert manifolds initiated by fuzzy partition

The goals are:

- Propose a manifold organization of space (universe) based on a system of local coordinates that arose from a fuzzy partition;

- Use the theory of Riemannian-Hilbert manifolds as a framework;

- Define Laplace operators using the Laplace-Beltrami approach;

- Characterize the Laplace spectrum

Short bio

Professor Irina Perfilieva, Ph.D., received the degrees of M.S. (1975) and Ph.D (1980) in Applied Mathematics from the Lomonosov State University in Moscow, Russia. At present, she is full professor in the University of Ostrava (CZ) and a Head of Theoretical Research Department in the Institute for Research and Applications of Fuzzy Modeling (IRAFM). She is: the author and co-author of six books on mathematical principles of fuzzy sets, fuzzy logic and their applications;

area editor of International Journal of CIS (IJCIS), Soft Computing, editorial board member of the journals: Fuzzy Sets and Systems, Journal of Uncertain Systems, IEEE Transaction on Fuzzy Systems, Advances in Artificial Intelligence and Machine Learning. She works as a member of Program Committees of the most prestigious International Conferences and Congresses in the area of fuzzy and knowledge-based systems. She is an EUSFLAT Honorary Member, and the IFSA Fellow. She received a special price at the 2010 Seoul International Invention Fair and several awards for the best paper, IFSA 2019 as the last. She has two patents. Her scientific interests lie in the area of applied mathematics and mathematical modeling where she successfully uses modern as well as classical approaches. For the past five years, she has been working in the field of fuzzy integro-differential equations, image processing, pattern recognition and the theoretical foundations of deep learning.

Ruy Ribeiro

Los Alamos National Laboratory

USA

Email: ruy@lanl.gov

Dynamical models of within-host viral replication

Mathematical models of viral replication in vivo, and viral interactions with the host afforded a dynamical understanding of viral biology. Application of these ideas, for example during primary infection or following drug treatment, has been used in the last two decades to study the biology of diverse virus. I will discuss, with examples from HIV and hepatitis C virus (HCV) infection, the principles and approach of this methodology. I will also present recent examples of insights into the biology of these viruses and SARS-CoV-2 gained with viral dynamics.

Short bio

Ruy M. Ribeiro got his Ph.D. in Mathematical Biology at the University of Oxford, UK. He then joined Los Alamos National Laboratory (LANL) in 2000, as a Postdoctoral Researcher, later becoming a staff scientist working on viral and immune system dynamics. His main research interests are the pathogenesis of infections, and the use of quantitative modeling tools to gain insight into viral and immune system dynamics. His work has always entailed close collaborations with experimental researchers to develop proper statistical and dynamic models to analyze experimental data. His modeling work spans multiple scales from the intracellular (eg. a model of the molecular details of HCV infection) to the epidemiological (including HIV and influenza epidemics). He was Professor of Statistics at the Medical School of the University of Lisbon, while on leave from LANL, between 2017 and 2020. Ruy Ribeiro has over 140 peer-reviewed papers in

this area, and he is/was the PI of several research projects funded by the National Institutes of Health, the European Union, and the Department of Energy.

ORCID ID: https://orcid.org/0000-0002-3988-8241

Jan Sieber

University of Exeter

United Kingdom

Email: j.sieber@exeter.ac.uk

An unusual tipping mechanism - Mid-Pleistocene Transition

The Mid-Pleistocene Transition (MPT) is a shift from 41,000-year to about 100,000-year ice age cycles that occured roughly 1,000,000 years ago, as shown in proxy records. It is often considered as a change in internal climate dynamics and studied using simple conceptual models such as the one proposed by Saltzman and Maasch (1988). We show for such a simple model that the astronomical forcing (changes in effective solar radiation incoming to the Earth) and internal bistability can lead to a form of tipping that replicates features of the MPT in the records. The tipping observed in the model is connected to the theory of quasiperiodically forced dynamical systems and strange non-chaotic attractors.

Short bio

Current and Previous Appointments, PhD
Since 2016 Associate Professor in Mathematics, University of Exeter
2001-2016 University of Portsmouth (UK), University of Aberdeen (UK), University of Bristol (UK),
Humboldt University of Berlin (Germany)
2001 PhD in Mathematics, Humboldt University of Berlin (Germany), Supervisors: L. Recke, K.R. Schneider

Research area:

Applications of Dynamical Systems (overall 56 publications, see http://empslocal.ex.ac.uk/people/staff/js543)

Tracking dynamically unstable phenomena in experiments
These methodologies have been taken up by experimenters in mechanical and civil engineering,

cell biology and fluid dynamics. The EPSRC (UK) Fellowship 2017-2021 expanded the scope of these methods to applications in complex systems in other areas such tipping points in Climate Science and Ecology. Generic stabilizability for time-delayed feedback control. PRSA 472 (2016), Controlling unstable chaos: Stabilizing chimera states by feedback. PRL. 112 (2014), Experimental continuation of periodic orbits through a fold. PRL. 100 (2008). Dynamical systems with delay. Rigorous mathematical results have informed contribution to development of the opensource software DDE-Biftool, which is widely used in the community (7,450 downloads since 2015). Temporal dissipative solitons in time-delay feedback systems. PRL 123 (2019). Finding periodic orbits in state-dependent delay differential equations as roots of algebraic equations. DCDS-A 32 (2012).

PhD students and Postdoctoral Researchers supervised
PhD students Paul D. L. Ritchie (graduated 2016), Courtney Quinn (2019), Robert E. Carroll, Asim Alawfi, John Osei
Postdocs Patricia Verrier (2011-2013), Ozkan Karabacak (2017-2018), Bert Wuyts (since 2018)

Public Support and Recognition
EPRSC (UK) funding
Fellowship Exploring instability in complex systems 2017-2021, Grant Control-based Bifurcation Analysis for Experiments, 2012-2014
EU funding ITN Critical Transitions in Complex Systems, 2015-2019, H2020 Project Tipping Points in Earth Systems, 2019-2023
2016 Plenary lecture at XXXVI European Dynamics Days, Corfu (Greece) 2016
2010-2021 Associate Editor on Editorial Board, SIAM Journal on Applied Dynamical Systems
Member of LMS, SIAM

Delfim F.M. Torres

University of Aveiro

Portugal

Email: delfim@ua.pt

Existence and uniqueness of solution for fractional differential equations with integral boundary conditions and the Adomian Decomposition Method

We propose an Adomian decomposition method to solve a class of nonlinear differential equations of fractional-order with Caputo derivatives and integral boundary conditions. Our approach uses the

integral boundary conditions to derive an equivalent nonlinear Volterra integral equation before establishing existence and uniqueness of solution and a recursion scheme for the solution. The convergence of the method is proved and an error analysis given. Two numerical examples are solved by obtaining a rapidly converging sequence of analytical functions to the solution. Joint work with: Om Kalthoum Wanassi (University of Aveiro) and Rim Bourguiba (University of Monastir).

Short bio

Delfim F. M. Torres was born 16 August 1971 in Portuguese East Africa. He is, since 2015, a Full Professor of Mathematics at University of Aveiro (UA), Director of the Center for Research and Development in Mathematics and Applications(CIDMA), the largest Portuguese Research Center in Mathematics, and Coordinator of the Systems and Control Group. He obtained a MSc in Optimization and Control Theory in 1998, a PhD Mathematics in 2002, and Habilitation in Mathematics in 2011. His main research area is calculus of variations and optimal control; optimization; fractional derivatives and integrals; dynamic equations on time scales; and mathematical biology. Torres has written outstanding scientific and pedagogical publications. In particular, he has authored and co-authored two books with Imperial College Press, three books with Springer, being also an Editor of books with Springer and Elsevier. He has strong experience in graduate and post-graduate student supervision and teaching in mathematics. Moreover, he has been team leader and member in several national and international R&D projects, including EU projects and networks. He is, since 2013, the Director of the Doctoral Programme Consortium in Mathematics and Applications (MAP-PDMA) of Universities of Minho, Aveiro, and Porto. Prof. Torres is married since 2003, and has one daughter and two sons. Professor Torres is a Distinguished University Professor, a Highly Cited Researcher in Mathematics (2015, 2016, 2017 and 2019), and Lifetime Member of The American Mathematical Society. He is one of the founders of fractional variational analysis and fractional optimal control, and has made tremendous contributions to the theory of variational analysis with applications to many other fields such as optimization, optimal control, time-scale analysis, and mathematical epidemiology and biology. Professor Delfim F. M. Torres is the recipient of several international awards, including the 325 Years of Fractional Calculus Award, in Testimony of the High Regard for His Achievements in the Area of Fractional Calculus and Its Applications, is included in the World's Top 2% Scientists 2020 by Stanford University, both as a Career-long Highly Cited Researcher and as a single calendar year Highly Cited Researcher, was considered by Thomson Reuters as one of the World's Most InfluentialScientific Minds, won a Publons Peer Review Award as a world's top peer reviewer, was recognized in the top 1% of reviewers, a Sentinel of Science Award, and so on. Many of his research works have beenconsidered top papers in the area, served as research highlights, and been awarded prizes. Besides being a great scholar, he is also a great teacher who has already educated twenty two Ph.D. students from all over the world. Special: https://www.mdpi.com/journal/axioms/special_issues/delfim

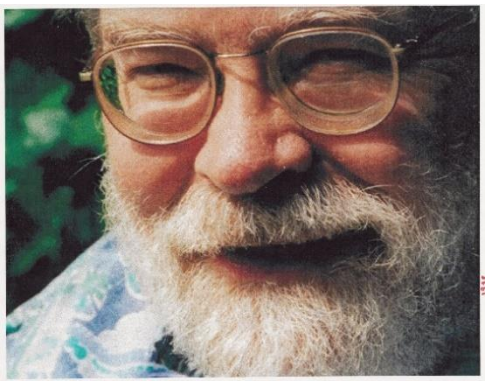

James Yorke

University of Maryland

USA

Email: yorke@umd.edu

Properties of "almost every" equation F(X)=C: pure math for the applied scientist

This work is in collaboration with Sana Jahedi, Tim Sauer, and Naghmen Akhaven.

We ask what are the properties that hold for ``almost every'' system of equations? What does "almost every" mean? "Almost every" is defined so as to be useful to the scientist. I think of this as pure math for the applied scientist. Systems of M equations in N unknowns are ubiquitous in mathematical modeling. These systems, often nonlinear, are used to identify equilibria of dynamical systems in ecology, genomics, control, and many other areas. Our goal is to describe the properties that will hold for ``almost every'' F that has some structure, and in particular the global properties of solutions for structured systems of smooth functions. As an application of these ideas I will show examples of Lotka-Volterra systems of differential equations. One example has 14 species. We show that 3 must die out exponentially fast. The technique is rather unique. We produce a "team" of 24 Lyapunov functions, each of which gives different information about which species will die out.

Short bio

A.B., Columbia University 1963; James Yorke has been at the University of Maryland since 1963. Ph.D. in Mathematics: University of Maryland at College Park 1966.

Currently: Distinguished University Research Professor of Mathematics and Physics, Univ. of Maryland, College Park, MD, USA. James Yorke is perhaps best known for coining the mathematical term chaos in his 1975 paper with Tien-Yien Li "Period Three Implies Chaos". He came to the University of Maryland as a math graduate student in 1963 hoping to explore interdisciplinary mathematics. Those hopes were fully realized after he received his Ph.D. and joined the faculty of the University of Maryland. He feels that a Ph.D. in mathematics is a license to investigate the universe. His current research interests include simple models for covid-19, for ecosystems, for ergodic chaotic systems with multiple instabilities. In 2003 he was awarded the Japan Prize jointly with Benoit Mandelbrot for their work in chaos and fractals in a ceremony presided over by the Emperor of Japan.

AWARDS

CAREER AWARD For extraordinary contributions in Nonlinear Dynamics

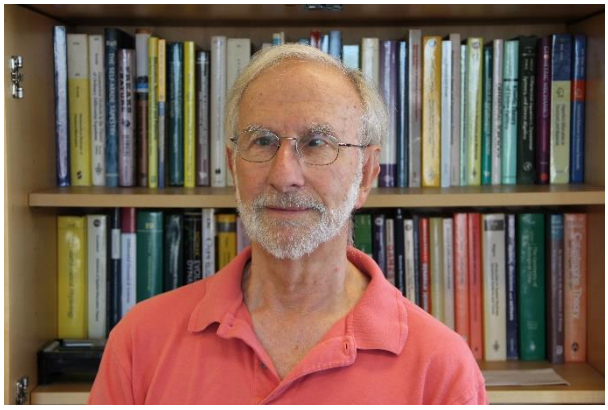

Professor Martin Golubitsky - Info

Hopf Bifurcation in Networks and Binocular Rivalry

J.A. TENREIRO MACHADO AWARD For breakthrough achievements in Fractional Calculus

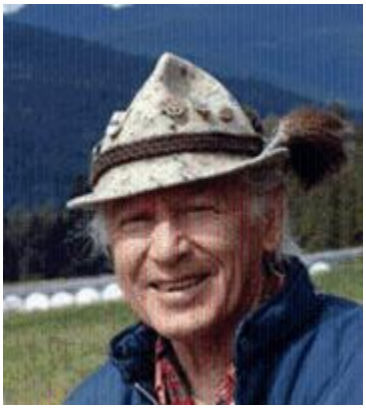

Professor Michele Caputo - Info

Memory, Mathematics and economics II

JAMES YORKE AWARD For breakthrough achievements in Nonlinear Dynamics and Chaos

Professor Miguel A.F. Sanjuán - Info

Partial Control and Beyond: Forcing Escapes and Controlling Chaotic Transients with the Safety Function

Abstract: A new control algorithm based on the partial control method has been developed. The general situation we are considering is an orbit starting in a certain phase space region Q having a chaotic transient behavior affected by noise, so that the orbit will definitely escape from Q in an unpredictable number of iterations. Thus, the goal of the algorithm is to control in a predictable manner when to escape. While partial control has been used as a way to avoid escapes, here we want to adapt it to force the escape in a controlled manner. We have introduced new tools such as escape functions and escape sets that once computed makes the control of the orbit straightforward. The partial control method aims to avoid the escape of orbits from a phase space region Q where the transient chaotic dynamics takes place. The technique is based on finding a special subset of Q called the safe set. The chaotic orbit can be sustained in the safe set with a minimum amount of control. We have developed a control strategy to gradually lead any chaotic orbit in Q to the safe set by using the safety function. With the technique proposed here, the safe set can be converted into a global attractor of Q. This is joint work with Gaspar Alfaro and Rubén Capeáns, URJC, Spain.

keywords: partial control; chaotic transients; safety function

[1] Juan Sabuco, Miguel A. F. Sanjuán and James A. Yorke. Dynamics of Partial Control. Chaos 22, 047507, (2012).

[2] Ruben Capeáns, Juan Sabuco, and Miguel A.F. Sanjuán. A new approach of the partial control method in chaotic systems. Nonlinear Dynamics 98, 873--887 (2019)

[3] Gaspar Alfaro, Rubén Capeáns, and Miguel A. F. Sanjuan. Forcing the escape: Partial control of escaping orbits from a transient chaotic region. Nonlinear Dynamics 104, 1603–1612 (2021)

[4] Rubén Capeáns and Miguel A. F. Sanjuán. Beyond partial control: Controlling chaotic transients with the safety function. Nonlinear Dynamics 107, 2903–2910 (2022)

BEST STUDENT PAPER For outstanding young scholars in Mathematical Analysis and Applications

Akhil Srivastav and Vanessa Steindorf, for their work on Complex dynamics in SIR model-type driven by disease enhancement factor and temporary immunity in secondary infections, BCAM - Basque Center for Applied Mathematics, Bilbao, Basque Country – Spain.

BEST POSTER For best poster presentation in Mathematical Analysis and Applications

Renato Colucci, Érika Diz-Pita and M. Victoria Otero-Espinar, for their work on The influence of indirect effect in the dynamics of a three-dimensional population model, Universitá Politecnica delle Marche, Ancona, Italy, and Universidade de Santiago de Compostela - CITMAga, Spain

LIST OF SYMPOSIA

- SYMPOSIUM #1: Impact of fractional calculus in modelling and control applications

  Carla Pinto[1], Eva Dulf[2], Cristina Muresan[2]

  [1]School of Engineering Polytechnic of Porto, Portugal, mailto:mcap@isep.ipp.pt

  [2]Technical University of Cluj-Napoca, Romania, mailto:mcristina.pop@aut.utcluj.ro

- SYMPOSIUM #2: State-of-the-art of fractional biological models

  Dumitru Baleanu[1], Carla Pinto[2], Devendra Kumar[3], Necati Ozdemir[4]

  [1]Cankaya University, Turkey and Institute of Space Sciences, Romania, dumitru@cankaya.edu.tr

  [2]School of Engineering Polytechnic of Porto, Portugal, mailto:mcap@isep.ipp.pt

  [3]University of Rajasthan, India, mailto:mdevendra.maths@gmail.com

  [4]Balikesir University, Turkey, mailto:mnozdemir@balikesir.edu.tr

- SYMPOSIUM #3: Fractional differential theory and applications

  M. Manuela Rodrigues[1], N. Loureiro Vieira[1], Milton Ferreira[2]

  [1]CIDMA, University of Aveiro, mailto:mmrodrigues@ua.pt

  [2]School of Technology and Management, Polytechnic Institute of Leiria & CIDMA, University of Aveiro.

- SYMPOSIUM #4: Mathematical analysis in medical applications

  Inês Domingues

  Medical Physics, Radiobiology and Radiation Protection Group, IPO Porto Research Centre (CI-IPOP), Portugal, mailto:minesdomingues@gmail.com

- SYMPOSIUM #5: Dynamical systems, special equations and applications

  Helena Reis[1], Júlio C. Rebelo[2]

  [1]Faculty of Economics, University of Porto and Centre for Mathematics, University of Porto, mailto:mhreis@fep.up.pt

  [2]University of Toulouse, mailto:mrebelo@math.univ-toulouse.fr

- SYMPOSIUM #6: Mathematical Modeling in Fuzzy-Structured Space

  Irina Perfilieva[1], Alireza Khastan[2], Stefania Tomasiello[3]

  [1]University of Ostrava, Czechia, mailto:mirina.perfilieva@osu.cz

  [2]Institute for advanced studies in basic sciences (IASBS), Zanjan, Iran, mailto:Khastan@iasbs.ac.ir

  [3]Institute of Computer Science, University of Tartu, Estonia, mailto:mstefania.tomasiello@ut.ee

- SYMPOSIUM #7: Symmetries and Conservation Laws for Nonlinear Partial Differential Equations with Applications

  Stephen Anco[1],Maria Santos Bruzón[2], Maria Luz Gandarias[2]

  [1]Department of Mathematics and Statistics Brock University, St. Catharina On l2s3a1, Canada, mailto:msanco@brocku.ca

  [2]Department of Mathematics, University of Cadiz, Puerto Real, Spain, mailto:mmarialuz.gandarias@uca.es

- SYMPOSIUM #8: Dynamics and Games

  Alberto Pinto[1], José Martins[2]

  [1]LIAAD-INESC TEC and Faculty of Sciences, University of Porto, Portugal, aapinto@fc.up.pt

  [2]LIAAD-INESC TEC and School of Technology and Management, Polytechnic Institute of Leiria, Portugal, mailto:mjmmartins@ipleiria.pt

- SYMPOSIUM #9: Difference & differential equations with applications

  Sandra Pinelas

Academia Militar, Portugal, mailto:msandra.pinelas@gmail.com

- SYMPOSIUM #10: Stochasticity, nonlinearity and complexity in science and engineering

Yong Xu[1], Stefano Lenci[2]

[1]Northwestern Polytechnical University, China, mailto:mhsux3@nwpu.edu.cn

[2]Polytechnic University of Marche, Italy

- SYMPOSIUM #11: Fractional viscoelasticity

Magda Rebelo[1], M. Luísa Morgado[2], Luís Lima Ferrás[3]

[1]Centro de Matemática e Aplicações (CMA) and Departamento de Matemática, Faculdade de Ciências e Tecnologia, Universidade NOVA de Lisboa, Portugal, mailto:mmsjr@fct.unl.pt

[2]CEMAT, Instituto Superior Técnico, Universidade de Lisboa & Departamento de Matemática, Universidade de Trás-os-Montes e Alto Douro, UTAD, Vila Real, Portugal, mailto:mluisam@utad.pt

[3]Centro de Matemática, Universidade do Minho (CMAT), Portugal, mailto:mluislimafr@gmail.com

- SYMPOSIUM #12: Advances in differential equations with uncertainties and modeling

Tomás Caraballo[1], Juan Carlos Cortés[2], Rafael Villanueva[2]

[1]Departamento de Ecuaciones Diferenciales y Análisis Numerico, Facultad de Matemáticas, Universidad de Sevilla, Spain, mailto:mcaraball@uv.es

[2]Instituto Universitario de Matemática Multidisciplinar, Universitat Politècnica de València, Spain, mailto:mjccortes@imm.upv.es and mailto:mrjvillan@imm.upv.es

- SYMPOSIUM #13: Mathematical models in epidemiology

Maíra Aguiar[1,2,*], Vanessa Steindorf[1], Akhil Kumar Srivastav[1]

[1]BCAM - Basque Center for Applied Mathematics, Bilbao, Basque Country, Spain

[2]Ikerbasque, Basque Foundation for Science, Basque Country, Spain

[3]Dipartimento di Matematica, Universita degli Studi di Trento, Italy

mailto:maguiar@bcamath.org and mailto:vsteindorf@bcamath.org and mailto:masrivastav@bcamath.org

- SYMPOSIUM #14: Mathematics Education

Carla Pinto[1], Jorge Mendonça[1], Fernando Carvalho[1], Lurdes Babo[2]

[1]School of Engineering Polytechnic of Porto, Portugal, mailto:cap@isep.ipp.pt

[2]Porto Accounting and Business School, Polytechnic of Porto, CEOS, Portugal, mailto:lbabo@iscap.ipp.pt

TABLE OF CONTENTS

Analysis of a model for epilepsy. 1

Candace M. Kent, David M. Chan

The interplay between sub-critical fluctuations and import: understanding COVID-19 dynamics and subsequent vaccination impact. 3

Nico Stollenwerk and Maira Aguiar

Spatial epidemiological models of infectious disease transmission: multiscale and heterogeneity . . . . . features.. 5

Damián Knopoff, Nicole Cusimano, Maíra Aguiar and Nico Stollenwerk

Rate-induced tipping in mathematical models in epidemiology 9

Jochen Merker

Complex dynamics in SIR model-type driven by disease enhancement factor and temporary immunity in secondary infections. 13

Vanessa Steindorf, Maíra Aguiar, Akhil Srivastav, Nico Stollenwerk and Bob Kooi

Understanding the immunological responses mediated by antibodies during primary dengue infection 17

Vizda Anam and Maíra Aguiar

Optimal vaccine allocation for the control of sexually transmitted infections 19

Fernando Saldaña, Vanessa Steindorf, Akhil Srivastav, Nico Stollenwerk and Maíra Aguiar

Optimal control of multi-strain host-vector dengue model 21

Akhil Kumar Srivastav, Vanessa Steindorf, Nico Stollenwerk, Bob W. Kooi and Maira Aguiar

A pragmatic view on chaotic dynamics and ergodicity in a SIR-like epidemic model 23

Bruno Valdemar Guerrero Borges, Maíra Aguiar and Nico Stollenwerk

Optimal strategies for mitigating the HIV/AIDS epidemic in the Philippines 25

Carlo Delfin S. Estadilla and Aurelio A. de Los Reyes

Stochastic differential equation models of animal growth and optimization in cattle raising 27

Carlos A. Braumann, Gonçalo Jacinto, Patrícia A. Filipe

Impact of travel restrictions on the spread of infection 31

Kjetil Holm, Swar Ramo, Josef Rebenda and Yuriy Rogovchenko

A deterministic model for Atlantic salmon life cycle 35

Kjetil Holm, Swar Ramo, Josef Rebenda and Yuriy Rogovchenko

Dynamics of a pituitary-adrenal model with distributed time delays 39

Roxana Matei, Eva Kaslik and Mihaela Neamtu

A mathematical model of CD19- relapses after CAR-T cell treatment in B cell leukemia 43

Salvador Chulián, Álvaro Martínez-Rubio, Ana Niño-López and María Rosa

Parameter estimation for a FSDE model of glucose control. 47

Simona Panunzi, Alessandro Borri, Elvin Moore and Andrea De Gaetano

A Mathematical Model of Acute Lymphoblastic Leukemia Development 49

Ana Niño-López, Álvaro Martínez-Rubio, Salvador Chulián and María Rosa

Stochastic cellular automaton for modeling benign and invasive tumor dynamics. 53

Carlos Alberto Valentim, José Antonio Rabi and Sergio Adriani David

A mathematical model of the population diffusion of Candida Auris within an Intensive Care Unit. . . .57

Cristina Perez Diukina, Rafael-Jacinto Villanueva, Carlos Andreu-Vilarroig and Juan-Carlos Cortes

Modelling antibiotic resistance from an agent-based modelling approach: an application to colistin-resistant A. baumannii 61

Carlos Andreu-Vilarroig, Rafael-Jacinto Villanueva, Juan-Carlos Cortés, Juan Carlos Orengo and Juan A. Aledo

A numerical scheme for a model of drug delivery enhanced by light 65

Jose Augusto Ferreira, Hugo Gómez and Luis Pinto

Stability and bifurcations in an infinite network of theta neurons. . . .. .69

Lavinia Birdac, Eva Kaslik and Raluca Muresan

Multi-parametric controlling cancer cell invasion in biological systems with memory of states.. 73

Larysa Dzyubak, Oleksandr Dzyubak and Jan Awrejcewicz

Global dynamics of a Kolmogorov predator-prey system.. 77

Érika Diz-Pita, Jaume Llibre and M. Victoria Otero-Espinar

From Duffing equation to bio-oscillations. 81

Felix Sadyrbaev

Modeling real noise in population dynamics with applications to the chemostat model 85

Javier López-de-la-Cruz

Exact solutions for a mathematical model of high-grade brains tumors through symmetry reductions. 89

María Rosa Durán, Salvador Chulián, Ana Niño-López, Álvaro Martínez-Rubio and María Luz Gandarias

A higher degenerated invasive-invaded species interaction. 93

José Luis Díaz Palencia

Auscultation chest locations are correlated with short term spectral features of pulmonary sounds. . .97

Sebastian Escobar-Pajoy and Juan Ugarte

Kurtosis vector for rotor detection in cardiac fibrillation. 101

Juan Alzate-Marulanda, Steven Giraldo-Mora, Catalina Tobón and Juan Ugarte

Symmetry reductions of a viscoelastic hyperbolic equation modelling biological processes 105

Almudena del Pilar Márquez, Elena Recio, Tamara María Garrido and María Luz Gandarias

Poisson stable dynamics of shunting inhibitory cellular neural networks 109

Marat Akhmet, Madina Tleubergenova, Akylbek Zhamanshin

Rayleigh function of energy dissipation in modelling oscillatory behaviour of moving sister chromatids in anaphase of mitosis 111

Andjelka N. Hedrih, Katica (Stevanović) Hedrih, Jasmina Bogdanovic-Jovanovic

Mathematical analysis of two strain epidemic model with crossover behavior. 115

Aziz Khan, Kamal Shah, Thabet Abdeljawad and Manar A. Alqudah

Age-Structured HIV Model Incorporating Cell to Cell Transmission with Latently Infected T Cells . . . 117

Manoj Kumar and Syed Abbas

Implementation strategies of event-based fractional order controllers in targeted drug delivery applications 119

Isabela Birs and Cristina Muresan

Fractional order tumor growth model 123

Eva-H. Dulf, Levente Kovacs and Lucian Mocan

Lipschitz stability analysis of impulsive delayed reaction-diffusion fractional neural network models. 127

Ivanka Stamova, Trayan Stamov and Gani Stamov

Stability of epidemic fractional models. 131

Cristiana J. Silva

Electrical potential of fractal structures in the point of view of fractional calculus. 135

Isabel S. Jesus and Ramiro S. Barbosa

On the fractional derivatives with an exponential kernel 139

Enyu Fan, Changpin Li, Jingshu Wu, Shaoying Zeng

Fractional versions of complex Wirtinger (d-bar) derivatives 143

Arran Fernandez and Chaima Bouzouina

On state variables and fractional derivatives 147

Blas M. Vinagre Inés Tejado Carlos M. Vinagre

Stability properties of multi-term fractional-differential equations with four fractional derivatives.. . 151

Oana Brandibur and Eva Kaslik

Solving the fractional Ambartsumian equation.. 155

Manuel Ortigueira and Gabriel Bengochea

Solving Prabhakar differential equations using Mikusiński's operational calculus.. 159

Noosheza Rani Arran Fernandez

Mittag-Leffler special function and its connection to special Lévy processes. 161

Janusz Gajda

Ψ-Hilfer fractional relaxation-oscillation equation. 163

Nelson Vieira, Milton Ferreira and M. Manuela Rodrigues

On a regular Ψ-fractional Sturm-Liouville problem. 167

Milton Ferreira, M. Manuela Rodrigues and Nelson Vieira

On a Hilfer-Hadamard fractional integro-differential inclusion. 171

Aurelian Cernea

On the Ulam, Hyers and Rassias stabilities for a Caputo fractional boundary value problem of order greater than two. 175

Luís Castro and Anabela Silva

A complete study of the fractional Hermite differential equation with uncertainties 179

Clara Burgos Simón, Juan Carlos Cortés López, Tomás Caraballo Garrido, Laura Villafuerte Altúzar and Rafael Jacinto Villanueva Micó

Fractional dependence in integer order PDE. 183

Daniel Cao Labora

Fractional derivative of the Lerch zeta function - further properties. 187

Emanuel Guariglia

Fractional derivative as normalization approach for clustering applications. 189

Diego Mauricio Murillo Gómez and Juan Ugarte

Beyond entropy: the Zeta function 193

Alain Mehauté, Philippe Riot, Alina Gavrilut, Dmitriii Tayurskii

Numerical methods for singular fractional integro-differential equations with constant coefficients.. 197

Kaido Lätt

Fractal-Fractional Order Modeling for the Disease Dynamics in both Prey and Predator. 201

Zubair Ahmad, Francesco Giannino, Gerardo Toraldo

Strichartz estimates for structurally damped equations of space-time-fractional type. 203

Nelson Faustino and Jorge Marques

Fractional Choquet Integral on Time-scale with respect to Non-additive Measure.. 207

Shekhar Singh Negi and Vicenc Torra

Well-posedness of stochastic time fractional 2D-Stokes models with finite and infinite delays. 209

Tomas Caraballo and Jiaohui Xu

Averaging principle for Caputo fractional stochastic differential equations with fractional Brownian motion. 213

Ruifang Wang, Yong Xu and Bin Pei

Fuzzy transform for fractional fuzzy problem 217

Irina Pefilieva and Thi Minh Tam Pham

Solution of fuzzy integral equations of the second kind. 221

Zahra Alijani and Urve Kangro

Collocation based approximations for fractional boundary value problems.. 225

Hanna Britt Soots, Kaido Lätt and Arvet Pedas

A Collocation Method Based on Central Part Interpolation for Fractional Integro-Differential Equations… 229

Margus Lillemäe, Arvet Pedas and Mikk Vikerpuur

Numerical solution of linear multi-term fractional differential equations.. 233

Arvet Pedas and Mikk Vikerpuur

An Efficient Matrix Method For Coupled Systems of Variable Fractional Order Differential Equations. 237

Kamal Shah, Thabet Abdeljawad and Iyad Suwan

Approximating Fractional Calculus Operators with General Analytic Kernel by Stancu Variant of Modified Bernstein-Kantorovich Operators.. 239

Mehmet Ali Özarslan

Bivariate Modified Bernstein-Kantorovich Operators for the Numerical Solution of Two-Dimensional Fractional Volterra Integral Equations. 241

Suzan Cival Buranay

Some representations for the eigenfunctions of the time-fractional wave operator 245

M. Manuela Rodrigues, Milton Ferreira and Nelson Vieira

Stable coalition formation for the preservation of public goods 249

Alberto Pinto and Elvio Accinelli

Firm Network Location-Price Game. 251

João P. Almeida and Alberto Pinto

The value of information search against fake news. 253

José Martins and Alberto Pinto

Local equilibria in price competition with positive network effects. 255

Renato Soeiro and Alberto Pinto

Bifurcation analysis for a discrete-time delayed dynamic Cournot mixed oligopoly model.. 257

Loredana-Camelia Culda, Eva Kaslik and Mihaela Neamțu

Evaluation of the utility loss due to habit formation: application to an environmental project. 261

Hidekazu Yoshioka, Motoh Tsujimura, Kunihiko Hamagami and Haruka Tomobe

Resolving a dynamic winner determination problem (WDP) by dynamic programming 265

Asli Larbi

Analysis of the effect of the randomized damping coefficient on the response of a SDOF system. . . . 269

Ana Navarro Quiles, Rossella Laudani and Givanni Falsone

Initial boundary value problem for hyperbolic equation with piecewise-constant argument or generalized type. 273

Анар Assanova

Dependence on the initial conditions of the numerical solution for the model of the flow and thermal explosion of a reactive micropolar real gas.. 277

Angela Bašić-Šiško

Godunov-Type Methods for Computing Homogeneous Mixture Flows 281

A. Qadi El Idrissi, Eric Goncalves da Silva and Dia Zeidan

Probabilistic analysis of a cantilever beam with random parameters via probability density functions 285

Juan Carlos Cortés López, Elena López Navarro, José Vicente Romero Bauset and María Dolores Roselló Ferragud

On the semilinear damped wave equations in Friedmann-Lemaitre-Robertson-Walker spacetime. . . 289

Jorge Marques and Marcelo Ebert

Exponential scaling and order preserving in a higher order operator with non-linear diffusion and reaction. 293

José Luis Díaz Palencia

On analogue of blow-up solutions for a discrete variant of second-order Emden-Fowler differential equation. 297

Josef Diblik and Evgeniya Korobko

Generalised Distributed-Order Maxwell Model: the case of a distributed-springpot and a dashpot . . 301

Magda Rebelo, Luis Ferrás and Maria Luísa Morgado

New Insights into the Generalised Distributed-Order Maxwell Model 305

Maria Luisa Morgado, Magda Rebelo and Luís Ferrás

A Heisenberg-Pauli-Weyl type inequality for a generalized wavelet transform 309

Luís Castro and Rita Guerra

On the solutions to differential equations with uncertainties: comparison of different approaches. . 313

Rosana Rodríguez-López

An Improved Integro-Differential Linear Viscoelastic Model 317

Luís Ferrás, Maria Luísa Morgado, Magda Rebelo, Rosalía Leiva, Juliana Bertoco, Alexandre Afonso and A. Castelo

On a boundary-value problem with parameter for differential equations with piecewise constant argument of generalized type. 321

Roza Uteshova

Solvability conditions for the special Cauchy problem.. 325

Sandugash Mynbayeva

On the well-posedness of the Cauchy problem for the quasi-linear controlled neutral functional differential equation. 329

Tea Shavadze

A Fuzzy q-Symmetric Variational Problem via Granular Differentiability Approach.. 333

Tri Truong, Linh Nguyen and Baruch Schneider

Probabilistic analysis of a general kinetic equation with uncertainty. 337

Juan Carlos Cortés, Ana Navarro Quiles and Sorina Madalina Sferle

Probability Density Evolution Simulation and its Applications in Random Differential Equations 341

Vicente Bevia, Juan Carlos Cortés and Rafael Jacinto Villanueva

Oscillation criteria for second-order half-linear neutral functional differential equations 345

Irena Jadlovska

Symmetric flow models of an ideal micropolar compressible and heat-conducting gas. 349

Ivan Dražić

F-transform-based Laplace Operator. 353

Hana Zámečníková and Irina Perfilieva

Unproportional mosaicking. 357

Vojtěch Molek, Petr Hurtik, Pavel Vlasanek and David Adamczyk

Prediction of dynamical systems driven by Lévy noise based on deep learning. 361

Zi-Fei Lin, Yan-Ming Liang and Jia-Li Zhao

Existence and approximation of solutions to a class of second-order functional differential equations 365

Rosana Rodríguez-López

On the Stochastic Linear Quadratic Optimal Control Problem by Piecewise Constant Controls. The Infinite Horizon Time Case 369

Vasile Dragan, Ioan-Lucian Popa and Samir Aberkane

A reaction-diffusion model of virus-immune system interaction: Lie symmetries. 373

Tamara María Garrido Letrán, Almudena del Pilar Márquez and Rafael de La Rosa

From unequal size sample sums to estimating the standard deviation 377

Miguel Casquilho and Jorge Buescu

Efficient Algorithms for Joint Approximate Diagonalization of Multiple Matrices. 381

Nela Bosner

Numerical Treatments for Some Stochastic-Deterministic Chaotic Systems 385
N. H. Sweilam, S. M. AL-Mekhla and N. R. Alsenaideh

Some 2-orthogonal polynomial eigenfunctions of differential operators 389

Teresa A. Mesquita

Poisson stability in Duffing equations.. 393

Akylbek Zhamanshin, Marat Akhmet and Madina Tleubergenova

Cosine and sine functions on time scales 397

Aldo Pereira

On some recent results from the theory of MHD equations. 399

Jiri Neustupa

Existence results for nonlinear boundary value problems with a generalized Laplacian 403

Miroslawa Zima

Exact solvability conditions for the model with a discrete memory effect. 405

Natalia Dilna

Some regularity results for solutions to the Navier-Stokes equations 409

Petr Kučera

Analysis of a stochastic differential equation with nonlocal discrete diffusion modeling life tables. . . 413

José Valero, Francisco Morillas and Tomás Caraballo

Point symmetries and conservation laws of the generalized Krichever-Novikov equation in 2+1 dimensions 417

Stephen Anco, James Hornick and Thomas Wolf

Exact solitary wave solutions for a coupled gKdV-NLS system. 421

Stephen Anco, James Hornick, Richard Zhao and Thomas Wolf

About the structure of attractors for a nonlocal Chafee-Infante problem. 425

Rubén Caballero Toro, Alexandre Carvalho, Pedro Marín-Rubio and José Valero

The conditional regularity of the weak solutions of the Navier-Stokes equations. 427

Zdenek Skalak

Precise Laplace approximation for mixed rough differential equation. 431

Yong Xu and Xiaoyu Yang

Virtual operators generated by operator families 435

Vladimir Vasilyev

A five dimensional model with two distributed time delays. 439

Loredana Flavia Vesa, Mihaela Neamtu, Eva Kaslik and Liliana Harding

Increasing the applicability of Chebyshev-Secant-type methods. 443

Nisha Yadav, Sukhjit Singh, Miguel Angel Hernández Verón and Eulalia Martínez

Second order semilinear inclusions without compactness. 447

Valentina Taddei and Martina Pavlackovà

A coupled finite-volume solver for numerical simulation of log-conformation tensor based viscoelastic flows 449

Célio Fernandes

Stability and flip bifurcation of a three dimensional exponential system of difference equations. . . .451

Chrysoula Mylona, Garyfalos Papaschinopoulos and Christos Schinas

High order schemes for a subdiffusion problem 453

Ercília Sousa and Carla Jesus

Weak Pontryagin's Maximum Principle for Optimal Control Problems Involving a General Analytic Kernel. 455

Faïçal Ndaïrou and Delfim F. M. Torres

Differential equations with state-dependent delays and their solution manifolds 457

Hans-Otto Walther

The effect of the same damping parameter presence in a system of linear and nonlinear oscillators. 459

Jamal Odysseas Maaita, Lazaros Laskaridis, Dimitrios Prousalis and Christos Volos

Prediction capabilities of data-driven operator based algorithms on some classes of differential equations. 461

Nelida Črnjarić -Žic, Senka Maćešić

Oscillation criteria for second order neutral delay differential equations. 463

Sandra Pinelas

Stability for time scale dynamics. 467

Sergey Kryzhevich

Exponential Lag Synchronization of Cohen-Grossberg Neural Networks with Discrete and Distributed Delays on Time Scales. 469

Vipin Kumar, Jan Heiland and Peter Benner

Partial Control and Beyond: Forcing Escapes and Controlling Chaotic Transients with the Safety Function 471

Miguel A. F. Sanjuán

Unpredictable solutions of quasilinear differential equations with generalized pircewise constant arguments 473

Zakhira Nugayeva, Marat Akhmet, Duygu Aruğaslan Çinçin and Madina Tleubergenova

Mathematical modelling and analysis of non-Newtonian nanofluid flows over stretching sheets 477

G. Bognár

Multi-class Semantic Segmentation for Prostate Cancer Radiotherapy Treatment Optimization.. … . .481

Bruno Mendes, Inês Domingues and João Santos

Fractal Brownian motion vs global assessment of cop excursion during impulse phase on standard MJV 485

Carlos Rodrigues, Miguel Correia, João Abrantes, Marco Aurélio Benedetti Rodrigues and Jurandir Nadal

Building a script that emulates VeriSoft® in the Gamma Analysis of Complex Radiotherapy Treatments 489

Leyla Ebrahimpour, Inês Domingues, Sofia Silva, Diana Pimparel, Joana Lencart, Bruno Mendes, Filipe Dias and João Santos

Calculating and employing Complexity Indexes to compare and improve the quality of the VMAT plan delivery in Radiotherapy Treatments 493

Leyla Ebrahimpour, Sofia Silva, Diana Pimparel, Joana Lencart, Bruno Mendes, Filipe Dias, Inês Domingues and João Santos

Using a Logit Approach to Determine the Occurrence of Barotrauma Under Hyperbaric Oxygen Therapy: a Case Study 497

M Filomena Teodoro and Sofia S. Teles

Attitute and Practice of Embarked Staff About Zika Virus 501

M. Filomena Teodoro, João Faria, Rosa Teodósio

Response models in experimental studies of fresh properties of cement pastes: Part I – typical approach through changes one-variable-at-a-time 505

Lino Maia

Response models in experimental studies of fresh properties of cement pastes: Part II – statistical approach based in a central composite design 509

Lino Maia

Inspection in the ceramics and glass industry 513

João Mendes, Nuno Ferreira and Victor Santos

Vision systems applied in the ceramic industry 517

André Santos and Nuno Ferreira

Development of grippers in the ceramic industry 521

Rogério Torres and Nuno Ferreira

Comparison of response models from full, fractionated and small central composite design of experiments in cement-based mortars. 525

Nara Cangussu, Ana Mafalda Matos and Lino Maia

Numerical modeling and optimization of self compacting mortars: central composite design approach with 529

Nara Cangussu, Ana Mafalda Matos and Lino Maia

Numerical methods for nonlocal and nonlinear parabolic equations with applications in hydrology and climatology 533

Łukasz Płociniczak

Transport models and internal transport barriers by stochastic solutions 535

R. Vilela-Mendes

Study of species' migration in biological population under symmetry analysis. 537

Dia Zeidan, Sumanta Shagolshem and B. Bira

Symmetry analysis and power series solution for cancer tumor model. 541

Dia Zeidan, B. Bira and S. Gimnitz Simon

The effect of boussinesq couple stress fluid flow with mass transpiration through a porous stretching sheet 545

K. N. Sneha, U. S. Mahabaleshwar and Dia Zeidan

An exact analytical solution of a mass transpiration due to stretching due to stretching/shrinking sheet with slip parameter. 549

R. Mahesh, K. N. Sneha, U. S. Mahabaleshwar and Dia Zeidan

Online Education of Future Mathematics Teachers in a Virtual Reality Environment. 553

Lilla Korenova and Angelika Schmid

An approach to signal filtering with mathematical transfer functions using Fourier series 557

Fernando Carvalho, Pedro Reis, Vítor Cardoso, Sandra Aires, Ana Costa, António Sousa and Pedro Guedes

Numerical approach to signal filtering with ODEs - classical programming and the Xcos didactic tool 561

Pedro Reis, Fernando Carvalho, Vítor Cardoso, Sandra Aires, Ana Costa, António Sousa and Pedro Guedes

Teaching differential equations for understanding 565

Svitlana Rogovchenko and Yuriy Rogovchenko

POSTERS

Modelling an electrical circuit using a system of differential equations. 569

Ana C. Meira Castro, António Sousa and Ana Júlia Viamonte

Mann's iteration scheme for Fredholm integral equation.. 573

Bahia Barache, Massinissa Souffit and Safia Hocine

Perturbation analysis of Probabilistic Boolean networks with gene perturbations 577

Massinissa Soufit, Baya Takhedmit and Karim Abbas

The influence of indirect effect in the dynamics of a three-dimensional population model 581

Renato Colucci, Érika Diz-Pita and M. Victoria Otero-Espinar

Geometric Properties of Analytic Functions Dened by (p,q) Derivative Operator Involving Poisson Distribution 585

S Santhiya and K Thilagavathi

Third Hankel Determinant Problem for Bounded Turning Functions, Starlike and Convex Functions Involving Pascal Distribution Series 587

S Santhiya and K Thilagavathi

The influence of the tail of claims distribution on the stability bounds of the univariate classical risk model 589

Safia Hocine, Djamil AÏssani and Aicha Bareche

International Conference on Mathematical Analysis and Applications in Science and Engineering
ICMA^{2}SC'22
ISEP Porto-Portugal, June 27 - 29, 2022

Analysis of a Model for Epilepsy

Candace M. Kent* **David M. Chan**

Virginia Commonwealth University, USA

*cmkent@vcu.edu

Abstract: In a monograph, we consider a phenomenological model of neuronal excitation intended to mimic the focal (i.e. regional) seizures of a common form of epilepsy, mesial (or middle) temporal lobe epilepsy. The model, originally introduced in a 2018 article by Chan and colleagues [1], is a nonautonomous, second-order, reciprocal difference equation with maximum and threshold functions:

$$x_{n+1} = \max\left\{\frac{A_n + D_n \cdot H_\epsilon(x_n)}{x_n}, \frac{B_n}{x_{n-1}}\right\}, \quad n = 0, 1, \ldots,$$

where H_ϵ is the Heaviside function defined by

$$H_\epsilon(x) = \begin{cases} 0, & 0 < x < \epsilon, \\ 1, & x \geq \epsilon. \end{cases}$$

We let the state variable x_n represent the density of activated, or excited, neurons at the nth time step in the middle structures of one of the temporal lobes of the brain. The parameter ϵ, which we call the "seizure threshold," and the initial densities of excited neurons, x_{-1} and x_0, are positive. The coefficient parameters $\{A_n\}_{n=0}^{\infty}$, $\{B_n\}_{n=0}^{\infty}$, and $\{D_n\}_{n=0}^{\infty}$ satisfy the following three hypotheses:

(H1) $\{A_n\}_{n=0}^{\infty}$ and $\{B_n\}_{n=0}^{\infty}$ are positive periodic sequences with minimal period 2.

(H2) $\{D_n\}_{n=0}^{\infty}$ is a positive periodic sequence with minimal period 3.

(H3) $A_0 + D_1, A_1 + D_1 < B_0, B_1 < A_0 + D_2, A_1 + D_2$.

Observe that $\{A_n + D_n\}_{n=0}^{\infty}$ is thus a positive periodic sequence with minimal period 6. Then this periodicity with minimal period a multiple of 3 and the inequalities in Hypothesis (H3) are the sufficient conditions for unboundedness and nonpersistence. In our talk, we will briefly discuss the following topics extensively covered in the monograph:

(i) Epilepsy and its associated seizures.

(ii) The connection between the model and epileptic seizures.

(iii) A foundation of analytic results showing that the model is consistent with reality.

keywords: max-type difference equation; eventual periodicity; epileptic seizures.

MSC2020: 39A20; 39A23; 39A60

References

[1] D.M. Chan, C.M. Kent, V.L. Kocić, and S. Stević. "Proposal for an application of a max-type difference equation to epilepsy." In: *Differential and Difference Equations with Applications*. Ed. by S. Pinelas, T. Caraballo, P. Kloeden, and J.R. Graef. New York: Springer, 2018, pp. 193–210.

THE INTERPLAY BETWEEN SUB-CRITICAL FLUCTUATIONS AND IMPORT: UNDERSTANDING COVID-19 DYNAMICS AND SUBSEQUENT VACCINATION IMPACT

Nico Stollenwerk[1⋆] **Maíra Aguiar**[1]

[1] BCAM, Bilbao, Spain

[1⋆]nico.biomath@gmail.com

Abstract: From previous analyses of COVID-19 dynamics in the Basque Country on the initial phases of exponential growth and first control measures in spring 2020 [1, 2, 3] we extended the analysis of the ongoing epidemiological data into summer and autumn 2020, observing and modelling the dynamics which by then was under control of community spreading, hence not in another exponential growth phase, but prone to isolated outbreaks due to external import via relaxation of travel restrictions.

In such scenarios one would expect on general grounds large fluctuations close to the critical threshold between community control and exponential explosion of cases [4], which could finally be modelled for the present case of COVID-19 and its data in the Basque Country [5]. The dynamics in autumn 2020 until close to the end of the year could be well described by the sub-critical fluctuations and import.

Based on this analysis we then developed models to describe and analyze the impact of the vaccination campaigns in the Basque Country, starting in January 2021, with various vaccines applied at the same time. One has to take into account that the different vaccines have different efficacies not only after full vaccination scheme, but especially between single dose and second does schemes. Here the question of protection against severe disease and against any infection [6] turned out to be very important in the overall outcome of the vaccination campaigns [7]. Especially, new variants of the virus challenge the vaccine efficacy, still reported to be high against severe disease, but with significantly lowering protection against mild and asymptomatic infection, well describable in SHAR and SHARUCD modelling frameworks, as set up as early as spring 2020 [1, 3]. Some first considerations will be made on such waning of vaccination immunity and its interplay with seasonal variation of infectivity in respiratory diseases, leading to new complex dynamics [8], the new normality we are living in, with COVID-19 as one of many seasonal respiratory diseases and its frequently appearing new variants.

keywords: epidemiology; critical thresholds; stochastic processes; large fluctuations; Bayesian statistics; chaotic dynamics; Lyapunov exponents.

MSC2020: 37A50; 37G15; 37N25; 60G07; 60J27; 62F15; 62P10; 92D25.

Acknowledgments

This research is supported by the Basque Government through the "Mathematical Modeling Applied to Health" Project, further the BERC 2018-2021 program and by Spanish Ministry of Sciences, Innovation and Universities: BCAM Severo Ochoa accreditation SEV-2017-0718. M. A. has also received funding from the European Union's Horizon 2020 research and innovation programme under the Marie Skłodowska-Curie grant agreement No 792494.

References

[1] Aguiar, M., Millán Ortundo, E., Bidaurrazaga Van-Dierdonck, J., Mar, J., & Stollenwerk, N. (2020) Modelling COVID-19 in the Basque Country from introduction to control measure response, *Nature Scientific Reports* **10**, 17306 (16 pages).

[2] Aguiar, M., Bidaurrazaga Van-Dierdonck, J., & Stollenwerk, N. (2020) Reproduction ratio and growth rates: measures for an unfolding pandemic, *PLoS ONE* **15**, e0236620 (14 pages).

[3] Aguiar, M., & Stollenwerk, N. (2020) SHAR and effective SIR models: from dengue fever toy models to a COVID-19 fully parametrized SHARUCD framework, *Commun. Biomath. Sci.* **3**, 60–89.

[4] Stollenwerk, N., & Jansen, V. (2011) *Population Biology and Criticality: From critical birth–death processes to self-organized criticality in mutation pathogen systems* (Imperial College Press, World Scientific, London).

[5] Stollenwerk, N., Bidaurrazaga Van-Dierdonck, J., Mar, J., Cusimano, N., Knopoff, D., Anam, V., & Aguiar, M. (2021) Critical fluctuations in epidemic models explain COVID-19 post-lockdown dynamics, *Nature Scientific Reports*, **11**, 13839 (12 pages).

[6] Stollenwerk, N., Bidaurrazaga Van-Dierdonck, J., Mar, J., & Aguiar, M. (2021) The role of mild and asymptomatic infections on COVID-19 vaccines performance: a modelling study, *accepted for publication in Journal of Advanced Research* (21 pages).
https : *//doi.org*/10.1016/*j.jare*.2021.10.012

[7] Stollenwerk, N., Mar, J., Bidaurrazaga Van-Dierdonck, J., Ibarrondo, O., Estadilla, C., & Aguiar, M. (2021) Modelling COVID-19 vaccine efficacy and coverage towards herd-immunity in the Basque Country, Spain, *medRxiv preprint, 12. July 2021*,
https : *//doi.org*/10.1101/2021.07.21260390

[8] Stollenwerk, N., Spaziani, S., Mar, J., Eguiguren Arrazabalaga, I., Knopoff, D., Cusimano, N., Anam, V., Shrivastava, A., & Aguiar, M. (2022) Seasonally forced SIR systems applied to respiratory infectious diseases, bifurcations and chaos, *Computational and Mathematical Methods*, **2022**, 3556043 (14 pages).

International Conference on Mathematical Analysis and Applications in Science and Engineering
ICMA^{2}SC'22
ISEP Porto-Portugal, June 27 - 29, 2022

SPATIAL EPIDEMIOLOGICAL MODELS OF INFECTIOUS DISEASE TRANSMISSION: MULTISCALE AND HETEROGENEITY FEATURES

Damián Knopoff[1,2⋆] **Nicole Cusimano**[1] **Maíra Aguiar**[1,3]
Nico Stollenwerk [1]

[1] Basque Center for Applied Mathematics (BCAM), Spain
[2] Centro de Investigaciones y Estudios de Matemática (CIEM-CONICET), Argentina
[3] Ikerbasque Foundation for Science, Spain

[1⋆]damian.knopoff@unc.edu.ar

Abstract: In this work, we provide a mathematical and computational framework to the modeling and simulation of the spatial dynamics of infectious disease contagion, spreading, control and prevention. Starting from lattice-based models, we present a stochastic cellular automata disease model based on the SHAR (**S**usceptible-**H**ospitalized-**A**symptomatic-**R**ecovered) compartmentalisation of the population, show some simulation results, and relate them to real-life data for influenza and COVID-19 provided by the Health Department and the Health Services of the Basque Country. By means of stochastic simulations, we perform a numerical study to have an insight into the critical threshold of the SHAR percolating system, as well as some numerical tools to seek infection clusters (groups of connected individuals who have been infected by the same index case), count them and monitor their sizes [1, 4]. Then, some concepts on network theory will be discussed in order to show how networks can be employed as a valuable tool to model spatial spreading. In particular, we discuss a kinetic model for the spread of a respiratory disease considering heterogeneous populations [2, 3], focusing on the role of the network structure and connectivity on the overall dynamics.

keywords: epidemiological models; spatial models; network theory; clusters.

MSC2020: 92C60; 92D30.

1 Introduction

Infectious diseases have shaped the global population throughout history, and (whether through devastating epidemics or recurrent outbreaks of endemic diseases) they have been -and often still are- responsible for a large number of deaths worldwide. The ongoing COVID-19 pandemic has certainly brought significant attention to the important contribution that mathematical modeling can have in monitoring the spread of infectious pathogens across a population, in better understanding its underlying mechanisms, and in exploring the effects of possible control measures aimed at containing the transmission of the considered disease (and possibly eradicating it from the observed population).

In this work, we firstly consider the SHAR extension of the SIR compartmental model and develop a cellular automata stochastic formulation to explicitly account for spatial effects in the considered framework. We discuss the role of import and study the behavior of the system in various parametric settings, determining the critical transmission threshold analytically in the nonspatial formulation and exploring the effect of spatial correlations on the more general spatiotemporal model. Then, we introduce the concept of infection clusters and investigate their evolution (in terms of the amount of clus- ters present in the system as well as their individual size) as a function of different parameter combinations. Finally, using a multiscale network-based model of contagion dynamics, we explore the role of heterogeneity in shaping and unfolding the overall diffusion process of an epidemic. An extensive simulation analysis considering different social network structures is performed to investigate the impact of interactions during the pandemic. Results are compared addressing the effectiveness of social distancing policies. The impact of an immunization strategy is also investigated to understand the effectiveness of the current COVID-19 vaccination policy prioritizing the most vulnerable individuals.

2 Results and discussion

Spatial epidemiological models

The SHAR model is an extension of the well-known SIR framework in which the I class is divided into two groups labelled H and A, respectively: H stands for individuals developing a severe form of the disease and likely being hospitalized, while A refers to infected individuals who are asymptomatic or have a mild form of the disease. The model dynamics is described by the following reaction scheme:

$$\begin{array}{ccc} S+H & \xrightarrow{\eta\beta} & H+H \\ S+H & \xrightarrow{(1-\eta)\beta} & A+H \\ S+A & \xrightarrow{\phi\eta\beta} & H+A \\ S+A & \xrightarrow{\phi(1-\eta)\beta} & A+A \\ S & \xrightarrow{\varrho\eta\beta} & H \\ S & \xrightarrow{\varrho(1-\eta)\beta} & A \\ H,A & \xrightarrow{\gamma} & R \\ R & \xrightarrow{\alpha} & S. \end{array} \tag{1}$$

In addition to the infection rate β, the recovery rate γ, and the waning immunity rate α (already present in the general SIR formulation), the SHAR approach includes two extra epidemiological parameters: the severity ratio η, that gives the fraction of infected individuals who develop severe symptoms, and the scaling factor ϕ, which differentiates the infectivity $\phi\beta$ of mild/asymptomatic infections with respect to the baseline infectivity β of severe/hospitalized cases. The value of ϕ can be tuned to describe different situations: a value of $\phi < 1$ indicates that severe cases have larger infectivity than mild cases (which in the case of an infectious respiratory disease, for example, could be linked to enhanced coughing and sneezing), while $\phi > 1$ would be used to describe the scenario in which asymptomatic individuals and mild cases contribute more to the spread of the infection (e.g., due to their higher mobility and possibility of interaction) than severe cases (that are more likely to be detected and isolated). It is important to consider as well the import factor ϱ which refers to the possibility of susceptible individuals contracting the disease via an undetected infection chain which started outside the studied population.

From the reaction scheme (1) we derived analytically the critical transmission threshold

$$\beta_c = \frac{\gamma}{\eta + \phi(1-\eta)}, \tag{2}$$

extending already existing results for the SIR model [1].

This transition of the dynamics from subcritical to supercritical regimes is also illustrated in Figure 1, where the mean-field solution is plotted for different values of β both in natural and log-log scales.

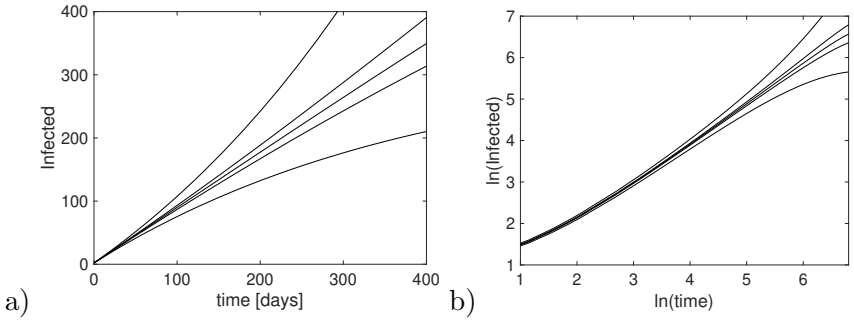

Figure 1: Mean-field solution for infected $H + A$ for different values of β in a) natural scale and b) log-log scale. From bottom to top $\beta = 0.95\beta_c$, $\beta = 0.99\beta_c$, $\beta = \beta_c$, $\beta = 1.01\beta_c$ and $\beta = 1.05\beta_c$.

The SHAR model was extended to a lattice structure in order to study the spatial propagation of a disease and the critical threshold in that scenario. Until now, we could infer that spatial correlations for the considered model contribute to keep disease transmission under control for larger values of the infectivity β, in comparison to the non-spatial model [4]. However, we have so far treated with quite small population sizes (lattices of about 60000 sites) due to the computational demand of the numerical simulations.

Multiscale models and heterogeneity

Modeling of epidemiological phenomena can be performed at different scales, from the so called *within-host* micro-scale to the macroscopic level of large populations with spatial distribution. We dealt with the multiscale model [3] based on the kinetic theory. The derivation of the mathematical structure can be obtained by a suitable balance of pedestrians in an elementary volume of the space of microscopic states, considering the net flow into such volume due to transport and interactions:

$$\partial_t f(t,x,u) + \mathrm{div}_x(v[\rho](t,x,u) f(t,x,u)) = \mathcal{J}[f](t,x,u), \qquad i = 1,\dots,n, \tag{3}$$

where $f(t,x,u)$ denotes the probability to find a particle, at time t, in an elementary volume surrounding position x and micro-state u, and v is the velocity. The left-hand term models the transport of particles, while $\mathcal{J}[f]$ represents transitions due to interactions.

Each single individual is seen as a particle, within which a competition dynamics between a pathogen and the immune system takes place. As a result, the individual may end up recovering or dying. This modeling approach is interesting since it let us introduce heterogeneity in a very simple way, for example just differentiating age or risk groups through a suitable choice of microscopic variables.

The model was further extended to networks [2], where we explored the role of heterogeneity in shaping and unfolding the overall diffusion process of an epidemic. We performed an extensive simulation analysis considering different social network structures is performed to investigate the impact of social interactions, addressing the effectiveness of social distancing policies, and the impact of immunization strategies, to understand the effectiveness of the current COVID-19 vaccination protocols prioritising the most vulnerable individuals.

The model is able to account for two forms of heterogeneity, namely between-individual heterogeneity on the basis of individual attributes influencing the epidemic growth, and social-structure

heterogeneity, introducing alternative forms of networks influencing the contact dynamics as well as different structured nodes within which contacts occur, namely schools, hospitals/nursing homes, workplaces and households.

3 Conclusions and Future work

The proposed models were able to provide important answers to questions arising in public health and epidemiology. There are, however, many open research lines to move forward. In particular, we are trying to give a more precise estimate of the critical threshold for this spatial model, considering larger lattice sizes (in order for the "abundance of susceptible" assumption to remain valid for longer times) and longer simulations (with the corresponding heavier computational burden), thus allowing to disambiguate between values of β corresponding to a super- or sub-critical regime. This requires further development of our algorithms.

Another topic to be developed within this line of research is the development of algorithms towards TTI (Testing, Tracing and Isolating) policies. The algorithm shall seek infection clusters (groups of connected individuals who have been infected by the same index case) through different tracing strategies. Clusters must be counted by means of a rapid routine (e.g., the Hoshen-Kopelman algorithm). Finally, the algorithm shall decide the kind of disease mitigation and containment actions to be adopted depending on the previous results. For example, isolation and vaccination of clusters can be included by reducing the infection rate of infected sites.

Finally, we plan to perform a coupling with economic variables, in order to quantify the costs and health outcomes of interventions (eg., lockdowns, vaccination, etc.) in a society through cost-effectiveness analyses.

Acknowledgments

This research was supported by the Basque Government through the "Mathematical Modeling Applied to Health" Project, BERC 2018-2021 program, by the Spanish Ministry of Sciences, Innovation and Universities: BCAM Severo Ochoa accreditation SEV-2017-0718, and by CONICET Project PIP 11220150100500 CO.

References

[1] Maíra Aguiar, Joseba Bidaurrazaga Van-Dierdonck, Javier Mar, Nicole Cusimano, Damián Knopoff, Vizda Anam, Nico Stollenwerk, Critical fluctuations in epidemic models explain COVID-19 post-lockdown dynamics, Nature Scientific Reports, **11** (2021), 13839.

[2] Maíra Aguiar, Giovanni Dosi, Damián Knopoff, Maria E. Virgillito, A multiscale network-based model of contagion dynamics: heterogeneity, spatial distancing and vaccination, Mathematical Models and Methods in Applied Sciences,**31**(12) (2021), 2425–2454.

[3] Nicola Bellomo, Richard Bingham, Mark Chaplain, Giovanni Dosi, Guido Forni, Damián Knopoff, John Lowengrub, Reydun Twarock, Maria E. Virgillito, A multiscale model of virus pandemic: Heterogeneous interactive entities in a globally connected world, Mathematical Models and Methods in Applied Sciences, **30**(8) (2020), 1591–1651.

[4] Damián Knopoff, Nicole Cusimano, Nico Stollenwerk, Maíra Aguiar, Spatially-extended SHAR epidemiological framework of infectious disease transmission, Computational and Mathematical Methods, **2022** (2022), 3304532.

International Conference on Mathematical Analysis and Applications in Science and Engineering
ICMA^{2}SC'22
ISEP Porto-Portugal, June 27 - 29, 2022

Rate-induced tipping and chaos in mathematical models in epidemiology

Jochen Merker[1⋆]

[1] Leipzig University of Applied Sciences, Germany

[1⋆]jochen.merker@htwk-leipzig.de

Abstract: We explore non-autonomous non-linear compartment models in epidemiology, particularly the occurrence of rate-induced tipping phenomena induced by basin instability, and of chaotic dynamics. If an autonomous compartment model in epidemiology has a unique asymptotically stable equilibrium attracting all interior points, then basin instability as well as rate-induced tipping can not occur for time-dependent parameters. Nonetheless, we discuss existence of non-smooth systems nearby, where a second equilibrium on the boundary attracts an open interior set and basin instability leads to rate-induced tipping. As a consequence, not only the measures taken against an epidemic but also the rate of implementation of these measures may have a drastic influence on the number of infectious. Moreover, (almost) periodically varying parameters may lead to a chaotic epidemic.

keywords: Mathematical models in epidemiology; Nonautonomous dynamical systems; Geometric methods in differential equations; Nonlinear equations and systems.

MSC2020: 37B55; 34A26; 34A34.

1 Introduction

We consider parameter-dependent compartment models in epidemiology given by an ODE

$$\dot{x}(t) = f(x(t), \lambda) \tag{1}$$

on the probability simplex

$$\Sigma^n := \{x \in \mathbb{R}^n \,|\, x \geq 0\,,\; 1^T x \leq 1\}\,, \tag{2}$$

and beneath positive invariance of Σ^n we assume persistence of a disease-free equilibrium (DFE) $x^* \in \partial\Sigma^n$ at a corner, i.e. we assume $f_i(x,\lambda) \geq 0$ for every $x \geq 0$ with $1^T x < 1$ and $x_i = 0$, $\sum_{i=1}^{n} f_i(x,\lambda) \leq 0$ for every $x \geq 0$ with $1^T x = 1$, and $f(x^*,\lambda) = 0$ for a corner $x^* \in \partial\Sigma^n$. After a generic local two-parameter bifurcation, where the formerly asymptotically stable DFE loses stability and another locally asymptotically stable equilibrium arises in Σ^n, we are mainly interested in two questions:

1. Does there exist a parameter path $\lambda(t)$, which connects $\lambda_- := \lim_{t\searrow-\infty} \lambda(t)$ sufficiently fast with $\lambda_+ := \lim_{t\searrow\infty} \lambda(t)$ without crossing a bifurcation parameter, such that for an initial state near the other locally asymptotically stable equilibrium the non-autonomous

system (1) with $\lambda = \lambda(t)$ tends to the DFE despite its instability, i.e. can rate-induced tipping from the other locally asymptotically stable equilibrium to the DFE occur? Or in other words, can implementing measures against an epidemic quickly enough lead to a die out of the disease that would otherwise have spread if implemented too slowly?

2. Can (almost) periodic parameter changes $\lambda = \lambda(t)$ lead to chaos, i.e. to chaotic outbreaks of epidemic waves?

2 Results and discussion

2.1 Smooth unfolding

If f is smooth and a bifurcation of co-dimension two occurs at x^* for $\lambda = \lambda^*$, then $\frac{\partial f}{\partial x}(x^*, \lambda^*)$ generically has a zero eigenvalue of algebraic multiplicity two, but geometric multiplicity one. On a two-dimensional center manifold, the ODE (1) generically has the unfolding

$$\begin{aligned} \dot{x} &= (\zeta - \gamma)x + \alpha y - \zeta xy - \zeta x^2 \\ \dot{y} &= (\beta - \alpha)y - \beta xy - \beta y^2 \,. \end{aligned} \tag{3}$$

with parameters $\alpha, \beta, \gamma, \zeta > 0$, and the two-parameter bifurcation occurs at $x^* = (0,0)^T$ for $\zeta = \gamma$ and $\beta = \alpha$. By the transformation $x = R = 1 - S - I$, $y = I$, this normal form (3) occurs in epidemiology as an extension of the SIRS model, where susceptibles become directly recovered with rate $\zeta > 0$ on contact with a recovered. Yet, regardless how the parameters are chosen, in this smooth case one equilibrium attracts all interior points of Σ^2. Thus, rate-induced tipping induced by basin instability in the sense of Definition 1 can not occur.

Definition 1 ([3]) *Suppose $A(\lambda)$ is a locally asymptotically stable equilibrium of the autonomous ODE (1) for every λ on a parameter path connecting λ_- with λ_+, and let $B(A(\lambda))$ denote the basin of attraction of $A(\lambda)$. Then, $A(\lambda)$ is said to be basin unstable on the parameter path, if there are two λ_1, λ_2 on the parameter path such that $A(\lambda_1)$ is outside the closure of the basin of attraction of $A(\lambda_2)$, i.e., $A(\lambda_1) \notin \overline{B(A(\lambda_2))}$.*

2.2 Non-smooth unfolding

This is different in the non-smooth case. Consider the non-smooth unfolding of the SIRS model

$$\begin{aligned} \dot{x} &= -\gamma x + \alpha y + g(x,y) \\ \dot{y} &= (\beta - \alpha)y - \beta xy - \beta y^2 - g(x,y) \,, \end{aligned} \tag{4}$$

with a continuous $g : \Sigma^2 \to \mathbb{R}$ smooth at every $(x,y) \neq (0,0)$ and satisfying $\lim_{x \searrow 0} \frac{g(x,0)}{x} = 0 = \lim_{y \searrow 0} \frac{g(0,y)}{y}$, but not necessarily totally differentiable at $x^* = (0,0)^T$, e.g.

$$g(x,y) := \begin{cases} \zeta \frac{xy}{x+y} & (x,y) \neq (0,0) \\ 0 & (x,y) = (0,0) \end{cases} \tag{5}$$

with $\zeta > 0$. Assume that g is such that the nullclines $\dot{x} = 0$, $\dot{y} = 0$, intersect exactly at one endemic equilibrium (ENE) in the interior of Σ^2 which is locally asymptotically stable. For (5), this is the case if for $\delta := \sqrt{\alpha(\alpha + 2\gamma + 2\zeta) + (\zeta - \gamma)^2}$ the inequalities $\gamma + \delta > \alpha + \zeta$ and

$(\beta+\gamma)(\delta-\alpha)+\beta(\zeta-\gamma) > (\delta+\alpha)\zeta+(\zeta-\gamma)^2$ are valid. Using polar coordinates $x = r(1-\phi)$, $y = r\phi$ for $r \geq 0$, $0 \leq \phi \leq 1$, w.r.t. the 1-norm on the simplex Σ^2, we obtain from (4)

$$\begin{aligned} \dot{r} &= r\left(\beta(1-r)\phi - \gamma(1-\phi)\right) \\ \dot{\phi} &= \phi\left((1-\phi)(\beta-\alpha-\beta r - \frac{1}{r\phi}g(r(1-\phi),r\phi)+\gamma) - \alpha\phi - \frac{1}{r}g(r(1-\phi),r\phi)\right) \end{aligned} \tag{6}$$

Thus, if both r and ϕ are small, then in the first equation the negative term $-\gamma(1-\phi)$ dominates the bracket. For a similar result in the second equation, we need $\beta-\alpha-\frac{1}{r\phi}g(r(1-\phi),r\phi)+\gamma < 0$ for r and ϕ suficiently small. For (5), this is the case iff $\beta-\alpha < \zeta-\gamma$. Therefore, in (4) the DFE attracts a subset with non-empty interior near the origin between the line $y = 0$ and the nullcline $\dot{y} = 0$. If now $\beta > \alpha$ and $\zeta > \gamma$ decrease, then the basin of attraction of the ENE shrinks so that the former ENE lies in the basin of attraction of the unstable DFE, i.e.

Proposition 1 *There exist parameter paths not crossing a bifurcation parameter on which the ENE of the non-smooth system* (4) *is basin unstable.*

Proposition 1 paves a way for irreversible rate-induced tipping: If the parameter change is sufficiently fast, then by the following theorem rate-induced tipping from the ENE to the DFE occurs in the non-autonomous system, and Question 1 can be positively answered.

Theorem 2 ([3]) *If a stable equilibrium $A(\lambda)$ of the autonomous frozen ODE* (1) *is basin unstable on a parameter path, then there is a time-varying external input $\lambda(t)$ of sufficiently fast rate that traces out the path and gives irreversible rate-induced tipping from $A(\lambda(t))$ in the non-autonomous system.*

2.3 Chaotic behaviour

To show chaotic dynamics for (almost) periodic parameter changes $\lambda = \lambda(t)$, let us consider (3) in the case $\zeta = 0$. After a scaling $x = \epsilon q$, $y = \epsilon^2 p$, $t = \tau/\epsilon$, $\gamma = \epsilon^2\nu$, $\beta-\alpha = \epsilon\mu$, a division of the second equation by p, a substitution of p for $\ln|p|$ and using $q = |q|$ for $q \geq 0$, we obtain

$$\begin{aligned} \dot{q} &= \alpha(1+p) - \epsilon\nu|q| + \alpha(\exp(p)-1-p) \\ \dot{p} &= 1 - \alpha|q| - \epsilon(\mu|q|+\alpha p) - \epsilon^2\mu p\,. \end{aligned} \tag{7}$$

For $\exp(p)-1-p$ of order ϵ and $\epsilon = 0$, (7) is a non-smooth Hamiltonian system with Hamiltonian $H(q,p) := \frac{\alpha}{2}(1+p)^2 - q + \frac{\alpha}{2}|q|q$, in which the equilibrium $(-\frac{1}{\alpha},-1)$ has a homoclinic orbit in the level set $H = \frac{1}{2\alpha}$ surrounding the equilibrium $(\frac{1}{\alpha},-1)$. An explicit calculation of this homoclinic orbit allows to apply Melnikov's method to conclude occurence of chaotic behaviour for certain (almost) periodic parameter changes $\lambda = \lambda(t)$, and Question 2 can be positively answered.

References

[1] Jochen Merker, Benjamin Kunsch, Rate-induced tipping phenomena in compartment models of epidemics, in: Agarwal P., Nieto J.J., Ruzhansky M., Torres D.F.M. (eds), Analysis of Infectious Disease Problems (Covid-19) and Their Global Impact, Springer, Singapore (2021), 307–328.

[2] Jochen Merker, Benjamin Kunsch, Gregor Schuldt, Nonlinear Compartment Models with Time-Dependent Parameters, Mathematics **9** (2021), 1657.

[3] P.E. O'Keeffe, S. Wieczorek, Tipping Phenomena and Points of No Return in Ecosystems: Beyond Classical Bifurcations, SIAM J. Appl. Dyn. Syst. **19** (2020), 2371–2402.

Complex dynamics in SIR model-type driven by disease enhancement factor and temporary immunity in secondary infections

Vanessa Steindorf[1⋆] **Akhil Kumar Srivastav**[1] **Nico Stollenwerk**[1,3]
Bob W. Kooi[4] **Maíra Aguiar**[1,2,3]

[1] BCAM - Basque Center for Applied Mathematics, Bilbao, Basque Country - Spain
[2] Ikerbasque, Basque Foundation for Science, Basque Country - Spain
[3] Dipartimento di Matematica, Universita degli Studi di Trento, Italy
[4] VU Amsterdam, Faculty of Science, Amsterdam, The Netherlands

vsteindorf@bcamath.org

Abstract: With the identification of a new human coronavirus, causing a severe respiratory disease which quickly spreading across the world and become a pandemic, mathematical models to understand and to predict the disease dynamics became an important tool to guide public health authorities during the implementation of the available intervention measures for disease control. In this work, a SIR (susceptible-infected-recovered) type-model is studied. Motivated by dengue fever epidemiology, two subsequent infections without pathogen structure and two biological features, temporary immunity period after a primary infection and disease enhancement in a secondary infection, are considered. The model has a rich dynamical behavior, including fixed points, and limit cycles. A detailed bifurcation analysis have shown a variety of bifurcation structures, including a backward bifurcation. The results presented here can be used as additional information for a more extended modeling development, for a better understanding of the biological mechanisms needed to generate such rich dynamical behaviour in very simple epidemic models.

keywords: bifurcation analysis; temporary immunity period; secondary infections; antibody-dependent enhancement factor.

MSC2020: 49-XX; 34-XX; 92-XX.

1 Introduction

In March 2020, the World Health Organization (WHO) [6] has declared COVID-19 a global pandemic emergency. As a major public health concern, experts around the globe have created modeling task forces to assist public health authorities to understand the dynamics of the disease in the population, giving projections on disease incidence cases, and monitoring disease while control measures were implemented over time.

Infectious disease outbreaks are part of human history, causing premature deaths and significant socio-economic problems. As of an example, dengue fever (DF) is a major public health problem, with more than one-third of the world population being at risk of acquiring the disease.

DF dynamics have been largely studied by Aguiar and Colleagues [1, 2, 3, 4, 5]. Using different extensions of the classical SIR (susceptible-infected-recovered) model including multiple strains combined with important biological features such as, temporary cross-immunity and the antibody-dependent enhancement (ADE) factor, the proposed models have shown complex dynamics, with various bifurcation structures been identified, such as Hopf, torus, and tangent bifurcations, including deterministic chaotic behaviour [3]. With a good qualitative agreement between model simulation and empirical data, the findings indicate that deterministic chaos is much more important in multi-strain models than previously thought.

Aiming to understand the role of biological mechanisms generating complex behavior in simple epidemiological models, we analyse a two infection SIR type model without strain structure, and consider two well known biological mechanisms observed in dengue epidemiology, the temporary immunity period, occurring after a primary infection, and the ADE effect, occurring during a secondary infection eventually changing the individual transmission rate. A detailed bifurcation analysis is performed showing that the combination of immunity and ADE factor play an important role in changing the dynamics in the system.

2 Results and discussion

The compartmental two infection model divides the total population into six classes: susceptible (S), infected for the first time (I_p), recovered from the first infection (R_p), susceptible with a previous infection (S_p), infected for the second time (I_s), and recovered from the second infection (R). The rate β represents the transmission rate. Individuals recover from the first infection with recovery rate γ, and after a temporary immunity period α, become susceptible again. Individuals can be reinfected transmitting the disease with infection rate $\phi\beta$. The parameter ϕ described the contribution of the secondary infections to the overall force of infection, where $0 < \phi < 1$ decreases the infectivity of secondary infection, while $\phi > 1$, enhances the infectivity of secondary infection. The complete ODE system can be written as

$$\frac{dS}{dt} = -\frac{\beta}{N} S(I_P + \phi I_S) + \mu(N - S) \tag{1}$$

$$\frac{dI_P}{dt} = \frac{\beta}{N} S(I_P + \phi I_S) - (\gamma + \mu) I_P \tag{2}$$

$$\frac{dR_P}{dt} = \gamma I_P - (\alpha + \mu) R_P \tag{3}$$

$$\frac{dS_P}{dt} = -\frac{\beta}{N} S_P(I_P + \phi I_S) + \alpha R_P - \mu S_P \tag{4}$$

$$\frac{dI_S}{dt} = \frac{\beta}{N} S_P(I_P + \phi I_S) - (\gamma + \mu) I_S \tag{5}$$

$$\frac{dR}{dt} = \gamma I_S - \mu R\,. \tag{6}$$

We analyzed qualitatively the ODE system, showing the existence of disease-free equilibrium and the disease endemic equilibrium. It is also demonstrated that the system can exhibit a backward bifurcation and has two unstable endemic equilibria if, $\mathcal{R}_0 = \frac{\beta}{\gamma+\mu} < 1$, and

$$\phi > \phi_c = \frac{\alpha + \mu}{\alpha} \frac{\gamma + \mu}{\gamma} > 1.$$

The tangent bifurcation was proved to occur at $\beta_T = \frac{\tilde{\gamma}}{4\tilde{\phi}\tilde{\gamma} - (\tilde{\phi} - \tilde{\gamma})^2}$, confirmed by numerical experiments, as shown in Figure 1.

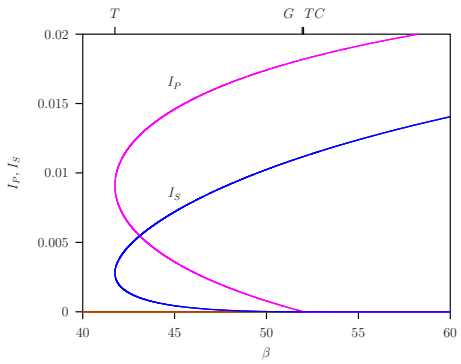

Figure 1: Backward bifurcation diagram. Tangent, transcritical and global homoclinic bifurcation represent by T, TC and G, respectively.

3 Conclusions and Future work

Motivated by dengue fever epidemiology, an extension of the classical SIR type model is studied. The model describes the transmission of an infection disease with two subsequent infections. With no strain structure, a temporary immunity period after a primary infection, and a disease enhancement during a secondary infection are assumed.

In order to investigate the role of the ADE effect on disease modelling, we fixed the temporary immunity period and varied the ADE factor as a bifurcation parameter. A backward bifurcation was found in a set of parameter regions generated by the change in the value of the ADE factor. Although a backward bifurcation was found, both endemic equilibria are unstable, and thus, the reproduction number still determines whether the disease persists or dies out.

Moreover, tangent, Hopf, and global homoclinic bifurcations were also identified and its occurrence are dependent on the force of infection and immunity period. For high force infection and high enhancement factor, Hopf bifurcation occurs, see Figure 2, thus periodic solutions are observed. In this case, it is possible to predict the periodicity of the new outbreaks. Furthermore, the numerical approach used is important since, without the restriction of non-negative solutions, a chaotic dynamic can be observed, see Figure 3.

This model allows the investigation of the role of real biological features acting as mechanisms that are able to generate rich dynamical behaviour in very simple models without additional migration factor, nor external forces. The temporary immunity period and the disease enhancement factor play an important role in changing the system dynamics and special attention should be taken to these epidemiological features for future disease modelling.

Numerical experiments in a more biological parameter space for temporary-protection period, considering, for example, $\alpha = 2\ y^{-1}$, i.e. six months, as observed on dengue disease, are ongoing, providing insights for public health intervention measures for disease control on epidemiological scenarios.

Acknowledgments

M. A. has received funding from the European Union's Horizon 2020 research and innovation programme under the Marie Skłodowska-Curie grant agreement No 792494. This research is also supported by the Basque Government through the "Mathematical Modeling Applied to Health" Project, BERC 2022-2025 program and by Spanish Ministry of Sciences, Innovation and Universities: BCAM Severo Ochoa accreditation SEV-2017-0718.

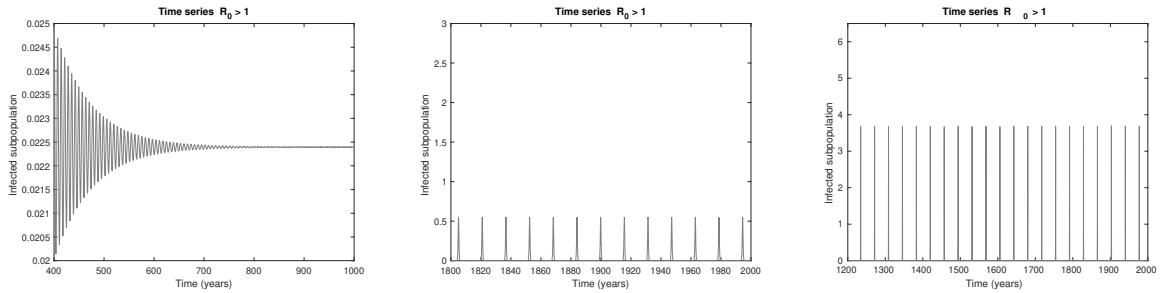

(a) $\phi = 1.4$ (b) $\phi = 1.8$ (c) $\phi = 2.6$

Figure 2: Time series for $\alpha = 52$ y^{-1}, $\gamma = 52$ y^{-1}, $\beta = 104$. Solution tend to (a) the endemic equilibrium, (b) and (c) limit cycle.

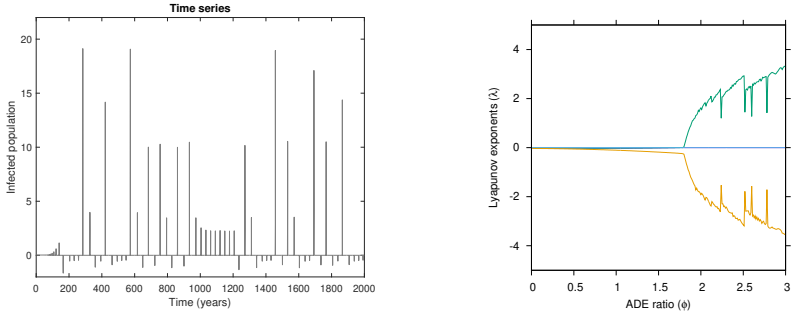

(a) Time series for $\phi = 2.6$. (b) Lyapunov exponent

Figure 3: Time series for $\alpha = 52$ y^{-1}, $\gamma = 52$ y^{-1}, $\beta = 104$ and $\phi = 2.6$ using ODE45 method without constraint of non-negative solution. Chaotic behavior demonstrated by a positive Lyapunov exponent ($\lambda = 1.271$).

References

[1] Maíra Aguiar, Bob W. Kooi, Nico Stollenwerk, Epidemiology of Dengue Fever: A model with temporary cross immunity and possibly secondary infection shows bifurcations and chaotic behaviors in wide parameter region, Mathematical Modelling of Natural Phenomena, **3**(4) (2008), 48–70.

[2] Maíra Aguiar, Nico Stollenwerk, Bob W. Kooi, Torus bifurcations, isolas and chaotic attractors in a simple dengue model with ADE and temporary cross immunity, International Journal of Computer Mathematics, **86** (2009), 1867–1877.

[3] Maíra Aguiar, Sebastien Ballesteros, Bob W. Kooi, Nico Stollenwerk, The role of seasonality and import in a minimalistic multi-strain dengue model capturing differences between primary and secondary infections: Complex dynamics and its implications for data analysis, Journal of Theoretical Biology, **289** (2011), 181–196.

[4] Maíra Aguiar, Nico Stollenwerk, Bob W. Kooi, Scaling of stochasticity in dengue hemorrhagic fever epidemics. Mathematical Modelling of Natural Phenomena, **7** (2012), 1–11.

[5] Maíra Aguiar, et al., Mathematical models for dengue fever epidemiology: a 10-year systematic review, Physics of Life Reviews, **40** (2022), 65–92.

[6] https://www.who.int/emergencies/diseases/novel-coronavirus-2019/situation-reports Accessed in March 2022.

International Conference on Mathematical Analysis and Applications in Science and Engineering
ICMA^{2}SC'22
ISEP Porto-Portugal, June 27 - 29, 2022

UNDERSTANDING THE IMMUNOLOGICAL RESPONSES MEDIATED BY ANTIBODIES DURING PRIMARY DENGUE INFECTION

Vizda Anam[1⋆] **Maíra Aguiar**[1,2,3]

[1] Basque Center for Applied Mathematics, BCAM, Bilbao, Spain
[2] Ikerbasque, Basque Foundation for Science, Bilbao, Spain
[3] Dipartimento di Matematica, Universita degli Studi di Trento, Italy

[1⋆]vanam@bcamath.org

Abstract: With more than a half of the world's population being at risk of dengue infection, at present dengue fever is a major public health problem in the tropics and subtropics. Nevertheless, a threat of possible outbreaks in Europe should not be underestimated. It is caused by four antigenically related but distinct serotypes (DENV-1 to DENV-4), infection by one serotype confers life-long immunity to that serotype and a period of temporary cross-immunity (TCI) to other serotypes. Although most of the cases recover following a self-limiting non-severe clinical course, there is good evidence that sequential infection increases the risk of developing severe disease, due to a process described as antibody-dependent enhancement (ADE). There is no specific treatment for dengue, and severe cases require hospitalization. A safe, effective and affordable dengue vaccine against the four strains would represent a significant advance for the control of the disease and could be an important tool for reducing disease transmission and mortality.
Mathematical modeling is often used for understanding infectious diseases dynamics and to evaluate the introduction of intervention strategies like vector control and vaccination. A careful review of deterministic dengue modeling was recently published [3], where three structural approaches were studied, the vector-host, the host-to-host and the within-host dynamic models. While the first two approaches aim to describe disease transmission at population level, the within-host framework is built to describe viral replication and antibody responses affecting the disease outcome in primary and recurrent infections, see e.g. [1, 2]. Understanding the immunopathogenesis of severe illness during recurring infections is critical for future research directions to evaluate the impact of dengue vaccines.
In this work, we analyse the deterministic and stochastic models describing the immunological responses mediated by antibodies during a primary dengue infection. A detailed sensitivity analysis of the parameters involved in the model is performed. The deterministic framework recently proposed by [1, 2] is extended to its stochastic counterpart for a better understanding of the variation observed in the available data following the same method used in [4]. Using numerical simulations, we investigate features of viral replication, antibody production and infection clearance over time. Results presented here will be used as baseline to investigate a more complex within-host dengue model, giving insights into the immunopathogenesis of severe diseases during secondary infections caused by heterologous serotypes.

keywords: Primary dengue infection ; Immune response; ADE; SDE.

MSC2020: 34A-25; 60G-07; 92-10.

Acknowledgments

M. A. has received funding from the European Union's Horizon 2020 research and innovation programme under the Marie Skłodowska-Curie grant agreement No 792494. This research is also supported by the Basque Government through the "Mathematical Modeling Applied to Health" Project, BERC 2022-2025 program and by Spanish Ministry of Sciences, Innovation and Universities: BCAM Severo Ochoa accreditation SEV-2017-0718..

References

[1] Anam, V., Sebayang, A.A., Fahlena, H., Knopoff, D., Stollenwerk, N., Soewono, E. and Aguiar, M., Modeling Dengue Immune Responses Mediated by Antibodies: Insights on the Biological Parameters to Describe Dengue Infections. Computational and Mathematical Methods, **(2022). https://doi.org/10.1155/2022/8283239**

[2] Sebayang, A.A., Fahlena, H., Anam, V., Knopoff, D., Stollenwerk, N., Aguiar, M. and Soewono, E., Modeling Dengue Immune Responses Mediated by Antibodies: A Qualitative Study. Biology, **10(9), (2021), p.941. https://doi.org/10.3390/biology10090941**

[3] Aguiar, M., Anam, V., Blyuss, K.B., Estadilla, C.D.S., Guerrero, B.V., Knopoff, D., Kooi, B.W., Srivastav, A.K., Steindorf, V. and Stollenwerk, N. Mathematical models for dengue fever epidemiology: a 10-year systematic review. Physics of Life Reviews. **(2022). https://doi.org/10.1016/j.plrev.2022.02.001**

[4] Srivasrav, A.K., Stollenwerk, N., Van-Dierdonck, J.B., Mar, J., Ibarrondo, O. and Aguiar, M., 2022. Modeling the initial phase of COVID-19 epidemic: The role of age and disease severity in the Basque Country, Spain. medRxiv. **https://doi.org/10.1101/2022.04.18.22273983**

Optimal vaccine allocation for the control of sexually transmitted infections

Fernando Saldaña[1⋆] **Vanessa Steindorf**[1] **Akhil Kumar Srivastav**[1]
Nico Stollenwerk[1] **Maíra Aguiar**[1]

[1] BCAM - Basque Center for Applied Mathematics, Spain

[1⋆]fsaldana@bcamath.org

Abstract: The burden of sexually transmitted infections (STIs) poses a challenge globally due to its high prevalence and its high health and economic intervention costs. Despite simple interventions and treatment efforts, vaccines are the main precaution for some viral STIs and for the prevention of diseases associated with these infections. In this work, the best way of distribution of prophylactic vaccines between sexes for the prevention and control of sexually transmitted infections in a heterosexual population is investigated. Various vaccination programs described by distinct budged constraints that mimic a scarce vaccine stockpile is compared. The vaccination programs are obtained as solutions to an optimal control problem subject to a two-sex Kermack-McKendrick-type model where the control variables are the daily vaccination rates for females and males, respectively. An important and novelty aspect of the approach taken in this work relies on conceptualizing a limited but specific vaccine stockpile via an isoperimetric constrain. The optimal control problem is solved via the Pontryagin Maximum Principle and a numerical approximation for the solution using a modified version of the forward-backward sweep method that handles the isoperimetric budget constraint in our formulation is obtained. Conclusively, the results suggest that for a limited and small vaccine supply ($20\% - 30\%$ vaccination coverage), one-sex vaccination appears to be more beneficial than the inclusion of both sexes into the vaccination program. On the other hand, if the vaccine supply is relatively large (enough to reach 40% coverage), vaccinating both sexes, with a slightly higher rate for females, is optimal and provides an effective and faster approach to reducing the prevalence of the infection.

keywords: Epidemic model; Optimal control; Vaccination strategies; HPV.

MSC2020: 92-D30.

Optimal control of multi-strain host-vector dengue model

Akhil Kumar Srivastav[1⋆] **Vanessa Steindorf**[1] **Nico Stollenwerk**[1]
Bob W. Kooi[4] **Maíra Aguiar** [1,2,3]

[1] Basque Center for Applied Mathematics, BCAM, Bilbao, Spain
[2] Ikerbasque, Basque Foundation for Science, Bilbao, Spain
[3] Dipartimento di Matematica, Universita degli Studi di Trento, Italy
[4]Faculty of Science, Vrije Universiteit Amsterdam, Amsterdam, The Netherlands

[1⋆]asrivastav@bcamath.org

Abstract: Dengue fever is caused by four dengue virus serotypes: DEN-1, DEN-2, DEN-3, and DEN-4. This study presents a mathematical host-vector model considering multiple strains of dengue fever and the dynamics between human and mosquito population. For this model, the sensitivity analysis (PRCC Method) is conducted in order to identify the key parameter that has more influence in the transmission of dengue. Further, in order to find the optimal strategies for suitable control interventions that reduce the dengue prevalence and economic burden, an optimal control problem is proposed by considering vaccination, use of preventive measures and killing mosquito population as control interventions. A weighted sum of various costs incurred in applied controls and the cost due to dengue disease (productivity loss) is incorporated in the proposed cost functional. The analysis of control system using Pontryagins Maximum Principle leads the existence of the optimal control profiles. Further, an exhaustive comparative study for three different control strategies is conducted numerically. Our findings ensure that every individual control strategy has their own impact on reducing the cumulative count of infection. The combined impact of all control interventions is highly effective in controlling the prevalence of dengue. We observed that the comprehensive use of controls keeps a strong tab on the infectivity even if the severity of epidemic is high.

keywords: dengue fever disease ; optimal control; multi strain vector-host model.

MSC2020: 34H-05, 49J-21 .

Acknowledgments

M. A. has received funding from the European Union's Horizon 2020 research and innovation programme under the Marie Skłodowska-Curie grant agreement No 792494. This research is also supported by the Basque Government through the "Mathematical Modeling Applied to Health" Project, BERC 2022-2025 program and by Spanish Ministry of Sciences, Innovation and Universities: BCAM Severo Ochoa accreditation SEV-2017-0718.

References

[1] P. Rashkov, B. W. Kooi, Complexity of host-vector dynamics in a two-strain dengue model, Journal of Biological Dynamics 15 (1) (2021) 35-72, DOI: 10.1080/17513758.2020.1864038

[2] Lenhart S, Workman JT. Optimal Control Applied to Biological Models: CRC Press; 2007, DOI: 10.1201/978142001141823.

[3] Pontryagin LS, Boltyanskii VG, Gamkrelidze RV, Mishchenko EF. The Mathematical Theory of Optimal Processes. New York: InterscicencePublishers; 1962.

[4] M. Aguiar, B. Kooi and N. Stollenwerk, Epidemiology of Dengue Fever:A Model with Temporary Cross-Immunityand Possible Secondary Infection Shows Bifurcationsand Chaotic Behaviour in Wide Parameter Regions, Mathematical Modelling of Natural Phenomena, 3(4) , 2008 , 48 - 70 DOI: 10.1051/mmnp:2008070

A pragmatic view on chaotic dynamics and ergodicity in a SIR-like epidemic model

Bruno V. Guerrero[1⋆] **Nico Stollenwerk** [1] **Maíra Aguiar**[1]

[1] MTB-Group, Basque Center for Applied Mathematics (BCAM), Spain

[1⋆]bguerrero@bcamath.org

Abstract: Epidemiological models, such as the prototypical compartmental SIR model, are widely used to describe the evolution of infectious diseases. Even though this kind of simplistic models fairly capture the phenomenology of the spreading disease, under certain circumstances are not capable of describing its long-term behavior. Sometimes, this lack of reproducibility of real data is not due to a deficiency of the model but to the non-linear nature of the phenomenon itself (associated with the emergence of chaos). A theoretical tool used to determine the stability of the solution and to define the prediction horizon are the Lyapunov's exponents λ_j (equal in number to the dimensionality of the phase space). In general, the solution is stable when the largest exponent is negative, while if at least one of the exponents is positive, it entails an exponential instability: infinitesimally close orbits in the phase space tend to separate exponentially in time with a rate λ (a hallmark of deterministic chaos). In particular, the unpredictability of chaos and the onset of complex dynamics that arises as a consequence of the seasonally modulation in the transmission rate [1, 2] poses a challenge when it comes to establishing timely seasonal control measures (such as seasonal vaccination campaigns or lock-downs) for recurrent disease outbreaks (i.e. influenza, dengue or COVID-19).

Stochastic versions of deterministic models are used to explore the effects of external noise or random environments (introduced as stochastic terms in the differential equations system or as fluctuations in the parameter values) in the simulated population dynamics. On average, the stochastic solution should match the deterministic one (mean-field approximation). But, when the system is not ergodic, *time*-averages of a given observable may not correspond with the obtained when using *ensemble*-averages (also known as *phase-space* averages).

In practice, the ergodicity of the problem is a feature often overlooked. However, the ergodicity breaking has implications that must be taken into account in order not to reach misleading or erroneous conclusions [3]. Here, from a practical point of view, the direct consequences of the non-ergodicity will be shown in a concrete physical example. From experimental measurements (physical observables of a granular system and some time variables), the ergodicity has been quantified in statistical terms (by means of diffusive properties) and rationalized (through a Continuous-Time Random Walk (CTRW) sub-diffusive model) [4].

Finally, our ongoing research will be presented and some preliminary results on the stability of a seasonally-driven SIR model with waning immunity and imported infected population, which has been characterized in terms of the Lyapunov spectrum, and to bring some thoughts on ergodicity from a merely pragmatic perspective.

keywords: ergodicity; chaos; infectious disease; modelling.

MSC2020: 37-06; 37A50; 92D25; 92D30.

References

[1] Nico Stollenwerk, Stefano Spaziani, Javier Mar, Irati Eguiguren Arrizabalaga, Damián Knopoff, Nicole Cusimano, Vizda Anam, Akhil Shrivastava, Maíra Aguiar, Seasonally Forced SIR Systems Applied to Respiratory Infectious Diseases, Bifurcations, and Chaos, Computational and Mathematical Methods, **2022** (2022), 3556043.

[2] Jorge Duarte, Cristina Januário, Nuno Martins, Jesús M. Seoane, Miguel A. F. Sanjuán, Controlling infectious diseases: The decisive phase effect on a seasonal vaccination strategy, International Journal of Bifurcation and Chaos, **31**(15) (2021), 2130044.

[3] Ralf Metzler, Jae-Hyung Jeon, Andrey G. Cherstvya, Eli Barkaid, Anomalous diffusion models and their properties: non-stationarity, non-ergodicity, and ageing at the centenary of single particle tracking, Physical Chemistry Chemical Physics, **16** (2014), 24128.

[4] Bruno. V Guerrero, Bulbul Chakraborty, Iker Zuriguel, Angel Garcimartín, Nonergodicity in silo unclogging: Broken and unbroken arches, Physical Review E, **100**(3) (2013), 032901.

OPTIMAL STRATEGIES FOR MITIGATING THE HIV/AIDS EPIDEMIC IN THE PHILIPPINES

Carlo Delfin S. Estadilla[1,2⋆] **Aurelio A. de los Reyes V**[2]

[1] Basque Center for Applied Mathematics, Spain
[2] University of the Philippines–Diliman, Philippines

[1⋆]cestadilla@bcamath.org

Abstract: The Human Immunodeficiency Virus (HIV) impairs a person's immune system, which can lead to Acquired Immunodeficiency Syndrome (AIDS), a condition marked by co-infection of other severe diseases. In the Philippines, HIV infections have more than doubled from 2010 to 2016, and a sterilizing cure is yet to be discovered. Here, we have constructed a mathematical model to capture the HIV dynamics in the Philippines. The model equilibria and basic reproduction number have been calculated, and public data have been used to identify model parameters. Under the framework of optimal control theory, the efficiency of precautionary measures, HIV screening, Anti-Retroviral Therapy, and Pre-Exposure Prophylaxis (PrEP) as disease controls has also been investigated. Each strategy, and combinations thereof have been compared in terms of their cost-effectiveness and ability to reduce infections. The PrEP-only scenario has been shown to be the most cost-effective strategy among all the possible combinations.

keywords: HIV; AIDS; optimal control; parameter identification.

MSC2020: 49-XX; 34-XX; 92-XX.

Acknowledgments

This work has been funded by the Philippine National Science Research Institute under the project number MAT-20-1-03.

References

[1] Carlo Delfin S. Estadilla, Aurelio A. de los Reyes V, Optimal strategies for mitigating the HIV/AIDS epidemic in the Philippines, Mathematical Methods in the Applied Sciences, **43**(18) (2020), 10690–10710.

International Conference on Mathematical Analysis and Applications in Science and Engineering
ICMA^{2}SC'22
ISEP Porto-Portugal, June 27 - 29, 2022

STOCHASTIC DIFFERENTIAL EQUATION MODELS OF ANIMAL GROWTH AND OPTIMIZATION IN CATTLE RAISING

Carlos A. Braumann[1⋆,2] **Gonçalo Jacinto**[1,2] **Patrícia A. Filipe**[1,3]

[1] Centro de Investigação em Matemática e Aplicações,
Instituto de Investigação e Formação Avançada, Universidade de Évora, Portugal
[2] Departamento de Matemática, Escola de Ciências e Tecnologia,
Universidade de Évora, Portugal
[3] Instituto Universitário de Lisboa (ISCTE - IUL), ISCTE Business School,
Quantitative Methods for Management and Economics Department, Portugal

[1⋆]braumann@uevora.pt

Abstract: The effect of environmental random fluctuations on the growth dynamics of individual animals is not captured by regression models and so we use stochastic versions of a quite general class of models that includes the classical growth curves as particular cases. They take the form of stochastic differential equations (SDE). These more realistic models can help farmers optimize the profit obtained by raising and selling an animal. To that end, we obtain the expected value and the standard deviation of the profit as a function of the selling age under the more general and realistic market situation where the feeding costs vary with the animal's weight and the selling price per kg paid to farmers depends on the animal's age and weight category. We apply results to real weight data from cattle males of the Mertolengo breed. Sensitivity analysis to model parameter estimates is also performed.

keywords: stochastic differential equations; cattle growth; profit optimization; sensitivity analysis; maximum likelihood estimators.

MSC2020: 60H10; 60E05; 62G07; 91B70; 92D99.

1 Introduction

The commonly used deterministic growth curve models for the size X_t of an animal or plant at age t can be obtained as solutions of particular cases of the general ODE model $dY_t = \beta(\alpha - Y_t)dt$, where $Y_t = h(X_t)$ is a modified size, with h a model specific monotonous C^1 function, α the asymptotic value of Y_t ($A = h^{-1}(\alpha)$ being the asymptotic actual size), and β a growth coefficient. Indeed, for $h(x) = x$, $h(x) = x^{-1}$, $h(x) = x^c$ ($c > 0$), and $h(x) = \ln x$, one obtains, respectively, the monomolecular, the logistic, the Bertalanffy-Richards, and the Gompertz models.
The traditional use of classical regression models (with mean given by deterministic growth curves) to handle random variations in data does not capture the dynamics of the growth process nor the effect produced by the environmental random fluctuations on such dynamics. So, as proposed by [6], we adopt the stochastic differential equation (SDE) version of the general ODE model:

$$dY_t = \beta(\alpha - Y_t)dt + \sigma dW_t, \tag{1}$$

with $\sigma > 0$ an environmental noise intesnsity parameter adn W_t a standard Wiener process. SDE models have been applied in forestry, agriculture and animal growth (e.g., [2, 3, 5, 6, 9, 10, 11, 12]). The solution of (1) with initial condition $Y_{t_0} = y_0$ is (see, for instance, [1]) $Y_t = \alpha - (\alpha - y_0)e^{-\beta(t-t_0)} + \sigma e^{-\beta t}\int_{t_0}^{t} e^{\beta s} dW_s$ and is Gaussian with mean $\alpha - (\alpha - y_0)e^{-\beta(t-t_0)}$ and variance $\frac{\sigma^2}{2\beta}\left(1 - e^{-2\beta(t-t_0)}\right)$. So, we know the p.d.f. $f_{X_t}(x)$ of $X_t = h^{-1}(Y_t)$.
Using the Markov property and independence among different animals, maximum likelihood parameter estimates for data from different animals can be seen in [2, 7]. For mixed models (not used here), in which the parameter α and/or the parameter β may vary randomly among animals to account for their genetic and other differences, a new parameter estimation method (delta method) and its comparison with existing methods can be seen in [8].
In order for farmers to optimize their profit, the use of more realistic stochastic models can be an important tool. In [4] these models were applied to the optimization of the mean profit (by age or by weight) obtained by raising and selling an animal, considering a simple raising cost structure and assuming a constant price per kg paid to the farmers.
This Talk, described by this Extended Abstract, is founded on our results in [7] and concerned with the more general, realistic and challenging profit structure where the price paid per kg to the farmers depends on the animal's age group and weight category and the feeding costs vary with the animal's weight. For this profit framework, we have obtained the expressions for the expected value and the standard deviation of the profit as a function of the selling age and developed the methodology to obtain the selling age that maximizes the expected profit.
We have applied the results to bovine males of the PDO (Protected Designation of Origin) Mertolengo breed raised in the Alentejo region of Portugal. Provided by the producer's association Associação de Criadores de Bovinos Mertolengos (ACBM), we have used two datasets, one from its database containing 16029 males having between 3 and 33 weight observations (at ages varying from birth to a maximum age ranging between 0.2 and 16 years, totaling 96204 observations), and the other from a test group of 18 animals (weighted monthly to an upper age ranging from 24 to 30 months). We have used the stochastic Gompertz model-SGM ($h(x) = \ln x$) and the stochastic Bertalanffy-Richards model-SBRM ($h(x) = x^{1/3}$). We also evaluate the sensitivity of the optimal selling age and the optimal expected profit to the parameter estimates.

2 Results and discussion

2.1 Optimization

The profit obtained from raising an animal since age t_0 (having a known weight $X_{t_0} = x_0$) in order to sell it at an age $t > t_0$ depends on t and on the animal's weight X_t (in kg) and is given by $L_t = L_t(X_t) = V_t(X_t) - C_t(X_t)$, where V_t is the selling price and C_t the acquisition (if it is the case) costs and the animal raising costs.
The carcass weight in kg is RX_t, where R is the dressing proportion (around 0.52 for Mertolengo males), and so $V_t(X_t) = P_t(X_t)RX_t$, where $P_t(X_t)$ is the sale price per unit carcass weight. Let $P_t(X_t) = P_{t,j}$ for an animal of age t having a carcass weight in the interval $[a_{t,j-1}, a_{t,j}[$ $(j = 1, \ldots, k)$, where $-\infty = a_{t,0} < a_{t,1} < \ldots < a_{t,k-1} < a_{t,k} = +\infty$. Then, using the indicator function I, $P_t(X_t) = \sum_{j=1}^{k} P_{t,j} I_{[a_{t,j-1}, a_{t,j}[}(RX_t) = \sum_{j=1}^{k} P_{t,j} I_{[a_{t,j-1}/R, a_{t,j}/R[}(X_t)$.
The raising costs are given by $C_t(X_t) = C_1 + C_2(t - t_0) + C_2 \int_{t_0}^{t} X_s ds$, where C_1 are the fixed costs (in Euros), C_2 the maintenance costs per unit time (in Euros/year) and C_3 the feeding costs per unit time and animal's weight (in Euros/(year $\times$ kg)).
This structure poses a challenging problem in determining the expected profit $\mathbb{E}[V_t]$ and the standard deviation of the profit as functions of the selling age t, but we were able in [7] solve this problem for the general model (general choice of the function h) and to give explicit expressions (not shown here) for the particular cases of the SGM ($h(x) = \ln x$) and the SBRM ($h(x) = x^{1/3}$).

2.2 Application

We obtain the parameter maximum likelihood (ML) estimates and their approximate 95% intervals for the SGM and the SBRM for the test group of 18 animals and for all 16029 database animals. We consider for this illustration the situation of the finishing phase starting at the typical weaning age of $t_0 = 0.7$ years with the animal weighting $x_0 = h^{-1}(y_0) = 170.5$ kg (typical average weight at that age) and look at the profit from raising the animal from that age up to the selling age to the meat market. According to the available data at the time, we have considered for the Mertolengo breed a fixed cost of $C_1 = 57.35$ Euros (commercialization and transportation, sanitation, Promert tax). Because it does not affect the optimal selling age, we ignore in the illustration the value of the animal at age t_0, but it can be considered as a cost and added to C_1. We assume handling costs of $C_2 = 0.435$ Euros per day and, due to lack of detailed information, we assume aa an approximation (that works quite well) that, during the finishing phase, the feeding cost is independent of the animal weight and amounts to $C_4 = 2.248$ Euros per day, so that $C(t) \approx C_1 + (C_2 + C_4)(t - t_0)$.
The price (in Euros) per kg of carcass weight, $P_t(X_t)$, varies according to the age group (there are 3 groups) and the carcass weight RX_t category (the lower age group has 5 carcass weight categories, the middle group has 3 categories and the older group has 7 categories). For example, the sale price per kg, $P_t(X_t)$, is 3.60 Euros for the age group 10 months$< t \leq$ 15 months and this group carcass weight category 160 kg$\leq RX_t <$ 180 kg.
Using the theoretical results in subsection 2.1, we determine and plot (see [7]) the expected value (and the standard deviation) of the profit V_t as a function of the selling age t. We determine the optimal selling age t and the corresponding optimal expected profit. For example, for the parameter values of the test group, we conclude that the typical average selling age of 1.16 years is slightly under the optimal selling age of 1.25 years (15 months), resulting in an expected profit 9 to 10 Euros (depending on the model) below the optimal expected profit.

2.3 Sensitivity to model parameters

Since the model parameters used are ML estimates and not the true parameter values, we use the test group data to study (see [7]) the sensitivity of results to their values. The parameter σ has a negligible influence. The parameters α and β have a considerable influence on the optimal expected profit but negligible or no influence on the optimal selling age. Similar conclusion arises when we study (by Monte Carlo simulation) the joint influence of the parameters.

3 Conclusions and Future work

Using an SDE general model for individual animal growth that takes into account random environmental fluctuations, we have obtained the expected profit (and also the standard deviation of the profit) as a function of the selling age for a farmer that raises and sells an animal under complex realistic cost and price structures. The theoretical results were applied to cattle males of the Mertolengo breed in order to determine the optimal selling age of an animal (slightly higher than the actual average selling age) and the corresponding (improved) optimal expected profit. A user friendly software was developed by RuralBit to made the optimization available to farmers. Sensitivity analysis w.r.t. model parameters showed that they have a negligible effect on the optimal selling age but, with the exception of σ, they have a sizable effect on the optimal expected profit.
Mixed models, in which the animal's growth parameters may depend on its genetic values (available in the database), are under study (with already preliminary results), so that optimization can be performed more precisely on an individual animal basis.

Acknowledgments

The authors work at the research center CIMA, supported by FCT (Fundação para a Ciência e a Tecnologia), project UID/04674/2020. This work was developed within the Operational Group PDR2020-1.0.1-FEADER-031130 - GoBovMais, funded by PDR 2020. We thank the ACBM and its head engineer José Pais for data and continuous support.

References

[1] Carlos A. Braumann, *Introduction to Stochastic Differential Equations with Applications to Modelling in Biology and Finance*. John Wiley & Sons, 2019.

[2] Patrícia A. Filipe, Carlos A. Braumann, Modelling individual animal growth in random environments. In: *Proceedings of the 23rd International Workshop on Statistical Modelling* (P. H. C. Eilers, Ed.), Utrecht, 2008, 232–237.

[3] Patrícia A. Filipe, Carlos A. Braumann, Nuno M. Brites, Carlos J. Roquete, Modelling animal growth in random environments: An application using nonparametric estimation, Biometrical Journal, **52**(5) (2010), 653–666.

[4] Patrícia A. Filipe, Carlos A. Braumann, Clara Carlos, Profit optimization for cattle growing in a randomly fluctuating environment. Optimization, **64**(6) (2015), 1393-1407.

[5] Patrícia A. Filipe, Carlos A. Braumann, Carlos J. Roquete, Multiphasic individual growth models in random environments, Methodology and Computing in Applied Probability, **14**(1) (2012), 49–56.

[6] Oscar García, A stochastic differential equation model for the height of forest stands, Biometrics, **3**9 (1983), 1059–1072.

[7] Gonçalo Jacinto, Patrícia A. Filipe, Carlos A. Braumann, Profit optimization of cattle growth with variable prices, Methodology and Computing in Applied Probability (2021), DOI: 10.1007/s11009-021-09889-z

[8] Nelson T. Jamba, Gonçalo Jacinto, Patrícia A. Filipe, Carlos A. Braumann, Likelihood function through the delta approximation in mixed SDE models, Mathematics, **10**(3) (2022), 385.

[9] Prajneshu, Himadri Ghosh, Stochastic differential equation models and their applications to agriculture: An overview, Statistics and Applications, **17**(1) (2019), 73–83.

[10] Qiming Lv., Jonathan W. Pitchford, Stochastic von Bertalanffy models, with applications to fish recruitment, Journal of Theoretical Biology, **244** (2007), 640–655.

[11] Keith Rennolls, Forest height growth modelling, Forest Ecology and Management, **71** (1995), 217–225.

[12] Hidekazu Yoshioka, Yuta Yaegashi, Yumi Yoshioka, Kentaro Tsugihashi, A short note on analysis and application of a stochastic open-ended logistic growth model, Letters in Biomathematics, **6**(1) (2019), 67–77.

International Conference on Mathematical Analysis and Applications in Science and Engineering
ICMA^{2}SC'22
ISEP Porto-Portugal, June 27 - 29, 2022

Impact of travel restrictions on the spread of infection

Kjetil Holm[1⋆], Swar Ramo[1], Josef Rebenda[1,2], Yuriy Rogovchenko[1]

[1] University of Agder, Norway
[2] Brno University of Technology, Czech Republic

[1⋆]kjetil_holm@live.no

Abstract: Travel facilitates the transmission of disease from areas affected by the virus to those less affected since the amount of contacts rises substantially. We suggest a mathematical model where susceptible cohort is split into two groups, those who currently travel and those who do not. Stability of infection-free equilibrium and endemic equilibrium is discussed and illustrated with numerical simulations.

keywords: SIR-model; travel patterns; basic reproduction number; stability; endemic equilibrium.

MSC2020: 92C60; 92D30.

1 Introduction

Mathematical models of infectious diseases have been used for centuries to analyze the mechanisms governing the spread of infection, predict possible outbreaks and the course of disease, and evaluate measures for preventing and controlling an epidemic [1, 2]. The design of the first mathematical model in epidemiology is attributed to Daniel Bernoulli who suggested a model in support of the inoculation against the smallpox back in 1760 [3]. Recent outbreak of Coronavirus pandemic in 2019 fuelled the interest in mathematical modeling in epidemiology and posed many questions which the research community attempted to answer with the modification of existing models and design of new ones.

2 Results and discussion

In this paper, we address the impact of travel patterns on the spread of infection. Our goal is to analyse how the restrictions on travel (or lack of such) impact the epidemic situation. Our default assumption is that individuals that travel have higher chances of getting infected because the number of other individuals encountered during the travel increases, whereas the environment (humidity, temperature, atmospheric pressure) may change quite rapidly, possibly accompanied with the travel stress. To explore this, we modify the classic SIR model [1, 2, 3]

dividing the susceptible cohort S into two, not traveling (S_1) and traveling (S_2). Individuals in the latter cohort are supposed to be traveling at time t and we assume that the transmission rate of infection for S_2 is higher than that for S_1. We do not exclude the possibility that some individuals completely recover after the disease and remain permanently immune to the infection afterwards but there always exists a possibility for reinfection for recovered patients who return to traveling and not traveling susceptible cohorts.

The epidemic situation we attempt to model is therefore described by the system of four differential equations for the four cohorts: not traveling susceptible S_1, traveling susceptible S_2, infected I, and recovered R. A modification of the classic SIR model to our case assumes the form

$$\dot{S}_1 = -\alpha I(t)S_1(t) - \gamma S_1(t) + \omega S_2(t) + \theta(1-\xi)R(t), \tag{1}$$

$$\dot{S}_2 = -\beta I(t)S_2(t) + \gamma S_1(t) - \omega S_2(t) + \theta\xi R(t), \tag{2}$$

$$\dot{I} = \alpha I(t)S_1(t) + \beta I(t)S_2(t) - \delta I(t), \tag{3}$$

$$\dot{R} = \delta I(t) - \theta R(t), \tag{4}$$

where the coefficients α and β are the rates of infection for not traveling and traveling individuals respectively, and the bidirectional flow between the not traveling and traveling cohorts is described in terms of inter-cohort transition rates γ and ω. Furthermore, individuals recover at the rate δ and θ is the transition rate from recovered to susceptible population, whereas ξ governs the distribution of individuals into traveling and not traveling cohorts after recovery with a possibility for further reinfection.

Observe that adding equations (1) - (4), we have $\dot{S}_1 + \dot{S}_2 + \dot{I} + \dot{R} = 0$ and thus in our model the total population $N(t) = S_1(t) + S_2(t) + I(t) + R(t)$ remains constant. This assumption is reasonable for our model since we consider the effect of the travel during relatively short periods of time. For convenience, we re-scale all variables so that $N(0) = 1$ and thus, for all $t \geq 0$,

$$S_1(t) + S_2(t) + I(t) + R(t) = 1. \tag{5}$$

Lemma 1. Assume that S_{1_0}, S_{2_0}, I_0, $R_0 \geq 0$. Then the solution $\vec{x}(t) = (S_1(t), S_2(t), I(t), R(t))^{\mathrm{T}}$ to the system (1) - (4) with the initial conditions

$$(S_1(0), S_2(0), I(0), R(0))^{\mathrm{T}} = (S_{1_0}, S_{2_0}, I_0, R_0)^{\mathrm{T}}$$

is non-negative for all $t \geq 0$.

We find equilibria for the system (1) - (4) by equating the right-hand sides of each of the differential equations to zero. The infection-free equilibrium E_0 is obtained when $I = 0$, in which case we have

$$E_0 = \left(\frac{\omega}{\gamma+\omega}, \frac{\gamma}{\gamma+\omega}, 0, 0\right).$$

For the endemic equilibrium $E_\star$ we look for a positive root I_* of the quadratic equation

$$A_2 I^2 + A_1 I + A_0 = 0 \tag{6}$$

where the coefficients A_2, A_1, and A_0 are defined as follows: $A_2 = \alpha\beta(\theta+\delta)$, $A_1 = \beta(\delta\theta - \delta\theta\xi + \gamma\theta + \gamma\delta) + \alpha(\omega\theta + \omega\delta + \delta\theta\xi - \beta\theta)$, $A_0 = \theta(\omega(\delta-\alpha) + \gamma(\delta-\beta))$.

Lemma 2. Assume that $0 < \delta < \alpha < \beta$. Then $A_0 < 0$ and quadratic equation (6) has two real roots of opposite signs.

Given the only positive root I_* of (6), the remaining three positive coordinates of the endemic equilibrium $E_\star$ can be computed. To analyse the stability properties of both equilibria, we

eliminate one of the equations in the system (1) - (4) using the property (5). The reduced system of three differential equations assumes the form

$$\begin{aligned}
\dot{I} &= \alpha I(t)S_1(t) + \beta I(t)S_2(t) - \delta I(t),\\
\dot{S_1} &= -\alpha I(t)S_1(t) - \gamma S_1(t) + \omega S_2(t) + \theta(1-\xi)(1-I-S_1-S_2),\\
\dot{S_2} &= -\beta I(t)S_2(t) + \gamma S_1(t) - \omega S_2(t) + \theta\xi(1-I-S_1-S_2).
\end{aligned}$$

Theorem 1. The infection-free equilibrium E_0 of the system (1) - (4) is locally asymptotically stable if the basic reproduction number

$$\mathcal{R}_0 = \frac{\alpha\omega + \beta\gamma}{\delta\,(\gamma+\omega)} < 1$$

and unstable if $\mathcal{R}_0 > 1$.

For analyzing the stability of the endemic equilibrium $E_* = (S_1^*, S_1^*, I_*, R_*)$, we calculate the Jacobian matrix at E_* and check the roots of the characteristic polynomial $p\,(\lambda) = \lambda^3 + b_2\lambda^2 + b_1\lambda + b_0$, where

$$\begin{aligned}
b_2 &= \gamma + \omega + \theta\xi + \alpha I_* + \beta I_* - \theta\,(\xi - 1)\,,\\
b_1 &= (\gamma + \alpha I_* - \theta\,(\xi-1))\,(\omega + \theta\xi + \beta I_*) - (\gamma - \theta\xi)\,(\omega + \theta\,(\xi-1))\\
&\quad + \alpha I_*\,(\alpha S_1^* - \theta\,(\xi-1)) + \beta I_*\,(\theta\xi + \beta S_2^*)\,,\\
b_0 &= \left(\theta\beta^2 S_2^* + \beta^2\gamma S_2^* + \alpha^2\omega S_1^* + \theta\beta\gamma + \theta\alpha\omega + \theta\alpha^2\xi S_1^*\right) I_*\\
&\quad - \left(\theta\beta^2\xi S_2^* + \alpha^2\beta I_* S_1^* - \alpha\beta^2 I_* S_2^* + \theta\alpha\beta I_*\right) I_*\\
&\quad + \left(-\theta\alpha\beta S_2^* + \alpha\beta\gamma S_1^* + \alpha\beta\omega S_2^* - \theta\alpha\beta\xi S_1^* + \theta\alpha\beta\xi S_2^*\right) I_*.
\end{aligned}$$

Theorem 2. The endemic equilibrium E^* for the system (1) - (4) is asymptotically stable if and only if the coefficients b_0, b_1 and b_2 of the characteristic polynomial $p\,(\lambda)$ are positive and satisfy the condition $b_2 b_1 > b_0$.

We explain the selection of important parameters in the system and their impact on the dynamics illustrating theoretical findings with numerical simulations. In the final part of the paper, we discuss how the presence of delay and periodic perturbation in the system (1) - (4) affect its evolution. The limitations of the model are also addressed.

Acknowledgments

KH, SR, and YR thank the Department of Mathematical Sciences, Faculty of Engineering and Science, and MatRIC, The Centre for Research, Innovation and Coordination of Mathematics Teaching at the University of Agder for financial support. JR greatefully acknowledges the support from the European Structural and Investment Funds, Operational Programme "Research, development and education" through the project "International Mobility of Researchers of Brno University of Technology," registration number CZ.02.2.69/0.0/0.0/18_053/0016962.

References

[1] F. Brauer, C. Castillo-Chavez, *Mathematical Models in Population Biology and Epidemiology*. Berlin: Springer Science, 2010.

[2] D.J. Daley, J. Gani, *Epidemic Modeling: An Introduction*. New York: Cambridge University Press, 2005.

[3] H.W. Hethcote, The mathematics of infectious diseases, SIAM Review. **42** (2000), 599–653.

International Conference on Mathematical Analysis and Applications in Science and Engineering
ICMA^{2}SC'22
ISEP Porto-Portugal, June 27 - 29, 2022

A deterministic model for Atlantic salmon life cycle

Kjetil Holm[1], Swar Ramo[1], Josef Rebenda[1,2,⋆], Yuriy Rogovchenko[1]

[1] University of Agder, Norway
[2] Brno University of Technology, Czech Republic

⋆rebenda@vutbr.cz

Abstract: The total export value of Norwegian Atlantic salmon in 2020 amounted to NOK 70,1 billion. Although mathematical modeling of salmon life cycle is challenging due to the impact of a large number of ecological and genetic factors and their variability, it is important for the sustainability of Norwegian fisheries. In this paper, we suggest a discrete model for Atlantic salmon life cycle based on the real data collected in a wild population inhabiting a Norwegian river. We analyse the dynamics of the model and discuss biologic and economic implications.

keywords: Atlantic salmon; discrete model; sensitivity; elasticity.

MSC2020: 39A60; 92D25.

1 Introduction

Mathematical modeling of Atlantic salmon population is challenging due to variability of biological parameters describing its life cycle [1, 2, 3]. Castellani et al. [2] pointed out the scarcity of research on the impact of numerous ecologic and genetic factors on the evolution of populations and emphasized an urgent need for new models incorporating these elements. They suggested an Individual-Based Salmon Eco-genetic Model (IBSEM) describing the demographic and population genetic change of an Atlantic salmon population through its entire life-cycle. IBSEM uses stochastic processes for simulating individuals' growth, maturation, and mortality. Empirical data were parameterized to match the environmental conditions and the characteristics of a wild population inhabiting a Norwegian river. Aas et al. [1] divide the life history of the Atlantic salmon in the wild into three main phases: embryonic, juvenile and oceanic (adult). The embryonic phase in freshwater splits into two sub-phases: egg and alevin. It is followed by the freshwater juvenile phase divided into two sub-phases: parr and smolt; these groups are structured according to their age. Parr stay in freshwater while smolts migrate to sea to enter the adult phase. In this paper, we suggest a deterministic model for Atlantic salmon population using discrete equations.

2 Results and discussion

We design a stage-structured model describing the life cycle of Atlantic salmon. The main source of data for our model is the paper [3, Tables 3-6] where useful estimates for the survival probabilities between different stages in the river are collected. As it is common for simpler models, several important factors (stochasticity, density dependence, immigration and emigration) are omitted. Although we balance between model error and parameter error due to simplifying assumptions and a limited set of data, the analysis of the model provides an important insight into the dynamics of the system. Following the description in [2], we model the life cycle of Atlantic salmon as shown in Figure 1 where the arrows represent transitions between stages. The numbers p_i are the probabilities that an individual survives to the next stage during the period between (t) and $(t+1)$, while the loop arrows mean that an individual remains at the same stage with the given survival probability. One important parameter not included in the diagram is the fecundity f_7 of a female adult individual.

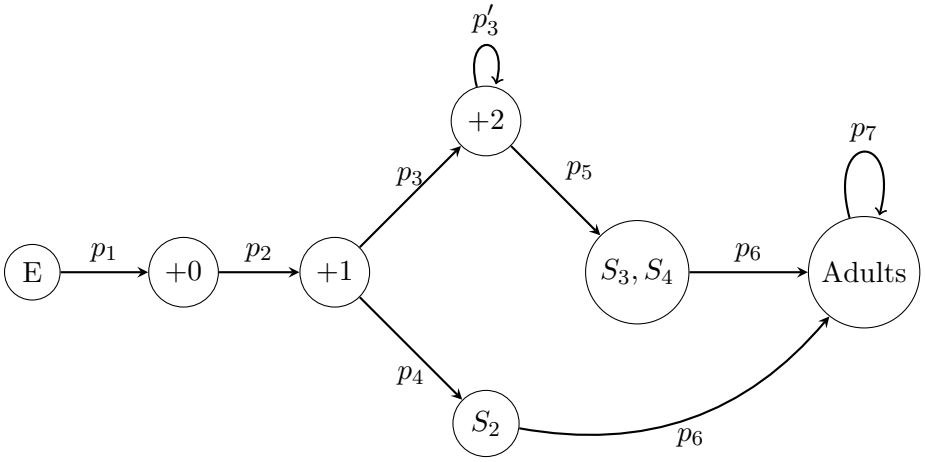

Figure 1: The transition between stages

Our model is described by the difference equation

$$N(t+1) = AN(t), \tag{1}$$

with the matrix A defined by

$$A = \begin{pmatrix} 0 & 0 & 0 & 0 & 0 & 0 & 7180.16 \\ 0.307 & 0 & 0 & 0 & 0 & 0 & 0 \\ 0 & 0.333 & 0 & 0 & 0 & 0 & 0 \\ 0 & 0 & 0.335 & 0.5 & 0 & 0 & 0 \\ 0 & 0 & 0.011 & 0 & 0 & 0 & 0 \\ 0 & 0 & 0 & 0.129 & 0 & 0 & 0 \\ 0 & 0 & 0 & 0 & 0.1 & 0.1 & 0.05 \end{pmatrix},$$

where the *reference values* are $f_7 = 7180.16$, $p_1 = 0.307$, $p_2 = 0.333$, $p_3 = 0.335$, $p_3' = 0.5$, $p_4 = 0.011$, $p_5 = 0.129$, $p_6 = 0.1$, $p_6' = 0.1$, and $p_7 = 0.05$. It is clear that the matrix A is neither a Leslie, nor a Lefkovitch matrix, and we deal with a general population projection matrix which accounts for several additional stages. Since A is non-negative, we first verify that it is irreducible. For this purpose we use the following results [4, Theorems 16 and 14].

Theorem 1 (i) *A non-negative square matrix A of order n is irreducible if and only if $I + A$ is primitive, where I is the unit square matrix of order n.*

(ii) *A necessary and sufficient condition for an irreducible square non-negative matrix A to be primitive is that A^m is positive for some positive integer m.*

Theorem 1 yields the following

Theorem 2 *The matrix A in equation* (1) *is irreducible and primitive.*

We also verify that A is primitive by computing successive powers of A until all elements of the matrix became positive for A^8 for the first time. Since A is primitive, Perron-Frobenius Theorem can be applied assuring the existence of a positive dominant eigenvalue with the corresponding positive eigenvector. In our case, the characteristic polynomial is

$$\lambda^7 - 0.55\,\lambda^6 + 0.025\,\lambda^5 - 0.80742044\,\lambda^2 - 2.7683511\,\lambda$$

and the spectral radius is equal to the dominant eigenvalue $\lambda_d = 1.3607 > 1$. This implies that the population is growing since the stable stage distribution is $N(t) \approx c_d \lambda_d^t v_d$ where v_d is the right eigenvector corresponding to the eigenvalue λ_d.

To explore the robustness of the salmon life cycle from the ecological point of view, we conducted a number of numerical experiments including "worst case scenarios" where the survival probabilities are taken one by one with minimal values found in [3]. It turns out that even in a "worst case scenario" the value of the dominant eigenvalue λ_d remains larger than 1 which ensures the persistent population growth.

Numerical experiments were done by using MATLAB; the results are collected in Table 1. The header of the table contains the list of all parameters in our model. We ran fourteen numerical experiments modifying the values of the elements in the matrix A as follows. In each row, the values colored red are fixed. All other values for parameters in that row are minimal values which ensure that the population is still growing in the long run provided that values of remaining parameters are set as the reference values from the top row.

Test	f_7	p_1	p_2	p_3	p_3'	p_4	p_5	p_6	p_6'	p_7
Ref.	7180.16	0.307	0.333	0.335	0.5	0.011	0.129	0.1	0.1	0.05
1.	960	0.0408	0.0443	0.0076	0	0	0.00291	0	0.00226	0.05
2.	1004	0.043	0.0466	0.011	0	0	0.00393	0	0.00304	0
3.	804	0.035	0.0373	0	0	0	0	0.1	0.0127	0.2
4.	302	0.013	0.014	0	0	0	0	0	0	0.7
5.	1576	0.0674	0.0775	0.0136	0.5	0	0.00525	0	0.00406	0.05
6.	1701	0.0728	0.07891	0.01499	0.01	0	0.0058	0	0.00446	0.05
7.	3590	0.0816	0.0885	0.0577	0.5	0	0.0223	0	0.0173	0.05
8.	3590	0.1455	0.1578	0.1143	0.01	0	0.044	0	0.0341	0.05
9.	718	0.4079	0.4424	0.4591	0.5	0.043	0.1768	0.3909	0.1371	0.05
10.	718	0.7271	0.7887	0.9089	0.01	0.0858	0.35	0.7798	0.2713	0.05
11.	1063	0.0454	0.0493	0.046	0.5	0	0.0177	0.01	0.0138	0.05
12.	2078	0.0888	0.0964	0.0909	0.01	0	0.035	0.01	0.0272	0.05
13.	4733	0.2023	0.2195	0.0753	0.5	0.0043	0.029	0.0391	0.01	0.05
14.	6050	0.2586	0.2805	0.1491	0.01	0.0086	0.0575	0.078	0.01	0.05

Table 1: Parameters in A: reference values and minimal values for the population growth.

Many components are important for the persistence of the species under different natural and man-affected ecologic changes. To identify these components, we conducted both sensitivity and elasticity analyses of the matrix A observing that the most significant parameters are f_7, p_1 and p_2, closely followed by p_3, p_5 and p_6'. We believe that our analysis provides an interesting insight into sustainability of the life cycle of Atlantic salmon presented schematically in Figure 1.

Acknowledgments

KH, SR, and YR thank the Department of Mathematical Sciences, Faculty of Engineering and Science, and MatRIC, The Centre for Research, Innovation and Coordination of Mathematics Teaching at the University of Agder for financial support. JR gratefully acknowledges the support from the European Structural and Investment Funds, Operational Programme "Research, development and education" through the project "International Mobility of Researchers of Brno University of Technology," registration number CZ.02.2.69/0.0/0.0/18_053/0016962.

References

[1] Ø. Aas, A. Klemetsen, S. Einum, J. Skurdal. *Atlantic Salmon Ecology*. Chichester: John Wiley & Sons, 2010.

[2] M. Castellani, M. Heino, J. Gilbey, H. Araki, T. Svåsand, K.A. Glover, IBSEM: An Individual-Based Atlantic Salmon Population Model. PLoS ONE **10**(9) (2015), e0138444. doi:10.1371/journal.pone.0138444.

[3] R. A. Cunjak, J. Therrien, Inter-stage survival of wild juvenile Atlantic salmon, Salmo salar L. Fisheries Management and Ecology, **5** (1998), 209–223.

[4] G. Giorgi, Nonnegative square matrices: irreducibility, reducibility, primitivity and some economic applications, Working Papers Series 2018-2020, Department of Economics and Management, University of Pavia, No. 175 (10-19), 2019. http://economiaweb.unipv.it/wp-content/uploads/2018/01/DEMWP0175.pdf

International Conference on Mathematical Analysis and Applications in Science and Engineering
ICMA^{2}SC'22
ISEP Porto-Portugal, June 27 - 29, 2022

Dynamics of a pituitary-adrenal model with distributed time delays

E. Kaslik[1,3] **R Matei**[1,⋆] **M. Neamţu**[2,3]

[1] Dept. of Mathematics and Computer Science, West University of Timişoara, Romania
[2] Dept. of Economics and Business Administration, West University of Timişoara, Romania
[3] Institute for Advanced Environmental Research, West University of Timişoara, Romania

⋆maria.matei91@e-uvt.ro

Abstract: The paper concerns the two-dimensional model of the pituitary-adrenal axis with general distributed delays based on the dynamical description of the concentrations of adrenocorticotropic hormone (ACTH) and cortisol. We prove the existence of a unique equilibrium point and study its local stability properties. Taking several types of delay kernels into account, such as Dirac kernels or weak Gamma kernels, we investigate the Hopf bifurcations and the stability of the bifurcating periodic solutions by using the method of multiple time scales. Numerical simulations are also included to exemplify the theoretical results.

keywords: pituitary-adrenal axis; stability analysis; Hopf bifuraction; distributed delays.

MSC2020: 34A34; 34C23; 34D20; 92B25.

1 Introduction

The hypothalamic-pituitary-adrenal (HPA) axis plays an essential role on how the body responds to stress and is influenced by the interactions of several hormones, such as corticotropin-releasing hormone (CRH), corticotropin (ACTH), and cortisol (CORT). The andrenal glands release cortisol in response to stress and the blood levels of cortisol vary throughout the day causing a fluctuation named the "circadian rhythm", which is a cycle that repeats every 24 hours. Additionally, we also have biological rhythms with a shorter period and higher frequency than the circadian rhythm named the 'ultradian rhythm'. In the past few decades, mathematical modelling has been used as a tool to gain a better understanding of hormonal behaviour and to seek explanation about endocrine and physiological regulation. Most of the existing models [2,4] considered so far in the literature have suggested that the circadian rhythm is the result of an external input to the HPA axis, which can only exhibit ultradian behaviour in the absence of an external input. In some of the studies [1,3] it has been shown that the ultradian rhythms are produced independently of the CRH secretion and based on this assumption, we will only consider a two-dimensional mathematical model involving the ACTH hormone and cortisol levels.

The main aim of this paper is accomplish a thorough analysis of the effect of different types of distributed time delays on the dynamics of the pituitary-adrenal axis. Time delays appear naturally in endocrine processes, due to the transportation of hormones between the endocrine

glands. Moreover, we consider distributed time delays in the proposed mathematical model, to provide a more accurate reflection of biological variability. It is important to emphasize that the exact delay distribution is not known, and consequently, approaches using general delay kernels may prove to be appropriate.

2 Results and discussion

The proposed mathematical model is based on the simplified HPA axis model considered in [2], which focuses on the interaction between ACTH and CORT. As described above, we include distributed time delays in this two-dimensional model. Denoting the concentrations of ACTH and cortisol by $A(t)$ and $C(t)$, we consider the following system of differential equations with distributed delays:

$$\begin{cases} \dot{A}(t) = f\left(\int_0^\infty h_c(s)C(t-s)ds\right) - \beta_a A(t) \\ \dot{C}(t) = g\left(\int_0^\infty h_a(s)A(t-s)ds\right) - \beta_c C(t) \end{cases} \tag{1}$$

The elimination constants β_a, β_c are positive real numbers. The functions $f, g : [0, \infty) \to (0, \infty)$ represent the negative and the positive feedback functions, respectively. The function f is assumed to be strictly decreasing, smooth and bounded on $[0, \infty)$ and the function g is assumed to be strictly increasing, smooth and bounded on $[0, \infty)$. Examples of such functions are given below:

$$f(x) = \gamma\left(1 - \mu\frac{x^m}{u^m + x^m}\right) \quad , \quad g(x) = \eta\frac{x^n}{v^n + x^n}$$

with $m, n \geq 1, \gamma > 0, u, v > 0$ and $\mu, \eta \in (0, 1)$.

The delay kernels $h_a, h_c : [0, \infty) \to [0, \infty)$ are probability density functions representing the probability that a particular time delay occurs, and they are assumed to be bounded and piecewise continuous.

An equilibrium point of system (1) is a solution of the following algebraic system:

$$\begin{cases} f(C) = \beta_a A \\ g(A) = \beta_c C \end{cases} \tag{2}$$

It follows that the system (1) has a unique equilibrium point $E = (A^\star, C^\star)$.

In what follows we study necessary and sufficient conditions for the local asymptotic stability of the equilibrium point. We construct the liniarized system at the equilibrium point E and we rely on the associated characteristic equation:

$$(z + \beta_a)(z + \beta_c) + bH_a(z)H_c(z) = 0 \tag{3}$$

where $H_i(z) = \int_0^\infty e^{-zs}h_i(s)ds$ represent the Laplace transforms of the delay kernels $h_i, i \in \{a, c\}$ and

$$b = -f'(A^\star)g'(C^\star) > 0.$$

We show that in the non-delayed case, the equilibrium point E is locally asymptotically stable. Additionally, we also determined the simple inequality $b < \beta_a\beta_c$ which guarantees that the equilibrium point E of system (1) is locally asymptotically stable for any delay kernels $h_a(t), h_c(t)$.

We also discuss the bifurcation analysis of system (1), considering two types of delay kernels: Dirac kernels and weak Gamma kernels. The bifurcation parameter that we take into account is $\tau = \tau_a + \tau_c,$, where τ_a and τ_c represent the average delays of the kernels h_a and h_c respectively. Hence, τ is the average time delay of the convolution of the kernels h_a and h_c.

Our main findings are as follows:

1. In the case of Dirac kernels, we have an infinity of critical values for the bifurcation parameter τ. However, relying on the transversality condition, we prove that the equilibrium point E is asymptotically stable if and only if

$$\tau < \frac{(\beta_a + \beta_c)\arccos(u_0)}{b\sqrt{1-u_0^2}} \quad \text{where} \quad u_0 = \frac{\sqrt{(\beta_a^2 - \beta_c^2)^2 + 4b^2} - (\beta_a + \beta_c)^2}{2b},$$

and there is no stability switching.

2. In the case of weak Gamma kernels, on the one hand, the condition $b < (\beta_a+\beta_c)(\sqrt{\beta_a}+\sqrt{\beta_c})^2$ implies that the equilibrium point E is asymptotically stable, for any $\tau > 0$. On the other hand, if the system parameters do not verify the previous inequality, there are exactly two critical values τ_1 and τ_2 (such that $\tau_1 < \tau_2$) of the bifurcation parameter τ, which are determined explicitly in terms of the system parameters. Again, relying on the transversality condition, we obtain that in this case, stability switching is observed and the equilibrium point E is asymptotically stable if and only if $\tau \in (0, \tau_1) \cup (\tau_2, \infty)$.

As limit cycles that appear due to Hopf bifurcations are naturally connected to the modelling of the circadian rhythm, we also investigate the stability of the resulting limit cycles and the criticality of the Hopf bifurcations, using the multiple time scales method.

3 Conclusions and Future work

The results of this paper emphasize the importance of including distributed time delays in mathematical models arising from endocrinology, such as the pituitary-adrenal model. Our theoretical results reveal that different dynamic properties are observed in system (1), based on the choice of delay kernels. On the one hand, if Dirac kernels are considered, stability switching does not occur and the positive equilibrium is locally asymptotically stable only for small values of the average time delays. However, if weak Gamma kernels are taken into account, stability switching is observed and local asymptotic stability of the positive equilibrium is also obtained for large values of the average time delays.

A different investigation of the pituitary-adrenal axis involving the stochastic approach may represent a direction for future research.

References

[1] A. Kalsbeek, R. van der Spek, J. Lei, E. Endert, R.M. Buijs, E. Fliers. "Circadian rhythms in the hypothalamo-pituitary-adrenal (HPA) axis" Mol. Cell. Endocrinol. **349** (1) (2012), 20-29.

[2] Kaslik, Eva, Mihaela Neamţu. "Stability and Hopf bifurcation analysis for the hypothalamic-pituitary-adrenal axis model with memory." Mathematical Medicine and Biology, **35** (2018), 49-78.

[3] Hamed Malek, Mohammad Mehdi Ebadzadeh, Reza Safabakhsh, Alireza Razavi. "Mathematical analysis of the role of pituitary-adrenal interactions in ultradian rhythms of the HPA axis." Nonlinear Computers in Biology and Medicine, **135** (2021), 104580.

[4] Yongli Song, Yanyan Han, Tonghua Zhang. "Stability and Hopf bifurcation in a model of gene expression with distributed time delays." Applied Mathematics and Computation, **243** (2014), 291-307.

International Conference on Mathematical Analysis and Applications in Science and Engineering
ICMA^{2}SC'22
ISEP Porto-Portugal, June 27 - 29, 2022

A mathematical model of CD19$^-$ relapses after CAR-T cell treatment in B cell leukemia

S. Chulián[1,2,⋆] **A. Martínez-Rubio**[1,2] **A. Niño-López**[1,2] **M. Rosa**[1,2]

[1] Department of Mathematics, Universidad de Cádiz, Puerto Real, Cádiz, Spain
[2] Biomedical Research and Innovation Institute of Cadiz (INiBICA)
Hospital Universitario Puerta del Mar, Cádiz, Spain

⋆salvador.chulian@uca.es

Abstract: B cell Acute Lymphoblastic Leukaemia (B-ALL) is the most common type of pediatric leukemia. Modern therapies have improved survival rates, but approximately 15-20 % of patients relapse. For such patients, a treatment possibility is chimeric antigenic receptor (CAR) T cells as it presents high rates of response. CAR T cells are able to recognize target cells with the antigen CD19, which is expressed in B-ALL. Here, we construct a mathematical model based on partial differential equations, where we simulate different scenarios regarding this therapy. We focus on how CAR-T cells therapy can lead to CD19$^-$ relapses, where leukemic cells loss the antigen and thus continue growing. We propose this model which could readily extend to other haematological malignancies considering this kind of immunotherapy.

keywords: partial differential equations; numerical simulation; CAR T cells; acute lymphoblastic leukemia; B cells; relapses

MSC2020: 37N25; 92B05.

1 Introduction

Chimeric antigen receptor (CAR) T cell therapy is an immunotherapy technique, key in personalised cancer treatment. It consists of genetically modified T-cells, able to recognize specific tumor antigens. Thus, these T lymphocytes recognise and can thus eradicate cancer cells. CAR T cells are obtained from blood, either from the patient or from a compatible donor, then is later modified and expanded in vitro, and finally re-infused into the patient [1]. CAR T cell therapy has a successful history in its application to B cell malignancies using the antigen CD19, expressed in the B cell lineage [2], with an early response of up to 92% in Acute Lymphoblastic Leukaemia (ALL) patients [3, 4, 5, 6].

Despite this success, 30 to 50% of patients still relapse after treatment [7]. This leads to two different types of post-CAR relapse: one where CD19 antigen is well expressed in post-CAR leukemic cells, and other where such leukemic cells lose expression of the CD19 antigen, therefore avoiding CAR T cells. In the first type of relapse (where the leukemic cells remain CD19$^+$), therapy fail may be due to the lack of expansion of CAR T cells or the quality of the product [8]. However, CD19$^-$ relapses demand a different approach, as recurrence occurs despite persistence of CAR T cells and continued B-cell aplasia, as healthy B cells also express CD19 antigen.

This is where mathematical modelling comes in hand. Some mathematical works have been focused on CAR-T cells (see a review in [9]), while the ones centered in ALL have mostly highlighted issues such as fratricide in T-cell ALL [10], or $CD19^+$ relapses in B-ALL [11]. In this work, we present a mathematical model derived from [12], and expand it to also consider the possibility of $CD19^-$ relapse after CAR T cell treatment.

2 Mathematical model

Our mathematical model accounts for the evolution over time of three interacting cellular populations. Here, $C(t)$ denote the function of CAR T cells number varying on time t. moreover, $L(t,x)$ and $B(t,x)$ represent the number of leukemic and healthy B-cells, depending both in time t and CD19 expression level x. Here, we consider $x \in [0,1]$, where 0 denotes a low intensity of CD19 ($CD19^-$ cells) and 1 as a high intensity of CD19 marker ($CD19^+$ cells). We work with the ODE-PDE system

$$\frac{dC(t)}{dt} = \rho_C C(t) \int_{x_{\min}}^{x_{\max}} (B(t,x) + L(t,x))\mathrm{d}x - \frac{C(t)}{\tau_C}, \tag{1a}$$

$$\frac{\partial L(t,x)}{\partial t} = \rho_L L(t,x) - f(x)\alpha C(t) L(t,x), \tag{1b}$$

$$\frac{\partial B(t,x)}{\partial t} = I_0(x) - f(x)\alpha C(t) B(t,x). \tag{1c}$$

Firstly, in Eq. (1a), $C(t)$ grows at a rate ρ_C, depending on the interaction between CAR T cells and the amount of cells expressing CD19 marker x. This is why we consider an integro-differential ODE accounting for all healthy (B) and leukemic (L) cells expressing CD19, and so integrate over a range of $x \in [x_{\min}, x_{\max}]$. This interval depends on how much CAR T cells are activated, and whether a low expression of CD19 ($x_{\min}$) is able to activate them, or levels over a high expression of CD19 ($x_{\max}$) exhausts T cells. Finally, CAR T cells die at a rate τ_C.

Secondly, in Eq.(1b), leukemic cells grow at a rate ρ_L, and die with rate α after the interaction with CAR T cells $C(t)$. This rate is scaled via a function $f(x)$, which should determine a direct relationship between the expression of CD19 (x) and the amount of cells that die after CAR T cell encounter. This is due to the fact that CAR T cells CD19 detection leads to target cells apoptosis. We choose then $f(x)$ to have a sigmoid form, i.e.,

$$f(x) = \frac{x}{x+h}, \tag{2}$$

with h as a Michaellis-Menten term.

Finally, in Eq.(1c), healthy cells are also target cells, and therefore die after encounter with CAR T cells with a rate α, scaled again via $f(x)$. However, healthy B-cells receive an input from stem cells at each time t, which we represent with the function $I_0(x)$.

3 Conclusions and Future work

In this work, we study a mathematical model for relapses in ALL after CAR-T cells treatment. The model includes a variable which consider the expression level of the antigen CD19, and therefore enables to consider the continuous existence of different maturity levels for healthy B cells, as well as different intensity of such antigen within the leukemic cell population. Such considerations leads to possibility of simulation of different scenarios, such as selection of preexisting $CD19^-$ leukemic subpopulations or CD19 downregulation.

Acknowledgments

This work has been partially supported by the Fundación Española para la Ciencia y la Tecnología (FECYT project PR214), the Asociación Pablo Ugarte (APU, Spain), Junta de Andalucía (Spain) group FQM-201, Ministry of Science and Technology, Spain (grant number PID2019-110895RB-I00, funded by MCIN/AEI/10.13039/501100011033). This work was also subsidized by a grant for the research and biomedical innovation in the health sciences within the framework of the Integrated Territorial Initiative (ITI) for the province of Cadiz (grant number ITI-0038-2019). ITI is 80% co-financed by the funds of the FEDER Operational Program of Andalusia 2014-2020 (Council of Health and Families).

References

[1] Levine BL, Miskin J, Wonnacott K, Keir C. Global manufacturing of CAR T cell therapy. Mol Ther Methods Clin Dev 2017; 4:92–101.

[2] Sadelain M. CD19 CAR T cells. Cell 2017; 171:1471.

[3] Feins S et al.An introduction to chimeric antigen receptor (CAR) T-cell immunotherapy for human cancer. Am J Hematol 2019; 94:S3-S9.

[4] Maude SL et al. Tisagenlecleucel in children and young adults with B-cell lymphoblastic leukemia. N Engl J Med 2018; 378:439-48.

[5] Pan J et al. High efficacy and safety of low-dose CD19-directed CAR-T cell therapy in 51 refractory or relapsed B acute lymphoblastic leukemia patients. Leukemia 2017; 12:2587-93.

[6] Militou AN, Papadopoulou LC. CAR T-cell therapy: a new era in cancer immunotherapy. Curr Pharm Biotechnol 2018; 19:5-18.

[7] Shah, NN, Fry TJ. Mechanisms of resistance to CAR T-cell therapy. Nat Rev Clin Oncol 2019; 16:372–385.

[8] Finney OC et al. CD19 CAR T-cell product and disease attributes predict leukemia remission durability. J Clin Investig 2019; 129:2123–2132.

[9] Chaudhury A et al. Antigen Receptor T-cell Therapies: A Review of Cellular Kinetic-Pharmacodynamic Modeling Approaches. J Clin Pharmacol 2020; 60:S147–S159.

[10] Pérez-García VM et al. (2021). CAR T cells for T-cell leukemias: Insights from mathematical models. Commun Nonlinear Sci Numer Simul 2021; 96:105684.

[11] Martínez-Rubio Á et al. (2021). A Mathematical Description of the Bone Marrow Dynamics during CAR T-Cell Therapy in B-Cell Childhood Acute Lymphoblastic Leukemia. Int J Mol Sci. 2021; 22(12):6371.

[12] León-Triana O et al. CAR T cell therapy in B-cell acute lymphoblastic leukaemia: Insights from mathematical models. Commun Nonlinear Sci Numer Simul 2021; 94:105570.

Parameter estimation for a FSDE model of glucose control

Simona Panunzi1[1] **Alessandro Borri**[1] **Elvin Moore**[2]
Andrea De Gaetano[1,3⋆]

[1] Consiglio Nazionale delle Ricerche
Istituto per l'Analisi dei Sistemi e Informatica (CNR-IASI), Rome, ITALY
[2] King Mongkut University of Technology North Bangkok
Dept. of Mathematics, Bangkok, THAILAND
[3] Consiglio Nazionale delle Ricerche
Istituto per la Ricerca e l'Innovazione Biomedica (CNR-IRIB), Palermo, ITALY

⋆andrea.degaetano@cnr.it

Abstract: In the quest for progressively more realistic mathematical representations of biomedical processes, fractional differential equations have the potential of summarizing, with an order that can in principle be estimated from data, different (presumably integer-order) interacting controls or influences upon the observed variable of interest. This is the case, for example, of transcutaneously measured glycemia, where besides glycemia itself (possibly decaying by first-order elimination) also unobserved factors (insulinemia, other hormones) may exert higher order effects. The problem is complicated by the fact that random events (food intake, exercise, emotions) may affect glycemia as well, leading to the formalization of the problem as a Fractional Stochastic Differential Equation. We use a simple FSDE model of glycemic control to exemplify a possible approach to model parameter estimation in this framework. Confidence regions on the estimates are obtained by Approximate Bayesian Computing and compared with the generating parameter values to assess the reliability of the approach.

keywords: Fractional Differential Equations; Stochastic Differential Equations; Parameter Estimation.

MSC2010: 26A##; 34A##; 93B##.

International Conference on Mathematical Analysis and Applications in Science and Engineering
ICMA^{2}SC'22
ISEP Porto-Portugal, June 27 - 29, 2022

A MATHEMATICAL MODEL OF ACUTE LYMPHOBLASTIC LEUKEMIA DEVELOPMENT

Ana Niño-López[1,3⋆] **Álvaro Martínez-Rubio**[1,2] **Salvador Chulián**[1,2]
María Rosa[1,2]

[1] Cádiz University , Spain
[2] Biomedical Research and Innovation Institute of Cadiz (INiBICA),
Hospital Universitario Puerta del Mar, Cádiz, Spain

⋆ana.nino@uca.es

Abstract: Leukemia is the most frequently type of cancer in pediatric age. Particularly, Acute Lymphoblastic Leukemia (ALL) brings about 80% of childhood leukemias. Even if its survival rate has increased in the recent years, about $15-20\%$ of treatments are unsuccessful, and patients relapse. For this reason, it is required to determine new therapeutic strategies to advance in this field. This work develops a mathematical model which describes leukemic cells behavior, and so establish the basis of future works about treatment. Therefore, we suggest a mathematical model which allows testing future alternative therapies. Methodology employed combines ordinary differential equations, numerical simulations and data analysis techniques, incluidng statistical tools for data processing with *Python*.

keywords: Mathematical model; Leukemia; Cancer.

MSC2020: 34A12; 92B05.

1 Introduction

Acute Lymphoblastic Leukemia (ALL) is a type of Leukemia, a disease originating in the bone marrow which arises from a disruption in the process in charge of blood cells production [1]. This process is known as hematopoiesis and it is considered as hierarchical tree where a stem cell can differentiate into lymphoid or myeloid branch. Acute Lymphoblastic Leukemia (ALL) is caused by cells with fast growth in the lymphoid branch, with special incidence in childhood [2, 3].

At present, mathematical models provide a wide variety of applications in medicine. Mathematical oncology is considered useful to understand and approach cells behavior. These works allow to study the healthy cells development in bone marrow [4, 5] to be able to include new assumptions.

In this work, we focus on the simulation of leukemic bone marrow. In terms of mathematical analysis, we study how both leukemic and healthy cells develop without treatment from a stability study of the model. This will allow us to propose future works related to drugs administration in optimal times.

2 A model which simulates a leukemic bone marrow

According to a previous paper which presents a study of lymphoid branch behaviour in a healthy bone marrow [5], we base our model on Model (1). This system represents the bone marrow development considering three cells compartment depending on their maturation states: Pro-B (C_1), Pre-B (C_2) and Transition cells (C_3), as shown in the following system:

$$\frac{dC_1}{dt} = \bar{s}\rho_1 C_1 - \alpha_1 C_1, \tag{1a}$$

$$\frac{dC_2}{dt} = \bar{s}\rho_2 C_2 + \alpha_1 C_1 - \alpha_2 C_2, \tag{1b}$$

$$\frac{dC_3}{dt} = \alpha_2 C_2 - \alpha_3 C_3, \tag{1c}$$

where ρ_1 and ρ_2 are the proliferation rates and α_1, α_2 and α_3 are transition rates. It is considered $\bar{s}$ as a regulatory signal which is in charge of controlling cells development.

Now, we take into account these three compartments and moreover, we consider leukemic cells as a new compartment L. We assume that this compartment is originated by an unique leukemic cell and it grows as a logistic function with carrying capacity is $L_{\max}$. The logistic growth rate is ρ_L and like in healthy cells, it is characterized by a maturation stage, [6, 7]. Depending on the stage where leukemia originates, $\rho_L = \rho_1$ if the first leukemic cell belongs to Pro-B compartment and if leukemia appears in Pre-B stage, $\rho_L = \rho_2$.

Therefore, we associate the following expression with the flux in the leukemic cells compartment:

$$\frac{dL}{dt} = s_L \rho_L L \left(1 - \frac{L}{L_{\max}}\right) - \gamma_L L. \tag{2}$$

In this case, signalling should be considered in two different situations. Healthy cells are influenced by the total amount of cells in bone marrow. However, leukemic cells do not control their own proliferation, in consequence, signal is only generated by healthy cells. Being

$$s = \frac{1}{1 + k\left(L + \sum_{i=1}^{3} C_i\right)}, \qquad s_L = \frac{1}{1 + k\sum_{i=1}^{3} C_i}, \tag{3}$$

we propose the Model (4) and we assume a constant influx of healthy stem cells c_0 in our initial compartment C_1 [8], both leukemic and healthy B cells behaviour are defined as follow:

$$\frac{dC_1}{dt} = c_0 + s\rho_1 C_1 - \alpha_1 C_1, \tag{4a}$$

$$\frac{dC_2}{dt} = s\rho_2 C_2 + \alpha_1 C_1 - \alpha_2 C_2, \tag{4b}$$

$$\frac{dC_3}{dt} = \alpha_2 C_2 - \alpha_3 C_3, \tag{4c}$$

$$\frac{dL}{dt} = s_L \rho_L L \left(1 - \frac{L}{L_{\max}}\right) - \gamma_L L, \tag{4d}$$

with s and s_L as in Eq. (3), where ρ_L depends on the origin of the leukemic clone [7].

Values obtained as solutions match with biological basis related to leukemia. Both cases for ρ_L are associated with stability values with biological sense. It has been studied the existence, boundedness and positivity of the solutions obtained and simulations for each case have been reproduced and interpreted.

3 Conclusions and Future work

Leukemia has the highest incidence cancer in childhood. Despite the fact that current protocols have improved survival rates, particularly in Acute Lymphoblastic Leukemia, there is a 20% of them which leads to a relapse. For that reason, we suggest an analysis of leukemic cells behavior with the goal of approximate the beginning of the disease along with the detection of the maturation state of the first leukemic cell. When leukemia is detected in a patient, leukemic cells population involves the 80% of the bone marrow [9]. It is important to analyze the behaviour from the beginning of the disease to obtain more information from blood or bone marrow extractions. Our intention is to find patterns in bone marrow along with drugs applied at the early stage of the disease. With this, it could be possible to predict relapses and improve current treatments.

Firstly, a healthy bone marrow model has been reviewed. That study allows us to include the assumption of the appearance of a leukemic cell. The strong development of leukemic cells match with their properties of malignant disease. The leukemic cell develops more or less accelerated depending on the inherited proliferation rate for ρ_L. The unique stable steady state obtained in the study is the one that represents the total occupancy of the bone marrow by leukemic cells and the rest of solutions are unstable. Therefore, Model (4) replicates reality and its study allows to adjust parameters related to leukemic population growth. In general, both cases have the same behavior. For the computed simulations, healthy and leukemic cells are able to coexist for a period of time. After such moment, leukemic cells take up all the bone marrow capacity, therefore, there is no space for healthy cells.

After studying leukemic cells behavior it is possible to analyze and advance in this area. Available clinical data are important to determinate parameters values according to different bone marrow samples from the same patient. Modeling current treatment in B cell leukemia leads to advances towards optimizing treatment.

Acknowledgments

This work has been partially supported by the Fundación Española para la Ciencia y la Tecnología (FECYT project PR214), the Asociación Pablo Ugarte (APU, Spain), Junta de Andalucía (Spain) group FQM-201, Ministry of Science and Technology, Spain (grant number PID2019-110895RB-I00, funded by MCIN/AEI/ 10.13039/501100011033). This work was also subsidized by a grant for the research and biomedical innovation in the health sciences within the framework of the Integrated Territorial Initiative (ITI) for the province of Cadiz (grant number ITI-0038-2019). ITI is 80% co-financed by the funds of the FEDER Operational Program of Andalusia 2014-2020 (Council of Health and Families).

References

[1] Stuart H. Orkin and Leonard I. Zon. Hematopoiesis: an evolving paradigm for stem cell biology. *Cell*, 132(4):631–644, 2008.

[2] Ching-Hon Pui, Dario Campana, and William E. Evans. Childhood acute lymphoblastic leukaemia–current status and future perspectives. *The lancet oncology*, 2(10):597–607, 2001.

[3] Ching-Hon Pui, Leslie L. Robison, and A. Thomas Look. Acute lymphoblastic leukaemia. *The Lancet*, (9617), 2008.

[4] Anna Marciniak-Czochra, Thomas Stiehl, Anthony D. Ho, Willi Jäger, and Wolfgang Wagner. Modeling of asymmetric cell division in hematopoietic stem cells regulation of self-renewal is essential for efficient repopulation. *Stem cells and development*, 18(3):377–386, 2009.

[5] Salvador Chulián, Alvaro Martínez-Rubio, Anna Marciniak-Czochra, Thomas Stiehl, Cristina Blázquez Goñi, Juan Francisco Rodríguez Gutiérrez, Manuel Ramirez Orellana, Ana Castillo Robleda, Víctor M. Pérez-García, and María Rosa. Dynamical properties of feedback signalling in b lymphopoiesis: A mathematical modelling approach. *Journal of Theoretical Biology*, 522:110685, 2021.

[6] Dominique Bonnet and John E. Dick. Human acute myeloid leukemia is organized as a hierarchy that originates from a primitive hematopoietic cell. *Nature medicine*, 3(7):730–737, 1997.

[7] Tommaso Lorenzi, Anna Marciniak-Czochra, and Thomas Stiehl. A structured population model of clonal selection in acute leukemias with multiple maturation stages. *Journal of mathematical biology*, 79(5):1587–1621, 2019.

[8] Álvaro Martínez-Rubio, Salvador Chulián, Cristina Blázquez Goñi, Manuel Ramírez Orellana, Antonio Pérez Martínez, Alfonso Navarro-Zapata, Cristina Ferreras, Victor M Pérez-García, and María Rosa. A mathematical description of the bone marrow dynamics during CAR T-cell therapy in B-cell childhood acute lymphoblastic leukemia. *International Journal of Molecular Sciences*, 22(12):6371, 2021.

[9] HM Amin, Y Yang, Y Shen, EH Estey, FJ Giles, SA Pierce, HM Kantarjian, SM O'Brien, I Jilani, and M Albitar. Having a higher blast percentage in circulation than bone marrow: clinical implications in myelodysplastic syndrome and acute lymphoid and myeloid leukemias. *Leukemia*, 19(9):1567–1572, 2005.

International Conference on Mathematical Analysis and Applications in Science and Engineering
ICMA^{2}SC'22
ISEP Porto-Portugal, June 27 - 29, 2022

Stochastic cellular automaton for modeling benign and invasive tumor dynamics

Carlos A. Valentim[1] **José A. Rabi**[1] **Sergio A. David**[1]

[1]Department of Biosystems Engineering, University of Sao Paulo at Pirassununga, Brazil.

carlos.valentim@usp.br
jrabi@usp.br
sergiodavid@usp.br

Abstract: Mathematical Oncology applies either continuous or discrete models to mathematically describe cancer-related phenomena. Although such models are usually expressed in terms of differential equations, tumor composition involves specific cellular structure while demonstrating probabilistic nature, thus often requiring tailor-made approaches. In this context, cell-based models are organized frameworks that allow monitoring independent single parameters, which might vary in both time and space. By relying on extant tumor growth models in the literature, the present work introduces cellular-automata simulation strategy that admits heterogeneous cell population while capturing both single-cell and cluster-cell behaviors. In this entirely stochastic computational model, tumor cells are limited to follow four possible courses of action, namely: proliferation, migration, apoptosis or quiescence. Despite this apparent simplicity, the resulting tumor can exhibit different complex features depending on parameter settings, which range from alternate dormancy periods to invading protrusions. Exploring those characteristics in virtualized scenarios, this work also addresses high-performance computing techniques implemented in Python code in view of forthcoming developments and extensions to simulate mechanistic features as well. The resulting stochastic-deterministic model is expected to support research in mathematical oncology towards tumor dynamics, thus improving diagnosis tools and/or personalized treatment.

keywords: Mathematical oncology; cancer dynamics; in-silico modeling; computational modeling.

MSC2020: 34-04; 92B05; 68Q80

1 Introduction

Mathematical oncology explores the development and application of models to cancer-related phenomena [5]. As an important advantage, mathematical models can test and reproduce several scenarios, which could be either unfeasible or impossible through in vitro experiments. Among extant approaches, cell-based or discrete models are organized frameworks that keep track of fully independent individual parameters depending on time and/or space, as an attempt to mathematically model heterogeneity and complex phenomena found in cancer. Computationally, they can rely on different approaches including (but not restricted to) Monte-Carlo simulations, energy minimization techniques, volume conservation laws and motion rules [3]. Virtualization (i.e. numerical simulation) involving cell-based models is often referred to as in-silico modeling because of their similarity and logical extension of in-vitro experimentation [2]. Concerning

cellular-automata (CA) models, relatively simple implementations can go a long way in providing emergent complex behavior [1, 4].
The model herein proposed is a stochastic framework in which a single cell originates a tumor exhibiting different characteristics depending on model configurations and its parameters. Every cell will obligatorily present one of the following exclusive behaviors: apoptosis, proliferation, migration, or quiescence. These behaviors have a predefined probability (which may itself vary with time) and they are checked in the aforesaid order. Healthy cells are absent spaces.
The model also comprises a heterogeneous tumor population, in which each cell can either be a regular tumor cell (RTC) or a stem tumor cell (STC). While RTC nonclonogenic cells compose the bulk of a tumor and are limited, STCs lack internal regulatory mechanisms regarding cell death, thus being immortal. They can be categorized as clonogenic (can only give birth to regular, i.e. mortal cells) or true stem cells (may also generate an identical true stem cell). Differences regarding aforementioned cells are depicted in Figure 1, in which STCs are represented in yellow whereas RTCs are depicted in shades of red. Figure 2 illustrates the degradation of proliferation potential after each replication. This mechanism only applies to RTC since they die (i.e. are removed from the model) after a finite number of duplications.

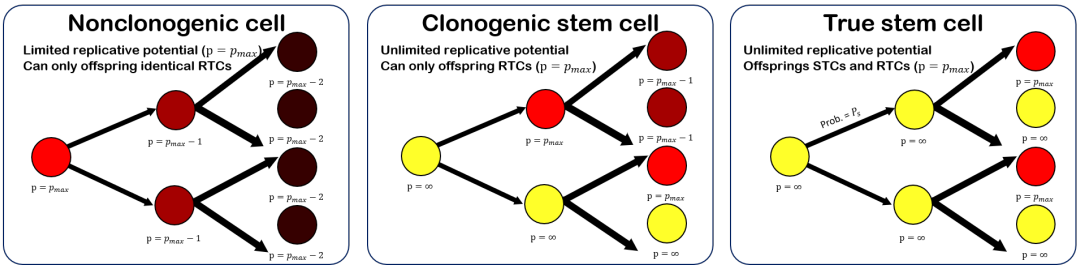

Figure 1: Populations considered in the model: Nonclonogenic, clonogenic and true stem cells.

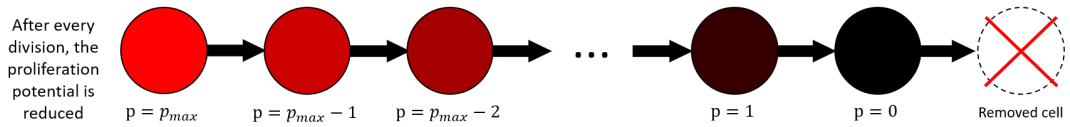

Figure 2: Proliferation potential in regular tumor cells.

2 Results and discussion

In this work, we implemented some high-performance techniques suggested by [4] as, for instance, coded-lattice and dynamically growing domains. The model was coded in Python due its versatility and accessible learning curve. By varying the progenitor cell type and each movement probability, the stochastic cellular automaton is able to simulate different scenarios such as tumor absence, benignity (stability), invasion (instability), and migrating tumors (clustering). Figure 3 depicts preliminary results related to the dynamics of two different tumors. The first, originated from a nonclonogenic cell, relates to some types of benign tumors, which can live in patients for up to decades and never reach a dangerous size or malignancy. The other originates from a true STC cell and is larger and unstable, such as an invasive tumor.

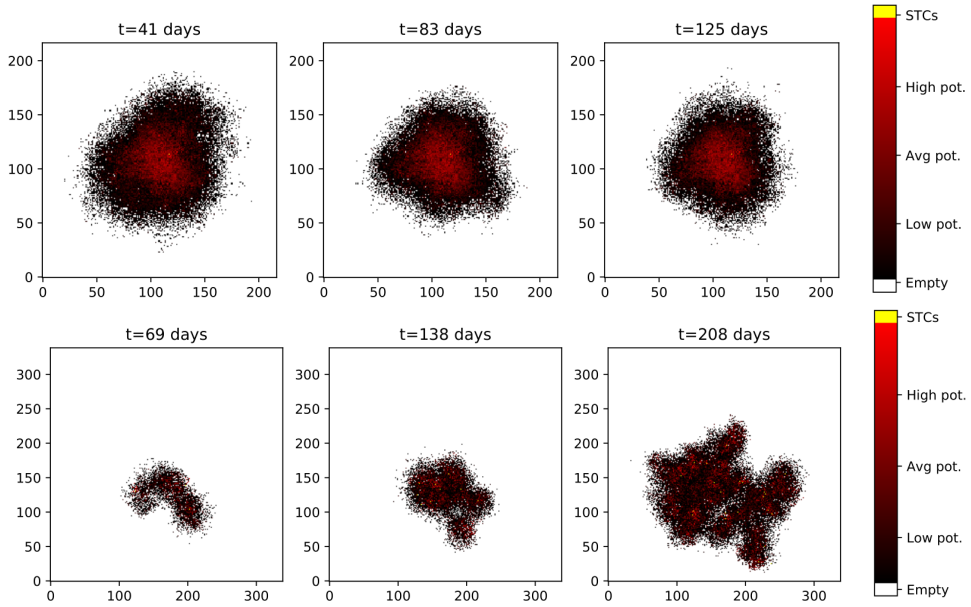

Figure 3: Virtualization of a benign tumor (above) and an invasive tumor (bellow)

3 Conclusions and Future work

In this paper, we have introduced and discussed the development of a stochastic cellular automaton for modeling tumor growth. The model created is capable to simulate different scenarios regarding tumor growth, figuring as an interesting tool for in silico modeling. We plan on expanding its features towards a hybrid model, incorporating deterministic and continuous characteristics. The idea is to increase the model's complexity as means to computationally simulate diverse tumor scenarios of clinical interest.

Acknowledgments

This study is financed in part by the Coordenação de Aperfeiçoamento de Pessoal de Nível Superior - Brasil (CAPES) - Finance code 001.

References

[1] Heiko Enderling, Alexander R.A. Anderson, Mark A.J. Chaplain, Afshin Beheshti, Lynn Hlatky, and Philip Hahnfeldt. Paradoxical dependencies of tumor dormancy and progression on basic cell kinetics. *Cancer Research*, 69(22):8814–8821, 2009.

[2] Fleur Jeanquartier, Claire Jean-Quartier, David Cemernek, and Andreas Holzinger. In silico modeling for tumor growth visualization. *BMC Systems Biology*, 10(1):1–15, 2016.

[3] John Metzcar, Yafei Wang, Randy Heiland, and Paul Macklin. A Review of Cell-Based Computational Modeling in Cancer Biology. *JCO Clinical Cancer Informatics*, (3):1–13, 2019.

[4] Jan Poleszczuk and Heiko Enderling. A High-Performance Cellular Automaton Model of Tumor Growth with Dynamically Growing Domains. *Applied Mathematics*, 05(01):144–152, 2014.

[5] Russell C. Rockne and Jacob G. Scott. Introduction to Mathematical Oncology. *JCO Clinical Cancer Informatics*, (3):1–4, nov 2019.

International Conference on Mathematical Analysis and Applications in Science and Engineering
ICMA^{2}SC'22
ISEP Porto-Portugal, June 27 - 29, 2022

A mathematical model of the population diffusion of Candida Auris within an Intensive Care Unit

Cristina Pérez-Diukina [1⋆] **Rafael-Jacinto Villanueva[1]**
Carlos Andreu-Vilarroig[1] **Juan-Carlos Cortés[1]**

[1] Universitat Politècncia de Valènica, Valencia, Spain

[1⋆]cperdiu@posgrado.upv.es

Abstract: The multi-drug resistant yeast Candida Auris (C.A.) poses a global threat to the healthcare environment. In this work, we have applied the Fisher Kolmogorov–Petrovsky–Piskunov (FKPP) equation to model the change in density trough time of C.A. inside an Intensive Care Unit (ICU). Such a model will allow us to evaluate the efficacy of well timed cleaning measures on C.A. population control.

keywords: Candida Auris; mathematical modelling; reaction-diffusion system .

1 Introduction

Candida Auris (C.A.) is a multi-drug resistant yeast that was discovered in 2009 [4]. This relatively new species of yeast is a public health concern in the healthcare settings and particularly in the Intensive Care Unit (UCI) environment across the globe [3].

As far as we know, the information available about C.A. is limited and heterogeneous. The mortality rates associated with C.A. vary greatly from study to study depending on the country and the environment in which infected subjects were located [2]. Furthermore, multi-drug resistance in C.A. and its ability to survive on plastic surface (for at least 2 weeks) are one of the most hard challenges for healthcare facilities. These microbiological characteristics are partly due to C.A.'s ability to form biofilms, making it resistant to multiple cleaning agents commonly used in healthcare settings [3],[6]. Because the ICU population is particularly vulnerable, these attributes pose a significant threat. After the colonization of an ICU patient with C.A., if no prevention measures were to be taken, it is estimated that the whole ICU would be colonized within 48h [1]. Therefore, ICU personnel have to undertake costly measures to control the spread of C.A. such as weekly testing of patients, isolation of detected colonized patients, and in depth cleaning.

To face this problem, mathematical models allow us to simulate the C.A. population spread in a environment such as ICU in a time and cost efficient manner. In this work, we propose to model the biological diffusion of C.A. within the ICU using with the Fisher Kolmogorov–Petrovsky–Piskunov (Fisher–KPP) model [5]. To calibrate the model's parameters, C.A. *in vitro* growth data and expert ICU medical personnel information has been used.

[1]information provided by chief ICU medical personnel

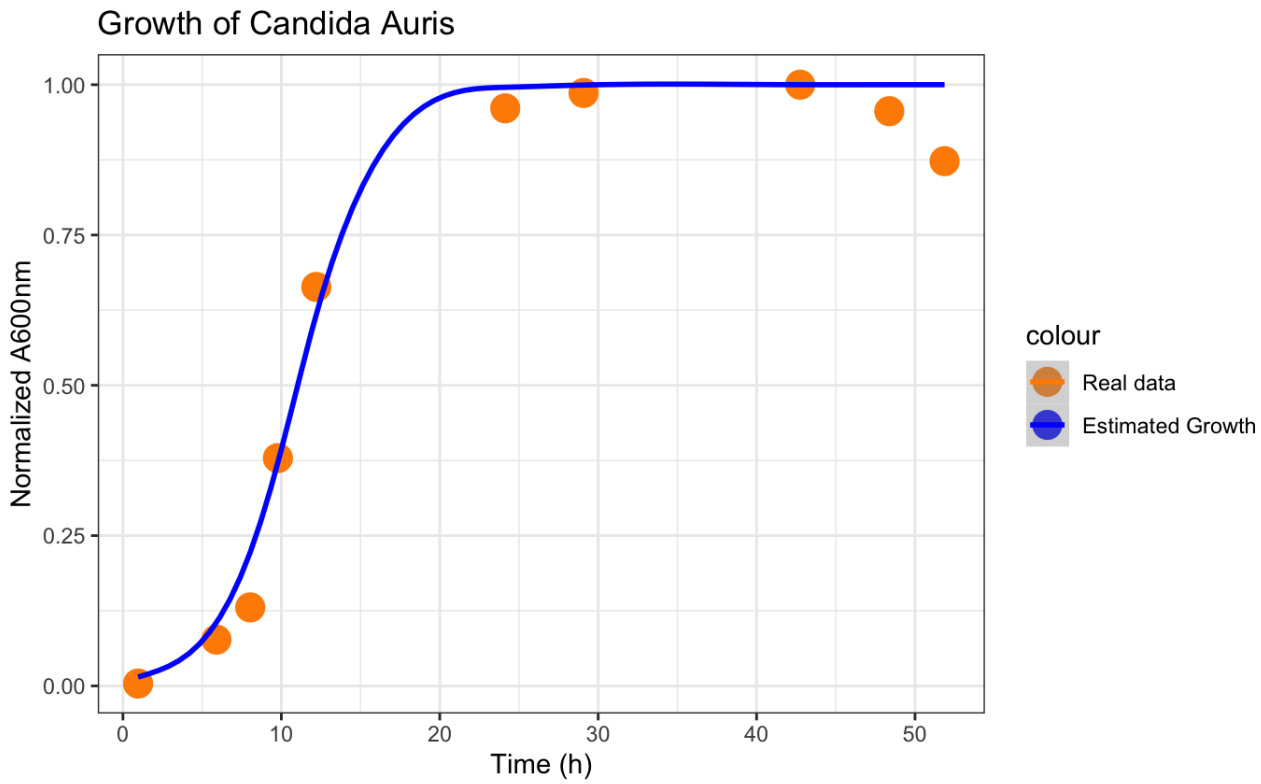

Figure 1: Observed *in vitro* growth of C.A. (in orange) and estimated logistic growth using nonlinear least squares.

2 Results and discussion

The 2-dimensional Fisher–KPP model is a reaction-diffusion system that is used to model population growth in a 2 coordinate space through time [5], given by the following equation:

$$\frac{\partial u}{\partial t} = D\left(\frac{\partial^2 u}{\partial x^2} + \frac{\partial^2 u}{\partial y^2}\right) + ru(1-u), \tag{1}$$

where x and y are the coordinates of a point on a plane, u is the density of the population at a given time t, $D > 0$ is the diffusion coefficient and $0 \leq r \leq 1$ is the growth rate. In this model the variation of the population density u through time is guided by both the diffusion term $D\left(\frac{\partial^2 u}{\partial x^2} + \frac{\partial^2 u}{\partial x^2}\right)$ which models microorganism's expansion in a plane, and the population growth term $ru(1-u)$, which indicates the amount of C.A. at a given time.

In order to estimate the growth rate r, a logistic growth model $du/dt = ru(1-u)$ has been fitted to C.A. *in vitro* growth data (under different conditions) [1] using nonlinear least squares (Figure 1). We have found the growth rate to be approximately $r = 0.416$, with a residual sum-of-squares of 0.03096. We then calibrated the diffusion coefficient D so that after 48h the density of u of C.A. is non 0 everywhere (except the 4 corners of the plane, that are the boundary conditions). This condition illustrates the situation where C.A. has colonized the entire environment. The best calibration result is $D = 0.005$.

With the best parameters found, we solved equation (1) numerically using explicit finite-differences and a smooth initial condition. In Figure 2 we can observe the diffusion of C.A. at different time instants.

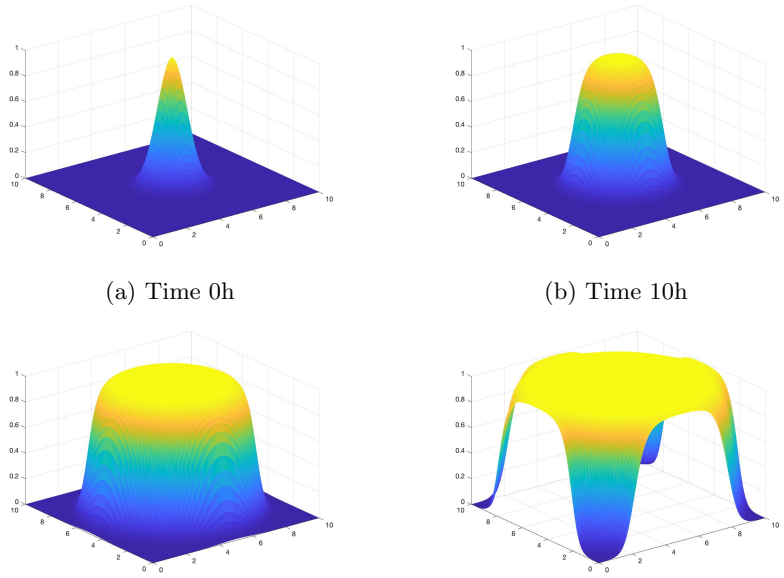

(a) Time 0h (b) Time 10h

(c) Time 30h (d) Time 48h

Figure 2: 3D plots of the Fisher-KPP numeric solutions when $D = 0.005$ and $r = 0.416$

3 Conclusions and Future work

C.A. is a global threat for healthcare facilities, and in particular the ICU environment. A great amount of economic and human labor is being put in ICU settings around the world to limit the colonization of patients by C.A. as much as possible. A mathematical model of the diffusion of C.A. density within a ICU using a Fisher–KPP model calibrated to real world data can, in the future, give us insight on the efficacy of well timed cleaning measures.

For future work, we will introduce a cleaning term in the model to simulate the effect of cleaning measures on C.A. population. We will also simulate multiple initial conditions to observe the different ways in which C.A. can spread in a ICU and how it may affect the efficacy of cleaning measures.

References

[1] Leiwen Fu, L Wang, H Guo, Z Liu, J Yang, Q Chen, J Hu, et al. Study on growth characteristics of candida auris under different conditions in vitro and its in vivo toxicity. *Zhejiang da xue xue bao. Yi xue ban= Journal of Zhejiang University. Medical Sciences*, 40(7):1049–1055, 2020.

[2] Shabir A Lone and Aijaz Ahmad. Candida auris—the growing menace to global health. *Mycoses*, 62(8):620–637, 2019.

[3] Johanna Rhodes and Matthew C Fisher. Global epidemiology of emerging candida auris. *Current opinion in microbiology*, 52:84–89, 2019.

[4] Kazuo Satoh, Koichi Makimura, Yayoi Hasumi, Yayoi Nishiyama, Katsuhisa Uchida, and Hideyo Yamaguchi. Candida auris sp. nov., a novel ascomycetous yeast isolated from the external ear canal of an inpatient in a japanese hospital. *Microbiology and immunology*, 53(1):41–44, 2009.

[5] Vladimir M Tikhomirov. *Selected Works of AN Kolmogorov: Volume I: Mathematics and Mechanics*, volume 25. Springer Science & Business Media, 1991.

[6] Rory M Welsh, Meghan L Bentz, Alicia Shams, Hollis Houston, Amanda Lyons, Laura J Rose, and Anastasia P Litvintseva. Survival, persistence, and isolation of the emerging multidrug-resistant pathogenic yeast candida auris on a plastic health care surface. *Journal of clinical microbiology*, 55(10):2996–3005, 2017.

International Conference on Mathematical Analysis and Applications in Science and Engineering
ICMA^{2}SC'22
ISEP Porto-Portugal, June 27 - 29, 2022

Modelling antibiotic resistance from an agent-based modelling approach: an application to colistin-resistant *A. baumannii*.

Carlos Andreu-Vilarroig[1⋆] Rafael-Jacinto Villanueva[1]
Juan-Carlos Cortés[1] Juan A. Aledo[2] Juan Carlos Orengo[3]

[1] Universitat Politècnica de València, Valencia, Spain
[2] University of Castilla la Mancha, Albacete, Spain
[3] Ponce Health Sciences University, Ponce, Puerto Rico, USA

[1⋆]caranvi1@upv.es

Abstract: Antimicrobial resistance (AMR) is one of the emerging global public health threat in the healthcare world. In this work, we propose an agent-based model to study the infection dynamics of the colistin-resistant *A. baumannii* bacterium in the population of the Valencia city and to predict its evolution in the coming years. In order to simulate a real scenario, demographic data from Valencia city have been used to create a realistic synthetic population. The individuals or agents in the synthetic population are characterized by a set of variables or states that evolve over time by changing randomly, according to a set of probabilistic rules. The unknown parameters of the model have been calibrated with Spanish clinical and epidemiological data by using the Particle Swarm Optimization (PSO) bio-inspired optimization algorithm. Finally, with the best parameter, a 20-year prediction has been simulated.

keywords: antimicrobial resistance (AMR); colistin; agent-based model; calibration; Particle Swarm Optimization; mathematical modelling.

MSC2020: 92D30; 68W50

1 Introduction

Antimicrobial resistance (AMR) is one of the emerging challenges in the healthcare world. AMR is defined as the ability of certain microorganisms to adapt to antibiotic treatments so that they no longer have an effect on them [11]. The World Health Organization (WHO), the United Nations and many scientific impact studies describe AMR as a global public health threat, as its development will mean that many infections will go untreatable. They also warn of the risk of continued uncontrolled use of antibiotics that create a favourable environment for the AMR spread [13, 5]. They also warn that to continue using antibiotics without control creates a favourable environment for the arise of AMR, and warn that, if no action is taken, it will generate a cost of 10 million human lives and an economic cost of 100 trillion dollars in 2050 [8].

Faced with this reality, mathematical modeling in epidemiology has proved to be a valuable resource for the prediction and control of disease dynamics in populations, public health decision making and their economic impact [9]. However, few mathematical models incorporate the AMR

factor, due to limitations such as the complexity of the phenomenon, the lack of real world clinical data, their incompleteness, or the great heterogeneity of the sources. For these reasons, AMR models are often focused on specific pathogens [7]. Among these, the *Acinetobacter baumannii* bacterium is characterized by its rapid adaptation to antibiotics and, therefore, is one of the most problematic nosocomial pathogens [10]. This fact has led to the use of certain old antibiotics, such as colistin, which were discarded years ago because of the serious side effects they caused in patients, but which are currently the only ones effective against *A. baumannii*, as a last resort [2].

2 Results and discussion

In this work, we propose an agent-based model to study the infection dynamics of the colistin-resistant *A. baumannii* in the population of the Valencia city and to predict its evolution in the coming years. Any agent-based model is composed of two elements: a synthetic population (a list of individuals with a series of states) and dynamics or behavioural rules of the individuals. In our case, the synthetic population has been generated by taking the population distribution by age groups of the inhabitants of the city of Valencia.

On the other hand, four additional states have been defined to govern the dynamics of individuals: *(i) environment* or individual location: hospital or outside hospital, i.e., community, *(ii) health status* with respect to *A. baumannii* disease: not infected or susceptible, infected by a sensitive strain, and infected by a resistant strain, *(iii) origin of infection*: no infection, community infection, or nosocomial infection and *(iv) hospital stay*, which depends on the individual age group (if individual is in the community, hospitalization time is 0). The dynamics for any individual in the population are as follows:

1. An individual located in community is admitted to hospital with an income probability and during a hospital stay depending on his/her age group.
2. Within the hospital, the cause of the admission is diagnosed. This may be due to a colistin-sensitive or colistin-resistant *A. baumannii* infection, or other causes.
3. If an individual is in hospital and does not have *A. baumannii* infection, he/she can become infected inside (nosocomial infection) during his stay.
4. Any individual located in the hospital leaves back to the community at the end of his/her hospital stay.

Some of the probabilities of these events have been found in the Spanish epidemiological data, but others, specifically four probabilities, have had to be calibrated. To do so, the PSO optimisation algorithm [6, 3, 4] has been applied, taking the set of unknown parameters as particles, and a set of four series of hospital infection prevalences as reference output. As all the states of the individuals at each instant in time were available, the prevalences of the model were calculated by counting cases of interest over the total number of cases. The algorithm has been run for 3000 iterations to ensure convergence, as observed. After calibration, a PSO-inspired selection algorithm [12, 1] has been applied to indicate the most representative solutions of the model (those that best estimate the confidence intervals of the reference prevalences). 50 best solutions have been selected and simulated for the time interval 2015 to 2035.

Results show that resistant cases, broken down by age group, are seen to increase in a sigmoid pattern, stabilising at around 10% from 2020 onwards (see Fig. 1). We also can observe that most of the sigmoidal growth of resistant cases is explained by the group over 60 years of age, while the number of cases in the group under 60 years of age is lower and the growth is smoother.

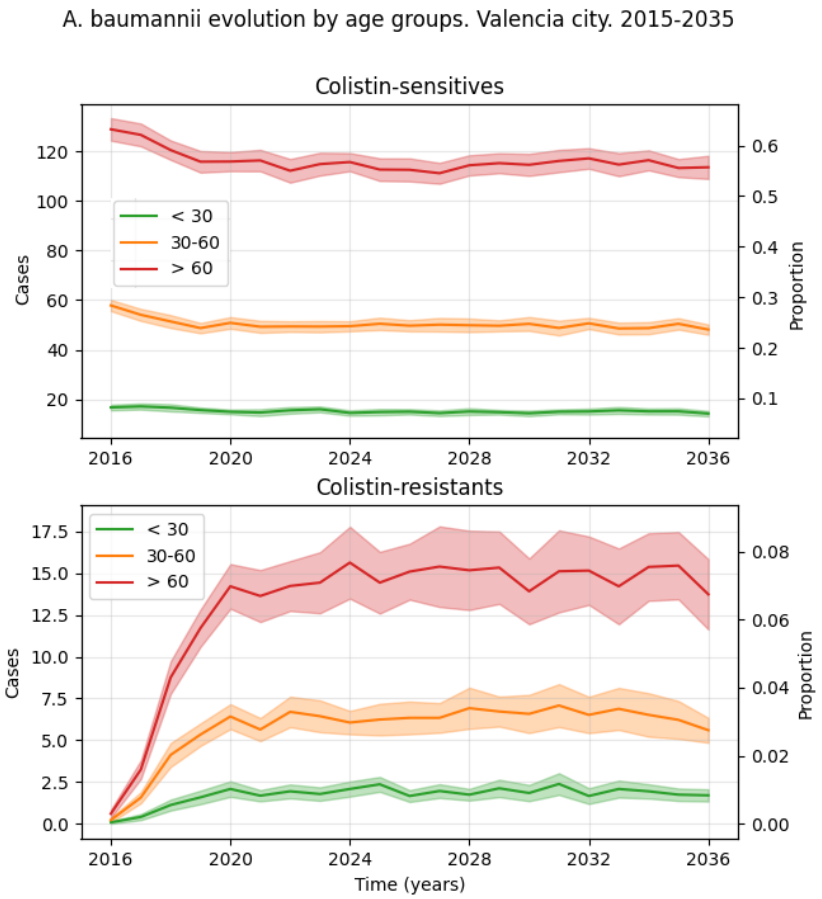

Figure 1: Mean (lines) and 95% *t*-student confidence intervals (bands) of cases of colistin-sensitive and colistin-resistant *A. baumannii* infections in the Valencia city in the period 2015-2035 by age groups.

3 Conclusions and Future work

The results of the 20-year forecasts show that colistin resistance will remain stable (under the same conditions as in recent years). The curves by age group indicate that the majority of cases are due to the over-60 age group, which is clearly related to the higher probability of these patients being admitted to the hospital (where most infections occur), and that their growth has been much faster than in other groups. Therefore, if a further increase in resistance is observed in the future, these groups should be prioritized for preventive actions. It is also important to consider other factors that can potentially influence it, such as antibiotic consumption. Although our predicted scenario is plausible, future research should focus on improving the model by incorporating new variables. Likewise, other limitations to be improved in future research on the model would be the incorporation of mortality in the population, and a more in-depth analysis of the dynamics of infection, in order to simulate modifications on these dynamics that imitate preventive actions. Hence, we should continue monitoring to ensure that the resistance does not increase, and the predictions performed should be revised.

Acknowledgments

This work has been partially supported by the grant PID2020-115270GB–I00 funded by MCIN/AEI/10.13039/501100011033 and the grant AICO/2021/302 (Generalitat Valenciana). Juan A. Aledo has been funded by the Government of Castilla-La Mancha and "ERDF A way of making Europe" through the project SBPLY/17/180501/000493. It is also part of the project PID2019–106758GB–C33 funded by MCIN/AEI.

References

[1] Clara Burgos, Juan Carlos Cortés, D Martínez-Rodríguez, and Rafael-Jacinto Villanueva. Computational modeling with uncertainty of frequent users of e-commerce in spain using an age-group dynamic nonlinear model with varying size population. *Advances in Complex Systems*, 22(04):1950009, 2019.

[2] Gabriela Jorge Da Silva and Sara Domingues. Interplay between colistin resistance, virulence and fitness in acinetobacter baumannii. *Antibiotics*, 6(4):28, 2017.

[3] James Kennedy and Russell Eberhart. Particle swarm optimization. In *Proceedings of ICNN'95-international conference on neural networks*, volume 4, pages 1942–1948. IEEE, 1995.

[4] Namrata Khemka and Christian Jacob. Exploratory toolkit for evolutionary and swarm-based optimization. *Mathematica Journal*, 11(3):376, 2008.

[5] Franklin D. Lowy. Antimicrobial resistance: the example of staphylococcus aureus. *Journal of Clinical Investigation*, 111(9):1265–1273, May 2003.

[6] Federico Marini and Beata Walczak. Particle swarm optimization (PSO). a tutorial. *Chemometrics and Intelligent Laboratory Systems*, 149:153–165, December 2015.

[7] Anna Maria Niewiadomska, Bamini Jayabalasingham, Jessica C Seidman, Lander Willem, Bryan Grenfell, David Spiro, and Cecile Viboud. Population-level mathematical modeling of antimicrobial resistance: a systematic review. *BMC medicine*, 17(1):1–20, 2019.

[8] J. O'Neill. Antimicrobial resistance: tackling a crisis for the health and wealth of nations. Technical report, Review on Antimicrobial Resistance, UK Governement, 07 2016. [Accessed: 31/10/2021].

[9] Lulla Opatowski, Didier Guillemot, Pierre-Yves Boëlle, and Laura Temime. Contribution of mathematical modeling to the fight against bacterial antibiotic resistance. *Current opinion in infectious diseases*, 24(3):279–287, 2011.

[10] Anahit Penesyan, Stephanie S Nagy, Staffan Kjelleberg, Michael R Gillings, and Ian T Paulsen. Rapid microevolution of biofilm cells in response to antibiotics. *NPJ biofilms and microbiomes*, 5(1):1–14, 2019.

[11] Fred C Tenover. Mechanisms of antimicrobial resistance in bacteria. *The American journal of medicine*, 119(6):S3–S10, 2006.

[12] Rafael-J Villanueva, J Ignacio Hidalgo, Carlos Cervigón, Javier Villanueva-Oller, and Juan-Carlos Cortés. Calibration of an agent-based simulation model to the data of women infected by human papillomavirus with uncertainty. *Applied Soft Computing*, 80:546–556, 2019.

[13] Richard Wise. Antimicrobial resistance: priorities for action. *Journal of Antimicrobial Chemotherapy*, 49(4):585–586, 04 2002.

International Conference on Mathematical Analysis and Applications in Science and Engineering
ICMA^{2}SC'22
ISEP Porto-Portugal, June 27 - 29, 2022

A numerical scheme for a model of drug delivery enhanced by light

J.A. Ferreira[1] **H.P Gomez**[1] **L. Pinto**[1]

[1] University of Coimbra, Portugal

[1]ferreira@mat.uc.pt, [1]hugopena@mat.uc.pt, [1]luisp@mat.uc.pt

Abstract: In this paper, we consider a numerical scheme for a nonlinear system of partial differential equations arising from the mathematical modeling of drug delivery enhanced by light. The system consists of diffusion-reaction equations for drug concentration and a diffusion equation for light propagation. Suitable initial conditions and Neumann-Dirichlet boundary conditions close the system. We numerically show that the scheme is second-order supraconvergent in space in a discrete H^1-norm and first-order convergent in time in a discrete L^2-norm.

keywords: Finite difference method; supraconvergence; drug delivery; numerical simulation.

MSC2020: 49-XX; 34-XX; 92-XX.

1 Introduction

In this paper we study a numerical scheme for the system of partial differential equations (1)-(3) where $D_I, D_d : \mathbb{R} \to \mathbb{R}$ are appropriate functions and $x \in \Omega$, $t \in (0, T]$. Let Ω be the set $\Omega = (0, 1)^2$. We denote the boundary of Ω by the union of its edges: $\partial\Omega = \bigcup \Gamma_i, i = l, u, r, d$ (edges left, up, right and down). To complete our problem, we impose the initial and boundary conditions (4)-(6).

$$\begin{cases} \frac{1}{\beta}\frac{\partial I}{\partial t} = \nabla \cdot (D_I \nabla I) - \mu_a I, & (1) \\ \frac{\partial c_f}{\partial t} = \nabla \cdot (D_d \nabla c_f) + \gamma c_b I, & (2) \\ \frac{\partial c_b}{\partial t} = -\gamma c_b I, & (3) \end{cases}$$

$$\begin{aligned} I(x,0) &= 0, \quad c_f(x,0) = 0, \\ c_b(x,0) &= c_{b,0}(x), \quad x \in \Omega, \end{aligned} \tag{4}$$

$$\begin{aligned} I(x,t) &= I_0(t), x \in \Gamma_l, t \in (0,T], \\ \nabla I(x,t) \cdot \eta &= 0, x \in \partial\Omega - \Gamma_l, t \in (0,T], \end{aligned} \tag{5}$$

$$\begin{aligned} \nabla c_f(x,t) \cdot \eta &= 0, x \in \partial\Omega - \Gamma_r, t \in (0,T], \\ c_f(x,t) &= 0, x \in \Gamma_r, \ t \in (0,T]. \end{aligned} \tag{6}$$

Drug delivery systems (DDS) have great potential for cancer treatment, in particular, those DDS that use near-infrared (NIR) light as an external stimuli to induce the drug release, since they allow not only spatio-temporal control of the drug but better penetretion in tissue [1]. We propose the model (1)-(6) to approximate the drug delivery dynamics from a polymeric matrix when light is used as enhancer. In equation (1), I is the light intensity. It is well known that light propagation through a scattering and absorbing medium can be described by the radiative

transfer equation (RTE) [3]. Depending on the magnitude of the absorption and scattering coefficients, μ_a and μ_s, respectively, different approaches can be considered to approximate the RTE. Following [2], we use the diffusion equation for light intensity (1), where D_I is the traditional light diffusion coefficient $D_I = 1/(3(\mu_a + \mu_s))$, $\mu_a I$ symbolize the absorption of light and β is the speed of light in the medium.
It is assumed that drug molecules are initially linked to the polymeric chains and the links are broken due to energy absorption, that is, the cleavage of the links occur by light irradiation. Equation (2) approximates the dynamics of the free drug c_f and the function $\gamma c_b I$ represents conversion of bound drug c_b into free drug that is allowed to be transported through the polymeric structure by diffusion. In (5) and (6), η denotes the unitary exterior normal.

Suppose that the diffusion coefficients in (1) and (2) are diagonal matrices with components bounded from below by a positive constant and are Lipschitz functions with Lipschitz constant L. Let Λ be a sequence of vectors $H = (h, k)$ with $h = (h_1, \ldots, h_{N_1})$, $k = (k_1, \ldots, k_{N_2})$ with positive entries, such that $\sum_{i=1}^{N_1} h_i = \sum_{i=1}^{N_2} k_i = 1$, with $H_{max} = \max\{h_{max}, k_{max}\} \to 0$, where $h_{max} = \max_{i=1,\ldots,N_1} h_i$ and $k_{max} = \max_{i=1,\ldots,N_2} k_i$.

Let $\overline{\Omega}_H$ be a non-uniform partition of $\overline{\Omega}$ defined by $\overline{\Omega}_H = \{(x_i, y_j), i = 0, \ldots, N_1, j = 0, \ldots, N_2\}$, where $x_i = x_{i-1} + h_i, i = 1, \ldots, N_1, y_j = y_{j-1} + k_j, j = 1, \cdots, N_2$, and and let $\Omega_H = \overline{\Omega}_H \cap \Omega$, $\partial\Omega_H = \overline{\Omega}_H \cap \partial\Omega$, and $\Gamma_{i,H} = \Omega_i \cap \partial\Omega_H, i = l, u, r, d$.

By D_{-x} we denote the usual backward finite difference (FD) operator and we introduce $D_x^* u_H(x_i, y_j) = \frac{u_H(x_{i+1}, y_j) - u_H(x_i, y_j)}{h_{i+\frac{1}{2}}}$, where $h_{i+\frac{1}{2}} = \frac{1}{2}(h_{i+1} + h_i)$, and $\nabla_H u_H = (D_{-x} u_H, D_{-y} u_H)$, $\nabla_H^* u_H = (D_x^* u_H, D_y^* u_H)$, where D_{-y} and D_y^* are the FD operators defined analogously.

Let $W(\overline{\Omega}_H)$ the space of grid functions defined in $\overline{\Omega}_H$ were we consider the inner product $(u_H, v_H)_H = \sum_{(x_i,y_j)\in\overline{\Omega}_H} |\square_{ij}| u_H(x_i, y_j) v_H(x_i, y_j)$, where $\square_{ij} = [x_{i-\frac{1}{2}}, x_{i+\frac{1}{2}}] \times [y_{j-\frac{1}{2}}, y_{j+\frac{1}{2}}] \cap \overline{\Omega}$, and $u_H, v_H \in W(\overline{\Omega}_H)$. The norm induced by this inner product is denoted by $\|\cdot\|_H$.

We also use the notations $(u_H, v_H)_{x,+} = \sum_{(x_i,y_j)\in\overline{\Omega}_H - \Gamma_{l,H}} |\square_{x,ij}| u_H(x_i, y_j) v_H(x_i, y_j)$, $\|u_H\|_{x,+} = \sqrt{(u_H, u_H)_{x,+}}$, where $\square_{x,ij} = [x_{i-1}, x_i] \times [y_{j-\frac{1}{2}}, y_{j+\frac{1}{2}}] \cap \overline{\Omega}$, and $u_H, v_H \in W(\overline{\Omega}_H - \Gamma_{l,H})$. Analogously, we define the notations $(u_H, v_H)_{y,+}$ and $\|u_H\|_{y,+}$ for $u_H, v_H \in W(\overline{\Omega}_H - \Gamma_{d,H})$.

For $u_H = (u_{H,1}, u_{H,2}), v_H = (v_{H,1}, v_{H,2})$, where $u_{H,1}, v_{H,1} \in W(\overline{\Omega}_H - \Gamma_{l,H})$, $u_{H,2}, v_{H,2} \in W(\overline{\Omega}_H - \Gamma_{d,H})$, we take $(u_H, v_H)_{H,+} = (u_{H,1}, v_{H,1})_{x,+} + (u_{H,2}, v_{H,2})_{y,+}$ and $\|u_H\|_+ = \sqrt{(u_H, u_H)_{H,+}}$.
The diffusion coefficients D_I and D_d are diagonal matrices with entries $D_{I,ii}, D_{d,ii}$, for $i = 1, 2$. To approximate the nonlinear diffusion coefficient we use the average operators $M_h u_H(x_i, y_j) = \frac{1}{2}\big(u_H(x_i, y_j) + u_H(x_{i-1}, y_j)\big)$, being M_k defined analogously. By $D_d(M_H u_H)$ we denote the diagonal matrix with diagonal entries $D_{d,11}(M_h u_H)$ and $D_{d,22}(M_k u_H)$.

To discretize the light intensity equation (1) and the boundary conditions (5) we need to consider the auxiliary point $x_{N_1+1} = x_{N_1} + h_{N_1}$, $y_{N_2+1} = y_{N_2} + k_{N_2}$ and $y_{-1} = -y_1$ and the fictitious points $\Gamma_{i,H}^{(I)}$, for $i = d, u, r$, see (7). Similarly, to discretize the free drug concentration equation (2) and the boundary condition (6) we need to introduce the auxiliary point $x_{-1} = -x_1$ and the fictitious points $\Gamma_{i,H}^{(c)}$, for $i = l, d, u$.

$$\begin{array}{ll} \Gamma_{d,H}^{(I)} = \{(x_i, y_{-1}), i = 1, \ldots, N_1\}, & \Gamma_{l,H}^{(c)} = \{(x_{-1}, y_j), j = 0, \ldots, N_2\}, \\ \Gamma_{u,H}^{(I)} = \{(x_i, y_{N_2+1}), i = 1, \ldots, N_1\}, & \Gamma_{d,H}^{(c)} = \{(x_i, y_{-1}), i = 0, \ldots, N_1 - 1\}, \\ \Gamma_{r,H}^{(I)} = \{(x_{N_1+1}, y_j), j = 0, \ldots, N_2\}, & \Gamma_{u,H}^{(c)} = \{(x_i, y_{N_2+1}), i = 0, \ldots, N_1 - 1\}. \end{array} \tag{7}$$

Let $W_{I,H}^*$ and $W_{c,H}^*$ be the space of grid functions defined in $\overline{\Omega}_H \cup (\cup_{i=d,r,u} \Gamma_{i,H}^{(I)})$ and $\overline{\Omega}_H \cup (\cup_{i=l,d,u} \Gamma_{i,H}^{(c)})$, respectively. Moreover, let $W_b(\overline{\Omega} - \Gamma_{r,H})$ be the space of grid functions defined in $\overline{\Omega} - \Gamma_{r,H}$.

2 Results and discussion

In the time domain $[0,T]$ we define the uniform grid $\{t_m, m = 0,\cdots,M\}$, with $t_0 = 0$, $t_M = T$ and $t_{m+1} = t_m + \Delta t$, for $m = 0,\cdots,M-1$. Moreover, define $D^{(I)}_{\eta_x} u_H(x_i,y_j) = \frac{1}{2}\big(D_{I,11}(M_h u_H(x_{i+1},y_j))D_{\text{-}x}u_H(x_{i+1},y_j) + D_{I,11}(M_h u_H(x_i,y_j))D_{\text{-}x}u_H(x_i,y_j)\big)$, for $(x_i,y_j) \in \Gamma_{r,H}$ and $D^{(I)}_{\eta_x} u_H(x_i,y_j) = 0$, for $(x_i,y_j) \in \partial\Omega_H - \Gamma_{r,H}$. Similarly, $D^{(I)}_{\eta_y} u_H(x_i,y_j)$ is defined as $D^{(I)}_{\eta_x}$ with the convenient adaptations. The boundary operators $D^{(c)}_{\eta_x}$ and $D^{(c)}_{\eta_y}$ are defined analogously. Let $\nabla^{(j)}_{H,\eta}$ be defined by $\nabla^{(j)}_{H,\eta} = (D^{(j)}_{\eta_x}, D^{(j)}_{\eta_y})$, for $j = I, c$.

We consider that the fully-discrete approximation $I^m_H \in W^*_{I,H}$, $c^m_{f,H} \in W^*_{c,H}$, $c^m_{b,H} \in W_b(\overline{\Omega}_H - \Gamma_{r,H})$ are solution of the system

$$\begin{cases} D_{\text{-}t} I^m_H = \nabla^*_H \cdot ((D_I(M_H I^m_H)\nabla_H I^{m+1}_H)) + G(I^m_H) & \text{in } \overline{\Omega}_H - \Gamma_{l,H} \quad (8)\\ D_{\text{-}t} c^m_{f,H} = \nabla^*_H \cdot ((D_d(M_H c^m_{f,H})\nabla_H c^{m+1}_{f,h})) + F(I^m_H, c^m_{f,H}, c^m_{b,H}) & \text{in } \overline{\Omega}_H - \Gamma_{r,H} \quad (9)\\ D_{\text{-}t} c^m_{b,H} = S(I^m_H, c^m_{f,H}, c^m_{b,H}) & \text{in } \overline{\Omega}_H - \Gamma_{r,H} \quad (10) \end{cases}$$

$$\text{with} \quad \begin{array}{ll} I^m_H & = R_H I_i(t_m) \text{ on } \partial\Omega_{l,H},\ \nabla^{(I)}_H I^m_H \cdot \eta = 0 \text{ on } (\partial\Omega_H - \Gamma_{l,H}) \times (0,T],\\ c^m_{f,H} & = 0 \text{ on } \Gamma_{r,H} \times (0,T],\ \nabla^{(c)}_H c^m_{f,H} \cdot \eta = 0 \text{ on } (\partial\Omega_H - \Gamma_{r,H}) \times (0,T]. \end{array} \quad (11)$$

Notice that system (8)-(11) is an IMEX (implicit-explicit) scheme. In example 1, we illustrate numerically the convergence rates in time and space for $c_{f,H}$ and $c_{b,H}$. We remark that I_H behaves in the same manner. The numerical solution of c_f for different values of $I_0(t)$ in the system (1)-(6) as well as the release rate of c_f are illustrated in example 2.

Example 1 *Let $\overline{\Omega} = [0,1]\times[0,1]$ and $T = 1$. In system (1)-(3) we consider the scalar diffusion coefficients $D_I(c_f) = 0.5\beta$ and $D_d(c_f) = 1 + c_f^2$. We set the parameters β, γ and μ_a equal to 1.*

The functions g_I, g_f and g_b were added to the right hand side of equations (1), (2) and (3), respectively, such that, the exact solution of the problem is $I(x,y,t) = \exp(t)\sin(xy)(x-1)(y-1)$, $c_f(x,y,t) = \exp(t)(x^2-x)(y^2-y)$ and $c_b(x,y,t) = \exp(t)x\cos(xy)$. The numerical approximations are computed using the IMEX scheme (8)-(10). For the approximations $c_{f,H}$ and $c_{b,H}$, the numerical error on a random mesh $\overline{\Omega}_H$ are defined, respectively by $Error^2_{f,H} = \max_{m=1,\ldots,M}\|E^m_{f,H}\|^2_h + \Delta t\sum_{k=1}^m \|D_{\text{-}x}E^k_{f,H}\|^2_+$ and $Error^2_{b,H} = \max_{m=1,\ldots,M}\|E^m_{b,H}\|^2_h$. The numerical convergence rate for $c_{f,H}$ is given by $Rate_{f,H} = \log_2(Error_{f,H}) - log_2(Error_{f,\frac{H}{2}})$, where $\frac{H}{2}$ denotes the mesh stepsizes obtained by halving the step sizes of the mesh H. The time step is chosen small enough (of the order of H^2_{max}) so that the spatial error dominates the time error. We take $N = N_1 = N_2$. The results are presented in table 1.

To get the numerical rate of convergence in time we fix $N_1 = N_2 = 500$ and successively halve the time step. We measure the numerical error by $Error^2_{\Delta t,j} = \max\limits_{m=1,\ldots,M}\|E^m_{j,H}\|^2_H$, for $j = f, b$. The rate of convergence is computed similarly as before.

M	N	H_{max}	$\text{Error}_{f,H}$	$\text{Rate}_{f,H}$	$\text{Error}_{b,H}$	$\text{Rate}_{b,H}$
82	12	1.1039E-1	7.2627E-5	-	1.2644E-5	-
328	24	5.5195E-2	2.7008E-6	2.3745	5.6640E-7	2.2402
1312	48	2.7598E-2	1.6714E-7	2.0071	3.8612E-8	1.9374
5251	96	1.3799E-2	1.0367E-8	2.0055	2.5305E-9	1.9658
21007	192	6.8994E-3	6.4455E-10	2.0038	1.6203E-10	1.9826
84030	384	3.4497E-3	4.0165E-11	2.0021	1.0251E-11	1.9912

M	$\text{Error}_{\Delta t,f}$	$\text{Rate}_{\Delta t,f}$	$\text{Error}_{\Delta t,b}$	$\text{Rate}_{\Delta t,b}$
4	1.3384E-2	-	6.8469E-3	-
8	3.8365E-3	0.9013	1.4678E-3	1.1109
16	1.0211E-3	0.9548	3.3167E-4	1.0729
32	2.6236E-4	0.9802	7.7990E-5	1.0442
64	6.6167E-5	0.9936	1.8721E-5	1.0293

Table 1: Space errors and convergence rates (on the left). Time errors and convergence rates (on the right).

Example 2 *This example intent to illustrate the behavior of the drug delivery system in the domain* $\Omega \times [0,T]$. *The initial conditions are* $c_b(x,0) = 1$ *for* $0 \leq x \leq 0.25$, $c_b(x,0) = 0$ *for* $x > 0.25$ *and* $c_f(x,0) = 0$, $I(x,0) = 0$ *for* $x \in \Omega$. *In figure 1, the values of* c_f *are plotted for different values of* $I(x,t) = I_0(t)$, $x \in \Gamma_l$, $t \in [0,T]$, *with* $T = 60s$. *In Figure 2 shows the* c_f *release rate for a bigger time domain with* $T = 3600s$. *For both figures the parameters values are* $\beta = 2.0689 \times 10^{10} cm/s$, $\mu_a = 4cm^{-1}$, $\mu_s = 13cm^{-1}$, $D_d = 4 \times 10^{-4} cm^2/s$. *From the results in Figure 1, an increase on the incidence light intensity leads to an increase on free drug.*

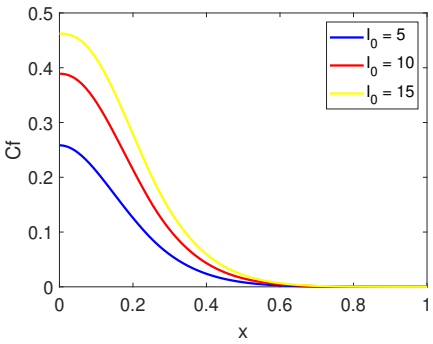

Figure 1: Free drug c_f for diferent I_0 values

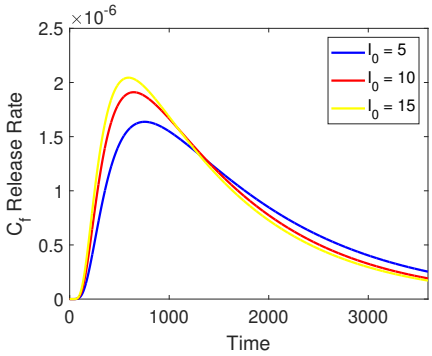

Figure 2: c_f release rate for $T = 3600s$.

3 Conclusions and Future work

We consider an IMEX time scheme combined with a finite difference discretization defined on nonuniform meshes. This method is considered to study a non-linear system modeling light-enhanced drug delivery. From the results presented here, we state that the method is first-order convergent in time with respect to a discrete L^2-norm and exhibits supraconvergence in space. By supraconvergence, we mean that the error is second-order convergent in a discrete H^1-norm despite the truncation error being first order in the L^∞-norm. In the near future we intent to show theoretically the results numerically observed.

Acknowledgments

This work was partially supported by the Centre for Mathematics of the University of Coimbra - UIDB/00324/2020, funded by the Portuguese Government through FCT/MCTES. H.P. Gómez was also supported by the FCT PhD grant PD/BD/150551/2019, funded by the Portuguese Government through FCT/MCTES.

References

[1] Xiaoying Wang, Zeliang Xuan, Xiaofeng Zhu et al. Near-infrared photoresponsive drug delivery nanosystems for cancer photo-chemotherapy. JNanobiotechnol 18, 108 (2020). https://doi.org/10.1186/s12951-020-00668-5

[2] L. Wang, H. Wu. Biomedical optics - principles and imaging, John Wiley and Songs,2007.

[3] A. Ishimaru. Wave Propagation ans Scattering in Random Media, Academic Press, 1978.

International Conference on Mathematical Analysis and Applications in Science and Engineering
ICMA^{2}SC'22
ISEP Porto-Portugal, June 27 - 29, 2022

Stability and bifurcations in an infinite network of theta neurons

L. Birdac[1*] **E. Kaslik**[1,2] **R.Muresan**[1*]

[1] Department of Mathematics and Computer Science, West University of Timişoara, Romania
[2] Institute for Advanced Environmental Research, West University of Timişoara, Romania

lavinia.birdac91@e-uvt.ro

Abstract: We consider an infinite network of identical theta neurons, all-to-all coupled by instantaneous synapses, modelled by a system of differential equations, which can be reduced to a low dimensional model, based on the Watanabe-Strogatz transformation. We determine the number of equilibria of this system with respect to two characteristic parameters and we discuss the possible bifurcations that can occur. A careful investigation also reveals the appearance of an exotic higher codimension bifurcation which involves a degenerate center.

keywords: Differential equations; stability; theta neuron; system; bifurcation.

MSC2020: 70K50;74H60.

1 Introduction

Let us consider a discrete model of a network of N identical theta neurons, all-to-all coupled via a synaptic current I, which acts by injecting current into neurons. We define the state of neuron j at time t as $\theta_j(t) \in [0, 2\pi]$. The dynamics of the network is given by:

$$\frac{d\theta_j}{dt} = 1 - \cos\theta_j + (1 + \cos\theta_j)(\eta + \kappa I), \quad j = \overline{1, N} \tag{1}$$

The input current to neuron j of the network is

$$I = \frac{1}{N}\sum_{k=1}^{N} P_n(\theta_k) \tag{2}$$

where $P_n(\theta) = a_n(1 - \cos\theta)^n$, $n \in \mathbb{N}$, and a_n is a normalization constant such that

$$\int_0^{2\pi} P_n(\theta)\, d\theta = 2\pi. \tag{3}$$

We assume that κ is the overall coupling strength for the whole network and η is the input current to all neurons when uncoupled. If $\eta < 0$ the neuron is excitable, if $\eta > 0$ the neuron fires periodically. Thus $\eta = 0$ is the threshold for firing. P_n has a maximum at $\theta = \pi$ and becomes more and more sharp as n increases [2, 4].

2 Main results and discussion

Defining $\omega = \eta + \kappa I + 1$ and $H = i(\eta + \kappa I - 1)$, system (1) can be written as

$$\frac{d\theta_j}{dt} = \omega + Im[He^{-i\theta_j}] \tag{4}$$

where ω is real and H is imaginary.

In this paper, the idea from Laing [1] is extended, where an infinite network of identical all-to-all coupled theta neurons is studied. We use the Watanabe-Strogatz ansatz transformation, [5, 6], to reduce the infinite network description to a system of three ODEs and a set of constants. The solution of the system (1)-(2) is constrained to lie on a three dimensional manifold with coordinates (ρ, Φ, Ψ), where:

$$\frac{d\rho}{dt} = \frac{1-\rho^2}{2} Re[He^{-i\Phi}] \tag{5}$$

$$\frac{d\Phi}{dt} = \omega + \frac{1+\rho^2}{2\rho} Im[He^{-i\Phi}] \tag{6}$$

$$\frac{d\Psi}{dt} = \frac{1-\rho^2}{2\rho} Im[He^{-i\Phi}] \tag{7}$$

Furthermore, in the case of an infinite number of identical neurons, we can reduce the dynamics of system (5)-(7) to a single complex equation considering $z = \rho e^{i\Phi}$ [3]:

$$\frac{dz}{dt} = i(\eta + kI)\frac{(1+z)^2}{2} - i\frac{(1-z)^2}{2} = i\omega z + \frac{H}{2} - \frac{\overline{H} z^2}{2} \tag{8}$$

where ω and H are as defined as above and from [1]

$$I = \frac{3}{2} - (z + \overline{z}) + \frac{(z^2 + \overline{z}^2)}{4} \tag{9}$$

We determine the number of equilibria of the reduced dynamical system with respect to the two characteristic parameters κ and η, and we study the local stability properties of each equilibrium, as well as possible bifurcations that may occur due to changes of the system's parameters. As a result, the occurrence of an exotic higher codimension bifurcation involving a degenerate center is also unveiled. To the best of our knowledge, this type of bifurcation has not been previousl analyzed in detail in the literature. Numerical results are also presented to illustrate complex dynamic behavior in this neural system. We illustrate the various dynamic behaviors that appear in this system, by considering several representative (κ, η) parameter combinations.

References

[1] Carlo R Laing. The dynamics of networks of identical theta neurons. *The Journal of Mathematical Neuroscience*, 8(1):1–24, 2018.

[2] Tanushree B Luke, Ernest Barreto, and Paul So. Complete classification of the macroscopic behavior of a heterogeneous network of theta neurons. *Neural computation*, 25(12):3207–3234, 2013.

[3] Edward Ott and Thomas M Antonsen. Low dimensional behavior of large systems of globally coupled oscillators. *Chaos: An Interdisciplinary Journal of Nonlinear Science*, 18(3):037113, 2008.

[4] Paul So, Tanushree B Luke, and Ernest Barreto. Networks of theta neurons with time-varying excitability: Macroscopic chaos, multistability, and final-state uncertainty. *Physica D: Nonlinear Phenomena*, 267:16–26, 2014.

[5] S. Watanabe and S. Strogatz. Constants of motion for superconducting josephson arrays. *Physica D*, 74:197–253, 1991.

[6] Shinya Watanabe and Steven H Strogatz. Integrability of a globally coupled oscillator array. *Physical review letters*, 70(16):2391, 1993.

International Conference on Mathematical Analysis and Applications in Science and Engineering ICMA²SC'22
ISEP **Porto-Portugal, June 27 - 29, 2022**

MULTI-PARAMETRIC CONTROLLING CANCER CELL INVASION IN BIOLOGICAL SYSTEMS WITH MEMORY OF STATES

Larysa Dzyubak[1,3*] Oleksandr Dzyubak[2*] Jan Awrejcewicz[1*]
[1]Department of Automation, Biomechanics and Mechatronics,
The Łódź University of Technology, Poland
[2]Ascension All Saints Cancer Center, USA
[3]Department of Applied Mathematics,
National Technical University "Kharkiv Polytechnic Institute", Ukraine
[1,3*]lpdzyubak@gmail.com [2*]Dzyubak.Oleksandr@gmail.com [1*]jan.awrejcewicz@p.lodz.pl

Abstract: A model for non-linear multi-scale diffusion cancer invasion was generalized for the case of biological systems with response delay. Modelling was based on the Masing–Bouc-Wen's framework with extra state variables (internal variables) added to simulate the memory of states. Chaotic attractors were quantified based on the wandering trajectories analysis. Comparison of the conditions leading to cancer invasion for the generalized model with and without memory is presented.

Keywords: biological system with memory of states; tumor growth; carcinogenesis; chaotic attractors; response delay

MSC2020: 34C28; 34H10; 34C55; 34A34; 34A36; 92-10.

1 Introduction

This work is the continuation of the earlier studies [1–2] in which the conditions controlling cancer invasion in a biological system were defined depending on parameters of the multi-parametric space as well as it was ascertained a significant influence of the biological system initial state to carcinogenesis. Due to presence of memory of states in these systems, the real biological systems exhibit their response to external perturbations with a certain delay. The biological system remembers in what initial state it was before the changes in functioning conditions and its transition to a new state depends on the pre-history of its behavior resulting in hysteresis (delayed response). The purpose of this study is to model the memory of states in the biological system and to evaluate how hysteretic properties define conditions leading to cancer invasion.

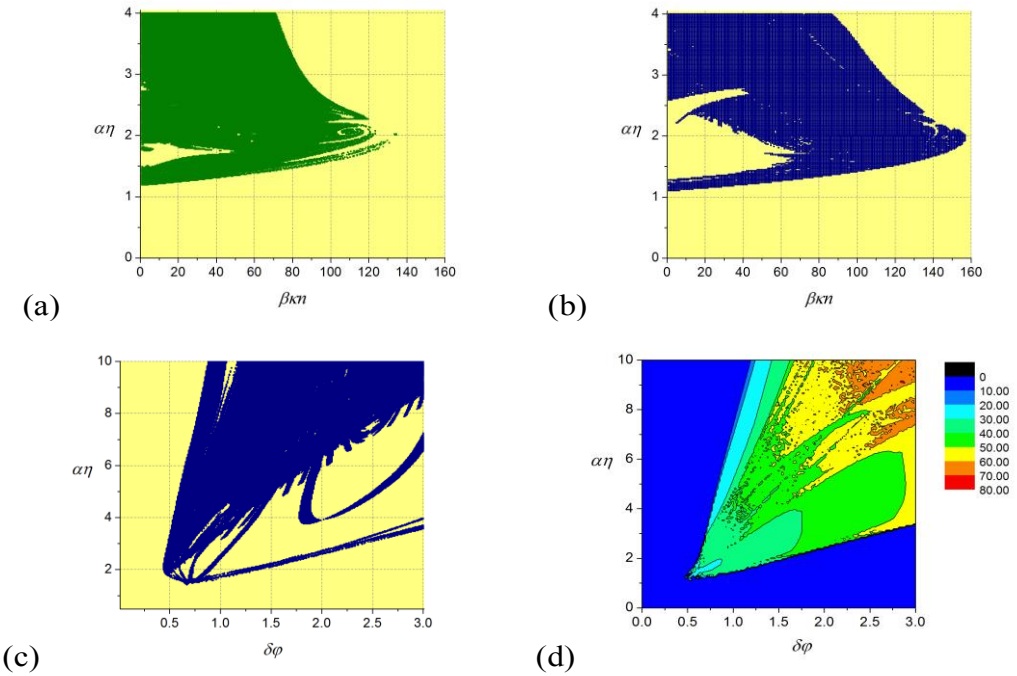

Fig. 1. Conditions leading to cancer invasion in the biological system with the memory of states (1)-(7): (a),(b) in control parameter plane ($\beta\kappa n$, $\alpha\eta$) – 'tumor cell volume vs glucose level' with values of the memorization parameters (a) h_f=0, h_m=0, h_c =0 – case of 'no memory'; and (b) h_f=0.9, h_m=0.9, h_c=0.9 – case 'with memory'; (c) in control parameter plane ($\delta\varphi$, $\alpha\eta$) – 'tumor cell volume vs diffusion saturation level' with corresponding (d) amplitude level contours of MM concentration.

2 Mathematical Model and Simulation Results

The generalized non-linear multi-scale diffusion cancer invasion model with additional state variables is governed by the inhomogeneous dissipative set of differential equations with discontinuities:

$$\dot{n} = 0, \tag{1}$$
$$\dot{f} = \alpha\eta(m - f) + h_f z_f, \tag{2}$$
$$\dot{z}_f = \left[A_f - \left(\gamma_f + \beta_f sgn(\dot{f})sgn(z_f)\right)|z_f|^{n_f}\right]\dot{f}, \tag{3}$$
$$\dot{m} = \beta\kappa n + f(\gamma - c) - m + h_m z_m, \tag{4}$$
$$\dot{z}_m = \left[A_m - \left(\gamma_m + \beta_m sgn(\dot{m})sgn(z_m)\right)|z_m|^{n_m}\right]\dot{m}, \tag{5}$$
$$\dot{c} = \upsilon fm - \omega n - \delta\phi c + h_c z_c, \tag{6}$$
$$\dot{z}_c = \left[A_c - \left(\gamma_c + \beta_c sgn(\dot{c})sgn(z_c)\right)|z_c|^{n_c}\right]\dot{c}. \tag{7}$$

The variables are defined as follows: n – tumor cell density; f – matrix–metalloproteinases (MM) concentration; m – matrix-degradative enzymes (MDE) concentration; c – oxygen concentration; z_f, z_m, z_c present the hysteretic part of the system considered. The fitting parameters are defined as follows: α – tumor cell volume; β – glucose level; γ – number of tumor cells; δ – diffusion saturation level; η and κ are coefficients describing a growth and decay of MM and MDE concentration, respectively; υ , ω, φ govern growth and decay of the oxygen concentration. The parameters (A_f, β_f, n_f), (A_m, β_m, n_m), (A_c, β_c, n_c)$\in R^+$ and γ_f , γ_m , $\gamma_c \in R$ govern the shape of the hysteresis loops. The memorization parameters h_f, h_m, h_c characterise a hysteresis contribution to the system considered.

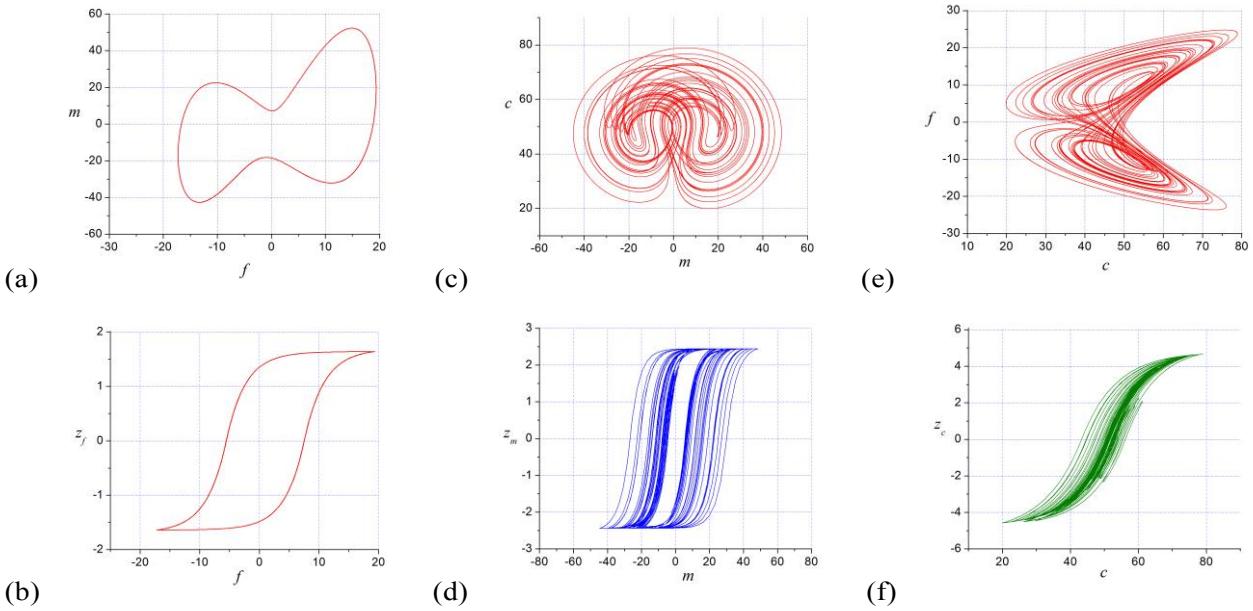

Fig. 2. Responses of the biological system with the memory of states (1)-(7) with memorization parameters h_f=0.5, h_m=0.4, h_c=0.3: (a) a chemical clock and (c),(e) chaotic attractors in MM, MDE and oxygen concentrations phase space projected to phase plane a) MDE vs MM; c) oxygen vs MDE; e) MM vs oxygen concentrations and (b),(d),(f) hysteretic loops associated with (b) MM, (d) MDE, (f) oxygen concentrations.

3 Concluding Remarks

Our numerical simulations confirmed that the suggested generalized non-linear multi-scale diffusion cancer-invasion model with additional state variables is well suited for simulations of the memory effects in the biological cancer system considered.

Analysis of the results demonstrated significant state memory influence on evolution of the conditions leading to cancer invasion in biological systems. For various memorization parameters, hysteresis loops and phase spaces projections of matrix–metalloproteinases, matrix-degradative enzymes and oxygen concentrations demonstrated a good agreement with the conditions leading to cancer invasion in biological systems. There were ascertained two effects of the memory of states: restraining and generating effects which control the conditions leading to cancer invasion in biological systems.

References

[1] L. Dzyubak, O. Dzyubak, J. Awrejcewicz, Controlling and stabilizing unpredictable behaviour of metabolic reactions and carcinogenesis in biological systems, Journal of Non-Linear Dynamics **97** (2019), 1853–1866.

[2] L. Dzyubak, O. Dzyubak, J. Awrejcewicz, Multi-parametric evolution of conditions leading to cancer invasion in biological systems, Applied Mathematical Modelling **90** (2021), 46–60.

[3] J. Awrejcewicz, L. Dzyubak, Hysteresis modelling and chaos prediction in one- and two-dof hysteretic models, Arch. of Appl. Mech. **77** (2007), 261–279.

[4] J. Awrejcewicz, L. Dzyubak, C.-H. Lamarque, Modelling of hysteresis using Masing–Bouc-Wen's framework and search of conditions for the chaotic responses, Communications in Nonlinear Science and Numerical Simulation **13** (2008), 939–958.

International Conference on Mathematical Analysis and Applications in Science and Engineering
ICMA^{2}SC'22
ISEP Porto-Portugal, June 27 - 29, 2022

Global dynamics of a Kolmogorov predator-prey system

Érika Diz-Pita[1⋆] **Jaume Llibre**[2] **M. Victoria Otero-Espinar**[1]

[1] Universidade de Santiago de Compostela - CITMAga, Spain
[2] Universitat Autónoma de Barcelona, Spain

[1⋆] erikadiz.pita@usc.es

Abstract: We consider a family of Kolmogorov systems depending on three parameters which models a predator-prey system, so it is interesting from an ecological point of view. We study the global dynamics of that family, obtaining their topologically distinct global phase portraits in the positive quadrant of the Poincaré disc.

keywords: predator-prey system; Kolmogorov system; global phase portrait.

MSC2020: 34C05; 37C15.

1 Introduction

Rosenzweig and MacArthur introduced in [5] the following predator-prey model

$$\begin{aligned} \dot{x} &= rx\left(1-\frac{x}{K}\right) - y\frac{mx}{a+x}, \\ \dot{y} &= y\left(-d+n\frac{mx}{a+x}\right), \end{aligned} \tag{1}$$

where we use the variable $x \geq 0$ for the prey density and the variable $y \geq 0$ for the predator density. In [3], Huzak has studied the Rosenzweig and MacArthur system but reducing it to a polynomial differential system, by means of some variable changes. The obtained system studied by Huzak is the following Kolmogorov system:

$$\begin{aligned} \dot{x} &= x(-x^2 + (1-a)x - y + a), \\ \dot{y} &= y((n-d)x - da). \end{aligned} \tag{2}$$

We want to study the dynamics of this Kolmogorov system and to do a classification of all their global phase portraits on the positive quadrant of the Poincaré disc, as this allows us to know the behavior near the infinity. This system has been proposed in [1], where we have initiated its study.

2 Results

We give the global classification except for the case in which the parameters satisfy the conditions $0 < ad < n-d$, $d(d(a+1)+n(a-1))^2 - 4n(n-d)^2(n-d(a-1)) < 0$ and $1+n-d-a-ad > 0$. In this case we make a conjecture about the expected global phase portrait.

We prove that the global phase portrait of system (2) in the closed positive quadrant of the Poincaré disc is topologically equivalent to one of the three phase portraits included in Figure 1. More precisely, if $ad \geq n-d$, the phase portrait is topologically equivalent to phase portrait (P1); if $0 < ad < n-d$ and $d(d(a+1)+n(a-1))^2 - 4n(n-d)^2(n-d(a-1)) \geq 0$, the phase portrait is topologically equivalent to phase portrait (P2); and if $0 < ad < n-d$, $d(d(a+1)+n(a-1))^2 - 4n(n-d)^2(n-d(a-1)) < 0$ and $1+n-d-a-ad < 0$, the phase portrait is equivalent to phase portrait (P3).

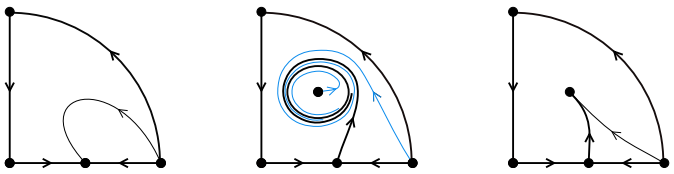

(P1) (P2) (P3)

Figure 1: Posiible phase portraits in the positive quadrant of the Poincaré disc for system (2)

We conjecture that the phase portrait of system (2) in the closed positive quadrant of the Poincaré disc if $0 < ad < n-d$ and $d(d(a+1)+n(a-1))^2 - 4n(n-d)^2(n-d(a-1)) < 0$ and $1+n-d-a-ad > 0$ is topologically equivalent to phase portrait (P3) in Figure 1.

We give a graphical representation of the parameters space in Figure 2. The different regions and surfaces correspond which each one of the phase portraits. The global phase portrait(P1) in Figure 1 appears when the parameters are in region I or over the surface S_1. The phase portrait (P2) in Figure 1 appears when the parameters are in region III. Note that we divide region II in two subregions, II-a and II-b, as only in one of them the results have been proved analytically. We have proved that phase portrait (P3) in Figure 1 appears when the parameters are in region II-a. Finally, based on numerical results, we conjecture that the phase portrait is also (P3) over the surfaces S_2 and S_3 and in the region II-b.

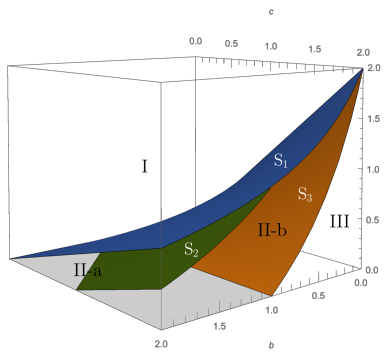

Figure 2: The regions and surfaces in the parameters space separating the different phase portraits: S_1 : $\{d = n/(a+1) \mid a, n \geq 0\}$, S_2 : $\{d = (1+n-a)/(a+1) \mid a, n \geq 0, (1+n-a)/(a+1) < n/(a+1)\}$ and S_3 : $\{d = n(1-a)/(1+a) \mid a, n \geq 0\}$

.

We begin by obtaining the singular points and determining their local phase portraits, both for the finite and infinite singular points.

First we deal with the finite singularities. The origin and the point $(1,0)$ are singular points for all the values of the parameters, and the point $P = \big(ad/(n-d), (-an(d+ad-n))/(n-d)^2\big)$ is a positive singular point if $n \neq d$ and $0 < ad < n-d$. We study the local phase portraits by applying Theorems 2.15 and 2.19 in [2].

Then, we consider the Poincaré compactification of system (2) which makes possible to study the behavior of the trajectories near infinity. We use the local charts of the sphere to obtain the compactification. In chart U_1 the only infinite singular point is the origin, and it is an unstable node. In chart U_2, the origin is also a singular point, but it is linearly zero, so we resort to the use of blow up's. We need to do a horizontal blow up and although we obtain a phase portrait which is not totally determined, the information it provides is sufficient. Specifically, there are two regions in the third and fourth quadrants, shaded in Figure 3, where the phase portrait is not defined, but we only need to determine the phase portrait of O_2 in the positive quadrant of the Poincaré disc, and this corresponds with the positive quadrant in the plane (u,v), in which the phase portrait is totally determined.

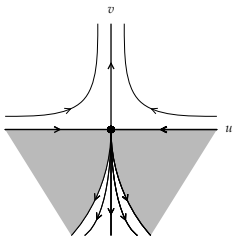

Figure 3: Phase portrait in a neighborhood of the origin of chart U_2.

Then we can state that the phase portrait at the infinite singular points is the same for all the values of the parameters: the origin of chart U_1 is an unstable node and the origin of chart U_2 on the positive quadrant of the Poincaré disc has only one sector which is hyperbolic, with one separatrix on $x = 0$ and the other at infinity.

Our objective is to obtain the global portraits from the local information, studying the separatrices and their possible connections, and depending on the values of the parameters we must distinguish several cases.

In the two cases in which there are no singular points in the first quadrant, there cannot exist a limit cycle. Therefore, once determined the local phase portrait at the finite and infinite singular points, we can determine the global portrait in the first quadrant of the Poincaré disc. In both cases, analyzing all the possible α and ω-limits, there is just one possibility, that all the orbits leave the singular point O_1 and go to the singular point $(1,0)$. The corresponding phase portrait is (P1) in Figure 1.

On the other hand, in the cases in which there is a singular point inside the first quadrant, we must study the existence of limit cycles. First, by the Poincaré-Bendixon Theorem we proof that if $0 < ad < n-d$ and $A > 0$, where $A = d(n-d) - ad(n+d)$, there exists at least one limit cycle surrounding the singularity P. We also proof, applying the results in [4], that in this case the limit cycle around the point P is unique.

We also study the Hopf bifurcation and prove that the equilibrium P of system (2) undergoes a supercritical Hopf bifurcation at $a_0 = (n-d)/(n+d)$. For $a > a_0$ the system has a unique stable limit cycle bifurcating from the equilibrium point P.

In the remaining cases, by the Bendixon-Dulac Theorem, we prove that if $0 < ad < n - d$, $A < 0$ and $1 + n < d + a + ad$, then system (2) does not have periodic orbits in the set $\{(x, y) \in \mathbb{R}^2 : x, z \geq 0\}$.

We conjecture, based on numerical evidence, that if $0 < ad < n-d$, $A < 0$ and $1+n > d+a+ad$, there are not limit cycles.

With these results and conjecture, and analyzing the possible alpha and omega-limits of the separatrices, we obtain the global phase portraits in the cases in which there is a singular point inside the first quadrant.

We recall that we are interested in the topological classification of the global phase portraits, so, even analytically we could obtain more phase portraits, all of them are topologically equivalent to one of the three phase portraits included in Figure 1.

3 Conclusions and future work

For system (2) we want to carry out a complete study of its dynamics. Regarding the global phase portraits in positive quadrant of the Poincaré disk, we have given a topological classification except for the case with conditions $1 + n - d - a - ad > 0$, $0 < ad < n - d$ and $d(d(a + 1) + n(a-1))^2 - 4n(n-d)^2(n-d(a-1)) < 0$. In this particular case we made a conjecture about the expected global phase portrait. Although we have numerical evidence supporting the conjecture, the analytical proof remains as an open problem for the future.

We are dealing with a modified system, changing the Holling type II functional response that appears in system 2 for Holling type III and IV functional responses. We think it is interesting to determine if considering these functional responses give rise to different or more complex dynamics.

Acknowledgments

The first and third authors are partially supported by the Ministerio de Ciencia e Innovación, Agencia Estatal de Investigación (Spain), grant PID2020-115155GB-I00 and the Consellería de Educación, Universidade e Formación Profesional (Xunta de Galicia), grant ED431C 2019/10 with FEDER funds. The first author is also supported by the Ministerio de Educación, Cultura y Deporte of Spain, contract FPU17/02125. The second author is partially supported by the Agencia Estatal de Investigación grant PID2019-104658GB-I00, and the H2020 European Research Council grant MSCA-RISE-2017-777911.

References

[1] E. Diz-Pita, J. Llibre, M. V. Otero-Espinar, Global phase portraits of a predator-prey system, Electronic Journal of Qualitative Theory of Differential Equations, **16** (2022), 1–13.

[2] F. Dumortier, J. Llibre and J.C. Artes, Qualitative Theory of Planar Differential Systems, UniversiText, Springer-Verlag, New York, 2006.

[3] R. Huzak, Predator-prey systems with small predator's death rate, Electronic Journal of Qualitative Theory of Differential Equations, **86** (2018), 1–16.

[4] L. P. Liou and K. S. Cheng, On the uniqueness of a limit cycle for a predator-prey system, SIAM J. Math. Anal, **19**(4), (1988), 867–878.

[5] M. Rosenzweig and R. MacArthur, Graphical representation and stability conditions of predator-prey interaction, American Naturalist, **97** (1963), 209–223

International Conference on Mathematical Analysis and Applications in Science and Engineering
ICMA^{2}SC'22
ISEP Porto-Portugal, June 27 - 29, 2022

FROM DUFFING EQUATION TO BIO-OSCILLATIONS

Felix Sadyrbaev[1,2]

[1] Institute of Mathematics and Computer Science, University of Latvia, Latvia
[2] Daugavpils University, Latvia

[1]felix@latnet.lv

Abstract: Two cases of irregular behavior of solutions to three-dimensional systems, arising in applications, are considered. The mechanism of this phenomena is analysed. Similarity of both cases is acknowledged.

keywords: chaotic behavior; dynamical systems; bio-oscillation.

MSC2020: 34C60; 34D45; 92B20.

1 Introduction

Systems of ordinary differential equations, exhibiting irregular behavior of solutions, appear in various fields, including engineering, mechanics, hydrodynamic and biology. The Duffing differential equation

$$x'' + \delta x' + \alpha x + \beta x^3 = h\cos\omega t$$

can be written also as a three-dimensional system

$$\begin{cases} x' = y, \\ y' = -\delta y - \alpha x - \beta x^3 - h\cos z, \\ z' = \omega. \end{cases} \tag{1}$$

The authors of [2] have considered the similar system

$$\begin{cases} x' = y, \\ y' = by + x - x^3 - kz, \\ z' = w(y - z) \end{cases} \tag{2}$$

In system (2) z is treated as "the third independent dynamical variable, w is its characteristic rate, and k is the feedback coefficient." The damping term in (2) has an opposite sign, compared to (1). The authors suggest that the negative damping yields additional spiral instability. A specific electrical circuit, imitating solutions of (2), is proposed in [2]. The simulation and experimental results were obtained for the oscillator (2) and the corresponding electronic device. The authors have observed the irregular behavior of time series and were led to the conclusion that system (2) can be chaotic.

We provide our own analysis of system (2) around the specific values of parameters. Our observations are used later for treatment of some system from the theory of genetic networks.

2 Results and discussion

Let $b = 1.9$, $k = 2.5$, $w \in (2.5, 3.85)$. The system (2) has exactly three critical points at $(-1, 0, 0)$, $(0, 0, 0)$, $(1, 0, 0)$. We examine the characteristics of these points under the change of the variable w from 3.85 to 2.55. Starting from the value $w = 3.55$ all three critical points are non-attractive. There are periodic trajectories around the two side critical points $(-1, 0, 0)$ and $(+1, 0, 0)$. The attractivity properties of these points are weakened, as the parameter w diminishes and finally trajectories start to travel between them, exhibiting irregular behavior and sensitivity to initial conditions.

The latter can be illustrated by the graphs of Lyapunov exponets, obtained using the program developed by M. Sandri [4].

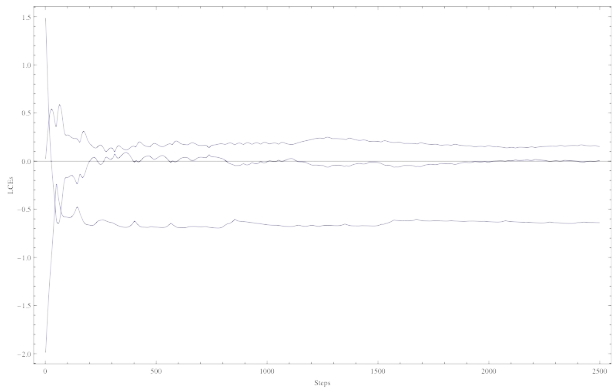

Figure 1: The Lyapunov exponents for the system 2, $b = 1.9$, $k = 2.5$, $w = 2.55$.

Recall that positivity of at least one Lyapunov Characteristic Exponents is the evidence of sensitive dependence of solutions to dynamical system to initial data.

Proposition 1. System (2) can be chaotic.

Consider the system

$$\begin{cases} x' = \frac{1}{1+e^{-\mu_1(w_{11}x+w_{12}y+w_{13}z-\theta_1)}} - x, \\ y' = \frac{1}{1+e^{-\mu_2(w_{21}x+w_{22}y+w_{23}z-\theta_2)}} - y, \\ z' = \frac{1}{1+e^{-\mu_3(w_{31}x+w_{32}y+w_{33}z-\theta_3)}} - z \end{cases} \tag{3}$$

which arises in the theory of genetic regulatory networks (GRN). It describes the three-element network with the elements x, y and z. They can influence each other, developing the collective response to some external threats. The system (3) has an invariant unit cube in the positive octant of the phase space. Therefore the system has an attractor. The knowledge of attractors, their locations and properties is of great theoretical and practical interest. We would like to claim that there are two stable periodic trajectories which attract other trajectories of the system. To show this, we consider the regulatory matrix of the special form. All other parameters can be selected so that the resulting system (3) have exactly three periodic trajectories like in Figure 2.

Proposition 2. System (3) can have at least two attractors in the form of stable closed trajectories.

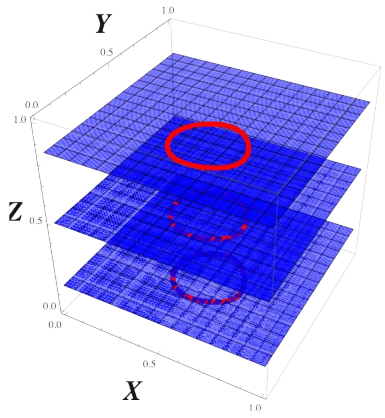

Figure 2:

3 Conclusions and Future work

Chaos in biological systems can be vitally important. Therefore this phenomenon needs further investigation, taking cue from similar mathematical models in other fields.

References

[1] Holmes, P. A nonlinear oscillator with a strange attractor. Philosophical Transactions of the Royal Society of London. Series A, Mathematical and Physical Sciences 292: 419–448, 1979 https://royalsocietypublishing.org/doi/10.1098/rsta.1979.0068

[2] Tamaševičius, A., Bumelienė, S., Kirvaitis, R., Mykolaitis, G., Tamaševičiūtė, E., Lindberg, E. Autonomous Duffing-Holmes Type Chaotic Oscillator Elektronika ir Elektrotechnika. 5 (93):43–46, 2009 https://www.eejournal.ktu.lt/index.php/elt/article/download/10178/5036

[3] Tamaševičiūtė, E., Tamaševičius, A., Mykolaitis, G., Bumelienė, S., Lindberg, E. Nonlinear Analysis:Modelling and Control, 2008, Vo. 13, No. 2, 241-252.

[4] Sandri, M. Numerical Calculation of Lyapunov Exponents. Mathematica J. 6, 78-84, 1996. http://library.wolfram.com/infocenter/Articles/2902

International Conference on Mathematical Analysis and Applications in Science and Engineering
ICMA^{2}SC'22
ISEP Porto-Portugal, June 27 - 29, 2022

Modeling real noise in population dynamics with applications to the chemostat model*

Javier López-de-la-Cruz

Departamento de Matemática Aplicada a las TIC
Escuela Técnica Superior de Ingenieros Informáticos
Campus de Montegancedo, Universidad Politécnica de Madrid
28660 Boadilla del Monte, Madrid, Spain

javier.lopez.delacruz@upm.es

Abstract: In this talk, some different ways to model random disturbances in biological systems will be presented, with applications to the chemostat model, that is considered as an idealization of nature for growing microorganisms in a cultured environment. We will perturb a parameter in the mathematical model, motivated by observations in real devices. To this end, we will use the well-known standard Wiener process (which will lead into some important drawbacks from the biological point of view) and then we will focus on modeling real noise by means of the Ornstein-Uhlenbeck process (which will allow us to provide conditions to ensure the persistence of the species, the main goal in practice). In addition, we will illustrate the theoretical results with several numerical simulations.

keywords: chemostat model; real noise; Wiener process.

MSC2020: 34A12; 34F05; 34D99.

1 Introduction

The chemostat is a laboratory device used for growing microorganisms in cultured environments. It is considered as an idealization of nature for growing microorganisms in a cultured environment. In addition, the chemostat has a huge number of applications in real life, for example, it can be used to study genetically altered organisms (see [13, 14]), models of mammalian large intestine (see [6, 7]), waste-water treatment processes (see [5, 9]) and models in ecology (see [8, 12]).

The classical chemostat apparatus consists of three tanks, the *feed bottle*, the *culture vessel* and the *collection vessel*, that are interconnected by means of pumps. The substrate is stored in the feed bottle and pumped from there to the culture vessel, where the interactions with the consumer species take place. In order to keep the volume of the culture vessel constant, another flow is pumped from the culture vessel to the collection vessel. Then, the goal is to investigate the dynamics of the substrate and the species in the culture vessel.

The mathematical model describing how the chemostat device works is the following system of ordinary differential equations

$$\frac{ds}{dt} = D(s_{in} - s) - \mu(s)x, \tag{1}$$

$$\frac{dx}{dt} = -Dx + \mu(s)x, \tag{2}$$

where $s = s(t)$ and $x = x(t)$ represent the concentration of substrate and species, respectively, $s_{in} > 0$ is the input concentration of substrate, $D > 0$ denotes the dilution rate and μ is a function that describes how the substrate is consumed by the species. We will consider in this talk the *Monod* consumption function

$$\mu(s) = \frac{ms}{a + s},$$

where $m > 0$ is the maximum specific growth rate of the microorganisms and $a > 0$ is the half-saturation constant.

The classical chemostat model (1)-(2) has been widely studied in the literature, since its invention by Monod (see [10]) and Novick and Szilard (see [11]) in the 1950s. Among the different assumptions when dealing with system (1)-(2), one is to assume that D is constant. However, it is very well-known that real life is often subject to random perturbations. In fact, measurements in real devices suggest that random perturbations on D should be considered to obtain a more realistic mathematical model.

2 Different ways of modeling random perturbations

Among the different ways to model random perturbations on the dilution rate D in the chemostat model (1)-(2), one could be replace D by $D + \alpha\dot{\omega}(t)$, where ω denotes the standard Wiener process and $\alpha > 0$ is the amount of noise. We refer readers to [2, 3], where Caraballo *et al.* investigate the resulting stochastic chemostat model by means of the theory of random dynamical systems and the concept of pullback convergence. In this case, since the standard Wiener process can take arbitrary large values (both positive and negative), several important drawbacks appear from the biological point of view, for instance, some state variables can take negative values, which is completely illogical in practice, and it is not possible to ensure the persistence of the species.

In order to avoid the previous drawbacks, another approach to model random perturbations on the dilution rate D in the chemostat model (1)-(2) consists of replacing D by $D + \Phi(z^*(\theta_t\omega))$, where $z^*(\theta_t\omega)$ denotes the well-known Ornstein-Uhlenbeck process (that is a mean reverting stochastic process) and Φ is an odd bounded real function.

This last way has proved to provide us a very powerful tool when modeling real noise, not only in the chemostat model, but also in other models in population dynamics. On the one hand, the realizations of the perturbed dilution rate $D + \Phi(z^*(\theta_t\omega))$ are very similar to the ones observed in real experiments. On the other hand, this way of modeling random perturbations allows us to provide conditions under which the consumer species persist, which is the most important goal in practice. In addition, in this case we do not need to use the theory of random dynamical systems and the concept of pullback convergence, but we can study the resulting random chemostat model for every fixed realization of the noise forwards in time. Every detail and proof concerning this way of modeling random perturbations can be found in [1, 3, 4].

References

[1] T. Caraballo, R. Colucci, J. López-de-la-Cruz, and A. Rapaport. A way to model stochastic perturbations in population dynamics models with bounded realizations. *Communications in Nonlinear Science and Numerical Simulation*, 77:239–257, oct 2019.

[2] T. Caraballo, M. J. Garrido-Atienza, and J. López-de-la-Cruz. *Some Aspects Concerning the Dynamics of Stochastic Chemostats*, volume 69, chapter 11, pages 227–246. Springer International Publishing, Cham, 2016.

[3] T. Caraballo, M. J. Garrido-Atienza, J. López-de-la-Cruz, and A. Rapaport. Modeling and analysis of random and stochastic input flows in the chemostat model. *Discrete & Continuous Dynamical Systems - Series B*, 24(8):3591–3614, 2018.

[4] Tomás Caraballo and J. López-de-la-Cruz. Survey on chemostat models with bounded random input flow. *Mathematical Modelling and Control*, 1(1):52–78, 2021.

[5] G. D'Ans, P. Kokotovic, and D. Gottlieb. A nonlinear regulator problem for a model of biological waste treatment. *IEEE Transactions on Automatic Control*, 16(4):341–347, aug 1971.

[6] R. Freter. *Human Intestinal Microflora in Health and Disease*, chapter Mechanisms that control the microflora in the large intestine, pages 33–54. Academic Press, New York, 1983.

[7] R. Freter. An understanding of colonization of the large intestine requires mathematical analysis. *Microecology and Therapy*, 16:147–155, 1986.

[8] J. Kalff and R. Knoechel. Phytoplankton and their dynamics in oligotrophic and eutrophic lakes. *Annual Review of Ecology and Systematics*, 9(1):475–495, nov 1978.

[9] J. W. M. La Rivière. Microbial ecology of liquid waste treatment. In *Advances in Microbial Ecology*, volume 1, pages 215–259. Springer US, 1977.

[10] J. Monod. La technique de culture continue: Théorie et applications. *Annales de l'Institute Pasteur*, 79:390–410, 1950.

[11] A. Novick and L. Szilard. Experiments with the chemostat on spontaneous mutations of bacteria. *Proceedings of the National Academy of Sciences*, 36(12):708–719, 1950.

[12] E. Rurangwa and M. C. J. Verdegem. Microorganisms in recirculating aquaculture systems and their management. *Reviews in Aquaculture*, 7(2):117–130, feb 2015.

[13] G. Stephanopoulos, R. Aris, and A.G. Fredrickson. A stochastic analysis of the growth of competing microbial populations in a continuous biochemical reactor. *Mathematical Biosciences*, 45(1-2):99–135, jul 1979.

[14] Frank Stewart and Bruce Levin. The population biology of bacterial plasmids: A priori conditions for the existence of conjugationally transmitted factors. *Genetics*, 87:209–228, 11 1977.

International Conference on Mathematical Analysis and Applications in Science and Engineering
ICMA^{2}SC'22
ISEP Porto-Portugal, June 27 - 29, 2022

Exact solutions for a mathematical model of high-grade brains tumors through symmetry reductions

M. Rosa[1,2,⋆] **S. Chulián**[1,2] **A. Niño-López**[1,2] **A. Martínez-Rubio**[1,2] **M.L. Gandarias**[1]

[1] Department of Mathematics, Universidad de Cádiz, Puerto Real, Cádiz, Spain
[2] Biomedical Research and Innovation Institute of Cadiz (INiBICA)
Hospital Universitario Puerta del Mar, Cádiz, Spain

[1⋆]maria.rosa@uca.es

Abstract: Malignant gliomas are the most frequent and deadly type of brain tumors. Over the last years, complex mathematical models of cancerous growths have been developed increasingly, especially on solid tumors, in which growth primarily comes from cellular proliferation. A nonlinear system of coupled Fisher-Kolmogorov equation has been considered by [1]. In this work, we study this model from the point of view of the theory of symmetry reductions in partial differential equations. We obtain the classical symmetries admitted by the system and we use the transformations groups to reduce the equations to ordinary differential equations. Finally, we obtain solutions for this model.

keywords: Lie symmetry; Exact solutions; Brain Tumors.

MSC2020: 34C20; 37N25; 92B05.

1 Introduction

High-grade gliomas are tumors of the glial cells, which are found in the brain and spinal cord. They are called "high-grade" because these tumors are fast-growing and they spread quickly through brain tissue, which makes them hard to treat. Median survival is generally less than one year from the time of diagnosis, and even in the most favorable situations, most patients die within two years [2].

Mathematical modeling is a powerful tool for analyzing biological problems. These models have the potential of becoming useful against cancer in three different ways: in personalized medicine, accessing unreachable scales and formulating novel hypothesis.

We consider a reduced continuous model describing the evolution of high grade gliomas in response to hypoxic events through the interplay of different cellular phenotypes. This model was studied in [1] in order to show how hypoxic events may have a role on the acceleration of the growth speed of high grade gliomas. The authors considered two cellular phenotypes to describe this model: One of them is more migratory and a second one is more proliferative. Therefore, $u(t, x, y, z)$ denotes a proliferative (or normoxic) phenotype and $v(t, x, y, z)$ denotes a migratory (or hypoxic) phenotype. The authors assumed that the model is based on a pair of coupled

Fisher-Kolmogorov equations, including a coupling term accounting for the decay of hypoxic cells into the normoxic phenotype [1]. The generalized model is as follows:

$$\begin{cases} F_1 \equiv u_t - d_1(u_{xx} + u_{yy} + u_{zz}) - c_1(1-u-v)u - g(v) = 0, \\ F_2 \equiv v_t - d_2(v_{xx} + v_{yy} + v_{zz}) - c_2(1-u-v)v + g(v) = 0, \end{cases} \tag{1}$$

where d_1, d_2 are the diffusion coefficients for the proliferative and migratory phenotypes, respectively. These parameters satisfy $d_2 > d_1$, and c_1, c_2 are the doubling times for both phenotypes with $c_1 > c_2$. The parameter a_1 corresponds to the typical time for the migratory phenotype to switch to the proliferate one once the hypoxic event has finished and in the present of sufficient oxygen. The densities u, v are taken in units of the maximal tissue density, typically around 10^3 cell/cm^3.

The search for exact solutions to nonlinear PDEs plays a fundamental role in the analysis of nonlinear physical phenomena. One of the most famous and established procedures for obtaining exact solutions of differential equations is the classical symmetries method, also called group analysis. Symmetries of nonlinear partial differential equations (PDEs) systems may be used to reduce the number of independent variables of the PDEs; in particular we might reduce the PDEs to ordinary differential equations (ODEs). The ODE systems may also have symmetries that allow us to reduce the order of one or of both ODEs and we can integrate to find exact solutions. Often solutions of the nonlinear PDE system will be asymptotic to the symmetry solutions. Explicit solutions (such as those found by symmetry methods) can also play an important role in the design and testing of numerical integrators [3].
In this study, by using Lie symmetry groups, we find analytical solutions for several models of high-grade brains tumors.

2 Lie Symmetries

We perform the corresponding Lie symmetry analysis for system (1). The method for finding Lie point symmetries is well known, see for example [3, 4, 5]. Let us consider a one-parameter Lie group of infinitesimal transformations in (t, x, y, z, u, v) given by

$$\begin{aligned} t^* &= t + \varepsilon\, \xi^1(t,x,y,z,u,v) + \mathcal{O}(\varepsilon^2), \\ x^* &= x + \varepsilon\, \xi^2(t,x,y,z,u,v) + \mathcal{O}(\varepsilon^2)\ , \\ y^* &= y + \varepsilon\, \xi^3(t,x,y,z,u,v) + \mathcal{O}(\varepsilon^2)\ , \\ z^* &= z + \varepsilon\, \xi^4(t,x,y,z,u,v) + \mathcal{O}(\varepsilon^2)\ , \\ u^* &= u + \varepsilon\, \eta^1(t,x,y,z,u,v) + \mathcal{O}(\varepsilon^2), \\ v^* &= v + \varepsilon\, \eta^2(t,x,y,z,u,v) + \mathcal{O}(\varepsilon^2), \end{aligned} \tag{2}$$

where ε is the group parameter.

The invariance of system (1) under a Lie group of transformations with infinitesimal generator of the form

$$X = \xi^1 \frac{\partial}{\partial t} + \xi^2 \frac{\partial}{\partial x} + \xi^3 \frac{\partial}{\partial y} + \xi^4 \frac{\partial}{\partial z} + \eta^1 \frac{\partial}{\partial u} + \eta^2 \frac{\partial}{\partial v} \tag{3}$$

yields a system of equations for the coordinates $\xi^1(t,x,y,z,u,v)$, $\xi^2(t,x,y,z,u,v)$, $\xi^3(t,x,y,z,u,v)$, $\xi^4(t,x,y,z,u,v)$, $\eta^1(t,x,y,z,u,v)$ and $\eta^2(t,x,y,z,u,v)$.

Applying the second prolongation $pr^{(2)}X$ to system (1) and solving the resultant overdetermined system of linear partial differential equations one obtains the following Lie points symmetries (Table 1):

i	g	X
1	Arbitrary	$X_1 = \partial_t$, $X_2 = \partial_x$, $X_13 = \partial_y$, $X_4 = \partial_z$, $X_5 = -y\partial_x + x\partial_y$, $X_6 = -z\partial_x + x\partial_z$, $X_7 = -z\partial_y + y\partial_z$.
2	$g_1 v + g_2 v \ln v$	X_1, X_2, X_3, X_4, X_5, X_6, X_7, $X_8 = -ve^{-g_2 t}\partial_u + ve^{-g_2 t}\partial_v$.
3	$g_1 v + g_2$	X_1, X_2, X_3, X_4, X_5, X_6, X_7, $X_8 = -e^{-g_1 t}(u+v)\partial_u + e^{-g_1 t}(u+v)\partial_v$, $X_9 = -e^{(g_2-g_1)t}(u+v-1)\partial_u + e^{(g_2-g_1)t}(u+v-1)\partial_v$, $X_{10} = \left(\frac{g_1^2}{g_2^2}v - \frac{g_1}{g_2}v - u - v + \frac{g_1}{g_2}\right)\partial_u - \left(\frac{g_1^2}{g_2^2}v - \frac{g_1}{g_2}v - u - v + \frac{g_1}{g_2}\right)\partial_v$.

Table 1: Symmetry classification for system (1) with g_1, g_2 arbitrary constants.

2.1 Symmetry reductions and exact solutions

We first solve the invariant surface condition by solving the corresponding characteristic equations

$$\frac{dt}{\xi^1} = \frac{dx}{\xi^2} = \frac{dy}{\xi^3} = \frac{dz}{\xi^4} = \frac{du}{\eta_1} = \frac{dv}{\eta_2}.$$

The similarity variable and similarity solutions can be found by solving the corresponding characteristic equations. We obtain similarity variable and similarity solutions

$$\xi = \lambda x + \mu y + \nu z + t, \quad u = U(\xi), \quad v = V(\xi). \tag{4}$$

The substitution of these variables into system (1) yields:

$$\begin{cases} -d_1\left(\lambda^2+\mu^2+\nu^2\right)U_{\xi\,\xi} + U_\xi - g(V) + c_1\,U^2 + (c_1 V - c_1)\,U = 0, \\ -d_2\left(\lambda^2+\mu^2+\nu^2\right)V_{\xi\,\xi} + V_\xi + g(V) + c_2\,V^2 + (c_1 U - c_1)\,V = 0. \end{cases} \tag{5}$$

Taking into account specializing $g(V) = b_1 V(\xi)$, we look for solutions of the form

$$V = -k_1 + k_1 \tanh^2(\xi).$$

By substituting into (5) we get

$$U = \frac{6\tanh^2(\xi)d_2k^2}{c_2} - k_1\tanh^2(\xi) - \frac{2d_2k^2}{c_2} + k_1 + \frac{2\tanh(\xi)}{c_2} - \frac{b_1}{c_2} + 1.$$

Taking into account (4), the corresponding solutions of system (1) are:

$$\begin{aligned} u &= \frac{6\tanh^2(\lambda x+\mu y+\nu z+t)d_2k^2}{c_2} - k_1\tanh^2(\lambda x+\mu y+\nu z+t) - \frac{2d_2k^2}{c_2} + k_1 \\ &+\frac{2\tanh(\lambda x+\mu y+\nu z+t)}{c_2} - \frac{b_1}{c_2} + 1, \\ v &= -k_1 + k_1\tanh^2(\lambda x+\mu y+\nu z+t). \end{aligned} \tag{6}$$

3 Conclusions and Future work

In this paper, we study a mathematical model of high-grade brains tumors using Lie symmetries. The complete symmetry classification has been performed with respect to the arbitrary functions $g(u)$. Once reduced system was obtained, we focused our attention in forms of $g(u)$ of the linear type. Finally, we find analytical solutions for this model.

Acknowledgments

This work has been partially supported by the Fundación Española para la Ciencia y la Tecnoloía (FECYT project PR214), the Asociación Pablo Ugarte (APU, Spain), Junta de Andalucía (Spain) group FQM-201, Ministry of Science and Technology, Spain (grant number PID2019-110895RB-I00, funded by MCIN/AEI/ 10.13039/501100011033). This work was also subsidized by a grant for the research and biomedical innovation in the health sciences within the framework of the Integrated Territorial Initiative (ITI) for the province of Cadiz (grant number ITI-0038-2019). ITI is 80% co-financed by the funds of the FEDER Operational Program of Andalusia 2014-2020 (Council of Health and Families).

References

[1] Pardo, R., Martínez-González, A., Pérez-García, V. M. Nonlinear ghost waves accelerate the progression of high-grade brain tumors. Communications in Nonlinear Science and Numerical Simulation, **39** (2016), 360–380.

[2] Stupp, R., Mason, W. P., Van Den Bent, M. J., Weller, M., Fisher, B., Taphoorn, M. J., & Mirimanoff, R. O. Radiotherapy plus concomitant and adjuvant temozolomide for glioblastoma. New England journal of medicine, **352**(10) (2005), 987–996.

[3] Olver P.J., Applications of Lie Groups to Differential Equations. Springer, Berlin, 1986.

[4] Bluman, G.W., Kumei, S. Symmetries and Differential Equations. Applied Mathematical Sciences, Springer, Berlin, 1989.

[5] Ibragimov N.H. Elementary Lie Group Analysis and Ordinary Differential Equations. Wiley, New York, 1999.

International Conference on Mathematical Analysis and Applications in Science and Engineering
ICMA^{2}SC'22
ISEP Porto-Portugal, June 27 - 29, 2022

A higher degenerated invasive-invaded species interaction

Jose Luis Diaz Palencia[1⋆]

[1] Universidad a Distancia de Madrid, Spain

[1⋆]joseluis.diaz.p@udima.es

Abstract: Invasive-invaded species problems are of relevance in mathematics applied to population dynamics. This kind of dynamics is introduced based on a fourth order parabolic operator together with coupled non-linear reaction terms. The order four operator allows modeling a heterogeneous diffusion, as introduced by the Landau-Ginzburg free energy approach. The non-linear reaction terms are given by a coupled non-linear effect with mortality in the invasive species (to account for mortality and limited resources) and by a non-Lipschitz term in the invaded species (to account for possible sprouts one the invasion occurs). The analysis starts by the proof of existence and uniqueness making use of the semi-group theory and a fixed point argument. Asymptotic solutions to the invasive species are explored with an exponential scaling. Afterwards, the problem is analyzed with travelling wave solutions where a region of positive solutions is explored

keywords: High order diffusion, Invasive-Invaded, Oscillations, Positive solutionn.

MSC2020: 35K92, 35K91, 35K55

1 Introduction

A systematic treatment of non-linear reaction-diffusion phenomena was initially studied by Fisher and Kolmogorov, Petrovskii and Piskunov (KPP). The principle introduced by the cited authors has been followed in many studies afterwards see [3] and [5]. The selection of an adequate diffusion requires analysis on the interactions. Diffusion has been founded on the Landau-Ginzburg energy principle in [1]. Other approaches to diffusion with spatial solutions have been provided in [4] where a fourth order operator is introduced as a perturbation term to a Fisher-Kolmogorov order two equation, resulting in the Extended Fisher-Kolmogorov equation (EFK). The introduction of such operator accounts for oscillating solutions in the proximity of the null stationary solution (see further in [9] and [8]). Note that invasive-invaded species dynamics has been a traditional area of research in mathematics applied to biological interactions, see [2] and [6]. In the proposed model, the invasive species concentration is referred as $v(x,t)$ while the invaded species concentration is $w(x,t)$. The following lines describe the interactions:

Assume that the invasive species time derivative is qualitatively high, otherwise the invasion will not succeed. In addition, a nonlinear reaction term in the invasive accounts for mortality with a maximum concentration at $v = h$. The reaction term in the invasive equation is hence: $f(v,w) = w^q(v-h)$, where the parameter $q > 1$ aims to correctly weight the invasive species response v_t to the invaded species state. To introduce the invaded species dynamics, assume

that the action of the invasive species over the invaded one will induce the invaded species concentration to decrease. In addition, if the concentration of invaded specie is such that $w \to 0^+$, the invasive species will annihilate the invaded one in a short time. As a consequence, a reaction term to the invaded species equation is: $f(v,w) = -v\,w^p,\ \ 0 < p < 1$.

The driving diffusion is formulated with a spatial order four operator to allow the modelling of heterogeneous spatial patterns in the proximity of the system critical states $v = h,\ w = 0$. Following the mentioned ideas, the problem is given by:

$$\begin{array}{c} v_t = -\Delta^2 v + w^q(h-v); \quad w_t = -\Delta^2 w - vw^p, \\ 0 < p < 1, \quad q > 1; \quad v_0(x), w_0(x) \in L^\infty(\mathbb{R}) \cap L^2_{loc}(\mathbb{R}) \cap H^4(\mathbb{R}), \end{array} \tag{1}$$

where H^4 is the classical Sobolev space up to the fourth derivative.

2 Results and discussion

The linear operator $-\Delta^2$ generates a strongly continuous semi-group. Assume that $\tau > 0$ is a single parameter linked to the semi-group, so that the following representation holds:

$$v(\tau) = e^{-\Delta^2\tau}v_0(x) + \int_0^\tau \left[e^{-\Delta^2(\tau-s)}w^q(s)(h-v(s))\right]ds;\ \ w(\tau) = e^{-\Delta^2\tau}w_0(x) - \int_0^\tau \left[e^{-\Delta^2(\tau-s)}v(s)w^p(s)\right]ds. \tag{2}$$

Given the problem $y_t = -\Delta^2 y$, with $y(x,0) = \delta(x)$, a solution under Fourier transformation is $\tilde{y}(\tau) = e^{-\omega^4\tau}\tilde{y}_0$. This supports the operator kernel construction as:

$$G(x,\tau) = F^{-1}(e^{-\omega^4\tau}) = \frac{1}{2\pi}\int_{\mathbb{R}} e^{-\omega^4\tau - i\omega x}d\omega = \frac{1}{2\pi}\int_{\mathbb{R}} e^{-\omega^4\tau}cos(\omega x)d\omega. \tag{3}$$

Note that the last integral is convergent for $\omega \in \mathbb{R}$. Hence, the expressions in (2) can be reformulated in terms of $G(x,\tau)$. To this end, assume the following mappings in a space of oscillating solutions H^4_Λ with norm $\|y\|^2_\Lambda = \int_{\mathbb{R}} \Lambda(\lambda)\sum_{k=0}^4 |D^k y(\lambda)|^2 d\lambda$, being $\Lambda(\lambda) = e^{a_0|\lambda|^{\frac{4}{3}}}$, and a_0 a small constant.

$$H_{v_0,\tau} : H^4_\Lambda(\mathbb{R}) \to H^4_\Lambda(\mathbb{R}); \quad I_{w_0,\tau} : H^4_\Lambda(\mathbb{R}) \to H^4_\Lambda(\mathbb{R}) \tag{4}$$

with the following structure (note that $*$ represent a convolution):

$$H_{v_0,\tau}(v) = G(x,\tau) * v_0(x) + \int_0^\tau G(x,\tau-s) * w^q(x,s)(h - v(x,s))ds, \tag{5}$$

$$I_{w_0,\tau}(w) = G(x,\tau) * w_0(x) - \int_0^\tau G(x,\tau-s) * v(x,s)w^p(x,s)ds. \tag{6}$$

The following lemma provides regularity results for each of the defined mappings.

Lemma 2.1. *The parametric operators $H_{v_0,\tau}$ and $I_{w_0,\tau}$ are bounded in the space of oscillating solutions $H^4_\Lambda(\mathbb{R})$.*

Another obtained result is the uniqueness of solutions that is built based on of a fix point argument to the following mapping:

$$T_{v_0,w_0,\tau} : H^4_\Lambda(\mathbb{R}) \times H^4_\Lambda(\mathbb{R}) \to H^4_\Lambda(\mathbb{R}) \times H^4_\Lambda(\mathbb{R}), \tag{7}$$

given by:

$$T_{v_0,w_0,\tau}(v,w) = \begin{pmatrix} G(x,\tau) * v_0(x) \\ G(x,\tau) * w_0(x) \end{pmatrix} + \begin{pmatrix} \int_0^\tau G(x,\tau-s) * w^q(x,s)(h-v(x,s))ds \\ -\int_0^\tau G(x,\tau-s) * v(x,s)w^p(x,s)ds \end{pmatrix}. \tag{8}$$

As a result, it is shown that a fix point argument holds of the form $(v, w) = T_{v_0,w_0,t}(v, w)$. Solutions are then explored based on an asymptotic analysis. This approach assumes that the invaded species concentration is small, i.e. $|w| < \varepsilon^{1/q} << 1\,, \varepsilon > 0$, so that w can be regarded as a perturbation in the equation to the invasive species in (1):

$$v_t = -\Delta^2 v + \varepsilon(h - v), \;\; v_0(x) \in L^\infty(\mathbb{R}) \cap L^2_{loc}(\mathbb{R}) \cap H^4(\mathbb{R}) \tag{9}$$

Consider the following non-linear scaling to the last equation (9):

$$v(x, t) = e^{\zeta(x,t)}. \tag{10}$$

This scaling has been applied in [10], [13] and [12]. It is possible to state that ζ is a complex map: $\zeta : Y \times [0, t] \to \mathbb{C}$, where $Y \subset \mathbb{R}$. Upon replacement in (9), ζ verifies the following Hamilton-Jacobi equation:

$$\zeta_t = F_4\left(\zeta, \frac{\partial \zeta}{\partial x}\right) + P_4\left(\zeta, \frac{\partial^j \zeta}{\partial x^j}\right), \quad j = 2, 3, 4, \quad F_4(\zeta) = -\zeta_x^2\zeta_x^2 + \varepsilon(h - e^\zeta), \tag{11}$$

and P_4 involves higher order spatial derivatives.

Eventually and in return to the scaling given in (10), a solution for $0 < T < \tau \leq t$:

$$v(x, \tau) = e^{3\tau^{-\frac{1}{3}}\left(\frac{1}{4}K(i)x\right)^{\frac{4}{3}}}, \tag{12}$$

Further, the problem (1) can be expressed under the travelling waves formulation by the change: $v(x, t) = \varphi(\xi)$, $w(x, t) = \psi(\xi)$, $\xi = x - at \in \mathbb{R}$, where a is the travelling wave velocity and $\varphi, \psi \in L^\infty(\mathbb{R})$ are the travelling wave profiles:

$$\begin{gathered} -a\varphi' = -\varphi^{(4)} + \psi^q(h - \varphi); \;\; -a\psi' = -\psi^{(4)} - \varphi\psi^p, \\ \varphi'(\xi) > 0\,,\, \psi'(\xi) < 0, \;\; \varphi(\infty) = 1\,,\, \psi(\infty) = 0. \end{gathered} \tag{13}$$

As another important result:

Lemma 2.2. *For any value in the travelling wave speed $a > 0$, the critical state $\varphi = h$, $\psi = 0$ represents a degenerate node in the phase space, where there exist: Three eigenvalues with positive real part (3-D set unstable), a null eigenvalue and Four eigenvalues with negative real part (4-D set stable).*

Travelling wave profiles have been obtained making use of the bvp4c in Matlab for the case of $q = 2$ and $p = 0.5$. The relation between a positive region and the travelling wave speed is $\xi_+ = 3.6391\, a^{-0.410}$.

3 Conclusions and Future work

Solutions to the proposed set of equations in (1) have been explored to describe an invasive-invaded species dynamics. Existence and uniqueness topics have been provided based on the semigroup theory and positivity conditions in the travelling waves approach. Following an exponential scaling to derive a Hamilton-Jacobi equation, an asymptotic solution has been obtained to the invasive specie. As a future research line, the set of equations in (1) may be formulated with a non-linear advection term. The author postulates that the advection would introduce a smoothing effect leading to additional positive regions.

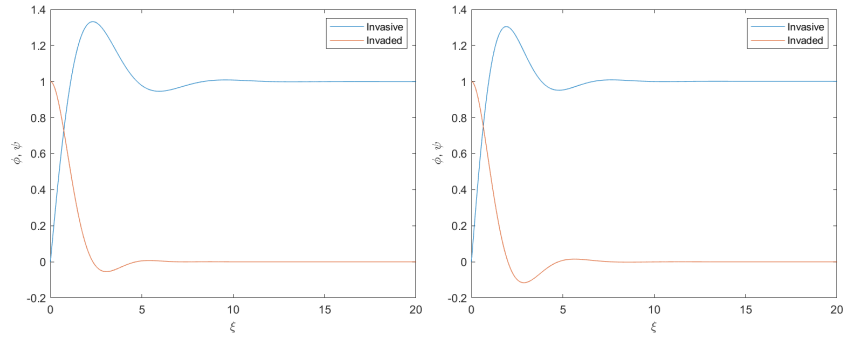

Figure 1: Travelling waves for $a = 1$ (left) and $a = 2$ (right). Note on the induced oscillation due to the order four operator while positivity holds for $\xi_+ = 3.862$ (left) and $\xi_+ = 2.7922$ (right).

References

[1] Cohen, D.S. and Murray, J.D. (1981). A generalized diffusion model for growth and dispersal in a population. *J. Math. Biology* 12, 237â249. https://doi.org/10.1007/BF00276132

[2] Perumpanani, J. A., Sherratt, J., Norbury and Byrne, H. (1999). A two parameter family of travelling waves with a singular barrier arising from the modelling of extracellular matrix mediated cellular invasion. *Physica D.* 126, 145â159.

[3] Aronson, D. (1980). Density-dependent interaction-diffusion systems. *Proc. Adv. Seminar on Dynamics and Modeling of Reactive System*, Academic Press, New York.

[4] RottschÃ¤fer, V. and Doelman, A. (1998). On the transition from the Ginzburg-Landau equation to the extended Fisher-Kolmogorov equation. *Physica D.* 118. 261 - 292.

[5] Aronson, D. and Weinberger, H. (1978). Multidimensional nonlinear diffusion arising in population genetics. *Adv. in Math.* 30, pp 33â76.

[6] Harley, K., Van Heijster, R., Marangell, R., Pettet, G., Roberts, T. and Wechselberger M. Instability of Travelling Waves in a Model of Haptotaxis. (2019) Preprint.

[7] Akveld, M.E. and Hulshof, J. (1998). Travelling Wave Solutions of a Fourth-Order Semilinear Diffusion Equation. *Appl. Math. Lett.* Vol. 11, No. 3, pp. 115-120.

[8] Bonheure, D. and SÃ¡nchez, L. (2006). *Heteroclinics Orbits for some classes of second and fourth order differential equations. Handbook of differential equations.* 3(06), 103-202.

[9] Peletier, L.A. and Troy, W.C.(2001). Spatial Patterns. Higher order models in Physics and Mechanics. *Prog. Nonlinear Differ. Equ. Their Appl.* 45. UniversitÃ© Pierre et Marie Curie.

[10] P. Bracken. The quantum HamiltonâJacobi formalism in complex space. Quantum Stud.: Math. Found. (2020) 7:389â403

[11] Chavez, M. and Galaktionov, V. (2001). Regional blow up for a higher-order semilinear parabolic equation. *Eur. J. Appl. Math.* 12. 601-623.

[12] R.A. Leacock, R.A., Padgett, M.S. Hamilton Jacobi action angle quantum mechanics. Phys. Rev. D28, 2491 (1983).

[13] R.A. Leacock, M.S. Padgett. Hamilton Jacobi theory and quantum action variables. Phys. Rev. Lett. 50, 3 (1983).

International Conference on Mathematical Analysis and Applications in Science and Engineering
ICMA^{2}SC'22
ISEP Porto-Portugal, June 27 - 29, 2022

Auscultation chest locations are correlated with short term spectral features of pulmonary sounds

Sebastian Escobar-Pajoy[1⋆] **Juan P. Ugarte**[1⋆]

[1] Universidad de San Buenaventura, Medellín, Colombia

[1⋆]juan.ugarte@usbmed.edu.co

Abstract: The digital stethoscope enables a computerized analysis of pulmonary sounds. Specific respiratory sounds can be captured by considering distinct recording sites on the chest surface. In this work, the correlation between the chest recording positions and quantitative features of pulmonary signals is assessed. For this purpose, pulmonary sounds simultaneously recorded from different chest regions are quantitatively characterized using different signal processing techniques. The analyzed respiratory sounds correspond to patients suffering from chronic obstructive pulmonary disease. A dimension reduction algorithm in combination with the Procrustes method are implemented for achieving a graphical representation of the high dimensional features space that characterizes the pulmonary data. The results evince that information about the chest locations, namely, trachea, posterior, lateral and posterior chest, can be recovered from the spectral features of the pulmonary recordings. However, such discrimination cannot be performed for left and right side chest positions. The correlation found between the quantitative features and the recording locations on the chest suggest that a multichannel, single-sided, simultaneous recording setup of pulmonary sounds, can provide non-redundant information about the lungs condition.

keywords: signal processing; dimension reduction; Procrustes analysis; pulmonary sounds; chronic obstructive pulmonary disease; computerized auscultation.

MSC2020: 49-XX; 34-XX; 92-XX.

1 Introduction

Pulmonary diseases are among the most common causes of death and identifying the respiratory symptoms and signs is important for an opportune diagnosis [1]. The standard procedure for assessing the pulmonary health is the auscultation, it consists of hearing through a stethoscope the sounds emitted by the respiratory system. These sounds are characterized by their tone or frequency, amplitude or sonority, timbre, and the body location at which they are captured [4]. Despite auscultation is routinely performed by physicians when examining patients it is a highly subjective process. In recent years, the use of digital stethoscopes enabled the option of recording and objectively analyzing respiratory sounds, by means of digital signal processing techniques. During auscultation, the recording site on the chest surface is an important factor due to specifics sounds can be captured. Recommended locations for sequential or simultaneous recordings are, the trachea, anterior left and right, posterior left and right and lateral left and right areas in the chest [5]. Stemming from these ideas, this work studies the correlation between the auscultated chest locations and short term quantitative features of respiratory signals.

1.1 Pulmonary sounds database

The set of signals from the ICBHI 2017 Respiratory Sound database [3] are used in this study. The database contains 6898 annotated respiratory cycles in 920 audio records corresponding to 126 patients. Two modalities of sound recording were adopted during the construction of the database, namely, single channel sequential and multichannel simultaneous. For the purposes of this work, only the data corresponding to 7 simultaneously captured respiratory sounds are analyzed, comprising 224 audio signals from 32 patients suffering from chronic obstructive pulmonary disease (COPD). The signals were recorded using an AKG C417L microphone. The chest locations are designated as Tc (Trachea), Al (Anterior left), Ar (Anterior right), Pl (Posterior left), Pr (Posterior right), Ll (Lateral left) and Lr (Lateral right). A preprocessing stage is applied to the raw data that includes, setting uniform sampling frequency to 4 kHz through signal resampling, signal segmentation according to the annotated respiratory cycles, and having respiratory cycle signals with zero mean and unit standard deviation by means of normalization.

1.2 Features extraction and dimension reduction

A signal processing approach is implemented so that, 13 Mel frequency Cepstral coefficients (MFCC) and 12 chroma features are estimated. In addition, 3 frequency bands are defined as low (60 Hz to 300 Hz), mid (300 Hz to 800 Hz), and high (800 Hz to 1800 Hz). For each frequency band, the following 11 spectral features are calculated: centroid, spread, skewness, kurtosis, crest factor, roll-off, flatness, decrease, flux, slope and entropy. A dynamical features extraction scheme is adopted for analyzing the respiratory cycles, by implementing short-term moving windows of 125 samples (i.e., 62 ms) and 90% of overlapping. Thus, the i-th respiratory cycle, recorded at the j-th chest location from a given patient, is characterized by a $58 \times L$ dimensional features matrix, $\Theta_i^{(j)}$, $i = 1, \ldots, M$, $j = 1, \ldots, 7$, where L and M represent the number of windows and respiratory cycles, respectively. Next, the $Q \times N$ dimensional matrix Φ is computed, where $Q = 7M$, $N = 58 \times 3$ and the rows of Φ are the N dimensional vectors $\phi_p(n)$, $n = 1, \ldots, N$, $p = 1, \ldots, Q$, composed by the mean, standard deviation and variation coefficient of the rows of $\Theta_i^{(j)}$. In addition, the n-th column of Φ is normalized by means of $\phi_p(n) \leftarrow \frac{\phi_p(n) - \mu_p}{\sigma_p}$, where, μ_p and σ_p are the values of mean and standard deviation calculted over the rows $p = 1, \ldots, Q$.

For each patient, let us define the Q-square matrix $\mathcal{D} = [d_{pq}]$ composed by the distances d_{pq} calculated between the rows $\phi_p(n)$ and $\phi_q(n)$, $p, q \in \{1, \ldots, Q\}$ of Φ. In this case, the Lorentzian distance (d_{pq}^{Lo}) and Pearson correlation (d_{pq}^{Pe}) are adopted. The distances matrix $\mathcal{D}$ is used as input of the uniform manifold projection (UMAP) analysis for dimension reduction [2]. The UMAP algorithm uses the distances between objects for assessing the connectivity of the manifold in which the data is embedded and mapping into a low dimensional space by preserving topological properties. In this manner, the high dimensional features space describing the respiratory signals can be visualized in 2 or 3 dimensional graphical representations. Bearing this in mind, a UMAP map is generated for each patient. Clusters are identified in each map and a centroid per cluster is defined by averaging the UMAP coordinates. Fynally, the centroids maps from the 32 patients are assembled by means of the Procrustes method, that performs linear transformations for maximizing the fit between individual maps.

2 Results and discussion

The resulting UMAP loci for two distinct patients are depicted in Figure 1, where different colors distinguish distinct chest locations. In both charts, four clusters can be identified, namely, $\mathcal{C}_1 = \{Al, Ar\}$, $\mathcal{C}_2 = \{Pl, Pr\}$, $\mathcal{C}_3 = \{Ll, Lr\}$, $\mathcal{C}_4 = \{Tc\}$. Such pattern suggests that the recordings from left and right locations are similar when captured at the anterior (posterior)

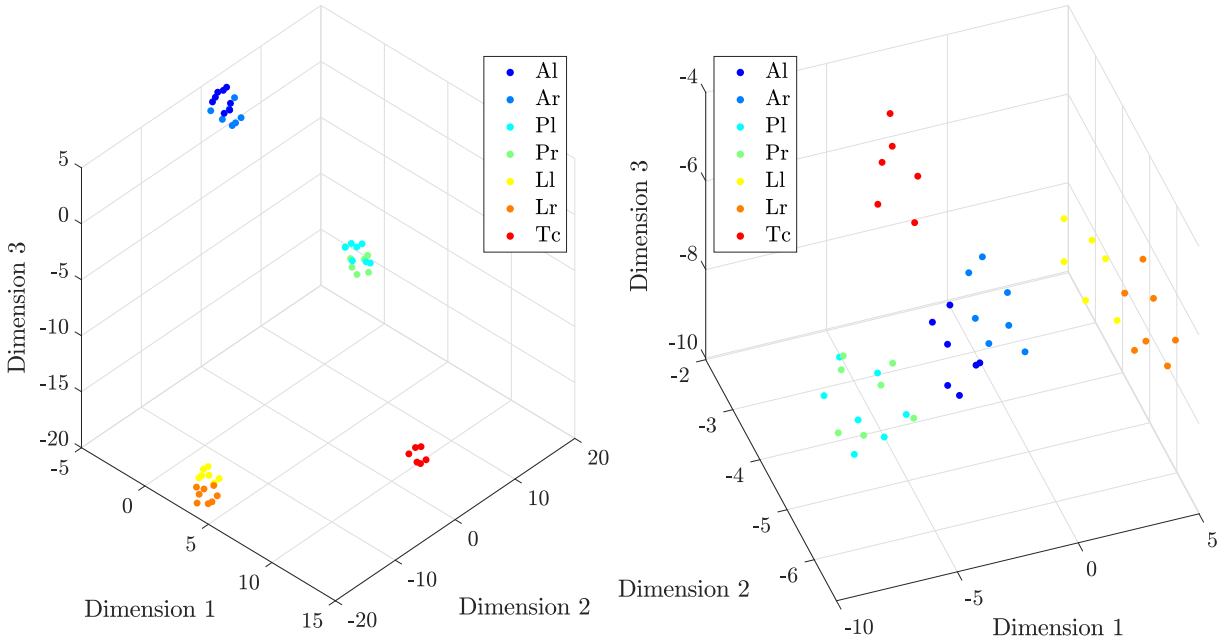

Figure 1: UMAP portraits corresponding to two distinct patients using d_{ij}^{Pe} distance.

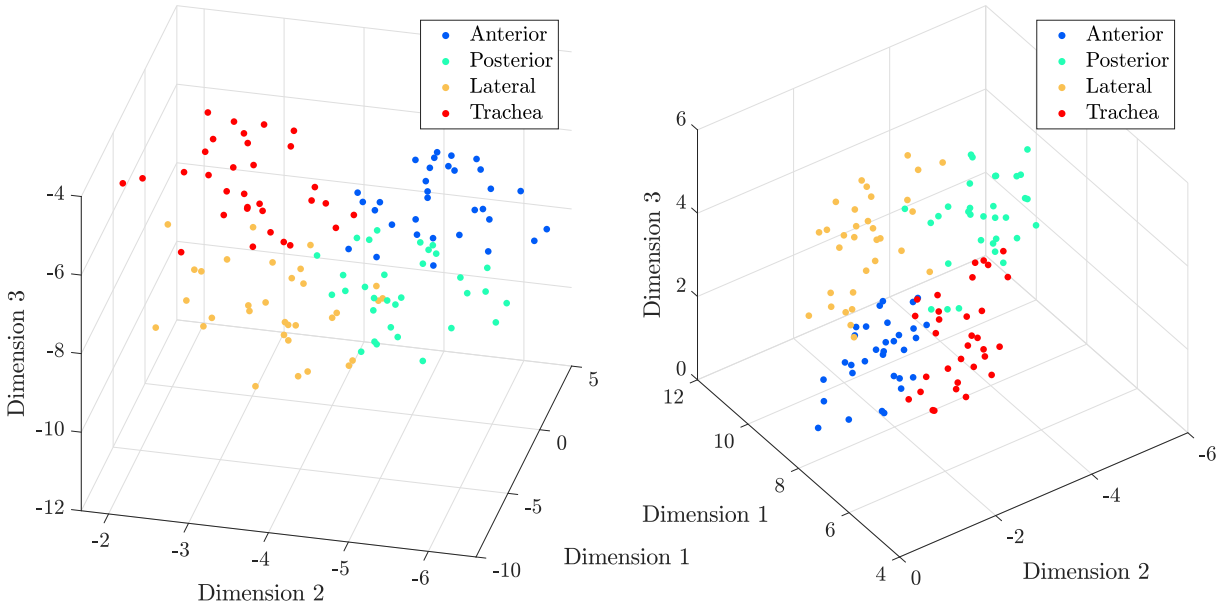

Figure 2: Assembled centroids from the 32 patients obtained by Procrustes for the d_{ij}^{Pe} (left) and d_{ij}^{Lo} (right) distances.

chest. On other hand, the trachea recordings exhibit strong dissimilarities with the rest of recordings. Bearing this in mind, each cluster $\mathcal{C}_i$, $i = 1, \ldots, 4$ can be described by single point, designated as the cluster centroid. In this manner, four centroids are estimated for each patient by means of the k-means algorithm. Figure 2 shows the centroids from all patients after Procrustes analysis for the d_{ij}^{Pe} (left) and d_{ij}^{Lo} (right) distances. Both charts evince that the centroids are organized according to the anterior, posterior, lateral and trachea recording locations. Although the distribution of points are somewhat affected by the distance, the pattern reflecting the chest location is preserved.

3 Conclusions and Future work

In this work the multichannel simultaneous recordings of pulmonary sounds are analyzed by extracting a set of short term features and three statistical moments of the resulting time series. The combined application of the UMAP algorithm and Procrustes method revealed that the features extracted from the respiratory signals are correlated with the recording locations on the chest. Such correlation is not sensitive to the side of the chest at which the auscultation is performed. Moreover, the trachea recordings present strong dissimilarities with the anterior, posterior and lateral positions, despite of being located at the anterior chest. These results supports the auscultation procedure of recording at different chest locations when looking for specific pulmonary sounds. Nonetheless, it seems that recording signals at both, left and right, sides of the chest does not add additional information with respect to the case in which single-sided analysis is performed. Further studies should be conducted to validate these results. Moreover, in this work, only COPD patients were considered. Thus, the effect of different pulmonary pathologies on the apparent non-sensitive of the quantitative information to the left or right recording positions must be validated.

References

[1] Forum of International Respiratory Societies. The global impact of respiratory disease. Third Edition. European Respiratory Society, 2021. Accessed 22 September, 2021. firsnet.org/images/publications/FIRS_Master_09202021.pdf.

[2] Leland McInnes, John Healy, and James Melville. UMAP: Uniform Manifold Approximation and Projection for Dimension Reduction. feb 2018.

[3] Bruno M Rocha, Dimitris Filos, Lu´Mendes, Gorkem Serbes, Sezer Ulukaya, Yasemin P Kahya, Nikša Jakovljevic, Tatjana L Turukalo, Ioannis M Vogiatzis, Eleni Perantoni, Evangelos Kaimakamis, Pantelis Natsiavas, Ana Oliveira, Cristina Jácome, Alda Marques, Nicos Maglaveras, Rui Pedro Paiva, Ioanna Chouvarda, and Paulo de Carvalho. An open access database for the evaluation of respiratory sound classification algorithms. *Physiological Measurement*, 40(3):35001, mar 2019.

[4] Malay Sarkar, Irappa Madabhavi, Narasimhalu Niranjan, and Megha Dogra. Auscultation of the respiratory system. *Annals of Thoracic Medicine*, 10(3):158–168, 2015.

[5] A. R.A. Sovijärvi, J. Vanderschoot, and J. E. Earis. Standardization of computerized respiratory sound analysis. *European Respiratory Review*, 10(77):585, 2000.

International Conference on Mathematical Analysis and Applications in Science and Engineering
ICMA^{2}SC'22
ISEP Porto-Portugal, June 27 - 29, 2022

Kurtosis vector for rotor detection in cardiac fibrillation

Juan Alzate-Marulanda[1] **Steven Giraldo-Mora**[1] **Catalina Tobón**[2]
Juan P. Ugarte[1⋆]

[1] Universidad de San Buenaventura, Colombia
[2] Universidad de Mededellín, Colombia

⋆juan.ugarte@usbmed.edu.co

Abstract: Atrial fibrillation (AF) is the most common arrhythmia in clinical practice. There is growing evidence supporting that AF is sustained by localized spiral propagating waves termed rotors. Thus, the rotor detection is a topic of interest for physicians in favor of a therapeutic strategy. In this work, the kurtosis for processing endocardial electrical recordings, known as electrograms (EGM), is assessed for characterizing the cardiac electrophysiological dynamics during AF. For this purpose, computational simulations are generated and virtual EGM are obtained according to a recording setup that resembles clinical procedures. Such setup represents a ring catheter with 10 recording electrodes. By exploiting the circular shape of the catheter structure, a kurtosis vector is estimated whose orientation lines up with the position of the rotor center. It can be evinced that the rotors can be spatially and temporally located through the kurtosis vector estimations made from EGM signals sequentially recorded. These results suggest that kurtosis can be used for characterizing rotors in a clinical scenario.

keywords: cardiac biophysics; signals processing; cardiac electrophysiology; rotors.

MSC2020: 49-XX; 34-XX; 92-XX.

1 Introduction

Atrial fibrillation (AF) is the most common supraventricular arrhythmia in clinical practice, affecting about 34 million individuals worldwide [4]. There is growing evidence supporting that the AF is sustained by localized sources, such as different types of reentries [5]. A rotor is a type of reentry, defined as a spiral wave propagating around a unexcitable core. Proper localization of rotors during AF episodes would allow more successful ablation strategies to revert the arrhythmia. Therefore, novel techniques for spotting rotors are part of an AF therapeutic research necessity that is currently unfolding. In the clinical context, rotors are detected using electrical recordings from the atrial endocardium, designated as electrograms (EGM). In addition to the analysis of the EGM time series, the adopted signal processing technique should also consider the spatial information given by the multiple EGM recording sites. The phase analysis is a well-accepted procedure for studying AF dynamics, through which propagation patterns, such as rotors, can be identified from phase singularities [2]. However, in practice, the high spatial resolution required for implementing such analysis imposes significant limitations. Thus,

there is an ongoing research effort oriented to unravel the information related with rotors from EGM features other than phase.

Bearing these ideas in mind, this work deals with the rotor detection problem by processing EGM signals using high order statistics. The statistical approach has been explored mainly by implementing entropy measures, on the basis of broader amplitude distributions are associated with irregular waveform signals [7]. Since information of the propagation dynamics is embedded on the EGM distribution, other statistics, such as kurtosis, have been proposed for localizing rotors. On this regard it has been reported that rotor detection through kurtosis yields an acceptable performance when using grid and star-shape EGM recording arrays [6]. In this study, kurtosis is assessed using a decapolar ring catheter for EGM recording, which is commonly used in clinical practice. For this purpose, simulated AF episodes are generated with distinct rotor dynamics. Moreover, the resulting kurtosis pattern outlined on the ring catheter is surveyed as a marker of the rotor core position.

1.1 Mathematical modeling and simulation of rotors

The mathematical formulation of the cardiac electrophysiology can be addressed through the two-dimensional monodomain model, which is described in terms of a reaction-diffusion equation with homogeneous Neumann boundary conditions [1]. The reactive term, that represents the membrane ionic kinetics of the cardiomyocyte, is estimated using the Fenton-Karma (FK) cardiomyocyte model [3]. The atrial tissue is modeled as a 2-dimensional rectangular domain $\Omega = \{(x,y)\,|(x,y) \in [0,L] \times [0,L]\}$, with $L = 4$ cm. The solution of the monodomain equation provides the membrane potential of each cell in Ω and it is numerically estimated using a finite difference scheme. The fibrillatory propagation is simulated by generating a rotor by implementing a S1-S2 cross-field stimulation protocol, as previously reported [7]. Three types of fibrillatory conduction with distinct propagation dynamics are simulated, namely, $\{F_1, F_2, F_3\}$, by configuring the FK model with the parameter sets 1, 4 and 6 from reference, respectively. Each resulting simulation has a duration of 12 s with time and spatial discretization steps of 10^{-2} ms and $4/149$ cm, respectively.

1.2 Virtual electrograms processing

Virtual EGM are obtained through a virtual electrode located at given point within Ω, where the extracellular potential is calculated by accounting the near and far field membrane potentials, with a sampling frequency of 1000 Hz [7]. A decapolar ring catheter with uniformly spaced electrodes, is used for defining the EGM recording points. Two catheter configurations are adopted, referred to as $\mathcal{Q}$ and $\mathcal{R}$, having diameters of 15 mm and 20 mm, respectively. Let us define a cartesian coordinate system in Ω with the origin located at the central point of the domain. Virtual EGM signals are sequentially recorded at the sets of points: $\mathcal{A} = \{a_1, \ldots, a_6|(0,0), (0.5\cos\theta_k, 0.5\sin\theta_k)\}$ and $\mathcal{B} = \{b_1, \ldots, b_6|(0,0), (\cos\theta_k, \sin\theta_k)\}$, where $\theta_k = 2\pi k/5$, $k = 0, \ldots, 4$, during 2 s at each position. It is noteworthy that the sets $\mathcal{A}$ and $\mathcal{B}$ include points belonging to a pair of concentric circumferences. In this manner, the motion of the catheter following two different trajectories is simulated. Taking into account the above description, let $\mathcal{S}^{(C,P)} = \{s_j^{(C,P)}, j = 1, \ldots, 10\}$ be the set of EGM signals recorded using the catheter configuration $C = \{\mathcal{Q}, \mathcal{R}\}$ along the trajectory $P = \{\mathcal{A}, \mathcal{B}\}$. The discrete signal $s_j^{(C,P)}(n)$, $n = 0, \ldots, N-1$, is quantitatively characterized using the kurtosis $\kappa_j^{(C,P)} = (1/N)\sum_{n=0}^{N-1}\left[\tilde{s}_j^{(C,P)}(n)\right]^4$, where $\tilde{s}_j^{(C,P)}(n)$ represents the standardized signal $s_j^{(C,P)}$ with zero mean and unit standard deviation. Thus, for a given catheter setup (C,P), the set of kurtosis values $\mathcal{K}^{(C,P)} = \{\kappa_j^{(C,P)}, j = 1, \ldots, 10\}$ is obtained. Additionally, the true location of

the rotor is pinpointed by implementing the phase singularity analysis, as reported in previous works [7].

2 Results and discussion

Figure 1A depicts the catheter $\mathcal{Q}$, from top to bottom, at the positions $\mathcal{A} = \{a_1, \ldots, a_6\}$, respectively, corresponding to fibrillatory simulation F_1. Each electrode is represented by a filled circle and different colors are related with the values of kurtosis normalized with respect to the maximum. It can be observed that low and high values of kurtosis gather on opposite sides of the ring catheter. This feature is used to define a kurtosis vector whose amplitude is proportional to the standard deviation of the 10 kurtosis values in the catheter and its direction is estimated as a weighted average of the angles described by all the line segments linking pairwise electrodes. The weights are determined by the pairwise kurtosis difference normalized to the sum of all pairwise kurtosis differences. Each map in Figure 1A shows the corresponding kurtosis vector depicted in blue color, where it can be seen that the vector direction indicates the kurtosis gradient from high to low values. The use of the kurtosis vector in the entire set of simulations and all catheter configurations is shown Figure 1B. Each plot shows the domain Ω where the yellow trace indicates the phase singularity. The singularity trajectories in F_1 and F_2 represent meandering and stable rotors, respectively, whereas, in F_2, the trajectory near the center corresponds to a relatively stable rotor and the remaining trajectories indicate other fibrillatory propagation patterns. Each plot portrays also the kurtosis vectors (depicted in blue color) of all catheter positions, where the red color circle pinpoints the center of the ring

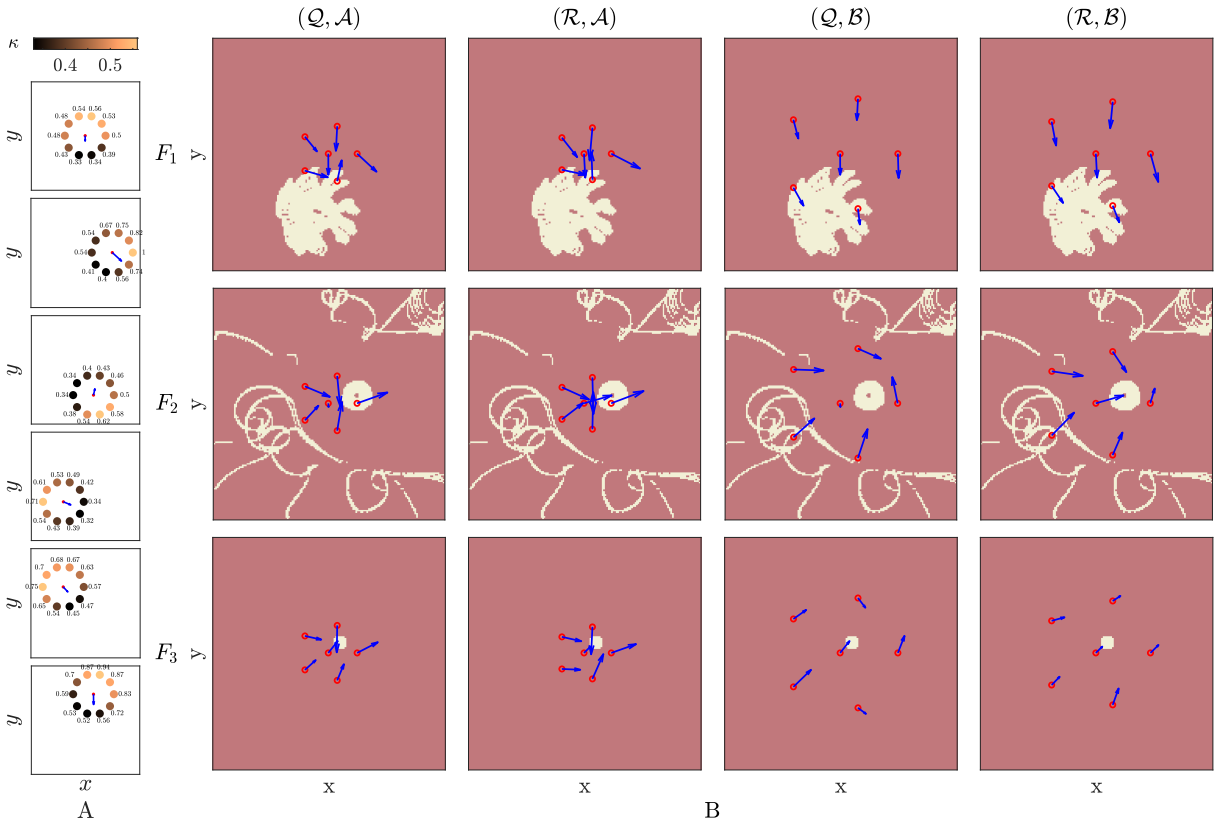

Figure 1: A. Kurtosis measures for catheter $\mathcal{Q}$ at the six positions in $\mathcal{A}$ depicted from top to bottom. B. Kurtosis vectors superposed to the maps of singularity trajectories for all fibrillation simulations.

catheter. One can observe that, kurtosis vectors points in direction of the rotor center location when the catheter motion defined by trajectory $\mathcal{A}$ is used, regardless the diameter of the ring catheter $(\mathcal{Q}, \mathcal{R})$. On the contrary, when the catheter moves along trajectory $\mathcal{B}$, which has a larger coverage field than $\mathcal{A}$, the kurtosis vectors evince difficulties in revealing the location of the rotor center. It is noteworthy that, the vectors observed in the simulation F_3 have the lowest magnitude among all vectors, indicating a decreased variability in the values of kurtosis along the catheter. Such behavior can be related to the fact that, F_3 contains a highly stable rotor and few or none EGM recording underlies the rotor center. These results suggest that the kurtosis vector, combined with the configuration of a ring catheter can provide information about the rotor dynamics during fibrillatory conduction.

3 Conclusions and future work

In this work, the kurtosis was assessed for processing EGM signals using AF computational models. The performed numerical experiments were conceived for resembling a clinical scenario, namely, distinct fibrillation dynamics, different configurations of a ring catheter for recording EGM and the sequential EGM recording by considering the motion of the catheter. Under such computational design, it was evinced that kurtosis can provide information about the rotor spatio-temporal dynamics by means of the kurtosis vector. Moreover, the kurtosis vector proved to be sensitive to the rotor stability. These results suggest that the proposed EGM kurtosis analysis can be useful in characterizing the fibrillation dynamics using an EGM recording setup commonly used in practice. Future studies should be conducted in order to further validate the proposed tool in 3D cardiac models and using EGM signals recorded from patients.

References

[1] R. H. Clayton, O. Bernus, E. M. Cherry, H. Dierckx, F. H. Fenton, L. Mirabella, a. V. Panfilov, F. B. Sachse, G. Seemann, and H. Zhang. Models of cardiac tissue electrophysiology: Progress, challenges and open questions. *Progress in Biophysics and Molecular Biology*, 104:22–48, 2011.

[2] Richard H. Clayton and Martyn P. Nash. Analysis of cardiac fibrillation using phase mapping. *Cardiac Electrophysiology Clinics*, 7(1):49–58, 2015.

[3] Flavio H. Fenton, Elizabeth M. Cherry, Harold M. Hastings, and Steven J. Evans. Multiple mechanisms of spiral wave breakup in a model of cardiac electrical activity. *Chaos*, 12:852–892, 2002.

[4] Jordi Heijman, Dominik Linz, and Ulrich Schotten. Dynamics of Atrial Fibrillation Mechanisms and Comorbidities. *Annual Review of Physiology*, 83:83–106, 2021.

[5] David E Krummen, Vijay Swarup, and Sanjiv M Narayan. The role of rotors in atrial fibrillation. *Journal of Thoracic Disease*, 7(2):142–151, feb 2015.

[6] Vasanth Ravikumar, Elizabeth Annoni, Preethy Parthiban, Sharon Zlochiver, Henri Roukoz, Siva K. Mulpuru, and Elena G. Tolkacheva. Novel mapping techniques for rotor core detection using simulated intracardiac electrograms. *Journal of Cardiovascular Electrophysiology*, 32(5):1268–1280, may 2021.

[7] Juan Ugarte, Catalina Tobón, and Andrés Orozco-Duque. Entropy Mapping Approach for Functional Reentry Detection in Atrial Fibrillation: An In-Silico Study. *Entropy*, 21(2):194, feb 2019.

International Conference on Mathematical Analysis and Applications in Science and Engineering
ICMA^{2}SC'22
ISEP Porto-Portugal, June 27 - 29, 2022

Symmetry reductions of a viscoelastic hyperbolic equation modelling biological processes

A. P. Márquez[1⋆] E. Recio[1] T. M. Garrido[1] M. L. Gandarias[1]

[1] Department of Mathematics, University of Cadiz, Spain

[1⋆]almudena.marquez@uca.es

Abstract: In this work, we consider a viscoelastic hyperbolic equation depending on nonlinear damping terms and nonlinear functions. The partial differential equation models the behaviour of viscoelasticity in physical processes such as viscoelastic fluids. Moreover, viscoelasticity and biology are closely related due to the fact that, for instance, living cells behave as a viscoelastic fluid. In addition, cellular mechanics and rheological properties are known to play an important role in biological processes, such as cell growth. The main aim of this study is to perform a Lie symmetry analysis of the viscoelastic hyperbolic equation. Afterwards, the optimal systems of one-dimensional subalgebras for each maximal Lie algebra are computed, by previously determining the commutator and adjoint relations. Then, symmetry reductions to ordinary differential equations are obtained using the one-dimensional subalgebras of the optimal systems.

keywords: Lie symmetries; optimal systems; symmetry reductions; viscoelastic equation.

MSC2020: 35B06; 35L25; 22E05.

1 Introduction

We study the nonlinear viscoelastic hyperbolic partial differential equation (PDE) with linear damping

$$u_{tt} - u_{xx} - w\, u_{txx} + f(u_t) + g(u) = 0, \tag{1}$$

where $w \geq 0$.

This model can also be considered removing one damping term ($w = 0$). In a previous paper [1], we considered the nonlinear viscoelastic wave equation

$$u_{tt} - u_{xx} + f(u_t) + g(u) = 0,$$

equal to equation (1), with $w = 0$, representing weak damping, but still presenting the damping term $f(u_t)$.

Several viscoelastic equations have been used to model biological processes. The mechanical behaviour of most biological processes is nonlinear viscoelastic rather than elastic. Therefore, there are many applications of nonlinear viscoelastic models. For instance, Freed and Rajagopal [2] studied numerical solutions of a viscoelastic equation describing the response of biological fibers. In general, viscoelastic behaviour has been observed and studied in several models of

biomechanics, e.g., describing the interaction with cells, skeletal muscle, bones, and ligaments [3].

Equation (1) has also been widely used as a model describing the behaviour of physical processes, such as viscoelastic fluids, processes of filtration through a porous media, fluids with temperature-dependent viscosity, etc. A particular case of equation (1) in a higher dimensional setting,

$$u_{tt} - \Delta u - w\,\Delta u_t + \mu u_t = |u^{p-2}|u, \tag{2}$$

with $\mu > 0$ and $p > 2$, is analysed by Guo and Liu [4], dealing with the lower bound for blow-up solutions to equation (2). The authors obtained as result a lower bound for blow-up time by establishing first-order differential inequality.

The present work is devoted to analysing the case of strong ($w > 0$) damping of equation (1), focusing on symmetries, optimal systems, and reductions.

2 Lie point symmetries

First of all, we perform a Lie symmetry analysis for equation (1). The theoretical basis are described in [5].

Lie point symmetries acting on the independent and dependent variables of the viscoelastic hyperbolic equation (1) are generated by vector fields

$$X = \tau(x,t,u)\partial_t + \xi(x,t,u)\partial_x + \eta(x,t,u)\partial_u. \tag{3}$$

The resulting transformation group, depending on the infinitesimal transformations $\tau(x,t,u)$, $\xi(x,t,u)$, $\eta(x,t,u)$, is a point symmetry if and only if

$$\mathrm{pr}^{(3)}X(u_{tt} - u_{xx} - w\,u_{txx} + f(u_t) + g(u))|_{\varepsilon} = 0, \tag{4}$$

where $\mathrm{pr}^{(3)}$ represents the third prolongation formula of the vector field (3) and ε the solution space of equation (1). The determining equation (4) splits with respect to derivatives of $u(x,t)$ leading to an overdetermined system of equations for the infinitesimals $\tau(x,t,u)$, $\xi(x,t,u)$, $\eta(x,t,u)$, together with $f(u_t)$ and $g(u)$, where $f(u_t)$ and $g(u)$ are not simultaneously linear functions.

As result, point symmetries are admitted by the viscoelastic hyperbolic equation (1), with $w > 0$ and $f(u_t)$, $g(u)$ not simultaneously linear functions, in the following cases:

1. For $f(u_t)$ and $g(u)$ arbitrary functions,

$$\begin{aligned} X_1 &= \partial_x, \\ X_2 &= \partial_t. \end{aligned}$$

2. For $f(u_t)$ arbitrary function and $g(u) = g_1 u + g_0$ linear function, with $g_1 > 0$ and g_0 arbitrary constants, in addition to X_1 and X_2,

$$\begin{aligned} X_3 &= e^{\sqrt{g_1}x}\,\partial_u, \\ X_4 &= e^{-\sqrt{g_1}x}\,\partial_u. \end{aligned}$$

3. For $f(u_t)$ arbitrary function and $g(u) = g_1 u + g_0$ linear function, with $g_1 < 0$ and g_0 arbitrary constants, in addition to X_1 and X_2,

$$\begin{aligned} X_5 &= sen(\sqrt{-g_1}x)\,\partial_u, \\ X_6 &= cos(\sqrt{-g_1}x)\,\partial_u. \end{aligned}$$

4. For $f(u_t)$ arbitrary function and $g(u) = g_0$ constant function, with $g_0 \neq 0$ arbitrary constant, in addition to X_1 and X_2,

$$\begin{aligned} X_7 &= x\,\partial_u, \\ X_8 &= \partial_u. \end{aligned}$$

In the above point symmetries, $g_1 \neq 0$.

3 Optimal systems and symmetry reductions

To determine non-equivalent solutions of equation (1) by action of the group, we calculate the one-dimensional optimal systems of subalgebras [5]. Hence, we obtain a classification of subalgebras, where each class contains equivalent solutions related through an element of the Lie symmetry group.

We construct the most general symmetry Lie algebra that PDE (1) admits, depending on functions $f(u_t)$ and $g(u)$, named the maximal Lie algebras. Then, we consider $\mathcal{L}$, a k-dimensional Lie algebra with basis constructed by generators X_k, $k = 1, \ldots, 8$. Next, we determine the commutation relations between each pair of elements in X_k, $k = 1, \ldots, 8$. This computation is done applying the well-known Lie bracket operator. Afterwards, we also determine the adjoint representations of each pair of elements in X_k, $k = 1, \ldots, 8$. This construction is done using the commutation relations obtained previously and summing the Lie series. Therefore, we state the subalgebras of the optimal systems.

Optimal systems of one-dimensional subalgebras for each maximal Lie algebra for equation (1), with $w > 0$ and $f(u_t)$, $g(u)$ not simultaneously linear functions, are given in the following cases:

1. For $f(u_t)$ and $g(u)$ arbitrary functions,

$$\{X_1, \lambda X_1 + X_2\}.$$

2. For $f(u_t)$ arbitrary function and $g(u) = g_1 u + g_0$ linear function, with $g_1 > 0$ and g_0 arbitrary constants,

$$\{X_1, X_3, X_4, \lambda X_1 + X_2, X_2 + X_3, X_2 + X_4, X_3 + X_4, X_2 + X_3 + X_4\}.$$

3. For $f(u_t)$ arbitrary function and $g(u) = g_1 u + g_0$ linear function, with $g_1 < 0$ and g_0 arbitrary constants,

$$\begin{aligned} \{X_1, X_5, X_6, \lambda X_1 + X_2, X_1 + X_5, X_1 + X_6, X_2 + X_5, X_2 + X_6, X_5 + X_6, \\ X_1 + X_2 + X_5, X_1 + X_2 + X_6, X_2 + X_5 + X_6\}. \end{aligned}$$

4. For $f(u_t)$ arbitrary function and $g(u) = g_0$ constant function, with $g_0 \neq 0$ arbitrary constant,

$$\begin{aligned} \{X_1, X_7, X_8, \lambda X_1 + X_2, X_1 + X_7, X_1 + X_8, X_2 + X_7, X_2 + X_8, X_7 + X_8, \\ X_1 + X_2 + X_7, X_1 + X_2 + X_8, X_2 + X_7 + X_8\}. \end{aligned}$$

In the above optimal systems, $g_1 \neq 0$ and λ are arbitrary constants.

Taking into account these optimal systems of one-dimensional subalgebras, we apply the method of characteristics to determine the invariants and reduced ODEs. The characteristic equations are defined by

$$\frac{dx}{\xi} = \frac{dt}{\tau} = \frac{du}{\eta}.$$

By solving these equations, the similarity variable and solution are obtained. Then, the substitution of these variables into the original PDE (1) yields the reduced ODEs.

As an example of the symmetry reductions, we present the travelling wave reduction. For $\lambda X_1 + X_2$, with $f(u_t)$ and $g(u)$ arbitrary functions, we obtain the invariants

$$z = x - \lambda t, \qquad u = h(z),$$

where $h(z)$ satisfies the equation

$$\lambda w h''' + (\lambda^2 - 1)h'' + f(-\lambda h') + g(h) = 0,$$

with λ an arbitrary constant.

4 Conclusions and Future work

In the present work we have found new results for the viscoelastic hyperbolic equation (1) for the strong damping case, with $w > 0$, modelling the behaviour of biological processes. The results are mainly related to symmetries, including optimal systems and symmetry reductions. Firstly, Lie point symmetries have been classified depending on functions $f(u_t)$ and $g(u)$. Then, we have constructed the maximal Lie algebras, and the commutator and adjoint relations. By using these actions and the point symmetries generators, we have constructed the optimal systems of one-dimensional subalgebras for each maximal Lie algebra. Finally, we have obtained the symmetry reductions to reduce the governing PDE to ODEs.

As future work, we will study conservation laws for the viscoelastic hyperbolic equation (1) for the strong damping case, with $w > 0$. In addition, to complete our previous paper of the weak damping case with $w = 0$, we will look for invariant conservation laws under translations and we will find new travelling wave solutions, by application of the recently proposed multi-reduction method.

Acknowledgments

The authors warmly acknowledge the financial support from the *Junta de Andalucía* FQM-201 group.

References

[1] A. P. Márquez, M. S. Bruzón, Lie point symmetries, traveling wave solutions and conservation laws of a non-linear viscoelastic wave equation, Mathematics, **9**(17) (2021), 2131.

[2] A. D. Freed, K. R. Rajagopal, A viscoelastic model for describing the response of biological fibers, Acta Mech., **227** (2016), 3367–3380.

[3] P. P. Provenzano, R. S. Lakes, D. T. Corre, R. Vanderby Jr., Application of nonlinear viscoelastic models to describe ligament behavior, Biomechan. Model. Mechanobiol., **1** (2002), 45–47.

[4] B. Guo, F. Liu, A lower bound for the blow-up time to a viscoelastic hyperbolic equation with nonlinear sources, Applied Mathematics Letters, **60** (2016), 115–119.

[5] P. J. Olver, *Applications of Lie groups to differential equations*. Springer: Verlag, 1986.

International Conference on Mathematical Analysis and Applications in Science and Engineering
ICMA^{2}SC'22
ISEP Porto-Portugal, June 27 - 29, 2022

Poisson stable dynamics of shunting inhibitory cellular neural networks

Marat Akhmet[1⋆] **Madina Tleubergenova**[2] **Akylbek Zhamanshin**[1,2]

[1] Middle East Technical University, Ankara, Turkey
[2] Aktobe Regional University, Aktobe, Kazakhstan

⋆marat@metu.edu.tr

Abstract: We consider shunting inhibitory cellular neural networks (SICNNS) with continuous time-varying rates and inputs. In the last decades, SICNNS have been extensively applied in robotics, speech, psychophysics, adaptive pattern recognition and image processing. In our study, the model is with compartmental passive decay rates, which consist of periodic and Poisson stable components. The first component guaranties the stability of the dynamics, while the second one causes irregular oscillations in the model [1]. The inputs are Poisson stable functions to take into account more sophisticated environment of the networks. To obtain the Poisson stable outputs, the rates and inputs are synchronized. Sufficient conditions for the existence of Poisson stable motions and their asymptotic properties are obtained. The efficient method has been developed to check the recurrence of the outputs [1, 2]. Discussions have been made to provide lights on relations of obtained results with practical and theoretical potentials of neuroscience. Numerical simulations show Poisson stable outputs as well as inputs. They are specific, since present the Poincare chaos. Technical parameters are suggested, which can be useful for the future applications of the results.

keywords: Shunting inhibitory cellular neural networks; compartmental passive decay rate; Poisson stable inputs, outputs and rates; Poincare chaos; asymptotic stability

MSC2020: 68T07; 34C15; 93D05.

References

[1] M. Akhmet, Domain Structured Dynamics: unpredictability, chaos, randomness, fractals, differential equations and neural networks, IOP Publishing, 2021.

[2] M. Akhmet, M. Tleubergenova, A. Zhamanshin, Modulo periodic Poisson stable solutions of quasilinear differential equations, Entropy, **23**(11) (2021) 1535.

International Conference on Mathematical Analysis and Applications in Science and Engineering
ICMA^{2}SC'22
ISEP Porto-Portugal, June 27 - 29, 2022

RAYLEIGH FUNCTION OF ENERGY DISSIPATION IN MODELLING OSCILLATORY BEHAVIOUR OF MOVING SISTER CHROMATIDS IN ANAPHASE OF MITOSIS

Andjelka N. Hedrih[1][1*] **Katica (Stevanović) Hedrih**[1][1,2] **Jasmina Bogdanovic-Jovanovic**[1][2]

[1] Department of Mechanics, Mathematical Institute of Serbian Academy of Science and Arts, Belgrade, Serbia
[2] University of Niš, Faculty of Mechanical Engineering, Niš, Serbia

[1*] handjelka@turing.mi.sanu.ac.rs; handjeka@hm.co.rs

Abstract: Cell division is in the basis of the regeneration processes. The special and very complex structure named the mitotic spindle ensures movements of chromosomes during mitosis. During some parts of this process chromosomes have to move through the cytoplasm that is considered a viscous fluid with a low Reynolds number. A mathematical model of the mitotic spindle based on the theory of oscillations is used to study chromosome movements during anaphase. A mitotic spindle is considered as a system of coupled oscillators. The assumptions of the model are given. To describe the forced oscillations of moving chromosomes in the metaphase plate in the cytoplasm as a viscous fluid with a low Reynolds number, Rayleigh function of energy dissipation and a system of coupled ordinary differential equations were used. We analyzed this oscillatory process through energy analysis of moving sister chromatids. Numerical analyses were done for masses of mouse chromosomes, for different parameters of the mitotic spindle.
The results show that the total energy of an oscillating pair of homologue chromosomes has an oscillatory character and is affected by the frequency of centrosome excitations and the spindle size. The obtained data could be of importance for understanding an asymmetric cell division and differentiating processes.

keywords: chromosomes movements; mitotic spindle; viscous fluid with a low Reynolds number; mathematical model; coupled oscillators, Rayleigh function of energy dissipation

MSC2020: 74-99, 70F35, 92C10, 74L10; 70Exx, 70KXX, 74M05, 37H20.

1 Introduction

There are specific patterns of chromosome movements during mitosis [1]. Their movements exhibit oscillatory properties [1, 2]. The age of centrosomes affects the stability of microtubules and the probability that centrosomes remain in the stem cell in asymmetric stem cell divisions [3].
The aim of this study is to explore how different oscillatory behaviors of centrosomes and different spindle sizes of metaphase plate affect the energy of pairs of homologue chromosomes in a system of mitotic spindle. The analyses were done in the scope of a mathematical model based on theory of oscillations [4] considering that sister chromatids are moving through the cytoplasm –a viscous fluid with a low Reynolds

number.

2 Results and discussion

For our numerical analysis we used a mathematical model, based on the theory of oscillations, which is explained in [4] in detail. Our model is based on dynamics of coupled systems that include the Rayleigh function of energy dissipation. According to this model, mitotic spindle is considered to be a system of coupled oscillators: each oscillator consists of:
- a homologue chromosome pair
- a pair of microtubules that are attached to homologue chromosomes and
- two centrosomes located on opposite poles of the cell.

Centrosomes are presented in the model as mass particles that represent two rheonomic centers of oscillations; microtubules are represented as standard light visco-elastic elements. Sister chromatids are represented as mass particles that are connected by a standard light massless elastic spring. Homologue chromosomes have equal masses and different chromosomes have different masses.

The resistance force resulting from the movement of chromosomes through the cytoplasm that is considered as a viscous fluid with a low Reynolds number is of the form: $F = \mu \dot{x}$.
The total Energy (Eq1) of each pair of sister chromatids is the sum of the kinetic (Eq2) and the potential (Eq3) energy modified for the energy dissipation that comes from the fluid resistance (Eq6).

$$E_{T,ik} = E_{k,ik} + E_{p,ip} \tag{1}$$

$$E_p = \frac{1}{2} c_{uik} x^2_{uik} + \frac{1}{2} c_{dik} x^2_{dik} + \frac{1}{2} c_{ik} [(y_{uO1} + y_{dO1}) + (x_{uik} \sin \alpha_{uik} + x_{dik} \sin \alpha_{dik})]^2 \tag{2}$$

$$\begin{aligned} \mathbf{E}_{K,ik} = {} & \frac{1}{2} m_{uik} \left[\left(\dot{x}_{uik} + \dot{y}_{uO1} \cos \alpha_{uik} \right)^2 + \left(\dot{y}_{uO1} \sin \alpha_{uik} \right)^2 \right] + \frac{1}{2} M_u \left(\dot{y}_{uO1} \right)^2 + \\ & + \frac{1}{2} m_{dik} \left[\left(\dot{x}_{dik} + \dot{y}_{dO2} \cos \alpha_{dik} \right)^2 + \left(\dot{y}_{dO2} \sin \alpha_{dik} \right)^2 \right] + \frac{1}{2} M_d \left(\dot{y}_{dO2} \right)^2 \end{aligned} \qquad i = 1, 2 \ldots 20 \tag{3}$$

As the influence of the fluid in which the system of mitotic spindle is immersed is expressed by a resistance force proportional to the velocity of each material particle (sister chromatids), the resulting fluid resistance forces of each of the material points are

$$F_{w,\mathrm{u}ik} = -m_{uik} \tilde{\mu} \sqrt{\left[\left(\dot{x}_{uik} + \dot{y}_{uO1} \cos \alpha_{uik} \right)^2 + \left(\dot{y}_{uO1} \sin \alpha_{uik} \right)^2 \right]} \tag{4}$$

$$F_{w,dik} = -m_{dik} \tilde{\mu} \sqrt{\left[\left(\dot{x}_{dik} + \dot{y}_{dO2} \cos \alpha_{dik} \right)^2 + \left(\dot{y}_{dO2} \sin \alpha_{dik} \right)^2 \right]} \tag{5}$$

For upper (Eq 4) and down (Eq 5) sister chromatid. Rayleigh function of total energy dissipation is:

$$\Phi_{ik}=\frac{1}{2}m_{gik}\mu\left[\left(\dot{x}_{uik}+\dot{y}_{uO1}\cos\alpha_{uik}\right)^2+\left(\dot{y}_{uO1}\sin\alpha_{uik}\right)^2\right]+\frac{1}{2}M_g\mu\left(\dot{y}_{gO1}\right)+$$
$$+\frac{1}{2}m_{dik}\mu\left[\left(\dot{x}_{dik}+\dot{y}_{dO2}\cos\alpha_{dik}\right)^2+\left(\dot{y}_{dO2}\sin\alpha_{dik}\right)^2\right]+\frac{1}{2}M_d\mu\left(\dot{y}_{dO1}\right)^2 \quad (6)$$

The Rayleigh function of the energy dissipation of the system is a measure of the decrease in the total energy of the system during the movement of the system. The system is non-conservative and the following theorem on the change of the total mechanical energy of the system is valid.

$$\frac{d\left(\mathbf{E}_{K,ik}+\mathbf{E}_{P,ik}\right)}{dt}=-2\Phi_{ik} \quad (7)$$

A system of ordinary differential equations that describes the oscillatory behavior of a single sister chromatid pair is:

$$\ddot{x}_{gik}+\left(\omega_{gik}^2+\bar{\omega}_{gik}^2\sin^2\alpha_{gik}\right)x_{gik}-\left(\bar{\omega}_{gik}^2\sin\alpha_{dik}\sin\alpha_{gik}\right)x_{dik}+\mu\dot{x}_{gik}=$$
$$=\left(\Omega_g^2h_{0,gik}-\bar{\omega}_{gik}^2\tilde{h}_{0,gik}\right)\cos\Omega_g t-\bar{\omega}_{gik}^2\tilde{\tilde{h}}_{0,gik}\cos\Omega_d t+\mu h_{0,gik}\Omega_g\cos\alpha_{uik}\sin\Omega_g t \quad (8)$$

$$\ddot{x}_{dik}+\left(\omega_{dik}^2+\bar{\omega}_{dik}^2\sin^2\alpha_{dik}\right)x_{dik}+\mu\dot{x}_{uik}-\left(\bar{\omega}_{dik}^2\sin\alpha_{gik}\sin\alpha_{dik}\right)x_{gik}=$$
$$=\left(\Omega_d^2h_{0,dik}+\bar{\omega}_{dik}^2\tilde{h}_{0,dik}\right)\cos\Omega_d t+\bar{\omega}_{dik}^2\tilde{\tilde{h}}_{0,dik}\cos\Omega_g t+\mu h_{0,dik}\Omega_d\cos\alpha_{dik}\sin\Omega_d t \quad (9)$$

Supposed particular solutions of Eq 8 and 9 are in the form:

$$x_{Pgik}=D_{gik}\cos\Omega_g t+\tilde{D}_{gik}\cos\Omega_d t+E_{gik}\sin\Omega_g t+\tilde{E}_{gik}\sin\Omega_d t \quad (10)$$

$$x_{Pdik}=D_{dik}\cos\Omega_g t+\tilde{D}_{dik}\cos\Omega_d t+E_{dik}\sin\Omega_g t+\tilde{E}_{dik}\sin\Omega_d t \quad (11)$$

3 Conclusions and Future work

Using the presented methodology, it is possible to numerically solve the cases when the sister chromatids are still connected, but also the case when their final separation occurs during anaphase II. In that case, each sister chromatid bound to the rheonomic center represents an oscillator with one degree of freedom of movement. The total oscillation energy of each sister chromatid is then expressed as a sum of kinetic energy, potential energy, and relation with the energy of the dissipation function Eq 7. In our further work, we will examine the change in the energy of movement of sister chromatids on the way to the centrosome/rheonomic center, assuming that the stiffness of microtubules/elastic springs increases by segments during shortening - moving towards the centrosome. Dalton et al [5] suggested "A gelation transition enables long-range microtubule transport causing the spindles to self-organize into two oppositely polarized microtubule gels" [5] as a possible explanation of chromosome dynamics during anaphase. In order to overcome the resistance force provided by fluid-cytoplasm, we are free to suggest that chromosomes and sister chromatids use relaxation oscillations as a possible mechanism of movements through the cytoplasm as a viscous fluid.

Acknowledgments

This work was supported by the Ministry of Education, Science and Technology Development of Republic of Serbia through the Mathematical Institute SANU, Belgrade,

Serbia. This paper is dedicated to Prof JA Tenreiro Machado, our dear friend and colleague who passed away in October 2021.

References

[1] Valentin Magidson, Christopher B. O'Connell, Jadranka Loncarek, Raja Paul, Alex Mogilner, and Alexey Khodjakov, The spatial arrangement of chromosomes during prometaphase facilitates spindle assembly, Cell, 146, (2011), 555–567.

[2] Ivan V. Maly, Systems biomechanics of centrosome positioning: A conserved complexity. Commun. Integr. Biol. 4, (2011), 230–235.

[3] Ivana Gasic, Purnima Nerurkar, and Patrick Meraldi, Centrosome age regulates kinetochore–microtubule stability and biases chromosome mis-segregation. Elife 4, (2015), 1–15.

[4] Andjelka Hedrih, Katica (Stevanovic) Hedrih, Relation between centrosome excitation and oscillatory energy of mitotic spindle in metaphase trough biomechanical oscillatory model of mitotic spindle, in: Antonov, I.., Serow, W.D. (Eds.), "Mathematics XXI Century & Natural Science". Envied Lecture. Book of Abstracts: IV International Seminar "Nonlinear henomenology Advances" (October 3−6, 2017); III International Wokshop "Scientific & Educational Problems of Belarusian Nuclear Power Plant. St. Petersburg: Publishing House of SPbPU., St. Petersburg, Russia, p. 27.

[5] Benjamin A. Dalton, David Oriola, Franziska Decker, Frank Jülicher and Jan Brugués, A gelation transition enables the self-organization of bipolar metaphase spindles. *Nat. Phys.*18**,** (2022), 323–331.

International Conference on Mathematical Analysis and Applications in Science and Engineering
ICMA^{2}SC'22
ISEP Porto-Portugal, June 27 - 29, 2022

MATHEMATICAL ANALYSIS OF TWO STRAIN EPIDEMIC MODEL WITH CROSSOVER BEHAVIOR

Aziz Khan[1,*], **Kamal Shah**[1,2], **Thabet Abdeljawad**[1,3*] **Manar A. Alqudah**[4]

[1]Department of Mathematics and Sciences, Prince Sultan University, P.O. Box 66833, 11586 Riyadh, Saudi Arabia
[2]Department of Mathematics, University of Malakand, Chakdara Dir(L), P.O.Box. 18000, Khyber Pakhtunkhwa, Pakistan
[3]Department of Medical Research, China Medical University, Taichung 40402, Taiwan
[4]Department of Mathematical Sciences, College of Science, Princess Nourah bint Abdulrahman University,Riyadh 11671, Saudi Arabia

[1*]akhan@psu.edu.sa

Abstract: The main objective of this article, to study qualitative theory of two strain epidemic model involving piecewise operator. Based on fixed pint theory to investigate existence results and unique solutions for the considered model. The numerical illustrations are established on a scheme developed with the help of Newton difference technique. A sudden changes we can see in many physical and natural phenomena. These characteristics have been found in the transmission of various infectious diseases, including the two-strain pandemic. As a result, the goal of this study is to use piecewise modeling to model the propagation of a two-strain pandemic. At the end numerical solutions are given for different fractional orders.

keywords: Two strain epidemic model; Piecewise operator; Fixed pint theory
Email addresses: kamalshah408@gmail.com,tabdeljawad@psu.edu.sa,maalqudah@pnu.edu.sa.

MSC2020: 26A33;34A08

International Conference on Mathematical Analysis and Applications in Science and Engineering
ICMA^{2}SC'22
ISEP Porto-Portugal, June 27 - July 1, 2022

Age-Structured HIV Model Incorporating Cell to Cell Transmission with Latently Infected T Cells

Manoj Kumar[1] **Syed Abbas**[1⋆]

[1] Indian Institute of Technology Mandi, India

[1⋆]abbas@iitmandi.ac.in

Abstract: The human immunodeficiency virus (HIV) can spread more efficiently when infected CD4+ T cells directly interact with uninfected T cells. This interaction forms virological synapses which lead to the cell to cell transmission of HIV. In this study we consider an age-structured HIV infection model with both virus to cell infection and cell to cell transmission. We also incorporate proportion of latently infected T cells. We derive steady state solutions to our model and also check the stability of steady states. Role of anti-retroviral therapy is also studied. Optimal treatment strategy is also discussed. To study the primary spread of virus, we solve our model numerically. Outcome of this work are new and complement the existing one.

keywords: Age-structured population model; HIV/AIDS model; Antiretroviral treatment.

MSC2010: 92D30; 35B35; 35q92; 35f61.

1 Introduction

Over the years, within host dynamics of HIV and antiretroviral therapy have attracted attention of many researchers. One of the first woks which describe the interaction between uninfected target cells, infected cells, and virus particles is done by Ho et al. [1] and Perelson et al. [2]. They considered a three dimensional ordinary differential equations based model to study the in host dynamics of HIV. It is often observed that the cell to cell transmission plays an important role in the spreading of HIV virus via formation of virological synapses. Also for some time period CD4+ T cells remain latently infected, so it is natural to consider HIV model with latently infected T cells [3]. There is enough literature available on age-structured HIV models which describe the in host dynamics of CD4+ T cells, for more details we refer to [4, 5].

When modeling the dynamics of infectious diseases, it is natural to divide the population into homogeneous subgroups. We consider an age-structured HIV model which describe the in host dynamics of HIV virus. Both virus to cell and cell to cell infection is considered. We show the existence of solution to our model by converting it into abstract framework. After deriving steady state solutions, we define a threshold parameter to our model. Global stability of infection free steady state is shown. Role of anti-retroviral therapy is also studied. For better visual illustration of our results, we solved our model numerically.

2 Results and Discussion

Existence and uniqueness of positive bounded solution is shown. We converted our problem into abstract form to show the existence and uniqueness of solution. Steady state solutions are derived to study the long term dynamics of solution. Stability of steady state solution is shown by constructing appropriate Lyapunov function. Effect of anti-retroviral therapy is also studied by incorporating an appropriate parameter for this. We numerically solve our model to study the primary spread of virus. Numerical simulation also validate our theoretical results.

3 Conclusions and Future work

It is important to consider both virus to cell infection and cell to cell transmission to study the dynamics of CD4+ T cells. Our theoretical results can help medical researchers and policy makers to take appropriate steps to reduce the harmful effects of HIV within human body. Also it is important to consider time since infection, that is, age-structured population models. Age-structured population models allow us to consider age dependent viral production kernel and mortality rate of latently infected and totally infected T cells. The results obtained are new and complement the existing one.

Some time it is necessary to consider random fluctuation in an age-structured population model for the in host dynamics of HIV. So, considering age-structured model with stochastic perturbation will be an interesting problem to study. Adding more compartments and comparing results with real time data will also be an interesting problem for future study.

References

[1] D.D. Ho, A.U. Neumann, A.S. Perelson, W. Chen, J.M. Leonard, M. Markowitz, *Rapid turnover of plasma virions and CD4+ lymphocytes in HIV-1 infection*. Nature 373 (1995) 123-126.

[2] A.S. Perelson, A.U. Neumann, M. Markowitz, J.M. Leonard, D.D. Ho, *HIV-1 dynamics in vivo: Virion clearance rate, infected cell life-span, and viral generation time*. Science 271 (1996) 1582-1586.

[3] M. Kumar, S. Abbas, *Global Dynamics of an Age-Structured Model for HIV Viral Dynamics with Latently Infected T Cells*. Math. Comput. Simulation, 2022 (Accepted).

[4] A. H. Abdel-Aty, M. M. Khater, H. Dutta, J. Bouslimi, M. Omri, Computational solutions of the HIV-1 infection of $CD4^+$ T-cells fractional mathematical model that causes acquired immunodeficiency syndrome (AIDS) with the effect of antiviral drug therapy. *Chaos Solitons Fractals* 139 (2020) 110092.

[5] A. Babaei, H. Jafari, M. Ahmadi, A fractional order HIV/AIDS model based on the effect of screening of unaware infectives. *Math. Methods Appl. Sci.* 42 (2019) 2334-2343.

IMPLEMENTATION STRATEGIES OF EVENT-BASED FRACTIONAL ORDER CONTROLLERS IN TARGETED DRUG DELIVERY APPLICATIONS

Isabela Birs[1⋆] **Cristina Muresan**[1]

[1] Automation Department, Technical University of Cluj-Napoca, Romania

[1⋆]Isabela.Birs@aut.utcluj.ro

Abstract: Targeted drug delivery is an emerging topic intensely studied in the biomedical field due to its multiple advantages in isolating and efficiently treating focus areas. Infallible and energy-efficient control strategies are required by this kind of processes. A possible solution for the process' requirements can be fractional order control that ensures a reliable closed loop behavior and its event based implementation that reduces energy consumption and computational effort. The current study presents two possibilities of implementing complex fractional order internal model control (FOIMC) strategies on a real life targeted drug delivery setup that mimics non-Newtonian blood characteristics. The velocity of a carrier submersible is controlled using the event-based FOIMC controller implemented using two novel implementation approaches. The first implementation strategy is based on separating the controller into an event-based integer order PID and a fractional order differintegral component. The second approach tackles the event-based FOIMC controller as a whole by using the Muir direct mapper to the discrete domain. Both implementation strategies are successfully validated on the biomedical process through reference tracking and disturbance rejection.

keywords: fractional calculus; targeted drug delivery; event-based control.

MSC2010: 26A33; 65R99; 65P99.

1 Introduction

Targeted drug delivery represents a state of the art biomedical solution to invasive medication treatments. The paradigm consists in isolating the area in need of treatment and applying substances exactly where they are needed. This leads to reduced side effects, lesser amounts of substances used, faster and more efficient treatment.

The present study combines the control needs of a carrier prototype with energy efficient solutions. The main tool in developing the control law is fractional calculus, a generalization of differentiation to any non-rational order, that brings multiple benefits in the fields of control engineering [1, 2]. Furthermore, the developed fractional order controller is implemented using event-based strategies for resource optimization purposes. However, the event-based implementation theory is lacking a fractional order generalization. Hence, two event-based implementation strategies are proposed to control the carrier prototype based on a FOIMC controller.

The novelty of this work lies in the fractional order event-based generalization as well as applying the obtained event-based controller to the targeted drug delivery process.

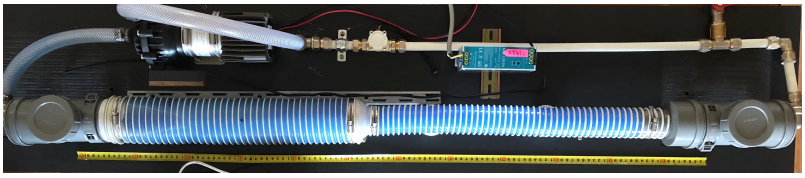

(a) Targeted drug delivery non-Newtonian environment

(b) Carrier prototype

Figure 1: Experimental setup

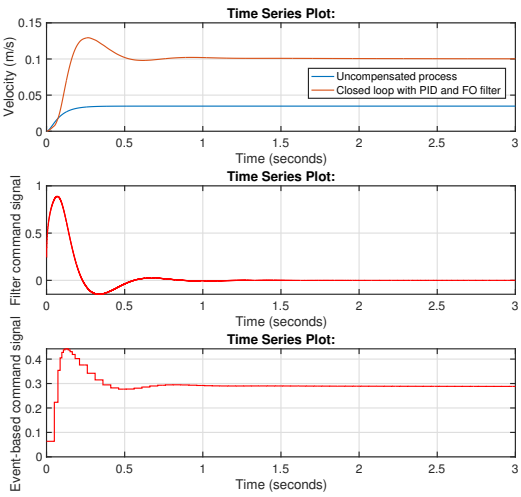

(a) Reference tracking

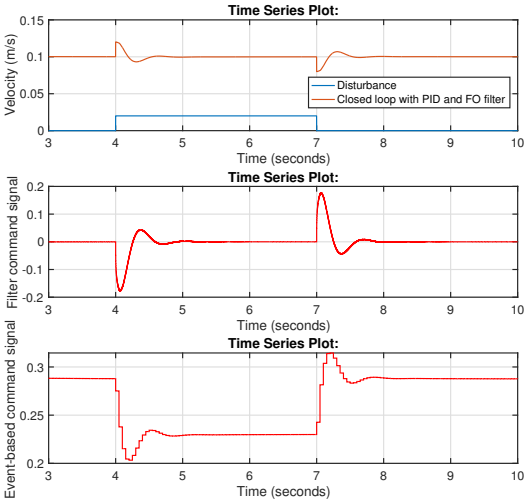

(b) Disturbance rejection

Figure 2: Validation of the PID and FO filter implementation approach

2 Results and discussion

The platform used for the development of the FOIMC control structure is presented in Fig. 1. The non-Newtonian environment features tubes of different diameters with steel insertions that expand and contract when a variable flow pump introduces non-Newtonian fluid into the pipes. The carrier prototype is able to transit the non-Newtonian environment using the propeller as the thrust unit. In a targeted drug delivery scenario, the carrier navigates to an area in need of treatment and releases a substance. The focus point of this study is controlling the velocity of the submersible in the two tubes. The robot's passing from the larger tube into the smaller one, or vice versa, represents a disturbance of the output velocity caused by the different flow rates.

An analytic model has been developed in [3] that connects the carrier's velocity to the PWM duty ratio engaging the propeller. An equivalent control structure featuring an FOIMC controller is computed for the velocity model as

$$H_c(s) = \frac{s^2 + 60.13s + 667.1}{232} \frac{1}{0.1013s^{1.2778}}. \tag{1}$$

The first implementation approach of the control structure involves separating the transfer function from (1) into a PID control of the form $k_p \left(1 + \frac{1}{T_i s} + T_d s\right)$ multiplied with a differintegral of the form $\frac{1}{s^\lambda}$. The FO component is implemented as a discrete transfer function using any viable discretization method, while the PID is implemented in its event-based form as presented by [4]. The implementation strategy is successfully validated in Fig. 2.

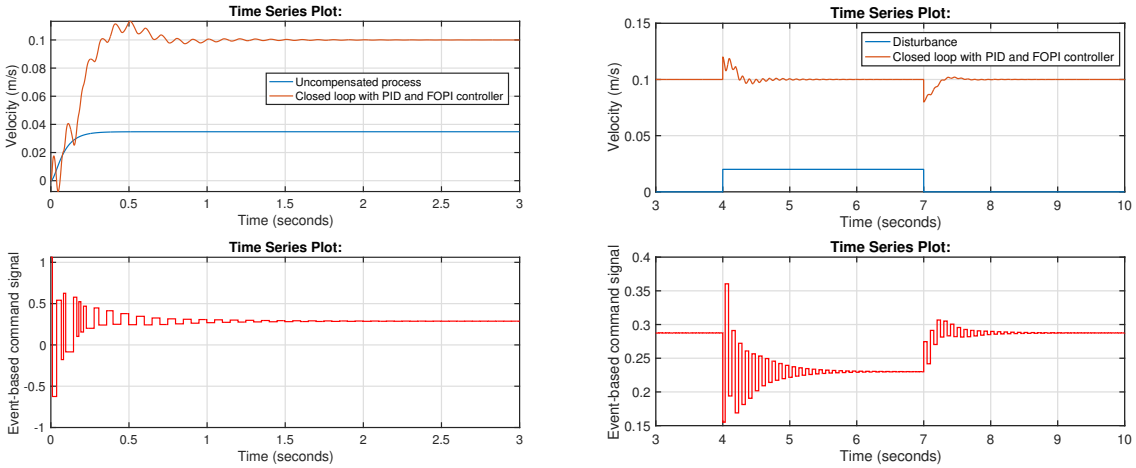

(a) Reference tracking

(b) Disturbance rejection

Figure 3: Validation of the event-based FOIMC implementation approach

The second approach involves separating the command computed by the equivalent structure into fractional order components: $\frac{k_p}{s^{0.2778}}$, $\frac{k_p}{T_i s^{1.2778}}$ and $k_p T_d s^{0.7222}$. Each differintegral is approximated to its discrete form using a direct discrete mapper based on the Muir formula. The implementation is a direct event-based fractional order control strategy. The validation of this method is presented in Fig. 3.

3 Conclusions and Future work

The papers presents a generalization of event-based controller implementations into the fractional order calculus field. Two approaches are proposed to control the velocity of a carrier prototype in a targeted drug delivery setting. Both strategies have been successfully validated through simulations, while future developments include their experimental validation.

Acknowledgments

This work was supported by a grant of the Romanian National Authority for Scientific Research and Innovation, CNCS/CCCDI-UEFISCDI, number PN-III-P1-1.1-TE-2016-1396, TE 65/2018.

References

[1] J. A. T. Machado, A. M. S. F. Galhao and J. J. Trujillo, *On development of fractional calculus during the last fifty years*, Scientometrics, Vol. 98, No. 577, 2014.

[2] W. Jifeng and L. Yuankai, *Frequency domain analysis and applications for fractional-order control systems*, Journal of Physics: Conference Series, Vol. 13, No. 1, 2005.

[3] I. Birs, C. Muresan, O. Prodan, S. Folea and C. M. Ionescu, Analytical modeling and preliminary fractional order velocity control of a small scale submersible, 2018 SICE International Symposium on Control Systems (SICE ISCS), pp. 157–162, Tokyo, 2018.

[4] J. Sanchez, A. Visioli and S. Dormido, Event-based PID control, *PID Control in the Third Millenium*, London: Springer, pp. 495–526, 2012.

International Conference on Mathematical Analysis and Applications in Science and Engineering
ICMA^{2}SC'22
ISEP Porto-Portugal, June 27 - 29, 2022

FRACTIONAL ORDER TUMOR GROWTH MODEL

Eva-H. Dulf[1,2*] **Levente Kovacs**[2] **Lucian Mocan**[3,4]

[3]

[1] Technical University of Cluj-Napoca, Romania
[2] ObudaUniversity, Hungary
[3] Iuliu Haţieganu University of Medicine and Pharmacy, Romania
[4] Regional Institute of Gastroenterology and Hepatology Cluj Napoca, Romania

[*]Eva.Dulf@aut.utcluj.ro

Abstract: Mathematical modelling of the tumor growth process is widely used to enhance quantitative understanding of biomedical phenomena. Recently, many investigators used fractional-order models for their proven efficiency in modelling biological phenomena. The present study compares two tumor growth models, defined from certain first-order ordinary differential equations with their fractional-order equivalents. The results highlight the advantages of fractional order differential equations. This study may provide clinicians with important insights on therapy strategies.

keywords: fractional order differential equation; tumor growth model; Bertalanffy-Pütter model

MSC2010: 26A##; 34A##; 93B##.

1 Introduction

Colorectal cancer ranks second in incidence among solid tumors in Europe (1499667 new cases in 2018) [1]. According to Eurostat official statistics for 2015, colorectal cancer was also responsible for 154 000 deaths in the EU-28, representing 11.7 % of all deaths from cancer. It is estimated that the market value for colon cancer therapies will reach as high as $11 billion by year 2025 [2] due to increase of branded therapies. Colorectal cancer represents one of the major health problems due to high incidence and mortality rates [1]. Diversity increase on treatment options as well as rising population need require novel prognostic tools. Longitudinal studies of tumor volume by mathematical growth models represent an important help in such prognostic.
Historically, the systematic application of mathematical models for tumor growth has begun in the 1960s [2]. In the meantime, many different approaches were developed. The Bertalanffy-Pütter model [3] unifies theme. It uses five parameters, amongst them two

exponents related to tumor metabolism and morphology [4]. On the other hand, fractional order models are characterized by a 'memory' property, which brings additional information to analyze the systems' dynamical behaviors, being very useful in describing biological processes [5]. In the last years a trend has been observed in the research community in employing tools from fractional calculus for use in modeling complex phenomena. However, only recently the usefulness of this tool has been recognized for analysis of complex systems in medicine [6, 7]. Since the classical mathematical models are special cases of the fractional order mathematical models, it implies that the results for the fractional mathematical model are more general and more accurate.
The goal of this paper is on longitudinal studies of tumor volume, which use tumor growth curves that are defined from fractional order differential equations. The authors investigate the advantages and disadvantages introduced by the fractional order model in the classical Bertalanffy-Pütter model and the differences in the prognosis.
The paper is structured in three parts. After this introductory part, section 2 discusses the obtained results. The work ends with concluding remarks.

2 Results and discussion

The classical Bertalanffy-Pütter model describes tumor volume v(t) in mm3 over time t in days, using five model parameters that are to be determined from fitting the model to size-at-age data [4]:

$$\frac{dv(t)}{dt} = p \cdot v(t)^a - q \cdot v(t)^b$$

Four parameters are displayed in the equations, namely the non-negative exponent-pair a < b and the constants p and q. A fifth parameter is the initial tumor volume at the start of monitoring, i.e. $v(0) = v_0 > 0$.
Introducing the fractional order derivative, we obtain a generalization of the model, additional information to analyze the systems' dynamical behavior.
There exist several definitions of fractional order derivative (or integral) [8]. One of theme is the Riemann–Liouville definition, which states that a fractional order integral of order $\mathcal{R}(\alpha) > 0$ is a natural consequence of Cauchy's formula for repeated integrals. The fractional-order derivative of order $\alpha \in$ R+ can be also defined using the Riemann–Liouville formula. Due to its importance in applications, it must be also enumerated the Grünwald–Letnikov's definition of the fractional-order derivative, based on the generalization of the backward difference.
In accordance with the above-described arguments, it is proposed the fractional order model

$$\frac{dv^{\alpha}(t)}{dt} = p \cdot v(t)^a - q \cdot v(t)^b$$

We aim at comparing the findings of [4] and we therefore use the data of that paper, which are originated of [9]. The simulation results obtained with these model exhibit different behaviors for different values of fractional order. Comparing the results with the classical model, are obvious the advantages. As examples are presented two data approximations, comparing the integer order models with the fractional order models, Figure 1 and Figure 2. For the first dataset the integer model is:

$$\frac{dv(t)}{dt} = 0.08 \cdot v(t)^{1.2} - 0.02 \cdot v(t)^{1.9} \quad (1)$$

for the treated case and

$$\frac{dv(t)}{dt} = 0.123 \cdot v(t)^{1.8} - 0.035 \cdot v(t)^{2.3} \quad (2)$$

for the control case, resulting a cumulative mean squared error of 0.5532 and 5.8569 respectively. The corresponding fractional order models implies a fractional order of 0.96. With these models the cumulative mean squared errors become 0.1079 and 0.4268.
For the second dataset the models are:

$$\frac{dv(t)}{dt} = 0.17 \cdot v(t)^{1.05} - 0.06 \cdot v(t)^{1.7} \quad (3)$$

and

$$\frac{dv(t)}{dt} = 0.188 \cdot v(t)^{0.75} - 0.01 \cdot v(t)^{0.69} \quad (4)$$

with cumulative mean squared errors 1.2142 and 1.6074. The corresponding fractional order models, with fractional order 0.96 leads to mean squared errors 0.2785 and 0.5601.

The advantage of the fractional order is obvious. The disadvantage of the models consists in the more complex calculus, which is not a major issue in today's computational power.

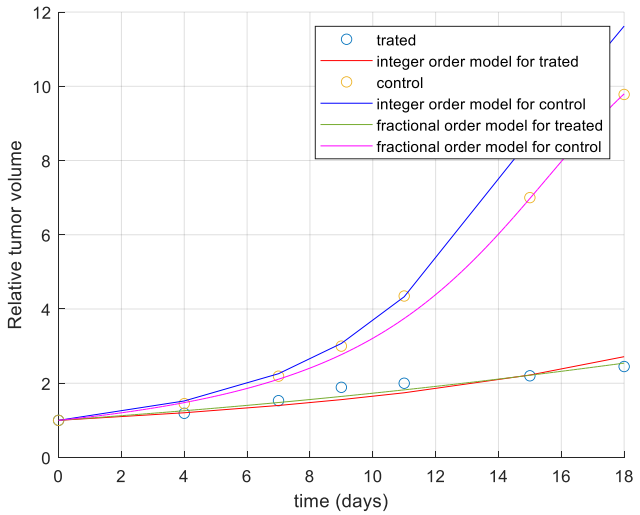

Figure 1. Comparison of results between integer order models and fractional order models, first dataset

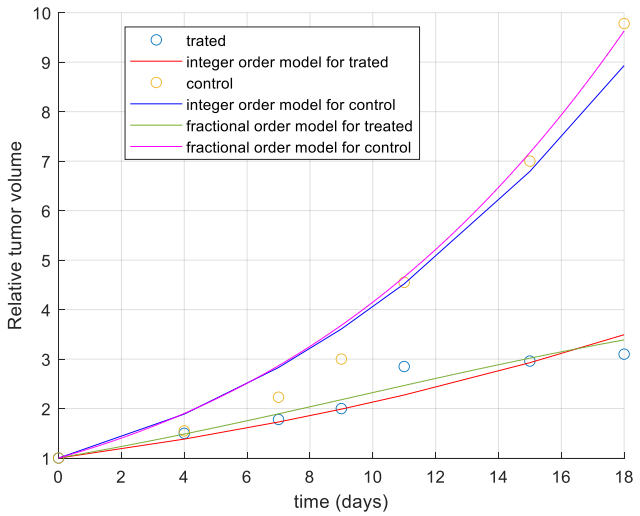

Figure 2. Comparison of results between integer order models and fractional order models, second dataset

3 Conclusions and Future work

The paper showed that the proposed fractional order models are able to better predict the treatment outcome than the integer order models. The provided models can be used for a more accurate prognosis. However, there is a large statistical uncertainty of the result due to the data used. Therefore, a future clinical study with a large number of patients is needed to confirm the findings. Future work is also needed to establish proper rules for the optimal fractional order for any dataset.

Acknowledgments

This research was funded by a grant of the Romanian Ministry of Research and Innovation, CCCDI – UEFISCDI, project number PN-III-P2-2.1-PED-2019-0844 (323PED/2020), PN-III-P2-2.1-PED-2019-2536 (557PED / 2020) and PN-III-P2-2.1-PED-2019-1660 (387PED2020).

References

[1] World Healt Organization, http://gco.iarc.fr/today accessed September 2019.
[2] M. Schwartz, A biomathematical approach to clinical tumor growth, *Cancer*. 14 (1961), 1272–1294.
[3] H.H/ Diebner, T. Zerjatke, M. Griehl, I. Roeder, Metabolism is the tie: The Bertalanffy-type cancer growth model as common denominator of various modelling approaches. *Biosystems* 167 (2018), 1–23.
[4] Manfred Kühleitner, Norbert Brunner, Werner-Georg Nowak, Katharina Renner-Martin, Klaus Scheicher, Best fitting tumor growth models of the von Bertalanffy-PütterType, *BMC Cancer*, 19 (2019), 683.
[5] Carla M. A. Pinto, Ana R. M. Carvalho, Dumitru Baleanu, Hari M. Srivastava, Efficacy of the Post-Exposure Prophylaxis and of the HIV Latent Reservoir in HIV Infection, *Mathematics*, 7(6), (2019, 515; https://doi.org/10.3390/math7060515
[6] Carla M.A. Pinto, J.A. Tenreiro Machado, Fractional model for malaria transmission under control strategies, Computers & Mathematics with Applications, **66**(5) (2013), 908–916.
[7] Joseph Páez Chávez, Burcu Gürbüz, Carla M.A. Pinto, The effect of aggressive chemother- apy in a model for HIV/AIDS-cancer dynamics, Communications in Nonlinear Science and Numerical Simulation, **75** (2019), 109–120.
[8] C. A. Monje, Y.Q. Chen, B. M. Vinagre, D. Xue, V. Feliu, *Fractional-order Systems and Controls*, DOI 10.1007/978-1-84996-335-0, Springer Verlag, (2010).
[9] H. Murphy, H. Jaafari, H.M. Dobrovolny, Differences in predictions of ODE models of tumor growth: a cautionary example, *BMC Cancer*, 6 (2016), 163–172. DOI https://doi.org/10.1186/s12885-016-2164-x.

International Conference on Mathematical Analysis and Applications in Science and Engineering
ICMA^{2}SC'22
ISEP Porto-Portugal, June 27 - 29, 2022

LIPSCHITZ STABILITY ANALYSIS OF IMPULSIVE DELAYED REACTION-DIFFUSION FRACTIONAL NEURAL NETWORK MODELS

Ivanka Stamova[1⋆] **Trayan Stamov**[2] **Gani Stamov**[1]

[1] University of Texas at San Antonio, USA
[2] Technical University of Sofia, Bulgaria

[1⋆]ivanka.stamova@utsa.edu

Abstract: In this paper the concept of Lipschitz stability is introduced to impulsive delayed reaction-diffusion neural network models of fractional order. Lipschitz stability analysis is performed and sufficient conditions for global uniform Lipschitz stability of the model are established. The introduced concept is also very useful in numerous inverse problems.

keywords: Lipschitz stability; reaction-diffusion neural networks; fractional; delays; impulses.

MSC2020: 26A33; 34A37; 34K20; 34K45; 34K60.

1 Introduction

During the last decades, the interest of researchers in fractional differential equations has been rapidly increasing and such equations are applied as modeling tools in engineering, physics, biology [1, 2, 7, 9].

A class of neural networks with reaction-diffusion terms is know to be very applicable in modeling of processes studied in epidemiology and virology [5], including fractional-order generalizations [8]. The extended reaction-diffusion neural networks of the Cohen–Grossberg type are also very well studied [4]. However, fractional generalizations of such models are not yet investigated.

In addition, results on impulsive Cohen–Grossberg reaction-diffusion neural networks of integer order are also reported in the literature [6]. However, the influence of impulsive factors to the qualitative behavior of fractional-order Cohen–Grossberg and reaction-diffusion neural network models has not been previously considered.

The extended concept of Lipschitz stability introduced in [3] is also applicable to fractional-order models [10]. However, the concept is not yet applied to fractional reaction-diffusion neural network models of Cohen–Grossberg type and this is the main goal of this paper.

2 Results and discussion

For $\mathcal{U}(t,x) = (\mathcal{U}_1(t,x),\mathcal{U}_2(t,x),\ldots,\mathcal{U}_m(t,x))^T \in \mathbb{R}^m$, $t \in \mathbb{R}_+$, $x \in \Omega$, Ω denotes an open and bounded set in $\mathbb{R}^n$ with smooth boundary $\partial\Omega$ and the measure expressed by mes$\Omega > 0$, $\mathbf{0} = (0,0,\ldots,0)^T \in \Omega$, we consider the norm $||\mathcal{U}(t,x)||_2 = \left[\int_\Omega \sum_{i=1}^m \mathcal{U}_i^2(t,x)dx\right]^{1/2}$.

Let $u \in C^1[\mathbb{R}_+ \times \Omega, \mathbb{R}]$. The time Caputo-type fractional derivative of order α, $0 < \alpha < 1$ with the lower limit 0 of the function u is defined by [7]

$$\frac{\partial^\alpha u(t,x)}{\partial t^\alpha} = \frac{1}{\Gamma(1-\alpha)}\int_0^t \frac{\partial u(s,x)}{\partial s}\frac{ds}{(t-s)^\alpha},\ t > 0,$$

where Γ is the Gamma function.

For $0 < t_1 < t_2 < \ldots$ and $\lim_{k\to\infty} t_k = \infty$ we consider the impulsive n-dimensional fractional-order delayed reaction-diffusion neural network model of Cohen–Grossberg type

$$\begin{cases} \dfrac{\partial^\alpha \mathcal{U}_i(t,x)}{\partial t^\alpha} = \displaystyle\sum_{q=1}^n \frac{\partial}{\partial x_q}\left(D_{iq}\frac{\partial \mathcal{U}_i(t,x)}{\partial x_q}\right) - a_i(\mathcal{U}_i(t,x))\Big[b_i(\mathcal{U}_i(t,x)) \\ \qquad\qquad - \displaystyle\sum_{j=1}^m c_{ij}(t)f_j\big(\mathcal{U}_j(t,x)\big) - \sum_{j=1}^m w_{ij}(t)g_j\big(\mathcal{U}_j(t-\tau_j(t),x)\big)\Big],\quad t \neq t_k, \\ \mathcal{U}_i(t_k^+,x) - \mathcal{U}_i(t_k,x) = J_{ik}(\mathcal{U}_i(t_k,x)), \end{cases} \tag{1}$$

where $i = 1,2,\ldots,m$, $m \geq 2$, $k = 1,2,\ldots$, $t > 0$, $x = (x_1,x_2,\ldots,x_n)^T \in \Omega$, $\mathcal{U}_i(t,x)$ denotes the state of the i-th neural unit at time t and in space x, the transmission time-varying delay $\tau_j(t)$ satisfies $\tau_j \in C[\mathbb{R},\mathbb{R}_+]$, $t > \tau_j$, $j = 1,\ldots,m$, $0 \leq \tau_j(t) \leq \tau$, the amplification functions $a_i \in C[\mathbb{R}\times\mathbb{R}^n,\mathbb{R}_+], = 1,2,\ldots,m$, is an amplification functions, $b_i \in C[\mathbb{R}\times\mathbb{R}^n,\mathbb{R}]$ is an appropriately behaved function, $i = 1,2,\ldots,m$, $c_{ij}(t)$ and $w_{ij}(t)$ are, respectively, the connection weight and time-varying delay connection weight matrices of j-th neuron on the i-th neuron, $c_{ij} \in C[\mathbb{R},\mathbb{R}]$, $w_{ij} \in C[\mathbb{R},\mathbb{R}]$, the activation functions $f_j, g_j \in C[\mathbb{R},\mathbb{R}]$, $i,j = 1,\ldots,m$, $D_{ik} = D_{iq}(t,x) \geq 0$ are the transmission diffusion coefficients along the i-th neuron, $q = 1,2,\ldots,n$, $J_{ik}(\mathcal{U}_i(t,x))$ are the impulsive functions.

Consider an initial function $\varphi_0 = (\varphi_{01},\varphi_{02},\ldots,\varphi_{0m})^T$, $\varphi_{0i} = \varphi_{0i}(\xi,x)$, $i = 1,2,\ldots,m$ defined on $[-\tau,0]\times\Omega$, which is piecewise continuous with respect to ξ. The set of all such functions will be denoted as $\mathcal{PC} = PC[[-\tau,0]\times\Omega,\mathbb{R}^m]$. The norm in the space $\mathcal{PC}$ will be defined as $|\varphi|_\tau = \sup||\varphi(\xi,x))||_2$, $(\xi,x) \in [-\tau,0]\times\Omega$.

The following assumptions will be used in our investigations:

A1. The functions a_i, $i = 1,2,\ldots,m$, are continuous on $\mathbb{R}$ and there exist positive constants $\underline{a}_i$ and $\overline{a}_i$ such that $\underline{a}_i \leq a_i(\chi) \leq \overline{a}_i$ for $\chi \in \mathbb{R}$, $i = 1,2,\ldots,m$.

A2. The functions b_i, $i = 1,2,\ldots,m$, are continuous, there exist continuous functions $B_i(t) > 0$, $t \in \mathbb{R}_+$, such that

$$b_i(\chi) \geq B_i(t)\chi,\ t \in \mathbb{R}_+$$

for $\chi \in \mathbb{R}$, and $\underline{B}_i = \inf_{t\in\mathbb{R}_+} B_i(t)$, $i = 1,2,\ldots,m$.

A3. The functions c_{ij}, w_{ij} $i,j = 1,2,\ldots,m$ are continuous on $\mathbb{R}_+$ and $\overline{c}_{ij} = \sup_{t\in\mathbb{R}_+} c_{ij}(t)$, $\overline{w}_{ij} = \sup_{t\in\mathbb{R}_+} w_{ij}(t)$.

A4. There exist positive constants L_j, M_j, $j = 1,2,\ldots,m$, with

$$|f_j(\chi_1) - f_j(\chi_2)| \leq L_j|\chi_1 - \chi_2|,\ |g_j(\chi_1) - g_j(\chi_2)| \leq M_j|\chi_1 - \chi_2|$$

for all $\chi_1,\chi_2 \in \mathbb{R}$, $\chi_1 \neq \chi_2$, and $f_j(0) = g_j(0) = 0$, $j = 1,2,\ldots,m$.

A5. The impulsive functions J_{ik} are continuous on $\mathbb{R}$ and $J_{ik}(0) = 0$ for all $i = 1, 2, \ldots, m$, $k = 1, 2, \ldots$.

A6. There exist constants $d_{iq} \geq 0$ such that $D_{iq}(t, x) \geq d_{iq}$ for $(t, x) \in \mathbb{R}_+ \times \Omega$, $i = 1, 2, \ldots, m$, $q = 1, 2, \ldots, n$.

We will adopt a Lipschitz stability definition given in [3] to the impulsive fractional-order neural network model (1).

Definition 1 *The fractional neural network reaction-diffusion model (1) of Cohen–Grossberg type is said to be globally uniformly Lipschitz stable, if there exists a positive constant $M > 0$ such that for any initial function $\varphi_0 \in \mathcal{PC} : \ ||\varphi_\prime||_\tau < \infty$ we have $||\mathcal{U}(t, x; 0, \varphi_0)||_2 \leq M||\varphi_0||_\tau$, $t \geq 0$, $x \in \Omega$.*

Consider the following comparison fractional-order impulsive equation

$$\frac{d^\alpha l(t)}{dt^\alpha} = g(t, l), \ t \neq t_k, \ \Delta l(t_k) = l(t_k^+) - l(t_k^-) = P_k(l(t_k)), \ t_k > 0, \tag{2}$$

where $g : \ \mathbb{R}_+ \times \mathbb{R}_+ \to \mathbb{R}$, $P_k : \ \mathbb{R}_+ \to \mathbb{R}_+$, $k = 1, 2, \ldots$.

The main results in our research are the following theorems.

Theorem 1 *Assume that Assumptions A1–A6 are fulfilled, and:*

1. The set $\Omega = \{x = (x_1, x_2, ..., x_n)^T : \ a_q \leq |x_q| \leq b_q\}$, where a_q, b_q $(q = 1, 2, \ldots, n)$ are positive constants, $\Lambda = \max\{b_q - a_q\}$ and $\overline{D}_i = \sum_{q=1}^n \frac{12 d_{iq}}{\Lambda^2}$, $i = 1, 2, \ldots, m$.

2. There exists a continuous for $t \in (t_{k-1}, t_k]$ function $\bar{g}(t)$, $k = 1, 2, \ldots$, that satisfies

$$\min_{1 \leq i \leq m} \left(2(\underline{a}_i \underline{B}_i + \overline{D}_i) - \sum_{j=1}^m (\overline{a}_i L_j |\overline{c}_{ij}| + \overline{a}_i M_j |\overline{w}_{ij}| + \overline{a}_j L_i |\overline{c}_{ji}|) \right) - \max_{1 \leq i \leq m} \left(M_i \sum_{j=1}^m \overline{a}_j |\overline{w}_{ji}| \right) > \bar{g}(t).$$

3. The impulsive functions J_{ik} are such that $J_{ik}(\mathcal{U}_i(t_k, x)) = -\gamma_{ik} \mathcal{U}_i(t_k, x), \ 0 < \gamma_{ik} < 2, \ i = 1, 2, \ldots, m, \ k = 1, 2, \ldots$.

4. The zero solution of equation (2) with $g(t, l) = \bar{g}(t) l$, $t, l \in \mathbb{R}_+$ and $P_k = 0$, $k = 1, 2, \ldots$, is globally uniformly Lipschitz stable.

Then the impulsive fractional reaction-diffusion neural network (1) of the Cohen–Grossberg type is globally uniformly Lipschitz stable.

Theorem 2 *If in Theorem 1 we let $\bar{g}(t) = 0$ for $t \in \mathbb{R}_+$, then the fractional impulsive reaction-diffusion neural network (1) of Cohen–Grossberg type is globally uniformly Lipschitz stable.*

Theorem 3 *Assume that:*

1. Assumptions A1–A6 and conditions 1 and 3 of Theorem 1 are fulfilled.

2. For $\underline{a} = \min_{1 \leq i \leq m} \underline{a}_i$, $\overline{a} = \max_{1 \leq i \leq m} \overline{a}_i$, we have $|1 - \gamma_{ik}| \leq \frac{a}{\overline{a}}$, $i = 1, 2, \ldots, m$, $k = 1, 2, \ldots$.

3. The model's parameters satisfy $\min_{1 \leq i \leq m} \left(\frac{\overline{D}_i}{\underline{a}} + \underline{B}_i - L_i \sum_{j=1}^m |\overline{c}_{ji}| \right) > \frac{\overline{a}}{\underline{a}} \max_{1 \leq i \leq m} \left(M_i \sum_{j=1}^m |\overline{w}_{ji}| \right)$.

Then the impulsive fractional reaction-diffusion neural network (1) of the Cohen–Grossberg type is globally uniformly Lipschitz stable.

3 Conclusions and Future work

In this paper, an impulsive reaction-diffusion neural network model of Cohen–Grossberg type is extended to the fractional-order case. The notion of Lipschitz stability is introduced to the model and criteria for global uniform Lipschitz stability are established. One of the directions for future research on the topic is related to the study of the effects of variable impulsive perturbations on the Lipschitz stability behavior and refinement of stabilization strategies.

Acknowledgments

We wish to acknowledge the support of the Department of Mathematics at the University of Texas at San Antonio, USA.

References

[1] D. Baleanu, J.A. Tenreiro Machado, A.C.J. Luo, Eds. *Fractional Dynamics and Control*. New York: Springer, 2011.

[2] Carla M.A. Pinto, J.A. Tenreiro Machado, Fractional model for malaria transmission under control strategies, Computers & Mathematics with Applications, **66**(5) (2013), 908–916.

[3] F.M. Dannan, S. Elaydi, Lipschitz stability of nonlinear systems of differential equations, Journal of Mathematical Analysis and Applications, **113** (1986), 562–577

[4] R. Li, J. Cao, A. Alsaedi, B. Ahmad, Passivity analysis of delayed reaction-diffusion Cohen–Grossberg neural networks via Hardy–Poincaré inequality, Journal of the Franklin Institute, **354** (2017), 3021–3038.

[5] Y. Luo, S. Tang, Z. Teng, L. Zhang, Global dynamics in a reaction-diffusion multi-group SIR epidemic model with nonlinear incidence, Nonlinear Analysis: Real World Applications, **50** (2019), 365–385.

[6] J. Pan, X. Liu, S. Zhong, Stability criteria for impulsive reaction-diffusion Cohen–Grossberg neural networks with time-varying delays, Mathematical and Computer Modelling, **51** (2010), 1037–1050.

[7] I. Podlubny, *Fractional Differential Equations*. San Diego: Academic Press, 1999.

[8] I.M. Stamova, S. Simeonov, S. Delayed reaction-diffusion cellular neural networks of fractional order: Mittag–Leffler stability and synchronization, Journal of Computational and Nonlinear Dynamics, **13** (2018), 011015-1.

[9] I.M. Stamova, G.T. Stamov, *Functional and Impulsive Differential Equations of Fractional Order: Qualitative Analysis and Applications*. Boca Raton: CRC Press, 2017.

[10] I. Stamova, G. Stamov, Lipschitz stability criteria for functional differential systems of fractional order, Journal of Mathematical Physics, **54** (2013), 043502.

International Conference on Mathematical Analysis and Applications in Science and Engineering
ICMA^{2}SC'22
ISEP Porto-Portugal, June 27 - 29, 2022

STABILITY OF EPIDEMIC FRACTIONAL MODELS

Cristiana J. Silva[1⋆]

[1] Center for Research and Development in Mathematics and Applications (CIDMA), Department of Mathematics, University of Aveiro, 3810-193 Aveiro, Portugal

[1⋆]cjoaosilva@ua.pt

Abstract: In this work we revisit local, uniform and global stability results applied to Caputo type fractional-order epidemic models, based on the works [2, 7]. We start by a fractional order model for HIV/AIDS transmission [7, 8] and prove the local and uniform asymptotic stability of the equilibrium points. We end by presenting a new result, proved in [2], for the global stability of the disease-free equilibrium in the fractional calculus context.

keywords: epidemic fractional models; uniform asymptotic stability; global stability of disease-free equilibrium.

MSC2020: 34C60; 34D23; 92D30.

1 Introduction

In this work, we start by considering a Caputo fractional order SICA epidemiological model with constant recruitment rate, mass action incidence and variable population size, for HIV/AIDS transmission, proposed in [7] (see also [8]). Using the results from [1] and [5], we prove the local asymptotic stability of the disease free equilibrium. Then, we extend the results of [4] and [9] and prove the uniform asymptotic stability of the disease free and endemic equilibrium points.

The study of global stability of the equilibrium points usually involves constructing suitable Lyapunov-like functions, which, sometimes, can be hard to find. This is the motivation to investigate a new method to study global asymptotic stability for dynamical systems described by fractional differential equations. In [2], a novel method was presented, by writing the system in a matricial form and analyzing the matrices involved is such procedure, under some simple assumptions, we can ensure that the equilibrium point is globally stable if the basic reproduction number $\mathcal{R}_0$ is less than 1. This result generalizes the main result of [3] to the fractional setting.

2 Main results

We start with local and uniform stability results applied to a HIV/AIDS fractional model.

2.1 Fractional SICA model: local and uniform stability analysis

Definition 1 (See [6]) *Let $a > 0$, $t > a$, and $\alpha, a, t \in \mathbb{R}$. The Caputo fractional derivative of order α of a function $f \in C^n$ is given by*

$$ {}_a^C D_t^\alpha f(t) = \frac{1}{\Gamma(n-\alpha)} \int_a^t \frac{f^{(n)}(\xi)}{(t-\xi)^{\alpha+1-n}} d\xi, \qquad n-1 < \alpha < n \in \mathbb{N}. $$

Let us consider the Caputo fractional order SICA epidemiological model for HIV/AIDS transmission with constant recruitment rate, mass action incidence, and variable population size (for more details on the model assumptions and parameters, please see [7]):

$$ \begin{cases} {}_{t_0}^C D_t^\alpha S(t) = \Lambda - \beta \left(I(t) + \eta_C C(t) + \eta_A A(t) \right) S(t) - \mu S(t), \\ {}_{t_0}^C D_t^\alpha I(t) = \beta \left(I(t) + \eta_C C(t) + \eta_A A(t) \right) S(t) - \xi_3 I(t) + \omega C(t) + \gamma A(t), \\ {}_{t_0}^C D_t^\alpha C(t) = \phi I(t) - \xi_2 C(t), \\ {}_{t_0}^C D_t^\alpha A(t) = \rho\, I(t) - \xi_1 A(t). \end{cases} \tag{1} $$

The biologically feasible region of system (1) is given by

$$ \Omega = \left\{ (S, I, C, A) \in \mathbb{R}_+^4 \, : \, N \leq \frac{\Lambda}{\mu} \right\}. $$

The model (1) has a disease free equilibrium given by

$$ \Sigma_0 = \left(S^0, I^0, C^0, A^0 \right) = \left(\frac{\Lambda}{\mu}, 0, 0, 0 \right). $$

Let R_0 denote the basic reproduction number of (1) which is given by

$$ R_0 = \frac{S^0 \beta \, \left(\xi_2 \left(\xi_1 + \rho\, \eta_A \right) + \eta_C \, \phi \, \xi_1 \right)}{\mu \, \left(\xi_2 \left(\rho + \xi_1 \right) + \phi \, \xi_1 + \rho \, d \right) + \rho \, \omega \, d} = \frac{S^0 \mathcal{N}}{\mathcal{D}}, \tag{2} $$

where $\xi_1 = \gamma + \mu + d$, $\xi_2 = \omega + \mu$, $\mathcal{N} = \beta \, \left(\xi_2 \left(\xi_1 + \rho\, \eta_A \right) + \eta_C \, \phi \, \xi_1 \right)$ and $\mathcal{D} = \mu \, \left(\xi_2 \left(\rho + \xi_1 \right) + \phi \, \xi_1 + \rho \, d \right) + \rho \, \omega \, d$.

Whenever $R_0 > 1$, the model (1) has a unique endemic equilibrium $\Sigma_* = (S^*, I^*, C^*, A^*)$ given by

$$ S^* = \frac{\mathcal{D}}{\mathcal{N}}, \quad I^* = \frac{\xi_1 \xi_2 (\Lambda \mathcal{N} - \mu \mathcal{D})}{\mathcal{D} \mathcal{N}}, \quad C^* = \frac{\phi \xi_1 (\Lambda \mathcal{N} - \mu \mathcal{D})}{\mathcal{D} \mathcal{N}}, \quad A^* = \frac{\rho \xi_2 \left(\Lambda \mathcal{N} - \mu \mathcal{D} \right)}{\mathcal{D} \mathcal{N}}. $$

The local asymptotic stability of the disease free equilibrium Σ_0, comes straightforward from [5] and [1]. Stronger stability results are stated next.

Theorem 1 (See [7]) *Let $\alpha \in (0, 1)$. The disease free equilibrium Σ_0, of the fractional order system (1), is uniformly asymptotically stable in Ω, whenever (2) satisfies $R_0 < 1$.*

Theorem 2 (See [7]) *Let $\alpha \in (0, 1)$ and (2) be such that $R_0 > 1$. Then the unique endemic equilibrium Σ_* of the fractional order system (1) is uniformly asymptotically stable in the interior of its invariant region Ω.*

2.2 Global stability of DFE for fractional epidemic models

Definition 2 *The (left-sided) Caputo fractional derivative of order α of function $f \in C^1(\mathbb{R}_0^+, \mathbb{R})$ is defined by*

$$ {}^{C}\mathbb{D}_{0+}^{\alpha} f(t) := \frac{1}{\Gamma(1-\alpha)} \int_0^t (t-\tau)^{-\alpha} f'(\tau)\, d\tau, \quad t > 0. $$

Definition 3 *The Mittag–Leffler function with two parameters is defined by*

$$ E_{\alpha,\beta}(t) := \sum_{k=0}^{\infty} \frac{t^k}{\Gamma(\alpha k + \beta)}, \quad t \in \mathbb{C}, $$

with $\alpha, \beta \geq 0$. When $\beta = 1$, we define the one parameter Mittag–Leffler function $E_\alpha(t) := E_{\alpha,1}(t)$.

Definition 4 *Given $A \in \mathbb{C}^{n\times n}$, the matrix Mittag–Leffler function with two parameters is defined through the convergent series*

$$ E_{\alpha,\beta}(A) := \sum_{k=0}^{\infty} \frac{A^k}{\Gamma(\alpha k + \beta)} $$

where $\alpha, \beta \geq 0$. If $\beta = 1$, we define the one parameter matrix Mittag–Leffler function $E_\alpha(A) := E_{\alpha,1}(A)$.

Suppose that the epidemiological model under study is described by the fractional differential system

$$ \begin{cases} {}^{C}\mathbb{D}_{0+}^{\alpha} X(t) = F(X, I) \\ {}^{C}\mathbb{D}_{0+}^{\alpha} I(t) = G(X, I) \\ G(X, 0) = 0 \end{cases} \tag{3} $$

with nonnegative initial conditions $X(0) = X_0 \in \mathbb{R}^m$ and $I(0) = I_0 \in \mathbb{R}^n$, where the components of the vector X denote the number of uninfected individuals (e.g., susceptible, recovered, vaccinated, etc.) and the components of I denote the number of the infected and infectious (the ones that can transmit the disease, such as the asymptomatic but infectious and active infected). In addition, we assume that function F is continuous, G is of class C^1, and the fractional differential system (3) with initial conditions $X(0) = X_0$ and $I(0) = I_0$ admits a unique solution.

Denote by $U_0 = (X^\star, 0) \in \mathbb{R}^{m+n}$ the disease-free equilibrium (DFE) point of the system (3), that is, $F(X^\star, 0) = G(X^\star, 0) = 0$.

Let $A := \frac{\partial G}{\partial I}(X^\star, 0)$ and assume that matrix A can be written in the form $A = M - D$, where M, D are two square matrices with $M \geq 0$ (all entries are nonnegative), and $D > 0$ is a diagonal matrix.

Theorem 3 (See [2]) *Suppose that*

1. *For ${}^{C}\mathbb{D}_{0+}^{\alpha} X(t) = F(X, 0)$, the vector $X^\star$ is globally asymptotically stable;*
2. *Function G can be written as $G(X, I) = A \cdot I - \hat{G}(X, I)$, where $\hat{G}(X, I) \geq 0$ for all (X, I), and $A = \frac{\partial G}{\partial I}(X^\star, 0)$ can be written as $A = M - D$, where $M \geq 0$ and $D > 0$ is a diagonal matrix;*

3. *Matrix A is diagonalizable, the real parts of the eigenvalues of A are nonpositive, and $E_{\alpha,\alpha}(A) \geq 0$,*

4. *$I(t) \geq 0$ for all $t > 0$ (nonnegativity of solutions).*

If $\mathcal{R}_0 < 1$, then the DFE, $U_0 = (X^\star, 0)$, is a globally asymptotically stable equilibrium of system (3), for all $0 < \alpha < 1$.

The proof of Theorem 3 is given in detail in [2] as well as three examples applied to different types of fractional epidemic models that may be applied to a wide range of infectious diseases.

Acknowledgments

This research is partially supported by the Portuguese Foundation for Science and Technology (FCT) by the project UIDB/04106/2020 (CIDMA). Cristiana J. Silva is also supported by FCT via the FCT Researcher Program CEEC Individual 2018 with reference CEECIND/00564/2018.

The results from [7] are a joint work with Delfim F. M. Torres and the ones from [2] are a joint work with Ricardo Almeida and Natália Martins, from CIDMA, Department of Mathematics, University of Aveiro, Portugal.

References

[1] E. Ahmed and A.S. Elgazzar, On fractional order differential equations model for nonlocal epidemics,Physica A: Statistical Mechanics and its Applications, **379** (2) (2007), 607–614.

[2] R. Almeida, N. Martins, C. J. Silva, Global stability condition for the disease-free equilibrium point of fractional epidemiological models, Axioms, **10** (4) (2021), article-number 238.

[3] C. Castillo–Chavez, Z. Feng, W. Huang, On the computation of R_0 and its role in global stability, IMA Vol. Math. Its Appl. **125** (2002), 229–250.

[4] H. Delavari, D. Baleanu, J. Sadati, Stability analysis of Caputo fractional-order nonlinear systems revisited, Nonlinear Dynam., **67** (4) (2012), 2433–2439.

[5] D. Matignon, Stability Results For Fractional Differential Equations With Applications To Control Processing, In: Computational Engineering in Systems Applications, 1996, 963–968.

[6] M. Michele, Linear models of dissipation whose Q is almost frequency independent. II, Fract. Calc. Appl. Anal., **11** (1) (2008), 4–14.

[7] C. J. Silva, D. F. M. Torres, Stability of a fractional HIV/AIDS model, Math. Comput. Simul. **164** (2019), 180–190.

[8] C. J. Silva, D. F. M. Torres, On SICA models for HIV transmission, In: Hattaf K., Dutta H. (eds) Mathematical Modelling and Analysis of Infectious Diseases. Studies in Systems, Decision and Control, vol 302. Springer, Cham., 2020.

[9] C. Vargas-De-León, Volterra-type Lyapunov functions for fractional-order epidemic systems, Commun. Nonlinear Sci. Numer. Simul., **24** (1-3) (2015), 75–85.

International Conference on Mathematical Analysis and Applications in Science and Engineering
ICMA^{2}SC'22
ISEP Porto-Portugal, June 27 - 29, 2022

ELECTRICAL POTENTIAL OF FRACTAL STRUCTURES IN THE POINT OF VIEW OF FACTIONAL CALCULUS

Isabel S. Jesus[1⋆] **Ramiro S. Barbosa**[1]

[1] GECAD −Research Group on Intelligent Engineering and Computing for Advanced Innovation and Development - Institute of Engineering of Porto - Polytechnic of Porto
R. Dr. António Bernardino de Almeida 431, 4249-015 Porto, Portugal

[1⋆]isj@isep.ipp.pt, [1]rsb@isep.ipp.pt

Abstract: The area of fractional calculus is employed in physics, engineering, biology, economy and other scientific fields. On the other hand, the fractional mathematical concept arises quite naturally, in the intrinsic parameterization of the fractal curve. In this paper we apply the theory of fractional calculus in the electromagnetic field, in particular in the electrical potential, with the electrical charges distribution inserted in the fractal structures. For that, we discuss the electrical potential for a distribution of charges, applied to different fractals structures, namely fractals with one, two and three dimensions. After that, we analyze the resulted electrical potential under the point of view of fractional calculus.

keywords: Fractional calculus; Electrical potential; Fractal geometries.

MSC2020: 49-XX; 34-XX; 92-XX.

1 Introduction

Recent studies have brought Fractional Calculus (FC) into prominence, revealing that many physical phenomena are modeled by fractional differential equations [1, 2]. An important area related with FC is the fractals. During the last century mathematicians verified the formal existence of certain "pathological curves", for example, Cantor, Peano, Sierpinski, Hausdorff, among others [3, 4]. Moreover, fractal geometry, provides a mean for quantifying this complexity, making possible to relate the dimension with the derivative order [5]. Experimental works has shown that the link between fractality and non-integral derivatives is essential to a proper approach to the reality in many fields where fractality plays an interesting role and introduces scaling laws. Tricot [6] showed that non-integral derivative provides a very efficient method for measuring the degree of irregularity of a fractal curve.

Bearing these ideas in mind, this paper analyzes the fractional-order dynamics of a electrical potential created by several electrical charges implemented in fractal structures, being organized as follows. Section 2 introduces the fundamental aspects of fractional calculus theory. Section 3 presents the fundamental static electrical potencial concepts. Section 4 makes the introduction to the fractals structures. Section 5 describes the methodology applied to this work and show the obtained results. Finally, section 6 draws the main conclusions and addresses perspectives towards future developments.

2 FUNDAMENTAL ASPECTS OF FRACTIONAL CALCULUS

Since the beginning of the theory of differential and integral calculus, mathematicians such as Euler and Liouville investigated their ideas on the calculation of non-integer order derivatives and integrals [1]. An important property revealed by the Grünwald-Letnikov definition is that while an integer-order derivative implies simply a finite series, the fractional-order derivative requires an infinite number of terms. This means that integer derivatives only need the actual values in opposition with fractional derivatives that have implicitly a memory of all past events.

On the other point of view, some authors [2, 7] verified that the well-known expressions for the electrical potential are related through fractional-order integral and derivatives, revealing advantages in their use in practical implementations.

3 STATIC ELECTRICAL POTENTIAL

In a linear media, that is isotropic and reveal homogenety, the electric potential φ at a point P produced by a single charge (1), a dipole (2), a quadrupole (3), an infinite straight filament carrying a charge λ per unit length (4), two opposite charged filaments (5), and a planar surface with charge density σ (6), are given by [7]:

$$\varphi = \frac{q}{4\pi\varepsilon_0}\frac{1}{r} + C \quad (1) \qquad \varphi = \frac{ql\cos\theta}{4\pi\varepsilon_0}\frac{1}{r^2} + C,\ r >> l \quad (2)$$

$$\varphi = \frac{ql^2\left(3\cos^2\theta - 1\right)}{4\pi\varepsilon_0}\frac{1}{r^3} + C,\ r >> l \quad (3) \qquad \varphi = -\frac{\lambda}{2\pi\varepsilon_0}\ln r + C \quad (4)$$

$$\varphi = \frac{\lambda l\cos\theta}{2\pi\varepsilon_0}\frac{1}{r} + C,\ r >> l \quad (5) \qquad \varphi = -\frac{\sigma}{2\varepsilon_0}r + C \quad (6)$$

where $C \in \Re$, ε_0 represents the permittivity, q the electric charge, l the length, r the radial distance and θ the corresponding angle with the axis.

Analyzing expressions (1)-(6) we verify the relationship $\varphi \sim r^{-3}, r^{-2}, r^{-1}, \ln r, r$, that corresponds to the application of integer-order derivatives and integrals [7].

4 FRACTAL STRUCTURES

In recent years, different definitions of fractals have been emerged. However, the fundamental definition of fractal was introduced by Benoit Mandelbrot in 1975 [3, 4, 5, 6], through the neologism "Fractal", which means irregular or broken.

One of the most important concepts of fractals is their dimension, also called Hausdorff dimension. Intuitively, a point has dimension 0, a line has dimension 1, a plane has dimension 2 and a cube has dimension 3. However, in fractal geometry we find mathematical objects that have a fractional dimension.

There are many examples of fractals particularly well known, namely the Cantor set, the Von Koch curve, the Sierpinski triangle, the Sierpinski carpet and the Sierpinski cube.

Table 1: Parameters correspondent to a power law approximation, for a Carpet Sierpinski distribution charges.

N°. of iterations	a	b	ε
0	1.000	-1.000	0.0000
1	1.041	-1.055	0.0011
2	1.050	-1.073	0.0032
3	1.052	-1.076	0.0037

5 SIMULATION AND RESULTS

The fractals major characteristic is their irregularity all over of its length. This irregularity is the reason of the non-integer dimensions of fractal sets, what unfortunately, it makes them very difficult to handle analytically since the usual calculus is inadequate to describe such structures and processes. In our study it is argued that a new calculus may be developed which includes intrinsically the fractal structure and the fractional order concepts. In this line of thought we study the electrical potential, applying charges in the fractal elements and try to find relations between fractional order systems and fractal geometries. For that, we have used the Cantor Set, the Sierpinski Carpet and the Sierpinski Cube, to place charges and calculate the corresponding electrical potential. We selected these three geometries, corresponding to different fractal dimensions, because we intended to study the influence of different distribution of charges in the electrical potential. So, in order to study the slope behavior of electrical potential, we placed the electrical charges in the fractal structure segments and calculated the resulting potential along the x-axis.

The fractal geometries used have different dimensions namely, for Cantor Set is given by $D = \log(2)/\log(3) = 0.63$, for the Carpet Sierpinski the value is $D = \log(8)/\log(3) = 1.89$ and for the Cube Sierpinski we have $\log(20)/\log(3) = 2.73$. In this work we developed experiments for all of these fractals, however due to the limited space in this abstract we only present the Carpet Sierpinski.

5.1 Carpet Sierpinski

In this subsection, we analyze the Carpet Sierpinski, which corresponds to a 2D-dimensional fractal. In this case, at iteration 0, we have one square with one unitary charge at the middle. At iteration 1, we subdivide the square in to 9 equal squares, and ignore the square located in the middle. The charges are located in the middle of the remain squares. In next iterations we subdivide the valid squares in new other 9 squares, and repeat the procedure described before. The number of squares is equal to $n_c = 8^{iter}$, and the value of the charges are Q/n_c.

To illustrate this case, we consider also the third iteration with the Carpete Sierpinski centered around the origin axis, with $-0.5 < x < 0.5$ $[m]$ and $-0.5 < y < 0.5$ $[m]$. Fig. 1 a) depicts one example of Carpet Sierpinski, namely for iteration 3, where the dots represent the charges. Fig. 1 b) shows the corresponding electrical potential. We verify that the potential has a slope$= -1$ for large distances of charges, and near them the slope presents some differences. Table 1 shows the corresponding parameter values obtained for a electrical potential power-law approximation, *i.e.* , $\varphi \sim ar^{-b}$, where φ represents the electrical potential, r is the distance to the measuring point and $b \in \Re$, as the number of iterations is increased. The value ε is the sum of squared errors between the actual potential and the approximation.

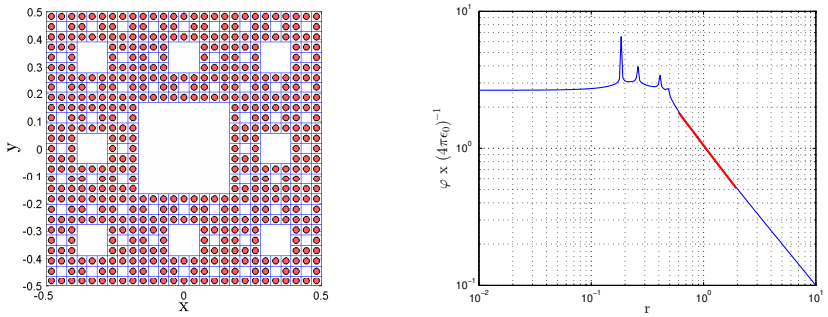

a) b)

Figure 1: Sierpinski Carpet ($Iter = 3$): a) with the charges (dots) in the middle of the valid squares, and b) Electrical potential.

6 Conclusions and Future work

This paper addressed several aspects of FC applied to electromagnetic potential. We conclude that the fractional calculus is another way to see the physical phenomena with a different concept of traditional methodologies usually applied. We analyzed the evolution of electrical potential system for different distribution of charges in a fractal field. For specific distribution of charges, we applied the theoretical concept of fractal to a geometry with two dimensions, and we analyzed the electrical potential and the fractal dimension of system. The study developed here could be extended to other fractals and for different arrangements of charges.

Acknowledgments

This work is supported by FEDER Funds through the Programa Operacional Factores de Competitividade - COMPETE program and by National Funds through FCT Fundacão para a Ciência e a Tecnologia under the project UIDB/00760/2020.

References

[1] Keith B. Oldham and Jerome Spanier, *The Fractional Calculus: Theory and Application of Differentiation and Integration to Arbitrary Order*. Academic Press Publishers, 1974.

[2] A. Oustaloup, *La Commande CRONE: Commande Robuste d'Ordre Non Entier*. Hermes Publishers, 1991.

[3] B.B. Mandelbrot, *The Fractal Geometry of Nature*, Jo Freeman,New York Pub, 1977.

[4] Abdon Atangana, Fractal−fractional differentiation and integration: Connecting fractal calculus and fractional calculus to predict complex system, Chaos, Solutions & Fractals Journal,**102**, (2017), 396–406.

[5] Frank B. Tatom, The Relationship Between Fractional Calculus and Fractals, Fractals Journal,**3**(1), (1995), 217–229.

[6] C. Tricot, *Curves and fractal dimension*, Springer, New York, Pub, 1993.

[7] Isabel S. Jesus and J. A. Tenreiro Machado, Implementation of Fractional-order electromagnetic potential through a genetic algorithm, Journal of Communications in Nonlinear Science and Numerical Simulation,**14**, Elsevier(2006), 1838–1843.

International Conference on Mathematical Analysis and Applications in Science and Engineering
ICMA^{2}SC'22
ISEP Porto-Portugal, June 27-29, 2022

On the fractional derivatives with an exponential kernel

Enyu Fan **Changpin Li*** **Jingshu Wu** **Shaoying Zeng**

Department of Mathematics, Shanghai University, Shanghai 200444, China

*lcp@shu.edu.cn

Abstract: This article mainly focuses on the fractional derivatives with an exponential kernel ("exponential fractional derivatives" for brevity). First, the several extended integral transforms of the exponential fractional derivatives are obtained, including the Fourier transform, the Laplace transform and the Mellin transform. Then the L2 discretisation for the exponential Caputo derivative with $\alpha \in (1, 2)$ is established. The estimation of truncation error and the properties of the coefficients are discussed. And a numerical example is given to verify the correctness of the L2 discretisation.

keywords: Exponential fractional derivative; integral transform; L2 discretisation; truncation error.

MSC2020: 26A33; 44A05.

1 Introduction

The fractional derivatives with an exponential kernel ("exponential fractional derivatives" for brevity) are introduced in [3], which mainly include the exponential Riemann-Liouville derivative and exponential Caputo derivative. In general, the fractional differential equation with exponential fractional derivative has exponentially asymptotical solution. Such a kind of fractional derivatives gradually attracts scholars' attention. For example, the blow-up of the solution to a semilinear time-space fractional diffusion equation with the α-th ($\alpha \in (0, 1)$) order exponential Caputo time fractional derivative and the s-th ($s \in (0, 1)$) order fractional Laplacian in space [2] is studied. On the other hand, some typical numerical discretisations of the exponential Caputo derivative except L2 discretisation derived in [1]. In this paper, the integral transforms for exponential derivatives and L2 discretisation for exponential Caputo derivative are displayed.

2 Results and discussion

Firstly, a function space is introduced below.

$$AC^n_{\delta_e}[a, b] = \big\{ f : [a, b] \to \mathbb{R} : \delta_e^{n-1} f(t) \in AC[a, b], \quad n \in \mathbb{Z}^+ \big\}, \tag{1}$$

where the operator $\delta_e^n = (e^{-t}\frac{\mathrm{d}}{\mathrm{d}t})^n = \delta_e(\delta_e^{n-1})$ with $\delta_e^0 = I$ and $AC[a, b]$ is a space of absolutely continuous function on the interval $[a, b]$. Next, the definitions of several fractional integral and derivatives are introduced as follows.

Definition 1 *For $\alpha > 0$ and $f(t) \in L^1(a,b)$, the exponential Riemann-Liouville fractional integral of $f(t)$ is defined by*

$$ {}_e\mathrm{D}_{a,t}^{-\alpha} f(t) = \frac{1}{\Gamma(\alpha)} \int_a^t \left(e^t - e^\tau\right)^{\alpha-1} f(\tau) e^\tau \mathrm{d}\tau,\ t > a. \tag{2} $$

Definition 2 *For $n-1 < \alpha < n \in \mathbb{Z}^+$ and $f(t) \in AC_{\delta_e}^n[a,b]$, the exponential Riemann-Liouville fractional derivative of $f(t)$ is defined by*

$$ {}_e\mathrm{D}_{a,t}^{\alpha} f(t) = \frac{1}{\Gamma(n-\alpha)} \delta_e^n \int_a^t \left(e^t - e^\tau\right)^{n-\alpha-1} f(\tau) e^\tau \mathrm{d}\tau,\ t > a, \tag{3} $$

where $\delta_e^n g(t)$ for a given function $g(t)$ is defined by

$$ \delta_e^n g(t) = \left(e^{-t} \frac{\mathrm{d}}{\mathrm{d}t}\right)^n g(t) = \delta_e \left(\delta_e^{n-1} g(t)\right), \quad \delta_e^0 g(t) = g(t). $$

Definition 3 *For $n-1 < \alpha < n \in \mathbb{Z}^+$ and $f(t) \in AC_{\delta_e}^n[a,b]$, the exponential Caputo fractional derivative of $f(t)$ is defined by*

$$ {}_{Ce}\mathrm{D}_{a,t}^{\alpha} f(t) = \frac{1}{\Gamma(n-\alpha)} \int_a^t \left(e^t - e^\tau\right)^{n-\alpha-1} \delta_e^n f(\tau) e^\tau \mathrm{d}\tau,\ t > a, \tag{4} $$

where $\delta_e^n f(\tau)$ is defined by

$$ \delta_e^n f(\tau) = \left(e^{-\tau} \frac{\mathrm{d}}{\mathrm{d}\tau}\right)^n f(\tau) = \delta_e \left(\delta_e^{n-1} f(\tau)\right), \quad \delta_e^0 f(\tau) = f(\tau). $$

The exponential Riemann-Liouville fractional derivative (3) and the exponential Caputo fractional derivative (4) have the relationship below [2]

$$ \begin{aligned} {}_{Ce}\mathrm{D}_{a,t}^{\alpha} f(t) &= {}_e\mathrm{D}_{a,t}^{\alpha} \left[f(t) - \sum_{k=0}^{n-1} \frac{\delta_e^k f(a)}{k!} \left(e^t - e^a\right)^k \right] \\ &= {}_e\mathrm{D}_{a,t}^{\alpha} f(t) - \sum_{k=0}^{n-1} \frac{\delta_e^k f(a)}{\Gamma(k-\alpha+1)} \left(e^t - e^a\right)^{k-\alpha}, \end{aligned} \tag{5} $$

where $n-1 < \alpha < n \in \mathbb{Z}^+$ and $\delta_e^k f(a) = \left(e^{-t} \frac{\mathrm{d}}{\mathrm{d}t}\right)^n f(t)\big|_{t=a}$. It is clear that if $\delta_e^k f(a) = 0$ for $k = 0, 1, \ldots, n-1$, then two exponential fractional derivatives are equivalent, i.e.,

$$ {}_{Ce}\mathrm{D}_{a,t}^{\alpha} f(t) = {}_e\mathrm{D}_{a,t}^{\alpha} f(t). $$

The traditional integral transforms such as Fourier transform, Laplace transform, and Mellin transform are hard to applied to the above integral and derivatives [4, 5, 7]. So the extended versions of the usual integral transforms have to be proposed. In this paper, the generalized Fourier, Laplace, and Mellin transforms are introduced and then applied to the exponential fractional integral and derivatives.

On the other hand, although there are many typical numerical methods for the exponential fractional derivatives, for example, [1] for exponential Caputo fractional derivative, there are still some missing. Here, we continue to use the most convenient way to approximate the exponential Caputo fractional derivative with order $\alpha \in (1,2)$, called L2 scheme. Here "L" means left (the above definitions of integral and derivatives are actually for left integral and derivatives), 2 means $\alpha \in (1,2)$. Such a naming rule comes from [6].

3 Conclusions and Future work

This paper emphatically studies two aspects of exponential fractional derivatives. Firstly, the generalized Fourier transform, Laplace transform, and Mellin transform of the exponential fractional integral and derivatives are obtained. Secondly, the L2 numerical formula is constructed to approximate the exponential Caputo fractional derivative with order $\alpha \in (1, 2)$. In the future, we shall devote to solving the exponential fractional differential systems using the results of this paper.

Acknowledgments

This work was partially supported by the National Natural Science Foundation of China under grant no. 11872234.

References

[1] E.Y. Fan, C.P. Li, Z.Q. Li, Numerical methods for the Caputo-type fractional derivative with an exponential kernel, revised.

[2] C.P. Li, Z.Q. Li, On blow-up for a time-space fractional partial differential equation with exponential kernel in temporal derivative, J. Math. Sci., in press.

[3] C.P. Li, Z.Q. Li, C.T. Yin, Which kind of fractional partial differential equations has solution with exponential asymptotics? In: A. Dzielinski, D. Sierociuk, P. Ostalczyk (eds), Proceedings of the International Conference on Fractional Differentiation and its Applications (ICFDA'21), ICFDA 2021, Lecture Notes in Networks and Systems, vol **452**, pp. 112–117, Springer, Cham, 2022.

[4] C.P. Li, F.H. Zeng, *Numerical Methods for Fractional Calculus.* Boca Raton: CRC Press, 2015.

[5] I. Podlubny, *Fractional Differential Equations.* San Diego: Academic Press, 1999.

[6] K.B. Oldham, J. Spanier, *The Fractional Calculus.* New York: Academic Press, 1974.

[7] S. Samko, A. Kilbas, O. Marichev, *Fractional Integrals and Derivatives: Theory and Applications.* Switzerland: Gordon and Breach, 1993.

International Conference on Mathematical Analysis and Applications in Science and Engineering
ICMA^{2}SC'22
ISEP Porto-Portugal, June 27 - July 1, 2022

Fractional versions of complex Wirtinger (d-bar) derivatives

Arran Fernandez[1⋆] **Chaima Bouzouina**[1]

[1] Eastern Mediterranean University, Northern Cyprus

[1⋆]arran.fernandez@emu.edu.tr

Abstract: Fractional calculus and complex analysis are two major and important subdivisions of mathematical analysis, but uniting or combining them both together has so far been done only in very limited ways. Complex orders of fractional differintegration are well known; fractionally differintegrating a function of a complex variable is also fairly standard; but there are many other facts and operations of complex analysis whose fractional versions have not yet been defined or studied. We propose a model of fractional Wirtinger derivatives, in particular, a fractional version of the complex d-bar derivative. This theory is demonstrated to possess natural properties when compared both with the original d-bar and Wirtinger derivatives and with the original fractional calculus. It is expected to find applications in modelling fractional (non-local) versions of the many real-world problems in which complex d-bar derivatives are invaluable, such as medical imaging of the brain.

keywords: fractional calculus; complex analysis; d-bar derivatives.

MSC2010: 26A33; 30G20.

1 Introduction

Fractional calculus is a major topic of mathematical research nowadays, extending in many different directions both within mathematics (generalised operators, applications to special functions, and so on) and for modelling in the applied sciences (systems with non-local behaviour, viscoelastic processes, and so on).

Complex analysis is one of the classical branches of mathematical analysis, majorly developed by Cauchy in the 19th century and now seen as a standard extension of real analysis, with many further extensions and generalisations possible (Clifford analysis, functions of several complex variables, and so on) as well as applications in solving partial differential equations which appear in many fields of science.

How have these two fields been combined?

- In fractional calculus, the order α of differentiation or integration can be not only an integer but any real or complex number. Extension of α into the complex plane is a standard part of fractional calculus, but doing complex analysis with respect to α is more uncommon.
- Less frequently seen is fractional derivatives and integrals applied to a function of a complex variable. The definition is a classical one [1, §22], but it is rarely used in the literature: many authors prefer to assume all variables are real as it makes the work easier.

- But the study of complex analysis is far richer than just allowing variables to take values in $\mathbb{C}$. Properties such as Cauchy's theorem, Liouville's theorem, the residue theorem, and so on, all ultimately stem from the Cauchy–Riemann equations, or equivalently the complex d-bar derivative. These notions have, so far, no fractional versions.

We aim to resolve this hole in the field, by introducing what we believe is a natural definition of fractional complex d-bar derivatives. We justify our definition by proving many of its properties, including a semigroup property and a fractional Leibniz rule.

2 Results and discussion

In complex analysis, a function $f(z)$ of a complex variable $z = x + yi \in \mathbb{C}$ can also be considered as a function $f(x, y)$ of two independent real variables $x, y \in \mathbb{R}$. The partial derivatives with respect to x and y give rise to "complex partial derivatives", with respect to z and its complex conjugate $\bar{z}$:

$$\frac{\partial f}{\partial z} = \frac{1}{2}\left(\frac{\partial f}{\partial x} - i\frac{\partial f}{\partial y}\right); \qquad \frac{\partial f}{\partial \bar{z}} = \frac{1}{2}\left(\frac{\partial f}{\partial x} + i\frac{\partial f}{\partial y}\right). \tag{1}$$

The function f is complex differentiable if and only if it is real differentiable and satisfies the Cauchy–Riemann equations, or equivalently if and only if the d-bar derivative $\frac{\partial f}{\partial \bar{z}}$ exists and is equal to zero. In this case, the "complex partial" derivative $\frac{\partial f}{\partial z}$ is equal to the usual complex derivative $\frac{\mathrm{d}f}{\mathrm{d}z}$, and the function is holomorphic and analytic. The operators of (1) can also be combined and raised to any natural-number power in order to obtain multiple and mixed complex partial derivatives, known in general as Wirtinger derivatives.

What would be an appropriate fractional form of these complex partial derivatives?

Definition 1 *The fractional complex partial derivatives of a smooth complex function $f(z) = f(x + yi)$ are defined by taking fractional powers (using the binomial theorem) of the operators defined in* (1)*. In each case (with respect to z and $\bar{z}$), there are two possible definitions:*

$${}^{1}_{c}\partial^{\alpha}_{z} f(z) := 2^{-\alpha} \sum_{n=0}^{\infty} \binom{\alpha}{n} e^{-i\pi n/2}\, {}^{RL}_{c}D^{\alpha-n}_{x} D^{n}_{y} f(x + yi), \tag{2}$$

$${}^{2}_{c}\partial^{\alpha}_{z} f(z) := 2^{-\alpha} \sum_{n=0}^{\infty} \binom{\alpha}{n} e^{-i\pi(\alpha-n)/2} D^{n}_{x}\, {}^{RL}_{c}D^{\alpha-n}_{y} f(x + yi); \tag{3}$$

$${}^{1}_{c}\partial^{\alpha}_{\bar{z}} f(z) := 2^{-\alpha} \sum_{n=0}^{\infty} \binom{\alpha}{n} e^{i\pi n/2}\, {}^{RL}_{c}D^{\alpha-n}_{x} D^{n}_{y} f(x + yi), \tag{4}$$

$${}^{2}_{c}\partial^{\alpha}_{\bar{z}} f(z) := 2^{-\alpha} \sum_{n=0}^{\infty} \binom{\alpha}{n} e^{i\pi(\alpha-n)/2} D^{n}_{x}\, {}^{RL}_{c}D^{\alpha-n}_{y} f(x + yi). \tag{5}$$

Theorem 1 (Semigroup property) *Let $\alpha, \beta \in \mathbb{C}$. If either $\alpha \in \mathbb{N}$ or $\mathrm{Re}(\beta) < 0$, then:*

$${}^{1}_{c}\partial^{\alpha}_{z}({}^{1}_{c}\partial^{\beta}_{z}[f(z)]) = {}^{1}_{c}\partial^{\alpha+\beta}_{z}[f(z)], \qquad {}^{2}_{c}\partial^{\alpha}_{z}({}^{2}_{c}\partial^{\beta}_{z}[f(z)]) = {}^{2}_{c}\partial^{\alpha+\beta}_{z}[f(z)];$$
$${}^{1}_{c}\partial^{\alpha}_{\bar{z}}({}^{1}_{c}\partial^{\beta}_{\bar{z}}[f(z)]) = {}^{1}_{c}\partial^{\alpha+\beta}_{\bar{z}}[f(z)], \qquad {}^{2}_{c}\partial^{\alpha}_{\bar{z}}({}^{2}_{c}\partial^{\beta}_{\bar{z}}[f(z)]) = {}^{2}_{c}\partial^{\alpha+\beta}_{\bar{z}}[f(z)].$$

I.e. we have a semigroup property both for repeated derivatives of fractional operators and for fractional operators of fractional integrals.

Theorem 2 (Leibniz rule)

$$
\begin{aligned}
{}_c^1\partial_z^\alpha\left(f(z)g(z)\right) &= \sum_{n=-\infty}^{\infty}\binom{\alpha}{n}\,{}_c^1\partial_z^{\alpha-n}f(z)\,{}_c^1\partial_z^n g(z),\\
{}_c^2\partial_z^\alpha\left(f(z)g(z)\right) &= \sum_{n=-\infty}^{\infty}\binom{\alpha}{n}\,{}_c^2\partial_z^{\alpha-n}f(z)\,{}_c^2\partial_z^n g(z);\\
{}_c^1\partial_{\bar z}^\alpha\left(f(z)g(z)\right) &= \sum_{n=-\infty}^{\infty}\binom{\alpha}{n}\,{}_c^1\partial_{\bar z}^{\alpha-n}f(z)\,{}_c^1\partial_{\bar z}^n g(z),\\
{}_c^2\partial_{\bar z}^\alpha\left(f(z)g(z)\right) &= \sum_{n=-\infty}^{\infty}\binom{\alpha}{n}\,{}_c^2\partial_{\bar z}^{\alpha-n}f(z)\,{}_c^2\partial_{\bar z}^n g(z).
\end{aligned}
$$

Both of these theorems show exactly the same behaviour as in the usual (Riemann–Liouville) model of fractional calculus, and thus our proposed definition appears to be a *natural* way to define complex partial derivatives, displaying the properties that would be expected. We therefore have a starting point for a theory of fractional complex analysis, just as the original d-bar derivative can be a starting point for the Cauchy–Riemann equations, complex differentiability, and all of complex analysis.

3 Conclusions and Future work

The existing combinations of fractional calculus and complex analysis may be called "complex fractional calculus": taking the usual fractional calculus and complexifying it. We are doing "fractional complex analysis": taking the usual complex analysis and fractionalising it. In this way, we can obtain fractional versions of important complex-analytic properties that have never been satisfactorily fractionalised before.

This project can proceed in many possible directions in the immediate future. We plan to explore the concept of "fractional analyticity" (what happens if the fractional d-bar derivative is zero), to propose corresponding fractional versions of complex integration (to investigate the possibility of a fractional Cauchy's theorem, fractional residue theorem, etc.), and to extend the theory to more advanced settings such as Clifford analysis.

The complex d-bar derivative has many applications: in solving partial differential equations [2]; in inverting transforms which are used in medical imaging of the brain [3]; and so on. Similarly, we expect to be able to apply the fractional complex derivatives in solving fractional PDEs and fractional pseudoanalytic equations.

References

[1] S. Samko, A. Kilbas, O. Marichev, *Fractional Integrals and Derivatives: Theory and Applications*. London: Gordon and Breach Science Publishers, 1993.

[2] A.S. Fokas, M.C. van der Weele, Complexification and integrability in multidimensions, Journal of Mathematical Physics **59** (2018), 091413.

[3] A.S. Fokas, L.Y. Sung, Generalized Fourier Transforms, Their Nonlinearization and the Imaging of the Brain, Notices of the American Mathematical Society, **52**(10) (2005), 1178–1192.

International Conference on Mathematical Analysis and Applications in Science and Engineering
ICMA^{2}SC'22
ISEP Porto-Portugal, June 27 - 29, 2022

ON STATE VARIABLES AND FRACTIONAL DERIVATIVES

Blas M. Vinagre **Inés Tejado** **Carlos M. Vinagre**

Universidad de Extremadura, Spain

{bvinagre,itejbal}@unex.es;cavinagre@alumnos.unex.es

Abstract: Control techniques in state space require the description of the system in such a domain, i.e., a state representation of the system to be controlled, but control strategies do not need that all state variables have a physical meaning. They only require something like this for those that have to be measured and that, habitually, we take as outputs. The use of observers releases us even from this requirement. Furthermore, the observers allow to look inside the system and obtain as much dynamic information as convenient for control purposes. When modeling, we always make a selective destruction of information. By using a historical perspective, this work revises the concept of state and explores the significance of the information granted by taking into account a richest concept of state, and how this information can be used.

keywords: fractional calculus, state space, feedback control, linear systems.

MSC2020: 26A33.

1 From the beginning

Phase space was used originally to describe specific types of dynamical systems, but today it has become synonymous with the idea of a large parameter set linked to the degrees of freedom of the considered system, like it was in the cradle. With [3], we will begin our story in the midst of XIX century. With no reference to dynamics, nor mention of phase space, Liouville in 1838 studied a system of n first-order differential equations, with the complete set of solutions

$$\frac{dx_i}{dt} = P(t, x_1, x_2, \cdots, x_n), \quad x_i = x_i(t, a_1, a_2, \cdots, a_n), \tag{1}$$

being a_i arbitrary constants. In 1842, Jacobi recognized that this kind of differential equations could describe mechanical systems, particularly those implying, in Hamiltonian dynamics, the position coordinates, x_i, and the momentum coordinates, p_i. But at this moment, there was no concept of space beyond our *physical three dimensions*. The idea of a generalized space took long time to access the minds, even of the most conspicuous mathematicians and scientists, the time required to extend the concept of variable from algebraic entities to coordinate axes, a way that culminates with Riemann in 1868 (see [3]). It was in Boltzmann's 1871 papers about the kinetic theory of gases, when he made the analogy between physical trajectories of particles in a two-dimensional space and Lissajous figures, and in 1872 used for the first time the term "phase". Then, in 1879, Maxwell adopted the Boltzmann's terminology to describe the "state" of a system. The final step, the putting of "phase" into "space", was given by Poincaré at the end of the century: the developments included in *Les méthodes nouvelles de la mécanique céleste* (1892-1899) established the foundations of the phase space and the state variables.

2 The Contribution of Rudolf Kalman

For Control Theory, the final step was given by Rudolf Kalman. In [2], Kalman deals with the mathematical descriptions on dynamical systems. Though the focus is in linear systems, the study is relevant for our purposes. He considers two models of physical systems, the one based on *vector differential equations*, i.e., phase space and state variables, and that based on transfer functions. Two different "languages" whose use was, at that time, "surrounded by confusion". In Kalman's view, "the difficulty is due to insufficient appreciation of the concept of a *dynamical system*. Control theory is supposed to deal with physical systems, and not merely with mathematical objects, such as a differential equation or a transfer function. We must therefore pay careful attention to relationship between physical system and their representation via differential equations, transfer functions, etc." [2, p. 152], i.e., we must pay careful attention to the relationship between reality and models, between the territory and the map. The Kalman's proposal can be read as follows:

1. To establish a precise, abstract definition of a (physical) dynamical system based on generalizations of the Newtonian causality.
2. To formulate the central problem, the problem of realization, as follows: given an (experimentally observed) impulse response matrix, how can we identify the (linear) dynamical system that generated it?
3. To give the conditions and procedures for obtaining the abstract description of the coupling between external variables (inputs and outputs) and the internal variables (states), and for being the system so described an irreducible realization of a given impulse matrix.

By translating Newton to modern terminology, we can say, with Kalman, that the numbers that specify the instantaneous position and momentum of each particle represent the *state* of the system, an abstract quantity figuring the "minimal amount of information about the past history of the system which suffices to predict the effect of the past upon the future. Further, we say that the forces acting on the particles are the *inputs* of the system. Any variable in the system which can be directly observed is an *output*." [2, p. 154]

For the purposes of this work, when we are considering dynamical systems, and chiefly for control, we can summarize the main results as follows [1]:

1. There are internal variables called *state variables* whose values at a fixed time $t = t_0$ form the *state*.
2. There are external variables that can drive the system called *inputs*.
3. There are external variables that can be directly observed called *outputs*.
4. The state is the smallest collection of numbers that must be known at time $t = t_0$ in order to be able to predict the outputs of the system for any time $t \geq t_0$, knowing the inputs.
5. A state space model is an abstract structure describing the coupling between the external variables and the internal variables.
6. Given an experimentally observed impulse-response matrix, we can identify a linear dynamical system that generated it. This system is called a *realization* of the impulse-response matrix.
7. Rigorously speaking, a state space model is an *irreducible* realization of the given impulse-response matrix, a realization with minimal dimension.

3 The cases for fractional derivatives

3.1 From physics

Suppose we perform an experiment obtaining the step response represented in Figure 1(L) in blue. This could be the result of an experiment where we have observed some kind of anomalous relaxation phenomena[1]. Then, it will be approximated by a sum of two exponential functions, i.e.,

$$y_1(t) = ae^{bt} + ce^{dt} \tag{2}$$

resulting the curve in red color. This first fitting, the usual one, leads to an impulse–response matrix composed by two exponential terms and, consequently, to a state–space description with two state variables. But we can try an impulse-response matrix composed by terms of the form

$$t^{\alpha-1}\mathcal{E}_{\alpha,\alpha}(-bt^{\alpha}) \tag{3}$$

where $\mathcal{E}_{\alpha,\alpha}(-bt^{\alpha})$ is the Mittag-Leffler function. Then, the transfer-function matrix will be composed by terms of the form

$$Z(s) = \frac{1}{s^{\alpha} + b} \tag{4}$$

and following the procedure developed by Kalman, we can obtain the dynamical equations

$$\frac{d^{\alpha}x}{dt} = F(t)x(t) + G(t)u(t) \tag{5}$$

$$y(t) = H(t)x(t) \tag{6}$$

where $\frac{d^{\alpha}x}{dt}$ is the Riemann-Liouville fractional derivative[2]. Now we have only one, *state or pseudo-state?.*

In green color, we can see the results. Because we have measured the impulse-response matrix $S(t,\tau)$ by applying to each input, with the system at rest, a very narrow and sharp pulse, and have observed the effects on the outputs, equations (5)–(6) are a realization of $S(t,\tau)$. In fact, we can build the system with the standard techniques of simulation. The question is: *is there any reason for considering the first model, the one based on exponentials, more 'realistic', with more 'physical meaning'.*

3.2 From mathematics

The idea behind this argument is illustrated in Figure 1(R). Basically, the advantage of state space based control methods is due to the use of more information about the system to be controlled compared to input–output (transfer function) based methods. System augmentation, or in general fractional derivatives, can be seen as having additional information available for control. (Details for this section can be found in [5]). For such a redefined system we can design a fractional order observer to estimate not only unmeasured original state variables but also unknown fractional order derivatives of those state variables. This gives us the possibility of using them for augmented state feedback control, and achieve another possibility to adjust the desired system dynamics, dynamics that is not possible to achieve by using only integer order systems (just like for the fractional PID regulators).

[1] Following Kalman's procedure, we start from the system step response. It was obtained in MATLAB by means of the command `fotf` and added a noise to be more realistic.

[2] It is worth to observe that we used in the above few lines the three big names mentioned at the beginning of the paper when talking about the origins of the state space concepts: Liouville, Riemann and Mittag-Leffler.

Remark 1 *It is important to bear in mind that: 1) the physical system remains at it was, because the augmented system procedure only affects to an* artificial mathematical object*, the observer; and 2) in terms of vector spaces, we have increased the dimension of the complete system, like in the traditional control strategy using observers (or integral control).*

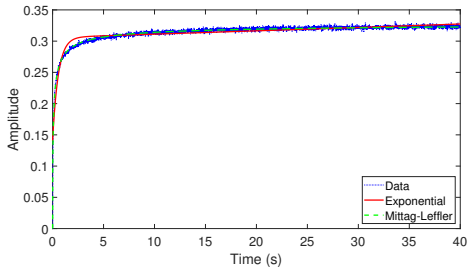

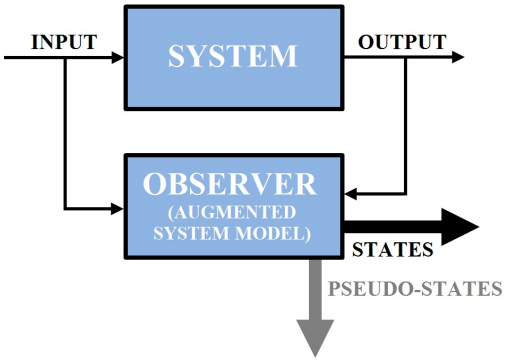

Figure 1: (L) Step response of an anomalous relaxation dynamic system: fitting results. (R) Block diagram of observer based on the augmented system.

4 Conclusions

Despite the many discussions about the meaning of fractional derivatives and their corresponding initial conditions (see, e.g., [4]), notwithstanding the appeal to the physical meaning of state variables, for control engineering purposes the state is a vector, the state space is a vector space, and no physical meaning is required as a necessary condition for its use and definitions. Furthermore, to consider as significant only the derivatives of integer order is to condemn many systems, their modeling and their control, to a limited bed of Procrustes.

References

[1] Rudolph E. Kalman. On the general theory of control systems. In *Proceedings of 1st International Congress on Automatic Control*, pages 481–492, 1960.

[2] Rudolph E. Kalman. Mathematical description of linear dynamical systems. *J.S.I.A.M. Control*, A1:152–191, 1963.

[3] David D. Nolte. The tangled tale of phase space. *Physics Today*, April:33–38, 2010.

[4] Manuel D. Ortigueira. A new look at the initial condition problem. *Mathematics*, 10:1771, 2022.

[5] Inés Tejado, Blas M. Vinagre, and Dominik Sierociuk. *Handbook of Fractional Calculus with Applications. Vol. 6: Applications in Control*, chapter State space methods for fractional controllers design, pages 175–199. De Gruyter, 2019.

International Conference on Mathematical Analysis and Applications in Science and Engineering
ICMA^{2}SC'22
ISEP Porto-Portugal, June 27 - 29, 2022

Stability properties of multi-term fractional-differential equations with four fractional derivatives

O. Brandibur[1*] **E. Kaslik**[1,2]

[1] Department of Mathematics and Computer Science, West University of Timişoara, Romania
[2] Institute for Advanced Environmental Research, West University of Timişoara, Romania

oana.brandibur@e-uvt.ro

Abstract: This paper presents stability and instability conditions for multi-term fractional-differential equations with four fractional derivatives of Caputo type. The stability and instability conditions of the considered fractional-order differential equation are expressed both with respect to the real part of the roots of the associated characteristic equations and with respect to the coefficients of the equations, dependent or independent of the fractional orders.

keywords: fractional-order differential equations; Caputo derivative; stability; instability.

MSC2020: 26A33; 03C45.

1 Preliminaries

We consider the following multi-term fractional differential equation

$$ {}^cD^q x(t) + \alpha {}^cD^{q_1} x(t) + \beta {}^cD^{q_2} x(t) + \gamma {}^cD^{q_3} x(t) + \delta x(t) = 0, \tag{1} $$

where $\alpha, \beta, \gamma, \delta$ are real numbers and q, q_1, q_2, q_3 are the fractional orders of the Caputo derivatives, with $0 < q_1 < q_2 < q_3 < q \leq 2$.

The initial condition associated to equation (1) is either

i. $x_i = x(0) = x_0 \in \mathbb{R}$, if $q \in (0, 1]$, or

ii. $x_i = (x(0), x'(0)) = (x_0, x_1) \in \mathbb{R}^2$ if $q \in (1, 2)$.

In what follows, $\varphi(t, x_i)$ denotes the unique solution of (1) satisfying one of the initial considered above. The existence and uniqueness of the solution of the initial value problem associated to the equation (1) can be proved similarly to the case of fractional-order systems of differential equations [3]. Equation (1) represents a generalized version of the equation studied in [1], where a three-term fractional-order differential equation was considered.

Due to the presence of the memory effect and hereditary properties, it is important to mention that the asymptotic stability of the trivial solution of equation (1) is not of exponential type [2, 4]. Instead, a non-exponential asymptotic stability concept is required in this case, called Mittag-Leffler stability [5]. Hereafter, in our work, we focus our attention on $\mathcal{O}(t^{-\alpha})$-asymptotic stability, which reflects the algebraic decay of the solution.

Definition 1 *The trivial solution of (1) is called* stable *if for any $\varepsilon > 0$ there exists $\delta = \delta(\varepsilon) > 0$ such that for every $\mathbf{x}_0 \in \mathbb{R}^n$ satisfying $\|\mathbf{x}_0\| < \delta$ we have $\|\varphi(t, \mathbf{x}_0)\| \leq \varepsilon$ for any $t \geq 0$.*

The trivial solution of (1) is called asymptotically stable *if it is stable and t here exists $\rho > 0$ such that $\lim_{t\to\infty} \varphi(t, \mathbf{x}_0) = 0$ whenever $\|\mathbf{x}_0\| < \rho$.*

*Let $\alpha > 0$. The trivial solution of (1) is called $\mathcal{O}(t^{-\alpha})$-*asymptotically stable *if it is stable and there exists $\rho > 0$ such that for any $\|\mathbf{x}_0\| < \rho$ one has:*

$$\|\varphi(t, \mathbf{x}_0)\| = \mathcal{O}(t^{-\alpha}) \quad \text{as } t \to \infty.$$

The characteristic equation is obtained:

$$s^q + \alpha s^{q_1} + \beta s^{q_2} + \gamma s^{q_3} + \delta = 0. \tag{2}$$

The main contribution of this work is the analysis of the distribution of roots of equation (2). Therefore, we consider the complex valued function

$$\Delta(s; \alpha, \beta, \gamma, \delta, q_1, q_2, q_3, q) = s^q + \alpha s^{q_1} + \beta s^{q_2} + \gamma s^{q_3} + \delta.$$

Theorem 1

i. Equation (1) is $\mathcal{O}(t^{-q'})$-asymptotically stable if and only if all the roots of the characteristic function $\Delta(s; \alpha, \beta, \gamma, q_1, q_2, q_3, q)$ are in the open left half-plane ($\Re(s) < 0$), where $q' = \min\{\{q_1\}, \{q_2\}, \{q_3\}, \{q\}\}$, with $\{q^*\} = q^* - \lfloor q^* \rfloor$, $q^* \in \{q_1, q_2, q_3, q\}$.

ii. If $\gamma \neq 0$ and the characteristic function $\Delta(s; \alpha, \beta, \gamma, \delta, q_1, q_2, q_3, q)$ has at least one root in the open right half-plane ($\Re(s) > 0$), equation (1) is unstable.

2 Fractional-order-dependent stability and instability results

In this section, we will assume that the fractional orders q_1, q_2, q_3, q are arbitrarily fixed inside the domain

$$D = \{(q_1, q_2, q_3, q) \in \mathbb{R}^4 \ : \ 0 < q_1 < q_2 < q_3 < q \leq 2\}.$$

Moreover, as $\delta < 0$ implies that the equation (1) is unstable, for any choice of the fractional orders q_1, q_2, q (as it will be shown in section 3), we will further assume that $\delta > 0$.

Lemma 2 *Let $(q_1, q_2, q_3, q) \in D$ and $\delta > 0$ arbitrarily fixed. Consider the parametric surface in the (α, β, γ)-space defined by*

$$S(\delta, q_1, q_2, q_3, q) \ : \ \begin{cases} \alpha = \delta^{1-\frac{q_1}{q}} h(\omega, \eta, q_1, q_2, q_3, q) \\ \beta = \delta^{1-\frac{q_2}{q}} h(\omega, \eta, q_2, q_1, q_3, q) \\ \gamma = \delta^{1-\frac{q_3}{q}} \eta \omega^{-\frac{q_3}{q}} \end{cases}, \quad \omega > 0, \eta \in \mathbb{R}$$

where $h : (0, \infty)^2 \times D \to (0, \infty)$ is given by:

$$h(\omega, \eta, q_1, q_2, q_3, q) = \omega^{-\frac{q_1}{q}} \left[\eta \rho(q_3 - q_2, q_2 - q_1) + \omega \rho(q - q_2, q_2 - q_1) - \rho(q_2, q_2 - q_1)\right]$$

with the function ρ defined as

$$\rho(a, b) = \frac{\sin \frac{a\pi}{2}}{\sin \frac{b\pi}{2}} \quad , \ \forall \ a \in [0, 2], \ b \in [-1, 0) \cup (0, 1].$$

The surface $S(\delta, q_1, q_2, q_3, q)$ lies outside the first octant ($\alpha > 0, \beta > 0, \gamma > 0$) of the (α, β, γ)-space.

Remark 1 *If* $q_1 = q_2 = q_3 =: q^*$, $S(\delta, q_1, q_2, q_3, q)$ *represents the plane*

$$\alpha + \beta + \gamma = -\frac{\gamma^{1-\frac{q^*}{q}} \sin\frac{q\pi}{2}}{\left(\sin\frac{q^*\pi}{2}\right)^{\frac{q^*}{q}} \left(\sin\frac{(q-q^*)\pi}{2}\right)^{1-\frac{q^*}{q}}}.$$

Proposition 3 *Let* $\delta > 0$, $(q_1, q_2, q_3, q) \in D$ *arbitrarily fixed. Consider the surface* $S(\delta, q_1, q_2, q_3, q)$ *defined in Lemma 2. The characteristic equation* (2) *has a pair of complex conjugated roots on the imaginary axis of the complex plane if and only if* $(\alpha, \beta, \gamma) \in S(\delta, q_1, q_2, q_3, q)$. *The surface* $S(\delta, q_1, q_2, q_3, q)$ *represents the boundary of the stability region of the equation* (1), *i.e. the set of parameters* (α, β, γ) *such that the trivial solution of equation* (1) *is asymptotically stable.*

3 Fractional-order-independent stability and instability results

Proposition 4 *If* $\delta < 0$ *or* $\alpha + \beta + \gamma + \delta + 1 \leq 0$, *the trivial solution of equation* (1) *is unstable, regardless of the fractional orders* q_1, q_2, q_3 *and* q.

The following Proposition provides a sufficient condition for the asymptotic stability of the equation (1), regardless of the fractional orders $(q_1, q_2, q_3, q) \in D$. In what follows, only the case $\delta > 0$ will be considered, as Proposition 4 states that if $\delta < 0$, the equation (1) is unstable, regardless of the fractional orders $(q_1, q_2, q_3, q) \in D$.

Proposition 5 *If* $\alpha > 0$, $\beta > 0$, $\gamma > 0$ *and* $\delta > 0$, *the trivial solution of equation* (1) *is asymptotically stable, for any fractional orders* q_1, q_2, q_3 *and* q.

References

[1] Oana Brandibur and Eva Kaslik. Stability analysis of multi-term fractional-differential equations with three fractional derivatives. *Journal of Mathematical Analysis and Applications*, 495(2):124751, 2021.

[2] J. Čermák and T. Kisela. Stability properties of two-term fractional differential equations. *Nonlinear Dynamics*, 80(4):1673–1684, 2015.

[3] K. Diethelm. *The analysis of fractional differential equations.* Springer, 2004.

[4] R. Gorenflo and F. Mainardi. Fractional calculus, integral and differential equations of fractional order. In A. Carpinteri and F. Mainardi, editors, *Fractals and Fractional Calculus in Continuum Mechanics*, volume 378 of *CISM Courses and Lecture Notes*, pages 223–276. Springer Verlag, Wien, 1997.

[5] Y. Li, Y.Q. Chen, and I. Podlubny. Mittag-Leffler stability of fractional order nonlinear dynamic systems. *Automatica*, 45(8):1965 – 1969, 2009.

International Conference on Mathematical Analysis and Applications in Science and Engineering
ICMA^{2}SC'22
ISEP Porto-Portugal, June 27 - 29, 2022

Solving the fractional Ambartsumian equation

Manuel D. Ortigueira[1⋆] **Gabriel Bengochea**[2]

[1] CTS-UNINOVA, Portugal.
[2] Universidad Autónoma de la Ciudad de México, México.

[1⋆]mdo@fct.unl.pt

Abstract: The fractional Ambartsumian equation is solved with all the generality for any order in the interval $(0, 2)$. The solution is expressed as a linear combination of Mittag-Leffler functions. The computation is performed with the fast Fourier transform.

keywords: Ambartsumian equation; Bilinear transformation; Mittag-Leffler function.

MSC2020: 49-XX; 34-XX; 92-XX.

1 Introduction

The original, integer order, Ambartsumian equation was introduced in the theory of surface brightness in milky way [1]. It assumes the form:

$$x'(t) + x(t) = \frac{1}{q}x(\frac{t}{q}) \tag{1}$$

under a suitable initial condition $x_0 = x(0)$. The parameter q is a real greater than 1. This equation was solved using different methodologies. In [2] a Taylor series was obtained. Alternatively, Bakodah and Ebaid [3], using the the "Laplace-Transform and Decomposition Method," got a solution in terms of a series with exponential terms. Alharbi and Ebaid obtained a similar solution [4].
The fractional Ambartsumian equation was studied first by Kumar et al. [5] using the Caputo derivative. The solution they found was essentially a fractional Taylor series, generalising the formulation in [2]. Two different papers obtained similar results generalising Bakodah and Ebaid result with the exponentials were subtituted by Mittag-Leffler functions.
Here, we will obtain a simpler formulation, also using Mittag-Leffler functions, but with a faster converging series. We use a simple implementation of the Mittag-Leffer function using the bilinear discrete-time equivalent [6].

2 Problem formulation and its solution

The fractional Ambartsumian equation we propose to solve assumes the general form

$$D^{\alpha}x(t) + x(t) = \frac{1}{q}x(\frac{t}{q}) \quad t \geq 0,\ q \geq 1, \tag{2}$$

under a suitable initial condition $x_0 = x(0)$. The derivative order α can assume any real value in the interval $(0, 2)$. We use the forward Grünwald-Letnikov [8, 7]

$$D^{\alpha}x(t) = \lim_{h \to 0^+} \frac{\sum_{n=0}^{\infty} \frac{(-\alpha)_n}{n!} x(t - nh)}{h^{\alpha}}, \tag{3}$$

Alternatively, we can use the Liouville derivatives, regularized or not [8]. The initial-condition is treated as in [9]. In terms of the bilateral Laplace transform (LT), the equation (2) becomes

$$s^{\alpha}X(s) - x_0 s^{\alpha-1} + X(s) = X(qs) \quad Re(s) > 0, \tag{4}$$

where $X(s) = \mathcal{L}x(t)$ and the scale property of the LT was used. It gives

$$X(s) = x_0 \frac{s^{\alpha-1}}{s^{\alpha}+1} + \frac{1}{s^{\alpha}+1} X(qs) \quad Re(s) > 0, \tag{5}$$

with $X(s) = \mathcal{L}x(t)$. Similarly to the procedure in [4, 3], we set

$$X(s) = \sum_{n=0}^{\infty} C_n \frac{s^{\alpha-1}}{s^{\alpha} + q^{-n\alpha}}, \tag{6}$$

where C_n are real paramters to be computed. With this formulation, the solution of (2) will assume the form

$$x(t) = \sum_{n=0}^{\infty} C_n E_{\alpha}\left(-q^{-n\alpha}t^{\alpha}\right), \quad t > 0, \tag{7}$$

where $E_{\alpha}(.)$ is the Mittag-Leffler function. We insert (6) into (4) to get

$$(s^{\alpha}+1)\sum_{n=0}^{\infty} C_n \frac{s^{\alpha-1}}{s^{\alpha} + q^{-n\alpha}} = x_0 s^{\alpha-1} + q^{-1}\sum_{n=1}^{\infty} C_{n-1} \frac{s^{\alpha-1}}{s^{\alpha} + q^{-n\alpha}}$$

On the other hand,

$$\frac{s^{\alpha}+1}{s^{\alpha}+q^{-n\alpha}} = \frac{s^{\alpha}+q^{-n\alpha}-q^{-n\alpha}+1}{s^{\alpha}+q^{-n\alpha}} = 1 + \frac{1-q^{-n\alpha}}{s^{\alpha}+q^{-n\alpha}}$$

that leads to

$$s^{\alpha-1}\sum_{n=0}^{\infty} C_n + \sum_{n=1}^{\infty} C_n \left(1 - q^{-n\alpha}\right) \frac{s^{\alpha-1}}{s^{\alpha} + q^{-n\alpha}} = x_0 s^{\alpha-1} + q^{-1}\sum_{n=1}^{\infty} C_{n-1} \frac{s^{\alpha-1}}{s^{\alpha} + q^{-n\alpha}}$$

from where, we obtain

$$C_n = \frac{1}{q\left(1 - q^{-n\alpha}\right)} C_{n-1}, \quad n = 1, 2, \cdots \tag{8}$$

where $x_0 = \sum_{n=0}^{\infty} C_n$. Starting with $C_0 =$ we obtain a sequence that has to be normalized so that its sum is equal to x_0. Let $S = \sum_{n=0}^{\infty} C_n$. Define a normalizing factor $F = \frac{x_0}{S}$. The normalized coefficients are given by $C_n \cdot F$.

3 Numerical aspects

As it can be verified, above a given n_{th}, the sequence becomes negligible, implying that the series solutions (7), or (6) have a finite number of meaningful terms, so that they can be truncated, disregarding the terms for $n > n_{th}$. From a numerical point of view, this means that they become comparable to the relative spacing between any two adjacent numbers in the machine's floating point system, "eps" in Octave/Matlab. We set $n_{th} = -log(eps)/log(q)/alfa$. Therefore, the series in (6) and (8) become finite summations. We have two different approaches not numerically equivalent to compute such summations:

1. Use of (8) together with a suitable algorithm for the computation of the needed Mittag-Leffler function [10]. This algorithm has a very severe drawback: the computational burden. For example, taking $q = 1.2$ it takes around 17 minutes to compute $x(t)$.

2. Work in frequency domain, using (6), followed by a transform inversion. To do it, we proceed according to the following steps

   (a) Use the $s \to z$ bilinear transformation [6] to pass from a continuous-time to a sampled (discrete) function. T is the sampling interval. With some work, we obtain the function

   $$X_d(z) = \frac{T}{2}\frac{1+z^{-1}}{1-z^{-1}}\sum_{n=0}^{n_{th}} C_n \frac{1}{1+q^{-n\alpha}\left(\frac{T}{2}\frac{1+z^{-1}}{1-z^{-1}}\right)^{\alpha}+}, \tag{9}$$

   Consider, for now, only the summation part, $\bar{X}_d(z)$

   (b) Set $z = e^{i\omega}$, $-\pi < \omega \leq \pi$ to obtain discrete-time Fourier transform $\bar{X}_d(e^{i\omega})$ of $\bar{x}(nT)$ [7] and sample it in a uniform grid, making $\omega_k = \frac{2\pi}{N}k$, $k = 0, 1, \cdots, N-1$, where N is enough high in agreement with T and the interval where we want to compute the function. In our simulations, we used $T = 0.01$ and $N = 2^12$.

   (c) Use the fast Fourier transform to compute the inverse of $\bar{X}_d(e^{i\omega_k})$, $\bar{x}(nT)$.

   (d) To get $x(nT)$, we use the following difference equation

   $$x(nT) = x\left((n-1)T\right) + \frac{T}{2}\left(\bar{x}\left(nT\right) + \bar{x}\left((n-1)T\right)\right)$$

   We must remark that this procedure, based on the inversion of a transform leads to $\frac{x(0)}{2}$ at the origin.

This procedure is very fast ($\approx 2s$) and the result is not visibly different from the direct approach based on the direct computation of the Mittag-Leffler function. In Figure 1 we illustrate the solution for 3 values of α and 2 of q.

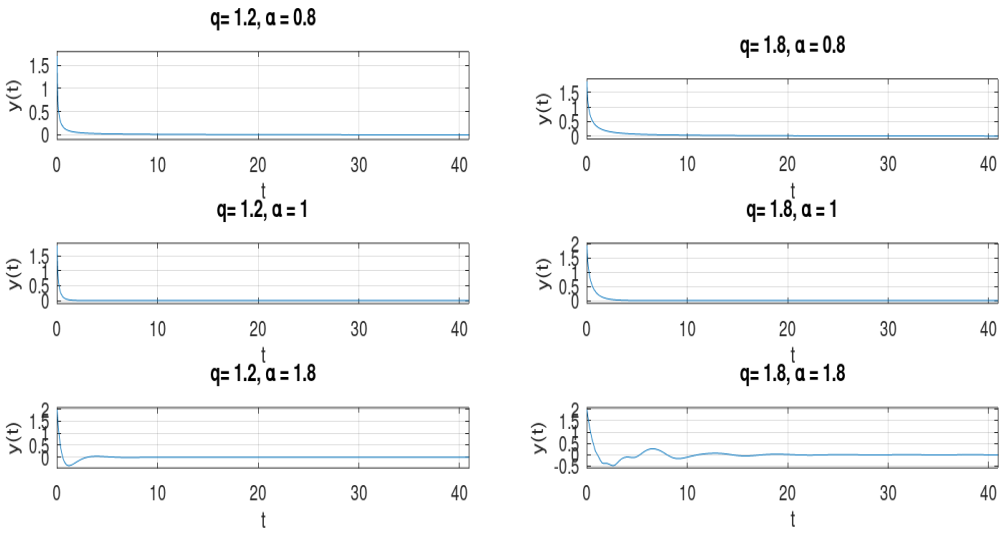

Figure 1: Numerical computation of $x(t)$.

4 Conclusions and Future work

We presented a simple solution for the Ambartsumian equation. We used a decomposition in terms of Mittag-Leffler functions. For the numarical computation we used the bilinear tarnsformation and the fast Fourier transform. This procedure will be used in other similar problems.

Acknowledgments

This work was funded by Portuguese National Funds through the FCT - Foundation for Science and Technology under the project UIDB/00066/2020.

References

[1] V. Ambartsumian, *On the fluctuation of the brightness of the milky way,* in: Dokl. Akad. Nauk SSSR, Vol. 44, 1944, pp. 223–226.

[2] J. Patade, S. Bhalekar, *On analytical solution of Ambartsumian equation,* National Academy Science Letters 40 (4) (2017) 291–293.

[3] H. O. Bakodah, A. Ebaid, *Exact solution of Ambartsumian delay differential equation and comparison with Daftardar-Gejji and Jafari approximate method,* Mathematics 6 (12) (2018) 331.

[4] F. M. Alharbi, A. Ebaid, *New analytic solution for Ambartsumian equation,* Journal of Mathematics and System Science 8, 182–186 (2018) .

[5] D. Kumar, J. Singh, D. Baleanu, S. Rathore, *Analysis of a fractional model of the Ambartsumian equation,* The European Physical Journal Plus 133 (7) (2018) 1–7.

[6] M. D. Ortigueira, J. A. T. Machado, *New discrete-time fractional derivatives based on the bilinear transformation: Definitions and properties*, Journal of Advanced Research 25 (2020) 1–10, recent Advances in the Fractional-Order Circuits and Systems: Theory, Design and Applications.

[7] M. D. Ortigueira, D. Valério, *Fractional signals and systems,* De Gruyter, 2020.

[8] M. D. Ortigueira, *Fractional Calculus for Scientists and Engineers,* Lecture Notes in Electrical Engineering, Springer, Dordrecht, Heidelberg, 2011.

[9] M. D. Ortigueira, F. J. Coito, *System initial conditions vs derivative initial conditions,* Computers & Mathematics with Applications 59 (5) (2010) 1782–1789.

[10] M. D. Ortigueira, A. M. Lopes, J. A. T. Machado, *On the numerical computation of the Mittag-Leffler function,* International Journal of Nonlinear Sciences and Numerical Simulation 20.

International Conference on Mathematical Analysis and Applications in Science and Engineering
ICMA^{2}SC'22
ISEP Porto-Portugal, June 27 - July 1, 2022

Solving Prabhakar differential equations using Mikusiński's operational calculus

Noosheza Rani **Arran Fernandez**

Eastern Mediterranean University, Northern Cyprus

nooshezarani@yahoo.com

Abstract: In this paper, we used Mikusiński's operational calculus to discuss the structure of the Prabhakar fractional derivative operator of Caputo type. The operational calculus allows us to construct explicit solutions for initial value problems for the general n-term linear equation with Caputo fractional derivatives of arbitrary order with constant coefficients.

keywords: fractional differential equations; operational calculus; Mikusiński's operational calculus; Mittag-Leffler functions; Prabhakar fractional calculus

MSC2010: 34A08; 44A40; 33E12

1 Introduction

As we know, differential equations play an important role to form a major part of applied mathematics. There exist several different ways to solve differential equations: sometimes an exact solution can be found explicitly, or for difficult cases a solution may be approximated numerically.

If the order of a differential equation is a non-integer real or complex number, then we get a so-called fractional differential equation. In the last two decades, fractional differential equations received increased interest both in pure and applied mathematics. There are many different methods for solving equations; some of them can easily extend to solve fractional differential equations with little modification, but some of them only work for special cases, e.g. rational-order operators.

In this paper we focus on Mikusiński's operational calculus. It is an algebraic interpretation of the operators of differentiation and integration, which gives rise to a method for solving fractional differential equations. This method is formally similar to the Laplace transform method, but easier to make mathematically rigorous, and applicable to more different types of functions. Since the 1990s, it has been applied to fractional calculus, including the basic Riemann-Liouville and Caputo fractional calculi as well as other types such as Hilfer fractional calculus, and recently fractional calculus with respect to functions and Prabhakar fractional calculus.

As we know, there are many different ways to define fractional integrals and derivatives, and in this paper we focus on the Prabhakar fractional calculus of Caputo type. It is important to address Caputo-type fractional differential equations, and this can be done by using Mikusiński's operational calculus. First of all we choose an appropriate function space setting, and make it a ring under addition and convolution. Secondly, extend the ring to its field of fractions, an

algebraic abstraction whose elements are not necessarily functions. Interpret integral operators as ring elements via convolution and derivative operators as field elements via inversion. Now many differential equations become algebraic equations. Solutions found algebraically in the ring, then written as functions.

2 Results and discussion

Definition 1 *For any $\eta \in \mathbb{R}$, the vector space C_η is defined to be the set of all functions $f(x)$, $x > 0$, expressible as $f(x) = x^p f_1(x)$ for some real number $p > \eta$ and function $f_1 \in C[0, \infty)$. Note that such functions f are not necessarily defined at $x = 0$ (if p is negative). Note also that, if $\eta \geq -1$, then $C_\eta \subseteq L^1[0, X]$ for any finite $X > 0$.*

Definition 2 *For any $\eta \in \mathbb{R}$ and $m \in \mathbb{N} \cup \{0\}$, the vector space C_η^m is defined to be the set of all functions $f(x)$, $x > 0$, such that f is m times differentiable and $f^{(m)} \in C_\eta$. Note that $C_\eta^0 \equiv C_\eta$.*

The Prabhakar fractional integral operator ${}_0^P I_x^{\alpha,\beta,\gamma,\delta}$ may be represented in the ring C_{-1} by multiplication with the element $P_{\beta,\gamma} = x^{\beta-1} E_{\alpha,\beta}^{\gamma}(\delta x^\alpha)$. Let $S_{\beta,\gamma}$ denote the algebraic inverse of $P_{\beta,\gamma}$ in the field M_{-1}.

Theorem 1 *Let $\alpha, \beta \in \mathbb{R}^+$ and $\gamma, \delta \in \mathbb{R}$ and $m = \lfloor \beta \rfloor + 1 \in \mathbb{N}$. For any $f \in C_\eta^m$ (where $\eta \geq -1$), its Prabhakar fractional derivatives of Riemann–Liouville and Caputo type are connected by the following relation:*

$$ {}_0^{PC} D_x^{\alpha,\beta,\gamma,\delta} f(x) = {}_0^{PR} D_x^{\alpha,\beta,\gamma,\delta} f(x) - \sum_{k=0}^{m-1} x^{k-\beta} E_{\alpha,k-\beta}^{\gamma}(\delta (x)^\alpha) f^{(k)}(0). \tag{1} $$

Theorem 2 *Let $\alpha, \beta \in \mathbb{R}^+$ and $\gamma, \delta \in \mathbb{R}$ and $m = \lfloor \beta \rfloor + 1 \in \mathbb{N}$. The Prabhakar fractional derivative operator ${}_0^{PC} D_x^{\alpha,\beta,\gamma,\delta}$ may be represented in the field M_{-1} in the form*

$$ {}_0^{PC} D_x^{\alpha,\beta,\gamma,\delta} f = S_{\beta,\gamma} \cdot f - S_{\beta,\gamma} \cdot Ff, \qquad f \in C_{-1}^m, \tag{2} $$

where the element Ff is given by initial values of f as

$$ Ff = \sum_{k=0}^{m-1} f^{(k)}(0^+) \cdot \frac{x^k}{k!}. $$

References

[1] J. Mikusiński, *Operational Calculus*, Pergamon Press, Oxford, 1959.

[2] H. G. Flegg, "Mikusinski's Operational Calculus", *International Journal of Mathematical Education in Science and Technology* 5(2) (1974), pp. 131–137.

[3] Y. Luchko, R. Gorenflo, "An operational method for solving fractional differential equations", *Acta Mathematica Vietnamica* 24 (1999), pp. 207–234.

[4] N. Rani, A. Fernandez, "Mikusinski's operational calculus for Prabhakar fractional calculus", *Integral Transforms and Special Functions* (2022), pp. 1–21.

[5] N. Rani, A. Fernandez, "Solving Prabhakar differential equations using Mikusinski's operational calculus", *Computational & Applied Mathematics* 41 (2022), 107.

International Conference on Mathematical Analysis and Applications in Science and Engineering
ICMA^{2}SC'22
ISEP Porto-Portugal, June 27 - 29, 2022

Mittag-Leffler special function and its connection to special Lévy processes.

Janusz Gajda[1⋆]

[1] Faculty of Economic Sciences, University of Warsaw
ul. Długa 44/50, 00-241 Warsaw, Poland

[1⋆]jgajda@wne.uw.edu.pl

Abstract: We investigate some generalizations of the Mittag-Leffler Lévy (ML) processes obtained via subordination or via Lévy measure extensions through the special Prabhakar function (which is a Mittag-Leffler with the additional parameters β and γ). We prove that this so-called Prabhakar process,for $\beta = 1$, can be represented as an α-stable process subordinated by an independent generalized gamma subordinator; thus it can be considered as an extension of the geometric stable process, to which it reduces for $\gamma = 1$. For other special cases of parameters, the Prabhakar process can be considered as an interpolation among various well-known and widely applied stochastic models.

keywords: Mittag-Leffler distribution; subordinated; stochastic processes.

MSC2020: 33E12; 26A33; 60G51; 60G52.

1 Introduction

We investigate some generalizations of the Mittag-Leffler (ML) Lévy processes obtained via subordination or via Lévy measure extension through the special Prabhakar function (which is a Mittag-Leffler with the additional parameters β and γ). We prove that this so-called Prabhakar process,for $\beta = 1$, can be represented as an α-stable process subordinated by an independent generalized gamma subordinator; thus it can be considered as an extension of the geometric stable process, to which it reduces for $\gamma = 1$. For other special cases of parameters, the Prabhakar process can be considered as an interpolation among various well-known and widely applied stochastic models. This work is based on papers [1, 2].

2 Results and discussion

Our main resulsts are related to construction of new classes of ML processes. We prove results related to subordination representation of such processes, their main properties like characteristic function, density of Lévy measure, characteristic function or fractional Fokker-Planck type equations describing their probability density functions. We illustrate our results with some numerical simulations.

References

[1] J. Gajda, Generalized Mittag-Leffler L´evy process and its connections to first passage times of L´evy subordinators, Communications in Statistics - Theory and Methods (2020) 1–9.

[2] J. Gajda, L. Beghin, Prabhakar L´evy processes, Statistics & Probability Letters 178 (2021) 109162.

International Conference on Mathematical Analysis and Applications in Science and Engineering
ICMA²SC'22
ISEP Porto-Portugal, June 27 - 29, 2022

ψ-Hilfer fractional relaxation-oscillation equation

N. Vieira[†,⋆] **M. Ferreira** [‡] **M. Manuela Rodrigues** [†]

[†] Department of Mathematics, University of Aveiro & CIDMA, Portugal
[‡] School of Technology and Management, Polytechnic Institute of Leiria & CIDMA, Portugal

[⋆] nloureirovieira@gmail.com

Abstract: In this work, we solve the ψ-Hilfer fractional relaxation-oscillation equation with a force term, where the time-fractional derivatives are in the ψ-Hilfer sense. The solution of the equation is presented in terms of bivariate Mittag-Leffler functions. An asymptotic analysis of the solution of the associated homogeneous equation is performed.

keywords: Fractional relaxation-oscillation equation; ψ-Hilfer derivative; Bivariate Mittag-Leffler function.

MSC2010: 35R11; 26A33; 34C26; 35B05.

1 Introduction

The relaxation and oscillation processes are of great relevance in physics. From a mathematical point of view, they are modelled by linear differential equations of first and second orders in time. In [2] the fractional relaxation and oscillation equations with Caputo derivatives were studied separately. The simultaneous consideration of time-fractional derivatives or first and second orders leads to the so-called fractional relaxation-oscillation phenomena, that we study in this paper.

2 Preliminaries

In this section, we recall some basic definitions about ψ-Hilfer fractional derivatives, special functions, and the ψ-Laplace transform, that are necessary for this work.

Definition 1 *(cf. [4, Def. 4]) Let (a,b) be a finite or infinite interval on the real line $\mathbb{R}$ and $\alpha>0$. Also let ψ be a monotone increasing and positive function on (a,b), having a continuous derivative ψ' in (a,b). The left Riemann-Liouville fractional integral of a function f with respect to another function ψ on $[a,b]$ is given by*

$$\left(I_{a^+}^{\alpha,\psi} f\right)(t) = \frac{1}{\Gamma(\alpha)} \int_a^t \psi'(w)\, (\psi(t)-\psi(w))^{\alpha-1}\, f(w)\, dw, \qquad t>a. \tag{1}$$

Next, we give the definition of the so-called ψ-Hilfer fractional derivative of a function f with respect to another function.

Definition 2 *(cf. [4, Def. 7]) Let $\alpha>0$ and $m=[\alpha]+1$, where $[\alpha]$ denotes the integer part of α. Let also $I=[a,b]$ be a finite or infinite interval on the real line and $f,\psi\in C^m[a,b]$ two functions such that ψ is a positive monotone increasing function and $\psi'(t)\neq 0$, for all $t\in I$. The left ψ-Hilfer fractional derivative ${}^{H}D_{a^+}^{\alpha,\mu;\psi}$ of order α and type $\mu\in[0,1]$ is defined by*

$$\left({}^{H}D_{a^+}^{\alpha,\mu;\psi} f\right)(t) = I_{a^+}^{\mu(m-\alpha),\psi} \left(\frac{1}{\psi'(t)}\frac{d}{dt}\right)^m I_{a^+}^{(1-\mu)(m-\alpha),\psi} f(t)\,. \tag{2}$$

We observe that when $\mu = 0$ we recover the left Riemann-Liouville fractional derivative of a function with respect to ψ (see [4, Def. 5]) and when $\mu = 1$ we obtain the left Caputo fractional derivative of a function with respect to ψ (see [4, Def. 6]). In Section 5 of [4] is presented a list of several fractional integrals and fractional derivatives that can be obtained from (1) and (2), respectively, for different choices of μ and ψ. The solution of the ψ-fractional relaxation-oscillation equation is presented in terms of the bivariate Mittag-Leffler function which has the following double series representation:

$$E_{(a_1,a_2),b}\left(z_1,z_2\right) = \sum_{l_1=0}^{+\infty}\sum_{l_2=0}^{+\infty}\frac{(l_1+l_2)!}{l_1!\,l_2!}\frac{z_1^{l_1}\,z_2^{l_2}}{\Gamma\left(b+a_1l_1+a_2l_2\right)}. \tag{3}$$

When $z_1 = -c_1t^{a_1}$, $z_2 = -c_2t^{a_2}$, with $a_1, a_2, c_1, c_2, b, t > 0$, we have the following asymptotic expansions near the origin and at the infinity:

$$E_{(a_1,a_2),b}\left(-c_1\,t^{a_1},-c_2\,t^{a_2}\right) \sim \frac{1}{\Gamma\left(b\right)} - \frac{c_1\,t^{a_1}}{\Gamma\left(b+a_1\right)} - \frac{c_2\,t^{a_2}}{\Gamma\left(b+a_2\right)}, \quad t \to 0^+, \tag{4}$$

$$E_{(a_1,a_2),b}\left(-c_1\,t^{a_1},-c_2\,t^{a_2}\right) \sim \frac{t^{-a_1}}{c_1\,\Gamma\left(b-a_1\right)}, \quad b \neq a_1,\ t \to +\infty. \tag{5}$$

The ψ-Laplace transform of a real valued function $f\left(t\right)$ with respect to ψ is defined by (see [3, Def. 13])

$$\mathcal{L}_\psi\left\{f\left(t\right)\right\}\left(\mathbf{s}\right) = \widetilde{f}_\psi\left(\mathbf{s}\right) = \int_0^{+\infty} e^{-\mathbf{s}\,\psi(t)}\,\psi'\left(t\right)\,f\left(t\right)\,dt, \quad \mathrm{Re}\left(\mathbf{s}\right) \in \mathbb{C},$$

where ψ is a non negative monotone increasing function in $\mathbb{R}_0^+$ and such that $\psi\left(0\right) = 0$. The ψ-Laplace transform may be written as the following composition operator involving the classical Laplace transform: $\mathcal{L}_\psi = \mathcal{L} \circ Q_{\psi^{-1}}$ where $\left(Q_{\psi^{-1}}f\right)\left(t\right) = f\left(\psi^{-1}\left(t\right)\right)$ (cf. [3, Thm. 4]). As a consequence of the previous relation, if f is a function whose classical Laplace transform is $\widetilde{f}$, the ψ-Laplace transform of $f\left(\psi\left(t\right)\right)$ is also $\widetilde{f}\left(\mathbf{s}\right)$ (see [3, Cor. 2]), that is,

$$\mathcal{L}\left\{f\left(t\right)\right\}\left(\mathbf{s}\right) = \widetilde{f}\left(\mathbf{s}\right) \quad \Rightarrow \quad \mathcal{L}_\psi\left\{f\left(\psi\left(t\right)\right)\right\}\left(\mathbf{s}\right) = \widetilde{f}\left(\mathbf{s}\right).$$

We observe that the definition of the ψ-Laplace can be adapted fon any interval $[a, +\infty[\subseteq \mathbb{R}_0^+$ with ψ satisfying $\psi\left(a\right) = 0$. This is important in our work in order to the ψ-Hilfer derivative encompasses the largest number of fractional derivatives. When the ψ-Laplace transform is applied to the ψ-Hilfer derivative we obtain (see [3, Thm. 6])

$$\mathcal{L}_\psi\left\{\,{}^{H}D_{a^+}^{\alpha,\mu;\psi}f\left(t\right)\right\}\left(\mathbf{s}\right) = \mathbf{s}^\alpha\,\widetilde{f}_\psi\left(\mathbf{s}\right) - \sum_{j=0}^{m-1}\mathbf{s}^{m-\mu(m-\alpha)-1-j}\left(I_{t,a^+}^{(1-\mu)(m-\alpha)-j;\psi}f\right)\left(a^+\right), \tag{6}$$

where $m = [\alpha] + 1$ and the initial-value terms $\left(I_{a^+}^{(1-\mu)(m-\alpha)-j,\psi}f\right)\left(a^+\right)$ are evaluated in the limit $t \to a^+$. The ψ-Laplace convolution operator of two functions is defined by (see [3, Def. 15])

$$\left(f *_\psi g\right)\left(t\right) = \int_0^t f\left(\psi^{-1}\left(\psi\left(t\right)-\psi\left(w\right)\right)\right)\,\psi'\left(w\right)\,g\left(w\right)\,dw, \quad t \in \mathbb{R}^+, \tag{7}$$

and the correspondent Convolution Theorem is (see [3, Thm. 8])

$$\mathcal{L}_\psi\left\{\left(f *_\psi g\right)\left(t\right)\right\}\left(\mathbf{s}\right) = \mathcal{L}_\psi\left\{f\right\}\left(\mathbf{s}\right)\,\mathcal{L}_\psi\left\{g\right\}\left(\mathbf{s}\right). \tag{8}$$

Moreover, from relation (17.6) in [1] we have that

$$\mathcal{L}_\psi\left\{\psi\left(t\right)^{\alpha-\gamma}\sum_{p=0}^{+\infty}\left(-a\,\psi\left(t\right)^{\alpha-\beta}\right)^p E_{\alpha,\alpha+(\alpha+\beta)p-\gamma+1}^{p+1}\left(-b\,\psi\left(t\right)^\alpha\right)\right\}\left(\mathbf{s}\right) = \frac{\mathbf{s}^{\gamma-1}}{\mathbf{s}^\alpha + a\mathbf{s}^\beta + b}, \tag{9}$$

where $\mathrm{Re}\left(\alpha\right), \mathrm{Re}\left(\beta\right), \mathrm{Re}\left(\gamma\right) \in \mathbb{R}^+$, $\left|\frac{a\mathbf{s}^\beta}{\mathbf{s}^\alpha+\beta}\right| < 1$, and provided that the series in (9) is convergent.

3 ψ-Hilfer fractional relaxation-oscillation equation

In this section, we solve the ψ-Hilfer fractional forced damped oscillator modelled by the following fractional differential equation

$$c_2\,{}^{H}D_{a^+}^{\alpha_2,\mu_2;\psi}u\left(t\right)+c_1\,{}^{H}D_{a^+}^{\alpha_1,\mu_1;\psi}u\left(t\right)+d^2\,u\left(t\right)\,=q\left(t\right), \tag{10}$$

and subject to the following initial conditions

$$\left(I_{t,a^+}^{(1-\mu_1)(1-\alpha_1);\psi}u\right)\left(a^+\right)=\kappa_1,\ \ \left(I_{t,a^+}^{(1-\mu_2)(2-\alpha_2);\psi}u\right)\left(a^+\right)=\kappa_2,\ \frac{d}{dt}\left[\left(I_{t,a^+}^{(1-\mu_2)(2-\alpha_2);\psi}u\right)\right]\left(a^+\right)=\kappa_3, \tag{11}$$

which are evaluated in the limit $t\to a^+$. Moreover, $c_2,c_1,d,\kappa_1,\kappa_2,\kappa_3\in\mathbb{R}$, $c_2\neq 0$, $t\in I$, with $I=[a,b]$ being a finite or infinite interval on $\mathbb{R}^+$, the partial time-fractional derivatives of orders $\alpha_1\in\,]0,1]$ and $\alpha_2\in]1,2]$, and types $\mu_1,\mu_2\in[0,1]$, respectively, are the ψ-Hilfer derivatives given by (2), q belongs to $L_1\left(I\right)$ (when $q\left(t\right)=0$ the solution of equation (10) corresponds to an unforced damped oscillator). We look for solutions u of our problem in the space $C^2\left(a,b\right)$.

When $\psi\left(t\right)=t$, with $t\in\mathbb{R}^+$, $\mu_1=\mu_2=1$, and $c_2=0$ or $c_1=0$ in equation (10), we obtain, respectively, the time-fractional relaxation/oscillation equations with Caputo fractional derivatives. These two equations were studied separately in [2]. Moreover, equation (10) is a particular case of the time-fractional telegraph equation with ψ-Hilfer derivatives studied in [5].

Now, we solve our relaxation-oscillation problem. Applying the ψ-Laplace transform to (10) and taking into account (11), we get

$$\left(c_2\,\mathbf{s}^{\alpha_2}+c_1\,\mathbf{s}^{\alpha_1}+d^2\right)\,\widetilde{u}_\psi\left(\mathbf{s}\right)-c_1\,\kappa_1\,\mathbf{s}^{-\mu_1(1-\alpha_1)}-c_2\,\kappa_2\,\mathbf{s}^{1-\mu_2(2-\alpha_2)}-c_2\,\kappa_3\,\mathbf{s}^{-\mu_2(2-\alpha_2)}=\widetilde{q}_\psi\left(\mathbf{s}\right). \tag{12}$$

Solving the above equation in order to $\widetilde{u}_\psi$, we obtain:

$$\widetilde{u}_\psi\left(\mathbf{s}\right)=\frac{\frac{c_1\,\kappa_1}{c_2}\,\mathbf{s}^{-\mu_1(1-\alpha_1)}+\kappa_2\,\mathbf{s}^{1-\mu_2(2-\alpha_2)}+\kappa_3\,\mathbf{s}^{-\mu_2(2-\alpha_2)}}{\mathbf{s}^{\alpha_2}+\frac{c_1}{c_2}\,\mathbf{s}^{\alpha_1}+\frac{d^2}{c_2}}+\frac{1}{c_2}\,\widetilde{q}_\psi\left(\mathbf{s}\right)\,\frac{1}{\mathbf{s}^{\alpha_2}+\frac{c_1}{c_2}\,\mathbf{s}^{\alpha_1}+\frac{d^2}{c_2}}. \tag{13}$$

Inverting the ψ-Laplace transform and taking into account (9), we have

$$\begin{aligned}
u\left(t\right)=&\frac{c_1\,\kappa_1}{c_2}\,\psi\left(t\right)^{\alpha_2-1+\mu_1(1-\alpha_1)}\sum_{p=0}^{+\infty}\left(-\frac{c_1}{c_2}\,\psi\left(t\right)^{\alpha_2-\alpha_1}\right)^p E_{\alpha_2,\alpha_2+(\alpha_2-\alpha_1)p+\mu_1(1-\alpha_1)}^{p+1}\left(-\frac{d^2}{c_2}\,\psi\left(t\right)^{\alpha_2}\right)\\
&+\kappa_2\,\psi\left(t\right)^{\alpha_2-2+\mu_2(2-\alpha_2)}\sum_{p=0}^{+\infty}\left(-\frac{c_1}{c_2}\,\psi\left(t\right)^{\alpha_2-\alpha_1}\right)^p E_{\alpha_2,\alpha_2+(\alpha_2-\alpha_1)p-1+\mu_2(2-\alpha_2)}^{p+1}\left(-\frac{d^2}{c_2}\,\psi\left(t\right)^{\alpha_2}\right)\\
&+\kappa_3\,\psi\left(t\right)^{\alpha_2-1+\mu_2(2-\alpha_2)}\sum_{p=0}^{+\infty}\left(-\frac{c_1}{c_2}\,\psi\left(t\right)^{\alpha_2-\alpha_1}\right)^p E_{\alpha_2,\alpha_2+(\alpha_2-\alpha_1)p+\mu_2(2-\alpha_2)}^{p+1}\left(-\frac{d^2}{c_2}\,\psi\left(t\right)^{\alpha_2}\right)\\
&+\frac{1}{c_2}\,q\left(\psi\left(t\right)\right)*_\psi\sum_{p=0}^{+\infty}\left(-\frac{c_1}{c_2}\,\psi\left(t\right)^{\alpha_2-\alpha_1}\right)^p\psi\left(t\right)^{\alpha_2-1}\,E_{\alpha_2,\alpha_2+(\alpha_2-\alpha_1)p}^{p+1}\left(-\frac{d^2}{c_2}\,\psi\left(t\right)^{\alpha_2}\right),
\end{aligned} \tag{14}$$

where the ψ-convolution is given by (7). From the definition of the bivariate Mittag-Leffler function (see (3)) we can rewrite (14) as

$$\begin{aligned}
u\left(t\right)=&\frac{c_1\,\kappa_1}{c_2}\,\psi\left(t\right)^{\alpha_2-1+\mu_1(1-\alpha_1)}E_{(\alpha_2,\alpha_2-\alpha_1),\alpha_2+\mu_1(1-\alpha_1)}\left(-\frac{d^2}{c_2}\,\psi\left(t\right)^{\alpha_2},-\frac{c_1}{c_2}\,\psi\left(t\right)^{\alpha_2-\alpha_1}\right)\\
&+\kappa_2\,\psi\left(t\right)^{\alpha_2-2+\mu_2(2-\alpha_2)}E_{(\alpha_2,\alpha_2-\alpha_1),\alpha_2-1+\mu_2(2-\alpha_2)}\left(-\frac{d^2}{c_2}\,\psi\left(t\right)^{\alpha_2},-\frac{c_1}{c_2}\,\psi\left(t\right)^{\alpha_2-\alpha_1}\right)
\end{aligned} \tag{15}$$

$$+\kappa_3\,\psi(t)^{\alpha_2-1+\mu_2(2-\alpha_2)}\,E_{(\alpha_2,\alpha_2-\alpha_1),\alpha_2+\mu_2(2-\alpha_2)}\left(-\frac{d^2}{c_2}\,\psi(t)^{\alpha_2},-\frac{c_1}{c_2}\,\psi(t)^{\alpha_2-\alpha_1}\right)$$

$$+\frac{1}{c_2}\,q(\psi(t))*_\psi\left[\psi(t)^{\alpha_2-1}\,E_{(\alpha_2,\alpha_2-\alpha_1),\alpha_2}\left(-\frac{d^2}{c_2}\,\psi(t)^{\alpha_2},-\frac{c_1}{c_2}\,\psi(t)^{\alpha_2-\alpha_1}\right)\right]. \tag{16}$$

Therefore, the solution involves series of three-parameter Mittag-Leffler functions of one variable or just bivariate Mittag-Leffler functions.

For the unforced case, the solution can be written as $u_h(t)=u_1(t)+u_2(t)+u_3(t)$, where u_1, u_2, u_3 corresponds to the first three terms in (16). These constitute a set of fundamental solutions of the homogeneous equation. Let us study the behaviour of u_h when $t\to a^+$ and $t\to+\infty$. From (4) we have the following asymptotic behaviour near the starting point $t=a$

$$u_h(t)\sim\frac{\kappa_2}{\Gamma(\alpha_2+\mu_2(2-\alpha_2)-1)}\,\psi(t)^{\alpha_2+\mu_2(2-\alpha_2)-2},\quad t\to a^+.$$

Moreover, from (5) we have the following asymptotic behaviour for large values of t

$$u_h(t)\sim\frac{\kappa_1}{\Gamma(\alpha_1+\mu_1(1-\alpha_1))}\,\psi(t)^{\mu_1(1-\alpha_1)-1},\quad t\to+\infty,$$

whenever $\mu_2(2-\alpha_2)-\mu_1(1-\alpha_1)<0$, for $\mu_1,\mu_2\in[0,1]$, $\alpha_1\in]0,1]$, and $\alpha_2\in]1,2]$.

4 Conclusions

In this work, we solved the ψ-Hilfer fractional relaxation-oscillation equation and we showed that the solution can be expressed in terms of bivariate Mittag-Leffler functions. We studied the asymptotic behaviour of the solution of the associated homogeneous equation. This is important to understand and classify the relaxation-oscillation phenomena. Our results generalise those presented in Section 3 of [2].

Acknowledgments

The work of the authors was supported by Portuguese funds through CIDMA-Center for Research and Development in Mathematics and Applications, and FCT–Fundação para a Ciência e a Tecnologia, within projects UIDB/04106/2020 and UIDP/04106/2020. N. Vieira was also supported by FCT via the 2018 FCT program of Stimulus of Scientific Employment - Individual Support (Ref: CEECIND/01131/2018).

References

[1] H.J. Haubold, A.M. Mathai, and R.K. Saxena, *Mittag-Leffler functions and their applications*, J. Appl. Math. **2011** (2011), Article No.298628 (51pp).

[2] F. Mainardi, *Fractional relaxation-oscillation and fractional diffusion-wave phenomena*, Chaos Solitons Fractals **7**-No.9 (1996), 1461–1477.

[3] J.V.C. Sousa, R.F. Camargo, E.C. Oliveira, and G.S.F. Frederico, *Pseudo-fractional differential equations and generalized g-Laplace transform*, J. Pseudo-Differ. Oper. Appl. **12** (2021), Article No.44 (27pp.).

[4] J.V.C. Sousa and E. C. Oliveira, *On the ψ-Hilfer derivative*, Commun. Nonlinear Sci. Numer. Simulat. **60** (2018), 72–91.

[5] N. Vieira, M. Ferreira, and M.M. Rodrigues, *Time-fractional telegraph equation in higher dimensions with ψ-Hilfer fractional derivatives*, submitted.

International Conference on Mathematical Analysis and Applications in Science and Engineering
ICMA^{2}SC'22
ISEP Porto-Portugal, June 27 - July 1, 2022

On a regular ψ-fractional Sturm-Liouville problem

M. Ferreira[‡,⋆] **M. Manuela Rodrigues**[†] **N. Vieira** [†]

[‡] School of Technology and Management, Polytechnic of Leiria & CIDMA, Portugal
[†] Department of Mathematics, University of Aveiro & CIDMA, Portugal

[⋆]milton.ferreira@ipleiria.pt

Abstract: In this short paper, we consider a ψ-fractional Sturm-Liouville eigenvalue problem by using left ψ-Caputo and right ψ-Riemann-Liouville fractional derivatives. We study the main properties of the eigenfunctions and the eigenvalues of the associated fractional boundary problem.

keywords: ψ-fractional derivatives; ψ-fractional Sturm-Liouville problem; Eigenvalues; Eigenfunctions.

MSC2010: 34B24; 26A33; 34L10.

1 Introduction

The classical regular Sturm-Liouville (S-L) problem is associated with the real second-order linear ordinary differential equation of the form:

$$\frac{d}{dx}\left(p(x)\frac{dy}{dx}\right) + q(x)\, y(x) = \lambda\, w(x)\, y(x),$$

where $p(x), w(x) > 0$, and $p(x), p'(x), q(x), w(x)$ are continuous functions on (a, b). The function $w(x)$, sometimes denoted by $r(x)$, is called the weight or density function. The unknown function $y(x)$ is continuous and differentiable on (a, b). In addition, $y(x)$ is required to satisfy some boundary conditions of the form $c_1 y(a) + c_2 y'(a) = 0$ and $d_1 y(b) + d_2 y'(b) = 0$, with $c_1^2 + c_2^2 \neq 0$ and $d_1^2 + d_2^2 \neq 0$. Finding the values of λ, known as eigenvalues, for which there exists a non-trivial solution $y(x)$, called eigenfunction associated to λ, constitutes the classical S-L problem. Fractional versions of this problem were already considered in the literature (see e.g. [3, 4] and references therein). Motivated by the unification given by the ψ-fractional calculus we study a regular ψ-fractional S-L problem.

2 Preliminaries

In this section, we introduce the concepts related to the ψ-fractional calculus necessary to this work (for more details see [5] and references therein).

Definition 1 *(cf. [5]) Let (a,b) be a finite or infinite interval on the real line $\mathbb{R}$ and $\alpha>0$. Also let ψ be a monotone increasing and positive function on (a,b), having a continuous derivative ψ' in (a,b). The left- and right-sided Riemnann-Liouville (RL) fractional integrals of a function f with respect to another function ψ on (a,b) are given respectively by*

$$I_{a^+}^{\alpha;\psi}f(x) = \frac{1}{\Gamma(\alpha)}\int_a^x \psi'(t)\,(\psi(x)-\psi(t))^{\alpha-1}\,f(t)\,dt, \qquad x>a, \tag{1}$$

$$I_{b^-}^{\alpha;\psi}f(x) = \frac{1}{\Gamma(\alpha)}\int_x^b \psi'(t)\,(\psi(t)-\psi(x))^{\alpha-1}\,f(t)\,dt, \qquad x<b. \tag{2}$$

Assuming further that $f,\psi\in C^n(a,b)$, where $n=[\alpha]+1$, and $\psi'(x)\neq 0$, for all $x\in(a,b)$, the corresponding inverse operators, i.e., the left- and right-sided ψ-RL fractional derivatives of order $\alpha>0$, are defined respectively by

$$D_{a^+}^{\alpha;\psi}f(x)=\left(\frac{1}{\psi'(x)}\frac{d}{dx}\right)^n I_{a^+}^{n-\alpha;\psi}f(x) \quad \text{and} \quad D_{b^-}^{\alpha;\psi}f(x)=\left(-\frac{1}{\psi'(x)}\frac{d}{dx}\right)^n I_{b^-}^{n-\alpha;\psi}f(x). \tag{3}$$

Moreover, the left- and right-sided ψ-Caputo fractional derivatives of order $\alpha>0$, are defined respectively by

$${}^{C}D_{a^+}^{\alpha;\psi}f(x)=I_{a^+}^{n-\alpha;\psi}\left(\frac{1}{\psi'(x)}\frac{d}{dx}\right)^n f(x) \quad \text{and} \quad {}^{C}D_{b^-}^{\alpha;\psi}f(x)=I_{b^-}^{n-\alpha;\psi}\left(-\frac{1}{\psi'(x)}\frac{d}{dx}\right)^n f(x). \tag{4}$$

Using the concepts of ψ-RL and ψ-Caputo fractional derivatives we can encompass in one definition several fractional derivatives known in the literature In [5], the authors listed several fractional derivatives that can be obtained for specific choices of the function ψ such as Caputo, RL, Hadamard, Katugampola, Chen, Jumarie, Prabhakar, Erdélyi-Kober, Weyl, among others.

Proposition 1 *Let $\alpha,\beta>0$ and $f\in C([a,b])$. Then the following relations hold*

$$I_{a^+}^{\alpha;\psi}I_{a^+}^{\beta;\psi}=I_{a^+}^{\alpha+\beta;\psi}, \qquad I_{b^-}^{\alpha;\psi}I_{b^-}^{\beta;\psi}=I_{b^-}^{\alpha+\beta;\psi},$$
$$D_{a^+}^{\alpha;\psi}I_{a^+}^{\alpha;\psi}f(x)=f(x), \qquad D_{b^-}^{\alpha;\psi}I_{b^-}^{\alpha;\psi}f(x)=f(x),$$
$${}^{C}D_{a^+}^{\alpha;\psi}I_{a^+}^{\alpha;\psi}f(x)=f(x), \qquad {}^{C}D_{b^-}^{\alpha;\psi}I_{b^-}^{\alpha;\psi}f(x)=f(x).$$

Moreover, for $f\in C^n([a,b])$, $n=[\alpha]+1$, and putting $f_\psi^{[k]}(x)=\left(\frac{1}{\psi'(x)}\frac{d}{dx}\right)^k f(x)$, we have

$${}^{C}D_{a^+}^{\alpha;\psi}f(x)=D_{a^+}^{\alpha;\psi}\left[f(x)-\sum_{k=0}^{n-1}\frac{f_\psi^{[k]}(a)}{k!}\left(\psi(x)-\psi(a)\right)^k\right],$$
$$I_{a^+}^{\alpha;\psi}\ {}^{C}D_{a^+}^{\alpha;\psi}f(x)=f(x)-\sum_{k=0}^{n-1}\frac{f_\psi^{[k]}(a)}{k!}\left(\psi(x)-\psi(a)\right)^k.$$

Proposition 2 *For $\alpha\in(0,1)$, the fractional differential operators (3) and (4) satisfy the following ψ-fractional integration by parts:*

$$\int_a^b f(x)D_{a^+}^{\alpha;\psi}g(x)\psi'(x)\,dx=\int_a^b {}^{C}D_{b^-}^{\alpha;\psi}f(x)g(x)\psi'(x)\,dx+f(x)I_{a^+}^{1-\alpha;\psi}g(x)\Big|_{x=a}^{x=b}, \tag{5}$$

$$\int_a^b f(x)D_{b^-}^{\alpha;\psi}g(x)\psi'(x)\,dx=\int_a^b {}^{C}D_{a^+}^{\alpha;\psi}f(x)g(x)\psi'(x)\,dx-f(x)I_{b^-}^{1-\alpha;\psi}g(x)\Big|_{x=a}^{x=b}. \tag{6}$$

For more properties of these ψ-fractional operators see [5] and references therein.

3 Regular ψ-fractional Sturm-Liouville problem

We consider the following ψ-fractional S-L equation

$$-D_{b^-}^{\alpha;\psi}\left(p\left(x\right)\,{}^{C}D_{a^+}^{\alpha;\psi}f\left(x\right)\right)+q(x)f(x)=\lambda\, w(x)\, f\left(x\right) \tag{7}$$

subject to the following boundary conditions

$$c_1\, f\left(a\right)+c_2\, I_{b^-}^{1-\alpha;\psi}\left(p(x)\,{}^{C}D_{a^+}^{\alpha;\psi}f(x)\right)\Big|_{x=a}=0,\quad c_1^2+c_2^2\neq 0, \tag{8}$$

$$d_1\, f\left(b\right)+d_2\, I_{b^-}^{1-\alpha;\psi}\left(p(x)\,{}^{C}D_{a^+}^{\alpha;\psi}f(x)\right)\Big|_{x=b}=0,\quad d_1^2+d_2^2\neq 0, \tag{9}$$

where $\alpha\in(0,1)$, $x\in[a,b]$, $p(x),w(x)>0$, for all $x\in[a,b]$, and p,q,w are real-valued continuous functions in $[a,b]$. Our problem consists in finding the values of λ such that the boundary-value problem (7)-(9) has a non-trivial solution. We denote by $\mathcal{L}^{\alpha;\psi}$ the ψ-fractional S-L operator associated to problem (7) given by

$$\mathcal{L}^{\alpha;\psi}:=-D_{b^-}^{\alpha;\psi}\left(p(x)\,{}^{C}D_{a^+}^{\alpha;\psi}\right)+q(x).$$

As suggested by the ψ-fractional integration by parts of Proposition 2 we will work in the weighted space $L_1([a,b],\psi'(x)dx)$. Using (6) and the boundary conditions (8)-(9) one can prove the following theorem.

Theorem 3 *The eigenvalues of our ψ-fractional problem (7)-(9) are real. Moreover, the eigenfunctions corresponding to distinct eigenvalues are orthogonal with respect to the sensity function $w(x)$ on $[a,b]$, that is*

$$\int_a^b f_{\lambda_1}(x)f_{\lambda_2}(x)w(x)\,\psi'(x)\,dx,\qquad \lambda_1\neq\lambda_2.$$

Our ψ-fractional S-L equation with boundary conditions can be written in integral form as the next proposition shows.

Proposition 4 *Let $\alpha>1/2$ and f_λ be an eigenfunction associated to the eigenvalue λ. On the space $C([a,b])$, the $\psi-$fractional S-L problem is equivalent to the integral equation*

$$f_\lambda(x)=-I_{a^+}^{\alpha;\psi}\Big(\frac{1}{p\left(x\right)}\,I_{b^-}^{\alpha;\psi}F_\lambda\left(f\right)\Big)+A\left(x\right)\int_a^b F_\lambda\left(f\right)\,dx+B\left(x\right)\left(I_{a^+}^{\alpha;\psi}\Big(\frac{1}{p\left(x\right)}\,I_{b^-}^{\alpha;\psi}F_\lambda\left(f\right)\Big)\right)\Big|_{x=b} \tag{10}$$

where the coefficients $A\left(x\right)$ and $B\left(x\right)$ are given by

$$A\left(x\right)=\frac{c_2}{\Delta}\left(d_2+d_1\Big(Y-\,I_{a^+}^{\alpha;\psi}\Big(\frac{\left(\psi\left(b\right)-\psi\left(x\right)\right)^{\alpha-1}}{p\left(x\right)\,\Gamma\left(\alpha\right)}\Big)\Big)\right),$$

$$B\left(x\right)=\frac{d_1}{\Delta}\left(c_1\,I_{a^+}^{\alpha;\psi}\Big(\frac{\left(\psi\left(b\right)-\psi\left(x\right)\right)^{\alpha-1}}{p\left(x\right)\,\Gamma\left(\alpha\right)}\Big)-c_2\right),$$

with $\Delta=c_1(d_1Y+d_2)-c_2d_1\neq 0$, $Y=I_{a^+}^{\alpha;\psi}\Big(\frac{(\psi(b)-\psi(x))^{\alpha-1}}{p(x)\,\Gamma(\alpha)}\Big)\,\Big|_{x=b}$, and $F_\lambda(f)=q(x)f_\lambda(x)-\lambda w(x)f_\lambda(x)$.

Sketch of the proof: Using composition rules we can write the equation (7) as follows:

$$D_{b^-}^{\alpha;\psi}\Big(p(x)\ {}^{C}D_{a^+}^{\alpha;\psi}\Big)\Big[f_\lambda(x)+I_{a^+}^{\alpha;\psi}\Big(\frac{1}{p(x)}I_{b^-}^{\alpha;\psi}F_\lambda(f)\Big)\Big]=0. \tag{11}$$

On the space $C([a,b])$ a general solution of (11) is given by

$$f_\lambda(x)+I_{a^+}^{\alpha;\psi}\Big(\frac{1}{p(x)}I_{b^-}^{\alpha;\psi}F_\lambda(f)\Big)=\xi_1+\xi_2\,I_{a^+}^{\alpha;\psi}\Big(\frac{(\psi(b)-\psi(x))^{\alpha-1}}{p(x)\,\Gamma(\alpha)}\Big),\quad \xi_1,\xi_2\in\mathbb{R}. \tag{12}$$

From [3, Eq. (34)] the fractional integral that is multiplied by ξ_2 gives a continuous function on $[a,b]$ only for $1/2<\alpha<1$. From (12) and using composition rules we obtain:

$$I_{b^-}^{1-\alpha;\psi}\Big(p(x)\ {}^{C}D_{a^+}^{\alpha;\psi}f_\lambda(x)\Big)=\xi_2-I_{b^-}^{1;\psi}F_\lambda(f). \tag{13}$$

Finally, from (13) and (12) and using the boundary conditions (8)-(9) we can relate the coefficients ξ_1,ξ_2 with the values $c_j,d_j,j=1,2$ in the boundary conditions to obtain (10).

Our final theorem gives the conditions under which the eigenfunctions exist and are unique. The proof follows similar arguments as the proof of [3, Thm. 9].

Theorem 5 *Let $\alpha>1/2$ and assume that $\Delta\neq 0$. Then our ψ-fractional problem has unique continuous eigenfunctions f_λ if the fixed point condition holds*

$$\|q(x)+\lambda\omega(x)\|<\frac{m_p}{\|\varphi(x)\|+\|B(x)\|\varphi(b)+m_p\|A(x)\|(\psi(b)-\psi(a))},$$

where $\varphi(x)=I_{a^+}^{\alpha;\psi}\Big(\frac{(\psi(b)-\psi(x))^{\alpha-1}}{p(x)\,\Gamma(\alpha)}\Big)$ and $m_p=\min_{x\in[a,b]}|p(x)|$.

4 Conclusion

In this work we showed how to use the ψ-fractional calculus to study a ψ-fractional S-L problem.

Acknowledgments

The work of the authors was supported by Portuguese funds through CIDMA-Center for Research and Development in Mathematics and Applications, and FCT–Fundação para a Ciência e a Tecnologia, within projects UIDB/04106/2020 and UIDP/04106/2020. N. Vieira was also supported by FCT via the 2018 FCT program of Stimulus of Scientific Employment - Individual Support (Ref: CEECIND/01131/2018).

References

[1] A. Zettl, *Sturm-Liouville Theory*, Mathematical Surveys and Monographs, Vol. 21. American Mathematical Society, 2005.

[2] A.A. Kilbas, H.M. Srivastava, and J.J. Trujillo, *Theory and applications of fractional differential equations*, North-Holland Mathematics Studies-Vol.204, Elsevier, Amsterdam, 2006.

[3] M. Klimek and O.P. Agrawal, *On a regular fractional Sturm-Liouville problem with derivatives of order in* $(0,1)$, in Proceedings of 13th International Carpathian Control Conference, ICCC, July, 2012.

[4] M. Ferreira, M.M. Rodrigues, and N. Vieira, *A fractional analysis in higher dimensions for the Sturm-Liouville problem*, Fract. Calc. Appl. Anal., **24**(2) (2021), 585–620.

[5] J.V.C. Sousa and E. C. Oliveira, *On the ψ-Hilfer derivative*, Commun. Nonlinear Sci. Numer. Simulat. **60** (2018), 72–91.

International Conference on Mathematical Analysis and Applications in Science and Engineering
ICMA^{2}SC'22
ISEP Porto-Portugal, June 27 - 29, 2022

ON A HILFER-HADAMARD FRACTIONAL INTEGRO-DIFFERENTIAL INCLUSION

Aurelian Cernea

Faculty of Mathematics and Computer Science, University of Bucharest, Romania

acernea@fmi.unibuc.ro

Abstract: A boundary value problem associated to a Hilfer-Hadamard fractional integro-differential inclusion is studied. The existence of solutions is established in the case when the set-valued map has nonconvex values.

keywords: differential inclusion; fractional derivative; boundary value problem.

MSC2020: 34A60; 34A12; 34A08.

1 Introduction

A generalization of both Riemann-Liouville and Caputo fractional derivatives was introduced by Hilfer in [3]. In fact, this derivative interpolates between Riemann-Liouville and Caputo derivatives. Several properties and applications of Hilfer fractional derivative may be found in [4]. The modification of Hilfer fractional derivative resulted in the concept of Hilfer-Hadamard fractional derivative. Similarly, the Hilfer-Hadamard fractional derivative covers the cases of Riemann-Liouville-Hadamard and Caputo-Hadamard fractional derivatives.

We consider the following problem

$$D_{HH}^{\alpha,\beta}x(t) \in F(t,x(t),V(x)(t)) \quad a.e.\ (I=[1,T]) \tag{1}$$

with boundary conditions of the form

$$x(1)=0, \quad x(T)=\sum_{j=1}^{m}\eta_j x(\xi_j)+\sum_{i=1}^{n}\zeta_i I_H^{\varphi_i}x(\theta_i)+\sum_{k=1}^{r}\lambda_k D_H^{\omega_k}x(\mu_k), \tag{2}$$

where $D_{HH}^{\alpha,\beta}$ is the Hilfer-Hadamard fractional derivative of order $\alpha\in(1,2]$ and type $\beta\in[0,1]$, $\xi_j,\theta_i,\mu_k\in(1,T)$, $\eta_i,\zeta_j,\lambda_k\in\mathbf{R}$, $j=\overline{1,m}, i=\overline{1,n}, k=\overline{1,r}$, I_H^{φ} is the Hadamard fractional integral of order $\varphi>0$, D_H^{ω} is the Hadamard fractional derivative of order $\omega>0$, $F:[1,T]\times\mathbf{R}\times\mathbf{R}\to\mathcal{P}(\mathbf{R})$ is a set-valued map and $V:C([1,T],\mathbf{R})\to C([1,T],\mathbf{R})$ is a nonlinear Volterra integral operator defined by $V(x)(t)=\int_0^t k(t,s,x(s))ds$ with $k(.,.,.):[1,T]\times\mathbf{R}\times\mathbf{R}\to\mathbf{R}$ a given function.

Our study is motivated by a recent paper [1]. Namely, in [1] three existence results for problem (1)-(2) may be found in the case when F does not depends on the last variable. All the results in [1] are proved by using several suitable theorems from fixed point theory.

Our goal is to obtain the existence of solutions for problem (1)-(2) in the case when the set-valued map F has nonconvex values but it is assumed to be Lipschitz in the second and third variable. Our result use Filippov's techniques ([2]); namely, the existence of solutions is obtained by starting from a given "quasi" solution. In addition, the result provides an estimate between the "quasi" solution and the solution obtained.

The Hadamard fractional integral of order $q > 0$ of a Lebesgue integrable function $f : [1, \infty) \to \mathbf{R}$ is defined by

$$I_H^q f(t) = \frac{1}{\Gamma(q)} \int_1^t \left(\ln \frac{t}{s} \right)^{q-1} \frac{f(s)}{s} ds$$

provided the integral exists and $\Gamma(.)$ is the (Euler's) Gamma function defined by $\Gamma(q) = \int_0^\infty t^{q-1} e^{-t} dt$.

The Hadamard fractional derivative of order $q > 0$ of a function $f : [1, \infty) \to \mathbf{R}$ is defined by

$$D_H^q f(t) = t \frac{d^n}{dt^n} (I_H^{n-q} f)(t),$$

provided the integral exists and $n = [q] + 1$, $[q]$ is the integer part of q.

The Hilfer-Hadamard fractional derivative of order $\alpha \in (n-1, n)$, $n \geq 2$ *and type* $\beta \in [0, 1]$ of a function $f \in L^1(I, \mathbf{R})$ is defined by

$$D_{HH}^{\alpha,\beta} f(t) = (I_H^{\beta(n-\alpha)} D_H^\gamma f)(t), \quad \gamma = \alpha + n\beta - \alpha\beta.$$

When $\beta = 0$ the Hilfer-Hadamard fractional derivative gives Hadamard fractional derivative and when $\beta = 1$ the Hilfer-Hadamard fractional derivative gives Caputo-Hadamard fractional derivative.

2 Results and discussion

Hypothesis 1. i) $F(.,.) : I \times \mathbf{R} \times \mathbf{R} \to \mathcal{P}(\mathbf{R})$ *has nonempty closed values and is* $\mathcal{L}(I) \otimes \mathcal{B}(\mathbf{R} \times \mathbf{R})$ *measurable.*

ii) *There exists* $L(.) \in L^1(I, (0, \infty))$ *such that, for almost all* $t \in I, F(t, ., .)$ *is* $L(t)$*-Lipschitz*

iii) $k(., ., .) : I \times \mathbf{R} \times \mathbf{R} \to \mathbf{R}$ *is a function such that* $\forall x \in \mathbf{R}$, $(t, s) \to k(t, s, x)$ *is measurable.*

iv) $|k(t, s, x) - k(t, s, y)| \leq L(t)|x - y| \quad a.e.\ (t, s) \in I \times I, \quad \forall\, x, y \in \mathbf{R}.$

We use next the following notations $M(t) := L(t)(1 + \int_1^t L(u)du), \quad t \in I, \quad K_0 = \int_1^T M(t)dt,$

$$M = \frac{(\ln T)^{\alpha-1}}{\Gamma(\alpha)} + \sum_{j=1}^m \frac{(\ln T)^{\gamma-1} (\ln \xi_j)^{\alpha-1}}{|\Lambda|\Gamma(\alpha)} + \sum_{i=1}^n \frac{(\ln T)^{\gamma-1} |\zeta_i| (\ln \theta_i)^{\alpha+\varphi_i-1}}{|\Lambda|\Gamma(\alpha+\varphi_i)}$$
$$+ \sum_{k=1}^r \frac{(\ln T)^{\gamma-1} |\lambda_k| (\ln \mu_k)^{\alpha-\omega_k-1}}{|\Lambda|\Gamma(\alpha-\omega_k)} + \frac{(\ln T)^{\alpha+\gamma-2}}{|\Lambda|\Gamma(\alpha)}.$$

Theorem 2. *Let* $\alpha \in (1, 2]$, $\beta \in [0, 1]$ *and* $0 < \omega_k \leq \alpha - 1$, $k = \overline{1, r}$. *Assume that Hypothesis 1 is satisfied and* $MK_0 < 1$. *Let* $y(.) \in C(I, \mathbf{R})$ *be such that* $y(1) = 0$, $y(T) = \sum_{j=1}^m \eta_j y(\xi_j) + \sum_{i=1}^n \zeta_i I_H^{\varphi_i} y(\theta_i) + \sum_{k=1}^r \lambda_k D_H^{\omega_k} y(\mu_k)$ *and there exists* $p(.) \in L^1(I, \mathbf{R}_+)$ *with* $d(D_{HH}^{\alpha,\beta} y(t), F(t, y(t), V(y)(t))) \leq p(t)$ *a.e.* (I).

Then there exists $x(.) : I \to \mathbf{R}$ *a solution of problem (1)-(2) satisfying for all* $t \in I$

$$|x(t) - y(t)| \leq \frac{M}{1 - MK_0} ||p(.)||_1.$$

Corollary 3. *Let $\alpha \in (1,2]$, $\beta \in [0,1]$ and $0 < \omega_k \leq \alpha - 1$, $k = \overline{1,r}$. Assume that Hypothesis 1 is satisfied, $d(0, F(t,0,0) \leq L(t)$ a.e. (I) and $MK_0 < 1$. Then there exists $x(.)$ a solution of problem (1)-(2) satisfying for all $t \in I$ $|x(t)| \leq \frac{M}{1-MK_0}||L(.)||_1$.*

Hypothesis 4. i) *$F(.,.) : I \times \mathbf{R} \to \mathcal{P}(\mathbf{R})$ has nonempty closed values and is $\mathcal{L}(I) \otimes \mathcal{B}(\mathbf{R})$ measurable.*

ii) *There exists $L(.) \in L^1(I, (0,\infty))$ such that, for almost all $t \in I$, $F(t,.)$ is $L(t)$-Lipschitz*

Denote $L_0 = \int_1^T L(t)dt$.

Corollary 5. *Let $\alpha \in (1,2]$, $\beta \in [0,1]$ and $0 < \omega_k \leq \alpha - 1$, $k = \overline{1,r}$. Assume that Hypothesis 4 is satisfied, $d(0, F(t,0) \leq L(t)$ a.e. (I) and $ML_0 < 1$. Then there exists $x(.)$ a solution of the fractional differential inclusion*

$$D_{HH}^{\alpha,\beta} x(t) \in F(t, x(t)) \quad a.e.\ (I),$$

with boundary conditions (2) satisfying for all $t \in I$

$$|x(t)| \leq \frac{ML_0}{1 - ML_0}. \tag{3}$$

Remark 6. A similar result to the one in Corollary 5 may be found in [1]; namely, Theorem 7. The proof of Theorem 7 in [1] is done by using the set-valued contraction principle. Our approach improves the hypothesis concerning the set-valued map in [1]. More exactly, we do not require for the values of F to be compact as in [1] and we do not require that the Lipschitz constant of F to be a mapping from $C(I, \mathbf{R})$ as in [1]. Moreover, Theorem 7 in [1] does not contains a priori bounds for solutions as in (3).

3 Conclusions and Future work

Our result improve an existence theorem in [1] in the case when the right-hand side is Lipschitz in the second variable. Moreover, our result may be viewed as a generalization to the case when the right-hand side contains a nonlinear Volterra integral operator. Even if the method we use here is known in the theory of differential inclusions it is largely ignored by the authors that are dealing with such problems in favor of fixed point approaches, most probably, because it is much easier to handle the applications of classical fixed point theorems.

It is worth mentioning that our results may be a basic tool in the study of optimal control problems defined by such kinds of fractional differential inclusions.

References

[1] B. Ahmad, S. K. Ntouyas, Hilfer-Hadamard fractional boundary value problems with non-local mixed boundary conditions, Fractal and Fractional, **5**(195) (2021), 1–25.

[2] A. F. Filippov, Classical solutions of differential equations with multivalued right hand side, SIAM Journal on Control, **5** (1967), 609–621.

[3] R. Hilfer, *Applications of Fractional Calculus in Physics*. Singapore: World Scientific, 2000.

[4] R. Hilfer, Y. Luchko, Z. Tomovski, Operational method for the solution of fractional differential equations with generalized Riemann-Liouville fractional derivative, Fractional Calculus and Applied Analysis, **12** (2009), 299–318.

International Conference on Mathematical Analysis and Applications in Science and Engineering
ICMA^{2}SC'22
ISEP Porto-Portugal, June 27 - 29, 2022

ON THE ULAM, HYERS AND RASSIAS STABILITIES FOR A CAPUTO FRACTIONAL BOUNDARY VALUE PROBLEM OF ORDER GREATER THAN TWO

Luís P. Castro[1] **Anabela S. Silva**[1⋆]

[1] CIDMA – Center for Research and Development in Mathematics and Applications, University of Aveiro, Portugal

⋆anabela.silva@ua.pt

Abstract: We analyse a boundary value problem determined by the usual derivative and a Caputo fractional derivative of order greater than two. Our main goal is to present conditions under which the fractional boundary value problem has the Ulam-Hyers and Ulam-Hyers-Rassias stabilities.

keywords: Fractional boundary value problem, Caputo fractional derivative, fixed point, Ulam-Hyers stability, Ulam-Hyers-Rassias stability

MSC2020: 26A33, 47H10, 34D20.

1 Introduction

The importance of fractional calculus as a powerful method in the mathematical modeling of several problems in other areas of knowledge is now well-known. In fact, fractional calculus has been strongly applied in engineering and other scientific areas such as biology, chemistry, economics, physics, image and signal processing, etc. (cf., e.g., [5, 2, 4, 9]). In this framework, various properties of consequent fractional boundary value problems (FBVP) have been and continue to be studied. This includes the analysis of existence and uniqueness of solutions, as well as their different possible notions of stability (cf., e.g., [8, 6, 7, 10, 1]).

Having in mind [3], we present here a study for the Ulam-Hyers and the Ulam-Hyers-Rassias stabilities for a class of boundary value problems involving Caputo fractional derivative ${}^{C}\mathcal{D}_a^{\alpha}$ of order $\alpha \in (2,3)$, and the usual derivative, defined in the following way:

$$({}^{C}\mathcal{D}_a^{\alpha}x)(t) + p(t)x'(t) + q(t)x(t) = g(t), \quad a < t < b, \;\; 2 < \alpha < 3, \tag{1}$$

with $x(a) = x'(a) = x(b) = 0$, where p, q and $g \in C^2([a,b])$.

For each $\alpha \in \mathbb{R}^+$, we recall that the Riemann-Liouville fractional integral of order α of a function u may be defined by

$$I_a^{\alpha}u(t) = \frac{1}{\Gamma(\alpha)} \int_a^t (t-s)^{\alpha-1} u(s)\mathrm{d}s$$

(provided the right-hand side is pointwise defined on (a,∞)), where Γ is the well-known Euler Gamma function. In a certain counterpoint, we may define the Caputo fractional derivative of order $\alpha > 0$ of a continuous function u as

$$ {}^{C}\mathcal{D}_a^{\alpha} u(t) = \frac{1}{\Gamma(n-\alpha)} \int_a^t \frac{u^{(n)}(s)}{(t-s)^{\alpha-n+1}} \mathrm{d}s, $$

where $n \in \mathbb{N}$ is such that $n-1 < \alpha < n$ (and being clear that for the case of $\alpha \in \mathbb{N}$, we have the classical situation of ${}^{C}\mathcal{D}_a^{\alpha} u(t) = \left(\frac{\mathrm{d}}{\mathrm{d}t}\right)^{\alpha} u(t)$).

Our main mathematical spaces framework will be developed in $C^n([a,b])$, the space of n-times continuously differentiable functions x on $[a,b]$, with the norm

$$ \|x\|_{C^n} = \sum_{k=0}^{n} \sup_{t\in[a,b]} |x^{(k)}(t)|. $$

It is well-known that $(C^n([a,b]), \|\cdot\|_{C^n})$ is a Banach space. Anyway, one of our main techniques in the deductions of our results will be done on generalized complete metric spaces and using there the consequent Banach contraction principle – which we recall as follows:

Theorem 1 (Banach contraction principle) *Let (X,d) be a generalized complete metric space, and $T : X \to X$ be a strictly contractive operator, i.e., $d(Tx,Ty) \leq Ld(x,y)$, $\forall x,y \in X$, for some constant $0 \leq L < 1$. Then the mapping T has a unique fixed point $x^* = Tx^*$ and*

$$ d(x,x^*) \leq \frac{1}{1-L} d(x,Tx), \qquad x \in X. $$

2 Results and Discussion

It turns out that it is possible to characterize the form of the solutions of our FBVP, and this is done in the following way:

Proposition 2 *The function $x \in C^2([a,b])$ is a solution of the boundary value problem* (1) *if and only if x satisfies the integral equation*

$$ \begin{aligned} x(t) &= \frac{(t-a)^2}{(b-a)^2\Gamma(\alpha)} \int_a^b (b-s)^{\alpha-1} \left(p(s)x'(s) + q(s)x(s) - g(s)\right) \mathrm{d}s \\ &\quad - \frac{1}{\Gamma(\alpha)} \int_a^t (t-s)^{\alpha-1} \left(p(s)x'(s) + q(s)x(s) - g(s)\right) \mathrm{d}s. \end{aligned} $$

For the sake of simplicity and shortening of the formulas, we will fix the following notations:

$$ \begin{aligned} \mu &:= \max_{t\in[a,b]} \{|p(t)|, |q(t)|\}, \\ \eta &:= 2\frac{(b-a)^{\alpha}}{\Gamma(\alpha+1)} + \frac{(b-a)^{\alpha-1}}{\Gamma(\alpha)} + \frac{(b-a)^{\alpha-2}}{\Gamma(\alpha-1)} + 2\frac{(b-a)^{\alpha-1}}{\Gamma(\alpha+1)} + 2\frac{(b-a)^{\alpha-2}}{\Gamma(\alpha+1)}. \end{aligned} $$

Taking into consideration the operator $T : C^2([a,b]) \to C^2([a,b])$ defined by

$$ \begin{aligned} (Tx)(t) &:= \frac{(t-a)^2}{(b-a)^2\Gamma(\alpha)} \int_a^b (b-s)^{\alpha-1} \left(p(s)x'(s) + q(s)x(s) - g(s)\right) \mathrm{d}s \\ &\quad - \frac{1}{\Gamma(\alpha)} \int_a^t (t-s)^{\alpha-1} \left(p(s)x'(s) + q(s)x(s) - g(s)\right) \mathrm{d}s, \end{aligned} $$

and using the Banach contraction principle, we are able to conclude that T has a unique fixed point and that T is strictly contractive, when $\eta\,\mu < 1$, which allows the basis to deduce the following conclusion.

Theorem 3 *If $\eta\,\mu < 1$, then the FBVP* (1) *has a unique solution in $x \in C^2([a,b])$.*

We shall now recall the notions of Ulam-Hyers and Ulam-Hyers-Rassias stabilities when considering our FBVP.

Definition 1 *The FBVP* (1) *is Ulam-Hyers stable if there exists a real constant $k > 0$ such that, for each $\epsilon > 0$ and for each solution $y \in C^2([a,b])$ of the inequality problem*

$$\begin{cases} \left|({}^C\mathcal{D}_a^\alpha y)(t) + p(t)y'(t) + q(t)y(t) - g(t)\right| \leq \epsilon, \quad t \in [a,b] \\ y'(a) = y(a) = y(b) = 0, \end{cases}$$

there exists a solution $x \in C^2([a,b])$ of the problem (1) *such that $\|y - x\|_{C^2} \leq k\epsilon$.*

Definition 2 *The FBVP* (1) *is Ulam-Hyers-Rassias stable with respect to $\varphi : [a,b] \to \mathbb{R}^+$ if there exists a real constant $k_\varphi > 0$ such that, for each $\epsilon > 0$ and for each solution $y \in C^2([a,b])$ of the inequality problem*

$$\begin{cases} \left|({}^C\mathcal{D}_a^\alpha y)(t) + p(t)y'(t) + q(t)y(t) - g(t)\right| \leq \epsilon\varphi(t), \quad t \in [a,b] \\ y'(a) = y(a) = y(b) = 0, \end{cases}$$

there exists a solution $x \in C^2([a,b])$ of the problem (1) *with $\|y - x\|_{C^2} \leq k_\varphi \epsilon\varphi(t)$, $t \in [a,b]$.*

Finally, as the main result of this presentation, we state sufficient conditions under which – having in mind Definition 1 and Definition 2 – we are able to conclude that the FBVP (1) is Ulam-Hyers stable and Ulam-Hyers-Rassias stable.

Theorem 4 *Suppose that $\eta\,\mu < 1$, let $x(t)$ be the solution of the FBVP* (1) *and $y(t)$ be such that $y(a) = y'(a) = y(b) = 0$ and, in addition:*

(i) if $\left|({}^C\mathcal{D}_a^\alpha y)(t) + p(t)y'(t) + q(t)y(t) - g(t)\right| \leq \epsilon$, $t \in [a,b]$, where $\epsilon > 0$, then there exists a constant $k > 0$ such that

$$\|y - x\|_{C^2} \leq k\epsilon, \quad t \in [a,b];$$

(ii) if $\left|({}^C\mathcal{D}_a^\alpha y)(t) + p(t)y'(t) + q(t)y(t) - g(t)\right| \leq \epsilon\varphi(t)$, $t \in [a,b]$, where $\epsilon > 0$ and the function $\varphi : [a,b] \to \mathbb{R}^+$ satisfies the properties

$$(I_a^\tau \varphi)(t) \leq \varphi(t) \text{ and } \varphi(t) \geq \varphi(b), \;\; t \in [a,b], \;\; \tau = \alpha, \alpha-1, \alpha-2, \;\; \alpha \in (2,3),$$

then there exists a constant $k_\varphi > 0$ such that

$$\|y(t) - x(t)\|_{C^2} \leq k_\varphi \epsilon\varphi(t), \quad t \in [a,b].$$

3 Conclusions and Future Work

We analysed the Caputo fractional boundary value problem (1), which englobes the usual (integer) derivative and a Caputo fractional derivative of order greater than two. Having started by rewriting this fractional boundary value problem as an equivalent integral equation (cf. Proposition 2), we used this to define an appropriate operator to which was applied the Banach contraction principle.

That was the stating point to deduce sufficient conditions to ensure the uniqueness of the solution, and also to deduce sufficient conditions that guarantee the Ulam-Hyers and the Ulam-Hyers-Rassias stabilities of the FBVP (cf. Theorem 4).

If a system is Ulam-Hyers or Ulam-Hyers-Rassias stable, then significant properties are valid around the exact solution, which constitutes an important tool in many applications of diverse areas. In the future, we intend to explore some of those properties, mainly from a mathematical point of view, but also to envision implementations of applications to cases of interest in other sciences.

Acknowledgments

This work is supported by the Center for Research and Development in Mathematics and Applications (CIDMA) through the Portuguese Foundation for Science and Technology (FCT - Fundação para a Ciência e a Tecnologia), reference UIDB/04106/2020. A. Silva is also funded by national funds (OE), through FCT, I.P., in the scope of the framework contract foreseen in the numbers 4, 5 and 6 of the article 23, of the Decree-Law 57/2016, of August 29, changed by Law 57/2017, of July 19.

References

[1] A. Zada, J. Alzabut, H. Waheed, P. Loan-Lucian, Ulam-Hyers stability of impulsive integrodifferential equations with Riemann-Liouville boundary conditions, Adv. Differ. Equ. **1** (2020), 1–50.

[2] A.A. Kilbas, H.M. Srivastava, J.J. Trujillo, *Theory and Applications of Fractional Differential Equations*, Elsevier, Amsterdam, 2016.

[3] E. Pourhadi, M. Mursaleen, A new fractional boundary value problem and Lyapunov-type inequality, J. Math. Inequalities **15**(1) (2021), 81–93.

[4] F. Metzler, W. Schick, H.G. Kilian, T.F. Nonnenmacher, Relaxation in filled polymers: A fractional calculus approach, J. Chem. Phys. **103** (1995), 7180–7186.

[5] K. Diethelm, A.D. Freed, On the solution of nonlinear fractional order differential equations used in the modeling of viscoplasticity. In: Keil, F., Mackens, W., Voss, H., Werther, J. (eds.) Scientific Computing in Chemical Engineering II-Computational Fluid Dynamics, Reaction Engineering and Molecular Properties, Springer, Heidelberg, (1999), 217–224.

[6] L.P. Castro, A.M. Simões, Hyers-Ulam-Rassias stability of nonlinear integral equations through the Bielecki metric, Math. Methods Appl. Sci.**41**(17) (2018), 7367–7383.

[7] L.P. Castro, A.M. Simões, A Hyers-Ulam stability analysis for classes of Bessel equations, Filomat **35**(13) (2021), 4391–4403.

[8] M. Ahmad, A. Zada, J. Alzabut, Hyers-Ulam stability of coupled system of fractional differential equations of Hilfer-Hadamard type, Demonstr. Math. **52** (2019), 283–295.

[9] S. Samko, A. Kilbas, O. Marichev, *Fractional Integrals and Derivatives: Theory and Applications*. London: Gordon and Breach Science Publishers, 1993.

[10] Y. Guo, X. Shu, Y. Li, F. Xu, The existence and Hyers-Ulam stability of solution for an impulsive Riemann-Liouville fractional neutral functional stochastic differential equation with infinite delay of order $1 < \beta < 2$, Bound. Value Prob. **59** (2019), 1–18.

International Conference on Mathematical Analysis and Applications in Science and Engineering
ICMA^{2}SC'22
ISEP Porto-Portugal, June 27 - 29, 2022

A complete study of the fractional Hermite differential equation with uncertainties

C. Burgos[1⋆] J. C. Cortés [1] T. Caraballo [2] L. Villafuerte [3] R. J. Villanueva[1]

[1] Instituto Universitario de Matemática Multidisciplinar.
Universitat Politècnica de València.
Camino de Vera s/n, 46022, Valencia, Spain
[2] Departamento de ecuaciones diferenciales y análisis numérico.
Universidad de Sevilla.
Avenida Reina Mercedes s/n, 41012, Sevilla, Spain
[3]Deparment of Mathematics.
University of Texas at Austin.
USA.

[1⋆]clabursi@posgrado.upv.es

Abstract: In this contribution a complete probabilitsic analisys for the random fractional Hermite differential equation has been performed. We first construct a solution stochastic process by applying the random fractional Fröbenius method. Then, we take advantage of this random power series to obtain reliable approximations for the mean, the standard deviation and the first probability density functions of the solution.

keywords: Random fractional Hermite differential equation; Uncertainty Quantification; Fractional Calculus.

This abstract is included in **Syposium #12: Advances in Differential Equations with Uncertainties and Modeling.**

1 Introduction

The Hermite differential equation appears in quantum dynamics to describe atomic iterations [REF]. Nevertheless, there are complex non-linear and non-local dynamics that the classical Hermite differential equation is unable to properly describe. Fractional operators play an important role in modeling of complex dynamics. Despite the physical meaning of fractional operators is still under discussion, recent studies confirm their usefulness.

On the other hand, it is also important to underline that real-world phenomena are often subject to randomness. To obtain an appropriate description of this kind of problems, uncertainties must be considered in the model formulation.

The goal of this contribution is to present a complete probabilistic analysis of the random fractional Hermite differential equation,

$$\begin{cases} ({}^{C}D_0^{2\alpha}Y)(t) - 2t^{\alpha}({}^{C}D_0^{\alpha}Y) + \lambda Y(t) = 0, \\ Y(0) = Y_0, \\ Y'(0) = Y_1, \end{cases} \tag{1}$$

where the model parameters λ, Y_0 and Y_1 are random variables and $({}^C D_0^{\alpha} Y)(t)$ denotes the fractional Caputo derivative in mean square (m.s.) sense [1] of order $\alpha \in]0,1]$. The operator $({}^C D_0^{2\alpha} Y)(t)$ is defined by [2]

$$({}^C D_0^{2\alpha} Y)(t) := {}^C D_0^{\alpha} \left({}^C D_0^{\alpha} Y(t) \right).$$

To perform a complete study of this random fractional initial value problem (RFIVP), we will fist construct a m.s. convergent solution using the random fractional Fröbenius method, [3, Ch. 4]. Then, we will obtain approximations for the mean and the standard deviation of the solution. Afterwards, we will go a step further computing the first probability density function (1-PDF) of the solution taking advantage of the Random Variable Transformation (RVT) technique [3, Ch. 2].

2 Computing the solution stochastic process, their mean, standard deviation and the first probability density functions

This section is devoted to apply the random fractional Fröbenius method to compute the solution stochastic process of the RFIVP (1). Then, taking advantage of this expression, we will approximate the two first statistical moments (mean and standard deviation). Finally, the 1-PDF of the solution is obtained using RVT technique.

The fractional Fröbenius method allows us to obtain a solution in terms of a generalized power series,

$$Y(t) = \sum_{m=0}^{\infty} Y_m t^{\alpha m}. \tag{2}$$

Then, substituting this expression in the IVP (1), after some cumbersome computations we can obtain the coefficients Y_m, hence obtaining the solution

$$\begin{aligned} Y(t) =& Y_0 \left(1 + \sum_{m=1}^{\infty} \left[\frac{t^{2m\alpha}}{\Gamma(2\alpha m + 1)} \left(\sum_{i=0}^{m-1} \lambda^{i+1} (-1)^{i+1} G_{m-1,i} \right) \right] \right) \\ &+ Y_1 \left(t^{\alpha} + \sum_{m=1}^{\infty} \left[\frac{\Gamma(\alpha+1) t^{(2m+1)\alpha}}{\Gamma((2m+1)\alpha + 1)} \left(\sum_{i=0}^{m} \lambda^{i} (-1)^{i} \hat{G}_{m,i} \right) \right] \right), \end{aligned} \tag{3}$$

where

$$G_{m,i} = \begin{cases} \displaystyle\sum_{j_1 < j_2 < \ldots < j_{m-i}} 2\frac{\Gamma(2j_1\alpha+1)}{\Gamma((2j_1-1)\alpha+1)} \cdot 2\frac{\Gamma(2j_2\alpha+1)}{\Gamma((2j_2-1)\alpha+1)} \cdots \ldots 2\frac{\Gamma(2j_{m-i}\alpha+1)}{\Gamma((2j_{m-i}-1)\alpha+1)}, & \text{if } i < m, \\ 1, & \text{if } m = i, \\ 0, & \text{otherwise,} \end{cases} \tag{4}$$

and

$$\hat{G}_{m,i} = \begin{cases} \displaystyle\sum_{j_1 < j_2 < \ldots < j_{m-i}} 2\frac{\Gamma((2j_1-1)\alpha+1)}{\Gamma((2j_1-2)\alpha+1)} \cdot 2\frac{\Gamma((2j_2-1)\alpha+1)}{\Gamma((2j_2-2)\alpha+1)} \cdots 2\frac{\Gamma((2j_{m-i}-1)\alpha+1)}{\Gamma((2j_{m-i}-2)\alpha+1)}, & \text{if } i < m, \\ 1, & \text{if } m = i, \\ 0, & \text{otherwise.} \end{cases} \tag{5}$$

As it can be observed, the solution is given by a generalized random power series and it is required to establish its convergence in m.s. sense. With this end, we will assume the following hypotheses

- **H1:** The data Y_0, Y_1 and λ are independent random variables

- **H2:** The data λ is bounded random variable, i.e. exist b_1 and b_2 finite such that $b_1 < \lambda(\omega) < b_2$ for each $\omega \in \Omega$.

Now we compute reliable approximations for the mean and the standard deviation of the solution. At this point it must emphasized that the mean square convergence of the random series (3)-(5) guarantees the convergence of the approximations of the mean and the standard deviation by truncating at a specific order, say $M > 0$ integer, the series solution, [3, Th. 4.3.1]. This leads to the following approximations for the mean and for the second order moment

$$\begin{aligned}\mathbb{E}[Y_M(t)] =&\mathbb{E}[Y_0]\left(1+\sum_{m=1}^{M}\left[\frac{t^{2m\alpha}}{\Gamma(2\alpha m+1)}\left(\sum_{i=0}^{m-1}\mathbb{E}[\lambda^{i+1}](-1)^{i+1}G_{m-1,i}\right)\right]\right)\\ &+\mathbb{E}[Y_1]\left(t^{\alpha}+\sum_{m=1}^{M}\left[\frac{\Gamma(\alpha+1)t^{(2m+1)\alpha}}{\Gamma((2m+1)\alpha+1)}\left(\sum_{i=0}^{m}\mathbb{E}[\lambda^{i}](-1)^{i}\hat{G}_{m,i}\right)\right]\right)\end{aligned} \tag{6}$$

and

$$\begin{aligned}\mathbb{E}[Y_M^2(t)] =&\mathbb{E}[Y_0^2]\left(1+2\sum_{m=1}^{M}\left[\frac{t^{2\alpha m}}{\Gamma(2\alpha m+1)}\left(\sum_{i=0}^{m-1}\mathbb{E}[\lambda^{i+1}](-1)^{i+1}G_{m-1,i}\right)\right]\right.\\ &\left.+\left(\sum_{m=1}^{M}\sum_{n=1}^{M}\left[\frac{t^{2\alpha(m+n)}}{\Gamma(2\alpha m+1)\Gamma(2\alpha n+1)}\left(\sum_{i=0}^{m-1}\sum_{j=0}^{n-1}\mathbb{E}[\lambda^{i+j+2}](-1)^{i+j+2}G_{m-1,i}G_{n-1,j}\right)\right]\right)\right)\\ &+\mathbb{E}[Y_1^2]\left(t^{\alpha}+2t^{\alpha}\sum_{m=1}^{M}\left[\frac{\Gamma(\alpha+1)t^{(2m+1)\alpha}}{\Gamma((2m+1)\alpha+1)}\left(\sum_{i=0}^{m}\mathbb{E}[\lambda^{i}](-1)^{i}\hat{G}_{m,i}\right)\right]\right.\\ &\left.+\sum_{m=1}^{M}\sum_{n=1}^{M}\left[\frac{\Gamma(\alpha+1)^2t^{(2n+2m+2)\alpha}}{\Gamma((2m+1)\alpha+1)\Gamma((2n+1)\alpha+1)}\left(\sum_{i=0}^{m}\sum_{j=0}^{n}\mathbb{E}[\lambda^{i+j}](-1)^{i+j}\hat{G}_{m,i}\hat{G}_{n,i}\right)\right]\right)\\ &+2\mathbb{E}[Y_0]\mathbb{E}[Y_1]\left(t^{\alpha}+t^{\alpha}\sum_{m=1}^{M}\left[\frac{t^{2\alpha m}}{\Gamma(2\alpha m+1)}\left(\sum_{i=0}^{m-1}\mathbb{E}[\lambda^{i+1}](-1)^{i+1}G_{m-1,i}\right)\right]\right.\\ &+\sum_{m=1}^{M}\left[\frac{\Gamma(\alpha+1)t^{(2m+1)\alpha}}{\Gamma((2m+1)\alpha+1)}\left(\sum_{i=0}^{m}\mathbb{E}[\lambda^{i}](-1)^{i}\hat{G}_{m,i}\right)\right]\\ &\left.+\sum_{m=1}^{M}\sum_{n=1}^{M}\left[\frac{\Gamma(\alpha+1)t^{2\alpha m}t^{(2n+1)\alpha}}{\Gamma((2n+1)\alpha+1)\Gamma(2\alpha m+1)}\left(\sum_{i=0}^{m-1}\sum_{j=0}^{n}\mathbb{E}[\lambda^{i+j+1}](-1)^{i+j+1}G_{m-1,i}\hat{G}_{n,j}\right)\right]\right),\end{aligned} \tag{7}$$

respectively.

Taking into account (6) and, (7) and $\sigma[Y_M(t)] = \sqrt{E[Y_M(t)^2] - E[Y_M(t)]^2}$, we can compute the standard deviation.

So far, approximations for the two first statistical moments have been obtained. Nevertheless, sometimes higher one-dimensional moments are also required. The 1-PDF of the solution allows us to compute these higher moments by integration. The 1-PDF will be approximated by applying the Random Variable Transformation technique [3, Ch. 2] to the truncated solution of order M. After some involved computations, we have obtained

$$f_{Y_M(t)}(y) = \int_{\mathcal{D}(Y_1,\lambda)} f_{Y_0}\left(\frac{y - y_1\left(t^\alpha + \sum_{m=1}^{M}\left[\frac{\Gamma(\alpha+1)t^{(2m+1)\alpha}}{\Gamma((2m+1)\alpha+1)}\left(\sum_{i=0}^{m}\lambda^i(-1)^i\hat{G}_{m,i}\right)\right]\right)}{1 + \sum_{m=1}^{M}\left[\frac{t^{2\alpha m}}{\Gamma(2\alpha m+1)}\left(\sum_{i=0}^{m}\lambda^{i+1}(-1)^{i+1}G_{m-1,i}\right)\right]}\right) f_{Y_1}(y_1) f_\lambda(\lambda)$$
$$\cdot \frac{1}{\left|1 + \sum_{m=1}^{M}\left[\frac{t^{2\alpha m}}{\Gamma(1\alpha m+1)}\left(\sum_{i=0}^{m-1}\lambda^{i+1}(-1)^{i+1}G_{m-1,i}\right)\right]\right|}\mathrm{d}y_1\mathrm{d}\lambda. \tag{8}$$

Assuming that the PDF of random variable Y_0, f_{Y_0}, is Lipschitz, it can be rigorously proved that (8) converges to the 1-PDF of the solution stochatic process, $Y(t)$, as $M \to \infty$.

3 Acknowledgements

This work has been supported by

- Grant $PID2020-115270GB-I00$ funded by $MCIN/AEI/10.13039/501100011033$
- Grant $AICO/2021/302$ (Generalitat Valenciana)

References

[1] C. Burgos, J.C. Cortés, L. Villafuerte, R. J. Villanueva. *Extending the deterministic Riemann Liouville and Caputo operators to the random framework: A mean square approach with applications to solve random fractional differential equations.* Chaos, Solitons Fractals. Elsevier. 2017, 102, 305-318.

[2] M. Al-Refai, M. Syam, Q. Al-Mdallal. (2017). *On the fractional Legendre equation and fractional Legendre functions.* Progr Fract Differ Appl. 2017 3(2), 93-102.

[3] T. T. Soong. *Random differential equations in science and engineering.* Academic Press. 1973. ISBN: 9780080956121

International Conference on Mathematical Analysis and Applications in Science and Engineering
ICMA^{2}SC'22
ISEP Porto-Portugal, June 27 - 29, 2022

Fractional dependence in integer order PDE

Daniel Cao Labora

Universidade de Santiago de Compostela, Spain

daniel.cao@usc.es

Abstract: Fractional Calculus has been proved to be of huge applicability in the recent years. In this sense, fractional integral and differential equations have been used to model issues of very diverse nature. Nevertheless, it also happens that fractional operators can arise easily in phenomena which are governed by a usual PDE, with no fractional orders imposed *a priori*. We will follow the ideas in [1], and [2] to present a general framework where this fractional dependence can be found, leaving two open questions.

keywords: Bagley-Torvik equation; Euler-Lagrange beam equation; fractional dependence in PDE.

MSC2020: 26A33; 35R11; 74S40.

1 Introduction

Fractional Calculus (FC) is known to have a wide spectrum of possible applications in many diverse scientific areas, as it can be seen in the rest of this book of abstracts. Nevertheless, from the point of view of the author, among all possible applications of FC one of these models is extremely special: the Bagley-Torvik equation, described in [1].

In a few words, the equation describes the movement of an ideal fluid that is induced by the motion of a plate over its surface. Thus, the partial differential equation (PDE) describes the movement of the liquid in horizontal layers, since the velocity field only depends on the time and depth. Besides, it is well-known that the shear stress at any point and time can be computed as the product of two magnitudes: the viscosity, that it is assumed to be constant, and the derivative of the velocity with respect to the depth. However, under certain assumptions, and using the properties of the Laplace transform (LT) in FC (that can be checked at [3]) it is possible to conclude that the shear stress can be also computed as a multiple of the time derivative of the velocity with order $\frac{1}{2}$.

This application for FC is of considerable interest, since it shows a time-fractional dependence for a physical magnitude without imposing any fractional derivative in the original equation *a priori*. This means that it is not necessary to consider a PDE with fractional orders to deduce that some magnitudes depend on fractional derivatives. In other words, fractional operators may arise naturally in phenomena governed by PDE that only involve standard derivatives in their formulation.

A few decades later, the author, together with professors Tenreiro and Lopes, extended the previous idea for another PDE in [2]: the Euler-Lagrange beam equation. In order to do so, we had to impose homogeneous initial conditions and make certain assumptions about the boundary

values and the Young modulus. We were able to obtain a similar result to the one in [1], but for the shear force of the beam. However, the restrictions that were assumed in order to provide a rigorous mathematical deduction made our conclusion a bit restrictive and of a limited practical applicability.

2 Results and discussion

The fluid and beam examples suggest that the previous argument can be done under a more general situation. We will sketch how to prove the aforementioned "fractional dependence" for any PDE of the form

$$c^n \frac{\partial^n f}{\partial t^n}(t,x) = \frac{\partial^m f}{\partial x^m}(t,x), \tag{1}$$

under suitable conditions, where n and m are different natural numbers, and $c > 0$. Besides, without loss of generality we can assume that $n < m$ and $c = 1$. From now on, t will denote a variable defined on $[0,\infty)$ (usually time), and x will be a variable defined on some compact interval (usually some spatial magnitude). As we have mentioned, and recalling that $c = 1$, the goal is to show the relation

$$\frac{\partial^k f}{\partial t^k}(t,x) = \text{constant} \cdot \frac{\partial^{k\frac{m}{n}} f}{\partial x^{k\frac{m}{n}}}(t,x). \tag{2}$$

In order to apply the procedure, we shall assume that our problem has homogeneous initial values, namely

$$f(0,x) = \frac{\partial f}{\partial t}(0,x) = \cdots = \frac{\partial^{n-1} f}{\partial t^{n-1}}(0,x) = 0. \tag{3}$$

The idea for arriving to (2) reads as follows.

1. First, thanks to (3), we observe that it is possible to apply the LT to the previous equation (1). We get

$$s^n\, F(s,x) = \frac{\partial^m F}{\partial x^m}(t,x), \tag{4}$$

   after replacing t for the new variable s, and changing f by the transformed function F.

2. Second, we remark that the solutions for (4) conform a module M of dimension m with respect to the ring of bounded functions in $[0,\infty)$, whose elements can be described as

$$F(s,x) = \sum_{j=0}^{m-1} F_j(s,x) = \sum_{j=0}^{m-1} C_j(s)\, e^{\sqrt[m]{s}^{\,n} \exp\left(\frac{2\pi i}{m} j\right) x}, \tag{5}$$

   where the $C_j(s)$ are free, but would be determined after imposing boundary conditions at (1). Besides, in this transformed domain, it is straightforward to check that the basis of the solutions described in (5) fulfil

$$\frac{\partial^k F_j}{\partial x^k}(s,x) = \sqrt[m]{s}^{\,n\cdot k} \exp\left(\frac{2\pi i}{m} j\, k\right) F_j(s,x). \tag{6}$$

3. Finally, we invert the LT. We highlight that, in order to do so, we need an exponential decay property for $F(s,x)$ when $s \to +\infty$. In this sense, we prove Theorem 1, that ensures the existence of a subbasis of M where we have the desired vanishing property. Taking this into account, we get (2) from the inversion formula of the LT applied to (6).

Theorem 1 *The m-dimensional module M described in* (5) *admits a subbasis of functions that decay exponentially when $s \to +\infty$. This subbasis is formed for R_m elements, where R_n is defined as*

$$R_m = \frac{m-2}{2}, \text{ if } m \equiv 0 \mod 4, \quad R_m = \frac{m-1}{2}, \text{ if } m \equiv 1 \mod 4,$$
$$R_m = \frac{m}{2}, \text{ if } m \equiv 2 \mod 4, \quad R_m = \frac{m+1}{2}, \text{ if } m \equiv 3 \mod 4.$$

Indeed, using a more compact notation, the formula for the dimension yields

$$R_n = \frac{3+(-1)^{j+1}}{2} + 2\left\lfloor \frac{m-2}{4} \right\rfloor \quad \forall m \in \mathbb{N}. \tag{7}$$

3 Conclusions and Future work

The main conclusion of this work is the proof that, for some solutions of a certain type of PDE (1), it is possible to show a fractional relation between the derivatives of the solution with respect to its two different variables. With respect to lines of future work, we can highlight two main directions.

- On the one hand, the arguments that we have shown permit to deduce "fractional dependences" in integer order PDE via LT. However, it is a natural question if this fractional relation can be observed directly, without masking the proof with integral transforms. Indeed, this is not just about "unmasking" the deduction by avoiding LT, but about finding another path for our argument that imposes less restrictions on the problem. More specifically, the deduction via integral transforms implies the necessity of adding some artificial hypotheses. As we have already seen, these hypotheses involve the vanishing of some coefficients in the transformed domain, in order to ensure the validity of the inverse LT. In principle, these additional assumptions could not be necessary to show the aforementioned fractional relation, provided that we use a different tool for their proof.

- On the other hand, under the government of a PDE of integer order from a certain family, we have provided a general remark that shows a fractional dependence between the derivatives of its solution with respect to different variables. Nevertheless, in order to ensure the practical interest and real applicability of this result, it is quite relevant to provide examples of equations of the form (1) that appear in nature, physics, engineering... In case we do so, we will be able to provide several examples of situations where fractional differential equations appear naturally, as a consequence of a phenomenon which is governed by a well-established PDE, as it is the case with the derivation of the Bagley-Torvik equation.

Acknowledgments

I would like to acknowledge the indirect role of professors J. A. Tenreiro Machado and António M. Lopes. This work is based on the paper [2], that we three developed together almost four years ago, during my PhD stay at Porto. Without their help and kindness, this would not be possible. Thank you.

References

[1] P.J. Torvik, R.L. Bagley, On the appearance of the fractional derivative in the behavior of real materials, Journal of Applied Mechanics, **51**(2) (1984), 294–298.

[2] Daniel Cao Labora, Antonio M. Lopes, J.A. Tenreiro Machado, Time-fractional dependence of the shear force in some beam type problems with negative Young modulus, Applied Mathematical Modelling, **80** (2020), 668–682.

[3] S. Samko, A. Kilbas, O. Marichev, *Fractional Integrals and Derivatives: Theory and Applications*. London: Gordon and Breach Science Publishers, 1993.

Fractional derivative of the Lerch zeta function – further properties

Emanuel Guariglia

Institute of Biosciences, Letters and Exact Sciences
São Paulo State University (UNESP)
Rua Cristóvão Colombo 2265
15054-000 São José do Rio Preto, SP
Brazil

email: emanuel.guariglia@gmail.com

Abstract: This work concerns the fractional derivative of the Lerch zeta function. The author already dealt with its functional equation. He reduced its computational cost and proved an approximate functional equation for this fractional derivative. Here, we study the statistical properties of this fractional derivative. Moreover, we also investigate its properties of universality and distribution of zeros.

Keywords: Lerch zeta function, Grünwald-Letnikov fractional derivative, statistical properties, universality, distribution of zeros.

MSC2020: Primary 26A33, 11M35; Secondary 30D05.

References

[1] Guariglia, E.: Fractional calculus of the Lerch zeta function. Mediterr. J. Math. **19**(1), 109 (2022).

[2] Garunkštis, R., Tamošiūnas, R.: Symmetry of zeros of Lerch zeta-function for equal parameters. Lith. Math. J. **57**(4), 433–440 (2017).

[3] Garunkštis, R.: Approximation of the Lerch zeta-function. Lith. Math. J. **44**(2), 140–144 (2004).

[4] Guariglia, E.: Riemann zeta fractional derivative – functional equation and link with primes. Adv. Difference Equ. **2019**(1), 261 (2019).

[5] Li, C., Dao, X., Guo, P.: Fractional derivatives in complex planes. Nonlinear Anal. **71**(5-6), 1857–1869 (2009).

[6] Machado, J.A.T., Kiryakova, V., Mainardi, F.: Recent history of fractional calculus. Commun. Nonlinear Sci. Numer. Simul. **16**(3), 1140–1153 (2011).

[7] Ortigueira, M.D., Trujillo, J.J.: Generalized GrÃ$\frac{1}{4}$nwald–Letnikov fractional derivative and its Laplace and Fourier transforms. J. Comput. Nonlinear Dyn. **6**(3), 034501 (2011).

[8] Srivastava, H.M.: Operators of basic (or q-) calculus and fractional q-calculus and their applications in geometric function theory of complex analysis. Iran. J. Sci. Technol. Trans. A Sci. **44**(1), 327–344 (2020).

International Conference on Mathematical Analysis and Applications in Science and Engineering
ICMA^{2}SC'22
ISEP Porto-Portugal, June 27 - 29, 2022

FRACTIONAL DERIVATIVE AS NORMALIZATION APPROACH FOR CLUSTERING APPLICATIONS

Diego Mauricio Murillo Gómez[1⋆] **Juan Pablo Ugarte Macias**[2]

[1] Asociación Colombiana de Higiene Ocupacional, Capítulo Antioquia, Colombia
[2] Universidad de San Buenaventura, Medellín, Colombia

[1⋆]dmurillo@conhintec.com

Abstract: This paper addresses a fractional calculus application to clustering problems. The results indicate that the fractional generalization of the logarithm as a normalization technique improves the general performance of the clustering algorithm for different distances. Future studies should be further validate the behavior of the normalization tool assessed in this work for large and different datasets.

keywords: Clustering; Fractional Derivative; Normalization.

MSC2020: 49-XX; 34-XX; 92-XX.

1 Introduction

Clustering is a well-established technique for supervised and non-supervised classification problems [Alauddin and Mohammad, 2006, Sinaga, 2020]. It relays on the analysis of distance's relations in between features in a n-dimensional space. Its main advantages correspond to a relative simplicity in the algorithm implementation, versatility for several types of problems and convergence [Madhulatha, 2012].

Normalization is a common stage in the preparation of the data to ensure that all features are bounded by same scale [Patel, 2011]. Otherwise, some features dominate due to the range of its magnitude, thus introducing bias in the analysis. This is a relevant aspect in clustering problems, where some distances (e.g., Euclidean) are sensitive to larger differences within the data magnitudes. Normalization is usually performed through the z-score [Mohamad, 2013], which yields zero mean and unitary standard deviation. The min-max normalization considers the minimum and maximum of each feature to scale them into a range within 0 and 1 [Virmani, 2013]. Finally, for sets containing only positive data, the use of a logarithmic normalization is also another feasible approach [Uragun, 2011].

A generalization of the logarithmic normalization can be adopted as follows. The first order derivative and integral of the logarithm is $1/x$ and $[log(x) - 1]x$, respectively. Since the integral, in terms of derivatives, corresponds to an operator of order -1, a generalization of the logarithmic

function can be formulated by considering the fractional order derivatives of $log(x)$ between -1 and 1. According to the theory of fractional calculus, the α order derivative of the logarithm has the following expression [Machado, 2014]:

$$\frac{d^{\alpha}}{dx^{\alpha}}\log(\mathbf{x}) = \frac{x^{-\alpha}}{\Gamma(1-\alpha)}\left[\log(\mathbf{x}) + \psi(1) - \psi(1-\alpha)\right], \tag{1}$$

where, $\alpha \in [-1, 1]$, $\Gamma(\cdot)$ and $\Psi(\cdot)$ are the gamma and digamma functions, respectively. It is noteworthy that for $\alpha = 0$ the logarithmic function is recovered.

Bearing this ideas in mind, this work discusses the implementation of the fractional order derivative as a normalization approach of datasets for clustering problems.

2 Results and discussion

The Fisher dataset [Fisher, 2021] has been used for the analysis. The numerical experiment consists of 52 trials that combines 4 normalization types, i.e., z-score, logarithmic, min-max and fractional generalization of logarithm, with 13 distance metrics, namely, Euclidean, Manhattan, Tchebychev, Cosine, Lorentzian, Sorensen, Canberra, Clark, Divergence, Jaccard, Dice, Weierstrass and Meehl [Pandit, 2011]. The distances are used for feeding a k-means algorithm. The data is divided by a relation of 80/20, where 80% of the data is used for training the clustering algorithm and the remaining 20% for testing. Figure 1 shows performance metrics using the testing data grouped by the type of normalization. Figure 2 illustrates the performance metrics for each distance and normalization type.

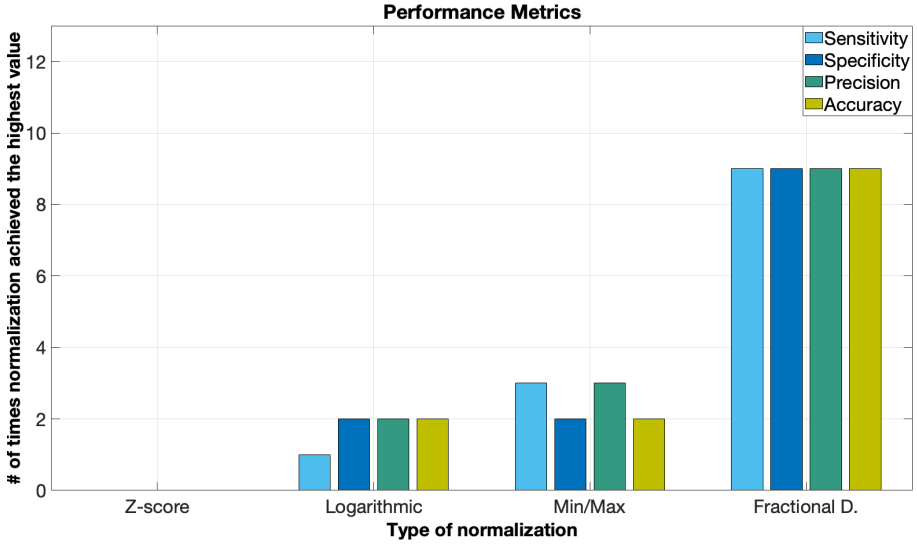

Figure 1: Normalization leading to the best performance for each type of distance.

The results indicate that the Fractional Derivative as normalization tool yield the best performance metrics in most of the cases (9 of 13 distances). Furthermore, the mean value for the 4 metrics is 91%, which supports the robustness of this normalization regardless the distance selected. The minimum value achieved corresponds to 75% in sensitivity corresponding to the Sorensen distance.

A study of how normalization affects the structure of the clusters is carried out using Multi Dimensional Scaling (MDS) [Cox, 2001] to reduce the dimensionality of the Fisher's Dataset from

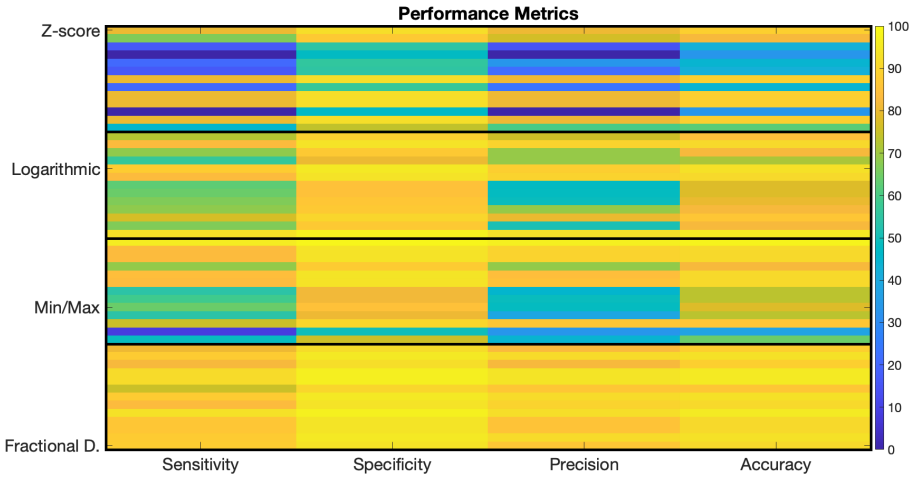

Figure 2: Performance metrics for each type of distance and normalization.

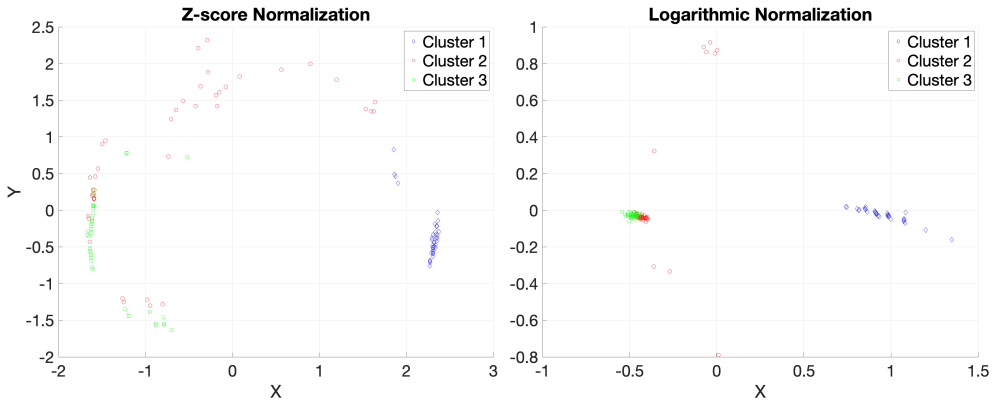

Figure 3: Clustering structure for Z-score and Logarithmic Normalization - Divergence Distance.

4 to 2 dimensions. Figures 3 and 4 depicts the data mapped into a 2 dimensional space for the Divergence distance. These results evince that the type of normalization affects significantly the data is distributed in the high dimensional space. This has a relevant incidence in the clustering algorithm as the basis for grouping data is the distance relation between objects. In the case of the fractional derivative, the data is generally scattered in three clearly distinguishable clusters, thus reducing the overlapping compared to the other 3 normalization techniques. Furthermore, the transition area between clusters are less dense, which reduce the probability of incorrect assignments.

3 Conclusions and Future work

The use of the Fractional Derivative as normalization method shows good results for the 13 distances considered. Whereas performance in the other normalizations varies according to the selected distance, high values for sensitivity, specificity, precision and accuracy were obtained with the Fractional Derivative for all cases. Future studies should be conducted to further validate the effect of the fractional generalization of the logarithm in the pre-processing stage of clustering tasks.

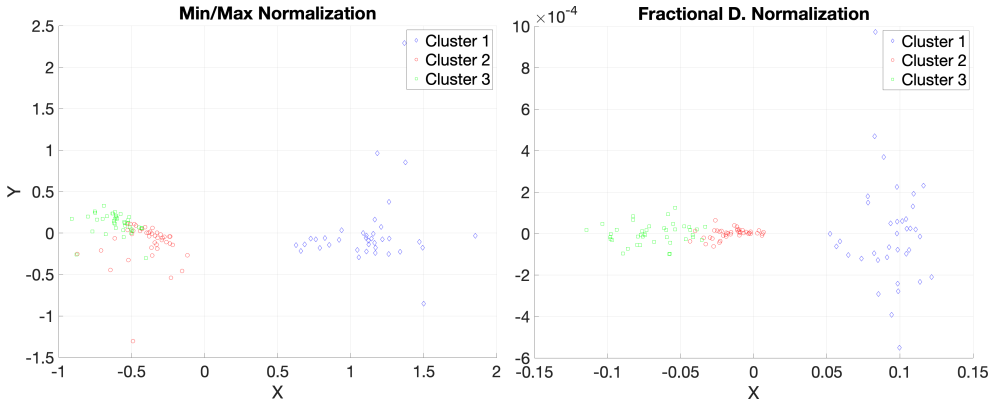

Figure 4: Clustering structure for Min/Max and Fractional D. Normalization - Divergence Distance.

References

[Alauddin and Mohammad, 2006] Alauddin, Y. and Mohammad, S., A new approach of clustering based machine-learning algorithm, Knowledge-Based Systems, 19(4), p. 248-258, 2006.

[Sinaga, 2020] Sinaga K. and Yang M.,"Unsupervised K-Means Clustering Algorithm, IEEE Access, 8, pp. 80716-80727, 2020.

[Madhulatha, 2012] Madhulatha, T., An Overview on Clustering Methods, IOSR Journal of Engineering, 2(4), p. 719-725, 2012.

[Patel, 2011] Patel V. and Mehta, R., Impact of outlier removal and normalization approach in modified k-means clustering algorithm, International Journal of Computer Science Issues, 8(5), p. 331,2011.

[Mohamad, 2013] Mohamad, I. and Usman, D., Standardization and its effects on K-means clustering algorithm. Research Journal of Applied Sciences, Engineering and Technology, 6(17), p. 3299-3303, 2013.

[Virmani, 2013] Virmani D., Taneja S., Malhotra G., Normalization based K means Clustering Algorithm, International Journal of Advanced Engineering Research and Science, 3, p. 5, 2015.

[Uragun, 2011] Uragun B., Rajan R., Developing an Appropriate Data Normalization Method, 10th International Conference on Machine Learning and Applications and Workshops; Honolulu, 2011.

[Machado, 2014] Machado J., Fractional order generalized information, Entropy. 16, p. 2350-2361, 2014.

[Fisher, 2021] Fisher R., Iris Data Set, consulted on 01/10/2021, https://archive.ics.uci.edu/ml/datasets/iris.

[Pandit, 2011] Pandit, S., and Gupta, S. A comparative study on distance measuring approaches for clustering, International Journal of Research in Computer Science, 2(1), p. 29-31, 2011.

[Cox, 2001] Cox T., Cox M., Multidimensional Scaling, Chapman & Hall/CRC, Boca Raton, 2001.

International Conference on Mathematical Analysis and Applications in Science and Engineering ICMA²SC'22

ISEP **Porto-Portugal, June 27 - July 1, 2022**

BEYOND ENTROPY: THE ZETA FUNCTION

Alain Le Méhauté[1*], **Philippe Riot**[2], **Alina Gavrilut**[3], **Dmitriii Tayurskii**[4]

[1] Materials Design & KFU 1, France
[2] Zeta Innovation Group 2, France
[3] Ioan Cuza University 3, Romania
[4] Kazan Federal University (KFU) 4 Russia

[1*] alm@materialsdesign.com

Abstract: Can the concept of "arrow of time" make sense in standard physical framework? It will be presumed that, for an arguing only backed on ZFC axioms and set theory, and except in a very particular case (2-metric and "thermal time" in quantum mechanics) the answer is undecidable. The use of category theory, in particular of the concept of Grothendieck's topos and monad, allows an access to a new stand point about this issue. As illustration, and using the links with the Riemann zeta function, this note analyses the breakthrough offered, in temporal matter, by the open fractional dynamics (in fractal fold structure 1<d<2). The analysis highlights the link between a "proper time" based on zeta function and the concept of entanglement and entropy. Taking priority over Noetherian energy in the physics of open systems, thus dual (internal-external/direct-anti), entropy appears related to a coarse graining bundled by arithmetic properties expressed through zeta Riemann function.

keywords: Fractal. Zeta function. Entropy. Topos. Monads. Arrow of time

MSC2010: 26E05; 34A10; 49J52.

1 Introduction

The concept of "arrow of time" is a concept open to many speculations. Since consciousness is a macroscopic characteristic, would it be possible to prove its existence using standard and non-quantum physical problems? If such an arrow exists, it is very probably related to the concept of entropy, to date the only oriented function in physics. Its foundation is combinatorial, which too much naturally links its expression to probabilities and therefore to a theory of additive and normalized measures (opposed to non-additive and none able to be normalized). In the spirit of the Maxwellian paradoxes about global irreversibility emerging from a local reversibility through a change of scales, and although quantum dynamics appeals an absolute reversible Newtonian time, Connes and Rovelli were able to design an arrow of so-called Thermal Time [1]. Its existence is based on the fact that quantum mechanics involves so-called von Neumann algebras (algebra attached to the laws governing the transitions between quantum states). In this algebraic framework, automorphisms only depend on a single parameter (Tomita Takesaki theorem). This parameter is such that if we consider the conjunction of two idempotent operators applied over a basis of canonical states of representation (cycles) a non-commutativity arises. It is only attached to the single control parameter. A link can then be established with the KMS principle (Kubo, Martin and Schwinger) which, in

physics, leads the same type of non-commutativity for Hamiltonian systems subject to thermal uncertainty [2 see many references inside]. The conservation of the identity of the structures is then expressed as a time shift, namely an "arrow of time" (for A. Connes linked to the temperature of the fossil radiation). Since, the non-trivial zeros of the zeta function are related to the transitions matrices between stable states [3] and the path integrals of Quantum Mechanics reveal that the underlying synthetic metric is of dimension $d=2$ (Peano metric: r,t), the authors decided to focus the analysis on the links between the functional properties of the zeta function and of Extensity Transfers on Fractal Interfaces of lower dimension $d<2$, for open irreversible systems. The canonical dynamics are then controlled by fractional differential equations and give rise to universal transfer functions involving power laws and a paradoxical delegitimization of the notion of energy (due to a revocation of Noether principles). The most emblematic of these universal transfer functions is the Cole and Cole whose singular dispersions properties and causality are linked to « $\alpha=1/d$ » [4].

2 Results and discussion

Among the most interesting results obtained, we note firstly the fact that Cole and Cole transfer function $Z_\alpha(\iota\omega)$, as pure hyperbolic geodesic in frequency space, is a stacking basis giving birth to the Riemann zeta function $\zeta_\alpha(s)$. The stalking parameter « θ » is none other than the one involved in the complex parameterization of the zeta function: $s=\alpha+\iota\theta$.

The second result relates to the incompleteness (of the representation backed on the only fractional transfer function with "α" parameter $Z_\alpha(\omega\tau)$. This function has no inverse Fourier transform so there is no one-parameter automorphism for this kind of fractional dynamics. Time as a usual dynamic deployment over an order parameter is not able to be locally relevant. Automorphisms, -because there are obviously some, for instance via renormalization-, are backed on sheaves of arithmetic correlations which destroy the absolute external order of the dynamics. These sheaves are based on a dual function stated: $Z_{1-\alpha}(\iota\tau)$. Itself is the basis of a stalking giving birth to $\zeta_{1-\alpha}(1-s)$. But, the stalk is now parametrized by « -θ » then $s=\alpha-\iota\theta$. This change in the signature is without consequence if $d=2$, but if $d<2$, the breaking of symmetry $\alpha \rightleftharpoons (1-\alpha)$, leads radical upshots; namely $\zeta^*_{1-\alpha}(s) \neq \zeta_{1-\alpha}(s^*)$. However, the categorical adjunction $\alpha \rightleftharpoons (1-\alpha)$ gives rise to a Grothendieck topos. This topos allows to understand why and how $\zeta_\alpha(s)$ and $\zeta_{1-\alpha}(1-s)$ unfold over dual universal varieties; all degeneracies involved by the internal arithmetic correlations are hidden behind $Z_\alpha(\omega\tau)$.

The third important result is the following: we confirm that the usual *Space-Time* coupling either linear ($v=Lt^{-1}$), diffusive ($D=L^2t^{-1}$), Lorentzian or other flat dispersions, comes from a more general form based on *Scale-Frequency* monad: namely based on $[C=(1/\Lambda)\,N^\alpha]_{Z\alpha(\omega)}$ characterized by $N: N=\iota\omega\tau=\iota\Pi p_i^{r_i}$ where r_i are integers and p_i are prime numbers. If we add that Scale-Frequency structure is dual with $[C'=(1/\Lambda')\,\tau^{1-\alpha}]_{Z1-\alpha(\tau)}$ the role of arithmetic correlations (sheaves) in a structure appears and then the zeta functions, as a representation of a covering (stalking) of the dual monads. Ultimately, this approach leads the functional relation on zeta functions $\zeta_\alpha(s)=F[\zeta_{1-\alpha}(1-s)]$, relation whose analytic complexity comes from the symmetry breaking between $Z_\alpha(\omega\tau)$ and $Z_{1-\alpha}(\tau)$ over the hyperbolic geodesic. While joining discrete and continuous structure, duality which structures the Grothendick topos restore the final role of the energy through the completion or the dual amalgam.

The fourth result brings us back to the arrow of time. In above approach, the parameter « θ » plays the role of a "proper time". It can be shown that the asymmetry between $+\theta$ and $-\theta$ is due to the appearance of a phase angle which two folds the complex plane of

representation. This angle may be associated physically with an increase in internal entropy and a production of external anti-entropy aimed at balancing the duality. From this new dynamic site, any creative process requires an increase of dissipation and an increase of the "time constants" of the processes implemented (downing of frequencies namely an increasing of the uncertainty), approach opposite to any local optimization. In the case *d=2* the process is only controlled by chance and the creative process is reduced to serendipity. The important point is that this is not so if d<2 and thought then become a world of human consciousness and representation, subject to the will of creation.

3 Conclusions and Future work

Above approach could appear purely theoretical but it is not so. Indeed historically this approach based in fine on category theory finds its origin at the end of the seventies in the design of the early lithium batteries [5]. Far from quantum mechanics framework [1], the mathematical foundations of our approach remain to be strengthened, in particular concerning the role of the zeta function as the result of a stalking of a fractional transfer function (via sheaves) , and as "bridging category" between discrete and continuous representations based not only on fractal geometries [6-7] but on number and measure theory. For instance, it can be proved that the Riemann hypothesis is undecidable in the framework of set theory under ZFC axioms. Nevertheless, David A. Martin axiom, extended to a so call Martin-Riemann axiom, guarantees that this passage is carried out in a regular way by respecting the Baire category theorem and zero dimension of Lebesgue measure for the countable approach of the continuous [8]. The link with non-standard analysis must be considered in this frame.
Moreover, the work of physical origins about the link between the arrow of time and the extension of Kan, highlighted by the authors, should be the subject of in-depth mathematical work in relation with non-commutative geometries [9]. In addition, the current works are centered on the metric, therefore the curvatures; nevertheless, beyond this aspect, arises the question of the singular topologies of open systems related to stalked fractal geometries [7] in relation with multi-connex graphs. So a considerable amount of mathematical studies to support new approaches.
In addition, this work could lead to physical applications (in particular in the field of materials with paradoxical properties and in quantum devices) but also in the fields of pedagogy and management (disappearance of optimization principles through figures, double quality plan, relationship to working time, new principles of econo-physics etc). Morover and finally analysis opens new perspectives between mathematic and philosophy [10,11,12].

Acknowledgments

Erich Wimmer and Benoit Leblanc among many others for scientific support. This note is dedicated to the memory of Jose Tenreiro Machado who was a friend with whom we often discussed the link between the notion of fractal and entropy.

References

[1] Carlo Rovelli and Matteo Smerlak, *Thermal time and Tolman Ehrenfest effect : Temperature as the speed of time*, https:// hal.archives-ouvertes.fr / hal-00686093;
[2] Philippe Riot and Alain Le Méhauté, *From the arrow of time in Badiali's quantum approach to the dynamic meaning of Riemann's hypothesis*, Condensed Matter Physics (2017) Vol. **20**, No 3, 33001: 1–13.

[3] Keating J.P., Snaith N.C., Random matrix theory, Commun. Math. Phys., (2000), **214**, 57–89
[4] Alain Le Méhauté, *Les géométries fractales et applications* Ed. Hermes Paris 1990 (in English *Fractal Geometry and applications*, Penton Press London 1991)
[5] Alain le Méhauté and Frédéric Héliodore, *The history of invention of Lithium Batteries (1970-1985): Example of Zeta management, Hyperion International Journal of Econo-physics and New Economy* (2020) **13**, issue 2, 7- 44.
[6] P. Riot,, A. Le Méhauté, D. Tayurskii, *Fractional Dynamics, Riemann Zeta Function and Self Similarity through Category Theory*, in Advances in Special Functions and Analysis of Differential Equations (Chapter 14) Agarwal Praveen, Agarwal Ravi P., Ruzhansky M. Editors. CRC Press Deleware, 2019.
[7] Alina. Gavrilut, Ioan. Merches, Maricel Agop, *Atomicity through fractal measure theory*, Springer, Zurich, 2019
[8] Philippe Riot, *Une nouvelle approche des hypothèses de Riemann et de Goldbach*, Entropie série Géométrie, Information et Entropie (to be published 2022),
[9] Alain Connes, *Noncommutative geometry*, Academic press San Diego C.A. 1994
[10] Franck Jedrzejewski, *Ontologie des catégories*, l'Harmattan Paris 2011
[11] Alain Badiou, *Mathematics of the transcendental*, Blomsbury, N.Y. 2014
[12] Simona Modreanu, Alina Gavrilut, Gabriel Crumpei and Maricel Agop, *αtom: a transdisplinary and transcultural insight*, Atlas publishing N.Y. 2022

International Conference on Mathematical Analysis and Applications in Science and Engineering
ICMA^{2}SC'22
ISEP Porto-Portugal, June 27 - 29, 2022

Numerical methods for singular fractional integro-differential equations with constant coefficients

Kaido Lätt[1⋆]

[1] Institute of Mathematics and Statistics, University of Tartu, Estonia

[1⋆]kaido.latt@ut.ee

Abstract: We consider singular fractional integro-differential equations with constant coefficients. In the talk we present some results about the unique solvability of such equations and introduce a collocation based scheme for finding the numerical solution of the problem under consideration. We also give results of numerical experiments.

keywords: fractional derivatives; singular fractional integro-differential equations; numerical methods.

MSC2020: 34A08; 65R20

1 Introduction

Fractional derivatives and equations containing them have fascinated scientists for a very long time. Over the last few decades interest in the field has increased significantly because of new applications in Physics, Chemistry, Electrical Networks and so on [1, 3].

For the Banach space of continuous functions u on $[0,T]$ we use the notation $C[0,T]$, $\|u\|_\infty = \sup\{|u(t)| : 0 \le t \le b\}$. By $L^1(0,1)$ we denote the Banach space consisting of real or complex valued functions φ defined on the interval $(0,1)$ such that $\|\varphi\|_{L^1(0,1)} = \int_0^1 |\varphi(x)|dx < \infty$.

In [2] the unique solvability of singular fractional differential equations was studied. We now consider singular fractional integro-differential equations of the form

$$(M^\beta D_0^\beta u)(t) = \sum_{k=1}^{l} a_k (M^{\beta_k} D_0^{\beta_k} u)(t) + a(V_\varphi u)(t) + f(t),\ 0 < t \le T. \tag{1}$$

Here the multiplication operator M^β, $\beta \in \mathbb{R} = (-\infty, \infty)$, is defined as $(M^\beta u)(t) = t^\beta u(t)$ $(0 < t \le T)$ for $u \in C[0,T]$,

$$(V_\varphi u)(t) = \int_0^t \frac{1}{t}\varphi\left(\frac{s}{t}\right) u(s)ds = \int_0^1 \varphi(x)u(tx)dx, \quad 0 \le t \le T, \quad u \in C[0,T],$$

i.e. $V_\varphi : C[0,T] \to C[0,T]$ is a cordial Volterra integral operator with core $\varphi \in L^1(0,1)$ [4], $\beta, \beta_k, a, a_k \in \mathbb{R}$ and

$$0 < \beta < 1, \quad \beta > \beta_k \ge 0, \quad f \in C[0,T], \quad k = 1, 2, \dots, l, \quad l \in \mathbb{N} = \{1, 2, \dots\}. \tag{2}$$

In equation (1) the fractional differential operator D_0^β, of the order $\beta \in [0,\infty)$, is defined as the inverse of the Riemann-Liouville integral operator $J^\beta : C[0,T] \to C[0,T]$ given by (in the following Γ denotes the Euler gamma function)

$$(J^\beta u)(t) = \frac{1}{\Gamma(\beta)} \int_0^t (t-s)^{\beta-1} u(s) ds, \quad u \in C[0,T], \quad t > 0,\ \beta > 0; \quad J^0 = I,$$

on the space $J^\beta C[0,T]$, i.e. $D_0^\beta v = (J^\beta)^{-1} v$, where v belongs to the range $J^\beta C[0,T]$ of J^β, $\beta \geq 0$.

2 Results and discussion

2.1 The unique solvability of the equation

We make in (1) the change of variables $v = M^\beta D_0^\beta u$, i.e. $u = (M^\beta D_0^\beta)^{-1} v = J^\beta M^{-\beta} v$, obtaining with respect to v the equation

$$v = \sum_{k=1}^{l} a_k V_{\psi_{\beta,\beta_k}} v + a V_{\varphi_\beta} v + f, \tag{3}$$

where

$$\psi_{\beta,\beta_k}(x) = \frac{1}{\Gamma(\beta-\beta_k)} (1-x)^{\beta-\beta_k-1} x^{-\beta}, \quad 0 < x < 1, \quad k = 1,2,\ldots,l, \tag{4}$$

and

$$\varphi_\beta(x) = \int_x^1 \frac{1}{\Gamma(\beta)} \varphi(y) x^{-\beta} (y-x)^{\beta-1} dy, \quad 0 < x < 1. \tag{5}$$

Equation (3) is a cordial Volterra integral equation with ψ_{β,β_k} and φ_β belonging to $L^1(0,1)$. Based on some results from the theory of cordial Volterra integral operators (see, e.g., [4]), we can show that the following theorem holds.

Theorem 1 *Let $\varphi \in L^1(0,1)$, $a, a_k, \beta, \beta_k \in \mathbb{R}$, $0 < \beta < 1$, and $\beta > \beta_k \geq 0$, $k = 1,2,\ldots,l$. For any $f \in C[0,T]$, equation (3) has a unique solution $v \in C[0,T]$ if and only if*

$$\sum_{k=1}^{l} a_k \frac{\Gamma(\lambda-\beta+1)}{\Gamma(\lambda-\beta_k+1)} + a\widehat{\varphi}(\lambda) \frac{\Gamma(\lambda-\beta+1)}{\Gamma(\lambda+1)} \neq 1,\ \forall \lambda \in \mathbb{C} \text{ with } \mathrm{Re}\lambda \geq 0.$$

Here $\widehat{\varphi}(\lambda) = \int_0^1 x^\lambda \varphi(x) dx$ for such $\lambda \in \mathbb{C} = \mathbb{R} + \mathrm{i}\mathbb{R}$ ($\mathrm{i} = \sqrt{-1}$ is the imaginary unit), where the integral converges.

2.2 Numerical method

We will now give a brief description of a numerical method for solving equation (1) under the conditions (2).

Let $N \in \mathbb{N}$. Introduce a uniform grid $\{t_0,\ldots,t_N\}$ for the interval $[0,T]$ with grid points

$$t_j = jh, \quad j = 0,\ldots,N, \quad h = T/N. \tag{6}$$

For $m \in \mathbb{N}$, define the standard space $S_N^{m-1}[0,T] = \{v : v|_{[(i-1)h,ih]} \in \mathcal{P}_{m-1},\ i = 1,\ldots,N\}$ of piecewise polynomial functions. Here $v|_{[(i-1)h,ih]}$, $i = 1,\ldots,N$, is the restriction of $v : [0,T] \to \mathbb{C}$

onto the subinterval $[(i-1)h, ih]$ and $\mathcal{P}_{m-1}$ is the space of polynomials of degree not exceeding $m-1$. Note that an element of the space $S_N^{m-1}[0,T]$ may have at interior knots ih, $i = 1,\dots,N-1$, two values so that $v|_{[(i-1)h,ih]} \in C[(i-1)h, ih]$, $i = 1,\dots,N$.

In every interval $[(i-1)h, ih]$, $i = 1,\dots,N$, we introduce $m \in \mathbb{N}$ interpolation (collocation) points:

$$t_{i\lambda} = t_{i-1} + \tau_\lambda h, \quad \lambda = 1,\dots,m,\ i = 1,\dots,N, \tag{7}$$

where τ_λ, $\lambda = 1,\dots,m$, are some fixed parameters that do not depend on either i or N but satisfy the condition

$$0 \le \tau_1 < \tau_2 < \cdots < \tau_m \le 1.$$

We are looking for an approximate solution of equation (1) in the form $u_N = J^\beta M^{-\beta} v_N$, where $v_N \in S_N^{m-1}[0,T]$ is such that the collocation conditions

$$v_N(t_{i\lambda}) = \sum_{k=1}^{l} a_k (V_{\psi_{\beta,\beta_k}} v_N)(t_{i\lambda}) + a(V_{\varphi_\beta} v_N)(t_{i\lambda}) + f(t_{i\lambda}), \quad \lambda = 1,\dots,m,\ i = 1,\dots,N, \tag{8}$$

are satisfied.

The collocation conditions (8) lead to a system of equations to uniquely determine the function $v_N \in S_N^{m-1}[0,T]$, the exact form the system of equations depends on the choice of basis in the space $S_N^{m-1}[0,T]$. If we use the Lagrange fundamental polynomial representation, then

$$v_N(t) = \sum_{j=1}^{N} \sum_{\mu=1}^{m} c_{j\mu} L_{j\mu}(t), \quad t \in [0,T], \tag{9}$$

where, for $j = 1,\dots,N$, $\mu = 1,\dots,m$,

$$L_{j\mu}(t) = \begin{cases} 0, & \text{if } t \notin [t_{j-1}, t_j], \\ \prod_{i=1, i\ne\mu}^{m} \frac{t - t_{ji}}{t_{j\mu} - t_{ji}}, & \text{if } t \in [t_{j-1}, t_j]. \end{cases} \tag{10}$$

Note that if we define v_N with (9) and (10), then $v_N \in S_N^{m-1}[0,T]$ and $v_N(t_{i\lambda}) = c_{i\lambda}$ for $\lambda = 1,\dots,m$, $i = 1,\dots,N$. To find the coefficients $c_{i\lambda}$, $i = 1,\dots,N$, $\lambda = 1,\dots,m$, in (9), we have to solve with respect to $c_{i\lambda}$ a system of linear algebraic equations

$$c_{i\lambda} = \sum_{j=1}^{N} \sum_{\mu=1}^{m} \left[\sum_{k=1}^{l} a_k (V_{\psi_{\beta,\beta_k}} L_{j\mu})(t_{i\lambda}) + a(V_{\varphi_\beta} L_{j\mu})(t_{i\lambda}) \right] c_{j\mu} + f(t_{i\lambda}), \tag{11}$$

where $i = 1,\dots,N$, $\lambda = 1,\dots,m$.

By finding coefficients $c_{i\lambda}$, $i = 1,\dots,N$, $\lambda = 1,\dots,m$, we determine the approximate solution $v_N(t) = \sum_{j=1}^{N} \sum_{\mu=1}^{m} c_{j\mu} L_{j\mu}(t)$, $t \in [0,T]$, of equation (3). To find the approximate solution of u_N of (1), we use

$$u_N(t) = (J^\beta M^{-\beta} v_N)(t) = \frac{1}{\Gamma(\beta)} \sum_{j=1}^{N} \sum_{\mu=1}^{m} c_{j\mu} \int_0^t (t-s)^{\beta-1} s^{-\beta} L_{j\mu}(s)\, ds, \quad 0 < t \le T. \tag{12}$$

Example 1 *Consider the equation*

$$(M^{\frac{1}{6}} D_0^{\frac{1}{6}} u)(t) = (M^{\frac{1}{10}} D_0^{\frac{1}{10}} u)(t) + \left(\frac{\Gamma\left(\frac{39}{10}\right)}{\Gamma\left(\frac{56}{15}\right)} - \frac{\Gamma\left(\frac{39}{10}\right)}{\Gamma\left(\frac{38}{10}\right)} \right) t^{\frac{29}{10}}, \quad 0 < t \le 1. \tag{13}$$

We see that (13) is an equation of the form (1), where $\beta = \frac{1}{6}$, $\beta_1 = \frac{1}{10}$, $a_1 = 1$, $a = 0$, $l = 1$ *and the last term on the right hand side of (13) is* f.

We use the collocation method described above to find the numerical solution of equation (13). Let $N \in \mathbb{N}$. *We introduce for the interval* $[0, 1]$ *a uniform grid defined by (6) and use collocation points (7), where the collocation parameters are defined in the following way: 1) if* $m = 2$, *then* $\tau_1 = \frac{1}{4}$ *and* $\tau_2 = \frac{3}{4}$; *2) if* $m = 3$, *then* $\tau_1 = \frac{1}{4}$, $\tau_2 = \frac{2}{4}$ *and* $\tau_3 = \frac{3}{4}$.

In the numerical results below the errors ε_N, $N \in \mathbb{N}$, *are calculated in the following way:*

$$\varepsilon_N := \max_{j=1,\dots,N} \max_{k=0,\dots,10} |u(s_{jk}) - u_N(s_{jk})|.$$

Here $u(t) = t^{\frac{29}{10}}$ $(0 < t \leq 1)$ *is the exact solution of equation (13),* u_N *is the approximation of* u *determined by (12), and the knots* $\{s_{jk}\}$ *are calculated as follows:* $s_{jk} := t_{j-1} + \frac{k}{10}h$, *for* $k = 0, \dots, 10$, $j = 1, \dots, N$ *with* $t_j = jh$, *for* $j = 0, \dots, N$ *and* $h = \frac{1}{N}$. *To demonstrate the numerical convergence rate, we compute the ratios* $\Theta_N := \frac{\varepsilon_{N/2}}{\varepsilon_N}$, $N = 2^j$, $j \geq 2$.
In the following table some results of numerical experiments for different values of parameters N *and* m *are presented.*

	$m = 2$		$m = 3$	
N	ε_N	Θ_N	ε_N	Θ_N
4	$8.39 \cdot 10^{-2}$		$6.35 \cdot 10^{-2}$	
8	$1.38 \cdot 10^{-2}$	6.093	$1.27 \cdot 10^{-2}$	4.984
16	$1.92 \cdot 10^{-3}$	7.153	$2.56 \cdot 10^{-3}$	4.965
32	$2.59 \cdot 10^{-4}$	7.434	$5.18 \cdot 10^{-4}$	4.953
64	$1.04 \cdot 10^{-4}$	2.487	$1.05 \cdot 10^{-4}$	4.940
128	$4.02 \cdot 10^{-5}$	2.591	$2.13 \cdot 10^{-5}$	4.930

3 Conclusions and Future work

We introduced a collocation based scheme for finding the numerical solution of singular fractional integro-differential equations with constant coefficients and presented results of some numerical experiments. Our aim in the future is to carry out a detailed convergence analysis of the introduced method.

Acknowledgments

This work was supported by the Estonian Research Council grant PRG864.

References

[1] K. Diethelm, *The Analysis of Fractional Differential Equations*. Berlin: Springer-Verlag, 2010.

[2] K. Lätt, A. Pedas, G. Vainikko, A smooth solution of a singular fractional differential equation, Z. Anal. Anwend., **34** (2015), 127–146.

[3] I. Podlubny, *Fractional Differential Equations*. San Diego: Academic Press, 1999.

[4] G. Vainikko, Cordial Volterra integral equations 2, Numer. Funct. Anal. Optim., **31** (2010), 191 – 219.

International Conference on Mathematical Analysis and Applications in Science and Engineering
ICMA^{2}SC'22
ISEP Porto-Portugal, June 27 - 29, 2022

FRACTAL-FRACTIONAL ORDER MODELING FOR THE DISEASE DYNAMICS IN BOTH PREY AND PREDATOR

Zubair Ahmad[1⋆] **Francesco Giannino**[2] **Gerardo Toraldo**[1]

[1] 1 Department of Mathematics and Physics, University of Campania âLuigi Vanvitelliâ, Caserta, 81100, Ita
[2] Department of Agricultural Sciences, University of Naples Federico II, Portici 80055, Italy

[1⋆]zubair.ahmad@unicampania.it

Abstract: In mathematical ecology, the Lotka-Volterra equations (they are known as a predator-prey model) is being explored by many researchers by adding different physical parameters to make it more realistic and some of them connected these models to the disease epidemiology. In the present article, we have developed a model of prey and predator with the consideration of carrying capacity and disease dynamics in both the species. The predation, migration and loss of immunity is considered in both the species. Both the species are interconnected with each other through nonlinear ordinary differential equations. The integer-order model is then transformed to the fractalfractional model through the fractal-fractional differential operator of Mittag-Leffler function. Positivity, boundedness, basic reproduction number, equilibrium points, stability analysis is also performed for the considered model. The graphical solution is achieved through numerical scheme based on Newton polynomial interpolation technique while the existence and uniqueness of the solution is also proved theoretically. Some physical results for different embedded parameters are displayed and discussed in detail while some concluding remarks has been drawn from the results.

keywords: Fractal-Fractional Derivative; ODE; Mittag-Leffler Kernel; Basic Reproduction Number; Prey-Predator.

MSC2020: 49M99; 34A08; 92B99; 26A33; 93A30; 37M05

International Conference on Mathematical Analysis and Applications in Science and Engineering
ICMA²SC'22
ISEP Porto-Portugal, June 27 - 29, 2022

Strichartz estimates for structurally damped equations of space-time-fractional type

Nelson Faustino[1,2⋆] **Jorge Marques**[1,3]

[1] Faculty of Economics (FEUC), University of Coimbra, Portugal
[2] Center for R&D in Mathematics and Applications (CIDMA), University of Aveiro, Portugal
[3] Centre for Business and Economics Research (CeBER), University of Coimbra, Portugal

[1,2⋆]nelson@fe.uc.pt
[1,3]jmarques@fe.uc.pt

Abstract: We obtain Strichartz estimates for a wide class of space-time-fractional evolution equations arising in applications towards the theory of structural damping plate equations. We focus on the case where the damping term $\mu(-\Delta)^{\frac{\sigma}{2}}\partial_t^\alpha u(t,x)$, involving a coefficient $\mu > -2$, is described in terms of the time fractional derivative ∂_t^α of order α taken in the Caputo-Djrbashian sense and of the fractional Laplacian $-(-\Delta)^{\frac{\sigma}{2}}$ of order σ in the space variable. Our results heavily rely on the study of the pseudo-differential representation for the resolvent $E_{\alpha,\beta}(-\lambda(-\Delta)^{\frac{\sigma}{2}}t^\alpha)$ in terms of the Mittag-Leffler functions $E_{\alpha,\beta}$.

keywords: Fractional differential equations; Strichartz estimates; structural damping.

MSC2020: 26A33; 33C10; 33E12; 42B15; 44A20

1 Introduction

The investigation of Strichartz estimates dates back to the fundamental paper [7] of R. Strichartz on the Fourier restriction problem. Nowadays they have been revealing to be a cornerstone tool in the study of Schrödinger equations, wave equations and alike. In great extent, because they permit us to obtain sharp estimates for the size and the decay for the solutions of PDEs on mixed Lebesgue spaces $L_t^r L_x^q$ (cf. [5]). To study it, from a fractional calculus perspective, we briefly introduce the main mathematical objects, which allows us to study properly our model problem.

Let us denote by $E_{\alpha,\beta}$ $(\Re(\alpha), \Re(\beta) > 0)$ the two-parameter Mittag-Leffler function, and by $-(-\Delta)^{\frac{\gamma}{2}}$ $(\gamma > 0)$ the fractional Laplacian of order γ. Through the aid of the Fourier transform, $\mathcal{F}$, and its inverse, $\mathcal{F}^{-1}$, we define for a function φ with membership in the Schwartz space $\mathcal{S}(\mathbb{R}^n)$ s.t. $\widehat{\varphi} = \mathcal{F}\varphi$, the resolvent operator $\varphi \mapsto E_{\alpha,\beta}(-\lambda(-\Delta)^{\frac{\sigma}{2}}t^\alpha)\varphi$ in terms of the Fourier inversion formula, valid for each $(t,x) \in [0,\infty)\times\mathbb{R}^n$:

$$E_{\alpha,\beta}(-\lambda(-\Delta)^{\frac{\sigma}{2}}t^\alpha)\varphi(x) = \frac{1}{(2\pi)^n}\int_{\mathbb{R}^n} E_{\alpha,\beta}(-\lambda|\xi|^\sigma t^\alpha)\widehat{\varphi}(\xi)e^{ix\cdot\xi}d\xi, \quad \Re(\lambda) > 0. \tag{1}$$

Our main goal is to report that the pseudo-differential representation (1) can be used to solve and to obtain Strichartz estimates for the class of evolution equations

$$\partial_t^{2\alpha}u(t,x) + \mu(-\Delta)^{\frac{\sigma}{2}}\partial_t^\alpha u(t,x) + (-\Delta)^\sigma u(t,x) = 0, \quad (t,x) \in \mathbb{R}^n \times (0,\infty). \tag{2}$$

We note that the space-time-fractional equation (2) seamlessly represents a time-fractional regularization for the class of structurally damped $\sigma-$evolution equations in the semi-critical case, studied by so many authors (cf. [4]), by replacing the first and second partial derivatives ∂_t and ∂_t^2 by the so-called Caputo-Djrbashian derivatives ∂_t^γ of order $\gamma = \alpha$ and $\gamma = 2\alpha$, respectively.

Such model problem is original motivated by the theory of structurally damped plate equations ($\sigma = 2\alpha = 2$) in a way that $(-\Delta)^\sigma$ shall be interpreted as a space-fractional regularization for the biharmonic operator Δ^2, whereas $\mu(-\Delta)^{\frac{\sigma}{2}}\partial_t^\alpha u(t,x)$ – appearing on the evolution equation (2) – as a space-time regularization for the strong damping term $-\mu\Delta\partial_t u(t,x)$. For further details, we refer to [3] and to the references therein.

2 Results and discussion

In order to obtain a solution representation for (2), we will take into account Laplace transform identities involving the Caputo-Djrbashian derivatives ∂_t^α resp. $\partial_t^{2\alpha}$ (cf. [6, Chapter 2]) and the Mittag-Leffler functions $E_{\alpha,\beta}$ as well (cf. [6, Chapter 1]). In the following theorems, the constants λ_+ and λ_- denote the algebraic roots of the polynomial $P(\lambda) = \lambda^2 - \mu\lambda + 1$.

Theorem 1 (Case I) *Let $0 < \alpha \leq \frac{1}{2}$, $\mu > -2$ and $u_0 \in \mathcal{S}(\mathbb{R}^n)$. Then*

$$v_{\alpha,\sigma}(t,x) = \begin{cases} \dfrac{E_{\alpha,1}(-\lambda_+ (-\Delta)^{\frac{\sigma}{2}} t^\alpha)u_0(x)}{(\lambda_+)^2 - 1} + \dfrac{E_{\alpha,1}(-\lambda_- (-\Delta)^{\frac{\sigma}{2}} t^\alpha)u_0(x)}{(\lambda_-)^2 - 1} & , \ \mu \neq 2 \\ \\ E_{\alpha,1}(-(-\Delta)^{\frac{\sigma}{2}} t^\alpha)u_0(x) + \dfrac{|\xi|^\sigma t^\alpha}{\alpha} E_{\alpha,\alpha}(-(-\Delta)^{\frac{\sigma}{2}} t^\alpha)u_0(x) & , \ \mu = 2. \end{cases}$$

solves the Cauchy problem for eq. (2) with initial condition $u(0,x) = u_0(x)$.

Theorem 2 (Case II) *Let $\frac{1}{2} < \alpha \leq 1$, $\mu > -2$ and $u_0, u_1 \in \mathcal{S}(\mathbb{R}^n)$, and set $v_{\alpha,\sigma}$ as in* **Theorem 1** *&*

$$w_{\alpha,\sigma}(t,x) = \begin{cases} t\ \dfrac{\lambda_+ E_{\alpha,2}(-\lambda_+ (-\Delta)^{\frac{\sigma}{2}} t^\alpha)u_1(x) - \lambda_- E_{\alpha,2}(-\lambda_- (-\Delta)^{\frac{\sigma}{2}} t^\alpha)u_1(x)}{\lambda_+ - \lambda_-} & , \ \mu \neq 2 \\ \\ \dfrac{t}{\alpha}\left(E_{\alpha,1}(-(-\Delta)^{\frac{\sigma}{2}} t^\alpha)u_1(x) - (\alpha-1)E_{\alpha,2}(-(-\Delta)^{\frac{\sigma}{2}} t^\alpha)u_1(x)\right) & , \ \mu = 2, \end{cases}$$

Then, $u(t,x) = v_{\alpha,\sigma}(t,x) + w_{\alpha,\sigma}(t,x)$ solves the Cauchy problem for eq. (2) with initial data $u(0,x) = u_0(x)$ and $\partial_t u(0,x) = u_1(x)$.

Our next step is to derive Strichartz estimates for the solutions obtained in Theorem 1 and Theorem 2 from $L^p - L^q$ estimates of (1). Starting with the estimates obtained for $E_{\alpha,\beta}(-z)$ in [1, Proposition 4.] (case of $z > 0$) and in [6, Theorem 1.6] (case of $z \in \mathbb{C} \setminus \mathbb{R}$), we obtain the following proposition.

Proposition 3 *For every $0 < \alpha \leq 1$, $\sigma > 0$ and $\frac{n}{\sigma} < r < \infty$ one has*

$$\left(\int_0^\infty |E_{\alpha,\beta}(-\lambda\rho^\sigma t^\alpha)|^r \, \rho^{n-1} d\rho\right)^{\frac{1}{r}} \leq \frac{(\ C_{r,\sigma,n}(\alpha,\beta,\lambda)\ )^{\frac{1}{r}}}{\Gamma(\beta)}\ t^{-\frac{\alpha n}{r\sigma}},$$

where $C_{r,\sigma,n}(\alpha,\beta,\lambda)$ is a constant depending on the parameters $r, \sigma, n, \alpha, \beta$ and λ.

Afterwards, we obtain Proposition 4 by a direct application of Young's inequality to the convolution representation of (1):

$$E_{\alpha,\beta}(-\lambda(-\Delta)^{\frac{\sigma}{2}}t^{\alpha})\varphi = \varphi * E_{\alpha,\beta}(-\lambda(-\Delta)^{\frac{\sigma}{2}}t^{\alpha})\delta.$$

We follow [2, Proposition 2.1] to deduce L^r estimates for $E_{\alpha,\beta}(-\lambda(-\Delta)^{\frac{\sigma}{2}}t^{\alpha})\delta$ in terms of the operator norm of the Hankel transform, $\widetilde{\mathcal{H}}_{\frac{n}{2}-1}$. Indeed, by substituting $\varphi(x) = \delta(x)$ on both sides of eq. (1) (i.e. $\widehat{\varphi}(\xi) = 1$), one readily gets

$$E_{\alpha,\beta}(-\lambda(-\Delta)^{\frac{\sigma}{2}}t^{\alpha})\delta = \frac{1}{(2\pi)^{\frac{n}{2}}}\widetilde{\mathcal{H}}_{\frac{n}{2}-1}f, \text{ with } f(\rho) = E_{\alpha,\beta}(-\lambda\rho^{\sigma}t^{\alpha}).$$

Proposition 4 *Under the conditions of Proposition 3 and of [2, Proposition 2.1], the following L^p-L^q estimate fulfils for every $\sigma > \frac{n}{2}$, $\max\left\{1, \frac{n}{\sigma}\right\} < r \leq 2$ and $1 \leq p, q \leq \infty$ s.t. $\frac{1}{r}+\frac{1}{p} = \frac{1}{q}+1$:*

$$\left\| E_{\alpha,\beta}(-\lambda(-\Delta)^{\frac{\sigma}{2}}t^{\alpha})\varphi \right\|_q \leq \frac{(\omega_{n-1}C_{r,\sigma,n}(\alpha,\beta,\lambda))^{\frac{1}{r}}}{(2\pi)^{\frac{n}{2}}\Gamma(\beta)}\ t^{-\frac{\alpha n}{r\sigma}}\ \|\varphi\|_p,$$

where ω_{n-1} denotes the $(n-1)-$dimensional volume of the sphere $\mathbb{S}^{n-1}$.
Moreover, $\varphi \in L^p(\mathbb{R}^n)$ implies $E_{\alpha,\beta}(-\lambda(-\Delta)^{\frac{\sigma}{2}}t^{\alpha})\varphi \in L^q(\mathbb{R}^n)$ whenever

$$\max\left\{0, \frac{n-\sigma}{n}\right\} < \frac{1}{p} \leq 1 \quad \wedge \quad \frac{1}{p} - \frac{1}{2} \leq \frac{1}{q} < \frac{1}{p} - \max\left\{0, \frac{n-\sigma}{n}\right\}.$$

Acknowledgments

Nelson Faustino was supported by The Center for Research and Development in Mathematics and Applications (CIDMA) through the Portuguese Foundation for Science and Technology (FCT), references UIDB/04106/2020 and UIDP/04106/2020;

Jorge Marques was supported by Centre for Business and Economics Research (CeBER) through the Portuguese Foundation for Science and Technology (FCT), reference UIDB/05037/2020.

References

[1] L. Boudabsa, T. Simon, Some properties of the Kilbas-Saigo function, Mathematics (2021) 9, 217.

[2] L. De Carli, On the L^p–L^q norm of the Hankel transform and related operators, Journal of mathematical analysis and applications, **348(1)** (2008), 366-382.

[3] R. Denk, R. Schnaubelt, A structurally damped plate equation with Dirichlet-Neumann boundary conditions, Journal of Differential Equations, **259** (4) (2015)., 1323–1353.

[4] T. P. Duong, , M. K. Mezadek, M. Reissig, Global existence for semi-linear structurally damped σ-evolution models. Journal of Mathematical Analysis and Applications, **431(1)** (2015), 569–596.

[5] M. Keel, T. Tao, Endpoint Strichartz Estimates, American Journal of Mathematics, **120(5)** (1998), 955-980.

[6] I. Podlubny, *Fractional Differential Equations*. New York: Academic Press, 1999.

[7] R. S. Strichartz, Restrictions of Fourier transforms to quadratic surfaces and decay of solutions of wave equations, Duke Mathematical Journal, **44(3)** (1977), 705-714.

International Conference on Mathematical Analysis and Applications in Science and Engineering
ICMA^{2}SC'22
ISEP Porto-Portugal, June 27 - 29, 2022

Fractional Choquet Integral on Time-scale with respect to Non-additive Measure

Shekhar Singh Negi[1⋆] **Vicenç Torra**[2]

[1 2] Umeå universitet, Sweden

[1⋆]shekharsinghnegi2017@gmail.com

Abstract: In 1954 [1], G. Choquet was the first to introduce the Choquet integral with respect to non-additive measures. It is a more general integral than the Lebesgue integral and a useful technique for dealing with uncertainty in imprecise probability theory, decision theory, and cooperative game studies, among other things. In the paper, we are going to study a fractional-Choquet integral with respect to non-additive measure. In which, we are first going to define a fractional Choquet integral on a time scale with respect to the distorted Δ-Lebesgue measure. Some properties of this integral will be discussed. The main motive of this paper is to discuss the calculation of the fractional-Choquet integral of the increasing, decreasing, convex and concave functions. In the end, results are illustrated by various examples.

keywords: Choquet Integral; Fractional derivatives and Integral; Non-additive Measure; Dynamic equation on time scale; Lebesgue Measure.

MSC2020: 46A55;26A33;28E10;28E10.

References

[1] Choquet, G., 1954. Theory of capacities. In Annales de l'institut Fourier, 5, pp. 131-295.

International Conference on Mathematical Analysis and Applications in Science and Engineering
ICMA^{2}SC'22
ISEP Porto-Portugal, June 27 - 29, 2022

WELL-POSEDNESS OF STOCHASTIC TIME FRACTIONAL 2D-STOKES MODELS WITH FINITE AND INFINITE DELAYS

Tomás Caraballo[1⋆] **Jiaohui Xu**[1]

[1] Universidad de Sevilla, Sevilla, Spain

⋆caraball@us.es

Abstract: In this work, the well-posedness of a stochastic delay time fractional 2D-Stokes equation with nonlinear multiplicative noise is analyzed. The main tool to prove the existence and uniqueness of mild solutions is based on fixed point arguments. The results are proved when the time fractional order $\alpha \in (1/2, 1)$, and the global existence in time has to be shown only when the noise is additive. The analysis is carried out separately in two cases, namely, bounded or unbounded delay. In addition, this model can be considered as a first approximation to the challenging model of stochastic time fractional Navier-Stokes (with or without delay) which so far remains as an open problem.

keywords: Stochastic time fractional 2D-Stokes equations; Mild solutions; Bounded and unbounded delay.

MSC2020: 35R11; 35Q30; 65F08; 60H15; 65F10.

1 Introduction

The well-posedness of the following stochastic delay time fractional 2D-Stokes equations of order $\alpha \in (0, 1)$ with nonlinear multiplicative noise will be investigated:

$$\begin{cases} \partial_t^\alpha u - \kappa\Delta u + \nabla p = f(t, u_t) + g(t, u_t)\frac{dW(t)}{dt} & \text{in } \mathbb{R}^2,\ t \geq 0, \\ \nabla \cdot u = 0 & \text{in } \mathbb{R}^2,\ t \geq 0, \\ u(t, x) = \varphi(t, x) & \text{in } \mathbb{R}^2,\ t \in (-h, 0], \end{cases} \tag{1}$$

where f and g are external forcing terms containing some hereditary or delay characteristics, φ is the initial data in the interval of time $t \in (-h, 0]$, h is a fixed positive number (in the case of bounded delay) or $h = \infty$ (for unbounded delay), and $W(t)$ is a standard scalar Brownian motion/Wiener process on an underlying complete filtered probability space $\{\Omega, \mathcal{F}, \{\mathcal{F}_t\}_{t\geq 0}, \mathbb{P}\}$.

Actually, this is a first linear approximation of the following challenging problem: stochastic time fractional 2D-Navier-Stokes equations with delay,

$$\begin{cases} \partial_t^\alpha u - \kappa\Delta u + u \cdot \nabla u + \nabla p = f(t, u_t) + g(t, u_t)\frac{dW(t)}{dt} & \text{in } \mathbb{R}^2,\ t \geq 0, \\ \nabla \cdot u = 0 & \text{in } \mathbb{R}^2,\ t \geq 0, \\ u(t, x) = \varphi(t, x) & \text{in } \mathbb{R}^2,\ t \in (-h, 0], \end{cases} \tag{2}$$

which, so far, it is not known how to handle satisfactorily. The deterministic model (i.e. $f = g = 0$) has been analyzed by Carvalho-Neto and Planas in [1] and they proved the existence and uniqueness (and eventual uniqueness) of mild solutions to (2) . However, mainly due to the difficulties generated by the nonlinear term $u \cdot \nabla u$, new techniques, how to handle the stochastic problem (2) in an appropriate way, are needed to propose.

The main result proved in this work ensures the global existence and uniqueness of mild solutions to problem (1).

2 Results and discussion

We can rewrite the time fractional stochastic 2D-Stokes delay differential equations (1) in the following abstract form:

$$\begin{cases} D_t^\alpha u = -Au + F(t, u_t) + G(t, u_t)\frac{dW(t)}{dt}, & t > 0, \\ u(t) = \varphi(t), & t \in (-h, 0], \end{cases} \tag{3}$$

where $A = -P\Delta = -\Delta P$, $F(t, u_t) = Pf(t, u_t)$ and $G(t, u_t) = Pg(t, u_t)$. Here, $P : L^2 \to L^2_\sigma$ is the Helmholtz-Leray projector and $A : D(A) \subset L^2_\sigma \to L^2_\sigma$ is the Stokes operator.

Recall now the definition of mild solutions to problem (3).

Definition 1 (**Mild solution**). *Let $\mathcal{S} = (\Omega, \mathcal{F}, \mathbb{P}, \{\mathcal{F}\}_{t\geq 0})$ be a fixed stochastic basis generated by a standard Brownian motion W and $T > 0$. Consider $\alpha \in (1/2, 1)$, let φ be an initial function which is an appropriate $\mathcal{F}_0$-measurable random variable (relative to $\mathcal{S}$). A mild solution to problem (3) on $(-h, T]$ is a stochastic process u such that $u(t) = \varphi(t)$ for $t \in (-h, 0]$, and fulfills*

$$\begin{aligned} u(t) = \mathbf{E}_\alpha(-t^\alpha A)\varphi(0) + \int_0^t (t-s)^{\alpha-1}\mathbf{E}_{\alpha,\alpha}(-(t-s)^\alpha A)F(s, u_s)ds \\ + \int_0^t (t-s)^{\alpha-1}\mathbf{E}_{\alpha,\alpha}(-(t-s)^\alpha A)G(s, u_s)dW(s), \ \mathbb{P}\text{-}a.s., \quad \text{for every } t \in [0, T]. \end{aligned} \tag{4}$$

Here, $\mathbf{E}_\alpha(-t^\alpha A)$ and $\mathbf{E}_{\alpha,\alpha}(-t^\alpha A)$ are the Mittag-Leffler families (see [2] for more details).

First we need to introduce suitable Banach spaces, which aim to capture the essence of problem (3). For any $\alpha \in (1/2, 1)$ and fixed $T > 0$, consider the Banach space $\mathcal{X}_2^T$ which is the set of continuous functions $u : [-h, T] \to L^2(\Omega; L^2_\sigma)$ equipped with its natural norm

$$\|u\|_{\mathcal{X}_2^T} = \left(\sup_{t\in[-h,T]} \mathbb{E}\|u(t)\|^2 \right)^{\frac{1}{2}}.$$

Next, we state the hypotheses imposed on external forcing terms in our problem. Suppose, for F, $G : [0, +\infty) \times C([-h, 0]; L^2(\Omega; L^2_\sigma)) \to L^2(\Omega; L^2_\sigma)$,

- (A_1) For each $\xi \in C([-h, 0]; L^2(\Omega; L^2_\sigma))$, the mappings $t \in [0, +\infty) \to F(t, \xi)$ and $t \in [0, +\infty) \to G(t, \xi)$ are measurable.
- (A_2) $F(t, 0) = G(t, 0) = 0$ (for simplicity).
- (A_3) There exist positive constants L_F and L_G, such that for all $t \in [0, \infty)$, and for all $\xi, \eta \in C([-h, 0]; L^2(\Omega; L^2_\sigma))$,

$$\|F(t, \xi) - F(t, \eta)\|^2_{L^2(\Omega;L^2_\sigma)} \leq L_F\|\xi - \eta\|^2_{C([-h,0];L^2(\Omega;L^2_\sigma))}.$$

$$\|G(t, \xi) - G(t, \eta)\|^2_{L^2(\Omega;L^2_\sigma)} \leq L_G\|\xi - \eta\|^2_{C([-h,0];L^2(\Omega;L^2_\sigma))}.$$

We can now establish a first result on local existence and uniqueness of mild solutions to problem (3) by a fixed point argument.

Theorem 1 *Let $\alpha \in (1/2, 1)$. Assume that (A_1)-(A_3) hold and $\varphi \in C([-h, 0]; L^2(\Omega; L^2_\sigma))$ is an $\mathcal{F}_0$-measurable random variable. Then there exists $T > 0$ (small enough) such that problem (3) admits a unique mild solution u in the sense of Definition 1 on $[-h, T]$.*

Additional results can be found in [3].

Acknowledgments

This research has been partially supported by the Spanish Ministerio de Ciencia, Innovación y Universidades, Agencia Estatal de Investigación (AEI), Fondo Europeo de Desarrollo Regional (FEDER) under the project PGC2018-096540-B-I00 and the Junta de Andalucía and FEDER under the project P18-FR-4509.

References

[1] P.M. Carvalho-Neto, G. Planas, Mild solutions to the time fractional Navier-Stokes equations in $\mathbb{R}^N$, J. Differential Equations **259** (2015), 2948–2980.

[2] J.H. Xu, Z. Zhang, T. Caraballo, Mild solutions to time fractional stochastic 2D-Stokes equations with bounded and unbounded delay, J. Dynamics Diff. Equ. **34** (2022), 583–603.

[3] J.H. Xu, T. Caraballo, Well-posedness of stochastic time fractional 2D-Stokes models with finite and infinite delay, preprint (submitted).

International Conference on Mathematical Analysis and Applications in Science and Engineering
ICMA^{2}SC'22
ISEP Porto-Portugal, June 27 - 29, 2022

Averaging principle for Caputo fractional stochastic differential equations with fractional Brownian motion

Ruifang Wang[1] **Yong Xu**[12⋆] **Bin Pei**[1]

[1] School of Mathematics and Statistics,
Northwestern Polytechnical University, Xi'an, 710072, China
[2] MIIT Key Laboratory of Dynamics and Control of Complex Systems,
Northwestern Polytechnical University, Xi'an, 710072, China

⋆hsux3@nwpu.edu.cn

Abstract: This paper investigates the averaging principle for a type of Caputo fractional stochastic differential equations driven by fractional Brownian motion with Hurst parameter $1/2 < H < 1$. Under suitable assumptions, the averaged fractional stochastic differential equations are defined and the averaging principle is shown to hold such that the solution of the original equation converges to the solution of the averaged equation in some Hölder continuous space.

keywords: Averaging principle; Caputo fractional derivative; fractional Brownian motion; generalised Riemann-Stieltjes integral.

MSC2020: 34A08; 60G22; 34C29.

1 Introduction

The averaging principle is a powerful tool for researching the asymptotic behavior of dynamical systems and the first related result about stochastic case is studied by Khasminskii [2]. Since then, many investigators have developed the theory of averaging principle for the stochastic system.

In this paper, consider that fractional Brownian motion (fBm) can describe the disturbance with long-range dependence, we focus on the averaging principle for the following fractional stochastic differential equations (SDEs):

$$D_t^\gamma X_t^\epsilon = f\big(\frac{t}{\epsilon}, X_t^\epsilon\big)dt + g\left(X_t^\epsilon\right) dB_t^H, \qquad X_0^\epsilon = X_0 \in \mathbb{R}^n, \tag{1}$$

where $0 < \epsilon \ll 1, 1/2 < H < 1, \max\{H, 2-2H\} < \gamma < 1$ and D_t^γ is the Caputo derivative. The processes $B^H = \left\{B_t^H, t \in [0,T]\right\}$ $(1/2 < H < 1)$ is d-dimensional fBm and the integral of fBm as a generalised Riemann-Stieltjes integral in the sense of Zähle [3] in this work. Moreover, initial variables X_0 are fixed and independent of B^H and the maps $f : [0,\infty)\times\mathbb{R}^n \to \mathbb{R}^n; g : \mathbb{R}^n \to \mathbb{R}^{n\times d}$ are continuous. Then, consider the following assumptions on the coefficients:

(A1) There exist constants $0 < \theta \leq 1$, such that for any $s, t \in [0, T]$ and $x, y \in \mathbb{R}^n$, have

$$\begin{aligned} |f(t,x) - f(t,y)| + |g(x) - g(y)| + |\nabla_x g(x) - \nabla_x g(y)| &\leq C|x-y|, \\ |f(t,x)| + |g(x)| &\leq C(1+|x|), \\ |f(t,x) - f(s,x)| &\leq C|t-s|^{\theta}, \end{aligned}$$

where ∇_x is the standard gradient with respect to the variable x.

Under the above assumption, by proceeding as the proof of Han and Yan [1], we can prove that for any $1/2 < H < 1$ and $\max\{H, 2-2H\} < \gamma < 1$, if $2 - H - \gamma < \alpha < H$, there exists a unique solution $X^{\epsilon} \in C^{1-\alpha}(0, T; \mathbb{R}^n)$ for equation (1):

$$X_t^{\epsilon} = X_0 + \frac{1}{\Gamma(\gamma)} \int_0^t (t-u)^{\gamma-1} f\big(\frac{u}{\epsilon}, X_u^{\epsilon}\big) du + \frac{1}{\Gamma(\gamma)} \int_0^t (t-u)^{\gamma-1} g(X_u^{\epsilon}) dB_u^H. \tag{2}$$

Moreover, for any $p \geq 1$, if in addition $\alpha + \gamma > 7/4$, there exist constant $C_{\alpha,\gamma,T,|X_0|}$ such that

$$\mathbb{E}\|X^{\epsilon}\|_{1-\alpha}^p \leq C_{\alpha,\gamma,p,T,|X_0|}, \tag{3}$$

where $C^{1-\alpha}(0, T; \mathbb{R}^n)$ is the space of $1-\alpha$-Hölder continuous functions $\sigma : [0, T] \to \mathbb{R}^m$ such that

$$\|\sigma\|_{1-\alpha} := \sup_{t \in [0,T]} |\sigma_t| + \sup_{0 \leq s < t \leq T} \frac{|\sigma_t - \sigma_s|}{(t-s)^{1-\alpha}} < \infty.$$

2 Averaging principle

To establish the averaging principle, we introduce the following assumption:

(A2) There exist a averaging function $\bar{f} : \mathbb{R}^n \to \mathbb{R}^n$ such that

$$\sup_{t \geq 0} \frac{1}{T} \int_t^{t+T} \big|f(u,x) - \bar{f}(x)\big|^2 du \leq \varphi(T)\big(1 + |x|^2\big), \quad x \in \mathbb{R}^n, \tag{4}$$

where $\varphi : \mathbb{R} \to \mathbb{R}$ is a convergence rate function and satisfies $\lim_{T \to \infty} \varphi(T) = 0$.

Remark 2.1 *For any $x, y \in \mathbb{R}^n$, thanks to assumptions (A1) and (A2), it is easy to get that*

$$\big|\bar{f}(x) - \bar{f}(y)\big| \leq C|x-y| \quad \textit{and} \quad \big|\bar{f}(x)\big| \leq C(1+|x|).$$

Further, we define the following averaged fractional SDEs:

$$D_t^{\gamma} \bar{X}_t = \bar{f}\big(\bar{X}_t\big) dt + g\big(\bar{X}_t\big) dB_t^H, \qquad \bar{X}_0 = X_0 \in \mathbb{R}^n. \tag{5}$$

Smilarly, thanks to the assumption (A1) and remark 2.1, we also can prove that for any $1/2 < H < 1$ and $\max\{H, \ 2-2H\} < \gamma < 1$, if $2 - H - \gamma < \alpha < H$, there exists a unique solution $\bar{X} \in C^{1-\alpha}(0, T; \mathbb{R}^n)$ for equation (5) [1]:

$$\bar{X}_t = X_0 + \frac{1}{\Gamma(\gamma)} \int_0^t (t-u)^{\gamma-1} \bar{f}\big(\bar{X}_u\big) du + \frac{1}{\Gamma(\gamma)} \int_0^t (t-u)^{\gamma-1} g\big(\bar{X}_u\big) dB_u^H, \tag{6}$$

and for any $p \geq 1$, if in addition $\alpha + \gamma > 7/4$, there exist constant $C_{\alpha,\gamma,p,T,|X_0|}$ such that

$$\mathbb{E}\big\|\bar{X}\big\|_{1-\alpha}^p \leq C_{\alpha,\gamma,p,T,|X_0|}. \tag{7}$$

Finally, we prove that the solution of fractional SDEs (1) converges to the solution of averaged fractional SDEs (5) in the mean square sense as $\epsilon \to 0$:

Theorem 2.2 *Under the assumptions (A1)-(A2), for any* $3/4 < H < 1$ *and* $\max\{H, 7/4 - H\} < \gamma < 1$, *if* $7/4 - \gamma < \alpha < H$, *we have*

$$\lim_{\epsilon \to 0} \mathbb{E} \left\| X^{\epsilon} - \bar{X} \right\|_{1-\alpha}^{2} = 0. \tag{8}$$

3 Conclusions

We main investigates the averaging principle for a type of Caputo fractional SDEs with fBm in this work. Under suitable assumptions, we define the averaged fractional SDEs as equation (5). Further, we use a different estimation method to prove that the solution of the original fractional SDEs (1) converges to the solution of the proposed averaged fractional SDEs (5) in the mean square sense.

Acknowledgments

This work was partly supported by the Key International (Regional) Joint Research Program of the NSF of China (12120101002), the National Natural Science Foundation of China (12072264) and the Shaanxi Provincial Key R&D Program (2019TD-010).

References

[1] Jingqi Han and Litan Yan. A time fractional functional differential equation driven by the fractional Brownian motion. *J. Appl. Anal. Comput.*, 9:547–567, 2019.

[2] R. Khasminskii. On the averaging principle for stochastic differential Itô equations. *Kybernetika.*, 4:260–279, 1968.

[3] M Zähle. Integration with respect to fractal functions and stochastic calculus. *Prob. Theory Relat. Fields*, 111(3):333–374, 1998.

International Conference on Mathematical Analysis and Applications in Science and Engineering
ICMA^{2}SC'22
ISEP Porto-Portugal, June 27 - 29, 2022

Fuzzy transform for fractional fuzzy problem

Irina Pefilieva[1⋆] **Thi Minh Tam Pham**[2]

[1] Institute for Research and Applications of Fuzzy Modeling, University of Ostrava, Czech Republic,
[2] Department of Mathematics, Faculty of Science, University of Ostrava, Czech Republic

[1⋆]Irina.Perfilieva@osu.cz

Abstract: In this research, we are focused on linear fractional fuzzy differential equation. Fractionality and fuzziness are both complex formalisms. We reduce the problem to the case that involves ordinary functions. The operational method named F-transform is applied to obtain an approximate solution in the numerical form.

keywords: Fuzzy; Fractional; Differential equations.

MSC2020: 34A08; 34A07; 34A25.

1 Introduction

Integral equations with fuzzy-valued parameters attract researchers from AI community due to the increasing role of high-dimensional systems in data analysis, see [4, 5, 6, 7, 8]. By this we mean deep learning neural networks with regularization as a preprocessing and convolution as a main transformation step which require thousands of initial parameters and operate in high-dimensional spaces. A suitable model of their inputs corresponding to their intermediate images is a fuzzy-valued function. We remind that fuzzy numbers and arithmetic operations over them was introduced in [9], and further elaborated in [10].
Recently, both of the aforementioned tools have appeared together in modeling with fuzzy fractional differential equations (FFDE) and their systems have gained attention.
We consider a system of linear fractional fuzzy fractional differential equations (linear FFDE) of the form

$$^{C}D^{\beta}y(t) = Ay(t) + u(t), \quad t \in [0,T], y(0) = y_0, \tag{1}$$

where $^{C}D^{\beta}$ is a Caputo-type fuzzy fractional derivative of order $0 < \beta \leq 1$, A is a $\nu \times \nu$ matrix of real numbers, $u = [u_1, ..., u_\nu]^T$ is a vector of fuzzy (source) functions, and $y = [y_1, ..., y_\nu]^T$ is an unknown vector of fuzzy functions. Finally, $y_0 = [y_{01}, ..., y_{0\nu}]^T$ is a given vector of fuzzy numbers with ν as a dimension.
To solve FFDE, in [2], they use Operational Chebyshev method. This is a very effective method. In this method, Chebyshev polynomials are used to estimate the function, in which the estimate becomes more accurate when the number of zeros of Chebyshev polynomial $T_{N+1}(x)$ increases. This requires the degree of the polynomial to be high for the estimate to be accurate. Hence, the cost will be high.
To overcome the above disadvantage, in this research, we use F^1-transform to solve FFDE. The nodes in partition of F^1-transform are arbitrary, therefore, it does not require large degree polynomials and the degree of approximated function is 1.

2 Results and discussion

2.1 Reduction of the original problem to the ordinary case

Base on [1], the original problem (1) can be rewrite as follow

Theorem 1 *1. Assume that system* (1) *is solvable and its solution y is an fn-valued ν-dimensional vector-function on $t \in [0,T]$, such that for each $r \in [0,1]$, the corresponding interval-valued vector-functions $y(.,r)$ are l-increasing and continuously* 1*-differentiable. Then, system* (1) *is equivalent with the following system of ordinary fractional differential equations over real valued functions.*

$$\begin{aligned} {}^{C}D^{\beta}\underline{y}(t) &= \underline{Ay(t)+u(t)}, \\ {}^{C}D^{\beta}\overline{y}(t) &= \overline{Ay(t)+u(t)}, \quad t \in [0,T], \\ \underline{y(0)} &= \underline{y}_0, \\ \overline{y(0)} &= \overline{y}_0. \end{aligned} \tag{2}$$

2. Assume that system (1) *is solvable and its solution y is an fn-valued ν-dimensional vector-function on $t \in [0,T]$, such that for each $r \in [0,1]$, the corresponding interval-valued vector-functions $y(.,r)$ are l-decreasing and continuously* 1*-differentiable. Then, system* (1) *is equivalent with the following system of ordinary fractional differential equations over real valued functions.*

$$\begin{aligned} {}^{C}D^{\beta}\overline{y}(t) &= \underline{Ay(t)+u(t)}, \\ {}^{C}D^{\beta}\underline{y}(t) &= \overline{Ay(t)+u(t)}, \quad t \in [0,T], \\ \overline{y(0)} &= \underline{y}_0, \\ \underline{y(0)} &= \overline{y}_0. \end{aligned} \tag{3}$$

As an important corollary of Theorem 1, we note that the original system (1), depending on the assumptions about solutions, reduces to two systems of ordinary fractional differential equations (2) and (3), which are equal up to the flipping. Below, we formulate this assertion explicitly.

Corollary 2 *Let the system* (1) *be solvable and its solution y fulfill assumptions given in Theorem 1. Then, the equivalent to* (1) *systems of ordinary fractional differential equations* (2) *and* (3) *have the following parametric forms:*

$$[\underline{y}_1, ..., \underline{y}_\nu, \overline{y}_1, ..., \overline{y}_\nu]^T = A^{\pm}\mathcal{J}^{\beta}y(t) + y(0) + \mathcal{J}^{\beta}u(t), \tag{4}$$

$$[\underline{y}_1, ..., \underline{y}_\nu, \overline{y}_1, ..., \overline{y}_\nu]^T = A^{\mp}\mathcal{J}^{\beta}y(t) + y(0) + \mathcal{J}^{\beta}u^f(t) \tag{5}$$

By an iteration method we obtain where all vectors in the right-hand sides are parametric forms of the corresponding fn-valued vector functions.

As an advantage of our approach, we emphasize that two systems of ordinary fractional differential equations (4) and (5) can be easily unified into the following general form:

$$y(t) = \mathcal{A}\mathcal{J}^{\beta}y(t) + y(0) + \mathcal{J}^{\beta}u(t), \quad t \in [0,T], \tag{6}$$

where $\mathcal{A}$ denotes a real matrix, and u is a vector of real functions.

2.2 Function approximation

In this section, we focus on finding approximate solutions for (6), where this equation contains the Riemann-Liouville integral applied to real vector functions. Let $x_0, ..., x_N$ are $\frac{T}{N}$-equidistant such that $a = t_0, b = t_N$. Let $A_1(t), ..., A_N(t)$ be $\frac{T}{N}$-uniform partition of interval $[0, T]$ which is defined on [1]. For arbitrary function f, for all $k = 1, ..., N$, let $c_{k,0} = \frac{\int_{t_{k-1}}^{t_{k+1}} (x-t_k)^2 A_k(x)dx}{h}$, F-transform of f has the form

$$f(t) \approx \sum_{k=1}^{N} c_{k,0} A_k(t). \tag{7}$$

Apply equation (7) for $y(t)$, $u(t)$, for all integer $k \in \{1, 2, ..., N\}$, for $j = 1, ..., \nu$ we have

$$y^j(t_k) \approx Y_k^j, \qquad u^j(t_k) \approx U_k^j \tag{8}$$

where $(Y_k^j)_{k=1,...,N}$, $(U_k^j)_{k=1,...,N}$ are components of F-transform of y^j and u^j.

Lemma 3 *For arbitrary function $y : [0, T] \to \mathbb{R}$, fraction $0 < \beta < 1$, and $[0, T]$ has its partition $A_1, ..., A_N$ with the nodes $t_0, t_1, ..., t_N, t_{N+1}$, we have*

$$\mathcal{J}^\beta y(t_k) \approx \frac{1}{\Gamma(\beta+1)} \sum_{i=1}^{k} c_{i,0}\big((k-i+1)^\beta - (k-i)^\beta\big)h^\beta, \tag{9}$$

where $(c_{i,0})_{i=1,...,N}$ is components of F-transform of f and $k = 1, ..., N$.

2.3 Main result

Theorem 4 *Let interval $[0, T]$ has its $\frac{T}{N}$-uniform partition $A_1, ..., A_N$ with the nodes $t_0, ..., t_{N+1}$. Let us denote*

$$Y = \begin{pmatrix} Y_1^1 & Y_2^1 & .... & Y_N^1 \\ ... & & & \\ Y_1^\nu & Y_2^\nu & ... & Y_n^\nu \end{pmatrix}^T, \qquad U = \begin{pmatrix} U_1^1 & U_2^1 & .... & U_N^1 \\ ... & & & \\ U_1^\nu & U_2^\nu & ... & U_n^\nu \end{pmatrix}^T, \qquad Y_0 = \begin{pmatrix} y_{01} & y_{01} & .... & y_{01} \\ ... & & & \\ y_{0\nu} & y_{0\nu} & ... & y_{0\nu} \end{pmatrix}^T,$$

$$L = \begin{pmatrix} a_{11} & a_{12} & .... & a_{1n} \\ 0 & a_{22} & ... & a_{2n} \\ .... & & & \\ 0 & 0 & ... & a_{nn} \end{pmatrix}$$

where Y_k^j and U_k^j are defined as equation (8) and

$$a_{i,k} = \frac{1}{\Gamma(\beta+1)}\big((k-i+1)^\beta - (k-i)^\beta\big)h^\beta.$$

Let us denote $H := Y_0 + U^T L$, the problem (6) can be rewritten as follows:

$$(Y^T - \mathcal{A}Y^T L) = H. \tag{10}$$

To solve (10), use the vectorization operator *vec* to obtain a system of linear algebraic equations in the standard form of a matrix equation. Thus, the system (10) can be converted to the standard form

$$(I_n \otimes I_\nu - L^T \otimes \mathcal{A})vec(Y^T) = vec(H), \tag{11}$$

where $\otimes$ is the Kronecker product and I_n is identity matrix with n rows and columns, and $vec(Y^T)$ is the unknown vector.
To solve (11), we apply LU (Lower-Upper) decomposition to the matrix of coefficients and obtain the (exact) solution $vec(Y_k)$ directly by forward and backward substitution.

3 Conclusions and Future work

In this result, we approximate successfully the Fractional integral of arbitrary function f by using F-transform. From there, the complex problem is simply approximated to the matrix equation. From here, we can develop by applying the F^1-transform to get more accurate results.

Acknowledgments

This work was supported by the ERDF/ESF project âCentre for the development of Artificial Intelligence Methods for the Automotive Industry of the regionâ No.CZ.02.1.01/0.0/0.0/17 â 049/0008414 and by SGS20/PrF-MF/2022 of the University of Ostrava.

References

[1] I. Perfilieva, M. Dankova, B. Bede, Towards a higher degree F-transform, Fuzzy Sets and Systems, **180** (2011), 3–19.

[2] I. Perfilieva, B. Shiri, Z. Alijani, D. Baleanu, Combination of fractionality and fuzziness in one model of a real problem: analysis of the stability of solutions, Knowledge-Based Systems, (2021).

[3] I. Perfilieva, T. Pham, Fuzzy Transform for Fuzzy Fredholm Integral Equation, Soft Computing: Biomedical and Related Applications (2021), 233–249.

[4] R. P. Agarwal, D. Baleanu, J.J. Nieto, D. F. Torres and Y. Zhou, A survey on fuzzy fractional differential and optimal control nonlocal evolution equations, Journal of Computational and Applied Mathematics, **339** (2018), 3–29.

[5] Z. Alijani and U. Kangro, Collocation Method for Fuzzy Volterra Integral Equations of the Second Kind, Mathematical Modelling and Analysis, **25** (2020), 1097–1108.

[6] A. Khastan, Z. Alijani and I. Perfilieva,k Fuzzy transform to approximate sulution of two-point boundary value problems, Mathematical Methods in the Applied Sciences, **40** (2017), 6147–6154.

[7] B. Shiri, I. Perfilieva, Z. Alijani: Classical approximation for fuzzy Fredholm integral equation, Fuzzy Sets and Systems, **404** (2020), 159–177.

[8] S.Tomasiello, J. E. Macias-Diaz, A. Khastan and Z. Alijani, New sinusoidal basis functions and a neural network approach to solve nonlinear Volterra-Fredholm integral equations, Neural Computing and Applications, **31** (2019), 4865–4878.

[9] L. A. Zadeh, The concept of a linguistic variable and its application to approximate reasoning, Information Science, **8** (1975), 199–249.

[10] D. Dubois and H. Prade, Operations on fuzzy numbers, International Joural of Systems Science, **9** (1978), 613–626.

International Conference on Mathematical Analysis and Applications in Science and Engineering
ICMA^{2}SC'22
ISEP Porto-Portugal, June 27 - July 1, 2022

Solution of fuzzy integral equations of the second kind

Zahra Alijani[1⋆] Urve Kangro [2]

[1] Institute for Research and Applications of Fuzzy Modeling, University of Ostrava
[2] Institute of Mathematics and Statistics, University of Tartu, Estonia

[1⋆]zahraalijani2@gmail.com

Abstract: We present the existence and uniqueness theorem for a fuzzy Volterra integral equations with a weakly singular kernel. A method of successive approximation and fuzziness of the approximate solution is the main tool in our analysis. For a numerical solution, we propose piecewise spline collocation methods with a graded mesh. By increasing the collocation points we show that the numerical solution exist and converges to the exact solution. Consequently, by the convergence property, we study the fuzziness of the approximate solution. The proposed method is illustrated by numerical examples, which confirm the theoretical convergence estimates.

keywords: weakly singular kernel; fuzzy integral equation.

MSC2010: 26A##; 34A##; 93B##.

1 Introduction

Integral equations arise in scientific and engineering problems. A large class of initial and boundary value problems can be transformed into Volterra or Fredholm integral equations. The theory of Volterra integral equations is thoroughly considered in the recent monograph by Brunner [1]. Most Volterra integral equations can not solve analytically. Hence there is a need to use a numerical solution to these equations. Integral equations with weak singular kernels have received considerable interest in the mathematical literature because of their applications in many fields of science, such as the theory of hydrodynamics, fractional differential equations, and the physical problems with memory properties [1, 2].

A linear fuzzy Volterra integral equation of the second kind is given by

$$g(t) = f(t) + \int_0^t K(t,s)g(s)ds, \quad t \in [0,T], \tag{1}$$

where $K\colon D_T \to \mathbb{R}$ is a given kernel with domain $D_T = \{(t,s)\colon 0 \le s < t \le T\}$, $T \in \mathbb{R}$, f is a given fuzzy function, and g is an unknown fuzzy function. The main achievement of this work is to study the fuzzy Volterra integral equation (1) with a weakly singular kernel. First, we transform the fuzzy Volterra integral equation (1) with a weakly singular kernel to a system of Volterra integral equations with weakly singular kernels. We obtain the existence and uniqueness of solutions based on this transformation, and then we show that the corresponding solution is

a fuzzy function that satisfies the equation (1). When analyzing the convergence of a numerical method for a given integral equation, one needs information about the smoothness of the exact solution. Then we introduce collocation methods on piecewise polynomial spaces for solving the corresponding system of Volterra integral equations. We provide the conditions for the fuzziness of the numerical solutions, and we obtain the convergence analysis.

2 Results and discussion

2.1 Class of kernels

In the literature, weak singularity of the kernel K may have different definitions. We follow here the definition of [3], where it was introduced for Fredholm integral equations. We are interested in kernels that are $\mathcal{C}^m$- smooth outside the diagonal which was introduced in [3], following smoothness-singularity class $S^{m,\alpha}$ of kernels. Let $T \in \mathbb{R}$. Denote $D_T = \{(t,s)\colon 0 \le s < t \le T\}$ and $\mathbb{N}_0 = \{0,1,2,...\}$.

Definition 1 *For given $m \in \mathbb{N}_0$, denote by $S^{m,\alpha} = S^{m,\alpha}(D_T)$ the set of m times continuously differentiable functions K on D_T, where $D_T = \{(t,s)\colon 0 \le s < t \le T\}$, $T \in \mathbb{R}$, that satisfy there for all $j,l \in \mathbb{N}_0$, $j+l \le m$, the inequality*

$$\left|\left(\frac{\partial}{\partial t}\right)^j \left(\frac{\partial}{\partial t}+\frac{\partial}{\partial s}\right)^l K(t,s)\right| \le C_{K,m} \begin{cases} 1 & \text{if } \ j+\alpha<0, \\ 1+|\log(t-s)| & \text{if } \ j+\alpha=0, \\ (t-s)^{-j-\alpha} & \text{if } \ j+\alpha>0. \end{cases} \tag{2}$$

A kernel $K \in S^{m,\alpha}$ is called weakly singular if $\alpha < 1$.

2.2 Parametric and operator form of the integral equation

Let $(\underline{f}(t,r), \overline{f}(t,r))$ and $(\underline{g}(t,r), \overline{g}(t,r))$, $(t,r) \in [0,T] \times [0,1]$ be parametric forms of $f(t)$ and $g(t)$. Then equation (1) can be rewritten as a system of Volterra integral equations:

$$\begin{cases} \underline{g}(t,r) = \underline{f}(t,r) + \displaystyle\int_0^t (K_+(t,s)\underline{g}(s,r) - K_-(t,s)\overline{g}(s,r)ds), \\ \\ \overline{g}(t,r) = \overline{f}(t,r) + \displaystyle\int_0^t (K_+(t,s)\overline{g}(s,r) - K_-(t,s)\underline{g}(s,r)ds), \end{cases} \tag{3}$$

where

$$K_+(t,s) = \begin{cases} K(t,s), & K(t,s) \ge 0, \\ 0, & \text{otherwise}, \end{cases}$$

and

$$K_-(t,s) = \begin{cases} -K(t,s), & K(t,s) \le 0, \\ 0, & \text{otherwise}. \end{cases}$$

We write this system as

$$G = F + \mathcal{K}G, \tag{4}$$

where $G = [g_1, g_2]^T$, $g_1 = \underline{g}$, $g_2 = \overline{g}$, $F = [f_1, f_2]^T$, $f_1 = \underline{f}$, $f_2 = \overline{f}$ and

$$\mathcal{K} = \begin{pmatrix} \mathcal{K}_+ & -\mathcal{K}_- \\ -\mathcal{K}_- & \mathcal{K}_+ \end{pmatrix}. \tag{5}$$

We also use the notation

$$\mathcal{K}G = \int_0^t \mathbf{K}(t,s)G(s,r)ds, \tag{6}$$

where

$$\mathbf{K}(t,s) = \begin{pmatrix} K_+(t,s) & -K_-(t,s) \\ -K_-(t,s) & K_+(t,s) \end{pmatrix}.$$

We call the vector G a fuzzy function if (g_1, g_2) is a fuzzy function.

Theorem 1 *Suppose that $K \in S^{m,\alpha}$, $m \geq 0$, $\alpha < 1$ and $F \in (\mathcal{C}[0,T])^2$. Then equation (4) has a unique solution G in $(\mathcal{L}^\infty(0,T))^2$ and $G \in (\mathcal{C}[0,T])^2$.*

Theorem 2 *Let $K \in S^{0,\alpha}$ with $\alpha < 1$. Let f be a fuzzy function such that $f \in C([0,T]; E)$. Then the solution $G = (\underline{g}, \overline{g})^T$ of (3) is a continuous fuzzy function.*

3 Conclusions and Future work

In this paper, we investigated a fuzzy Volterra integral equation with a weakly singular kernel. The existence, regularity and the fuzziness of the exact solution is studied. Collocation methods on discontinuous piecewise polynomial space are proposed. A convergence analysis obtained. The fuzziness of the approximate solution is investigated. Numerical method provided to support the theoretical. Some examples showed the sharpness of the result in the sense that we can not improve the convergent order in the discussed spaces.

Acknowledgments

The work is supported by the project "Centre for the development of Artificial Intelligence Methods for the Automotive Industry of the region" No. CZ.02.1.01/0.0/0.0/17-049/0008414

References

[1] H. Brunner, Volterra integral equations. An introduction to theory and applications. Cambridge Monographs on Applied and Computational Mathematics, 30. Cambridge University Press, 2017.

[2] G. Vainikko, Multidimensional weakly singular integral equations. Springer; 2006 Nov 15.

[3] G. Vainikko, Weakly singular integral equations, Lecture notes, HUT, UT, 2006-2007, http://kodu.ut.ee/ gen/WSIElecturesSIAM.pdf.

International Conference on Mathematical Analysis and Applications in Science and Engineering
ICMA²SC'22
ISEP Porto-Portugal, June 27 - 29, 2022

Collocation based approximations for fractional boundary value problems

Hanna Britt Soots[1⋆] **Kaido Lätt**[1] **Arvet Pedas**[1]

[1] University of Tartu, Estonia

[1⋆]hanna.britt.soots@ut.ee

Abstract: A boundary value problem for fractional integro-differential equations with weakly singular kernels is considered. The problem is reformulated as an integral equation of the second kind with respect to $z = D^{\alpha}_{\mathrm{Cap}}y$, the Caputo fractional derivative of y of order α, with $1 < \alpha < 2$, where y is the solution of the original problem. Using this reformulation, the regularity properties of both y and its Caputo derivative z are studied. Based on this information a piecewise polynomial collocation method is developed for finding an approximate solution z_N of the reformulated problem. Using z_N, an approximation y_N for y is constructed and a detailed convergence analysis of the proposed method is given. In particular, the attainable order of convergence of the proposed method for appropriate values of grid and collocation parameters is established. To illustrate the performance of our approach, results of some numerical experiments are presented.

keywords: Fractional weakly singular integro-differential equation; Caputo derivative; Boundary value problem; Collocation method; Graded grid.

MSC2020: 34A08; 65L10; 65R20

1 Introduction

Differential equations containing derivatives of fractional (i.e., of any real positive) order are useful in various fields of science and engineering, especially when modelling real-life processes with memory properties [1, 5]. We construct a high order method for the numerical solution of fractional weakly singular integro-differential equations in the form

$$(D^{\alpha}_{\mathrm{Cap}}y)(t) + h(t)y(t) + \int_0^t L_\kappa(t,s)y(s)ds = f(t),\ 0 \le t \le b,\ 0 < b < \infty, \tag{1}$$

subject to the conditions

$$a_{11}y(0) + a_{12}y(b_1) = \gamma_1; \quad a_{21}y'(0) + a_{22}y(b_1) = \gamma_2. \tag{2}$$

Here y is the unknown function, $D^{\alpha}_{\mathrm{Cap}}$ is the Caputo fractional differential operator of order α with $1 < \alpha < 2$, $b_1 \in (0, b]$ and $a_{11}, a_{12}, a_{21}, a_{22}, \gamma_1, \gamma_2 \in \mathbb{R} = (-\infty, \infty)$. For our approach below we assume that $b_1 a_{11} a_{22} + a_{11} a_{21} + a_{12} a_{21} \neq 0$. The functions h, f belong to $C[0, b]$ and the function L_κ is defined by the formula

$$L_\kappa(t,s) = \begin{cases} [1 + \log(t-s)]K(t,s) & \text{for } \kappa = 0, \\ (t-s)^{-\kappa}K(t,s) & \text{for } 0 < \kappa < 1, \end{cases} \tag{3}$$

where $0 \le s \le t \le b$ and $K \in C(\Delta)$, $\Delta = \{(t,s) : \ 0 \le s \le t \le b\}$.
By $C^m[0,b]$ and $C^m(\Delta)$, with $m \in \mathbb{N}_0 = \{0\} \cup \mathbb{N}$, $\mathbb{N} = \{1,2,\dots\}$, we denote the sets of m times continuously differentiable functions on $[0,b]$ and Δ, respectively; for $m = 0$ we set $C^0[0,b] = C[0,b]$ and $C^0(\Delta) = C(\Delta)$. In particular, $C[0,b]$ will denote the Banach space of continuous functions $u : [0,b] \to \mathbb{R}$ with the norm $\|u\|_\infty = \sup\{|u(t)| : 0 \le t \le b\}$.
For given $b \in \mathbb{R}$, $b > 0$, $q \in \mathbb{N}$ and $\nu \in \mathbb{R}$, $\nu < 1$, by $C^{q,\nu}(0,b]$ we denote the set of continuous functions $y : [0,b] \to \mathbb{R}$ which are q times continuously differentiable in $(0,b]$ such that for all $t \in (0,b]$ and $i = 1,\dots,q$, the following estimate holds:

$$|y^{(i)}(t)| \le c \begin{cases} 1 & \text{if } i < 1-\nu, \\ 1 + |\log t| & \text{if } i = 1-\nu, \\ t^{1-\nu-i} & \text{if } i > 1-\nu. \end{cases}$$

We have $C^n[0,b] \subset C^{n,\nu}(0,b] \subset C^{m,\mu}(0,b] \subset C[0,b]$ for $n \ge m \ge 1$, $\nu \le \mu < 1$. The Caputo fractional differential operator D^δ_{Cap} of order $\delta \in (1,2)$ can be defined by formula (see, e.g., [2, 4])

$$(D^\delta_{\mathrm{Cap}} y)(t) = (D^2 J^{2-\delta}(y - T_1 y))(t), \quad t \in [0,b], \quad y \in C^1[0,b],$$

where $T_1 y$ is the Taylor polynomial of degree 1 at the point 0 and J^δ is the Riemann-Liouville integral operator of order δ, defined by

$$(J^\delta y)(x) = \frac{1}{\Gamma(\delta)} \int_0^x (x-t)^{\delta-1} y(t) dt, \quad x \in [0,b], \ y \in L^\infty(0,b), \ \delta > 0; \ J^0 = I, \tag{4}$$

where I is the identity mapping and Γ the Euler gamma function.
We are interested in solutions $y \in C^1[0,b]$ of problem (1)–(2) such that $D^\alpha_{\mathrm{Cap}} y \in C[0,b]$, $\alpha \in (1,2)$. Due to [2] we cannot expect that a solution of a fractional differential equations with Caputo differential operator will be smooth on the closed interval of integration and this is a challenge for constructing high order methods for the numerical solution of such equations. Therefore, we reformulate the problem (1)–(2) as an integral equation: $z = Tz + g$, with $z = D^\alpha_{\mathrm{Cap}} y$. T is an integral operator and g is a function, both we'll detail in our presentation. By reformulating the problem as an integral equation of the second kind, the regularity properties of the solution of the original problem and its Caputo derivative are studied. Using the obtained knowledge about the behaviour of the solution an algorithm is constructed for finding approximate solutions of the original problem. Our approach is based on some ideas of [3].

2 Results and discussion

In this section we will give a brief overview of the proposed numerical method, formulate our main result and also present results of our numerical experiments. Let $N \in \mathbb{N}$, we introduce a partition (a graded grid) $\Pi_N = \{t_0, \dots, t_N\}$ of the interval $[0,b]$ with the grid points

$$t_j = b \left(\frac{j}{N} \right)^r, \quad j = 0, 1, \dots, N, \tag{5}$$

where the so-called grading exponent r belongs to $[1,\infty)$. For a given integer $k \in \mathbb{N}_0$, by $S_k^{(-1)}(\Pi_N)$ we denote the space of piecewise polynomial functions $S_k^{(-1)}(\Pi_N) = \{v : \quad v|_{[t_{j-1},t_j]} \in \pi_k, \ j = 1,\dots,N\}$. Here, $v|_{[t_{j-1},t_j]}$ is the restriction of function $v : [0,b] \to \mathbb{R}$ onto the subinterval $[t_{j-1},t_j] \subset [0,b]$ and π_k denotes the set of polynomials of degree not exceeding k. Observe that the elements of the space $S_k^{(-1)}(\Pi_N)$ may have jump discontinuities at the interior points $t_1,\dots,t_{N-1}$ of Π_N.

In every interval $[t_{j-1}, t_j]$, $j = 1, \ldots, N$, we define $m \in \mathbb{N}$ collocation points

$$t_{jk} = t_{j-1} + \eta_k(t_j - t_{j-1}), \quad k = 1, \ldots, m, \quad j = 1, \ldots, N, \tag{6}$$

with some fixed collocation parameters $0 \le \eta_1 < \eta_2 < \ldots < \eta_m \le 1$.
We find approximations $z_N \in S_{m-1}^{(-1)}(\Pi_N)$ $(m, N \in \mathbb{N})$ to the exact solution z of equation $z = Tz + g$ by collocation conditions

$$z_N(t_{jk}) = (Tz_N)(t_{jk}) + g(t_{jk}), \quad k = 1, \ldots, m, \quad j = 1, \ldots, N, \tag{7}$$

with $\{t_{jk}\}$ defined by (6). Having found z_N by the formula $y_N(\tau) = (J^\alpha z_N)(b_1)k_{00} + k_{01} + [(J^\alpha z_N)(b_1)k_{10} + k_{11}]\tau + (J^\alpha z_N)(\tau)$ (constants k_{00}, k_{01}, k_{10} and k_{11} will be detailed in our presentation) we determine the approximation y_N to y, the solution of problem (1)–(2).

Theorem 1 *Let $m, N \in \mathbb{N}$, $r \ge 1$ and assume that the problem (1)–(2) with $f = 0$ and $\gamma_1 = \gamma_2 = 0$ has in $C[0, b]$ only the trivial solution. Let $K \in C^{m+1}(\Delta)$, $h, f \in C^{m+1,\mu}(0, b]$, $\mu \in (-\infty, 1)$. Assume that $\eta_1, \ldots, \eta_m$ used are such that a quadrature approximation $\int_0^1 F(x)dx \approx \sum_{k=1}^m w_k F(\eta_k)$ with appropriate weights $\{w_k\}$ is exact for all polynomials of degree m.*
Then problem (1)–(2) has a unique solution $y \in C^1[0, b]$ such that y and $D^\alpha_{Cap} y$ belong to $C^{m+1,\nu}(0, b]$. There exists an integer $N_0 > 0$ such that, for $N \ge N_0$ the following error estimate holds:

$$\|y - y_N\|_\infty \le c \begin{cases} N^{-m-1} & \text{for} \quad m < 2 - \nu, \quad r \ge 1, \\ N^{-m-1}(1 + \log N)^2 & \text{for} \quad m = 2 - \nu, \quad r = 1, \\ N^{-m-1}(1 + \log N) & \text{for} \quad m = 2 - \nu, \quad r > 1, \\ N^{-r(2-\nu)} & \text{for} \quad m > 2 - \nu, \quad 1 \le r < \dfrac{m+1}{2-\nu}, \\ N^{-m-1} & \text{for} \quad m > 2 - \nu, \quad r \ge \dfrac{m+1}{2-\nu}. \end{cases} \tag{8}$$

Here $\nu = \max\{\kappa, \mu\}$ if $K \ne 0$ and $\nu = \max\{1 - \alpha, \mu\}$ otherwise; r is the grading exponent used in (5) and c is a positive constant not depending on N.

We present in the tables below some results of numerical experiments for different values of parameters m, N and r. The errors ε_N are calculated as follows:

$$\varepsilon_N = \max_{j=1,\ldots,N} \max_{k=0,\ldots,10} |y(\tau_{jk}) - y_N(\tau_{jk})|, \tag{9}$$

where $\tau_{jk} = t_{j-1} + k(t_j - t_{j-1})/10$, $k = 0, \ldots, 10$, $j = 1, \ldots, N$, with the gridpoints t_j defined by (5). The ratios $\Theta_N = \frac{\varepsilon_{\frac{N}{2}}}{\varepsilon_N}$, characterising the observed convergence rate, are also presented. The values given in the last row of the Table 1 are the theoretical estimates of the ratios Θ_N according to Theorem 1.
Example 1. Consider the following problem:

$$(D^{\frac{21}{20}}_{\mathrm{Cap}} y)(t) + h(t)y(t) + \int_0^t (t - s)^{-\frac{3}{4}} K(t, s)y(s)ds = f(t), \quad t \in [0, 1], \tag{10}$$

$$y(0) + y\left(\frac{1}{10}\right) = \left(\frac{1}{10}\right)^{\frac{11}{10}}; \quad y'(0) + y\left(\frac{1}{10}\right) = \left(\frac{1}{10}\right)^{\frac{11}{10}}, \tag{11}$$

with

$$h(t) = t, \quad K(t, s) = ts, \quad f(t) = \frac{\Gamma\left(\frac{21}{10}\right)}{\Gamma\left(\frac{21}{20}\right)} t^{\frac{1}{20}} + t^{\frac{21}{10}} + \frac{\Gamma\left(\frac{1}{4}\right)\Gamma\left(\frac{31}{10}\right)}{\Gamma\left(\frac{67}{20}\right)} t^{\frac{67}{20}}, \quad t \in [0, 1], \quad s \in [0, t].$$

The exact solution of (10)–(11) is $y(t) = t^{\frac{11}{10}}$. Clearly, $f, h \in C^{q,\mu}(0, 1]$ with $\mu = \frac{19}{20}$ and arbitrary $q \in \mathbb{N}$. Therefore $\nu = \max\{\kappa, \mu\} = \frac{19}{20}$.

	$r=1$		$r=2$		$r=3$		$r=4$	
N	ε_N	Θ_N	ε_N	Θ_N	ε_N	Θ_N	ε_N	Θ_N
4	4.85E-04		8.77E-05		4.30E-05		4.73E-05	
8	2.01E-04	2.42	2.03E-05	4.31	4.61E-06	9.34	4.18E-06	11.33
16	9.55E-05	2.10	4.07E-06	5.00	4.33E-07	10.64	1.77E-07	23.65
32	4.37E-05	2.19	8.42E-07	4.83	3.66E-08	11.83	1.07E-08	16.49
64	2.00E-05	2.19	1.73E-07	4.87	3.64E-09	10.05	6.64E-10	16.12
128	9.11E-06	2.19	3.77E-08	4.58	3.58E-10	10.17	4.13E-11	16.10
256	4.15E-06	2.19	8.80E-09	4.29	3.81E-11	9.39	2.61E-12	15.84
		2.07		4.29		8.88		16.00

Table 1: Numerical results for problem (10)-(11) with $m = 3$.

3 Conclusions

We have introduced and analysed a high order numerical method for solving boundary value problems for linear fractional weakly singular integro-differential equations with a Caputo fractional derivative. The performed numerical experiments were in accordance with theoretical results.

Acknowledgements

This work was supported by the Estonian Research Council grant (PRG864).

References

[1] D. Baleanu, K. Diethelm, E. Scalas, and J. J. Trujillo. *Fractional Calculus: Models and Numerical Methods.* World Scientific, Boston, 2016.

[2] K. Diethelm. *The Analysis of Fractional Differential Equations: An Application-Oriented Exposition Using Differential Operators of Caputo Type.* Springer-Verlag, Berlin, Heidelberg, 2010.

[3] A. Pedas, E. Tamme, and M. Vikerpuur. Spline collocation for fractional weakly singular integro-differential equations. *Applied Numerical Mathematics*, 110:204–214, 2016.

[4] G. Vainikko. Which functions are fractionally differentiable? *Zeitschrift für Analysis und ihre Anwendungen*, 35(4):465–487, 2016.

[5] M. P. Velasco, D. Usero, S. Jiménez, L. Vázquez, J. L. Vázquez-Poletti, and M. Mortazavi. About some possible implementations of the fractional calculus. *Mathematics*, 8(6):893, 2020.

International Conference on Mathematical Analysis and Applications in Science and Engineering
ICMA^{2}SC'22
ISEP Porto-Portugal, June 27 - 29, 2022

A Collocation Method Based on Central Part Interpolation for Fractional Integro-Differential Equations

Margus Lillemäe[1,a)] **Arvet Pedas**[1] **Mikk Vikerpuur**[1]

[1] Institute of Mathematics and Statistics, University of Tartu, Estonia

[a)] margus.lillemae@ut.ee

Abstract: A collocation method based on the central part interpolation by continuous piecewise polynomials on the uniform grid for the numerical solution of a class of linear fractional integro-differential equations with weakly singular kernels is constructed. Optimal convergence order of the proposed method is established and confirmed by numerical experiments.

keywords: Fractional integro-differential-equation; Caputo fractional derivative; weakly singular integral equation; central part interpolation; collocation method.

MSC2020: 34A08, 65L05.

1 Introduction

We consider a fractional initial value problem

$$(\mathrm{D}^{\alpha}_{Cap}u)(t) + r(t)u(t) + \int_0^t (t-s)^{-\kappa}K(t,s)u(s)\,\mathrm{d}s = f(t), \quad 0 \le t \le 1; \quad u(0) = u_0, \qquad (1)$$

where $0 < \alpha < 1$, $0 \le \kappa < 1$, $u_0 \in \mathbb{R} := (-\infty, \infty)$ and $\mathrm{D}^{\alpha}_{Cap}u$ is the α order Caputo fractional derivative of the unknown function u (see [1]):

$$(\mathrm{D}^{\alpha}_{Cap}u)(t) = \frac{1}{\Gamma(1-\alpha)}\frac{\mathrm{d}}{\mathrm{d}t}\int_0^t (t-s)^{-\alpha}[u(s)-u(0)]\,\mathrm{d}s, \quad 0 \le t \le 1,$$

with $\Gamma(x) := \int_0^{\infty} e^{-s}s^{x-1}\,\mathrm{d}s$, $x > 0$. We assume that the functions r, f and K are continuous: $r, f \in C[0,1]$, $K \in C(\Delta)$, $\Delta := \{(x,y) : 0 \le s \le t \le 1\}$. Then problem (1) possesses a unique solution $u \in C[0,1]$ such that $\mathrm{D}^{\alpha}_{Cap}u \in C[0,1]$ [2]. However, we cannot expect that the solution u belongs to $C^q[0,1]$ ($q \in \mathbb{N} := \{1,2,\ldots\}$) for $r, f \in C^q[0,1]$ and $K \in C^q(\Delta)$. More precisely, if $K \in C^q(\Delta)$, $r, f \in C^{q,\mu}(0,1]$, $q \in \mathbb{N}$, $\mu \in \mathbb{R}$, $\mu < 1$, then u and its derivative $\mathrm{D}^{\alpha}_{Cap}u$ belong to $C^{q,\nu}(0,1]$, where $\nu = \max\{1-\alpha, \mu, \kappa\}$ [2, 3]. Here, by $C^{q,\mu}(0,1]$ ($q \in \mathbb{N}$, $\mu \in \mathbb{R}$, $\mu < 1$) we denote the set of functions $u \in C[0,1] \cap C^q(0,1]$ such that

$$|u^{(i)}(t)| \le c \left\{ \begin{array}{ll} 1 & \text{if } i < 1-\mu \\ 1 + |\log t| & \text{if } i = 1-\mu \\ t^{1-\mu-i} & \text{if } i > 1-\mu \end{array} \right\}, \quad 0 < t \le 1, \quad i = 1, \ldots, m,$$

where c is a positive constant.

Thus, we see that, in general, the usual derivatives of the exact solution u of problem (1) may be unbounded at the left endpoint 0 of the interval $[0,1]$. This complicates the construction of high order methods for the numerical solution of problem (1). Below we construct a high order method for solving (1) based on improving the boundary behavior of the exact solution with the help of a change of variables, and on central part interpolation by polynomial splines on the uniform grid.

2 Integral equation reformulation of the problem

We start by converting problem (1) to an equivalent integral equation with respect to u:

$$u = Tu + g, \tag{2}$$

where

$$(Tu)(t) = -\frac{1}{\Gamma(\alpha)}\int_0^t (t-s)^{\alpha-1}u(s)\,\mathrm{d}s - \frac{1}{\Gamma(\alpha)}\int_0^t (t-s)^{\alpha-\kappa}L(t,s)u(s)\,\mathrm{d}s, \quad 0 \le t \le 1,$$
$$g(t) = \frac{1}{\Gamma(\alpha)}\int_0^t (t-s)^{1-\alpha}f(s)\,\mathrm{d}s + u_0, \quad 0 \le t \le 1,$$

with $L(t,s) := \int_0^1 \sigma^{-\kappa}(1-\sigma)^{\alpha-1}K((t-s)\sigma+s,s)\,\mathrm{d}\sigma$ for $0 \le s \le t \le 1$. To improve the possible singular behavior of derivatives of the solution to problem (1) (equation (2)) we perform in equation (2) the change of variables $t = \varphi(\tau)$, $s = \varphi(\sigma)$, where $\varphi : [0,1] \to [0,1]$ is defined by

$$\varphi(\tau) = \frac{1}{c_p}\int_0^\tau \xi^{p-1}(1-\xi)^{p-1}\,\mathrm{d}\xi, \quad c_p = \int_0^1 \xi^{p-1}(1-\xi)^{p-1}\,\mathrm{d}\xi, \quad p \in \mathbb{N}. \tag{3}$$

Clearly, $\varphi(0) = 0$, $\varphi(1) = 1$ and $\varphi'(x) > 0$, $x \in (0,1)$, thus there exists a continuous inverse $\varphi^{-1} : [0,1] \to [0,1]$. After the change of variables, equation (2) takes the form

$$u_\varphi = T_\varphi u_\varphi + g_\varphi, \quad (T_\varphi u_\varphi)(\tau) = \int_0^\tau K_\varphi(\tau,\sigma)u_\varphi(\sigma)\,\mathrm{d}\sigma, \quad 0 \le \tau \le 1, \tag{4}$$

where $K_\varphi(\tau,\sigma) = K(\varphi(\tau),\varphi(\sigma))\varphi'(\sigma)$ and $g_\varphi(\tau) = g(\varphi(\tau))$. The solution u of (2) and the solution u_φ of (4) are related by the equalities $u_\varphi(\tau) = u(\varphi(\tau))$ and $u(t) = u_\varphi(\varphi^{-1}(t))$.

It turns out that if

$$p > m \quad \text{for} \quad \nu \le 0; \quad p > \frac{m}{1-\nu} \quad \text{for} \quad 0 < \nu < 1, \tag{5}$$

then for $u \in C^{m,\nu}(0,1]$ we have $u_\varphi \in C^m[0,1]$ and $u_\varphi^{(j)}(0) = u_\varphi^{(j)}(1) = 0$, $j = 1,\dots,m$. Extending $u_\varphi(\tau)$ for $\tau < 0$ by the constant value $u_\varphi(0)$ and for $\tau > 1$ by the constant value $u_\varphi(1)$, the extended function is m times continuously differentiable on $\mathbb{R}$. This is helpful for the "central part" interpolation by piecewise polynomials that is considered in the next section.

3 Collocation method based on central part interpolation

Following some ideas of [4, 5] we construct a high-order method for the numerical solution of (1). Let $N, m \in \mathbb{N}$, $m \ge 2$. Let $\mathcal{P}_{m-1}$ be the set of polynomials of degree less than or equal to $m-1$. We introduce in $\mathbb{R}$ the uniform grid $\{jh : j \in \mathbb{N}\}$, where $h = \frac{1}{N}$. Given a function $u \in C[-\delta, 1+\delta]$, $\delta > 0$, we define a piecewise polynomial interpolant $\Pi_{h,m}u \in C[0,1]$ for

$h = \frac{1}{N} < \frac{1}{2\delta}$ as follows. On every subinterval $[jh, (j+1)h]$, $0 \le j \le N-1$, the function $\Pi_{h,m}u$ is defined independently from other subintervals as a polynomial $\Pi_{h,m}^{[j]}u \in \mathcal{P}_{m-1}$ by the conditions

$$\Pi_{h,m}^{[j]}u(lh) = u(lh), \text{ for } l \in \mathbb{Z} \text{ such that } l - j \in \mathbb{Z}_m, \quad \mathbb{Z}_m = \{k \in \mathbb{Z} : -\frac{j}{2} < k \le \frac{j}{2}\}. \tag{6}$$

For an "interior" knot jh, $1 \le j \le N-1$, interpolation conditions (6) contain the condition $\Pi_{h,m}^{[j-1]}(jh) = u(jh)$ as well as the condition $\Pi_{h,m}^{[j]}(jh) = u(jh)$, thus $\Pi_{h,m}u$ is uniquely defined at the interior knots jh, $1 \le j \le N-1$, and $\Pi_{h,m}u$ is continuous on $[0,1]$. Introducing the Lagrange fundamental polynomials $L_{k,m}(t) = \prod_{l \in \mathbb{Z}_m \setminus \{k\}} \frac{t-l}{k-l}$, $t \in \mathbb{R}$, $k \in \mathbb{Z}_m$, we get $L_{k,m} \in \mathcal{P}_{m-1}$ and

$$\left(\Pi_{h,m}^{[j]}u\right)(t) = \sum_{k \in \mathbb{Z}_m} u((j+k)h)L_{k,m}(Nt - j), \quad t \in [jh, (j+1)h], \quad 0 \le j \le N-1.$$

On $[jh, (j+1)h]$ the interpolant $\Pi_{h,m}u = \Pi_{h,m}^{[j]}u$ for a function $u \in C[-\delta, 1+\delta]$ coincides with the Lagrange interpolation polynomial of degree $m-1$ that interpolates u at m grid points lh for integers l satisfying $l - j \in \mathbb{Z}_m$. The Lagrange polynomial is exploited only for one subinterval of length h in the center of the interpolation interval $[a_j, b_j]$, where $a_j = (j - (m-1)/2)h$, $b_j = (j + (m+1)/2)h$ in the case of even m, and $a_j = (j - m/2)h$, $b_j = (j + m/2)h$ in the case of odd m. Moreover, $[jh, (j+1)h]$ is contained in the central part of $[a_j, b_j]$ on which the interpolation error can be estimated more precicely than on the whole interval [4, 5].

For $m = 2$, the interpolant $\Pi_{h,2}u$ is the usual piecewise linear function joining for $0 \le j \le n-1$ the pair of points $(jh, u(jh)) \in \mathbb{R}^2$ and $((j+1)h, h) \in \mathbb{R}^2$ by a straight line. For $m \ge 3$, we consider the extension operator $E_\delta : C[0,1] \to C[-\delta, 1+\delta]$, $\delta \ge \frac{m}{2}h$, putting $(E_\delta u)(t) = u(0)$ for $-\delta \le t < 0$, $(E_\delta u)(t) = u(t)$ for $0 \le t \le 1$ and $(E_\delta u)(t) = u(1)$ for $1 < t \le 1+\delta$. Then E_δ maintains the smoothness of u and the operator $P_{h,m} := \Pi_{h,m}E_\delta : C[0,1] \to C[0,1]$ is well defined, $P_{h,m}^2 = P_{h,m}$, and for any $u \in C[0,1]$ we have $\max_{0 \le t \le 1} |u(t) - (P_{h,m}u)(t)| \to 0$ as $N \to \infty$ [4, 5].

Using $P_{h,m}$ we approximate equation $u_\varphi = T_\varphi u_\varphi + g_\varphi$ (see (4)) by equation

$$u_{\varphi,h} = P_{h,m}T_\varphi u_{\varphi,h} + P_{h,m}g_\varphi. \tag{7}$$

Equation (7) is equivalent to a system of linear algebraic equations with respect to $u_{\varphi,h}(ih)$, $i = 0, \dots, N$. Having obtained the solution $u_{\varphi,h}$ of equation (7), we find an approximation u_h of u, the solution of problem (1), as follows:

$$u_h(t) = u_{\varphi,h}(\varphi^{-1}(t)), \quad 0 \le t \le 1. \tag{8}$$

For the proposed method we can prove the following result.

Theorem 1 (i) *Assume that* $0 < \alpha < 1$, $0 \le \kappa < 1$, $K \in C(\Delta)$, $r, f \in C[0,1]$. *Let the smoothing transformation* $\varphi : [0,1] \to [0,1]$ *be defined by* (3) *and let* $m \in \mathbb{N}$, $m \ge 2$. *Then there exists an* $N_0 \in \mathbb{N}$ *such that for* $N \ge N_0$ *the collocation equation* (7) *has a unique solution* $u_{\varphi,h} \in C[0,1]$ *such that*

$$\max_{t \in [0,1]} |u(t) - u_h(t)| = \max_{t \in [0,1]} |u_\varphi(t) - u_{\varphi,h}(t)| \to 0 \quad \textit{for} \quad N \to \infty,$$

where $u \in C[0,1]$ *is the solution of* (2) *(of problem* (1)*),* $u_\varphi(t) = u(\varphi(t))$ *(*$0 \le t \le 1$*) is the solution of* (4) *and* $u_h \in C[0,1]$ *is defined by the formula* (8).

(ii) *In addition to* (i), *let* $K \in C^m(\Delta)$, $r, f \in C^{m,\nu}(0,1]$, $m \ge 2$, $\nu \in \mathbb{R}$, $\nu < 1$ *and let the parameter* $p \in \mathbb{N}$ *of the smoothing transformation* $\varphi : [0,1] \to [0,1]$ *defined by* (3) *satisfy* (5) *where* $\nu = \max\{1 - \alpha, \mu, \kappa\}$. *Then the following error estimate holds:*

$$\max_{t \in [0,1]} |u(t) - u_h(t)| \le ch^m, \quad h = \frac{1}{N}, \quad N \ge N_0.$$

Here c *is a constant which is independent of* h *(of* N*).*

4 Numerical example

Consider the following initial value problem:

$$(\mathrm{D}^{0.5}_{Cap}u)(t) - tu(t) + \int_0^t (t-s)^{-0.3}u(s)\,\mathrm{d}s = f(t), \quad t \in [0,1], \quad u(0) = -1, \tag{9}$$

where $f(t) = \frac{\Gamma(2.1)}{\Gamma(1.6)}t^{0.6} + t - t^{2.1} + \frac{\Gamma(0.7)\Gamma(2.1)}{\Gamma(2.8)}t^{1.8} + \frac{10}{7}t^{0.7}$ for $t \in [0,1]$. The exact solution of problem (9) is $u(t) = t^{1.1} - 1,\ t \in [0,1]$.

To find the numerical solution to problem (9) via the method proposed above (see (7)-(8)), the parameter p in the smoothing transformation (3) has to be chosen greater than $\frac{m}{1-\nu}$, where $\nu = \max\{1-\alpha, \mu, \kappa\} = 0.5$, since $\alpha = 0.5,\ \mu = 0.4,\ \kappa = 0.3$. Thus we have to take $p > 2m$ to achieve the expected convergence order $O(h^m)$ given by Theorem 1.

In Table 1, the errors $\varepsilon_N := \max_{0\le i\le 10N} |u(\frac{i}{10N}) - u_h(\frac{i}{10N})|$ are presented. Here u is the exact solution of problem (9) and u_h is an approximation for u. Additionally, the quotients $\varepsilon_{N/2}/\varepsilon_N$ for different values of m, N and p are presented. Due to Theorem 1, the expected limit value of $\varepsilon_{N/2}/\varepsilon_N$ is 2^m. These values are given in the last row of Table 1. As we can see, the obtained numerical results are in accord with the theoretical results.

Table 1: Numerical results for problem (9).

	$m=2,\ p=5$		$m=3,\ p=7$		$m=4,\ p=9$	
N	ε_N	$\varepsilon_{N/2}/\varepsilon_N$	ε_N	$\varepsilon_{N/2}/\varepsilon_N$	ε_N	$\varepsilon_{N/2}/\varepsilon_N$
8	$2.58\cdot10^{-2}$		$1.82\cdot10^{-2}$		$1.10\cdot10^{-2}$	
16	$6.79\cdot10^{-3}$	3.80	$2.46\cdot10^{-3}$	7.37	$1.11\cdot10^{-3}$	9.85
32	$1.73\cdot10^{-3}$	3.90	$3.14\cdot10^{-4}$	7.85	$7.87\cdot10^{-5}$	14.20
64	$4.40\cdot10^{-4}$	3.94	$3.93\cdot10^{-5}$	7.97	$5.06\cdot10^{-6}$	15.55
128	$1.10\cdot10^{-4}$	3.97	$4.95\cdot10^{-6}$	7.95	$3.19\cdot10^{-7}$	15.83
256	$2.77\cdot10^{-5}$	3.98	$6.19\cdot10^{-7}$	7.99	$2.01\cdot10^{-8}$	15.88
		4		8		16

Acknowledgments

This research was supported by Estonian Research Council Grant PRG864.

References

[1] K. Diethelm, *The Analysis of Fractional Differential Equations* (Springer, Berlin, 2010).

[2] A. Pedas, E. Tamme and M. Vikerpuur, *Spline collocation for fractional weakly singular integro-differential equations*, Appl. Numer. Math. **110** (2016), 204-214.

[3] A. Pedas and M. Vikerpuur, *Spline collocation for multi-term fractional integro-differential equations with weakly singular kernels*, Fractal Fract. **5**, 90 (2021).

[4] K. Orav-Puurand and G. Vainikko, *Central part interpolation schemes for integral equations*, Numer. Func. Anal. Opt. **30**, 352-370 (2009).

[5] K. Orav-Puurand, A. Pedas and G. Vainikko, *Central part interpolation schemes for integral equations with singularities*, J. Integral Equations Appl. **29**, 401-440 (2017).

International Conference on Mathematical Analysis and Applications in Science and Engineering
ICMA^{2}SC'22
ISEP Porto-Portugal, June 27 - 29, 2022

Numerical solution of linear multi-term fractional differential equations

Arvet Pedas[1] **Mikk Vikerpuur**[1⋆]

[1]University of Tartu, Estonia

[1⋆]mikk.vikerpuur@ut.ee

Abstract: We consider general linear multi-term Caputo fractional integro-differential equations with weakly singular kernels subject to local or non-local boundary conditions. Based on the obtained regularity properties and spline collocation techniques, we then construct a high-order method for the numerical solution of the underlying problem. A numerical illustration about the proposed method is also presented.

keywords: Fractional differential equation; Weakly singular kernel; Caputo derivative; Boundary value problem; Collocation method; Graded grid.

MSC2020: 34A08, 65L10.

1 Problem formulation

Following [1], we consider a class of fractional weakly singular integro-differential equations

$$(D^{\alpha_p}_{Cap}y)(t)+\sum_{i=0}^{p-1}d_i(t)(D^{\alpha_i}_{Cap}y)(t)+\sum_{i=0}^{q}\int_0^t(t-s)^{-\kappa_i}K_i(t,s)(D^{\theta_i}_{Cap}y)(s)ds=f(t),\quad 0\le t\le b, \tag{1}$$

subject to the conditions

$$\sum_{j=0}^{n_0}\beta_{ij0}\,y^{(j)}(0)+\sum_{k=1}^{l}\sum_{j=0}^{n_1}\beta_{ijk}\,y^{(j)}(b_k)+\beta_i\int_0^{\bar b_i}y(s)ds=\gamma_i\,,\quad i=0,\dots,n-1,\quad n:=\lceil\alpha_p\rceil. \tag{2}$$

Here D^{δ}_{Cap} is the Caputo fractional differential operator of order $\delta>0$ and by $\lceil\delta\rceil$ we denote the smallest integer greater or equal to a real number δ. We assume that

$$\begin{aligned}
&0\le\alpha_0<\alpha_1<\dots<\alpha_p\le n,\quad p\in\mathbb{N}:=\{1,2,\dots\},\quad n=\lceil\alpha_p\rceil,\\
&0\le\theta_j<\alpha_p,\quad 0\le\kappa_j<1,\quad j=0,\dots,q,\quad q\in\mathbb{N}_0:=\{0\}\cup\mathbb{N},\\
&0<b_1<\dots<b_l\le b,\quad l\in\mathbb{N},\quad 0<\bar b_i\le b,\quad i=0,\dots,n-1,\\
&n_0,n_1\in\mathbb{N}_0,\quad n_0<n,\ n_1<n,\quad \beta_{ij0},\beta_{ijk},\beta_i,\gamma_i\in\mathbb{R}:=(-\infty,\infty),\\
&d_i\in C[0,b]\ (i=0,\dots,p-1),\quad f\in C[0,b],\\
&K_j\in C(\Delta),\quad j=0,\dots,q,\quad \Delta:=\{(t,s):0\le s\le t\le b\},\\
&\text{where } C(\Omega) \text{ is the set of continuous functions on } \Omega.
\end{aligned} \tag{3}$$

2 Existence, uniqueness and smoothness of the solution

To characterize the possible singular behaviour of a solution of a fractional differential equation, we introduce a weighted space $C^{m,\nu}(0,b]$ of smooth functions on $(0,b]$.

Definition 1 *For given $m \in \mathbb{N}$ and $\nu \in \mathbb{R}$, $\nu < 1$, by $C^{m,\nu}(0,b]$ we denote the set of continuous functions $u : [0,b] \to \mathbb{R}$ which are m times continuously differentiable in $(0,b]$ such that*

$$\left|u^{(i)}(t)\right| \le c \left\{ \begin{array}{lll} 1 & \text{if} & i < 1-\nu \\ 1+|\log t| & \text{if} & i = 1-\nu \\ t^{1-\nu-i} & \text{if} & i > 1-\nu \end{array} \right\}, \quad 0 < t \le b, \quad i = 1, \ldots, m,$$

where $c = c(u)$ is a positive constant.

The following theorem describes the existence, uniqueness and regularity properties of the solution of (1)–(2).

Theorem 1 (i) *Suppose that assumptions* (3) *hold. Moreover, assume that problem* (1)–(2) *with $f = 0$ and $\gamma_i = 0$ $(i = 0, \ldots, n-1)$ has in $C[0,b]$ only the trivial solution $y = 0$, and from all polynomials y of degree $n-1$ only $y = 0$ satisfies the conditions* (2) *with $\gamma_i = 0$ $(i = 0, \ldots, n-1)$.*

Then problem (1)–(2) *has a unique solution $y \in C^{n-1}[0,b]$ with $D^{\alpha_p}_{Cap} y \in C[0,b]$.*

(ii) *Assume that* (i) *holds and let $d_i \in C^{M,\mu}(0,b]$ $(i = 0, \ldots, p-1)$, $f \in C^{M,\mu}(0,b]$, $K_j \in C^M(\Delta)$ $(j = 0, \ldots, q)$, where $M \in \mathbb{N}$, $\mu \in \mathbb{R}$, $\mu < 1$.*

Then problem (1)–(2) *possesses a unique solution $y \in C^{n-1}[0,b]$ such that $y \in C^{M,\nu}(0,b]$ and $D^{\alpha_p}_{Cap} y \in C^{M,\nu}(0,b]$, where*

$$\nu := \max\{\mu, \nu_1, \nu_2, \nu_3, \nu_4\}, \tag{4}$$

with

$$\begin{aligned} \nu_1 &:= \max\{1 - (\alpha_p - \alpha_i) : \ \alpha_p - \alpha_i \notin \mathbb{N}, \ i = 0, \ldots, p-1\}, \\ \nu_2 &:= \max\{1 - (\lceil \alpha_i \rceil - \alpha_i) : \ \alpha_i < n-1, \ \alpha_i \notin \mathbb{N}_0, \ i = 0, \ldots, p-1\}, \\ \nu_3 &:= \max\{\kappa_i - (\lceil \theta_i \rceil - \theta_i) : \ \theta_i \le n-1, \ i = 0, \ldots, q\}, \\ \nu_4 &:= \max\{\kappa_i - (\alpha_p - \theta_i) : \ i = 0, \ldots, q\}. \end{aligned}$$

3 Numerical method and convergence results

We begin the construction of a numerical solution to problem (1)–(2) by reformulating the problem as a Volterra integral equation of the second kind with respect to the fractional derivative $z := D^{\alpha_p}_{Cap} y$, where y is the exact solution of the original problem. We aim to first find an approximation for z. To this end, in order to take into account the potential non-smoothness of the exact solution $z = z(t)$ at the origin $t = 0$, we introduce on the interval $[0,b]$ a graded grid $\Pi_N := \{t_0, \ldots, t_N\}$ with the grid points

$$t_j := b \left(\frac{j}{N}\right)^r, \quad j = 0, 1, \ldots, N. \tag{5}$$

Here $r \in \mathbb{R}$, $r \ge 1$ is the so-called grading exponent. If $r = 1$, then the grid points (5) are distributed uniformly; for $r > 1$ the points (5) are more densely clustered near the left endpoint

of the interval $[0,b]$. Next, let $m \in \mathbb{N}$. In every subinterval $[t_{j-1}, t_j]$ $(j = 1, \ldots, N)$ we define m collocation points $t_{j1}, \ldots, t_{jm}$ by

$$t_{jk} := t_{j-1} + \eta_k (t_j - t_{j-1}), \quad k = 1, \ldots, m, \ j = 1, \ldots, N, \tag{6}$$

where $\eta_1 \ldots, \eta_m \in [0,1]$ are some fixed numbers (the so-called collocation parameters) which do not depend on j and N and satisfy $0 \le \eta_1 < \eta_2 < \ldots < \eta_m \le 1$. We search for the approximate solution z_N of the exact solution z in the standard space of piecewise polynomial functions, that is, in the space $S_{m-1}^{(-1)}(\Pi_N) := \left\{ v : v\big|_{[t_{j-1},t_j]} \in \pi_{m-1},\, j = 1, \ldots, N \right\}$. Here $v\big|_{[t_{j-1},t_j]}$ is the restriction of $v : [0,b] \to \mathbb{R}$ onto the subinterval $[t_{j-1}, t_j] \subset [0,b]$ and π_{m-1} denotes the set of polynomials of degree not exceeding $m-1$. Note that the elements of $S_k^{(-1)}(\Pi_N)$ may have jump discontinuities at the interior points $t_1, \ldots, t_{N-1}$ of the grid Π_N.

We determine an approximation $z_N \in S_{m-1}^{(-1)}(\Pi_N)$ of the exact solution z by demanding that z_N satisfy the reformulated integral equation at collocation points (6), forming a system of so-called collocation conditions. After a choice of basis in $S_{m-1}^{(-1)}(\Pi_N)$, these conditions form a system of $N \times m$ linear algebraic equations with $N \times m$ unknowns, uniquely determining an approximate solution z_N. The approximation y_N to y, the exact solution of (1)–(2), we find by the formula

$$y_N(t) = \frac{1}{\Gamma(\alpha_p)} \int_0^t (t-s)^{\alpha_p - 1} z_N(s) ds + \sum_{i=0}^{n-1} \xi_i \, t^i, \quad 0 \le t \le b. \tag{7}$$

Here $\xi_i = \xi_i(z_N)$ $(i = 0, \ldots, n-1)$ are constants which depend on z_N but are independent of t. A more detailed explanation for finding z_N and y_N will be given in the talk (the exact form of them can be found in [1]).

The convergence and convergence order of the proposed algorithm is given by the following theorem.

Theorem 2 (i) *Let $m, N \in \mathbb{N}$, $r \ge 1$ and assume that the grid points* (5) *with collocation points* (6) *and arbitrary parameters $\eta_1, \ldots, \eta_m$ satisfying $0 \le \eta_1 < \cdots < \eta_m \le 1$ are used. Assume that conditions* (i) *of Theorem 1 are satisfied.*

Then problem (1)–(2) *has a unique solution $y \in C^{n-1}[0,b]$ such that $D_{Cap}^{\alpha_p} y \in C[0,b]$. There exists an integer N_0 such that for all $N \ge N_0$ the proposed method constructs a unique approximation y_N to y, the solution of* (1)–(2), *and* $\max_{0 \le t \le b} |y_N(t) - y(t)| \to 0 \quad \text{as} \quad N \to \infty$.

(ii) *In addition to* (i), *assume that conditions* (ii) *of Theorem 1 are fulfilled for $M = m+1$. Moreover, assume that the collocation parameters $\eta_1, \ldots, \eta_m$ are chosen so that the quadrature approximation $\int_0^1 F(x)\,dx \approx \sum_{k=1}^m w_k F(\eta_k)$ with appropriate weights $\{w_k\}$ is exact for all polynomials F of degree m. Finally, assume that* $\min\{\alpha_p - \alpha_{p-1}, \alpha_p - n_1\} \ge 1$.

Then for all $N \ge N_0$ the following error estimate holds:

$$\max_{0 \le t \le b} |y_N(t) - y(t)| \le c \begin{cases} N^{-m-1} & for \quad m < 2-\nu, \quad r \ge 1, \\ N^{-m-1}(1+\log N)^2 & for \quad m = 2-\nu, \quad r = 1, \\ N^{-m-1}(1+\log N) & for \quad m = 2-\nu, \quad r > 1, \\ N^{-r(2-\nu)} & for \quad m > 2-\nu, \quad 1 \le r < \frac{m+1}{2-\nu}, \\ N^{-m-1} & for \quad m > 2-\nu, \quad r \ge \frac{m+1}{2-\nu}. \end{cases}$$

Here ν is determined by (4), *r is the grid parameter in* (5) *and c is a positive constant independent of N.*

Remark 1 *In the case* $\min\{\alpha_p - \alpha_{p-1}, \alpha_p - n_1\} < 1$ *a similar error estimate can be made (see Theorem 3 in [1]).*

Table 1: Numerical results for problem (8)-(9) with $m = 3$.

	$r = 1$		$r = 2$		$r = 3$		$r = \frac{40}{11}$	
N	ε_N	Θ_N	ε_N	Θ_N	ε_N	Θ_N	ε_N	Θ_N
4	$9.34 \cdot 10^{-4}$		$1.79 \cdot 10^{-4}$		$7.89 \cdot 10^{-5}$		$8.54 \cdot 10^{-5}$	
8	$4.11 \cdot 10^{-4}$	2.28	$3.41 \cdot 10^{-5}$	5.26	$6.99 \cdot 10^{-6}$	11.3	$5.34 \cdot 10^{-6}$	16.0
16	$1.79 \cdot 10^{-4}$	2.29	$7.05 \cdot 10^{-6}$	4.84	$6.17 \cdot 10^{-7}$	11.3	$3.21 \cdot 10^{-7}$	16.6
32	$7.82 \cdot 10^{-5}$	2.29	$1.52 \cdot 10^{-6}$	4.64	$5.75 \cdot 10^{-8}$	10.7	$1.92 \cdot 10^{-8}$	16.8
64	$3.40 \cdot 10^{-5}$	2.30	$3.30 \cdot 10^{-7}$	4.61	$5.55 \cdot 10^{-9}$	10.4	$1.15 \cdot 10^{-9}$	16.6
128	$1.48 \cdot 10^{-5}$	2.30	$7.18 \cdot 10^{-8}$	4.60	$5.48 \cdot 10^{-10}$	10.1	$6.97 \cdot 10^{-11}$	16.5
256	$6.79 \cdot 10^{-6}$	2.18	$1.56 \cdot 10^{-8}$	4.60	$5.47 \cdot 10^{-11}$	10.0	$4.23 \cdot 10^{-12}$	16.5
512	$3.17 \cdot 10^{-6}$	2.14	$3.40 \cdot 10^{-9}$	4.60	$5.50 \cdot 10^{-12}$	9.94	$2.58 \cdot 10^{-13}$	16.4
		2.14		4.16		9.85		16.0

4 Numerical example

Consider the following boundary value problem:

$$(D^{\frac{11}{10}}_{Cap} y)(t) + d_0(t)y(t) + \int_0^t (t-s)^{-\frac{1}{2}} (D^{\frac{1}{10}}_{Cap} y)(s) ds = f(t), \quad 0 \le t \le 1, \tag{8}$$

$$y(0) = 0, \quad y'(0) = 0, \tag{9}$$

with

$$d_0(t) = t^{\frac{1}{5}}, \quad f(t) = \frac{\Gamma(\frac{11}{5})}{\Gamma(\frac{11}{10})} t^{\frac{1}{10}} + t^{\frac{7}{5}} + \frac{\Gamma\left(\frac{11}{5}\right)\Gamma(\frac{1}{2})}{\Gamma(\frac{8}{5})} t^{\frac{3}{5}}, \quad 0 \le t \le 1.$$

Clearly, $d_0, f \in C^{m,\mu}(0,1]$ with $\mu = \frac{9}{10}$ and arbitrary $m \in \mathbb{N}$. Therefore, we have by (4) that $\nu = \max\{\mu, 1-\alpha_1, \kappa_0 - (1-\theta_0), \kappa_0 - (\alpha_1 - \theta_0)\} = \max\{\frac{9}{10}, -\frac{1}{10}, -\frac{4}{10}, -\frac{5}{10}\} = \frac{9}{10}$.

In Table 1 some results of numerical experiments for $m = 3$ and for different values of the parameters N and r are presented, using the knots of the Gaussian quadrature approximation for $m = 3$ as collocation parameters $\eta_1, \ldots, \eta_3$. The errors ε_N in Table 1 are calculated by the formula

$$\varepsilon_N := \max_{j=1,\ldots,N} \max_{k=0,\ldots,10} |y(\tau_{jk}) - y_N(\tau_{jk})|,$$

where $\tau_{jk} := t_{j-1} + k(t_j - t_{j-1})/10$, $y(t) = t^{\frac{6}{5}}$ ($t \in [0,1]$) is the exact solution to (8)-(9) and y_N is found by the proposed method (see (7)). The ratios $\Theta_N := \varepsilon_{N/2}/\varepsilon_N$, characterizing the observed convergence rate, are also presented. The expected limit values of Θ_N, as given by Theorem 2, are shown in the last row of the table. As we can see, the numerical results are in good accord with the theoretical results.

Acknowledgments

This research was supported by Estonian Research Council Grant PRG864.

References

[1] A. Pedas, M. Vikerpuur, Spline collocation for multi-term fractional integro-differential equations with weakly singular kernels, Fractal and Fractional, **5**(3) (2021), 90.

International Conference on Mathematical Analysis and Applications in Science and Engineering
ICMA^{2}SC'22
ISEP Porto-Portugal, June 27 - 29, 2022

An Efficient Matrix Method For Coupled Systems of Variable Fractional Order Differential Equations

Kamal Shah[1,2,⋆] **Thabet Abdeljawad**[2,3,⋆] **Iyad Suwan**[4]

[1] Department of Mathematics and Sciences, Prince Sultan University, Riyadh, Saudi Arabia
[2] Department of Mathematics, University of Malakand, Khyber Pakhtunkhwa, Pakistan
[3]Department of Medical Research, China Medical University, Taichung 40402, Taiwan
[4]Department of Mathematics and Statistics, Arab American University, Palestine

[1,2⋆]kshah@psu.edu.sa

Abstract: We establish a powerful numerical algorithm to compute numerical solutions of coupled systems of variable fractional order differential equations (FODEs). Our numerical procedure is based on Bernstein polynomials (BPs). The mentioned polynomials are non-orthogonal and have the ability to produce good numerical results as compared to some other numerical method like wavelet. By variable fractional order differentiation and integration, some operational matrices are formed. On using the obtained matrices, proposed coupled systems are reduced to systems of algebraic equations. Using Matlab, we solve the given systems for required results. Graphical presentations and maximum absolute errors are given to illustrate the results. Some useful features of our sachem are those that we need no discretization or collocation technique prior to develop operational matrices. Due to these features the computational complexity is much more reduced. Further, the efficacy of the procedure is enhanced by increasing the scale level. We also compare our results with that of Haar wavelet method to justify the usefulness of our adopted method.

keywords: Variable FODEs; BPs; Coupled system.

MSC2020: 26A33; 34A08 ; 45L05.

International Conference on Mathematical Analysis and Applications in Science and Engineering
ICMA^{2}SC'22
ISEP Porto-Portugal, June 27 - 29, 2022

Approximating Fractional Calculus Operators with General Analytic Kernel by Stancu Variant of Modified Bernstein-Kantorovich Operators

Mehmet Ali Ozarslan

Department of Mathematics, Faculty of Arts and Sciences, Eastern Mediterranean University, Famagusta, North Cyprus, via Mersin 10, Turkey

mehmetali.ozarslan@emu.edu.tr

Abstract: Fractional calculus (FC) has its roots in 1695, and have been an attractive investigation area of mathematics. Obtained results during the last 327 years are important for pure mathematics and applied fields. Especially in the last three decades, several application areas of FC have been appeared. Because of this reason, lots of numerical approximation techniques have been developed in various function spaces [1]. Recently, linear approximation operators have been introduced with the help of auxiliary linear positive operators to approximate the bivariate FC operator based on the bivariate Mittag-Leffler function [2, 3]. On the other hand, in [4], general FC operator have been proposed based on the general analytic kernel which include the iterated integral, Riemann-Liouville integral, Caputo derivative and Atangana-Baleanu Caputo derivative when the function is replaced by its derivative, generalized proportional fractional integral and Prabhakar integral.
The main purpose of this paper is to approximate the FC operator with general analytic kernel by using auxiliary newly defined linear positive operators namely Stancu variant of modified Bernstein-Kantorovich operators. Our first intention in this paper is to investigate the approximation properties of this interesting newly defined auxiliary operators and based on the obtained results to prove the main theorems on the approximation of these general FC operators. We also obtain some quantitative estimates for this approximation in terms of modulus of continuity and Lipschitz class functions. Additionally, we exhibit our approximation results for well known fractional calculus operators such as Riemann-Liouville, and Prabhakar.

keywords: Modified Bernstein-Kantorovich operator; Riemann-Liouville operator; Prabhakar operator; modulus of continuity.

MSC2020: 26A33; 41A36.

References

[1] D. Baleanu, K. Diethelm, E. Scalas, J.J. Trujillo, Fractional calculus. Models and numerical methods. Series on Complexity, Nonlinearity and Chaos, 3. World Scientific Publishing Co. Pte. Ltd., Hackensack, NJ, (2012).

[2] M.A. Ozarslan, C. Kurt, Bivariate Mittag-Leffler functions arising in the solutions of convolution integral equation with 2D-Laguerre-Konhauser polynomials in the kernel. Appl. Math. Comput. 347 (2019), 631–644.

[3] C. Kurt, M.A. Ozarslan, A. Fernandez, On a certain bivariate Mittag-Leffler function analysed from a fractional-calculus point of view. Math. Methods Appl. Sci. 44 (2021), no. 3, 2600–2620.

[4] A. Fernandez, M.A. Ozarslan, D. Baleanu, On fractional calculus with general analytic kernels. Appl. Math. Comput. 354 (2019), 248–265.

International Conference on Mathematical Analysis and Applications in Science and Engineering
ICMA^{2}SC'22
ISEP Porto-Portugal, June 27 - 29, 2022

Bivariate Modified Bernstein-Kantorovich Operators for the Numerical Solution of Two-Dimensional Fractional Volterra Integral Equations

Suzan Cival Buranay

Department of Mathematics, Faculty of Arts and Sciences, Eastern Mediterranean University, Famagusta, North Cyprus, via Mersin 10, Turkey

suzan.buranay@emu.edu.tr

Abstract: It is well known that two-dimensional fractional Volterra integral equations (2D-FVIEs) may have non-smooth solution since the derivatives of the solution may be unbounded near the integral domain boundary. Therefore, in this study smoothing transformations are employed to change a class of two-dimensional linear fractional Volterra integral equations (2D-LFVIEs) into a new transformed 2D-LFVIEs with better regularity. Consequently, Bivariate Modified Bernstein-Kantorovich (B-MBK) operators are introduced and applied to develop a transformed B-MBK scheme that reduces the transformed integral equation to a system of algebraic equations by using discretization. Subsequently, an inverse transformation is applied to obtain the approximate solution of the original equation.

keywords: Fractional Volterra integral equations; Bivariate Modified Bernstein-Kantorovich operators; Smoothing transformation; Convergence analysis.

MSC2020: 65R20; 65D30; 45D05; 41A36.

1 Introduction

One important class of two-dimensional fractional integral equations (2D-FIEs) is the two-dimensional linear fractional Volterra integral equations (2D-LFVIEs) of second kind

$$u(x) = \Psi u(x) + g(x) := \int_S K(x;y)\, u(y)\, dy + g(x),\ \ x \in D_{l_1 l_2} \tag{1}$$

where, $x = (x_1, x_2)$ and $y = (y_1, y_2) \in D_{l_1 l_2}$, and $S := [0, x_1] \times [0, x_2]$, $D_{l_1 l_2} := [0, l_1] \times [0, l_2] \subset \mathbb{R}^2$ with $l_p > 0$ $(p = 1, 2)$ being constant, $u(x) = u(x_1, x_2)$ is the solution to be found and $g(x) = g(x_1, x_2)$ is a known function on $D_{l_1 l_2}$. Here, Ψ is the integral operator with a fractional exponential kernel function of the form

$$K(x;y) = \frac{(x_1 - y_1)^{\nu_1 - 1} (x_2 - y_2)^{\nu_2 - 1}}{\Gamma(\nu_1)\Gamma(\nu_2)} \widetilde{K}(x;y), \tag{2}$$

where, $(\nu_1, \nu_2) \in (0, \infty) \times (0, \infty)$ with $\nu_p, p = 1, 2$ being fractional, $\Gamma(.)$ is the Gamma function and the function $\widetilde{K}(x;y)$ is continuously differentiable on $D_{l_1 l_2} \times D_{l_1 l_2}$ up to $m - th$ derivative $m \in \mathbb{N}$. We remark that when $(\nu_1, \nu_2) \in (0, 1) \times (0, 1)$ the kernel K has weak singularity along

the diagonals $x_1 = y_1$ and $x_2 = y_2$. Furthermore, when $(\nu_1, \nu_2) \in (1, \infty) \times (1, \infty)$ although K is continuous on $D_{l_1 l_2} \times D_{l_1 l_2}$ its derivative may be singular along the diagonal.

During the last half century significant progress has been made in the numerical analysis of the one-dimensional Volterra integral equations with weakly singular kernels or other non-smooth kernels. Such as an early study of the collocation method on graded meshes in [1] and a recent study of convergence properties of spline collocation and iterated collocation methods for a linear weakly singular Volterra integral equation associated with certain heat conduction problems in [2].

On the other hand, there are few studies dealing with the derivation and analysis of general numerical methods for the approximate solutions of the two-dimensional Volterra integral equations (2D-VIEs) with non-smooth solution specifically 2D-FVIEs.

Some problems leading to multidimensional weakly singular integral equations and the smoothness of the solution were analyzed in [3]. Later, operational matrix methods were used to develop some numerical schemes to solve two-dimensional nonlinear fractional Volterra integral equations (2D-NFVIEs), while Fredholm integral equations were also considered. Such as block pulse operational matrix in regard with the properties of two-dimensional block pulse functions given in [4]. Recently, in [5] the transformed bivariate barycentric rational interpolation method for 2D-NFVIEs was given based on the barycentric rational interpolation and some smoothing transformations.

In this research B-MBK operators are introduced and asymptotic rate of convergence analysis are given. Then the smoothing transformations used in [5] are employed to change the 2D-LFVIEs in (1) into a new form. Further, the transformed equation is reduced to a system of algebraic equations by using the B-MBK operators and discretization. Subsequently, an inverse transformation is applied to obtain numerical solution of the original equation.

2 Transformed B-MBK scheme

For solving one-dimensional Volterra and Fredholm integral equations with continuous kernel and solution satisfying the required smoothness conditions, the use of Modified Bernstein-Kantorovich (MBK) operators was given in [6]. Let $D_{1,1} := [0,1] \times [0,1]$ and $\alpha = (\alpha_1, \alpha_2)$, $\alpha_i > 0, (i = 1, 2)$. We take $z = (z_1, z_2)$, that $z_p = \frac{y_p}{l_p}$, and $w^* = (w_1^*, w_2^*)$ where, $w_p^* = \frac{k_p + (z_p)^{\alpha_p}}{n_p + 1} l_p$, $p = 1, 2$ and introduce the Bivariate Modified Bernstein-Kantorovich (B-MBK) operators $K_{n_1,n_2}^{\alpha_1,\alpha_2}(u; x)$ for $u \in C(D_{l_1,l_2})$ as follows

$$K_{n_1,n_2}^{\alpha_1,\alpha_2}(u(y_1, y_2); x) = \sum_{k_2=0}^{n_2} \sum_{k_1=0}^{n_1} P_{0,l_1}^{n_1,k_1}(x_1) P_{0,l_2}^{n_2,k_2}(x_2) \int_{D_{1,1}} u(w^*)\, dz, \tag{3}$$

where,

$$P_{0,l_p}^{n_p,k_p}(x_p) = \binom{n_p}{k_p} \left(\frac{x_p}{l_p}\right)^{k_p} \left(1 - \frac{x_p}{l_p}\right)^{n_p - k_p}, \ p = 1, 2, \tag{4}$$

and $\binom{n_p}{k_p} = \frac{n_p!}{k_p!(n_p - k_p)!}$ and $n_p \in \mathbb{N}$ for $p = 1, 2$. Let $\omega = (\omega_1, \omega_2)$ that $\omega_p \in [1, \infty), p = 1, 2$. We consider the following smoothing transformation used in [5],

$$x_p = \phi_p(t_p) = l_p^{1-\omega_p} t_p^{\omega_p}, \ 0 \le t_p \le l_p, \ p = 1, 2, \tag{5}$$

such that $\phi_p \in C^m[0, l_p]$ and

$$\left|\phi_p^{(m_p)}(t_p)\right| \le \widetilde{c}_p t_p^{\omega_p - m_p}, 0 \le m_p \le \omega_p \le m, \tag{6}$$

$$|\phi_p(t_p) - \phi_p(s_p)| \ge \widehat{c}_p |t_p - s_p| \left(t_p^{\omega_p - 1} + s_p^{\omega_p - 1}\right), \tag{7}$$

where, $\widetilde{c}_p, \widehat{c}_p (p = 1, 2)$ are constants independent of $t_p, s_p \in [0, l_p]$. We consider the transformations in (5) for $\omega_p > 1, p = 1, 2$ for a better smoothing property of the transformed function. Since $\phi_p(t_p) \in C[0, l_p]$, $\phi_p(0) = 0$, and $\phi_p(l_p) = l_p$ additionally, $\phi_p'(t_p) = \omega_p l_p^{1-\omega_p} t_p^{\omega_p - 1} > 0$ it follows that ϕ_p maps $[0, l_p]$ into $[0, l_p]$ and has the following continuous inverse transformations

$$t_p = \phi_p^{-1}(x_p) = l_p^{(\omega_p - 1)/\omega_p} x_p^{1/\omega_p}, 0 \leq x_p \leq l_p, \ p = 1, 2. \tag{8}$$

Using the smoothing transformation (5) we have $x_1 = \phi_1(t_1) = l_1^{1-\omega_1} t_1^{\omega_1}$ and $x_2 = \phi_2(t_2) = l_2^{1-\omega_2} t_2^{\omega_2}$. Also $y_1 = \phi_1(s_1) = l_1^{1-\omega_1} s_1^{\omega_1}$ and $y_2 = \phi_2(s_2) = l_2^{1-\omega_2} s_2^{\omega_2}$. Then the 2D-LFVIE given in (1) becomes

$$u_\phi(t) = \Psi_\phi u_\phi(t) + g_\phi(t) := \int_{S_\phi} K_\phi(t; s) u_\phi(s) ds + g_\phi(t), \ t \in D_{l_1, l_2}, \tag{9}$$

where, $t = (t_1, t_2), s = (s_1, s_2)$ and $S_\phi := [0, t_1] \times [0, t_2]$. Further,

$$g_\phi(t) = g_\phi(t_1, t_2) = g(\phi_1(t_1), \phi_2(t_2)), \tag{10}$$

$$u_\phi(t) = u_\phi(t_1, t_2) = u(\phi_1(t_1), \phi_2(t_2)), \tag{11}$$

$$\Psi_\phi u_\phi(t) = \int_{S_\phi} K_\phi(t; s) u_\phi(s) ds, \tag{12}$$

and the transformed kernel K_ϕ is

$$K_\phi(t; s) = K(\phi_1(t_1), \phi_2(t_2); \phi_1(s_1), \phi_2(s_2)) \phi_1'(s_1) \phi_2'(s_2). \tag{13}$$

Then we use the B-MBK operators in (3) to approximate the unknown function u_ϕ in (9) as

$$K_{n_1, n_2}^{\alpha_1, \alpha_2}(u_\phi; t) = \int_{S_\phi} K_\phi(t_1, t_2; s_1, s_2) K_{n_1, n_2}^{\alpha_1, \alpha_2}(u_\phi; s) ds + g_\phi(t_1, t_2), \ t \in D_{l_1, l_2}. \tag{14}$$

Next we take the Chebyshev collocation points

$$t_{1,i} = l_1 \left(1 - \cos\left(\frac{i\pi}{2n_1}\right)\right), \ i = 0, 1, 2, ..., n_1, \tag{15}$$

$$t_{2,j} = l_2 \left(1 - \cos\left(\frac{j\pi}{2n_2}\right)\right), \ j = 0, 1, 2, ..., n_2, \tag{16}$$

and the transformation points $x_{1,i} = l_1^{1-\omega_1} t_{1,i}^{\omega_1}$ and $x_{2,j} = l_2^{1-\omega_2} t_{2,j}^{\omega_2}$ accordingly. Let $S_{\phi,i,j} := [0, t_{1,i}] \times [0, t_{2,j}]$, subsequently we obtain the transformed B-MBK scheme as

$$K_{n_1, n_2}^{\alpha_1, \alpha_2}(u_\phi; t_{1,i}, t_{2,j}) = \int_{S_{\phi,i,j}} K_\phi(t_{1,i}, t_{2,j}; s_1, s_2) K_{n_1, n_2}^{\alpha_1, \alpha_2}(u_\phi; s) ds + g_\phi(t_{1,i}, t_{2,j}). \tag{17}$$

By solving the algebraic system of equations obtained in (17) and the B-MBK operators in (3) we obtain the approximate solution $K_{n_1, n_2}^{\alpha_1, \alpha_2}(u_{\phi, n_1, n_2}; t)$. Then the approximate solution $u_{n_1, n_2}(x)$ of the original 2D-LFVIE given in (1) is obtained by using the inverse transformation in (8).

3 Numerical Investigation

Let

$$E_{n_1, n_2}^{\alpha_1, \alpha_2}(x) = u(x) - K_{n_1, n_2}^{\alpha_1, \alpha_2}(u_{n_1, n_2}; x), \ x \in D_{l_1, l_2}. \tag{18}$$

$M(K_{n_1, n_2}^{\alpha_1, \alpha_2})$ presents the given approach by using the B-MBK operators $K_{n_1, n_2}^{\alpha_1, \alpha_2}$.

$x=(x_1,x_2)$	$AE_{8,8}^{10,10}(x_1,x_2)$
$(0,0)$	0
$(0.1,0.1)$	9.64506×10^{-15}
$(0.2,0.2)$	2.93765×10^{-13}
$(0.3,0.3)$	5.21666×10^{-12}
$(0.4,0.4)$	2.13410×10^{-11}
$(0.5,0.5)$	5.12533×10^{-11}
$(0.6,0.6)$	9.85914×10^{-11}
$(0.7,0.7)$	1.85626×10^{-10}
$(0.8,0.8)$	3.80571×10^{-10}
$(0.9,0.9)$	8.32515×10^{-10}
$(1,1)$	1.80797×10^{-9}

Table 1: The absolute errors for the Example 1 obtained by the proposed method $M\left(K_{8,8}^{10,10}\right)$ for $\omega=(4,4)$.

$AE_{n_1,n_2}^{\alpha_1,\alpha_2}(x_1,x_2)$ is the absolute error at the point (x_1,x_2) defined as $\left|E_{n_1,n_2}^{\alpha_1,\alpha_2}(x_1,x_2)\right|$.

Example 1 *([5])*

$$u(x_1,x_2)=\int_0^{x_1}\int_0^{x_2}\frac{(x_1-y_1)^{\frac{3}{2}}(x_2-y_2)^{\frac{3}{2}}}{\Gamma\left(\frac{5}{2}\right)\Gamma\left(\frac{5}{2}\right)}u(y_1,y_2)\,dy_2dy_1+g(x_1,x_2)$$

where,

$$g(x_1,x_2)=x_1^{\frac{3}{2}}+x_2^{\frac{3}{2}}-\frac{113\pi}{21300}\left(x_1^4x_2^{\frac{5}{2}}+x_1^{\frac{5}{2}}x_2^4\right),$$

$x\in D_{1,1}$, *and* $D_{1,1}:=[0,1]\times[0,1]\subset\mathbb{R}^2$ *and the exact solution is* $u(x_1,x_2)=x_1^{\frac{3}{2}}+x_2^{\frac{3}{2}}$.

References

[1] H. Brunner, The numerical solution of weakly singular Volterra integral equations by collocation on graded meshes, Math. Comp., 45 (1985)417–437.

[2] T. Diago, Collocation and iterated collocation methods for a class of weakly singular Volterra integral equations, Journal of Computational and Applied Mathematics, 229 (2009) 363–372.

[3] G. Vaĭnikko, Multidimensional Weakly Singular Integral Equations, Springer-Verlag Berlin Heidelberg, 1993.

[4] S. Najafalizadeh, R. Ezzati, Numerical methods for solving two-dimensional nonlinear integral equations of fractional order by using two-dimensional block pulse operational matrix, Applied Mathematics and Computation, 280 (2016) 46–56.

[5] H. Liu, J. Huang, X. He, Bivariate barycentric rational interpolation method for two dimensional fractional Volterra integral equations, Journal of Computational and Applied Mathematics, 389 (2021) 113339 1–13.

[6] S.C. Buranay, M.A. Özarslan, S.S. Falahhesar, Numerical solution of the Fredholm and Volterra integral equations by using Modified Bernstein-Kantorovich Operators, Mathematics, 9 1193 (2021) 1–32.

International Conference on Mathematical Analysis and Applications in Science and Engineering
ICMA^{2}SC'22
ISEP Porto-Portugal, June 27 - July 1, 2022

Some representations for the eigenfunctions of the time-fractional wave operator

M. Manuela Rodrigues[†,⋆] M. Ferreira [‡] N. Vieira [†]

[†] Department of Mathematics, University of Aveiro & CIDMA, Portugal
[‡] School of Technology and Management, Polytechnic Institute of Leiria & CIDMA, Portugal

⋆ mrodrigues@ua.pt

Abstract: In this work we present some new representations for the eigenfunctions of the time-fractional wave operator with the time-fractional derivative in the Caputo sense.

keywords: Time-fractional wave operator; Eigenfunctions; Caputo fractional derivative.

MSC2010: 35R11; 26A33; 35C15.

1 Introduction

The time-fractional wave equations are obtained from the standard wave equation by replacing the time derivative by a fractional derivative of order $\beta \in]1,2]$. This equation models anomalous wave propagation phenomena and has been studied over the last years by several authors. In the one-dimensional it has been studied comprehensively in several papers (see e.g. [5] and references therein). For the multidimensional case there are some works in this direction (see e.g. [2, 3] and references therein). In [2] it was obtained a representation for the eigenfunctions of the time-fractional diffusion-wave equation in terms of Kampé de Fériet and Lauricella series. In this paper, we focused in the one-dimensional case and we show alternative representations for the eigenfunctions of the time-fractional wave operator in terms of radial integrals, H-functions of two variables, and double series. Moreover, we present some plots of the eigenfunctions for some particular choices of the order of derivation and the eigenvalue.

2 Preliminaries

In this section we recall some basic definitions about fractional derivatives and special functions that are necessary for this work.

Definition 1 *(cf. [6, Def. 4]) Let (a,b) be a finite or infinite interval on the real line $\mathbb{R}$ and $\alpha > 0$. Also let ψ be a monotone increasing and positive function on (a,b), having a continuous derivative ψ' in (a,b). The left Riemann-Liouville fractional integral of a function f with respect to another function ψ on $[a,b]$ is given by*

$$\left(I_{a^+}^{\alpha,\psi} f\right)(t) = \frac{1}{\Gamma(\alpha)} \int_a^t \psi'(w)\, (\psi(t) - \psi(w))^{\alpha-1}\, f(w)\, dw, \qquad t > a. \tag{1}$$

Next, we give the definition of the so-called ψ-Hilfer fractional derivative of a function f with respect to another function.

Definition 2 *(cf. [6, Def. 7]) Let $\alpha > 0$ and $m = [\alpha] + 1$, where $[\alpha]$ denotes the integer part of α. Let also $I = [a, b]$ be a finite or infinite interval on the real line and $f, \psi \in C^m[a, b]$ two functions such that ψ is a positive monotone increasing function and $\psi'(t) \neq 0$, for all $t \in I$. The left ψ-Hilfer left fractional derivative ${}^H\mathbb{D}^{\alpha,\mu;\psi}_{t,a^+}$ of order α and type $\mu \in [0, 1]$ is defined by*

$$\left({}^H\mathbb{D}^{\alpha,\mu;\psi}_{a^+} f\right)(t) = I^{\mu(m-\alpha),\psi}_{a^+} \left(\frac{1}{\psi'(t)} \frac{d}{dt}\right)^m I^{(1-\mu)(m-\alpha),\psi}_{a^+} f(t).$$

We observe that when $\mu = 1$ and $\psi(t) = t$ with $t \in \mathbb{R}^+$, we recover the left Caputo fractional derivative of order $\alpha > 0$ on $[a, b] \subset \mathbb{R}$ (see [6, Sec. 5]), which is defined by

$$\left({}^C D^{\alpha}_{a^+} f\right)(t) = \frac{1}{\Gamma(m-\alpha)} \int_a^t \frac{f^{(m)}(w)}{(t-w)^{\alpha-m+1}}\, dw. \tag{2}$$

One of the integral representations presented in this work involves the bivariate Mittag-Leffler function which has the following double series representation:

$$E_{(a_1,a_2),b}(z_1, z_2) = \sum_{l_1=0}^{+\infty} \sum_{l_2=0}^{+\infty} \frac{(l_1+l_2)!}{l_1!\, l_2!} \frac{z_1^{l_1}\, z_2^{l_2}}{\Gamma(b + a_1 l_1 + a_2 l_2)}.$$

We recall the H-function of two variables, which is defined via a double Mellin-Barnes type integral by (see [1])

$$H^{0,n_1;\, m_2,n_2;\, m_3,n_3}_{p_1,q_1;\, p_2,q_2;\, p_3,q_3} \left[\begin{array}{c|l} z_1 & (a_j;\alpha_j,A_j)_{1,p_1}\,;\,(c_j,\gamma_j)_{1,p_2}\,;\,(e_j,E_j)_{1,p_3} \\ & \\ z_2 & (b_j;\beta_j,B_j)_{1,q_1}\,;\,(d_j,\delta_j)_{1,q_2}\,;\,(f_j,F_j)_{1,q_3} \end{array} \right]$$

$$= \frac{1}{(2\pi i)^2} \int_{\mathcal{L}_2} \int_{\mathcal{L}_1} \phi(s,w)\, \phi_1(s)\, \phi_2(w)\, z_1^s\, z_2^w\, ds\, dw,$$

where

$$\phi(s,w) = \frac{\prod_{i=1}^{n_1} \Gamma(1 - a_i + \alpha_i s + A_i w)}{\prod_{i=n_1+1}^{p_1} \Gamma(a_i - \alpha_i s - A_i w) \prod_{j=1}^{q_1} \Gamma(1 - b_j + \beta_j s + B_j w)},$$

$$\phi_1(s) = \frac{\prod_{j=1}^{m_2} \Gamma(d_j - \delta_j s) \prod_{i=1}^{n_2} \Gamma(1 - c_i + \gamma_i s)}{\prod_{j=m_2+1}^{q_2} \Gamma(1 - d_j + \delta_j s) \prod_{i=n_2+1}^{p_2} \Gamma(c_i - \gamma_i s)}, \phi_2(w) = \frac{\prod_{j=1}^{m_3} \Gamma(f_j - F_j w) \prod_{i=1}^{n_3} \Gamma(1 - e_i + E_i w)}{\prod_{j=m_3+1}^{q_3} \Gamma(1 - f_j + F_j w) \prod_{i=n_3+1}^{p_3} \Gamma(e_i - E_i w)},$$

and where an empty product is interpreted as 1, $x, y \in \mathbb{C}$, $m_i, n_i, p_i, q_i \in \mathbb{Z}$ such that $0 \leq m_i \leq q_i$, $0 \leq n_i \leq p_i$ $(i = 1, 2, 3)$; $a_i, b_j, c_i, d_j, e_i, f_j \in \mathbb{C}$, $\alpha_i, A_i, \beta_j, B_j, \gamma_i, \delta_j, E_i, F_j \in \mathbb{R}^+$ and the sequence of parameters (a_j), (b_j), (c_j), (d_j), (e_j) and (f_j) are restricted that none of the poles of the integrand coincide. For more details about the convergence conditions of this function the interested reader can consult [1].

3 Integral and series representations for the eigenfunctions

In this section, we present some representations for the eigenfunctions of the time-fractional wave operator in terms of double Mellin-Barnes integrals, H-functions of two variables, and double series. Let us start considering the eigenfunction equation for the time-fractional wave operator

$$\left({}^C\partial^{\beta}_{t,0^+} - c_0^2\, \partial^2_{xx}\right) u^{\beta}_{\lambda}(x,t) = \lambda\, u^{\beta}_{\lambda}(x,t), \tag{3}$$

subject to the following initial conditions

$$u^{\beta}_{\lambda}(x,0) = \delta(x) \qquad \text{and} \qquad \partial_t u^{\beta}_{\lambda}(x,0) = 0, \tag{4}$$

where $x \in \mathbb{R}$, $t \in \mathbb{R}^+$, $\lambda \in \mathbb{C}$, $\delta(x)$ is the distributional Dirac delta functions, and ${}^{C}\partial^{\beta}_{t,0^+}$ is the partial time-fractional derivative in the Caputo sense of order $1 < \beta \leq 2$ (see (2)). Problem (3)-(4) can be seen as a particular case of the problem studied in [4] where the authors solved the Cauchy problem associated to the time-fractional telegraph equation with ψ-Hilfer derivatives in $\mathbb{R}^n \times \mathbb{R}^+$:

$$c_2\, {}^{H}\partial^{\alpha_2,\mu_2;\psi}_{t,a^+} u(x,t) + c_1\, {}^{H}\partial^{\alpha_1,\mu_1;\psi}_{t,a^+} u(x,t) - c_0^2\, \Delta_x u(x,t) + d\, u(x,t) = q(x,t), \tag{5}$$

with appropriate initial conditions. If we consider in (5)

$$n = 1, \quad c_2 = 1, \quad c_1 = -\lambda, \quad d = 0, \quad q(x,t) = 0, \quad \psi(t) = t, \quad \mu_1 = \mu_2 = 1, \quad \alpha_2 = \beta, \qquad \alpha_1 = 0 \tag{6}$$

we recover immediately the one-dimensional case (3). In this sense, assuming (6) and the initial conditions (4) in some of the results presented in [4] we obtain the following representations of u^{β}_{λ}:

- In the form of radial integrals:

$$u^{\beta}_{\lambda}(x,t) = \frac{1}{\pi} \sum_{p=0}^{+\infty} \left(\lambda t^{\beta}\right)^p \int_0^{+\infty} E^{p+1}_{\beta,\beta p+1}\left(-c_0^2 w^2 t^{\beta}\right) \cos(|x|w)\, dw$$

$$- \frac{\lambda\, t^{\beta}}{\pi} \sum_{p=0}^{+\infty} \left(\lambda\, t^{\beta}\right)^p \int_0^{+\infty} E^{p+1}_{\beta,\beta(1+p)+1}\left(-c_0^2 w^2 t^{\beta}\right) \cos(|x|w)\, dw;$$

- In the form of H-functions of two variables:

$$u^{\beta}_{\lambda}(x,t) = \frac{1}{\sqrt{\pi}\,|x|} H^{0,1;0,1;1,0}_{1,1;1,0;0,1}\left[\begin{array}{c|c} \dfrac{4c_0^2 t^{\beta}}{|x|^2} & (0;1,1)\,;\left(\dfrac{1}{2},1\right);-- \\ -\lambda t^{\beta} & (0;\beta,\beta)\,;--;(0,1) \end{array}\right]$$

$$- \frac{\lambda t^{\beta}}{\sqrt{\pi}\,|x|} H^{0,1;0,1;1,0}_{1,1;1,0;0,1}\left[\begin{array}{c|c} \dfrac{4c_0^2 t^{\beta}}{|x|^2} & (0;1,1)\,;\left(\dfrac{1}{2},1\right);-- \\ -\lambda t^{\beta} & (-\beta;\beta,\beta)\,;--;(0,1) \end{array}\right]; \tag{7}$$

- In the form of double series:

$$u^{\beta}_{\lambda}(x,t) = \frac{1}{2c_0 t^{\frac{\beta}{2}}} \sum_{p=0}^{+\infty}\sum_{r=0}^{+\infty} \frac{\left(\frac{1-r}{2}\right)_p}{\Gamma\left(1-\frac{\beta}{2}+\beta p-\frac{\beta r}{2}\right) p!\, r!} \left(\lambda t^{\beta}\right)^p \left(-\frac{|x|}{c_0 t^{\frac{\beta}{2}}}\right)^r$$

$$- \frac{\lambda t^{\beta}}{2c_0} \sum_{p=0}^{+\infty}\sum_{r=0}^{+\infty} \frac{\left(\frac{1-r}{2}\right)_p}{\Gamma\left(1+\frac{\beta}{2}+\beta p-\frac{\beta r}{2}\right) p!\, r!} \left(\lambda t^{\beta}\right)^p \left(-\frac{|x|}{c_0 t^{\frac{\beta}{2}}}\right)^r. \tag{8}$$

4 Graphical representation of the eigenfunctions

In this section, we present and discuss some plots of the eigenfunctions u^{β}_{λ} for some particular choices of the fractional parameter β and the eigenvalue λ. For the generation of the plots we consider the series representation (8) with $c_0 = 1$, $x \in [-3,3]$, and $t \in [0,2]$.

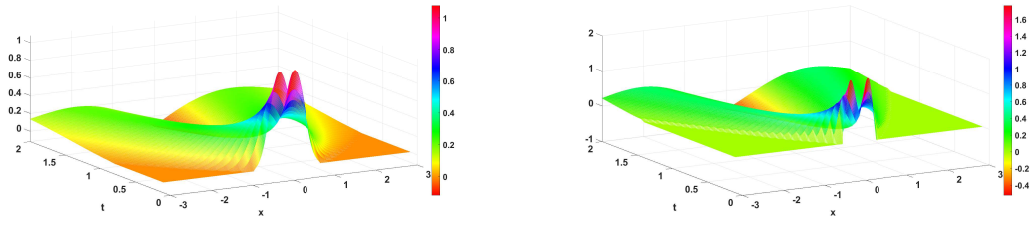

Figure 1: Plots of u^{β}_{λ} for $\beta = 1.25$ and $\lambda = 0.5$ (right), and $\beta = 1.50$ and $\lambda = 1$ (left).

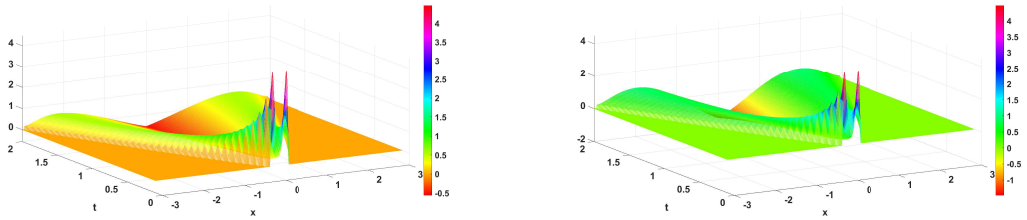

Figure 2: Plots of u_λ^β for $\beta = 1.75$ and $\lambda = 1$ (right), and $\beta = 1.75$ and $\lambda = 2$ (left).

From the analysis of Figures 1 and 2 we conclude that the eigenfunctions attain two symmetric maxima which decrease with time, and attains a minimum at $x = 0$. For all values of λ the eigenfunctions are continuous and differentiable with respect to the space variable. The obtained plots are in agreement with those obtained in [2].

5 Conclusions

In this work, we presented several representations for the eigenfunctions of the time-fractional wave equation in $\mathbb{R} \times \mathbb{R}^+$: in the form of radial series, in terms of H-functions of two variables, and as double series. The representation (7) coincides with the one presented in [2] when $n = 1$ (see expression (3.6)). For particular values of β and λ, some plots of the eigenfunctions were presented and discussed.

Acknowledgments

The work of the authors was supported by Portuguese funds through CIDMA-Center for Research and Development in Mathematics and Applications, and FCT–Fundação para a Ciência e a Tecnologia, within projects UIDB/04106/2020 and UIDP/04106/2020. N. Vieira was also supported by FCT via the 2018 FCT program of Stimulus of Scientific Employment - Individual Support (Ref: CEECIND/01131/2018).

References

[1] R.G. Buschman, *H-functions of two variables I*, Indian J. Math. **20** (1978), 132–153.

[2] M. Ferreira, Yu. Luchko, M. M. Rodrigues, and N. Vieira, Eigenfunctions of the time-fractional diffusion-wave operator, Math Meth Appl Sci. **44**(2) (2021), 1713–1743.

[3] M. Ferreira and N. Vieira, *Fundamental solutions of the time fractional diffusion-wave and parabolic Dirac operators*, J. Math. Anal. Appl. **447**(1) (2017), 329–353.

[4] N. Vieira, M. Ferreira, and M.M. Rodrigues, *Time-fractional telegraph equation in higher dimensions with ψ-Hilfer fractional derivatives*, submitted.

[5] Yu. Luchko, Fractional wave equation and damped waves, J. Math. Phys. **54**(3) (2013), Article ID: 031505 (16pp).

[6] J.V.C. Sousa and E. C. Oliveira, *On the ψ-Hilfer derivative*, Commun. Nonlinear Sci. Numer. Simulat. **60** (2018), 72–91.

International Conference on Mathematical Analysis and Applications in Science and Engineering
ICMA^{2}SC'22
ISEP Porto-Portugal, June 27 - 29, 2022

Stable coalition formation for the preservation of public goods

A. Pinto[1,2⋆] **Elvio Accinelli**[3]

[1] LIAAD - INESC TEC, Portugal
[2] University of Porto, Portugal
[3] Universidad Autónoma de San Luís Potosí, México

[1⋆]aapinto@fc.up.pt

Abstract: Baliga and Maskin introduced a model of contributions to the conservation of clean air that can be extended to consider the provision or preservation of public goods. In this paper we consider an extension of such model, a fact that will allow us to analyze the effects of the change in the behavior of economic agents with respect to the preservation of a public good, in particular, when the parameter α, which we will call preservation intensity, is modified. This parameter is considered constant and equal to $1/2$ in their work, we consider cases where $0 < \alpha < 1$. Baliga and Maskin [1] introduced a model of contributions for the provisions of public goods. In this paper we consider an extension of their model and we analyze the effects of the intensity of preservation parameter $0 < \alpha < 1$ ($\alpha = 1/2$ in their case). We show the formation of stable coalitions which are absorbing states of a bargaining Markov chain, where agents join/leave coalitions according to their cooperation/free-riding incentives. We show that there is a stable high coalition consisting of a set of agents most preferring/valuing the public good. The increase of the intensity of preservation parameter α increases the size of the stable high coalition that changes from a single member (competitive coalition as shown in Baliga and Maskin's paper) to the grand coalition. However, the utility of the members of the stable coalition can be very small compared to the utility of the free-riders, making the formation of the stable coalitions very difficult without an external mechanism. We show that Barrett's paradox of cooperation holds except when the free-riders have a very low preference for the public good, which also facilitates the formation of the stable coalition, or there are no free-riders.

keywords: public and common goods; free-riding; coalitions.

MSC2020: 91-10; 91B18; 91B69.

References

[1] Baliga, Sandeep and Maskin, Eric, Mechanism design for the environment, Handbook of environmental economics, Eds. K.G. Maler and J. Vincent, Elsevier Science/North Holland, 2003.

Firm Network Location-Price Game

João P. Almeida[1⋆] **Alberto Pinto**[2]

[1] Cedri and Polytechcinc Institute of Bragança, Portugal
[2] LIAAD-INESC TEC and University of Porto, Portugal

[1⋆]jpa@ipb.pt

Abstract: We develop a theoretical framework to study the location-price competition of firms in network game. The game is an extension of the classical Hotelling model in the line, where consumers face linear transportation costs along with firms' prices. We show the existence of a pure Nash equilibrium price if, and only if, some explicit conditions on the production costs and on the network structure hold. Furthermore, we prove that the localizations of the local firms are optimal at the cross-roads of the town. In addition, we extend the results to the case were Firms know their production costs but are uncertain about the production costs of the competitor firms.

keywords: Networks; Two stage game; Location; Hotelling game.

MSC2020: 91A43; 91A06; 91A80, 91A44.

References

[1] d'Aspremont, C., Jaskold Gabszewicz, J. and Thisse, J.-F. (1979), On On Hotelling's "Stability in Competition". Econometrica **47**(5) 1145–1150.

[2] Biscaia, R., and Mota, I. (2013), Models of spatial competition: A critical review. Papers in Reginal Science, **92**(4) 851–871.

[3] Hotelling H., (1929), Stability in Competition. Economic Journal. (39) 41–57.

[4] Pinto, A.A., J.P. Almeida and T. Parreira (2016), Local market structure in a Hotelling town. Journal of Dynamics and Games, **3**(1) 75–100.

International Conference on Mathematical Analysis and Applications in Science and Engineering
ICMA^{2}SC'22
ISEP Porto-Portugal, June 27 - 29, 2022

The value of information search against fake news

José Martins[1,2⋆] **Alberto Pinto**[1,3]

[1] LIAAD - INESC TEC, Portugal
[2] Polytechnic of Leiria, Portugal
[3] University of Porto, Portugal

[1⋆]jmmartins@ipleiria.pt

Abstract: We introduce the evolutionary information search dynamics and characterize its stable equilibria. Inspired in Daley-Kendall [1] and Goffman-Newill [2] models, we propose an Ignorant-Believer-Unbeliever rumor spreading model with the following characteristics: (i) a network contact between the individuals that determine the spread of the rumors; (ii) a value (benefits versus costs) for the individuals to search truthful information; (iii) a payoff for the individuals depending on the value of information search and depending on the risk of believe on false rumors. Since the rumors are false, fake news are the best example. For each value of information search, we compute the evolutionary stable information search strategy that is the attractor of the information search dynamics; and the optimal information search strategy that maximizes the expected information payoff of the population. Three distinct scenarios occur: (i) when the benefits are higher than the costs, we show that both strategies coincide and all individuals search for truthful information; (ii) when the benefits are slightly lower than the costs, we show that both strategies coincide and all individuals do not search for truthful information.

keywords: Fake news; Rumors spreading; Nash equilibrium.

MSC2020: 91A35; 91A40; 91A80.

References

[1] DJ Daley, DG Kendall, Epidemics and rumours. Nature (1964) 204:1118.

[2] W Goffman, VA Newill, Generalization of epidemic theory: an application to the transmission of ideas. Nature (1964) 204:225-228.

International Conference on Mathematical Analysis and Applications in Science and Engineering
ICMA^{2}SC'22
ISEP Porto-Portugal, June 27 - 29, 2022

Local equilibria in price competition with positive network effects

Renato Soeiro[1,2⋆] **Alberto Adrego Pinto**[1,2]

[1] Inesc Tec, Portugal
[2] University of Porto, Portugal

[1⋆]rsoeiro@fe.up.pt

Abstract: The study of network effects in models of price competition is usually a perturbation of an (equilibrium) demand function, which is either a primitive or a specification arising from a standard model. When network effects are positive and depend on the aggregate of choices, such a construction is necessary to control the bandwagon effect and avoid ending up in a corner solution. We show that in duopolies where network effects depend on a partition into groups, some influence structures produce a local (pure price) duopoly equilibrium where both firms profit. The local solution can be part of a subgame-perfect equilibrium if firms' are afraid that a price outside the interval that supports the local optimum will tip the market to their rival. It may be particularly suitable for some fickle popularity phenomena. It also shows it is possible to take network effects as the microeconomic foundation for demand and then perturb that solution with other effects if deemed necessary.

keywords: Bertrand Model; Duopoly; Network effects; Imperfect Competition; Pricing; Nash equilibrium.

MSC2020: 91B24; 91A80; 91A40.

Acknowledgments

The authors thank the financial support through National Funds by the FCT - Fundacao para a Ciencia e a Tecnologia, I.P. (Portuguese Foundation for Science and Technology) within the project MDG, with reference PTDC/MAT-APL/31753/2017.

International Conference on Mathematical Analysis and Applications in Science and Engineering
ICMA^{2}SC'22
ISEP Porto-Portugal, June 27 - 29, 2022

Bifurcation analysis for a discrete-time delayed dynamic Cournot mixed oligopoly model

Loredana Camelia Culda[1] **Eva Kaslik**[1,2] **Mihaela Neamţu**[2,3]

[1] Dept. of Mathematics and Computer Science, West University of Timişoara, Romania
[2] Institute for Advanced Environmental Research, West University of Timişoara, Romania
[3] Dept. of Economics and Economic Modelling, West University of Timişoara, Romania

[1]loredana.culda@e-uvt.ro; [2]eva.kaslik@e-uvt.ro;[3] mihaela.neamtu@e-uvt.ro

Abstract: In this paper, we investigate a discrete-time Cournot game with three time delays, where the interactions of one public firm and n private firms on the market are considered. The mathematical model is described by a nonlinear delayed system of $n+1$ difference equations, which admits two equilibrium points. The local stability analysis shows that the boundary equilibrium point is a saddle point, while the positive equilibrium is asymptotically stable for any time delays, if some conditions on the system parameters are fulfilled. The bifurcation phenomena which occur in a neighborhood of the positive equilibrium are also analyzed, considering the time delays as bifurcation parameters. Numerical simulations illustrate the complex dynamic behaviour of the system.

keywords: Cournot oligopoly, local stability, bifurcation, time delay, simulation

MSC2020: 39A28; 91A05; 91A50.

1 Introduction

Dynamic Cournot oligopoly games have been widely studied in the literature. For example, in [2], three concurrent firms with bounded rationality are considered, based on the utility CES function and complex dynamic behavior is reported. In [5] a mixed triopoly game is analyzed, illustrating the competition between a public firm and two private firms. In [1] the competition of n firms is investigated, in a context of isoelastic demand with non-unitary elasticity and the stability of the Nash equilibrium is discussed. In addition, in [4] it is highlighted that state-owned public firms are significant for their market competitors and private firms might face financial difficulties that could lead to their nationalization.

Motivated by the mixed competition setting, as well as the delay in the information collection and decision making processes, we focus on the analysis of the influence of the number of private firms and the time delays on the dynamics of a Cournot oligopoly model. With this aims, we consider one public firm and n private firms producing differentiated products. The firms have two types of strategies: naive for the private firms and bounded rationality for the public firm. The public firm makes the output's decision based on the social surplus, taking into account the past production levels of the private firms [5]. On the other hand, the outputs of each private firm is adjusted using the reaction functions and the past production levels of the public firm and the other private firms. The main result of this paper is related to the stability and bifurcation analysis of the Nash equilibrium, with respect to the number of the private firms, the degree of product differentiation, the adjustment parameter and the time delays.

2 Results and discussion

We consider competitors' time delays in the terms of the bounded rationality, reflected on the ideas presented in [3]. The production of the public firm is adjusted based on the past production levels of the private firms (at time $t-\tau_1$, $\tau_1>0$). However, the aim of this study is to focus on the case when the productions of each private firms are updated with respect to the past production (at time $t-\tau_0$, $\tau_0>0$) of the public firm, as well as the past production (at time $t-\tau_2$, $\tau_2>0$) of the other private firms. Therefore, in this paper, we investigate the following nonlinear discrete-time mathematical model with time delays:

$$\begin{cases} q_0(t+1) = q_0(t) + \alpha q_0(t)\left[a_0 - bq_0(t) - b\delta\sum\limits_{i=1}^{n} q_i(t-\tau_1)\right] \\ q_j(t+1) = \dfrac{a_1}{2b} - \dfrac{\delta}{2}q_0(t-\tau_0) - \dfrac{\delta}{2}\sum\limits_{i=1,i\neq j}^{n} q_i(t-\tau_2) \quad , \quad j=\overline{1,n}. \end{cases} \tag{1}$$

The discrete dynamical system (1) has two equilibrium points (nonnegative fixed points):

$$E_0 = (0, q^\star, q^\star, ..., q^\star) \qquad \text{and} \qquad E_+ = (q_0^\star, q_1^\star, q_1^\star ..., q_1^\star),$$

where

$$\begin{aligned} q^\star &= \frac{a_1}{b[2+(n-1)\delta]}, \\ q_0^\star &= \frac{[2+(n-1)\delta]a_0 - n\delta a_1}{b[2+(n-1)\delta - n\delta^2]}, \\ q_1^\star &= \frac{a_1 - \delta a_0}{b[2+(n-1)\delta - n\delta^2]}. \end{aligned}$$

As $\delta \in (0,1)$, it follows that E_+ is a positive equilibrium point if and only if the following assumptions are satisfied:

$$\begin{aligned} &(\text{A.1}) \qquad [2+(n-1)\delta]a_0 > n\delta a_1 \ , \\ &(\text{A.2}) \qquad a_1 > \delta a_0 \ . \end{aligned}$$

The characteristic equation associated to the liniarized system at one of the equilibrium points $E=(q_0^e, q_1^e, q_1^e, ..., q_1^e) \in \{E_0, E_+\}$ is of the form:

$$\left(\lambda - \frac{\delta}{2}\lambda^{-\tau_2}\right)^{n-1}\left[nb\alpha q_0^e\frac{\delta^2}{2}\lambda^{-\tau_0-\tau_1} - (\lambda - 1 - \alpha(a_0 - 2bq_0^e - nb\delta q_1^e))\left(\lambda + (n-1)\frac{\delta}{2}\lambda^{-\tau_2}\right)\right] = 0. \tag{2}$$

Assuming that the assumption $(A.1)$ is satisfied, we easily obtain that the boundary equilibrium point E_0 is a saddle point, regardless of the the time delays τ_0, τ_1, τ_2.

For the positive equilibrium, as $q_0^e = q_0^\star$ and $q_1^e = q_1^\star$, based on the characteristic equation (2), the local stability analysis reduces to studying the distribution of the roots with respect to the unit circle of the following equation:

$$n\beta\frac{\delta^2}{2}\lambda^{-\tau_0-\tau_1} - (\lambda - 1 + \beta)\left(\lambda + (n-1)\frac{\delta}{2}\lambda^{-\tau_2}\right) = 0, \tag{3}$$

where

$$\beta = \alpha\frac{[2+(n-1)\delta]a_0 - n\delta a_1}{2+(n-1)\delta - n\delta^2} > 0. \tag{4}$$

If assumptions $(A.1)$ and $(A.2)$ hold, using the Schur-Cohn stability criterion, we show that when $\tau_0 = \tau_1 = \tau_2 = 0$, the positive equilibrium point E_+ is asymptotically stable if and only if the following inequalities are satisfied:

$$\delta < \frac{2}{n-1} \qquad \text{and} \qquad \beta < \frac{4-2(n-1)\delta}{2-(n-1)\delta+n\delta^2}. \tag{5}$$

Moreover, we also prove that when $\tau_2 = 0$, inequalities (5) represent sufficient conditions for the asymptotic stability of the positive equilibrium point E_+, for any time delays τ_0 and τ_1.

We also analyze the bifurcation phenomena occurring in a neighborhood of the positive equilibrium E_+, considering the three time delays as bifurcation parameters.

3 Conclusions and Future work

This work generalizes existing findings recently reported in the literature [5], concerning the stability and bifurcation analysis of a discrete-time Cournot oligopoly game involving one public firm and several private firms. Numerical simulations reveal complex dynamic behavior and the presence of chaotic regimes for sufficiently large values of the time delays.

On the one hand, understanding the possible routes towards chaotic behavior in terms of the number of private firms and the time delays and on the other hand, investigating a similar mathematical model in which the n private firms do not have all-to-all connection are possible directions for future research.

References

[1] J. Andaluz, A. A. Elsadany, G. Jarne, Dynamic Cournot oligopoly game based on general isoelastic demand, Nonlinear Dynamics, **99** (2020), no. 2, 1053–1063.

[2] S. S. Askar, M. F. El-Wakeel, M. Alrodaini, Exploration of complex dynamics for Cournot oligopoly game with differentiated products, Complexity, **2018** (2018), ID 6526794, 1–13.

[3] A. Elsadany, Dynamics of a delayed duopoly game with bounded rationality, Journal of computational mathematics, **52** (2010), no. 9-10, 1479–1489.

[4] J. Haraguchi, T. Matsumura, Cournot–Bertrand comparison in a mixed oligopoly, Journal of Economics, **117** (2016), no. 2, 117–136.

[5] J. Wang, Z. Bao, J. Huang, Y. Song, Complex Dynamics of Mixed Triopoly Game with Quantity and Price Competition, Discrete Dynamics in Nature and Society, **2021** (2021), ID 9532340, 1–15.

[6] L.C. Culda, E. Kaslik, M. Neamtu, A dynamic Cournot mixed oligopoly model with time delay for competitors, Carpathian Journal of Mathematics, (2022), in press.

Evaluation of the utility loss due to habit formation: application to an environmental project

Hidekazu Yoshioka[1*] **Motoh Tsujimura**[2] **Kunihiko Hamagami**[3] **Haruka Tomobe**[4]

[1] Shimane University, Japan
[2] Doshisha University, Japan
[3] Iwate University, Japan
[4] Tokyo Institute of Technology, Japan

[1*]yoshih@life.shimane-u.ac.jp

Abstract: Habit formation is a relaxation mechanism of control policies in making decisions. It prevents the decision-maker from rapidly changing his/her control variables. Our contribution presents and analyzes a new mathematical model of a modern environmental policy-making problem with a habit formation.

keywords: habit formation; time-average control; sediment replenishment

MSC2020: 93E03; 49L20; 60J76.

1 Introduction

Habit formation as a relaxation mechanism of control variables is a central research topic in mathematical finance, economics, and insurance [1], while not so in civil and environmental engineering despite their importance. The relaxation prevents the decision-maker from rapidly changing his/her control variables, possibly leading to the loss of utility to be maximized by the project implementation. Adaptive environmental management, even if it is theoretically optimal, would be often repelled. This is considered due to technical difficulties in the project implementation and/or aversion of the decision-maker against the rapid adaptation. However, the loss of utility due to the habit formation in this aspect has not been evaluated.

We formulate an environmental management problem with a habit formation focusing on the modern sediment replenishment [2]. As a new attempt, the sediment transport (i.e., volume decrease of a sediment lump in time) is described by an avalanche model [3] as a simple model of decreasing processes having a unique scaling property. The objective of the sediment replenishment is to supply sand to a sediment-starved river reach, such as a river reach downstream of a dam, which is a costly project necessary for the conservation of aquatic ecosystems. We formulate a time-average control problem to find the cost-efficient replenishment policy with and without the habit formation.

2 Results and discussion

We work in a continuous-time setting where state variables are normalized for simplicity. The presentation in this material is formal, and will be formulated more rigorously in its full paper version. The time is denoted as $t \geq 0$. The sediment storage in a target river reach at time t is denoted as $X_t \in [0,1]$, which is assumed to follow the stochastic differential equation (SDE) [3]

$$\mathrm{d}X_t = -\begin{Bmatrix} q & (X_{t-} > 0) \\ 0 & (X_{t-} = 0) \end{Bmatrix} \mathrm{d}t - \mathrm{d}N_t, \ t > 0, \ X_0 \in [0,1] \tag{1}$$

when there is no replenishment. Here, $q > 0$ is a constant, N_t is a state-dependent compound Poisson process such that its jump intensity is a constant $\lambda > 0$. At each its jump time τ of N_t, with $\beta \in (0,1)$ the jump size is βX_t (resp., $(1-\beta)X_t$) with the probability $(1-\beta)X_t$ (resp., βX_t), and the jump size is 0 with the probability $1 - X_t$. The first and second terms of (1) describe gradual and sudden transport of the sediment to the downstream reach, the latter being due to flood events. The non-smoothness of the first term prevents the sediment storage from falling below 0. The first term of (1) is not appearing in [3]. With this term, the sediment storage becomes 0 in a finite time.

We consider a time-average control problem by a decision-maker who wants to increase the sediment storage so that it does not become empty. We assume that the replenishment chances arrive following a Poisson process P_t with the intensity $\omega > 0$ mutually independent from N_t. The volume of storable sediment is 1. At each jump time s of P_t, the range of the sediment volume η_s to be replenished should be $A \equiv [0, 1 - X_s]$.

The habit formation enters the proposed model as a restriction of the control range A. Here, we consider the particular case such that the control range A is restricted by another state variable $Y_t \in [0,1]$, the habit, as $A \equiv [0, \min\{Y_s, 1 - X_s\}]$, where the governing equation of the habit is given by the linear relaxation

$$\mathrm{d}Y_t = -\mu(Y_t - 1)\mathrm{d}t, \ t > 0, \ Y_0 \in [0,1] \tag{2}$$

when there is no replenishment, where $\mu > 0$ is the relaxation parameter of habit. At the time s of replenishment, the habit is updated as $Y_s = \eta_s$. In this way, the habit formation with a finite μ restricts the control range so that the decision-making of the latest sediment replenishment is affected by the past. There exist the two extreme cases. Firstly, the limit $\mu \to +\infty$ corresponds to the decision-maker without any habit, where the control range is $A \equiv [0, 1 - X_s]$. Secondly, the limit $\mu \to +0$ is the ratcheting case that does not allow for increasing the volume of replenishment in the future; namely, $Y_t = \min_{0 \leq s \leq t} \{Y_0, \eta_s\}$. The case where the lower bound of the control range is restricted by forming the habit can also be formulated analogously, but is not presented here.

The expectation conditioned on $(X_0, Y_0) = (x, y)$ is denoted as $\mathbb{E}^{x,y}$. Given the dynamics augmented by the control, set the minimization problem [2]

$$\text{minimize } \limsup_{T \to +\infty} \frac{1}{T} \mathbb{E}^{x,y} \left[\int_0^T \mathbb{I}_{\{X_s = 0\}} \mathrm{d}s + \sum_{s_i \leq T} \left(d\mathbb{I}_{\{\eta_{s_i} > 0\}} + c\eta_{s_i} \right) \right] \text{ by choosing } \{\eta_{s_i}\}_{i=0,1,2,\ldots}, \tag{3}$$

where $\mathbb{I}_B$ is the indicator function of the generic set B, $c>0$ is the proportional cost, $d>0$ is the fixed cost, and η_{s_i} is the amount of sediment replenishment at ith jump time of P_t. The first term of (3) penalizes the sediment depletion, while the second term evaluates the total cost of the replenishment.

Under a Markovian control framework, if the minimum value $H \geq 0$ of the objective function in (3) exists as a constant, then the optimality equation associated with the control problem is

$$H + q\mathbb{I}_{\{x>0\}}\frac{\partial \Phi}{\partial x} + \mu(y-1)\frac{\partial \Phi}{\partial y} + \lambda x\left(\Phi - \beta\Phi(\beta x, y) - (1-\beta)\Phi\left((1-\beta)x, y\right)\right) + \omega\left(\Phi - \min_{\eta\in[0,\min\{1-x,y\}]}\left\{\Phi(x+\eta,\eta) + d\mathbb{I}_{\{\eta>0\}} + c\eta\right\}\right) - \mathbb{I}_{\{x=0\}} = 0 \quad , \ 0 \leq x, y \leq 1. \quad (4)$$

A solution to this equation is a couple (H,Φ) where the potential $\Phi:[0,1]^2 \to \mathbb{R}$ is a sufficiently regular function. The meaning of "solution" should be discussed from a standpoint of viscosity solutions, which will be left in the forthcoming work and here we present computational results of Φ and a candidate of the Markovian optimal control

$$\eta_s^* = \eta^*(X_s, Y_s) = \underset{\eta\in[0,\min\{1-X_s,Y_s\}]}{\arg\min}\left\{\Phi(X_s+\eta,\eta) + d\mathbb{I}_{\{\eta>0\}} + c\eta\right\}. \quad (5)$$

For the numerical discretization of (4), we use the local Lax-Friedrichs finite difference scheme on a uniform 200×200 mesh, and the resulting nonlinear system is resolved by a fast-sweeping method [2], which is truly applicable to a constant H (see, the discussion below). The parameter values are chosen as $\lambda = 0.25$, $\beta = 0.2$, $q = 0.1$, $\omega = 0.3$, $c = 0.21$, $d = 0.28$. We fix $\Phi(0,0) = 0$ to resolve a non-uniqueness issue of Φ.

Figure 1 compares the numerical solution for different values of μ. The optimized objective H is computed as 0.205 for $\mu = +\infty$ and 0.212 for $\mu = 0.1$. The convergence failed for $\mu = 0$. Habit formation with a larger relaxation parameter μ thus leads to a larger loss of the utility here appearing as the increase of the optimized objective H. Numerical solutions do not contain any spurious oscillation for $\mu = +\infty$ and $\mu = 0.1$, and the computed Φ are monotone in both x and y directions. In particular, in the case $\mu = +\infty$, both Φ and η^* do not depend on the habit y as expected.

The ratcheting case $\mu = 0$ is interesting because the aforementioned numerical method failed, suggesting that some of its assumptions are not satisfied in this case. We therefore applied a vanishing-discount method as a different approach to compute time-average stochastic control problems. This method has already been examined against the other cases. The right panel of **Figure 1** shows the computed value function multiplied by the discount rate 0.005, which is still denoted as $H = H(x,y)$. The computed H is clearly state-dependent, suggesting a non-constant H. Indeed, if the infimum of (3) is a constant, then the computed $H(x,y)$ should be close to a constant. The non-constant H is considered due to the modeling consequence that the sediment is never replenished when $Y_0 = 0$, while it is possible otherwise. This may cause the existence of multiple attractors depending on Y_0. The issue of non-constant H will be addressed in future.

3 Conclusions and future work

We presented and analyzed a time-average control problem of the sediment replenishment subject to habit formation. The model was fairly simple, while its analysis results implied a complex dependence of the optimal control on the habit formation. In the future, the model will be more sophisticated by introducing a more realistic sediment transport mechanism, a more complicated performance index considering benthic water environmental conditions, and a more flexible observation policy.

We will improve the avalanching term by modulating the state-dependent jump size and frequency so that the decreasing speed of the sediment storage becomes better consistent with the existing data. As an example, we are currently investigating the state-dependent α-stable subordinator having the jump kernel, as an extension of [2]:

$$\nu\left(X_{t-};\mathrm{d}z\right)=f\left(X_{t-}\right)\frac{\mathrm{d}z}{z^{\alpha+1}},\ \text{jump size } z>0,\ \text{a parameter } \alpha\in(0,1) \text{ and some function } f. \quad (6)$$

Some additional computational results will be presented in the conference and a corresponding paper.

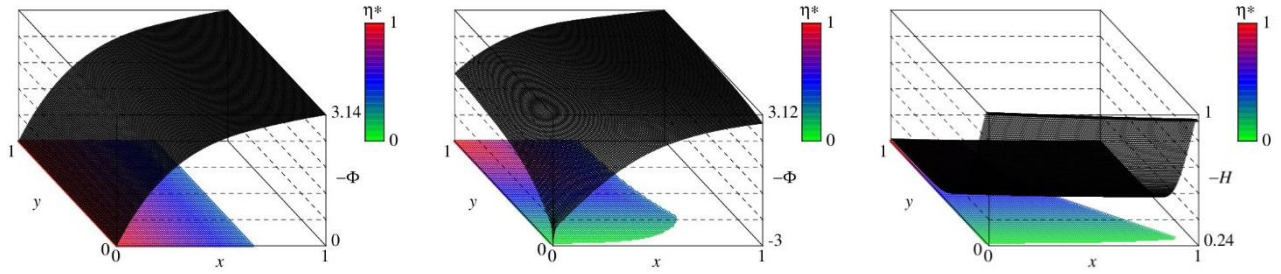

Figure 1. Computed $\Phi=\Phi(x,y)$ (surface plot, left and middle), $H=H(x,y)$ (surface plot, right), and optimal control η^{*}. Here, μ is set as $+\infty$ (left), 0.1 (middle), and 0 (right). The right panel was computed using a vanishing-discount method.

Acknowledgments

This work was supported by the Yanmar Environmental Sustainability Support Association No. KI0212021 and the Japan Society for the Promotion of Science No. 22K14441.

References

[1] He L., Liang Z., Song Y., Ye Q., Optimal asset allocation, consumption and retirement time with the variation in habitual persistence, Insurance: Mathematics and Economics, **102** (2022), 188–202.

[2] Yoshioka H., Tsujimura M., Yaegashi Y., Analytical and numerical solutions to ergodic control problems arising in environmental management, Mathematical Methods in the Applied Sciences, in press.

[3] Beznea L., Deaconu M., Lupaşcu-Stamate O., Scaling property for fragmentation processes related to avalanches, *International Conference on Applications of Mathematics and Informatics in Natural Sciences and Engineering*, 37–45. Springer, Cham, 2019.

International Conference on Mathematical Analysis and Applications in Science and Engineering
ICMA^{2}SC'22
ISEP Porto-Portugal, June 27 - 29, 2022

Resolving a dynamic winner determination problem (WDP) by dynamic programming

Asli Larbi[1]

[1] University of Bejaia, Algeria

[1⋆]larbi.asli@univ-bejaia.dz

Abstract: In this paper, we propose a mathematical formulation model for the dynamic winner determination problem (DWDP), in combinatorial auctions. This model is developed for the purpose of implementing the web, the model reflects the English auction mechanism. We have developed an optimal resolution algorithm, which is based on the temporal analysis of the bid status in order to avoid to the maximum to the combinatorial resolution. We use the dynamic programming if need be, According to state of the bid. The algorithm gives at every time of the auction period, a temporary list of winners, Articles sold and the temporary gain. A numerical experiment using this algorithm on simulated data gives rise to satisfactory results.

keywords: English combinatorial auction, dynamic programming, temporary winners list, final winner, winner determination problem, WDP.

MSC2020: 26A33; 34A60; 34G25; 93B05.

1 Introduction

An English combinatorial auction is described by a number m of items in limited quantities for each one, which are offered for sale to potential buyers. These buyers have a limited period of time and opportunity to update their bids.
Each bid is a combination of items, formulated as a vector of dimension $m + 1$, which contains m quantise of items desired by the bidder and the price offered for this bid. Knowing the bids of each other, the algorithm that we will develop will list the temporary winners at every moment, which leaves to the bidders the opportunity to respond accordingly.

2 DWDP mathematical model

This model have for objective the maximization of the total profit obtained by the auction, Subjected to constraints of the availability. It reproduces the behavior of an English auction where each bidder has the right to update his bid during the exercise period T.
The model is built in a dynamic way, It starts at $t = 0$, once the first bidder proposes a first bid $S_1 = (c_1(t), a_{i1}(t))$. Each bid is formed by a list of items A^j with corresponding prices c_j. At this moment, The problem will contain a single variable and be 1-dimensional.
So, and as long as, other bidders come, the model is completed with the possibility that each

bid previously given can be changed depending on the status of the auction.
The full model at time $t \in [0, T]$ is:

$$WDP_t \left| \begin{array}{lll} f_t(x) = & \max \sum_{j=1}^{k} c_j(t) x_j & \\ & \sum_{j=1}^{k} a_{ij}(t) x_j & \leq \beta_i \\ i = 1, \ldots, m; & j = 1, \ldots, k; x_j & \in \{0, 1\} \quad . \end{array} \right. \tag{1}$$

During this phase a bidder can modify his offer as needed, he can vary the amount c_j or quantities a_j desired, to better position himself in the list of winners.
At the end of the exercise period $t = T$, the auction will stop, and the model will be final and contain n bidders.

2.1 DP: the description

Let a set of states Q be defined as

$$Q = \{q(0), q(1), \ldots, q(b)\} \tag{2}$$

The state $q(k), k = 0, \ldots, b$, represents all nonnegative integer solutions of the $DWDP$, i.e.

$$q(k) = \{x \in \{0, 1\}^k : ax = k\} \tag{3}$$

Note that for the initial state $q(0)$ we get $q(0) = \{0\}$ independently from the weight vector a and the objective coefficients. Since there may occur solutions in all states the set of final states Q_F is given by:

$$Q_F = \{q(0), q(1), \ldots, q(b)\} \tag{4}$$

The decision of increasing a variable x_j by 1 for a solution $x \in q(k)$ results in an increase of the right-hand side k by a_j and thus corresponds to a transition of x from the state $q(k)$ to the state $q(k + aj)$. Let $G(q(k)), k = 0, 1, \ldots, b$ be the set of all solutions of the $k - DWDP$. Then the original $DWDP$ can be solved applying the following recursive equations:

$$\left| \begin{array}{l} G(q(0)) = \{0\} \\ G(q(k)) = vmax\{G(q(k - a_j)) + c_j : j \in S; k - a_j \geq 0\} k = 1, \ldots, b. \end{array} \right. \begin{array}{l} ; \\ . \end{array} \tag{5}$$

where $S = \{1, \ldots, n\}$ denotes the index set of the variables $x_j, j = 1 \ldots, n$, and operation $vmax$ computes the solutions in the set being the algebraic sum of the cost vector c_j and the set of all the solutions of the $(k - a_j) - DWDP$. Since all the states are final, the set of vector costs of all solutions Y_e is obtained as the maximum of the union of the sets. $G(q(k)), k = 1, \ldots, b$, i.e.

$$Y_e = vmax \bigcup_{k=0,1,\ldots,b} G(q(k)) \tag{6}$$

References

[1] B. Villarreal and M. H. Karwan. Multicriteria integer programming: A (hybrid) dynamic programming recursive approach. Mathematical Programming, 21:204-223, 1981.

[2] Riikka-Leena Leskelä, Bidder support in iterative multiple-unit combinatorial auctions, DissertationHelsinki University of Technology, Department of Industrial Engineering and Management, Doctoral Dissertation Series 2009/12. Espoo 2009

[3] L. Asli et M. Aïder ; El-Ghazali Talbi. Solving a dynamic combinatorial auctions problem by a hybrid metaheuristic based on a fuzzy dominance relation. EDP sciences, RAIRO-Oper. Res, (2019), vol. 53, no. 1, pages 207-221. 2019.

International Conference on Mathematical Analysis and Applications in Science and Engineering
ICMA^{2}SC'22
ISEP Porto-Portugal, June 27 - 29, 2022

Analysis of the effect of the randomized damping coefficient on the response of a SDOF system

Giovanni Falsone[1] **Rossella Laudani**[1] **Ana Navarro Quiles**[2⋆]

[1] Universita degil Studi di Messina, Italy
[2] Universitat de Valencia, Spain

[1⋆]ana.navarro@uv.es

Abstract: In this work, a full probabilistic description of the response of a randomized SDOF system is done. Considering that the damping of the structure does not simply relate to any single physical phenomenon, the sensitivity of the response to the randomness of the damping parameter is investigated. The stochastic analysis is conducted via the Probability Transformation Method therefore the first probability density function of the response is evaluated. The effect of the uncertain damping coefficient on the response of the SDOF system has been investigated through several numerical examples.

keywords: Single Degree-of-Freedom system; Uncertainty quantification; Random damping coefficient; Probability density function

MSC2020: 34F05; 37H10.

1 Introduction

The dynamic analysis of structural systems depends on external actions as well as on the physical-geometrical properties of the structures, which are usually described using deterministic parameters. In many cases, these quantities have such a highlevel of uncertainty as to produce random variations in the dynamic response [1]. For this reason, it is more advisable to study the probabilistic behavior of the stochastic response functions given by the randomization of the structural system. In this work we consider the harmonic oscillator, because it is certainly the simplest but one of the most interesting models to examine the characteristics of dynamical systems in engineering and applied sciences. In the last years, many authors providing studies on the oscillator's response due to random loadings, see for example [2]. This model depends on three parameters: the mass, the stiffness and the damping. Among these parameters, the estimation of the damping value of a structural system is the most difficult task for a design engineer. Given the fact that there is almost always uncertainty about the energy dissipation during dynamic motion of a mechanical or structural system, the damping of a system may vary significantly from its "design" value. In fact, unlike mass and stiffness values, damping is not related to a uniqueand well-defined physical phenomenon. For this reason, damping is surely the most uncertain parameter influencing the dynamic responses of structures, and its incorrect estimation results in a large error in theresponse [3].

The main objective of this contribution is to analyze how the damping parameter affects the response function of a Single Degree-of-Freedom (SDOF) system when it is assumed to be a random variable (RV). In particular, a fully stochastic characterization of the system response in terms of probability density function (PDF) has been performed by applying the Probability Transformation Method (PTM), [4].

2 Results and discussion

Consider a rigid girder with mass m which is supported by columns with combined stiffness k being the internal friction between the girder and the columns described by a viscous dashpot damper with damping coefficient c. Suppose that the girder is also subjected to an externally applied force $f(t)$. Therefore, denoting by $k/m = \omega_0^2$ and $c/m = 2\xi\omega_0$, the equation of motion of an SDOF, written in the standard form in the theory of vibration, is

$$\ddot{x}(t) + 2\xi\omega_0\dot{x}(t) + \omega_0^2 x(t) = \frac{f(t)}{m}, \tag{1}$$

ω_0 being the natural circular frequency and ξ the non-dimensional damping coefficient. Let the following initial conditions

$$x(0) = x_0, \qquad \dot{x}(0) = x_1, \tag{2}$$

where, without loss of generality, the initial time is equal to zero.

Assuming that the damping coefficient is random rather than deterministic, we analyze the behavior of the response of the system (1) which, in this case, is a stochastic process (SP). In the initial value problem (IVP) (1)–(2), the damping parameter $\xi(\theta)$ and the initial conditions, $x_0(\theta)$ and $x_1(\theta)$, are assumed to be an absolutely continuous RVs defined on a complete probability space $(\Omega, \mathcal{F}, \mathbb{P})$. We are going to carry out the analysis of the randomization of IVP (1)–(2) in the time domain and in the frequency domain. The corresponding random IVP is

$$\begin{cases} \ddot{x}(t,\theta) + 2\xi(\theta)\omega_0\dot{x}(t,\theta) + \omega_0^2 x(t,\theta) = \dfrac{f(t)}{m}, \\ x(0,\theta) = x_0(\theta), \qquad \dot{x}(0,\theta) = x_1(\theta). \end{cases} \tag{3}$$

It is important to note at this point that, in most structural and mechanical vibration problems, values of the parameter ξ smaller than 0.05 are needed. Furthermore, in some particular cases, such as those for which the energy of the input is located at frequencies lower than the natural frequency, if $\xi \geq 2^{-1/2}$, the power spectral density of the response $S_{XX}(\omega)$, if it exists, simply decays monotonically from $S_{XX}(0)$, see [2]. Thus, in this paper we assume the following domain to the random damping coefficient $\mathcal{D}(\xi(\theta)) = [0, 1)$ and the system described in the IVP (3) is an underdamped system with probability one (w.p.1). Regarding the distribution of the initial conditions, no restrictions are assumed. In addition, for sake of generality, we assume that all RVs are dependent with a known joint PDF $f_{x_0,x_1,\xi}(x_0, x_1, \xi)$.

As previously indicated, under some considerations the first PDF of the response function can be calculated in both the time and frequency domain using the PTM method. We will now show what happens in the particular case where the force is periodic and of the form $f(t) = F_0 \sin(\phi t)$. We choose the following distributions for the random parameters which, for sake of simplicity in the calculations, will be assumed independent:

- The initial conditions $x_0(\theta)$ and $x_1(\theta)$ have an Uniform distribution in the interval $[1 - 10^{-10}, 1 + 10^{-10}]$, i.e., $x_i(\theta) \sim \mathrm{U}([1 - 10^{-10}, 1 + 10^{-10}])$, $i = 1, 2$.
- We compare different scenarios to the parameter $\xi(\theta)$ depending on the proportion of variability respect to the mean, p. We consider that the random parameter $\xi(\theta)$ follows an Uniform distribution in a given interval, i.e., $\xi(\theta) \sim \mathrm{U}([\xi_0(1-p), \xi_0(1+p)])$ with $\xi_0 = 0.02$ and $p \in \{0.05, 0.3, 0.5\}$.

Regarding the deterministic parameters, the undamped angular frequency is $\omega_0 = 46.13$ rad/s, the force $f(t) = 200\sin(t)$ and the mass $m = 36\,000$ kg.

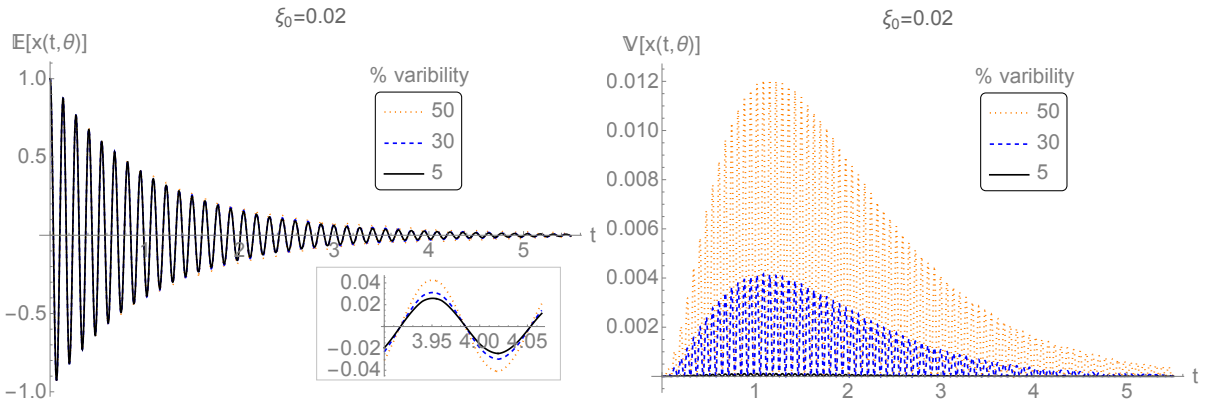

Figure 1: Mean (left) and variance (right) of the response of the system (3), $x(t,\theta)$, when the damping parameter has a fixed mean $\xi_0 = 0.02$, and to different values of the percentage of variability, $p \in \{0.05, 0.3, 0.5\}$.

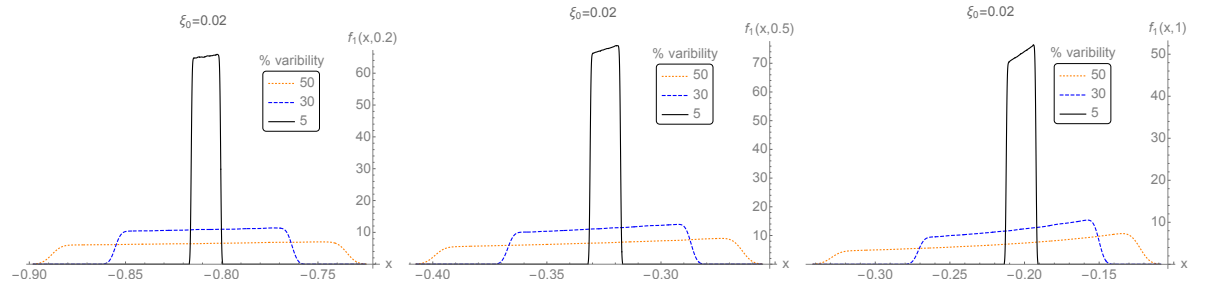

Figure 2: 1-PDF of the response of the system $x(t,\theta)$, $f_1(x,t)$, when the damping parameter has a fixed mean $\xi_0 = 0.02$ comparing different values of the percentage of variability, $p \in \{0.05, 0.3, 0.5\}$ at the time instants $t \in \{0.2, 0.5, 1\}$ (left, center and right, respectively).

In Fig. 1 mean and variance of the response of the system (3), $x(t,\theta)$, have been plotted when the mean of the damping parameter has is $\xi_0 = 0.02$, and to different values of the variability $p \in \{0.05, 0.3, 0.5\}$. From these graphical representations, it can be appreciated that the damping has a significant effect on the variance of the response. In particular, in Fig. 1 it can be noted a significant difference in the mean and in the variance of the system response for the higher percentage of the variability of the damping parameter ($p = 0.5$). Moreover, in Fig. 2 the 1-PDF of the response of the system at the time instants $t \in \{0.2, 0.5, 0.7\}$ has been plotted. From these graphs it is possible to appreciate the non-linear relation between the input random parameter and the response of the system. Therefore the choice of using a stochastic tool, as the PTM, that allows the definition of the PDF of the output functions system, is certainly recommended because the first two order statistics are not sufficient to describe the output probabilistically.

3 Conclusions and Future work

The linear dynamic analysis of a harmonic oscillator with uncertain damping parameter subjected to deterministic excitation has been investigated. The obtained results give interesting food for thought for a design engineer. It can be observed that the role of random damping plays a significant effect on the response functions. That is, the uncertainty in the damping coefficient has a significant influence on system response. Therefore, the main conclusion from this study is that for dynamic analysis of systems, a design engineer should be taken into consideration the possibility to do a stochastic analysis instead of a deterministic one especially for systems characterized by a low value of damping. Finally, in the authors' opinion, cause a non-linear relation between the random input and the output of the system occurs, a complete stochastic characterization of the response in terms of PDF is recommended, and the use of the PTM confirms again how the stochastic method is an adequate and competitive tool for the probabilistic characterization of the structural response.

Acknowledgments

This work has been supported by the grant PID2020–115270GB–I00 funded by MCIN/AEI/10.13039/501100011033 and the grant AICO/2021/302 (Generalitat Valenciana). Ana Navarro Quiles acknowledges the Conselleria de Innovación, Universidades, Ciencia y Sociedad Digital of the Generalitat Valenciana for its contribution through the grant BEST/2021/143.

References

[1] L. Lutes, S. Sarkani, *Random Vibrations: Analysis of Structural and Mechanical Systems*, Elsevier, Oxford, 2004.

[2] M. Gitterman, Classical harmonic oscillator with multiplicative noise, Phys. A352 **(2-4)** (2005) 309–334.

[3] A. Kareem, K. Gurley, Damping in structures: its evaluation and treatment of uncertainty, J. Wind Eng. Ind. Aerodyn. **59 (2-3)** (1996) 131–157.

[4] T.T. Soong, *Random Differential Equations in Science and Engineering*, AcademicPress, New York, 1973.

International Conference on Mathematical Analysis and Applications in Science and Engineering
ICMA^{2}SC'22
ISEP Porto-Portugal, June 27 - 29, 2022

INITIAL-BOUNDARY VALUE PROBLEM FOR HYPERBOLIC EQUATION WITH PIECEWISE-CONSTANT ARGUMENT OF GENERALIZED TYPE

Anar Assanova[1⋆]

[1] Institute of Mathematics and Mathematical Modeling, Kazakhstan

[1⋆]anartasan@gmail.com

Abstract: Initial-boundary value problem for system of hyperbolic equations with piecewise-constant argument of generalized type is considered. The domain is divided into N parts, the values of a solution at the interior lines of the subdomains are considered as additional functional parameters, and the initial-boundary value problem for system of hyperbolic equations with piecewise-constant argument of generalized type is reduced to an equivalent problem for system of hyperbolic equations with parameters on the subdomains. Based on the solution these problems, and continuity conditions of a partial derivative of solution at the interior lines of the partition, the system of linear functional equations with respect to parameters is composed. Methods for solving initial-boundary value problem for system of hyperbolic equation with piecewise-constant argument of generalized type are proposed, which are based on the solving of the equivalent problem.

keywords: Initial-boundary value problem; hyperbolic equations with piecewise-constant argument of generalized type; solvability.

MSC2020: 35L53, 35R05, 34A12, 35Q92.

1 Introduction

On the domain $\Omega = [0, T] \times [0, \omega]$ we consider a system of hyperbolic equations with piecewise-constant argument of generalized type in the following form

$$\frac{\partial^2 u}{\partial t \partial x} = A(t,x)\frac{\partial u}{\partial x} + B(t,x)\frac{\partial u}{\partial t} + C(t,x)u(t,x) + f(t,x) + \\ + A_0(t,x)\frac{\partial u(\gamma(t),x)}{\partial x} + B_0(t,x)\frac{\partial u(\gamma(t),x)}{\partial t} + C_0(t,x)u(\gamma(t),x), \qquad (1)$$

where $u(t,x) = colon(u_1(t,x), u_2(t,x), ..., u_n(t,x))$ is unknown vector function, the $n \times n$ matrices $A(t,x)$, $B(t,x)$, $C(t,x)$, $A_0(t,x)$, $B_0(t,x)$, $C_0(t,x)$ and n vector function $f(t,x)$ are continuous on Ω;

$\gamma(t) = \zeta_j \quad$ if $\quad t \in [\theta_j, \theta_{j+1}), \quad j = \overline{0, N-1}; \quad \theta_j \le \zeta_j \le \theta_{j+1} \quad$ for all $\quad j = 0, 1, ..., N-1;$

$0 = \theta_0 < \theta_1 < ... < \theta_{N-1} < \theta_N = T.$

We impose conditions on the characteristics

$$u(0,x)=\varphi(x), \qquad x\in[0,\omega], \tag{2}$$

$$u(t,0)=\psi(t), \qquad t\in[0,T], \tag{3}$$

where the n vector function $\varphi(x)$ is continuously differentiable on $[0,\omega]$, the n vector function $\psi(t)$ is continuously differentiable on $[0,T]$.

Let $C(\Omega,\mathbb{R}^n)$ be the space of continuous on Ω vector functions $u(t,x)$ with the norm

$||u||_0=\max\limits_{(t,x)\in\Omega}||u(t,x)||$, $||u(t,x)||=\max\limits_{i=\overline{1,n}}|u_i(t,x)|$.

A vector function $u(t,x)\in C(\Omega,\mathbb{R}^n)$ is a solution to problem (1)–(3) if:

(i) $u(t,x)$ has partial derivatives $\frac{\partial u(t,x)}{\partial x}\in C(\Omega,\mathbb{R}^n)$, $\frac{\partial u(t,x)}{\partial t}\in C(\Omega,\mathbb{R}^n)$;

(ii) the mixed partial derivative $\frac{\partial^2 u(t,x)}{\partial t\partial x}$ exists at each point $(t,x)\in\Omega$ with the possible exception of the points (θ_j,x), $j=\overline{0,N-1}$, for all $x\in[0,\omega]$, where the one-sided mixed partial derivatives exist;

(iii) system of hyperbolic equations (1) is satisfied for $u(t,x)$ on each subdomain $(\theta_j,\theta_{j+1})\times[0,\omega]$, $j=\overline{0,N-1}$, and it holds for the right mixed partial derivative of $u(t,x)$ at the points (θ_j,x), $j=\overline{0,N-1}$, $x\in[0,\omega]$;

(iv) boundary conditions (2), (3) are satisfied for $u(t,x)$ at the lines $t=0$, $x=0$, respectively.

Differential equations are an important tool for understanding real world problems because they mathematically represent real process. However, modeling of problems using differential equations is often not enough. This is due to the neglect of the gap effects in mathematical models, while the results of a qualitative analysis of such models may be far from reality. This question led to the need to introduce and develop the theory of differential equations with discontinuities. A special class of such equations constitute differential equations with deviating arguments that, in turn, include functional-differential equations, delay differential equations, differential equations with piecewise constant argument [1].

Differential equations with piecewise-constant argument of generalized type are introduced in the works [2]–[5]. Mathematical modeling of real processes often leads to differential equations with piecewise-constant argument of generalized type. Therefore, the questions of solvability of boundary value problems for such equations are of great importance and relevance.

In the present paper we propose a new approach for solving problem (1)–(3) based on Dzhumabaev's parameterization method [6].

2 Results and discussion

Further, we apply Dzhumabaev's parametrization method.

Denote by $\Delta_N(\omega)$ a partition of the domain Ω: $\Omega=\bigcup\limits_{r=1}^{N}[\theta_{r-1},\theta_r)\times[0,\omega]$ by lines $t=\theta_j$, $j=\overline{1,N-1}$.

Let

$C([0,\omega],\mathbb{R}^n)$ be the space of continuous on $[0,\omega]$ vector functions $\varphi(x)$ with the norm

$||\varphi||_1=\max\limits_{x\in[0,\omega]}||\varphi(x)||$;

$C(\Omega, \Delta_N(\omega), \mathbb{R}^{nN})$ be the space of functions systems $u([t], x) = (u_1(t, x), u_2(t, x), \ldots, u_N(t, x))'$, where $u_r : [\theta_{r-1}, \theta_r) \times [0, \omega] \to \mathbb{R}^n$ are continuous and have finite left-hand side limits $\lim\limits_{t \to \theta_r - 0} u_r(t, x)$ for all $r = \overline{1, N}$ and $x \in [0, \omega]$ with norm $\|u([\cdot], x)\|_2 = \max\limits_{r=\overline{1,N}} \sup\limits_{t \in [\theta_{r-1}, \theta_r)} ||u_r(t, x)||$.

Denote by $u_r(t, x)$ a restriction of function $u(t, x)$ on r-th subdomain $\Omega_r = [\theta_{r-1}, \theta_r) \times [0, \omega]$, i.e.

$$u_r(t, x) = u(t, x) \quad \text{for} \quad (t, x) \in \Omega_r, \quad r = \overline{1, N}.$$

Then the function system $u([t], x) = (u_1(t, x), u_2(t, x), \ldots, u_N(t, x))$ belongs to $C(\Omega, \Delta_N(\omega), \mathbb{R}^{nN})$, and its elements $u_r(t, x)$, $r = \overline{1, N}$, satisfy the following system of hyperbolic equations with piecewise-constant argument of generalized type

$$\frac{\partial^2 u_r}{\partial t \partial x} = A(t, x)\frac{\partial u_r}{\partial x} + B(t, x)\frac{\partial u_r}{\partial t} + C(t, x)u_r(t, x) + f(t, x) + A_0(t, x)\frac{\partial u_r(\zeta_{r-1}, x)}{\partial x} + \\ + B_0(t, x)\frac{\partial u_r(t, x)}{\partial t}\Big|_{t=\zeta_{r-1}} + C_0(t, x)u(\zeta_{r-1}, x), \qquad (t, x) \in \Omega_r, \quad r = \overline{1, N}, \quad (4)$$

and conditions

$$u_1(0, x) = \varphi(x), \qquad x \in [0, \omega], \quad (5)$$

$$u_r(t, 0) = \psi(t), \qquad t \in [\theta_{r-1}, \theta_r), \quad r = \overline{1, N}, \quad (6)$$

$$\lim_{t \to \theta_p - 0} \frac{\partial u_p(t, x)}{\partial x} = \frac{\partial u_{p+1}(\theta_p, x)}{\partial x}, \qquad p = \overline{1, N-1}, \qquad x \in [0, \omega]. \quad (7)$$

In (4) we take into account that $\gamma(t) = \zeta_j$ if $t \in [\theta_j, \theta_{j+1}), \quad j = \overline{0, N-1}$. Conditions (7) are the continuity conditions of partial derivative of function $\frac{\partial u(t,x)}{\partial x}$ at the lines $t = \theta_p$, $p = \overline{1, N-1}$.

Introduce an additional functional parameters [7]–[8] $\lambda_r(x) = u_r(\zeta_{r-1}, x)$ for all $r = \overline{1, N}$ and $x \in [0, \omega]$. Making the substitution $\widetilde{u}_r(t, x) = u_r(t, x) - \lambda_r(x)$ on every r-th subdomain Ω_r, we obtain the system of hyperbolic equations with parameters

$$\frac{\partial^2 \widetilde{u}_r}{\partial t \partial x} = A(t, x)\frac{\partial \widetilde{u}_r}{\partial x} + B(t, x)\frac{\partial \widetilde{u}_r}{\partial t} + C(t, x)\widetilde{u}_r(t, x) + f(t, x) + [A(t, x) + A_0(t, x)]\dot{\lambda}_r(x) + \\ + B_0(t, x)\frac{\partial \widetilde{u}_r(t, x)}{\partial t}\Big|_{t=\zeta_{r-1}} + [C(t, x) + C_0(t, x)\lambda_r(x), \qquad (t, x) \in \Omega_r, \quad r = \overline{1, N}, \quad (8)$$

initial conditions

$$\widetilde{u}_r(\zeta_{r-1}, x) = 0, \qquad x \in [0, \omega], \qquad r = \overline{1, N}, \quad (9)$$

$$\widetilde{u}_r(t, 0) = \psi(t) - \psi(\zeta_{r-1}), \qquad t \in [\theta_{r-1}, \theta_r), \quad r = \overline{1, N}, \quad (10)$$

boundary condition

$$\frac{\partial \widetilde{u}_1(0, x)}{\partial x} + \dot{\lambda}_1(x) = \dot{\varphi}(x), \qquad x \in [0, \omega], \quad (11)$$

and continuity conditions

$$\lim_{t \to \theta_p - 0} \frac{\partial \widetilde{u}_p(t, x)}{\partial x} + \dot{\lambda}_p(x) = \frac{\partial \widetilde{u}_{p+1}(\theta_p, x)}{\partial x} + \dot{\lambda}_{p+1}(x), \qquad p = \overline{1, N-1}, \qquad x \in [0, \omega]. \quad (12)$$

We also have initial conditions with respect to λ_r:

$$\lambda_r(0) = \psi(\zeta_{r-1}), \qquad r = \overline{1, N}. \quad (13)$$

Problem (8)–(10) is a initial-boundary value problems for system of hyperbolic equations with parameters on the subdomains Ω_r, $r = \overline{1, N}$. For any fixed $\lambda_r(x) \in C([0, \omega], \mathbb{R}^n)$ and r, the problem (8)–(10) has a unique solution $\widetilde{u}_r(t, x, \lambda_r)$, and the function system $\widetilde{u}[t, x, \lambda] = (\widetilde{u}_1(t, x, \lambda_1), \widetilde{u}_2(t, x, \lambda_2), \ldots, \widetilde{u}_N(t, x, \lambda_N))$ belongs to $C(\Omega, \Delta_N(\omega), \mathbb{R}^{nN})$. Equations (11), (12) with conditions are Cauchy problems for ordinary differential equations according to $\lambda_r(x)$.

Methods for solving initial-boundary value problem for system of hyperbolic equations with piecewise-constant argument of generalized type are proposed, which are based on the solving of problems (8)–(13).

3 Conclusions and Future work

In the paper we investigated initial-boundary value problem for system of hyperbolic equations with piecewise-constant argument of generalized type. We offered a new approach for solving this problem. We can extend this approach for study nonlocal problems for system of hyperbolic equations with piecewise-constant argument of generalized type. We also propose other method for initial-boundary value problem for system of hyperbolic equations with piecewise-constant argument of generalized type based on new general solution to the family of differential equations with piecewise-constant argument of generalized type [9].

Acknowledgments

This research is funded by the Science Committee of the Ministry of Education and Science of the Republic of Kazakhstan (Grant No. AP08855726).

References

[1] J. Wiener, *Generalized Solutions of Functional Differential Equations*. Singapore: World Scientific, 1993.

[2] M.U. Akhmet, Integral manifolds of differential equations with piecewise constant argument of generalized type, Nonlinear Analysis, **66** (2007), 367–383.

[3] M.U. Akhmet, On the reduction principle for differential equations with piecewise constant argument of generalized type, Journal of Mathematical Analysis and Applications, **336** (2007), 646–663.

[4] M.U. Akhmet, Almost periodic solutions of differential equations with piecewise constant argument of generalized type, Nonlinear Analysis: Hybrid Systems and Applications, **2** (2008), 456–467.

[5] M.U. Akhmet, Stability of differential equations with piecewise constant argument of generalized type, Nonlinear Analysis: Theory, Methods and Applications, **68** (2008), 794–803.

[6] D.S. Dzhumabayev, Criteria for the unique solvability of a linear boundary-value problem for an ordinary differential equation, U.S.S.R. Computational Mathematics and Mathematical Physics, **29**(1) (1989), 34–46.

[7] A.T. Assanova, D.S. Dzhumabaev, Well-posedness of nonlocal boundary value problems with integral condition for the system of hyperbolic equations, Journal of Mathematical Analysis and Applications, **402**(1) (2013), 167–178.

[8] A.T. Assanova, N.B. Iskakova, N.T. Orumbayeva, On the well-posedness of periodic problems for the system of hyperbolic equations with finite time delay, Mathematical Methods in the Applied Sciences, **43**(2) (2020), 881–902.

[9] A.T. Assanova, Hyperbolic equation with piecewise-constant argument of generalized type and solving boundary value problems for it, Lobachevskii Journal of Mathematics, **42**(15) (2021), 3584-3593.

International Conference on Mathematical Analysis and Applications in Science and Engineering
ICMA^{2}SC'22
ISEP Porto-Portugal, June 27 - 29, 2022

Dependence on the initial conditions of the numerical solution for the model of the flow and thermal explosion of a reactive micropolar real gas.

Angela Bašić-Šiško

University of Rijeka, Faculty of Engineering, Croatia

abasicsisko@riteh.hr

Abstract: We consider a one-dimensional model of the flow and thermal explosion of a reactive micropolar real gas. The micropolar model is an extension of the classical fluid model, where local microeffects in the continuum are taken into account. The model describes the behavior of a gas mixture during combustion, where we assume a generalized equation of state due to the extreme conditions that prevail during the reaction. In this paper we study the properties of the numerical solution of this problem, more precisely the dependence on the initial conditions. The numerical scheme we study here is based on the Faedo-Galerkin method, and we investigate its quality in terms of the smoothness of the initial functions. The method turns out to be generally valid, but suboptimal when the initial conditions are not smooth.

keywords: micropolar real gas; numerical solution; dependence on the initial conditions.

MSC2020: 76A05; 65M12; 35B30.

1 Introduction

The governing system for one-dimensional flow and thermal explosion of a reactive micropolar real gas in Lagrangian mass coordinates reads

$$\begin{aligned}
&\partial_t \rho = -\frac{1}{L}\rho^2 \partial_x v,\\
&\partial_t v = -\frac{R}{L}\partial_x(\rho^p \theta) + \frac{\lambda+2\mu}{L^2}\partial_x(\rho \partial_x v),\\
&j_I \partial_t \omega = \frac{c_0+2c_d}{L^2}\partial_x(\rho \partial_x \omega) - 4\mu_r \frac{\omega}{\rho},\\
&c_v \partial_t \theta = \frac{\kappa}{L^2}\partial_x(\rho \partial_x \theta) - \frac{R}{L}\rho^p \theta\, \partial_x v + \frac{\lambda+2\mu}{L^2}\rho(\partial_x v)^2 + \frac{c_0+2c_d}{L^2}\rho(\partial_x \omega)^2 + 4\mu_r \frac{\omega^2}{\rho} + \delta r(\rho,\theta,z),\\
&\partial_t z = \frac{\sigma}{L^2}\partial_x\left(\rho^2 \partial_x z\right) - r(\rho,\theta,z).
\end{aligned}$$

Here ρ is the mass density, v is the velocity, ω is the microrotation velocity, θ is the absolute temperature, and z is the fraction of unburned fuel. Corresponding initial conditions associated with the system are

$$\rho(x,0) = \rho_0(x),\ v(x,0) = v_0(x),\ \omega(x,0) = \omega_0(x),\ \theta(x,0) = \theta_0(x),\ z(x,0) = z_0(x).$$

We also consider the following homogeneous boundary conditions

$$v(0,t) = v(1,t) = 0,\ \omega(0,t) = \omega(1,t) = 0,\ \partial_x\theta(0,t) = \partial_x\theta(1,t) = 0,\ \partial_x z(0,t) = \partial_x z(1,t) = 0.$$

It is shown in [4] that the model has a generalized solution locally in time (in a sufficiently small time interval) if certain mild conditions apply (see [4] for details). To prove this result, a set of approximate semidiscretized initial problems was constructed using the Faedo-Galerkin method:

$$\rho^n(x,t) = L\rho_0(x)\left(L + \rho_0(x)\sum_{i=1}^{n}\zeta_i^n(t)i\pi\cos(\pi ix)\right)^{-1}, \tag{1}$$

$$v^n(x,t) = \sum_{i=1}^{n} v_i^n(t)\sin(\pi ix),\ \omega^n(x,t) = \sum_{i=1}^{n}\omega_i^n(t)\sin(\pi ix), \tag{2}$$

$$\theta^n(x,t) = \sum_{i=0}^{n}\theta_i^n(t)\cos(\pi ix),\ z^n(x,t) = \sum_{i=0}^{n} z_i^n(t)\cos(\pi ix), \tag{3}$$

$n = 1, 2, 3, \ldots$, where v_i^n, ω_i^n, θ_i^n, z_i^n, and ζ_i^n are unknown functions that satisfy the following conditions

$$\dot{v}_i^n(t) = 2\int_0^1\left[-\frac{R}{L}\partial_x((\rho^n)^p\theta^n) + \frac{\lambda+2\mu}{L^2}\partial_x(\rho^n\partial_x v^n)\right]\sin(\pi ix)dx, \tag{4}$$

$$\dot{\omega}_i^n(t) = 2\int_0^1\left[\frac{c_0+2c_d}{L^2 j_I}\partial_x(\rho^n\partial_x\omega^n) - 4\frac{\mu_r}{j_I}\frac{\omega^n}{\rho^n}\right]\sin(\pi ix)dx, \tag{5}$$

$$\begin{aligned}\dot{\theta}_j^n(t) = \lambda_j\int_0^1\Bigg[&\frac{\kappa}{L^2c_v}\partial_x(\rho^n\partial_x\theta^n) - \frac{R}{Lc_v}(\rho^n)^p\theta^n\partial_x v^n + \frac{\lambda+2\mu}{L^2c_v}\rho^n(\partial_x v^n)^2 + 4\frac{\mu_r}{c_v}\frac{(\omega^n)^2}{\rho^n}\\ &+ \frac{c_0+2c_d}{L^2c_v}\rho^n(\partial_x\omega^n)^2 + \frac{\delta}{c_v}\epsilon(\rho^n)^{m-1}(z^n)^m\exp\frac{\theta^n-1}{\epsilon\theta^n}\Bigg]\cos(\pi jx)dx,\end{aligned} \tag{6}$$

$$\dot{z}_j^n(t) = \lambda_j\int_0^1\left[\frac{\sigma}{L^2}\partial_x\left((\rho^n)^2\partial_x z^n\right) - \epsilon(\rho^n)^{m-1}(z^n)^m\exp\frac{\theta^n-1}{\epsilon\theta^n}\right]\cos(\pi jx)dx, \tag{7}$$

$$\dot{\zeta}_i^n(t) = v_i^n(t), \tag{8}$$

$$\begin{aligned}&v_i^n(0) = 2\int_0^1 v_0(x)\sin(\pi ix)dx,\quad \omega_i^n(0) = 2\int_0^1\omega_0(x)\sin(\pi ix)dx,\\ &\theta_j^n(0) = \lambda_j\int_0^1\theta_0(x)\cos(\pi ix)dx,\quad z_j^n(0) = \lambda_j\int_0^1 z_0(x)\cos(\pi ix)dx,\quad \zeta_i^n(0) = 0,\end{aligned} \tag{9}$$

for $i = 1, \ldots, n$ and $j = 0, 1, \ldots, n$, where $\lambda_0 = 1$, and $\lambda_j = 2$ for $j \geq 1$. It was shown that functions (1)–(3), whereby (4)–(9) holds, converge to a generalized solution of the observed initial-boundary value problem. The numerical scheme for solving the observed problem is obtained by fully discretizing the problem, i.e., numerically approximating the integral on the right-hand side in (4)–(7) and applying the numerical method to solve the resulting system of ordinary differential equations. In particular, we used the Gauss-Legendre quadrature formula of order 20 and an ODE solver based on the backward differentiation formula. For details see [5] where similar problem was considered.

2 Results and discussion

In this section we test the numerical method described in the previous section with respect to the smoothness of the initial conditions. In all examples, we assume the following parameter values:

$$\begin{aligned}&L = 1,\ c_d = c_0 = c_v = 1,\ R = 1,\ j_I = 1,\ \lambda = -2, \mu_r = 1,\ \mu = 3,\ \kappa = 0.024,\\ &p = 4,\ \sigma = 1,\ \delta = 1, \epsilon = 0.2,\ m = 2.\end{aligned} \tag{10}$$

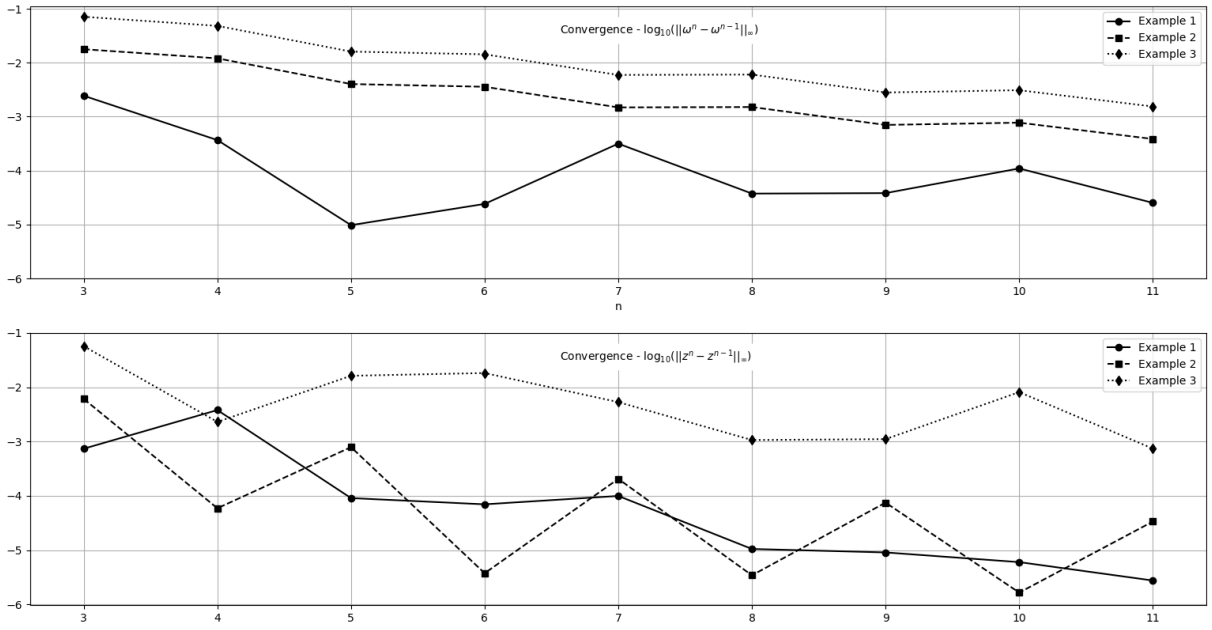

Figure 1: Convergence test

In the first example, we consider simple initial conditions where the functions have a finite Fourier series expansion:

$$\rho_0(x) = 1, \quad v_0(x) = \sin(\pi x), \quad \omega_0(x) = \sin(2\pi x), \quad \theta_0(x) = 2 + \cos(\pi x), \quad z_0(x) = 1.$$

In the second example, the initial functions are smooth but do not have a finite Fourier expansion, i.e., the corresponding coefficients are approximated numerically:

$$\rho_0(x) = 1,\ v_0(x) = x - x^2,\ \omega_0(x) = x^2 - x^4,\ \theta_0(x) = 2x^3 - 3x^2 + 2,\ z_0(x) = 2x^3 - 3x^2 + 1.$$

In the third example, the initial functions are continuous but not smooth:

$$\rho_0(x) = |x^2 - 0.25| + 1,\ v_0(x) = 0,\ \omega_0(x) = 4(x^2 - x^4),\ \theta_0(x) = 0.1,$$
$$z_0(x) = \begin{cases} 1, & x < 0.2 \\ -2x + 1.4, & 0.2 \le x \le 0.7 \\ 0, & x > 0.7 \end{cases}.$$

Figure 1 shows the result of the convergence test for all three examples for ω and z, and Table 1 contains the CPU times needed for the simulations.

3 Conclusions and Future work

From the numerical test performed, it appears that the smoothness of the initial conditions affects the convergence of the numerical method. For initial conditions that have finitely many nontrivial terms of Fourier expansion, the convergence is fastest, as expected. In the case of smooth functions, the convergence is similar in magnitude or slightly slower, but the problem of oscillations may occur. In the case of non-smooth initial conditions, the convergence is the slowest.

Based on these results we can conclude that the method works for all initial conditions, but in order to compute more accurate simulations faster, it is necessary to develop a more efficient

n	Example 1	Example 2	Example 3
3	2.38	2.72	2.74
4	3.19	3.75	5.10
5	4.93	4.13	6.71
6	5.11	5.89	6.47
7	8.12	6.62	7.79
8	8.31	8.23	11.47
9	8.87	8.62	16.44
10	9.70	9.35	18.43
11	9.64	12.90	18.00

Table 1: CPU times (s)

numerical method for the described problem. One possible improvement in terms of convergence rate and avoiding oscillation problems is to use the finite difference method as was used for a similar model in [8].

Acknowledgments

Author of this work is supported by the University of Rijeka, Croatia under the project uniri-prirod-18-118-1257 (Analysis of mathematical models of fluid mechanics and technical systems using data-driven algorithms for Koopman operator).

References

[1] G. Lukaszewicz, *Micropolar FluidsTheory and Applications (Modeling and Simulation in Science, Engineering and Technology)*. Boston: Birkhäuser, 1999.

[2] S. N. Antontsev, A. V. Kazhikhov, V. N. Monakhov, *Boundary value problems in mechanics of nonhomogeneous fluids, Studies in Mathematics and its Applications* (vol. 22). Amsterdam: North-Holland Publishing Co., 1990.

[3] M. Lewicka, P. Mucha, On temporal asymptotics for the pth power viscous reactive gas, Nonlinear Anal. **57** (2004), 951–969.

[4] A. Bašić-Šiško, I. Dražić, Local existence for viscous reactive micropolar real gas flow and thermal explosion with homogeneous boundary conditions, J. Math. Anal. Appl. **509**(2) (2022), 125988.

[5] A. Bašić-Šiško, I. Dražić, L. Simčić, One-dimensional model and numerical solution to the viscous and heat-conducting micropolar real gas flow with homogeneous boundary conditions, Math. Comput. Simulation **195**(2) (2022), 71–87.

[6] A. Bašić-Šiško, I. Dražić, Uniqueness of generalized solution to micropolar viscous real gas flow with homogeneous boundary conditions, Math. Methods Appl. Sci. **44**(6) (2021), 4330–4341.

[7] A. Bašić-Šiško, I. Dražić, Global solution to a one-dimensional model of viscous and heat-conducting micropolar real gas flow, J. Math. Anal. Appl. **495**(1) (2021), 124690.

[8] N. Črnjarić-Žic, N. Mujaković, Numerical analysis of the solutions for 1d compressible viscous micropolar fluid flow with different boundary conditions, Math. Comput. Simulation **126** (2016), 45–62.

International Conference on Mathematical Analysis and Applications in Science and Engineering
ICMA^{2}SC'22
ISEP Porto-Portugal, June 27 - 29, 2022

Godunov-Type Methods for Computing Homogeneous Mixture Flows

A. Qadi El Idrissi[1] **Eric Goncalves da Silva**[2] **Dia Zeidan**[3⋆]

[1] National School of Applied Sciences, Hassan 1st University, Morocco
[2] Institut Pprime UPR 3346 CNRS, ISAE-ENSMA, France
[3] School of Basic Sciences and Humanities, German Jordanian University, Jordan

[3⋆]dia.zeidan@gju.edu.jo

Abstract: In this paper, we present numerical simulations of the two-phase gas-liquid mixture using two finite difference methods, namely, Lax-Friedrichs and Richtmyer methods. The main objective is to evaluate the performance of such methods by comparison with an exact Riemann solver developed recently for the Riemann problem in gas-liquid mixture. Accuracy and robustness of the proposed numerical methods have been validated and good agreement found between the analytical Riemann solutions and the numerical results obtained by these numerical methods.

keywords: Lax-Friedrichs; Richtmyer; Hyperbolic system; Riemann problem

MSC2020: 35L65, 76L05, 76T10

1 Introduction

Two-phase mixture of liquid and gas flows remains a subject of many theoretical and numerical investigations. Such mixtures encountered in engineering and industrial applications such as medical, energy and petroleum industries [1, 3, 4]. The present work concerns with the interesting case of the bubbly flow constituted with small gas bubbles dispersed in liquid. In the literature, this two-phase flow has been studied extensively either numerically and/or experimentally. In most cases, the modelling is based on the Homogeneous Equilibrium Model (HEM), where the governing equations are defined by the conservation of mass and momentum. For the purpose of the current work, we assume that there is no-slip between the liquid and gas bubbles. We also assume that the two-phase mixture is isothermal with two compressible phases. This yields to express the Homogeneous Equilibrium Model as a conservative system defined by two conservations laws for mass, and a conservation law for the mixture momentum. We aim by this study to evaluate the performance of the Richtmyer and Lax-Friedrichs methods by comparing their numerical computations with the analytical solution of the Riemann problem for a bubbly flow dealing with small gas bubbles dispersed in liquid. As known, the solution of this theoretical problem is a collocation of elementary waves such as rarefaction waves, shock waves and contact discontinuities. Finally, validations are performed by considering the four cases of the Riemann solution involving the rarefaction, contact discontinuity and shock waves.

2 Governing Equations

We investigate a compressible two-phase flow consisting of small gas bubbles dispersed in liquid, and moving in an elastic pipe. To model this two-phase flow mixture, we propose the Homogeneous Equilibrium Mixture Model defined by [2]:

Conservation of mass

$$\frac{\partial}{\partial t}(A\rho_g\alpha) + \frac{\partial}{\partial x}(A\rho_g\alpha u) = 0, \tag{1}$$

$$\frac{\partial}{\partial t}(A\rho_l(1-\alpha)) + \frac{\partial}{\partial x}(A\rho_l(1-\alpha)u) = 0, \tag{2}$$

where ρ_k, α, u and A denote, respectively, the density of phase k (g, l), the volume fraction of the gas, the velocity of both phases and the pipe cross-sectional area.

Conservation of momentum for the mixture

$$\frac{\partial}{\partial t}(A\rho u) + \frac{\partial}{\partial x}(A\rho u^2) + A\frac{\partial p}{\partial x} = AT^w - A\,\rho\, g\, \sin\theta, \tag{3}$$

in which ρ, p, T^w, g and θ are the density of the mixture, the common pressure of gas and liquid phases, the term of friction on the pipe wall, the gravitational acceleration and the angle of inclination of the pipe, respectively. Further, these are defined as:

Mixture density: $\rho = \rho_g\alpha + \rho_l(1-\alpha)$.

Equilibrium of pressures: $p_g = p_l = p$, where p_k is the pressure of the phase k =g,l.

Compressibility of phases: $\frac{1}{\rho_k}\frac{d\rho_k}{dp} = \frac{1}{K_k}$, where K_k is the bulk modulus of the phase k.

Cross-sectional area: $\frac{1}{A}\frac{dA}{dp} = \frac{D}{eK}$. e, K and D stands for the thickness of the pipe wall, the Young's modulus for the pipe material and the circle pipe diameter, respectively.

Viscous stress: $T^w = -\frac{1}{2}\lambda\rho_l\frac{u|u|}{D}$, with λ is the friction coefficient.
For the purpose of this paper, the compressibility of gas and liquid is taken as:

$$K_g = p \quad \text{and} \quad K_l = \text{Constant},$$

which yields to $\rho_g(p) = \frac{p}{a^2}$ and $\rho_l(p) = \rho_{l,0}e^{(p-p_0)/K_l}$ with the following cross-sectional found as a function of the pressure:

$$A(p) = \frac{A_0}{\left(1 - \frac{D_0}{2eK}(p-p_0)\right)^2}.$$

Further details about the mathematical nature and physical parameters are not stated here due to space limitation. For additional information, please see [2].

3 Numerical Experiment and Discussion

In this section, we describe the Lax-Friedrichs and Richtmyer methods, two numerical methods widely used in the simulation of the hyperbolic systems of conservative laws related to single-phase flows. The advantage of these numerical methods is the simple formulation of their numerical flux and also, the low cost of their computations compared to finite volume methods. It is well-known that the Lax-Friedrichs scheme is very dissipative and Richtmyer scheme is known as dispersive. Yet, within such small dissipation in their behaviour they remain to be high frequency when one investigate bubbly flows.

Lax-Friedrichs scheme: is an explicit, first order scheme defined as

$$\mathcal{W}_j^{n+1} = \mathcal{W}_j^n - \frac{\Delta t}{\Delta x}\Big(F_{j+1/2}^n - F_{j-1/2}^n\Big),$$

where

$$F_{j+1/2}^n = \frac{1}{2}\Big(F(\mathcal{W}_j^n + F(\mathcal{W}_{j+1}^n))\Big) - \frac{\Delta t}{2\Delta x}\Big(\mathcal{W}_{j+1}^n - \mathcal{W}_j^n\Big),$$

together with the stability of this scheme holds if $\frac{\Delta t}{\Delta x} max|\lambda_j| < 1$, where λ_j denotes the wave speed [2].

Richtmyer scheme: is an explicit predictor-corrector scheme of second-order defined by the following steps

Step 1. Predictor: $\mathcal{W}_j^* = \frac{1}{2}\Big(\mathcal{W}_j^n + \mathcal{W}_{j+1}^n\Big) - \frac{\Delta t}{2\Delta x}\Big(F(\mathcal{W}_{j+1}^n) - F(\mathcal{W}_j^n)\Big)$.

Step 2. Corrector: $\mathcal{W}_j^{n+1} = \mathcal{W}_j^n - \frac{\Delta t}{\Delta x}\Big(F(\mathcal{W}_j^*) - F(\mathcal{W}_{j-1}^*)\Big)$, where the stability holds if $\frac{\Delta t}{\Delta x} max|\lambda_j| < \frac{1}{2}$. See [5] for both methods.

Further, we present the numerical resolution for the Riemann problem related to two-phase mixture composed of liquid and small air bubbles. To evaluate the performance of the proposed numerical methods, a comparative study is carried out between the numerical results obtained by the Richtmyer and Lax-Friedrichs schemes and those obtained analytically for the Riemann problem. Figure 1 depicts the transient evolution of the pressure corresponding to the four cases of the Riemann solution. These solutions include three wave functions defined by the rarefaction, contact discontinuity and shock waves. For all the computations, the distance increment is taken to be $\Delta x = L/600$, L =295m being the pipe length. The time increment is evaluated at each iteration through the CFL criterion. As illustrated by figure 1, the numerical simulations reproduce accurately the exact Riemann solution. In addition to that, the comparison between theoretical and numerical results indicates a good agreement with the analytical solutions of the rarefaction and shock waves. We observe that the Richtmyer scheme gives a better simulation compared to the Lax-Friedrichs scheme. Despite its good agreement, the Richtmyer scheme appears to be highly oscillatory due to its dispersive property of second order accurate.

4 Conclusions and Future work

The robustness and accuracy of the proposed numerical methods have been clearly demonstrated by the different comparisons made between the numerical results and those provided analytically for the Riemann problem. The simulation also indicates that the Richtmyer scheme is the most accurate and efficient numerical method compared to the Lax-Friedrich scheme. The perspective

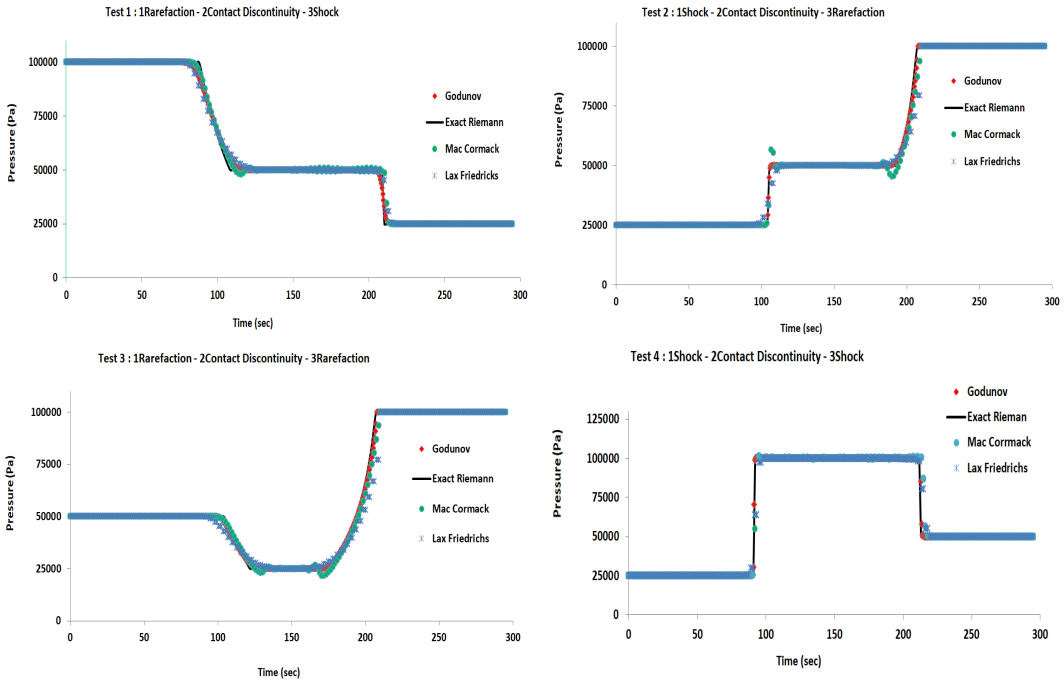

Figure 1: Comparison between Exact Riemann solver and Numerical Resolutions at time $t = 0.065$

of this work is the extension of the numerical schemes for the case of two-dimensional two-phase mixture and the resolution of the spurious oscillations by considering exact or approximate Riemann solvers.

Acknowledgments The authors gratefully acknowledge the support provided by the University Hassan 1, Morocco, Institut Pprime UPR 3346 CNRS, ISAE-ENSMA, France, and the German Jordanian University, Amman, Jordan.

References

[1] S. Ouffa, D. Zeidan, D. Seba. The WAF scheme for the isentropic drift-flux model of compressible two-phase flows. Journal of Computers and Fluids, **229** (2021), 105091.

[2] A. Qadi El Idrissi. Exact Riemann Solver for a nonlinear hyperbolic system of equations modelling a compressible two-phase flow in pipes. Journal of Mathematical Analysis and Applications, **505**(1) (2022), 125580.

[3] A. Qadi el Idrissi, B. Achchab, A. Agouzal. Numerical simulations for non conservative hyperbolic system. Application to transient two-phase flow with cavitation phenomenon. Journal of Mathematical Modelling and Analysis, **24**(2) (2019), 218-235.

[4] D. Zeidan, E. Romenski, Arezki Slaouti, E. F. Toro. Numerical study of wave propagation in compressible two-phase flow. International journal for numerical methods in fluids. Vol. 54(4)(2007),393-417.

[5] E. F. Toro. Riemann solvers and numerical methods for fluid dynamics, 2nd edition, New York: Springer, 1999.

International Conference on Mathematical Analysis and Applications in Science and Engineering
ICMA^{2}SC'22
ISEP Porto-Portugal, June 27 - 29, 2022

Probabilistic analysis of a cantilever beam with random parameters via probability density functions

J.-C. Cortés[1] **E. López-Navarro**[1⋆] **J.-V. Romero**[1] **M.-D. Roselló**[1]

[1] Instituto Universitario de Matemática Multidisciplinar,
Universitat Politècnica de València, València, Spain

[1⋆]ellona1@doctor.upv.es

Abstract: The aim of this contribution is to perform a probabilistic analysis of the deflection of a cantilever beam by means of a full randomization of the classical governing fourth-order differential equation with boundary conditions. The probabilistic study is based on the calculation of the first probability density function, via the Random Variable Transformation method, of the solution stochastic process as well as the density function of further quantities of interest associated with this engineering problem such as the maximum slope and deflection at the free end of the cantilever beam, which are treated as random variables.

keywords: Random Variable Transformation method; Cantilever beam; Probability density function; Maximum deflection; Maximum slope.

This abstract is included in **Syposium #12: Advances in Differential Equations with Uncertainties and Modeling.**

1 Introduction

In this contribution we deal with the stochastic analysis of the deflection experienced by a load-carrying beam. It is well-known that this phenomenon can be mathematically described by means of the following fourth-order differential equation [1]

$$\frac{\mathrm{d}^4 Y(x)}{\mathrm{d}x^4} = \frac{W(x)}{EI}, \quad 0 < x < l, \tag{1}$$

where $Y(x)$ represents the deflection curve of the beam, E is the Young's modulus of elasticity of the material of the beam, I denotes the moment of inertia of the cross section of the beam around a horizontal line through the centroid of the cross section, l is the length of the beam and $W(x)$ represents the density of downward force acting vertically on the beam at the space point x, which can be interpreted as load per unit length acting on the beam. For the latter, we will assume that $W(x)$ consists of two different loads, represented by W_0 and W_1, that occupy the same space on the beam, i.e.

$$W(x) = W_0 \left(\mathcal{U}(x) - \mathcal{U}(x - l/2)\right) + W_1 \left(\mathcal{U}(x - l/2) - \mathcal{U}(x - l)\right), \tag{2}$$

where $\mathcal{U}(\cdot)$ is the unitary Heaviside function.

Depending on the type of beam, we will have different boundary conditions. The case we are going to study is a cantilever beam (a beam firmly fastened at the origin, $x = 0$, but with no support at the end, $x = l$). In Fig. 1 we show a graphical scheme of the model. Therefore, hereinafter the following boundary conditions will be assumed

$$Y(0) = 0, \;\; Y'(0) = 0, \;\; Y''(l) = 0, \;\; Y'''(l) = 0. \tag{3}$$

Due to the heterogeneity of the material, the mathematical nature of the Young's modulus is random rather than deterministic as it has been reported in different investigations [3, 4]. Additionally, in practice the value of $W(x)$ on the whole spatial domain is approximated via measurements, so containing epistemic errors. All these considerations lead to rigorously treat (1) as a random differential equation. We are going to consider E an absolutely continuous random variable and $W(x)$ represents two uniform loads characterized by two independent random variables.

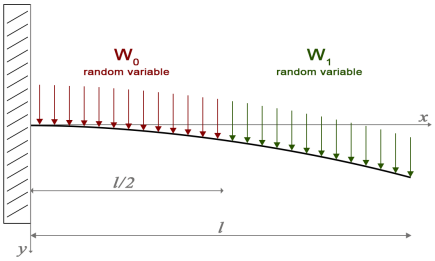

Figure 1: Cantilever beam with two loads modelled via random variables.

Under our approach, the solution of the randomized boundary problem (1)–(3) is a stochastic process, $Y(x)$, and our goal will be to determine the so-called first probability density function (1-p.d.f.) of the solution, $f_{Y(x)}(y)$, taking advantage of the Random Variable Transformation (RVT) technique (see [2, page 25]). The calculation of this function is of great usefulness from a practical standpoint since it permits determining all the one-dimensional moments and the probability that the solution lies on a certain interval of specific interest. We will also obtain the p.d.f. of other quantities of interest, such as the maximum deflexion and the maximum slope at the free end of the beam, since these quantities are of major interest when analyzing and designing cantilever beams in civil engineering.

In the stochastic analysis of civil engineering structures this information is of paramount importance since it permits evaluating the probability of breaking of a structure (like a bridge, a balcony, a crane, etc.) that is carrying on distributed or uniform forces. Indeed, this is done by calculating the probablity that the deflection of a beam lies within a certain *safety* interval.

2 Results and discussion

In order to obtain the 1-p.d.f., $f_{Y(x)}(y)$, taking advantage of the RVT technique (see [2, page 25]), we first need to explicitly calculate the stochastic solution of Eq. (1). To this end several techniques can be applied, here we shall apply the Laplace transform because of the well-known advantages of this integral transform. Then, the solution stochastic process, $Y(x)$, of model (1)–(3) is given by

$$Y(x)=\begin{cases}\dfrac{l^2W_0+3l^2W_1}{16EI}x^2-\dfrac{lW_0+lW_1}{12EI}x^3+\dfrac{W_0}{24EI}x^4, & 0<x\leq l/2,\\ \dfrac{l^2W_0+3l^2W_1}{16EI}x^2-\dfrac{lW_0+lW_1}{12EI}x^3+\dfrac{W_0}{24EI}x^4+\dfrac{W_1-W_0}{384EI}(l-2x)^4, & l/2<x\leq l,\end{cases} \tag{4}$$

Notice that the solution $Y(x)$ is differentiable, hence continuous at $x=l/2$, which is interesting from an engineering standpoint, since informs us that the deflection varies smoothly at the spatial point, $x=l/2$, where the load changes.

As $Y(x)$ is a piecewise function, the calculation of the 1-p.d.f. of $Y(x)$ will be done separately in the two subdomains $0<x\leq l/2$ and $l/2<x\leq l$. Then, applying the RVT method and expressing the obtained 1-p.d.f. in terms of the expectation operator w.r.t. random variables (W_0,W_1), the 1-p.d.f. for $0<x<l/2$ is given by

$$\begin{aligned}f_{Y(x)}(y) &= \mathbb{E}_{W_0,W_1}\left[f_E\left(\frac{1}{48yI}\left(3l^2W_0x^2+9l^2W_1x^2-4lW_0x^3-4lW_1x^3+2W_0x^4\right)\right)\right.\\ &\left.\cdot\frac{1}{48y^2I}\left|\left(3l^2W_0x^2+9l^2W_1x^2-4lW_0x^3-4lW_1x^3+2W_0x^4\right)\right|\right],\quad 0<x\leq l/2,\end{aligned} \tag{5}$$

and the 1-p.d.f. on the second piece of the domain $l/2 < x \leq l$ is given by,

$$f_{Y(x)}(y) = \mathbb{E}_{W_0,W_1}\left[f_E\left(\frac{1}{384yI}\left(-l^4(W_0-W_1)+8l^3(W_0-W_1)x+96l^2W_1x^2-64lW_1x^3+16W_1x^4\right)\right)\right.$$
$$\left.\cdot\frac{1}{384y^2I}\left|\left(-l^4(W_0-W_1)+8l^3(W_0-W_1)x+96l^2W_1x^2-64lW_1x^3+16W_1x^4\right)\right|\right]. \tag{6}$$

The maximum slope, Θ, and the maximum deflection, Δ, in a cantilever beam represent key information to account for safety and control measures [1] . In the case of a cantilever beam, it is clear they are calculated at the free end of the beam, i.e., $x = l$. It is easy to check that they are given by the following expressions

$$\Theta = Y'(l) = \frac{l^3}{48EI}\left(W_0+7W_1\right), \quad \Delta = Y(l) = \frac{l^4}{384EI}\left(7W_0+41W_1\right). \tag{7}$$

In our context, Θ and Δ are random variables, whose respective p.d.f.'s, $f_\Theta(\theta)$ and $f_\Delta(\delta)$, provide important information about its probabilistic behaviour. The RVT technique permits explicitly calculating them

$$f_\Theta(\theta) = \frac{l^3}{48\theta^2 I}\mathbb{E}_{W_0,W_1}\left[f_E\left(\frac{l^3}{48\theta I}\left(W_0+7W_1\right)\right)\left(W_0+7W_1\right)\right], \tag{8}$$

and

$$f_\Delta(\delta) = \frac{l^4}{384\delta^2 I}\mathbb{E}_{W_0,W_1}\left[f_E\left(\frac{l^4}{384\delta I}\left(7W_0+41W_1\right)\right)\left(7W_0+41W_1\right)\right]. \tag{9}$$

We point out that the results derived throughout this section can be extended, using the same reasoning, to a finite number of loads including the case that the loads occupy different lengths on the beam.

Example 1 *We take the following data for the deterministic parameters of the model* (1)*:* $l = 10$ *m and* $I = 722$ *cm*^{4}*, while for the random parameters, we will assume that the Young's modulus of elasticity,* E*, has a Gaussian distribution with mean* $210 \cdot 10^9$ Pa *(Pascals) and variance* $420 \cdot 10^7$ Pa^2*, i.e.* $E \sim \mathrm{N}(210 \cdot 10^9; 420 \cdot 10^7)$*. We assume that the loads are defined by random variables whose distributions are Gaussian,* $W_0 \sim \mathrm{N}\left(\mu_{W_0} = 40; \sigma^2_{W_0} = 0.4\right)$ *and* $W_1 \sim \mathrm{N}\left(\mu_{W_1} = 20; \sigma^2_{W_1} = 0.2\right)$*.*

Fig. 2 shows the graphical representation of the 1-p.d.f. given by expressions (5) *and* (6) *at different spatial points* $x \in \{1, ..., 10\}$*. As it is expected, we can observe that the variance increases as* x *does.*

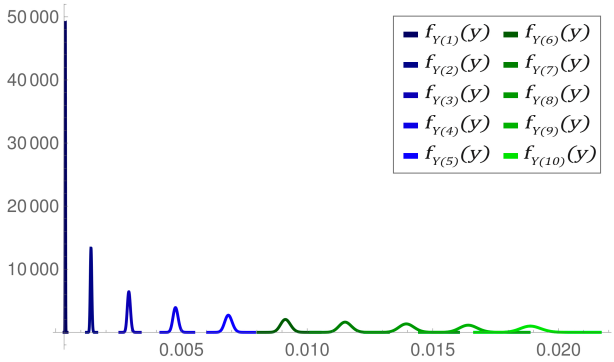

Figure 2: 1-p.d.f., $f_{Y(x)}(y)$, of the solution stochastic process (4), computed by (5) and (6), at different spatial points $x \in \{1, ..., 10\}$. Example 1.

In Table 1, we include the numerical results for the mean and the standard deviation of random variables Θ *and* Δ *obtained from expressions* (8) *and* (9)*.*

	Mean	Standard deviation
Slope at free end	0.0024742	0.00005343
Max. deflection	0.0189006	0.00040673

Table 1: Mean and standard deviation of the maximum slope and the maximum deflection of $Y(x)$ at the free end of the beam. Example 1.

3 Conclusions and Future work

Throughout the paper, we have studied, from a probabilistic standpoint, a foundational model to describe the deflection of a cantilever beam subject to two uniform loads characterized by two independent random variables. Our analysis has several advantages, first, it permits computing not only the mean and the standard deviation of deflection, but its probability density function that provides a fuller description. Besides, we have probabilistically characterized, via the corresponding densities, important quantities of interest as the slope and maximum deflection of the cantilever beam under mild hypotheses. We think that this approach can be promising to deal with, in future works, the stochastic analysis of the deflection of other kinds of beams than cantilevers and using different loads functions.

Acknowledgments

This work has been supported by the grant PID2020-115270GB-I00 funded by MCIN/AEI/ 10.13039/501100011033 and the grant AICO/2021/302 (Generalitat Valenciana) and the European Union through the Operational Program of the European Regional Development Fund (ERDF)/European Social Fund (ESF) of the Valencian Community 20142020, grant EDGJID/ 2021/185.

References

[1] A. Öchsner, *Classical Beam Theories of Structural Mechanics*. Springer, 2021.

[2] T. Soong, *Random Differential Equations in Science and Engineering*. New York: Academic Press, 1973.

[3] H. Khakurel, M.F.N. Taufique, A. Roy, G. Balasubramanian, G. Ouyang, J. Cui, D.D. Johnson, R. Devanathan, Machine learning assisted prediction of the Young's modulus of compositionally complex alloys, Scientific Reports, **11(1)** (2021).

[4] C. Soyarslan, M. Pradas, S.Bargmann, Effective elastic properties of 3d stochastic bicontinuous composites. Mechanics of Materials, **137** (2019), 103098.

International Conference on Mathematical Analysis and Applications in Science and Engineering
ICMA^{2}SC'22
ISEP Porto-Portugal, June 27 - 29, 2022

On the semilinear damped wave equations in Friedmann-Lemaître-Robertson-Walker spacetime

Jorge Marques[1,2] **Marcelo Ebert**[3]

[1] Faculty of Economics (FEUC), University of Coimbra, Portugal
[2] Centre for Business and Economics Research (CeBER), University of Coimbra, Portugal
[3] Department of Computing and Mathematics, University of São Paulo, Brazil

[1,2]jmarques@fe.uc.pt
[3]ebert@ffclrp.usp.br

Abstract: We study the Cauchy problem for the semilinear massless wave equation:

$$u_{tt}(t,x) - (1+t)^{-2\ell}\Delta u(t,x) + \frac{\beta}{1+t}u_t(t,x) = |u|^p$$

with $0 < \ell < 1$, $\beta > 0$ and $p > 1$, in FLRW spacetime. The solution u^0 of the corresponding linear Cauchy problem will be represented in the explicit form using Fourier multipliers operators with multipliers expressed in terms of special functions. Our main goal is to prove global (in time) existence of solutions in the case of decelerating expansion universe with small initial data belongs to $L^1(\mathbf{R}^n) \cap H^{k-1}(\mathbf{R}^n)$, $k \geq 1$. We are focused in finding the critical exponent of Fujita type: $p_c(n,\ell) = 1 + \frac{2}{n(1-\ell)}$. It means that, if $1 < p \leq p_c(n,\ell)$ there exist small data for which u blow-up in finite time while if $p > p_c(n,\ell)$ the global solution has the same long time behavior of u^0. We derive optimal $L^p - L^q$ estimates of u^0 and then we use Duhamel's principle to prove our results.

keywords: semilinear evolution equations, critical exponent, global existence, small data solutions

MSC2020: 35A01, 35B33, 35L05, 35L71

1 Introduction

We prove the global (in time) existence of small data solutions to the Cauchy problem for the semilinear wave equation with scale-invariant damping and decreasing in time propagation speed

$$\begin{cases} u_{tt}(t,x) - (1+t)^{-2\ell}\Delta u(t,x) + \frac{\beta}{1+t}u_t(t,x) = f(u(t,x)), & t \geq 0,\ x \in \mathbf{R}^n, \\ u(0,x) = 0 = u_0(x), & x \in \mathbf{R}^n, \\ u_t(0,x) = u_1(x), & x \in \mathbf{R}^n, \end{cases} \tag{1}$$

with $\ell \in (0,1)$, $\beta > 0$ and $f(u) = |u|^p$ for some $p > 1$ or, more in general, f satisfying the following local Lipschitz-type condition

$$|f(u) - f(v)| \leq C\,|u-v|\left(|u|^{p-1} + |v|^{p-1}\right). \tag{2}$$

We consider that this wave equation is represented in the family of FLRW spacetime, which is endowed with a metric written in the form

$$ds^2 = -dt^2 + \alpha^2(t)(dx_1^2 + \ldots + dx_n^2)$$

with an appropriate scale factor $\alpha(t)$. If $\frac{d}{dt}\alpha(t) > 0$ and $\frac{d^2}{dt^2}\alpha(t) < 0$ we can say that the universe is in decelerating expansion. Our model (1) is derived from $\alpha(t) = (1+t)^\ell$ with $\ell = \frac{2}{\gamma n}$ satisfying $\frac{2}{n} < \gamma \leq 2$, $n \geq 2$ (see [5]). We also have $\alpha(t) = (1+t)^{2/3}$ for the Einstein- de Sitter 4-dimensional spacetime, so that it is well known as a particular case of FLRW spacetime in a decelerating expansion universe model. Moreover, the case in which $\beta = 2$, $n = 3$ and $\ell = \frac{2}{3}$ in (1) it is called the covariant massless field in the Einstein- de Sitter spacetime with non-singular (at $t = 0$) coefficients (see [4]).

2 Results

Before stating our results, let us introduce a suitable notion of weak solution to the Cauchy problem (1).

Definition 1 *We say that $u \in \mathcal{C}([0,\infty), L^q)$, is a weak solution to (1) with $f(u) = |u|^p$ if, for any test functions $\psi \in \mathcal{C}_c^\infty([0,\infty))$ and $\varphi \in \mathcal{C}_c^\infty(\mathbf{R}^n)$, the following equality holds true:*

$$\begin{aligned} &\int_0^\infty \int_{\mathbf{R}^n} |u(t,x)|^p \, \psi(t)\, \varphi(x)\, dx\, dt + \psi(0) \int_{\mathbf{R}^n} u_1(x)\, \varphi(x)\, dx \\ &\quad = \int_0^\infty \int_{\mathbf{R}^n} u(t,x) \big(\partial_t^2 - (1+t)^{-2\ell}\Delta - \frac{\beta}{1+t}\partial_t + \frac{\beta}{(1+t)^2}\big)\psi(t)\varphi(x)\, dx\, dt. \end{aligned} \tag{3}$$

Indeed, if u is a smooth solution to (1), then (3) follows integrating by parts.
Let

$$p_c(n,\ell) \doteq p_F(n(1-\ell)) = 1 + \frac{2}{n(1-\ell)} \tag{4}$$

the critical exponent of Fujita type. In the next theorems, due to the fact that $p_c(n,\ell) \to \infty$ as $\ell \to 1$, the choice of the spaces of solutions is related to fixed ranges for $\ell \in [0,1)$ and the space dimensions $n \geq 2$. In theorems 2 and 3 we restrict our analysis to the case of small values for β, whereas the simple case of large values for β is treated in Theorem 1.

Theorem 1 *Let $\ell \in \big(1 - \frac{2}{n}, 1\big)$ for $n \geq 2$ and $k \doteq 1 + \frac{n\ell}{2}$.*
If $\beta \geq 2 - \ell + n(1-\ell)(1+\ell)$ and $p > \max\{p_c(n,\ell), k\}$, with $p_c(n,\ell)$ given by (4), then there exists $\delta > 0$ such that for any initial data

$$u_1 \in \mathcal{D} = H^{k-1}(\mathbf{R}^n) \cap L^1(\mathbf{R}^n), \qquad ||u_1||_{\mathcal{D}} \leq \delta,$$

there exists a unique weak solution $u \in C([0,\infty), H^k(\mathbf{R}^n))$ to (1), which satisfies the following estimates

$$||u(t,\cdot)||_{L^2} \lesssim (1+t)^{\frac{n}{2}(\ell-1)} ||u_1||_{\mathcal{D}}; \tag{5}$$

and

$$||u(t,\cdot)||_{\dot{H}^k} \lesssim ||u_1||_{\mathcal{D}} \begin{cases} (1+t)^{(\ell-1)\left(\frac{n}{2}+k\right)}, & \beta > \ell + n(1-\ell) + 2k(1-\ell) \\ (1+t)^{\frac{\ell-\beta}{2}} (\ln(e+t))^{\frac{1}{2}}, & \beta = \ell + n(1-\ell) + 2k(1-\ell). \end{cases} \tag{6}$$

Theorem 2 *Let $\ell \in \left(1-\frac{2}{n}, \frac{2}{n}\right)$ for $n=2,3$ or $\ell=\frac{2}{3}$ for $n=3$. If $\ell + n(1-\ell)(1+\ell) \leq \beta < 2-\ell+n(1-\ell)(1+\ell)$ and $p > p_c(n,\ell)$, with $p_c(n,\ell)$ given by (4), then there exists $\delta > 0$ such that for any initial data*

$$u_1 \in \mathcal{D} = H^{k-1}(\mathbf{R}^n) \cap L^1(\mathbf{R}^n), \qquad ||u_1||_{\mathcal{D}} \leq \delta,$$

with $k \doteq 1+\frac{n\ell}{2}$, there exists a unique weak solution $u \in C([0,\infty), H^k(\mathbf{R}^n))$ to (1), which satisfies the following estimates

$$||u(t,\cdot)||_{L^2} \lesssim (1+t)^{\frac{n}{2}(\ell-1)}||u_1||_{\mathcal{D}},$$

$$||u(t,\cdot)||_{\dot{H}^{k-1}} \lesssim h(t)||u_1||_{\mathcal{D}},$$

with

$$h(t) = \begin{cases} (1+t)^{(\ell-1)\left(\frac{n}{2}+k-1\right)}, & \ell + n(1-\ell)(1+\ell) < \beta < 2-\ell+n(1-\ell)(1+\ell), \\ (1+t)^{\frac{\ell-\beta}{2}}(\ln(e+t))^{\frac{1}{2}}, & \beta = \ell + n(1-\ell)(1+\ell), \end{cases}$$

and

$$||u(t,\cdot)||_{\dot{H}^k} \lesssim (1+t)^{\frac{\ell-\beta}{2}}||u_1||_{\mathcal{D}}.$$

In the following result we may consider the case $\ell \in \left(\frac{2}{3}, 1\right)$ for $n=3$, by looking for solutions with additional regularity $H^{\kappa(r_1)-1,r_2}(\mathbf{R}^3)$, with $\kappa(r_1) = 3\left(\frac{1}{2}-\frac{1}{r_1}\right)$ and r_1, r_2 satisfying

$$r_1 > \frac{2(3\ell-1)}{1-\ell}, \qquad 2 < r_2 < \frac{6}{2\kappa(r_1)-1}. \tag{7}$$

Theorem 3 *Let $n=3$, $\ell \in \left(\frac{2}{3}, 1\right)$, r_1, r_2 satisfying (7) with $\kappa(r_1) = 3\left(\frac{1}{2}-\frac{1}{r_1}\right)$. If $\ell + 6(1-\ell)\left(1-\frac{1}{r_1}\right) \leq \beta < 2-\ell+3(1-\ell)(1+\ell)$ and*

$$p_c(3,\ell) < p < 1 + \frac{r_1(2-\kappa(r_1))}{3}, \tag{8}$$

with $p_c(3,\ell)$ given by (4), then there exists $\delta > 0$ such that for any initial data

$$u_1 \in \mathcal{D} = H^{\kappa(r_1)-1}(\mathbf{R}^3) \cap L^1(\mathbf{R}^3), \qquad ||u_1||_{\mathcal{D}} \leq \delta,$$

there exists a unique weak solution $u \in C([0,\infty), H^{\kappa(r_1)}(\mathbf{R}^3) \cap \dot{H}^{\kappa(r_1)-1,r_2}(\mathbf{R}^3))$ to (1), which satisfies the following estimates

$$||u(t,\cdot)||_{\dot{H}^{j\kappa(r_1)}} \lesssim (1+t)^{(\ell-1)\left(\frac{n}{2}+j\kappa(r_1)\right)}||u_1||_{\mathcal{D}}, \quad j=0,1;$$

and

$$\|u(t,\cdot)\|_{\dot{H}^{\kappa(r_1)-1,r_2}} \lesssim (1+t)^{(\ell-1)\left(n\left(1-\frac{1}{r_2}\right)+\kappa(r_1)-1\right)}||u_1||_{\mathcal{D}}.$$

Acknowledgments

Jorge Marques is supported by Centre for Business and Economics Research (CeBER) through the Portuguese Foundation for Science and Technology (FCT), reference UIDB/05037/2020.

References

[1] D'Abbicco, M: The threshold of effective damping for semilinear wave equations. Math. Meth. Appl. Sci. **38 (6)**, 1032–1045 (2015).

[2] Ebert, M. R., Marques, J.: Critical Exponent for a Class of Semilinear Damped Wave Equations with Decaying in Time Propagation Speed. In: Cicognani M., Del Santo D., Parmeggiani A., Reissig M. (eds) Anomalies in Partial Differential Equations. Springer INdAM Series, vol 43. Springer, Cham (2021).

[3] Ebert, M. R., Marques, J.: Critical exponent of Fujita-type for semilinear wave equations in Friedmann-Lemaître-Robertson-Walker spacetime. [Submitted]

[4] Galstian, A., Yagdjian, K. : Global solutions for semilinear Klein-Gordon equations in FLRW spacetimes. Nonlinear Anal. **113**, 339–356 (2015).

[5] Tsutaya, K., Wakasugi, Y.: On heatlike lifespan of solutions of semilinear wave equations in Friedmann-Lemaître- Robertson-Walker spacetime. J. Math. Anal. Appl. **500**, 125133 (2021).

[6] Wirth, J: Solution representations for a wave equation with weak dissipation. Math. Meth. Appl. Sci. **27** (2004).

International Conference on Mathematical Analysis and Applications in Science and Engineering
ICMA^{2}SC'22
ISEP Porto-Portugal, June 27 - 29, 2022

Exponential scaling and order preserving in a higher order operator with non-linear diffusion and reaction

Jose Luis Diaz Palencia[1⋆]

[1] Universidad a Distancia de Madrid, Spain

[1⋆]joseluis.diaz.p@udima.es

Abstract: Fisher-KPP problems have been widely studied involving non-linear and non-homogeneous operators. In the present analysis, a Fisher-KPP problem with a fourth order operator and non-linear advection is introduced. The intention is to provide a systematic treatment to find asymptotic solutions based on an exponential scaling that ends into a Hamilton-Jacobi equation. Furthermore, positivity conditions are explored and a comparison principle introduced.

keywords: higher order diffusion, Hamilton-Jacobi, Positivity.

MSC2020: 35K92, 35K91, 35K55

1 Introduction

The Fisher or KPP model appears in numerous scenarios from theoretical perspective to applied scopes (see [1], [2] and [3]). Recently, the KPP models have been reformulated in terms of different evolution operators: see for example fractional operator [9] or higher order operator [6]. In addition, the higher order operators have been discussed as perturbed terms to a regular diffusion, see for example [8]. The equation under study is constituted by a non-homogeneous diffusion of fourth order, a non-linear advection and a reaction term of KPP type:

$$n_t = -n_{xxxx} + c(n^q)_x + n(a-n), \;\; n_0(x) \in L^2_{loc}(\mathbb{R}) \cap L^\infty(\mathbb{R}),\, n_{0,x} \in L^q(\mathbb{R}),\; q>0,\; a>0. \quad (1)$$

2 Results and discussion

The proposed equation (1) is discussed based on the following non-linear exponential scaling:

$$n(x,t) = e^{m(x,t)}. \quad (2)$$

The exponential scaling has been employed widely in the search of solutions for the Schrodinger equation and a whole formalism has been previously introduced (see [10] and [11]). The non-homogeneous evolution operator $\{\frac{\partial}{\partial t} + D_{xxxx}\}$ (where D represents spatial derivatives) is well-known to hold oscillatory profiles of solutions (see for example [5] and [6]). Hence, the function $m(x,t)$ is complex and defined as $m : X \times [0,T] \to \mathbb{C}$. Following some ideas in [4], the function $m(x,t)$ satisfies the following Hamilton-Jacobi equation:

$$m_t = H_4\left(m, \frac{\partial m}{\partial x}\right) + P_4\left(m, \frac{\partial^j m}{\partial x^j}\right), \quad j = 2,3,4, \quad (3)$$

$$H_4(m) = -m_x^2 m_x^2 + cqm_x e^{(q-1)m} + a - e^m, \tag{4}$$

and where P_4 involves the higher order derivatives:

$$\begin{aligned} P_4(m) = &- D_{xxxx}m - D_{xx}(D_x m\, D_x m) - 2D_x m D_{xxx}m - 2(D_x m\, D_x m)D_{xx}m \\ &- 2D_x m\, D_x(D_x m\, D_x m) - (D_{xx}m)^2. \end{aligned} \tag{5}$$

It is the intention to study a solution spanned up to the first spatial derivative. This given a smooth function $\gamma \in H^4(\mathbb{R})$ and for any $\lambda \in \mathbb{R}$, it holds $|P_4(\lambda\gamma)| = O(\lambda^3 \partial^\alpha \gamma) << H_4(\lambda\gamma) = O(\lambda^4\, \gamma_x)$, where $\alpha = 1, 2, 3, 4$. Considering only the leading terms, the equation (1) is expressed by:

$$m_t = -m_x^2 m_x^2 + cqm_x e^{(q-1)m} + a - e^m. \tag{6}$$

Based on the form of (2), standing waves solutions to (6) are explored. To this end, assume the standard separation of variables $m(x,t) = (\sigma + t)^{-\frac{1}{3}}\Theta(x)$, where $\sigma < t < T$ (for further details refer to [4]). Upon replacement in (6) with $\sigma \gg 1$:

$$-\frac{1}{3}\Theta = -\Theta_x^4 + cq(\sigma + t)\Theta_x + a^*, \tag{7}$$

where for any $\sigma \gg 1$ and any $t < k\sigma$, $k > 1$, $a^* = (a-1)\,(k+1)^{4/3}\,\sigma^{4/3}$. Note that $e^m = e^{(\sigma+t)^{-\frac{1}{3}}\Theta(x)} \to 1$, $e^{(q-1)m} = e^{(q-1)(\sigma+t)^{-\frac{1}{3}}\Theta(x)} \to 1$, for $\sigma \gg 1$. After balancing of the leading terms in (7) for $|\Theta_x| \ll 1$:

$$-\frac{1}{3}\Theta = cq(\sigma + t)\Theta_x + a^*. \tag{8}$$

Considering again $|\Theta_x| \ll 1$ for $\sigma \gg 1$, and searching for a propagation front where $\Theta = 0$, it holds:

$$|x| = 3\,c\,q\,\ln(a^*)\,(\sigma + t), \tag{9}$$

for t sufficiently close to σ. After balancing the first derivative with $|\Theta_x| \ll cq(\sigma + t) \ll |\Theta_x^4|$, the expression (7) is rewritten as $-\frac{1}{3}\Theta = -\Theta_x^4 + a^*$. The solution is $\Theta(x) = 3\left(\frac{1}{4}C(i)x\right)^{\frac{4}{3}} - 3a^*$, where $C(i) = (-1)^{\frac{1}{4}}$. Then, departing from σ and for any $t < k\sigma,\ k > 1$:

$$m(x,t) = 3\left(\left(\frac{1}{4}C(i)x\right)^{\frac{4}{3}} - a^*\right)t^{-\frac{1}{3}}. \tag{10}$$

Considering (2), a solution is $n(x,t) = e^{-3a^*t^{-\frac{1}{3}}}\, e^{3t^{-\frac{1}{3}}\left(\frac{1}{4}C(i)x\right)^{\frac{4}{3}}}$, in the oscillatory range while propagating along the front (9). Note that solutions are indeed oscillating given the complex $C(i)$.

The intention now is to explore the behaviour of the solution to (1) when evolving to the equilibrium $n = 0$ and for the envelope $(n^q)_x = 0$. Hence, the equation (1) can be studied based on the properties of the homogeneous:

$$n_t = -n_{xxxx}, \quad n_0(x) \in L^2_{loc}(\mathbb{R}) \cap L^\infty(\mathbb{R}). \tag{11}$$

To study the profiles close the null solutions, assume the initial function as a step-like Heaviside $n_0(x) = H(-x)$. The idea is to obtained a positive maximal kernel to the higher order operator. To this end, consider the following self-similar scaling:

$$\psi(y,t) = f(y)\, e^t t^{-\frac{1}{4}}, \quad y = \frac{x}{t^{\frac{1}{4}}}. \tag{12}$$

Introducing (12) into (11), the following elliptic equation holds:

$$-f^4 + \frac{1}{4}f'y + \frac{1}{4}f = 0; \quad \int_{\mathbb{R}} f(y)dy = 1. \tag{13}$$

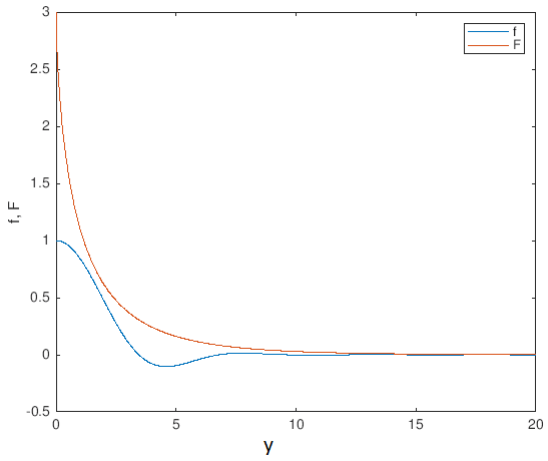

Figure 1: The monotone solution F is a maximal evolution to the oscillatory f for $C_1 = 3$ and $k_1 = 0.5$. This figure has been obtained based on numerical explorations to (13). Both solutions exhibit an asymptotic exponential decreasing rate.

Note that a bound holds for f (see [5]) :

$$|f(y)| \leq C_1 F(y), \quad F(y) = \xi_0 e^{-k_1 |y|^{\frac{4}{3}}} > 0, \quad \xi_0 = \left(\int_{\mathbb{R}} e^{-k_1 |y|^{\alpha}} dy \right)^{-1}. \tag{14}$$

The constant ξ_0 is introduced so that the maximal and positive F satisfies the normalization $\int_{\mathbb{R}} F(y) dy = 1$. Note that $C_1 > 0$ is the order deficiency, and shall be considered sufficiently big so that $C_1 F(y) > f(y)$. The Figure 1 provides values for C_1 and k_1 to keep the distance (no intersection) between both f, F while keeping the monotone and maximal evolution of F. The next step, in the characterization of the maximal kernel (F), is to obtain a suitable value for k_1. For this purpose, we use an asymptotic approach for the self-similar kernel elliptic ODE (13), so that:

$$y \to \infty; \ f \to 0 \Rightarrow -f^{(4)} + \frac{1}{4} y f' = 0. \tag{15}$$

A value for k_1 can be assessed by a Wentzel-Kramers-Brillouin (WKB) approximation. To this end, assume that the exponential decreasing rate exhibited in Figure 1 is expressed as $e^{-k_1 G(y)}$, where $G(y) = y^{\frac{4}{3}}$. Given the WKB approach and into (15):

$$\begin{aligned} &- \left(k_1 \frac{4}{3} \right)^4 y^{4/3} e^{-k_1 y^{4/3}} + \left(k_1 \frac{4}{3} \right)^3 e^{-k_1 y^{4/3}} + \frac{2}{3} \left(\frac{4}{3} \right)^2 k_1^3 e^{-k_1 y^{4/3}} \\ &+ k_1^3 \frac{16}{27} e^{-k_1 y^{4/3}} - \frac{1}{4} y k_1 \frac{4}{3} y^{1/3} e^{-k_1 y^{4/3}} = 0. \end{aligned} \tag{16}$$

Making the leading terms balance: $-\left(k_1 \frac{4}{3}\right)^4 - \frac{1}{4} k_1 = 0, \to k_1 = Re \left(-\frac{3^3}{2^8} \right)^{\frac{1}{3}}$. At this point, two solutions holds, one oscillatory (n) and one with a positive evolution (N) while keeping the exponential decreasing behaviour: $\psi(x,t) = t^{-\frac{1}{4}} e^t f(y), \quad \Psi(x,t) = t^{-\frac{1}{4}} e^t F(y), \quad y = \frac{x}{t^{\frac{1}{4}}}$. Now, based on the maximal and positive Ψ, a comparison principle holds. Indeed, assume an initial condition $\tilde{n}_0(x)$, such that $\tilde{n}_0(x) \geq n_0(x)$, then $\tilde{n}(x,t) \geq n(x,t)$.

$$\begin{aligned} \tilde{n}(t) - n(t) &= \Psi(t) * \tilde{n}_0 - \psi(t) * n_0 \geq \Psi(t) * \tilde{n}_0 - |\psi(t)| * |n_0| \\ &\geq \Psi(t) * \tilde{n}_0 - \Psi(t) * |n_0| = \Psi(t)(\tilde{n}_0 - |n_0|). \end{aligned} \tag{17}$$

considering $\tilde{n}_0 \geq |n_0|$, $\tilde{n}(t) \geq n(t)$. To introduce the spatial variable, assume symmetric conditions at $x = 0$, and evolving towards $x > 0$, i.e. $n_x(0,t) = n_{xxx}(0,t) = 0, \quad t > 0$. Similarly for

$\tilde{n}$. Then:

$$\begin{aligned}\tilde{n}(x) - n(x) &= \Psi(x) * \tilde{n}_0(t) - \psi(x) * n_0(t) \geq \Psi(x) * \tilde{n}_0 - |\psi(x)| * |n_0| \\ &\geq \Psi(x) * \tilde{n}_0 - \psi(x) * |n_0| = \Psi(x)(\tilde{n}_0 - |n_0|).\end{aligned} \tag{18}$$

Considering $\tilde{n}_0 \geq |n_0| \rightarrow \tilde{n}(x) \geq n(x)$, as intended to show.

3 Conclusions and future work

The asymptotic analysis, supported by the exponential scaling introduced, has permitted to study the behaviour of solutions to a order four operator. A comparison principle has been shown to hold for a maximal kernel that was obtained based on a self-similar and exponential scaling. In addition, dedicated values to the involved constant for the maximal kernel have been provided based on analytical (WKB approximation) and numerical evidences.

References

[1] Aronson, D. (1980). Density-dependent interaction-diffusion systems. *Proc. Adv. Seminar on Dynamics and Modeling of Reactive System*, Academic Press, New York.

[2] Aronson, D. Weinberger, H. (1975). Nonlinear diffusion in population genetics, combustion and nerve propagation. *Partial Differential Equations and Related Topic.* Pub., New York, 5â49.

[3] Aronson, D. Weinberger, H. (1978). Multidimensional nonlinear diffusion arising in population genetics. *Adv. in Math.* 30, pp 33â76.

[4] Chavez, M. and Galaktionov, V. (2001). Regional blow up for a higher-order semilinear parabolic equation. *Euro. Jnl of Applied Mathematics* vol 12, pp. 601-623.

[5] Galaktionov, V.A. (2001). On a spectrum of blow-up patterns for a higher-order semilinear parabolic equation. *Proceedings of the Royal Society A: Mathematical, Physical and Engineering Sciences.*

[6] Galaktionov, V. (2012). Towards the KPP–Problem and Log-Front Shift for Higher-Order Nonlinear PDEs I. Bi-Harmonic and Other Parabolic Equations. *Cornwell University arXiv:1210.3513.*

[7] Harley, K,; Van Heijster, R.; Marangell, R.; Pettet G.; Roberts, T. and Wechselberger M. Instability of Travelling Waves in a Model of Haptotaxis. (2019) Preprint.

[8] RottschÃ¤fer, V. and Doelman A. (1998). On the transition from the Ginzburg-Landau equation to the extended Fisher-Kolmogorov equation. *Physica D 118.* 261 - 292.

[9] X. Cabre, X. Roquejoffre, J. (2013. The influence of fractional diffusion in Fisher-KPP equations. *Comm. Math. Phys.* 320, pp 679â722.

[10] P. Bracken. The quantum HamiltonâJacobi formalism in complex space. Quantum Stud.: Math. Found. (2020) 7:389â403

[11] R.A. Leacock, M.S. Padgett. HamiltonâJacobi theory and quantum action variables. Phys. Rev. Lett. 50, 3 (1983).

International Conference on Mathematical Analysis and Applications in Science and Engineering
ICMA^{2}SC'22
ISEP Porto-Portugal, June 27 - 29, 2022

ON ANALOGUE OF BLOW-UP SOLUTIONS FOR A DISCRETE VARIANT OF SECOND–ORDER EMDEN–FOWLER DIFFERENTIAL EQUATION

Josef Diblík[1⋆] **Evgeniya Korobko**[2]

[1] Brno University of Technology, Brno, Czech Republic
[2] Brno University of Technology, Brno, Czech Republic

[1⋆]diblik@vut.cz, [2⋆]jakovi300195@yandex.ru, 222594@vut.cz

Abstract: A nonlinear second-order discrete equation of Emden–Fowler type

$$\Delta^2 v(k) = -k^s \left(\Delta v(k)\right)^3$$

is studied for $k \to \infty$, where $s \neq 1$ is a real number, v is an unknown function, $\Delta v(k) = v(k+1) - v(k)$, and $\Delta^2 v(k) = v(k+2) - 2v(k+1) + v(k)$. This equation is a discrete analogue of Emden–Fowler second-order differential equation

$$y''(x) = y^s(x),$$

having non-continuable blow–up solutions.

keywords: blow-up solution; Emden–Fowler equation; discrete equation.

MSC2020: 39A33; 39A22; 39A12.

1 Introduction

Differential equations of Emden–Fowler type are a class of nonlinear equations. One of the classic forms of Emden-Fowler equation, often investigated in the literature, is

$$y'' \pm x^\alpha y^m = 0, \tag{1}$$

where α and m are constants. Many investigations deal with the analysis of proper solutions [1, 2, 3, 5, 9]. Such solutions are unboundedly continuable to the right.

Nevertheless, equations of Emden–Fowler type can have non–continuable blow–up solutions [4]. To illustrate such a behaviour of solutions, consider an autonomous second-order Emden–Fowler type differential equation of the type (1)

$$y''(x) = y^s(x), \tag{2}$$

where $s \neq 1$ is a real number. Let us show that (2) can have blow–up solutions. Equation (2) is solvable and its general solution is

$$\int_{y_0}^{y(x)} \frac{dz}{\sqrt{2\int_{z_o}^{z} t^s\,dt + D}} = x - x_0, \tag{3}$$

where D is an arbitrary admissible constant and (x_0, y_0) is an arbitrary admissible point. If, for example, $s = 3$ and $D = 0$, then it is easy to derive from (3) a class of solutions

$$y(x) = \pm\frac{\sqrt{2}}{x + C},$$

where C is an arbitrary constant and one can see the blow-up phenomenon explicitly if $x \to -C$.

A direct transfer of equation (2) to a discrete equation is problematic since, in discrete equations, the discrete independent variable runs over a set of integers. Therefore, we prove the existence of blow–up solutions implicitly. Consider a change of variables

$$x = u(y). \tag{4}$$

If, for $y \to \infty$ we have $\lim_{y\to\infty} x = \lim_{y\to\infty} u(y) = 0$ (or the limit equals to a nonzero constant x^*), then one can expect that, for a suitable function $u(y)$ in (4), this property implies the existence of a blow–up solution such that $\lim_{x\to 0} y = \infty$ (or $\lim_{x\to x^*} y = \infty$) to equation (2). For u we derive

$$u'' = -y^s \left(u'\right)^3 \tag{5}$$

and equation

$$\Delta^2 v(k) = -k^s \left(\Delta v(k)\right)^3 \tag{6}$$

is its discrete variant. In (6), $k \in \mathcal{Z}_{k_0}^{\infty} := \{k_0, k_0 + 1, \dots\}$, k_0 is an integer, k is a discrete independent variable, $v\colon \mathcal{Z}_{k_0}^{\infty} \to \mathbb{R}$ is an unknown function, $\Delta v(k) = v(k + 1) - v(k)$ and $\Delta^2 v(k) = v(k + 2) - 2v(k + 1) + v(k)$.

As an equivalent problem to the existence of a blow–up solution for differential equation (2) can be considered one of proving the existence of a nontrivial solution to equation (5) such that $\lim_{y\to\infty} u(y)$ exists and is finite. This serves as a motivation for considering the problem of the existence of a nontrivial solution to equation (6) such that the limit $\lim_{k\to\infty} v(k)$ exists and is finite. More exactly, under condition $s > 1$, we prove the existence of a solution to equation (6) such that

$$\lim_{k\to\infty} v(k) = 0. \tag{7}$$

Trying to look for an approximate solution of discrete equation (6) with asymptotic behavior

$$v(k) \sim c \cdot k^{-\alpha} \tag{8}$$

for $k \to \infty$, where c and α are constants, assuming $c \neq 0$ and $\alpha \neq 0$, we obtain

$$\alpha = \frac{s-1}{2}\,, \quad c = \pm\frac{\sqrt{\alpha+1}}{\alpha} = \pm\frac{\sqrt{2s+2}}{s-1}\,. \tag{9}$$

2 Main result

Below, the notation "O" is used for Landau order symbol big "O". The main result of the paper is following.

Theorem 1 *Let $s > 1$. Let ε_i, γ_i, $i = 1, 2$ be fixed positive numbers such that $\varepsilon_2 < \varepsilon_1 < 1$, $\gamma_2 < \gamma_1 < 1$. Then, there exists a solution $v = v(k)$ to equation (6) such that*

$$-\varepsilon_1 |c| k^{-\alpha} < v(k) - ck^{-\alpha} < \gamma_1 |c| k^{-\alpha}, \tag{10}$$

$$-\varepsilon_2\gamma_2\Delta(|c|k^{-\alpha})) < \Delta v(k) - (\Delta(ck^{-\alpha})) < \gamma_2\Delta(|c|k^{-\alpha})) \tag{11}$$

and

$$\Delta^2 v(k) = O(1) \tag{12}$$

for all $k \in \mathcal{Z}_{k_0}^{\infty}$ provided that k_0 is sufficiently large.

Describe shortly the proof of the above theorem. The change of variables

$$v(k) = ck^{-\alpha}(1 + Y_1(k)), \tag{13}$$

$$\Delta v(k) = (\Delta(ck^{-\alpha}))(1 + Y_2(k)), \tag{14}$$

$$\Delta^2 v(k) = (\Delta^2 \left(ck^{-\alpha}\right))(1 + Y_3(k)), \tag{15}$$

where $Y_i(k)$, $i = 1, 2, 3$ are new dependent functions Y_i: $\mathcal{Z}_{k_0}^{\infty} \to \mathbb{R}$, c and α are defined by (9) transforms equation (6) into a system

$$\Delta Y_1(k) = (\Delta k^{-\alpha})(Y_2(k) - Y_1(k))(k+1)^{\alpha}, \tag{16}$$

$$\Delta Y_2(k) = (\Delta^2 k^{-\alpha})(\Delta(k+1)^{-\alpha})^{-1}(Y_3(k) - Y_2(k)), \tag{17}$$

where

$$Y_3(k) = \left[-k^s \frac{\alpha+1}{\alpha^2}(\Delta k^{-\alpha})^3(1 + 3Y_2(k) + 3Y_2^2(k) + Y_2^3(k)) - \Delta^2 k^{-\alpha}\right] \cdot (\Delta^2 k^{-\alpha})^{-1}. \tag{18}$$

Using equation (18), after some computations, system (16), (17) can be written as

$$\Delta Y_1(k) = \left(\frac{\alpha}{k} + \frac{\alpha(\alpha-1)}{k^2} + O\left(\frac{1}{k^3}\right)\right)(Y_1(k) - Y_2(k)), \tag{19}$$

$$\Delta Y_2(k) = -\left(\frac{\alpha+1}{k} + O\left(\frac{1}{k^2}\right)\right)\left(2Y_2(k) + 3Y_2^2(k) + Y_2^3(k) + O\left(\frac{1}{k}\right)\right). \tag{20}$$

Equation (20) is a scalar one and can be investigated using Theorem 4 in [7]. It can be proved that there exists a solution $Y_2 = Y_2^*(k)$ to equation (20) satisfying the inequality

$$-\varepsilon_2 < Y_2^*(k) < \gamma_2, \quad k \in \mathcal{Z}_{k_0}^{\infty}, \tag{21}$$

where k_0 is sufficiently large and the positive numbers ε_2, γ_2, $\varepsilon_2 < 1$, $\gamma_2 < 1$ are fixed. Note, that this solution is not trivial as follows, e.g., from analysing equations (17), (18). Using this solution in (19) we arrive at a scalar equation

$$\Delta Y_1(k) = \left(\frac{\alpha}{k} + \frac{\alpha(\alpha-1)}{k^2} + O\left(\frac{1}{k^3}\right)\right)(Y_1(k) - Y_2^*(k)). \tag{22}$$

Applying a slight modification of Theorem 1 in [8] or Theorem 2 in [6] we see that, if $s > 1$, there exists a nontrivial solution $Y_1 = Y_1^*(k)$ to equation (22) satisfying the inequality

$$-\varepsilon_1 < Y_1^*(k) < \gamma_1, \quad k \in \mathcal{Z}_{k_0}^{\infty}, \tag{23}$$

where k_0 is sufficiently large and the positive numbers ε_1, γ_1 satisfying $\varepsilon_2 < \varepsilon_1 < 1$, $\gamma_2 < \gamma_1 < 1$ are fixed. System (19), (20) has a solution $(Y_1(k), Y_2(k)) = (Y_1^*(k), Y_2^*(k))$ where $Y_1^*(k)$ and $Y_2^*(k)$ satisfy inequalities (23), (21). Using the change of variables (13)–(15), inequalities (23), (21), and equation (18), we derive the inequalities (10)–(12) in Theorem 1.

3 Conclusions and Future work

In the paper, discrete and differential second–order Emden–Fowler types equations are considered. Equation (2) has so–called blow–up solutions and the existence of such solutions is, within a specified meaning, studied for the discrete equation (6). The problem of the existence of blow-up solutions is transformed to one of the existence of vanishing solutions of (6) when $k \to \infty$.

It is an open question whether it is possible to prove the existence of blow–up solutions without auxiliary transformations used in the paper. To solve it we suggest the following approach - to develop a suitable discretization (instead considering discrete equation (6)) derived directly from differential second-order equation (2). Such a discretization should use a discrete increasing sequence of values of the independent variable with a finite limit point (where the blow–up phenomenon would occur). Then, a modification of the method used in the proof of Theorem 1 should be employed to derive the desired result on the existence of a blow–up solution.

Acknowledgments

This research has been partially supported by the project of specific university research at Brno University of Technology FEKT-S-20-6225 (Faculty of Electrical Engineering and Communication).

References

[1] R. Bellman, *Stability Theory of Differential Equations*, Dover Publications, Inc., New York, 2008.

[2] I. V. Astashova, Asymptotic behavior of singular solutions of Emden–Fowler type equations, Translation of Differ. Uravn., **55** (2019), 597–606, Differ. Equ., **55** (2019), 581–590, (Russian).

[3] I. Astashova, On asymptotic behavior of solutions to Emden–Fowler type higher-order differential equations, Math. Bohem., **4** (2015), 479–488.

[4] I. Astashova, On quasi-periodic solutions to a higher-order Emden-Fowler type differential equation. Bound. Value Probl. 2014, **2014**:174, 8 pp.

[5] I. V. Astashova, Uniqueness of solutions to second order Emden–Fowler type equations with general power–law nonlinearity, J. Math. Sci. (N.Y.), **255** (2021), 543–550.

[6] J. Diblík: Asymptotic behavior of solutions of discrete equations, Funct. Differ. Equ. **11**(1–2) 2004, 37–48.

[7] J. Diblík, Asymptotic behaviour of solutions of systems of discrete equations via Liapunov type technique, Comput. Math. Appl. **45** (2003), 1041–1057.

[8] J. Diblík, Discrete retract principle for systems of discrete equations, Comput. Math. Appl. **42** (2001), 515–528.

[9] I. T. Kiguradze, T. A. Chanturia, *Asymptotic Properties of Solutions of Nonautonomous Ordinary Differential Equations*, (Russian) Mathematics and its Applications (Soviet Series), **89**. Kluwer Academic Publishers Group, Dordrecht, 1993.

International Conference on Mathematical Analysis and Applications in Science and Engineering
ICMA^{2}SC'22

ISEP Porto-Portugal, June 27 - 29, 2022

Generalised Distributed-Order Maxwell Model: the case of a distributed-springpot and a dashpot

Magda Rebelo[1⋆] **Luis Ferrás**[2] **Maria Luísa Morgado**[3]

[1] Centro de Matemática e Aplicações (CMA) and NOVA School of Science and Technology, Portugal.
[2] FEUP, University of Porto & CMAT - Centre of Mathematics, University of Minho, Portugal.
[3] CEMAT, Instituto Superior Técnico & University of Trás-os-Montes e Alto Douro, UTAD, Portugal.

[1⋆]msjr@fct.unl.pt

Abstract: In this work we study the role of the weighting function ($c(\alpha)$) in a Generalised Distributed-Order Maxwell Model (GDOM model) consisting of a distributed spring pot and a dashpot in series. We analyse the GDOM model in simple flows: relaxation, creep compliance, steady shear viscosity and Small Amplitude Oscillatory Shear.

keywords: Fractional Calculus, Viscoelasticity, Maxwell Model.

MSC2020: 26A33; 74D05; 76A05; 76A10.

1 Introduction

One of the simplest viscoelastic models found in the literature is given by,

$$\sigma(t) = \int_0^t G(t-t')\frac{d\gamma(t')}{dt'}dt', \tag{1}$$

where σ is the stress, $\frac{d\gamma(t')}{dt'}$ is the rate of deformation tensor, t' is the elapsed time, and t is the current time. The stress and the rate of deformation, are related by a relaxation modulus $G(t-t')$, which controls how the stress evolves when a particular deformation occurs.

In previous works [1, 2], we consider a more complex relaxations modulus, that generalises the Maxwell and Fractional viscoelastic models.

In [1, 2], the proposed relaxation modulus is given by,

$$G\left(t-t'\right) = \int_0^1 \frac{c(\alpha)}{\Gamma(1-\alpha)}(t-t')^{-\alpha}\, d\alpha,$$

where $c(\alpha) \in C([0,1])$. The resulting distributed-order viscoelastic model is given by:

$$\sigma(t) = {}_0^{RL}\mathbb{D}_t\gamma(t), \quad t>0, \tag{2}$$

where ${}_0^{RL}\mathbb{D}_t$ is the Riemann-Liouville distributed-order fractional derivative,

$${}_0^{RL}\mathbb{D}_t f(t) = \int_0^1 c(\alpha)\,{}_0^{RL}D_t^{\alpha} f(t)\; d\alpha, \tag{3}$$

with ${}_0^{RL}D_t^{\alpha} f(t)$ the Riemann-Liouville differential operator:

$$ {}_0^{RL}D_t^{\alpha}(f(t)) = \frac{d}{dt}\frac{1}{\Gamma(1-\alpha)}\int_0^t \frac{f(s)}{(t-s)^{\alpha}}ds. \tag{4} $$

The function $c(\alpha)$, acting as a weight for the order of differentiation, is such that $c(\alpha) \geq 0$ and $\int_0^1 c(\alpha)\, d\alpha = C > 0$ and the dimensions of $c(\alpha)$ are $[time]^{\alpha} / [length]^2$.

The GDOM model considered in this work consists of a distributed springpot and a dashpot arranged in series. The distributed-springpot is represented by equation (2) and the dashpot obeys the Newton's law of viscosity

$$\sigma(t) = \eta\dot{\gamma}(t),$$

where η is the shear viscosity.

Since the stress, $\sigma(t)$, is the same in both elements, their respective strain expressions are given by ([2]):

$$\gamma_1(t) = \sigma(t) * \mathcal{L}^{-1}\left(\frac{1}{b(s)}; t\right), \quad \gamma_2(t) = \sigma(t) * \mathcal{L}^{-1}\left(\frac{1}{\eta s}; t\right),$$

where

$$b(s) = \int_0^1 c(\alpha)s^{\alpha}d\alpha. \tag{5}$$

The total deformation is therefore the sum of the deformations determined for the two elements in series $\gamma(t) = \gamma_1(t) + \gamma_2(t)$, and, it satisfies

$$\gamma(t) = \sigma(t) * \mathcal{L}^{-1}\left(\frac{\eta s + b(s)}{\eta s b(s)}; t\right). \tag{6}$$

Applying to both sides of equation (6) the Laplace transform and then the inverse Laplace transform, using the convolution theorem for the Laplace transform it follows that

$$\sigma(t) = \int_0^t \gamma(t-\theta)\mathcal{L}^{-1}\left(\frac{\eta s b(s)}{\eta s + b(s)}; \theta\right) d\theta. \tag{7}$$

The main goal of this work is to better understand the model and to catalogue the plethora of different behaviours of the model through the use of the distributed order derivative.

2 Results and discussion

In order to better understand the GDOM model, the following flows will be analysed: relaxation test, creep test, small amplitude oscillatory shear (SAOS) and a steady shear deformation. Note that the model used in this work (equation (7)) is linear and the steady shear deformation measures a nonlinear deformation.

Relaxation and Creep: limiting cases

Suppose that the stress is given by $\sigma(t) = \sigma_0 H(t)$, where H is the Heaviside step function. Then from (6) and using the properties of the Laplace transform it follows

$$\lim_{t\to 0}\gamma(t) = 0, \qquad \lim_{t\to+\infty}\gamma(t) = +\infty. \tag{8}$$

Note the fact that using a dashpot does not guarantee that the strain will converge to a plateau at long times.

Suppose now that the strain is given by $\gamma(t) = \gamma_0 H(t)$. From (7) we can prove that

$$\lim_{t\to 0} \sigma(t) = +\infty, \qquad \lim_{t\to+\infty} \sigma(t) = 0. \tag{9}$$

Thus, a distributed-springpot and a dashpot in series have complete stress relaxation (regardless of the weighting function used).

Steady Shear Viscosity

For the case of a steady shearing deformation the functional of the deformation imposed during steady shear is given by $\dot{\gamma}(t) = \dot{\gamma}_0 H(t)$, where $\dot{\gamma}_0$ is the steady shear rate applied at time $t = 0$, and we intend to analyse $\lim_{t\to+\infty} \sigma(t)$.
In this case we prove that

$$\lim_{t\to+\infty} \sigma(t) = \eta\dot{\gamma}_0. \tag{10}$$

Therefore, we have that the steady shear viscosity $\eta^+(t) = \frac{\sigma(t)}{\dot{\gamma}_0} \to \eta$ as expected (we are using a dashpot).

SAOS The storage (G') and loss (G'') moduli for a distributed-springpot and a dashpot in series is given by

$$G'(\omega) = \frac{\eta^2\omega^2 b_1(\omega)}{(b_1(\omega))^2 + (b_2(\omega) + \eta\omega)^2}, \tag{11}$$

$$G''(\omega) = \frac{\eta\omega\left((b_1(\omega))^2 + (b_2(\omega))^2\right) + (\eta\omega)^2 b_2(\omega)}{(b_1(\omega))^2 + (b_2(\omega) + \eta\omega)^2}, \tag{12}$$

respectively, where b_1 and b_2 are given by

$$b_1(\omega) = \int_0^1 c(\alpha)\omega^\alpha \cos\left(\frac{\pi}{2}\alpha\right) d\alpha, \tag{13}$$

$$b_2(\omega) = \int_0^1 c(\alpha)\omega^\alpha \sin\left(\frac{\pi}{2}\alpha\right) d\alpha. \tag{14}$$

For some specific $c(\alpha)$ functions, an explicit expression is possible to obtain for the storage and loss moduli. A few of these particular cases are presented next. It is possible to obtain more analytical expressions considering other weighting functions. Whenever this is not possible, the G' and G'' values for each ω must be obtained numerically.

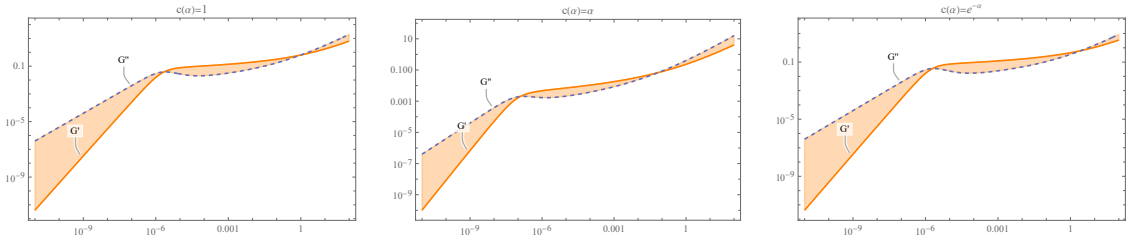

Figure 1: Plots of the storage and loss modulus for a distributed-springpot and a dashpot in series for $\eta = 40000$ Pa.s. The x axis shows the angular frequency, ω, in rad/s. Left: $c(\alpha) = 1$; Center: $c(\alpha) = \alpha$; Right: $c(\alpha) = e^{\alpha}$.

Due to the simple distributed contribution of all derivatives ($c(\alpha) = 1, \alpha, e^{-\alpha}$), we obtain quite similar profiles for G' and G'' (figure 1). We have a viscoelastic fluid behaviour ($G'' > G'$) for low

frequencies, a rubbery plateau and a transition region for higher frequencies. This shows that the model is robust, and allows for the modelling of a more complex behaviour, when compared to the single distributed-springpot (that shows a viscoelastic solid behaviour).

Figure 2 shows the effect of η on G' and G'', for $c(\alpha) = 1$. As expected, when the viscosity decreases, a fluid behaviour is dominant.

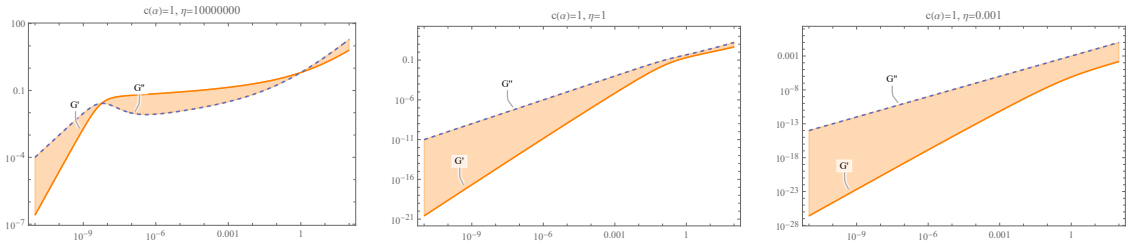

Figure 2: Plots of the storage and loss modulus for a distributed-springpot and a dashpot in series for $c(\alpha) = 1$. The x axis shows the angular frequency, ω, in rad/s. Left: $\eta = 10000000$ Pa.s; Center: $\eta = 1$ Pa.s; Right: $\eta = 0.001$ Pa.s.

3 Conclusions and Future work

We have developed a viscoelastic model (a distributed-springpot spring pot and a dashpot in series) that generalises the Maxwell model, the fractional viscoelastic fluid, and the three-parameter fluid model. The model predicts viscoelastic fluid behaviour for low frequencies and a rubbery plateau and transition region for higher frequencies. Therefore, the model appears to be appropriate for polymer systems.

The model is only valid for linear flows (is not invariant). Therefore, it will be adapted to non-linear flows in the future. Also the suitability to fit experimental data from different rheological experiments will be checked in the future.

Acknowledgments

This work is funded by national funds through the FCT-Fundação para a Ciência e a Tecnologia (Portuguese Foundation for Science and Technology) through the project UIDB/00297/2020 and UIDP/00297/2020 (Center for Mathematics and Applications)
L.L. Ferrás would also like to thank FCT for financial support through CMAT (Centre of Mathematics of the University of Minho) projects UIDB/ 00013/2020 and UIDP/00013/2020.
M.L. Morgado aknowledges funding by FCT through project UID/Multi/04621/2019 of CEMAT/IST-ID, Center for Computational and Stochastic Mathematics, Instituto Superior Técnico, University of Lisbon.

References

[1] L. Ferrás, M. Morgado, and M. Rebelo. A distributed order viscoelastic model for small deformations. In Proc. of the 5th International Conference on Numerical and Symbolic Computation: Developments and Applications (SYMCOMP 2021), pages 179-197. ECCOMAS, 2021.

[2] L. Ferrás, M. Morgado, and M. Rebelo. A generalised distributed-order Maxwell model. *Mathematical Methods in the Applied Sciences*, submitted 2022.

International Conference on Mathematical Analysis and Applications in Science and Engineering
ICMA^{2}SC'22

ISEP Porto-Portugal, June 27 - 29, 2022

New Insights into the Generalised Distributed-Order Maxwell Model

M.L. Morgado[1]⋆ M. Rebelo[2] L.L. Ferrás[3]

[1] CEMAT, Instituto Superior Técnico & University of Trás-os-Montes e Alto Douro, UTAD, Portugal.
[2] Centro de Matemática e Aplicações (CMA) and NOVA School of Science and Technology, Portugal.
[3] FEUP, University of Porto & CMAT - Centre of Mathematics, University of Minho, Portugal.

[1⋆]luisam@utad.pt

Abstract: In this work we introduce the Generalised Distributed-Order Maxwell (GDOM) Model, which consists of two distributed-order elements (distributed-springpots) connected in series. We present new insights into the use of the model and show that the model reduces to well-known classical and fractional viscoelastic models when a suitable weighting function of the order of the derivative is chosen.

keywords: Fractional Calculus, Distributed-Order Derivatives, Linear Viscoelasticity

MSC2020: 26A33; 74D05; 74D10; 76A05; 76A10.

1 Introduction

The stress ($\sigma(t)$) of a viscoelastic material can be written as [1],

$$\sigma\left(t\right)=\gamma_0 G(t)H(t)+\int_{0^+}^{t} G\left(t-t'\right)\frac{d\gamma}{dt'}dt', \tag{1}$$

where γ is the strain, $H(t)$ is the Heaviside function and $G(t)$ is known as the relaxation modulus. We assume that the state of stress at $t=0$ is not influenced by any kind of past ($t<0$) process.

Some materials show a fading memory that follows an algebraic decay, $G\left(t\right)=St^{-\alpha}$. Therefore, taking into account the different relaxations in the different regions of the complex material, we consider a combination of algebraic decays [2, 3], such as,

$$G\left(t\right)=S_1 t^{-\alpha_1}+S_2 t^{-\alpha_2}+...+S_n t^{-\alpha_n}, \tag{2}$$

with $0<\alpha_i<1$, $i=1,...,n$. Making $n\to\infty$, covering the open set $(0,1)$, we can write a continuous version of the previous finite combination of algebraic decays, which is given by:

$$G\left(t\right)=\int_0^1 S(\alpha)t^{-\alpha}\,d\alpha, \tag{3}$$

where $S(\alpha)$ is a function that interpolates $(\alpha_i, S_i)\, i = 1, ..., n$..
Let $c(\alpha)$ be a function such that $S(\alpha) = c(\alpha)/\Gamma(1-\alpha)$ ($c(\alpha)$ will be defined later), then, the relaxation modulus can be written in the form:

$$G\left(t-t'\right) = \int_0^1 \frac{c(\alpha)}{\Gamma(1-\alpha)}(t-t')^{-\alpha}\, d\alpha. \tag{4}$$

Inserting equation (4) into (1), for $t > 0$ we obtain:

$$\sigma\left(t\right) = {}_0^{RL}\mathbb{D}_t^{(c)}\left(\gamma(t)\right), \tag{5}$$

where ${}_0^{RL}\mathbb{D}_t^{(c)}$ is the Riemann-Liouville distributed-order fractional derivative given by,

$${}_0^{RL}\mathbb{D}_t^{(c)} f(t) = \int_0^1 c(\alpha)\, {}_0^{RL}D_t^{\alpha} f\left(t\right)\, d\alpha, \tag{6}$$

with ${}_0^{RL}D_t^{\alpha} f\left(t\right)$ the Riemann-Liouville differential operator defined by [4],

$${}_0^{RL}D_t^{\alpha}(f(t)) = \frac{d}{dt}\frac{1}{\Gamma(1-\alpha)}\int_0^t \frac{f(s)}{(t-s)^{\alpha}}ds = \frac{f(0)t^{-\alpha}}{\Gamma(1-\alpha)} + \frac{1}{\Gamma(1-\alpha)}\int_0^t \frac{f'(s)}{(t-s)^{\alpha}}ds. \tag{7}$$

The function $c(\alpha)$, acting as a weight for the order of differentiation, is such that $c(\alpha) \geq 0$ and $\int_0^1 c(\alpha)\, d\alpha = C > 0$ (see [5] for more details).

Since the Maxwell model consists of two elements in series (a spring and a dashpot), in this work we also consider two elements (two distributed-springpots) in series, as shown in figure 1.

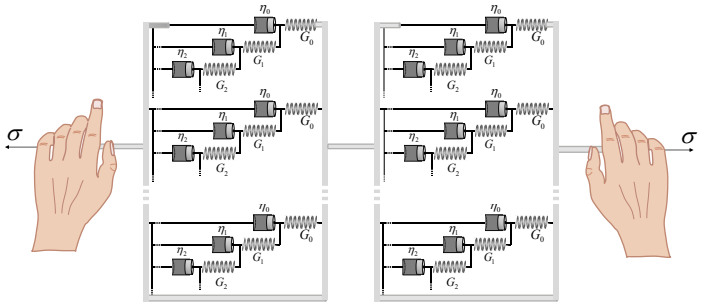

Figure 1: Two distributed-springpots in series: the GDOM Model.

Theorem 1.1 *[3] The strain $\gamma(t)$ that satisfies the distributed order equation (5) is described as a function of the stress, $\sigma(t)$, through the following equality*

$$\gamma(t) = \sigma(t) * \mathcal{L}^{-1}\left(\frac{1}{b(s)}; t\right), \tag{8}$$

where $*$ denotes the convolution of $\sigma(t)$ and $b(\cdot)$ is defined as $b(s) = \int_0^1 c(\alpha)s^{\alpha}\, d\alpha$.

If we consider two distributed-order elements in series, and that the stress is the same for both elements, the respective stress-strain relationships for two elements are given by

$$\gamma_1(t) = \sigma(t) * \mathcal{L}^{-1}\left(\frac{1}{b_1(s)}; t\right), \tag{9}$$

$$\gamma_2(t) = \sigma(t) * \mathcal{L}^{-1}\left(\frac{1}{b_2(s)}; t\right), \tag{10}$$

where $b_i(s) = \int_0^1 c_i(\alpha) s^\alpha ds$, and the functions c_i, $i = 1, 2$, correspond to the weighting functions related with the distributed derivative.

Assuming that the total deformation is given by the sum of the deformations obtained for the two elements in series ($\gamma(t) = \gamma_1(t) + \gamma_2(t)$), we obtain the Generalised Distributed-Order Maxwell Model (figure 1):

$$\sigma(t) = \int_0^t \gamma(t-y)\mathcal{L}^{-1}\left(\frac{b_1(s)b_2(s)}{b_1(s)+b_2(s)}; y\right) dy. \tag{11}$$

This is a complex expression requiring more than one integration, and simpler formulas are possible only for certain weighting functions $c_i(\alpha)$, as shown in the next section.

2 Results and discussion

This model differs from most common classical and fractional models in that a weighting function is used instead of a finite number of parameters. We will now show that the GDOM model generalises several viscoelastic models.

Let C_1 and C_2 be real positive constants, then:

- for $c_1(\alpha) = C_1\delta(\alpha-0)$ and $c_2(\alpha) = C_2\delta(\alpha-1)$ the model reduces to a spring and a dashpot in series, and we recover the classical Maxwell model (figure 2 (top-left)):

$$\sigma(t) + \frac{C_2}{C_1}\frac{d\sigma(t)}{dt} = C_2\frac{d\gamma(t)}{dt}. \tag{12}$$

- for $c_1(\alpha) = C_1\delta(\alpha-\beta_1)$ and $c_2(\alpha) = C_2\delta(\alpha-\beta_2)$ we recover the Fractional Maxwell Model [7] (figure 2 (top-right)):

$$\sigma(t) + \frac{C_2}{C_1}\frac{d^{\beta_2-\beta_1}\sigma(t)}{dt^{\beta_2-\beta_1}} = C_2\frac{d^{\beta_2}\gamma(t)}{dt^{\beta_2}}, \tag{13}$$

  where $\frac{d^{\beta_2-\beta_1}}{dt^{\beta_2-\beta_1}}$ is the fractional derivative according to Caputo, which coincides with the fractional derivative according to Riemann-Liouville (equation (7)) when $\gamma(0) = 0$.

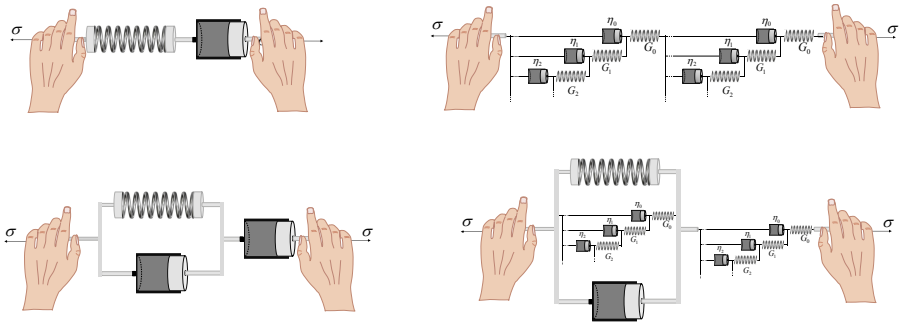

Figure 2: Particular cases of the GDOM model.

- for $c_1(\alpha) = C_1\delta(\alpha-1)+C_2\delta(\alpha-0)$ and $c_2(\alpha) = C_3\delta(\alpha-1)$ we have a distributed-springpot (that consists only of a spring and a dashpot in parallel - a standard linear solid) connected to a dashpot in series. This model is known as the *three parameter fluid model* (figure 2 (bottom-left)).

- for $c_1(\alpha) = C_1\delta(\alpha-1) + C_2\delta(\alpha-0) + C_3\delta(\alpha-\beta_1)$ and for $c_2(\alpha) = C_4\delta(\alpha-\beta_2)$ we have a distributed-springpot (that consists only of a spring, a dashpot and a springpot in parallel) connected to a springpot in series (figure 2 (bottom-right)).

3 Conclusions and Future work

We have developed a generalised Maxwell model that covers most classical and fractional viscoelastic models. The model advocates a different philosophy than previous models, by using a continuous weighting function instead of parameters.

In the future, we will investigate the influence of more complex weighting functions on the model behaviour and also perform fits to experimental data.

Acknowledgments

This work is funded by national funds through the FCT-Fundação para a Ciência e a Tecnologia, I.P. (Portuguese Foundation for Science and Technology) under the scope of the projects UIDB/00297/2020 and UIDP/00297/2020 (Center for Mathematics and Applications).
L.L. Ferrás would also like to thank FCT for financial support through CMAT (Centre of Mathematics of the University of Minho) projects UIDB/ 00013/2020 and UIDP/00013/2020.
M.L. Morgado aknowledges funding by FCT through projects projects UIDB/04621/2020 and UIDP/04621/2020 of CEMAT/ IST-ID, Center for Computational and Stochastic Mathematics, Instituto Superior Técnico, University of Lisbon.

References

[1] L.L. Ferrás, M.L. Morgado, M. Rebelo, A Distributed Order Viscoelastic Model for small Deformations, SYMCOMP 2021, 5th International Conference on Numerical and Symbolic Computation: Developments and Applications.

[2] R.C. Koeller, Polynomial operators, Stieltjes convolution, and fractional calculus in hereditary mechanics, Acta Mechanica, 58(3) (1986), 251-264.

[3] L.L. Ferrás, M. Morgado, and M. Rebelo. A generalised distributed-order Maxwell model. *Mathematical Methods in the Applied Sciences*, submitted 2022.

[4] K. Diethelm, *The Analysis of Fractional Differential Equations*, Lecture Notes in Mathematics book series (LNM, volume 2004) Springer, (2004)

[5] F. Mainardi, G. Pagnini, A. Mura, R. Gorenflo, Time-fractional diffusion of distributed order, J. Vib. Control, 14 (2008), 1267-1290.

[6] L.L. Ferrás, N. Ford, M. Luísa, M. Rebelo, G.H. Mckinley, J.M. Nóbrega, Theoretical and numerical analysis of unsteady fractional viscoelastic flows in simple geometries, Computers and Fluids, 174 (2018), 14-33.

[7] H. Schiessel, A. Blumen, Hierarchical analogues to fractional relaxation equations, Journal of Physics A: Mathematical and General, 26(19) (1993), 5057.

International Conference on Mathematical Analysis and Applications in Science and Engineering
ICMA^{2}SC'22
ISEP Porto-Portugal, June 27 - 29, 2022

A Heisenberg-Pauli-Weyl type inequality for a generalized wavelet transform

L. P. Castro[1] **R. C. Guerra**[2⋆]

[1] CIDMA – Center for Research and Development in Mathematics and Applications, University of Aveiro, Portugal
[2] CMUC – Center for Mathematics of University of Coimbra, University of Coimbra, Portugal

[2⋆]rita.guerra@mat.uc.pt

Abstract: We obtain a Heisenberg-Pauli-Weyl type inequality for a generalized wavelet transform which is presented in the form of an uncertainty principle for this integral transform. This is based on the consideration of a new convolution associated with the quadratic-phase Fourier transform, and a convenient use of some of its properties.

keywords: Heisenberg-Pauli-Weyl type inequality; quadratic-phase Fourier transform; wavelet transform; convolution; uncertainty principle.

MSC2020: 42A38; 42C20; 44A35.

1 Introduction

For many decades, we have witnessed several applications of the Fourier transform, and its related transforms, to multiple areas of knowledge. More recently, some Fourier transform generalizations have gained additional prominence due to their great application potential, as well as to their high flexibility (e.g. in the parameters that they use). This is the case of the quadratic-phase Fourier transform introduced by [5] which includes, as subcases, the fractional Fourier transform and the linear canonical transform (see also [4, 9] for complementary information).

We recall that the quadratic-phase Fourier transform is defined as

$$(\mathcal{Q}f)(x) = \frac{1}{\sqrt{2\pi}} \int_{\mathbb{R}} e^{iQ_{(a-e)}(x,y)} f(y)\, dy, \tag{1}$$

where $Q_{(a-e)}(x,y) := ax^2 + bxy + cy^2 + dx + ey$, with $a, b, c, d, e \in \mathbb{R}$ (and $b \neq 0$), for elements $f \in L^1(\mathbb{R})$ or $f \in L^2(\mathbb{R})$ (cf. [5]).

The inversion formula of (1) is given by

$$f(x) = \frac{b}{\sqrt{2\pi}} \int_{\mathbb{R}} e^{-iQ_{(a-e)}(y,x)} (\mathcal{Q}f)(y)\, dy,$$

for almost every $x \in \mathbb{R}$.

In this work, one of the goals is to interconnect the advantages of the quadratic-phase Fourier transform with the general structure of the wavelet transform. So, similarly to [7, 8], we construct

a new convolution associated with the quadratic-phase Fourier transform, that serves as a basis to construct a new wavelet transform. Here it is worth mentioning that new convolutions and their interactions with integral transforms of the most varied types have lately had many fruitful developments; cf., e.g., [2, 3].

Part of the interest in studying wavelet transforms is related to their applications to signal processing. In fact, the Fourier transform decomposes the signal into sines and cosines; and, in contrast, the wavelet transform can have a kernel chosen arbitrarily, since it obeys to some conditions. Consequently, with the Fourier transform, we obtain a representation of the signal in the frequency domain and, with the wavelet transform, we have a representation of the signal in both the time and frequency domains.

We will introduce a convolution associated with the quadratic-phase Fourier transform and, based on that convolution, we present a new generalized wavelet transform. This makes it possible to build a mathematical context for obtaining a Heisenberg-Pauli-Weyl uncertainty inequality for this new wavelet transform. Mathematically, uncertainty principles (or inequalities) may be realized as inequalities that, for example, for the Fourier transform, state that a nonzero function and its Fourier transform can not both be sharply localized. This fact is of significative importance, e.g., in the theory and applications of partial differential equations (cf. [1, 6]).

2 Results and discussion

We begin by introducing a new convolution associated with the quadratic-phase Fourier transform. We will do it by using an appropriate exponential weight function in the kernel of the classical convolution. Namely, for $c \in \mathbb{R}$, and $f, g \in L^2(\mathbb{R})$, we define

$$(f *_c g)(x) = \frac{1}{\sqrt{2\pi}} \int_{\mathbb{R}} f(u) g(x-u) e^{-ic(x^2-u^2)}\, du. \tag{2}$$

The next theorem gives us the factorization identity associated with the proposed convolution and the quadratic-phase Fourier transform, this is, when we apply the quadratic-Fourier transform to our new convolution, we can decouple the convolution into a product of two functions (that depend on the image of the quadratic-phase Fourier transforms of the initial two functions).

Theorem 1 *If $f, g \in L^2(\mathbb{R})$, then the convolution introduced in (2) has the following factorization identity:*

$$\left(\mathcal{Q}(f *_c g)\right)(x) = e^{-i(ax^2+dx)} (\mathcal{Q}f)(x) (\mathcal{Q}(e^{-ic(\cdot)^2} g))(x),$$

for almost every $x \in \mathbb{R}$.

Based on the introduced convolution, as well as on the properties that it exhibits, we define a new generalized wavelet transform as follows. For any $f \in L^2(\mathbb{R})$, we will call *generalized wavelet transform of f* (with respect to a wavelet $\psi \in L^2(\mathbb{R})$ and the parameter $c \in \mathbb{R}$) to

$$\left(\mathcal{W}_{\psi^c_{\alpha,\beta}} f\right)(\alpha, \beta) = \frac{1}{\sqrt{2\pi}} \int_{\mathbb{R}} f(x) \overline{\psi^c_{\alpha,\beta}(x)}\, dx, \tag{3}$$

where

$$\psi^c_{\alpha,\beta}(x) = \frac{1}{\sqrt{\alpha}} \psi\left(\frac{x-\beta}{\alpha}\right) e^{-ic(x^2-\beta^2)}.$$

For this new generalized wavelet transform, we obtain an uncertainty principle of Heisenberg-Pauli-Weyl type in the next theorem.

Theorem 2 *Let $(\mathcal{W}_{\psi^c_{\alpha,\beta}} f)(\alpha,\beta)$ be the generalized wavelet transform introduced in (3). Then, the following uncertainty inequality holds:*

$$\left[\int_{\mathbb{R}\times\mathbb{R}^+} \beta^2 \left|(\mathcal{W}_{\psi^c_{\alpha,\beta}} f)(\alpha,\beta)\right|^2 \frac{d\beta d\alpha}{\alpha^2}\right]\left[\int_{\mathbb{R}} x^2 \left|(\mathcal{Q}f)(x)\right|^2 dx\right] \geq \frac{C_\psi}{4|b|^2}\|f\|_2^4,$$

where

$$C_\psi = \int_{\mathbb{R}^+} \frac{|(\mathcal{Q}\Psi)(\alpha x)|^2}{\alpha} d\alpha < \infty,$$

for almost every $x \in \mathbb{R}$; and

$$\Psi(\alpha, x) = e^{-i(cx^2+e(x-\alpha x))}\overline{\psi(-x)}.$$

This uncertainty principle is obtained by starting to use the classical Heisenberg-Pauli-Weyl inequality for the quadratic-phase Fourier transform. Then, using that uncertainty principle and identifying $\mathcal{W}_{\psi^c_{\alpha,\beta}} f$ as a function of the time variable t, we obtain a new inequality that will be integrated with respect to $(d\alpha)/\alpha^2$. After this, we use the Cauchy-Schwartz inequality, the Parseval identity for the generalized wavelet transform and the relation between the generalized wavelet transform and the quadratic-phase Fourier transform to obtain the result.

3 Conclusions and future work

In this work, we introduce a new generalized wavelet transform and study some of its properties. The main result was a Heisenberg-Pauli-Weyl type uncertainty principle associated with this new transformation.

As future work, we hope to obtain more uncertainty principles associated with this new general transform that will allow us to further describe its relationships with its images and other integral and wavelet transforms. We also have the future objective of obtaining more generalizations for wavelet transforms, studying their properties and elaborating comparative studies (with what already exists) that allow us to show the possible advantages of such generalizations.

Acknowledgments

L. P. Castro was supported in part by FCT–*Portuguese Foundation for Science and Technology* through the *Center for Research and Development in Mathematics and Applications (CIDMA)* of Universidade de Aveiro, within project UIDB/04106/2020. R. C. Guerra was supported through the *Centre for Mathematics of the University of Coimbra (CMUC)* - UIDB/00324/2020, funded by the Portuguese Government through FCT/MCTES. R. C. Guerra also acknowledges a postdoctoral research fellowship supported by CMUC - UIDP/00324/2020.

References

[1] W. Beckner, Pitt's inequality and the uncertainty principle, *Proceedings of the American Mathematical Society*, 123(6) (1995), 1897–1905.

[2] L. P. Castro, N. Goel, A. S. Silva, A new convolution operator for the linear canonical transform with applications, *Comput. Appl. Math.* 40(3) (2021), Paper No. 95, 18 pp..

[3] L. P. Castro, R. C. Guerra, N. M. Tuan, New convolutions weighted by Hermite functions and their applications, *Math. Inequal. Appl.* 22(2) (2019), 719–745.

[4] L. P. Castro, M. R. Haque, M. M. Murshed, S. Saitoh, N. M. Tuan, Quadratic Fourier transforms, *Ann. Funct. Anal.*, 5(1) (2014), 10–23.

[5] L. P. Castro, L. T. Minh, N. M. Tuan, New convolutions for quadratic-phase Fourier integral operators and their applications, *Mediterranean Journal of Mathematics*, 15(1) (2018), 13, 17pp..

[6] C. Fefferman, The uncertainty principle, *Bulletin of the American Mathematical Society. New Series*, 9(2) (1983), 129–206.

[7] A. Prasad, P. B. Sharma, The quadratic-phase Fourier wavelet transform, *Mathematical Methods in the Applied Sciences*, 43 (2020), 1953–1969.

[8] F. A. Shah, W. Z. Lone, Quadratic-phase wavelet transform with applications to generalized differential equations, *Mathematical Methods in the Applied Sciences*, 45 (2022), 1153–1175.

[9] F. A. Shah, W. Z. Lone, A. Y. Tantary, Short-time quadratic-phase Fourier transform, *Optik - International Journal for Light and Electron Optics*, 245 (2021), 167689.

International Conference on Mathematical Analysis and Applications in Science and Engineering
ICMA^{2}SC'22
ISEP Porto-Portugal, June 27 - 29, 2022

On the solutions to differential equations with uncertainties: comparison of different approaches

Rosana Rodríguez-López[1,2⋆]

[1] CITMAga, 15782 Santiago de Compostela, Spain.
[2] Departamento de Estatística, Análise Matemática e Optimización, Facultade de Matemáticas, Universidade de Santiago de Compostela, 15782, Santiago de Compostela, Spain.

[1,2⋆]rosana.rodriguez.lopez@usc.es

Abstract: CONTRIBUTION IN MEMORY OF PROF. J.A. TENREIRO MACHADO, SUBMITTED TO SYMPOSIUM #12: ADVANCES IN DIFFERENTIAL EQUATIONS WITH UNCERTAINTIES AND MODELING
This contribution is devoted to compare two different approaches in the resolution of differential equations with uncertainties given by interval-valued and fuzzy-valued terms. The results presented are related to the reference [20], which is a joint work with A. Khastan.

keywords: differential equations with uncertainty; types of derivatives; differential inclusions.

MSC2020: 26E50; 34A07; 34A60.

1 Introduction

The work [22] provided a new framework to deal with the uncertainty due to subjective factors, namely, the concept of fuzzy set. Since then, differential equations of fuzzy type have been considered one possible way to predict the evolution of phenomena subject to uncertainty (see [10], for instance).

The obstacles found in the resolution of this type of differential equations with uncertainties led to the proposal of different perspectives and notions of solution. The most extensively used approaches are based on the concept of a derivative for a fuzzy function [8, 18], Zadeh's Extension Principle [17], differential inclusions [9], etc. Hence, several notions of derivative appeared, such as Hukuhara differentiability, strongly generalized differentiability, generalized Hukuhara differentiability, or metric-based derivatives, for instance, see [1, 2, 3, 4, 14, 15, 21], and different authors explored the relation between the approaches available [3, 5, 6, 7, 11, 12, 13, 19].

This contribution is devoted to compare two different approaches in the resolution of differential equations with uncertainties given by interval-valued (concept in [16]) and fuzzy-valued terms. In particular, we consider the perspective of differential calculus and differential inclusions (for details, see [20]).

2 Results and discussion

To start with, we recall from [20] the connection between the solutions to interval-valued problems under different perspectives. For this, consider a differential inclusion of the type

$$\dot{x} \in a(t)x + F(t),\ t \in [0,T], \qquad x(0) \in X_0, \tag{1}$$

for $F(t) = [f(t), g(t)]$, $f(t) \leq g(t)$, and $X_0 = [x_0, y_0]$ with $x_0 \leq y_0$.

With the aim of comparing the expression of the solution with those corresponding to some related linear problems under the perspective of strongly generalized derivative, we consider the following initial value problem:

$$x' = a(t)x + F(t),\ t \in [0,T], \qquad x(0) = X_0. \tag{2}$$

The simplest case arises when $a > 0$, where the solution of the differential inclusion (1) is exactly the same as the solution through the H-derivative ((i)-differentiability) to the problem (2).

By constrast, if $a < 0$ and $f(t) = g(t)$, then the solution to the differential inclusion (1) coincides with the solution to problem (2) from the point of view of the (ii)-differentiability. However, if $f(t) \neq g(t)$, this is not true.

If a is continuous, the study of the intervals of monotonicity of the diameter of the solution can give an interesting information. The solution to the equation via differential inclusions can exhibit a behavior changing from nondecreasing to nonincreasing diameter and conversely. Despite of this fact, the solution via differential inclusions does not coincide with the solution under the strongly generalized differentiability by using switching points in the derivative for an invariant equation. As we show in [20], it is also required to switch the equation to other differential problem, similar but non equivalent to the original one. This suggests us to consider the combination of different types of derivatives and problems depending on the sign of a, by the introduction of switching points, with a switch not only in the type of derivative but also in the differential problem (see [20]).

For the general equation (1), we have the following cases, where we assume that the corresponding problems make sense:

- If $a > 0$, the solution via differential inclusions coincide with the (i)-solution to (2).
- For $a < 0$, we have the solution to

  $$x' = F(t) \ominus (-a(t))x,\ t \in [0,T], \qquad x(0) = X_0, \tag{3}$$

  under (i)-differentiability, provided that the corresponding differences exist.
- If $a > 0$, and $F(t)$ is real, then we have the (ii)-differentiable solution to

  $$x' = F(t) \ominus (-a(t))x,\ t \in [0,T], \qquad x(0) = X_0, \tag{4}$$

  provided the differences exist. In this case, X_0 and the solution have also to be real.
- If $a < 0$ and $F(t)$ is real, the solution to (2) via differential inclusions is a (ii)-differentiable solution to the same problem (2).
- If $a < 0$ and $F(t)$ is non real, we have the (ii)-differentiable solution to

  $$x' = a(t)x \ominus (-F(t)),\ t \in [0,T], \qquad x(0) = X_0, \tag{5}$$

  provided that the corresponding differences exist.

Summarizing, if $F(t)$ is real, the solution to (2) via differential inclusions is the (i)-solution to the same equation on the intervals where $a > 0$ and the (ii)-solution to the equation on the intervals where $a < 0$. Note that the initial condition is updated at the switching points (in this case, the points where a changes its sign).

On the other hand, if $F(t)$ is non real, the solution to (2) via differential inclusions is the (i)-solution to the same equation on the intervals where $a > 0$ and, on the intervals where $a < 0$, it is the (i)-solution to the equation in (3) provided that this problem makes sense and the (ii)-solution to (5) provided that it makes sense.

In the fuzzy case, we consider the solution to $x' \in a(t)x + b(t)$ under differential inclusions' approach. In [20], it is proved that the solution to the differential inclusion is obtained by considering subsequent initial value problems defined by varying the type of differentiability and the type of right-hand side term in the expression $x' = F_i(t, x)$, where $i \in \{1, 2, 3\}$ and $F_1(t, x) = a(t)x + b(t)$, $F_2(t, x) = b(t) \ominus (-a(t))x$, and $F_3(t, x) = a(t)x \ominus (-b(t))$, provided that the corresponding differences exist. See [20], for further details.

3 Conclusions and Future work

We have compared the solutions under the approaches of strongly generalized differentiability and differential inclusions for some types of simple differential equations subject to uncertainty, study that can be extended to more general problems.

Acknowledgments

This research has been partially supported by grants PID2020-113275GB-I00 (AEI/FEDER, UE), and ED431C 2019/02 (GRC Xunta de Galicia).

References

[1] B. Bede, S. G. Gal, Generalizations of the differentiability of fuzzy-number-valued functions with applications to fuzzy differential equations, Fuzzy Sets and Systems **151** (2005), 581–599.

[2] B. Bede, S. G. Gal, Solution of fuzzy differential equations based on generalized differentiability, Communications in Mathematical Analysis **9** (2009), 22–41.

[3] B. Bede, I. J. Rudas, A. L. Bencsik, First order linear fuzzy differential equations under generalized differentiability, Information Sciences **177**(7) (2007), 1648–1662.

[4] B. Bede, L. Stefanini, Generalized differentiability of fuzzy-valued functions, Fuzzy Sets and Systems **230** (2013), 119–141.

[5] Y. Chalco-Cano, A. Khastan, R. Rodríguez-López, Normalized expression for solutions to linear fuzzy differential equations under combination of differences, in: J. M. Alonso, H. Bustince, M. Reformat, M. (eds.) Proceedings of the 2015 Conference of the International Fuzzy Systems Association and the European Society for Fuzzy Logic and Technology, pp. 1382–1388. Atlantis Press, Amsterdam, 2015.

[6] Y. Chalco-Cano, H. Román-Flores, Comparation between some approaches to solve fuzzy differential equations, Fuzzy Sets and Systems **160** (2009), 1517–1527 .

[7] Y. Chalco-Cano, H. Román-Flores, Some remarks on fuzzy differential equations via differential inclusions, Fuzzy Sets and Systems **230** (2013), 3–20.

[8] D. Dubois, H. Prade, Towards fuzzy differential calculus: part 3, differentiation, Fuzzy Sets and Systems **8** (1982), 225–233.

[9] E. Hüllermeier, An approach to modelling and simulation of uncertain dynamical systems, International Journal of Uncertainty, Fuzziness and Knowledge-Based Systems **5**, 117–137 (1997).

[10] O. Kaleva, A note on fuzzy differential equations, Nonlinear Analysis **64** (2006), 895–900.

[11] A. Khastan, J. J. Nieto, R. Rodríguez-López, Variation of constant formula for first order fuzzy differential equations, Fuzzy Sets and Systems **177(1)** (2011), 20–33.

[12] A. Khastan, R. Rodríguez-López, On the solutions to first order linear fuzzy differential equations, Fuzzy Sets and Systems **295(C)** (2016), 114–135.

[13] A. Khastan, R. Rodríguez-López, On linear fuzzy differential equations by differential inclusions' approach, Fuzzy Sets and Systems **387** (2020), 49–67.

[14] A. Khastan, R. Rodríguez-López, M. Shahidi, New differentiability concepts for set-valued functions and applications to set differential equations, Information Sciences **575** (2021), 355–378.

[15] A. Khastan, R. Rodríguez-López, M. Shahidi, New metric-based derivatives for fuzzy functions and some of their properties, Fuzzy Sets and Systems (2021).

[16] S. M Markov, Existence and uniqueness of solutions of the interval differential equation $X' = F(t, X)$, Comptes rendus de l'Academie bulgare des Sciences **31**(12) (1978), 1519–1522.

[17] M. T. Mizukoshi, L. C. Barros, Y. Chalco-Cano, H. Román-Flores, R. C. Bassanezi, Fuzzy differential equations and the extension principle, Information Sciences **177** (2007), 3627–3635.

[18] M. L. Puri, D. A. Ralescu, Differentials of fuzzy functions, Journal of Mathematical Analysis and Applications **91** (1983), 552–558.

[19] R. Rodríguez-López, On the existence of solutions to periodic boundary value problems for fuzzy linear differential equations, Fuzzy Sets and Systems **219** (2013), 1–26.

[20] A. Khastan, R. Rodríguez-López, Relation between strongly generalized solutions and solutions via differential inclusions: a study for linear fuzzy differential equations (2022).

[21] L. Stefanini, B. Bede, Generalized Hukuhara differentiability of interval-valued functions and interval differential equations, Nonlinear Analysis **71** (2009), 1311–1328.

[22] L. Zadeh, Fuzzy Sets, Information and Control **8** (1965), 338–353.

International Conference on Mathematical Analysis and Applications in Science and Engineering
ICMA^{2}SC'22

ISEP Porto-Portugal, June 27 - 29, 2022

An Improved Integro-Differential Linear Viscoelastic Model

L.L. Ferrás[1] **M.L. Morgado**[2] **M. Rebelo**[3] **R.T. Leiva**[4⋆] **J. Bertoco**[4]
A.M. Afonso[6] **A. Castelo**[4]

[1] FEUP, University of Porto & CMAT - Centre of Mathematics, University of Minho, Portugal.
[2] CEMAT, Instituto Superior Técnico & University of Trás-os-Montes e Alto Douro, UTAD, Portugal.
[3] Centro de Matemática e Aplicações (CMA) and NOVA School of Science and Technology, Portugal.
[4] Instituto de Ciências Matemáticas e de Computação-USP, São Carlos 13566-590, SP, Brazil.
[5]CEFT-Departamento de Engenharia Mecânica, FEUP, 4200-465 Porto, Portugal.

[1⋆]Rosalia.taboada@usp.br

Abstract: In this work, we present a generalisation of the integral Maxwell model by developing a new relaxation modulus based on the Mittag-Leffler function. The new model provides a better fit to linear experimental data compared to a classical 2-mode Maxwell model.

keywords: Maxwell Model, Linear Viscoelasticity, Mittag-Leffler.

MSC2020: 74D05; 74D10; 76A05; 76A10.

1 Introduction

The most elementary model for the constitutive response of viscoelastic fluids was proposed by Maxwell [1, 2] and is given by:

$$\boldsymbol{\sigma}(t) + \lambda \frac{d\boldsymbol{\sigma}(t)}{dt} = \eta \dot{\boldsymbol{\gamma}}(t), \tag{1}$$

with $\boldsymbol{\sigma}$ the stress tensor,

$$\dot{\boldsymbol{\gamma}}(t) = \frac{d\boldsymbol{\gamma}(t)}{dt} = \left(\nabla \boldsymbol{u} + (\nabla \boldsymbol{u})^T\right) \tag{2}$$

the rate of deformation tensor, $\mathbf{u}$ the velocity vector, λ the relaxation time of the fluid and η the zero shear-rate viscosity. The model can also be written in integral form as,

$$\boldsymbol{\sigma}(t) = \int_{-\infty}^{t} G_0 e^{-\frac{t-t'}{\lambda}} \frac{d\boldsymbol{\gamma}(t')}{dt'} dt' \tag{3}$$

where $G(t) = G_0 e^{\frac{-t}{\lambda}}$ is the relaxation modulus (the response of the stress to a jump in deformation), γ is the deformation tensor, and it is assumed that the fluid is at rest for $t < 0$. This is one specific form of the Boltzman integral for linear viscoelastic deformations of complex materials

[1]. This type of Maxwell-Debye relaxation (exponential decay) is observed in several complex viscoelastic fluids, but there are other materials showing a more complex fading memory that follows a more generalised exponential decay, that is,

$$G\left(t\right) = S_0\Gamma(\beta)E_{\alpha,\beta}\left(t\right), \tag{4}$$

where $E_{\alpha,\beta}$ is the Mittag-Leffler function (a generalisation of the exponential function), Γ is the Gamma function and the normalisation $\Gamma\left(\beta\right)$ is used to ensure that $G(0) = S_0$, for all choices of β. The Mittag-Leffler function is defined as,

$$E_{\alpha,\beta}\left(z\right) = \sum_{j=0}^{\infty} \frac{z^j}{\Gamma\left(\alpha j + \beta\right)}, \tag{5}$$

with α, β being real and positive. When $\alpha = \beta = 1$, the Mittag-Leffler function reduces to the exponential function, and when $\beta = 1$ the original one-parameter Mittag-Leffler function, $E_\alpha(\cdot)$ is obtained.

The new constitutive equation (Maxwell-ML model) is then given by:

$$\boldsymbol{\sigma}\left(t\right) = \int_{-\infty}^{t} S_0\Gamma(\beta)E_{\alpha,\beta}\left(-\frac{t-t'}{\lambda}\right)\frac{d\boldsymbol{\gamma}(t')}{dt'}dt' \tag{6}$$

where $G(t-t') = S_0\Gamma(\beta)E_{\alpha,\beta}\left(-\frac{t-t'}{\lambda}\right)$ is the relaxation modulus. This model has one or two new fitting parameters α and β, resulting in an additional fitting flexibility.

It should be remarked that a monotonic decay is expected. Therefore, we must impose restrictions on the α and β parameters, so that a proper relaxation is obtained.

Theorem 1.1 *[3] The function*

$$E_\alpha(-z), \quad z \in \mathbb{R}^+ \tag{7}$$

is completely monotonic for any $0 < \alpha \leq 1$.

Theorem 1.2 *[4] The function*

$$E_{\alpha,\beta}(-z), \quad z \in \mathbb{R}^+ \tag{8}$$

is completely monotonic for $\alpha > 0$ *and* $\beta > 0$ *if and only if* $0 < \alpha \leq 1$ *and* $\beta \geq \alpha$

These two theorems set the restriction imposed in the α, β parameters, that is: $0 < \alpha \leq 1$ and $\beta \geq \alpha$.

The Maxwell model can be written in both differential (Eq. 1) and integral (Eq. 3) forms. The new constitutive equation (given by Eq 6) is more complex, and can only be reduced to an integro-differential form.

Lemma 1.1 *The Maxwell-ML model can be written in integro-differential form, as:*

$$\frac{S_0\Gamma(\beta)}{\alpha\lambda}\int_{-\infty}^{t} A(t-t')\dot{\boldsymbol{\gamma}}(t')dt' + \frac{d\boldsymbol{\sigma}(t)}{dt} = S_0\dot{\boldsymbol{\gamma}}(t), \tag{9}$$

where $A(t-t') = E_{\alpha,\alpha+\beta-1}\left(\frac{t'-t}{\lambda}\right) + (1-\beta)E_{\alpha,\alpha+\beta}\left(\frac{t'-t}{\lambda}\right)$.

The main objective of this work is to develop new viscoelastic models that allow better modelling of complex materials, without the use of fractional derivatives that can lead to more complex numerical implementations (due to the presence of singular kernels). To better understand the newly proposed model, we perform fits to experimental data and compare the results with classical models.

2 Results and discussion

Since the Maxwell- ML model has four parameters, it is expected to provide additional flexibility in fitting a wider range of complex fluid rheology. To test this, we performed a fit using a Maxwell model, a 2-mode Maxwell model, and the Maxwell- ML model (with only one new parameter α) to the storage and loss modulus experimental data (G' and G'') obtained from the rheological characterization (small amplitude oscillatory shear at 230 °C) of a polystyrene [5].

The following lemma establishes the mathematical expressions of G' and G'' for the Mawell-ML model. These expressions were used to perform a fit to the experimental data shown in Fig. 1.

Lemma 2.1 *The storage (G') and loss (G") moduli for the 1D Maxwell-ML viscoelastic model are given by:*

$$G'(\omega) = \omega S_0 \Gamma(\beta) \int_0^\infty E_{\alpha,\beta}\left(\frac{-t}{\lambda}\right) \sin(\omega t)\ dt, \tag{10}$$

$$G''(\omega) = \omega S_0 \Gamma(\beta) \int_0^\infty E_{\alpha,\beta}\left(\frac{-t}{\lambda}\right) \cos(\omega t)\ dt. \tag{11}$$

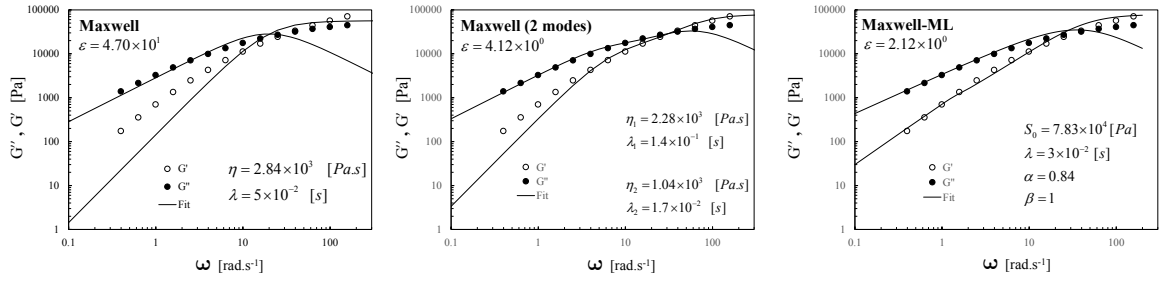

Figure 1: Fit of the elastic and viscous contributions G' and G'' to the linear viscoelastic modulus obtained from the rheological characterisation of a polystyrene extrusion grade, Polystyrol 158K from BASF using (a) Maxwell model; (b) Maxwell model with 2 modes; (c) The model proposed in this work, with the one parameter ML function $E_\alpha(\cdot)$ Maxwell-ML.

From the results shown in Fig. 1, it can be seen that using the Maxwell-ML model (with only three parameters) a better fit is obtained. To quantify the error incurred during the fitting process we used the mean square error given by,

$$\varepsilon = \sum_i \left[\log G_i^{'} - \log G_{fit}^{'}(\omega_i)\right]^2 + \sum_i \left[\log G_i^{''} - \log G_{fit}^{''}(\omega_i)\right]^2. \tag{12}$$

It should be remarked that the β parameter was not used in the fitting process. This means that we could achieve a better fit with 3 parameters when compared the Maxwell model with 2 modes (4 parameters).

3 Conclusions and Future work

We have developed a Maxwell-type linear viscoelastic model using the Mittag-Leffler in the relaxation modulus. The model has 4 parameters and allows a better fit to the storage and loss modulus data of polymer systems (even using only 3 parameters). The model is linear and is currently being improved to become frame invariant by using an invariant measure of deformation such as the Finger tensor $\boldsymbol{B}(t,t')$ [1] (instead of the infinitesimal strain $\boldsymbol{\gamma}(t,t')$). The invariant model is presently being implemented in the numerical code HiG-Flow [6, 7].

Acknowledgments

This work was funded by national funds through the FCT-Fundação para a Ciência e a Tecnologia, I.P. (Portuguese Foundation for Science and Technology) under the scope of the projects UIDB/00297/2020 and UIDP/00297/2020 (Center for Mathematics and Applications).
L.L. Ferrás would also like to thank FCT for financial support through CMAT (Centre of Mathematics of the University of Minho) projects UIDB/ 00013/2020 and UIDP/00013/2020.
M.L. Morgado aknowledges funding by FCT through projects projects UIDB/04621/2020 and UIDP/04621/2020 of CEMAT/ IST-ID, Center for Computational and Stochastic Mathematics, Instituto Superior Técnico, University of Lisbon.
A. Afonso aknowledges funding by FCT through projects UIDB/00532/2020 and UIDP/00532/2020 of CEFT (Centro de Estudos de Fenómenos de Transporte).
This work was also funded by Fapesp-Fundação de Amparo à Pesquisa do Estado de São Paulo, Fapesp-2017/21105-6 and 2013/07375-0.

References

[1] R.B. Bird, R.C. Armstrong, O. Hassager, *Dynamics of Polymeric Liquids. Fluid Mechanics, second ed., vol. I.* Wiley, 1987.

[2] N.W. Tschoegl, *The phenomenological theory of linear viscoelastic behavior: an introduction.* Springer Science & Business Media, 2012.

[3] H. Pollard, The completely monotonic character of the Mittag-Leffler function $E_\alpha(-x)$, Bulletin of the American Mathematical Society, 54(12) (1948), 1115-1116.

[4] W.R. Schneider, Completely monotone generalized Mittag-Leffler functions, Expo. Math. 14 (1996), 3-16

[5] L.L. Ferrás, N. Ford, M. Luísa, M. Rebelo, G.H. Mckinley, J.M. Nóbrega, Theoretical and numerical analysis of unsteady fractional viscoelastic flows in simple geometries, Computers and Fluids, 174 (2018), 14-33.

[6] F. Sousa, C. Lages, J. Ansoni, A. Castelo, A. Simao, A finite difference method with meshless interpolation for incompressible flows in non-graded tree-based grids, Journal of Computational Physics, 396 (2019), 848-866.

[7] A. Castelo, A.M. Afonso, W. De Souza Bezerra, A Hierarchical Grid Solver for Simulation of Flows of Complex Fluids, Polymers, 13(18) (2021), 3168.

International Conference on Mathematical Analysis and Applications in Science and Engineering
ICMA^{2}SC'22
ISEP Porto-Portugal, June 27 - 29, 2022

ON A BOUNDARY-VALUE PROBLEM WITH PARAMETER FOR DIFFERENTIAL EQUATIONS WITH PIECEWISE CONSTANT ARGUMENT OF GENERALIZED TYPE

Roza Uteshova

Institute of Mathematics and Mathematical Modeling, Kazakhstan
International IT University, Kazakhstan

r.uteshova@iitu.edu.kz

Abstract: We consider a linear boundary value problem with parameter for differential equations with piecewise constant argument of generalized type. We propose an algorithm based on the parametrization method and a new concept of general solution.

keywords: functional-differential equations; piecewise constant argument of generalized type; boundary-value problem with parameter.

MSC2020: 34K10; 34K35.

1 Introduction

The paper deals with the linear boundary value problem with parameter

$$\frac{dx}{dt} = A(t)x + B(t)x(\gamma(t)) + C(t)\mu + g(t), \quad t \in (0,T), \quad x \in \mathbb{R}^n, \quad \mu \in \mathbb{R}^m \tag{1}$$

$$K_0\mu + K_1x(0) + K_2x(T) = d, \quad d \in \mathbb{R}^{m+n}, \tag{2}$$

where $n\times n$ matrices $A(t)$, $B(t)$, $n\times m$ matrix $C(t)$ and $n-$dimensional vector $g(t)$ are continuous on $[0,T]$; the $(n+m)\times m$ matrix K_0 and $(n+m)\times n$ matrices K_1 and K_2 are constant; $\|x\| = \max\limits_{i=\overline{1,n}} |x_i|$. The argument $\gamma(t)$ is a step function defined as $\gamma(t) = \zeta_j$ if $t \in [\theta_j, \theta_{j+1})$, $\theta_j \le \zeta_j \le \theta_{j+1}$, $j = \overline{0, N-1}$, where $0 = \theta_0 < \theta_1 < \ldots < \theta_N = T$.

A solution of problem (1), (2) is a pair $(\mu^*, x^*(t))$, where $\mu^* \in \mathbb{R}^m$ and $x^*(t)$ is a function that satisfies the conditions: (i) $x^*(t)$ is continuous on $[0,T]$; (ii) $x^*(t)$ is continuously differentiable on $(0,T)$ with the possible exception of the points θ_j, where one-sided derivatives exist; (iii) $x^*(t)$ satisfies (1) with $\mu = \mu^*$ on each interval (θ_j, θ_{j+1}), $j = \overline{0, N-1}$; at the points θ_j Eq. (1) is satisfied by the right-hand derivatives of $x^*(t)$; (iv) $x^*(t)$ satisfies (2) with $\mu = \mu^*$.

In this paper, we develop an algorithm for solving problem (1), (2) that is based on the Dzhumabaev parametrization method [1]. This is a constructive method for studying and solving various types of boundary value problems. In particular, this method was applied to a two-point boundary-value problem for a second order differential equation with piecewise-constant

argument of generalized type [2]. We adapt a new approach to the concept of general solution of Eq. (1) proposed by Dzhumabaev (see [3]). The structure of the new general solution is based on the partition of [0,T] that takes into account the features of the problem. The new general solution contains $N+1$ arbitrary vectors and satisfies Eq. (1) everywhere on $(0,T)$ except the interior partition points. The question of solvability of the problem under consideration is reduced to that for a system of algebraic equations in $N+1$ parameters, which are the values of the unknown function x(t) at the points θ_j, $j=\overline{0,N}$.

2 Results

Let Δ_N denote the partition of $[0,T]$ into N subintervals by points θ_j, $j=\overline{0,N}$. We will denote by $C([0,T],\Delta_N,\mathbb{R}^{nN})$ the space of function systems $x[t]=(x_1(t),x_2(t),\dots,x_N(t))$ whose elements $x_r(t):[\theta_{r-1},\theta_r)\to\mathbb{R}^n$ are continuous and have left-hand limits $\lim\limits_{t\to\theta_r-0}x_r(t)$ for all $r=\overline{1,N}$, with the norm $\|x[\cdot]\|=\max\limits_{r=\overline{1,N}}\sup\limits_{t\in[\theta_{r-1},\theta_r)}\|x_r(t)\|$.

Suppose that a pair $(\mu,x(t))$ is a solution to Eq.(1) and $x_r(t)$ is the restriction of $x(t)$ to the rth subinterval of Δ_N, $r=\overline{1,N}$. Then the functions $x_r(t)$ satisfy the following system of equations:

$$\frac{dx_r}{dt}=A(t)x_r+B(t)x(\zeta_{r-1})+C(t)\mu+g(t),\quad t\in[\theta_{r-1},\theta_r),\quad r=\overline{1,N}.$$

A solution of this system is a pair $(\hat\mu,\hat x[t])$ with $\hat\mu\in\mathbb{R}^m$ and $\hat x[t]\in C([0,T],\Delta_N,\mathbb{R}^{nN})$ whose elements satisfy the equations of the system on the partition subintervals.

If $(\mu,x(t))$ is a solution of Eq.(1) and $x[t]=(x_1(t),x_2(t),\dots,x_N(t))$ is the system of the restrictions of $x(t)$ to the partition subintervals, then the components of this system must satisfy the continuity conditions at the interior points of Δ_N:

$$\lim_{t\to\theta_p-0}x_p(t)=x_{p+1}(\theta_p),\quad p=\overline{1,N-1}. \tag{3}$$

Let us introduce additional parameters $\lambda_r=x_r(\zeta_{r-1})$, $r=\overline{1,N}$, and make the substitutions $u_r(t)=x_r(t)-\lambda_r$ on every subinterval $[\theta_{r-1},\theta_r)$. We then obtain the system of Cauchy problems for ordinary differential equations with parameters μ and λ_r

$$\frac{du_r}{dt}=A(t)(u_r+\lambda_r)+B(t)\lambda_r+C(t)\mu+g(t),\quad t\in[\theta_{r-1},\theta_r),\quad u_r(\zeta_{r-1})=0,\quad r=\overline{1,N}. \tag{4}$$

Let ξ denote the vector of parameters $\xi=(\lambda_1,\lambda_2,\dots,\lambda_N,\mu)\in\mathbb{R}^{nN+m}$. For fixed r and ξ, each of Cauchy problems (4) has a unique solution $u_r(t,\xi)$, $t\in[\theta_{r-1},\theta_r)$. It is easily seen that $u[t,\xi]\in C([0,T],\Delta_N,\mathbb{R}^{nN+m})$. We will refer to $u[t,\xi]$ as a solution to the system of Cauchy problems with parameters (4).

Definition 1 *Let a function system $u[t,\xi]$ be a solution to the Cauchy problem (4) for some $\xi\in\mathbb{R}^{nN+m}$. Then the pair $x(\Delta_N,t,\xi)$ defined as*

$$x(\Delta_N,t,\xi)=\begin{cases}\lambda_r+u_r(t,\xi), & \text{if } t\in[\theta_{r-1},\theta_r),\ r=\overline{1,N},\\ \lambda_N+\lim\limits_{t\to T-0}u_N(t,\xi), & \text{if } t=T\end{cases}$$

is called the Δ_N-general solution to Eq.(1).

It follows from the definition that the Δ_N-general solution depends on $m+nN$ arbitrary constants and satisfies Eq.(1) for all $t\in(0,T)\setminus\{\theta_p,p=\overline{1,N-1}\}$.

Theorem 1 *Suppose a function $\tilde{x}(t)$ is piecewise continuous on $[0,T]$ with possible discontinuities at $t=\theta_p$, $p=\overline{1,N-1}$, continuously differentiable at $t\in(0,T)\setminus\{\theta_p, p=\overline{1,N-1}\}$, and satisfies Eq.(1) with some $\mu=\tilde{\mu}\in\mathbb{R}^m$. Then there exists a unique $\tilde{\xi}\in\mathbb{R}^{nN+m}$ such that the equality $\tilde{x}(t)=x(\Delta_N,t,\tilde{\xi})$ holds for all $t\in[0,T]$.*

Corollary 2 *Let a pair $(\mu^*,x^*(t))$ be a solution of Eq.(1) and $x(\Delta_N,t,\xi)$ be the Δ_N-general solution of Eq.(1). Then there exists a unique $\xi^*\in\mathbb{R}^{nN+m}$ such that the equality $x^*(t)=x(\Delta_N,t,\xi^*)$ holds for all $t\in[0,T]$.*

The solutions of the Cauchy problems (4) can be represented in the form

$$u_r(t,\mu,\lambda_r)=\Phi_r(t)\int_{\theta_r}^{t}\Phi_r^{-1}(\tau)\{[A(\tau)+B(\tau)]\lambda_r+C(\tau)\mu+g(\tau)\}d\tau,\quad t\in[\theta_{r-1},\theta_r),\quad r=\overline{1,N},$$

where $\Phi_r(t)$ is a fundamental matrix of the differential equation $\dfrac{dx_r}{dt}=A(t)x_r$.

Let us introduce the auxiliary Cauchy problems

$$\frac{dz}{dt}=A(t)z+P(t),\quad z(\zeta_{r-1})=0,\quad t\in[\theta_{r-1},\theta_r),\quad r=\overline{1,N},$$

where $P(t)$ is a continuous matrix or vector. Then the Δ_N-general solution to Eq.(1) can be represented in terms of solutions of auxiliary Cauchy problems in the following way:

$$x(\Delta_N,t,\xi)=\begin{cases}\lambda_r+a_r(A+B,t)\lambda_r+a_r(C,t)\mu+a_r(g,t), & \text{if } t\in[\theta_{r-1},\theta_r),\quad r=\overline{1,N},\\ \lambda_N+\lim\limits_{t\to T-0}u_N(t,\xi), & \text{if } t=T.\end{cases}\tag{5}$$

Let us now turn to the boundary value problem with a parameter (1),(2) and make use of the Δ_N-general solution to Eq.(1) in solving this problem. As mentioned above, the Δ_N-general solution depends on $m+nN$ arbitrary constants that are components of vector-valued parameters $\mu\in\mathbb{R}^m$ and $\lambda\in\mathbb{R}^{nN}$. By substituting $x(\Delta_N,t,\xi)$ into the boundary conditions (2) and the continuity conditions (3), we obtain the following system of linear algebraic equations in unknown parameters μ and λ:

$$[K_0+K_2a_N(C,T)]\mu+K_1\lambda_1+[K_2+K_2a_N(A+B,T)]\lambda_N=d-K_2a_N(g,T),$$
$$a_p(C,\theta_p)\mu+\lambda_p+a_p(A+B,\theta_p)\lambda_p-\lambda_{p+1}=-a_p(g,\theta_p),\quad p=\overline{1,N-1}.$$

Denoting by $Q^*(\Delta_N)$ the square matrix of order $m+nN$ corresponding to the left-hand side of this system, we rewrite the system in the matrix form:

$$Q^*(\Delta_N)\xi=-F^*(\Delta_N),\quad \xi\in\mathbb{R}^{m+nN},\tag{6}$$

where $F^*(\Delta_N)=(-d+K_2a_N(g,T),a_1(g,\theta_1),a_2(g,\theta_2),\dots,a_{N-1}(g,\theta_{N-1}))\in R^{m+nN}$.

Theorem 3 *The boundary value problem (1),(2) is uniquely solvable if and only if the matrix $Q^*(\Delta_N)$ is invertible.*

Based on the results obtained, we propose the following algorithm for finding a solution to the linear boundary value problem with parameter (1),(2).

1. Construct the Δ_N-general solution (5).

2. Set up the system of linear algebraic equations (6) by substituting the Δ_N-general solution into the boundary conditions (2) and continuity conditions (3). Find the solution $\xi^*\in\mathbb{R}^{m+nN}$ of system (6).

3. Substitute the components $\mu^*\in\mathbb{R}^m$ and $\lambda^*\in\mathbb{R}^{nN}$ of ξ^* into the Δ_N-general solution to get the solution $(\mu^*,x^*(t))$ to problem (1),(2).

Acknowledgments

This research is funded by the Science Committee of the Ministry of Education and Science of the Republic of Kazakhstan (Grant No. AP08855726).

References

[1] D.S. Dzhumabaev, Criteria for the unique solvability of a linear boundary-value problem for an ordinary differential equation, USSR Comput. Math. Math. Phys., **29** (1989), 34–46.

[2] A.T. Assanova, New general solution of second order differential equation with piecewise-constant argument of generalized type and its application for solving boundary value problems, Kazakh Math. J., **20**(4) (2020), 87–97.

[3] D.S. Dzhumabaev, Computational methods of solving the boundary value problems for the loaded differential and Fredholm integro-differential equations, Math. Meth. Appl. Sci., **41**(2018), 1439–1462.

International Conference on Mathematical Analysis and Applications in Science and Engineering
ICMA^{2}SC'22
ISEP Porto-Portugal, June 27 - 29, 2022

SOLVABILITY CONDITIONS FOR THE SPECIAL CAUCHY PROBLEM

Sandugash Mynbayeva

Institute of Mathematics and Mathematical Modeling, Kazakhstan
K.Zhubanov Aktobe Regional University, Kazakhstan

mynbaevast80@gmail.com

Abstract: The solvability of the special Cauchy problem arising when applying the D. Dzhumabaev parametrization method to the Fredholm integro-differential equation is investigated. Sufficient conditions for the existence of a unique solution to this problem are established.

keywords: nonlinear Fredholm integro-differential equation, special Cauchy problem, parametrization method

MSC2020: 34G20, 45J05, 47G20.

1 Introduction

We consider the Fredholm integro-differential equation (FIDE)

$$\frac{dx}{dt} = A(t)x + \sum_{k=1}^{m} \varphi_k(t) \int_0^T \psi_k(\tau) f_k(\tau, x(\tau)) d\tau + f_0(t), \quad t \in (0,T), \quad x \in R^n, \tag{1}$$

where the $n \times n$ matrices $A(t)$, $\varphi_k(t)$, $\psi_k(\tau)$, are continuous on $[0,T]$, $f_0 : [0,T] \to R^n$, $f_k : [0,T] \times R^n \to R^n$ are continuous, $k = \overline{1,m}$,; $\|x\| = \max\limits_{i=\overline{1,n}} |x_i|$.

Denote by $C\big([0,T], R^n\big)$ the space of all continuous functions $x : [0,T] \to R^n$ with the norm $\|x\|_1 = \max\limits_{t\in[0,T]} \|x(t)\|$. By a solution to equation (1) we mean a continuously differentiable on $(0,T)$ function $x(t) \in C\big([0,T], R^n\big)$ satisfying equation (1).

The special Cauchy problem plays an essential role in constructing the new general solutions for Fredholm IDEs [1], [2] and solving boundary value problems [3], [4], [5].

The goal of this work is to establish the solvability conditions of the special Cauchy problem resulting from the use of D. Dzhumabaev parametrization method for equation (1).

2 Results and discussion

Let Δ_N be a partition of the interval $[0,T)$ into N parts: $[0,T)=\bigcup\limits_{r=1}^{N}[t_{r-1},t_r)$ and $\overline{h}=\max\limits_{r=\overline{1,N}}(t_r-t_{r-1})$. Given a vector $\lambda^{(0)}=\left(\lambda_1^{(0)},\lambda_2^{(0)},\ldots,\lambda_N^{(0)}\right)\in R^{nN}$ and numbers $\rho_\lambda>0$, $\rho>\rho_\lambda$, $\rho_v\in(0,\rho-\rho_\lambda]$, we compose the sets:

$$S\big(\lambda^{(0)},\rho_\lambda\big)=\big\{\lambda=(\lambda_1,\lambda_2,\ldots,\lambda_N)\in R^{nN}:\big\|\lambda_r-\lambda_r^{(0)}\big\|\le\rho_\lambda,\quad r=\overline{1,N}\big\},$$

$$S\big(x_0(t),\rho\big)=\big\{x\in R^n:\big\|x-x_0(t)\big\|\le\rho\big\},$$

$$G^0(\rho)=\big\{(t,x):t\in[0,T],\big\|x-x_0(t)\big\|\le\rho\big\},$$

where a piecewise constant vector function $x_0(t)$ on $[0,T]$ is defined by the equalities $x_0(t)=\lambda_r^{(0)}$, $t\in[t_{r-1},t_r)$, $r=\overline{1,N}$, and $x_0(T)=\lambda_N^{(0)}$.

Condition A. *Let the following inequalities be fulfilled:*

(1) $\|f_0(t)\|\le M_0$, $t\in[0,T]$, $\|f_k(t,x)\|\le M_k$, $(t,x)\in G^0(\rho)$, M_k *is a constant,* $k=\overline{1,m}$*;*

(2) $D\overline{h}=\Big[\alpha(\rho+\|\lambda^{(0)}\|)+\sum\limits_{k=1}^{m}\max\limits_{t\in[0,T]}\|\varphi_k(t)\|\sum\limits_{j=1}^{N}\int\limits_{t_{j-1}}^{t_j}\|\psi_k(\tau)\|d\tau M_k+M_0\Big]\overline{h}<\rho,$

where $\alpha=\max\limits_{t\in[0,T]}\|A(t)\|$.

We construct the following sets:

$G_p^0(\rho)=\Big\{(t,x):t\in[t_{p-1},t_p),\|x-x_0(t)\|\le\rho-D(t_p-t)\Big\},\quad p=\overline{1,N-1},$

$G_N^0(\rho)=\Big\{(t,x):t\in[t_{N-1},t_N],\|x-x_0(t)\|\le\rho-D(t_N-t)\Big\}$, and

$G^0(\Delta_N,\rho)=\bigcup\limits_{r=1}^{N}G_r^0(\rho).$

Further, we choose $\rho_\lambda=\rho-D\overline{h}$ and $\rho_v=D\overline{h}$.

If a function $x(t)$ satisfies Eq.(1) and $(t,x(t))\in G^0(\Delta_N,\rho)$, then the functions $x_r(t)$, $r=\overline{1,N}$, being the restrictions of $x(t)$ to $[t_{r-1},t_r)$, satisfy the nonlinear IDEs

$$\frac{dx_r}{dt}=A(t)x_r+\sum_{k=1}^{m}\varphi_k(t)\sum_{j=1}^{N}\int_{t_{j-1}}^{t_j}\psi_k(\tau)f_k(\tau,x_j(\tau))d\tau+f_0(t),\ t\in[t_{r-1},t_r),\tag{2}$$

and $(t,x_r(t))\in G_r^0(\rho)$, $r=\overline{1,N}$. Introducing the parameters $\lambda_r\hat{=}x_r(t_{r-1})$ and making the substitutions $u_r(t)=x_r(t)-\lambda_r$, $t\in[t_{r-1},t_r)$, $r=\overline{1,N}$, we obtain the system of nonlinear IDEs with parameters

$$\frac{du_r}{dt}=A(t)(u_r+\lambda_r)+\sum_{k=1}^{m}\varphi_k(t)\sum_{j=1}^{N}\int_{t_{j-1}}^{t_j}\psi_k(\tau)f_k(\tau,u_j(\tau)+\lambda_j)d\tau+f_0(t),\quad t\in[t_{r-1},t_r),\tag{3}$$

subject to the initial conditions

$$u_r(t_{r-1})=0,\quad r=\overline{1,N}.\tag{4}$$

We will refer to problem (3), (4) as to the special Cauchy problem for the system of nonlinear IDEs with parameters on the subintervals.

Let $C\big([0,T],\Delta_N,R^{nN}\big)$ denote the space of all function systems $u[t]=\big(u_1(t),u_2(t),\dots,u_N(t)\big)$, where $u_r:[t_{r-1},t_r)\to R^n$ is continuous and has the finite left-sided limit $\lim\limits_{t\to t_r-0}u_r(t)$ for any $r=\overline{1,N}$, with the norm $\big\|u[\cdot]\big\|_2=\max\limits_{r=\overline{1,N}}\sup\limits_{t\in[t_{r-1},t_r)}\|u_r(t)\|$.

A solution to (3), (4), for a fixed parameter $\lambda=\lambda^*=\big(\lambda_1^*,\lambda_2^*,\dots,\lambda_N^*\big)\in R^{nN}$, is a function system $u[t,\lambda^*]=\big(u_1(t,\lambda^*),u_2(t,\lambda^*),\dots,u_N(t,\lambda^*)\big)\in C\big([0,T],\Delta_N,R^{nN}\big)$, where $u_r(t,\lambda^*)$, $r=\overline{1,N}$, are continuously differentiable with respect to t on their domains and satisfy the system (3) with $\lambda=\lambda^*$ and initial conditions (4).

System of IDEs (2) is equivalent to the special Cauchy problem with parameters on subintervals (3), (4).

In constructing a new general solution and in solving boundary value problems we will use the limit values of the solution to problem (3), (4), it is therefore reasonable to consider the following special Cauchy problem on the closed subintervals:

$$\frac{dv_r}{dt}=A(t)(v_r+\lambda_r)+\sum_{k=1}^{m}\varphi_k(t)\sum_{j=1}^{N}\int_{t_{j-1}}^{t_j}\psi_k(\tau)f_k(\tau,v_j(\tau)+\lambda_j)d\tau+f_0(t),\quad t\in[t_{r-1},t_r],\quad(5)$$

$$v_r(t_{r-1})=0,\quad r=\overline{1,N}.\qquad(6)$$

Denote by $\widetilde{C}\big([0,T],\Delta_N,R^{nN}\big)$ the space of all function systems $v[t]=\big(v_1(t),v_2(t),\dots,v_N(t)\big)$, where $v_r:[t_{r-1},t_r]\to R^n$ is continuous for all $r=\overline{1,N}$, with the norm $\big\|v[\cdot]\big\|_3=\max\limits_{r=\overline{1,N}}\max\limits_{t\in[t_{r-1},t_r]}\|v_r(t)\|$.

For the solutions to problems (3), (4) and (5), (6), the following relations are fulfilled:

$$u_r(t,\lambda)=v_r(t,\lambda),\quad t\in[t_{r-1},t_r),\quad\lim_{t\to t_r-0}u_r(t,\lambda)=v_r(t_r,\lambda),\quad r=\overline{1,N}.$$

At a fixed parameter $\widehat{\lambda}\in S\big(\lambda^{(0)},\rho_\lambda\big)$, we get

$$\frac{dv_r}{dt}=A(t)v_r+A(t)\widehat{\lambda}_r+\sum_{k=1}^{m}\varphi_k(t)\sum_{j=1}^{N}\int_{t_{j-1}}^{t_j}\psi_k(\tau)f_k(\tau,v_j(\tau)+\widehat{\lambda}_j)d\tau+f_0(t),t\in[t_{r-1},t_r],\quad(7)$$

$$v_r(t_{r-1})=0,\quad r=\overline{1,N}.\qquad(8)$$

Let us introduce the following notation:
$S\big(0,\rho_v\big)=\big\{v[t]=(v_1(t),v_2(t),\dots,v_N(t))\in\widetilde{C}\big([0,T],\Delta_N,R^{nN}\big):\|v[\cdot]\|_3\le\rho_v\big\}$.

Theorem 1 *Let Condition A be fulfilled and the following inequalities be valid:*

(i) $\big\|f_k(t,x')-f_k(t,x'')\big\|\le L_k\|x'-x''\|$, L_k *is a constant,* $(t,x'),(t,x'')\in G^0(\rho)$, $k=\overline{1,m}$;

(ii) $\Big(\alpha+\sum\limits_{k=1}^{m}\max\limits_{t\in[0,T]}\|\varphi_k(t)\|\sum\limits_{j=1}^{N}\int\limits_{t_{j-1}}^{t_j}\|\psi_k(\tau)\|d\tau L_k\Big)\overline{h}<1$;

(iii) $\overline{h}\Big(\alpha(\|\lambda^{(0)}\|+\rho)+\sum\limits_{k=1}^{m}\max\limits_{t\in[t_{r-1},t_r]}\big\|\varphi_k(t)\big\|\sum\limits_{j=1}^{N}\int\limits_{t_{j-1}}^{t_j}\big\|\psi_k(\tau)\big\|d\tau M_k+M_0\Big)\le\rho_v$.

Then, for any $\widehat{\lambda}\in S(\lambda^{(0)},\rho_\lambda)$, *there exists a unique function system* $v[t,\widehat{\lambda}]=(v_1(t,\widehat{\lambda}),v_2(t,\widehat{\lambda}),\dots,v_N(t,\widehat{\lambda}))$, *the solution to the special Cauchy problem* (7), (8) *in* $S(0,\rho_v)$.

3 Conclusions and Future work

The solvability conditions of the special Cauchy problem are obtained. The special Cauchy problem will be used in the study of Fredholm IDEs.

Acknowledgments

This research is funded by the Science Committee of the Ministry of Education and Science of the Republic of Kazakhstan, Grant No. AP 09258829.

References

[1] D.S. Dzhumabaev, New general solutions to linear Fredholm integro-differential equations and their applications on solving the boundary value problems, J. Comput. Appl. Math., **327** (2018), 79–108.

[2] D.S. Dzhumabaev, S.T. Mynbayeva, New general solution to a nonlinear Fredholm integro-differential equation, Eurasian Math. J., **10**(4) (2019), 24–33.

[3] D.S. Dzhumabaev, On one approach to solve the linear boundary value problems for Fredholm integro-differential equations, J. Comput. Appl. Math., **294** (2016), 342-357.

[4] D.S. Dzhumabaev, Necessary and sufficient conditions for the solvability of linear boundary value problems for the Fredholm integro-differential equations, Ukrainian Math. J., **66**(8) (2015), 1200–1219.

[5] D.S. Dzhumabaev, E.A. Bakirova, and S.T. Mynbayeva, A method of solving a nonlinear boundary value problem with a parameter for a loaded differential equation, Math. Methods Appl. Sci., **4** (2020), 1788–1802.

InternationalConferenceon Mathematical Analysis and Applicationsin ScienceandEngineering
ICMA²SC'22
ISEP Porto-Portugal,June27 - 29,2022

ON THE WELL-POSEDNESS OFTHE CAUCHYPROBLEM FOR THE QUASI-LINEAR CONTROLLED NEUTRAL FUNCTIONAL DIFFERENTIAL EQUATION

Tea Shavadze

I. Javakhishvili Tbilisi State University, Georgia

tea.shavadze@gmail.com

Abstract: for the controlled neutral functional differential equation whose right-hand side linear with respect to prehistory of the phase velocity the continuous dependence of a solution on the initial data and on the nonlinear term in right-hand side of equation is investigated. The perturbation nonlinear term and initial data are small in the integral and standard sense, respectively. Under initial data we mean the collection of delay parameters, the initial vector and function, the control function.

keywords: neutral functional differential equation; well-posedness; perturbation.

MSC2020:34K40;34K27.

1 Introduction

The neutral functional differential equation is a mathematical model of such system whose behavior at a given moment depends on the velocity and state of the system in the past. Many real processes are described by neutral functional differential equations and the theory of such equations is presented in [1-3]. For illustration, here we consider a model of economic growth. Let $p(t)$ be a quantity of a product produced at the moment t which is expressed in money units. The fundamental principle of the economic growth has the form

$$p(t) = a(t) + i(t), \tag{1.1}$$

where $a(t)$ is a quantity money for the salaries and social programs; $i(t)$ is a quantity money for the induced investment (purchase of new technologies and etc). We consider the case where the functions $a(t)$ and $i(t)$ have the form

$$a(t) = \alpha(t, p(t)), \tag{1.2}$$

$$i(t) = \beta(t, p(t-\tau), \dot{p}(t), \dot{p}(t-\tau)) + \gamma\, \ddot{p}(t) + \varsigma(t, p(t-h), \dot{p}(t), \dot{p}(t-h), v(t))\, \ddot{p}(t-\sigma), \tag{1.3}$$

where $v(t) \in [v_1, v_2]$ is a control function (investment from the government or from the private firms), with $v_2 > v_1 > 0$; $\gamma > 0$ is a given number; $\tau > 0, h > 0$ and $\sigma > 0$ are so-called delays. The formula (1.3) shows that the value of investment at the moment t depends: on the quantity of money at the moment $t-\tau$ and $t-h$ (in the past); on the velocity (production current) at the moments $t, t-\tau$ and $t-h$; on the acceleration at the moments t and $t-\sigma$. From formulas (1.1)-(1.3) we get the equation

$$\ddot{p}(t) = \frac{1}{\gamma}\left[p(t) - \alpha(t, p(t)) - \beta(t, p(t-\tau), \dot{p}(t), \dot{p}(t-\tau)) - \varsigma(t, p(t-h), \dot{p}(t), \dot{p}(t-h), v(t))\, \ddot{p}(t-\sigma)\right]$$

which is equivalent to the following controlled quasi-linear neutral functional differential equation:

$$\begin{cases} \dot{x}^1(t) = x^2(t), \\ \dot{x}^2(t) = \dfrac{1}{\gamma}\left[x^1(t) - \alpha(t, x^1(t)) - \beta(t, x^1(t-\tau), x^2(t), x^2(t-\tau)) \right. \\ \left. - \varsigma(t, x^1(t-h), x^2(t), x^2(t-h), v(t))\dot{x}^2(t-\sigma), \right. \end{cases}$$

here $x^1(t) = p(t)$.

In the paper, for the controlled neutral functional differential equation

$$\dot{x}(t) = A(t, x(t), x(t-h_0), u_0(t))\dot{x}(t-\sigma_0) + f_0(t, x(t), x(t-\tau_0)), \quad t \in I = [t_0, t_1]$$

with the initial condition

$$x(t) = \varphi_0(t), \ t < t_0, \ x(t_0) = x_{00}$$

the theorem on the continuous dependence of solution is given, when perturbations of the initial vector x_{00}, the initial function $\varphi_0(t)$, delay parameters h_0, σ_0, τ_0 and the control function $u_0(t)$ are small in the Euclidean topology, and a perturbation of the function $f_0(t, x, y)$ is small in the integral sense. Theorems of such a type play an important role in studying optimal control problems, in proving variation formulas of solution [3] and in the sensitivity analysis of models.

2 Results and discussion

Let $O \subset R^n$ be an open set and $U \subset R^r$ be a compact set; let $h_2 > h_1 > 0, \sigma_2 > \sigma_1 > 0$ and $\tau_2 > \tau_1 > 0$ be given numbers. Suppose that E is the set of functions $f : I \times O^2 \to R^n$ satisfying the following conditions: for each fixed $(x, y) \in O^2$ the function $f(\cdot, x, y) : I \to R^n$ is measurable; for each $f \in E$ and compact set $K \subset O$ there exist functions $m_{f,K}(t), L_{f,K}(t) \in L(I, [0, \infty))$, such that for almost all $t \in I$

$$|f(t, x, y)| \le m_{f,K}(t), \forall (x, y) \in K^2,$$

$$|f(t, x_1, y_1) - f(t, x_2, y_2)| \le L_{f,K}(t)\left(|x_1 - x_2| + |y_1 - y_2|\right), \forall (x_1, y_1) \in K^2, \forall (x_2, y_2) \in K^2.$$

Let Φ be the set of continuously differentiable initial functions $\varphi(t) \in O, t \in [\hat{\tau}, t_0]$, where $\hat{\tau} = t_0 - \min\{h_2, \sigma_2, \tau_2\}$, with $\|\varphi\|_1 = \sup\{|\varphi(t)| + |\dot{\varphi}(t)| : t \in [\hat{\tau}, t_0]\}$. By Ω denote the set of piecewise-continuous control functions $u(t) \in U, t \in I$, with $\|u\| = \sup\{|u(t)| : t \in I\}$. Let $A(t, x, y, u)$ be a given $n \times n$ matrix function satisfying Lipschitz's condition on the set $I \times O^2 \times U$.

To each element

$$w = (h, \sigma, \tau, x_0, \varphi(t), u(t), f) \in W = [h_1, h_2] \times [\sigma_1, \sigma_2] \times [\tau_1, \tau_2] \times O \times \Phi \times \Omega \times E$$

we assign the differential equation

$$\dot{x}(t) = A(t, x(t), x(t-h), u(t))\dot{x}(t-\sigma) + f(t, x(t), x(t-\tau)), \quad t \in I \tag{2.1}$$

with the initial condition

$$x(t)=\varphi(t),\ t\in[\hat{\tau},t_0),\ x(t_0)=x_0. \tag{2.2}$$

Definition. Let $w\in W$, a function $x(t)=x(t;w)\in O, t\in[\hat{\tau},t_1]$ is called a solution of Eq. (2.1) with the initial condition (2.2) or a solution corresponding to the element w and defined on the interval $[\hat{\tau},t_1]$ if it satisfies the condition (2.1) and absolutely continuous on the interval $[t_0,t_1]$ and satisfies Eq. (2.1) almost everywhere on $[t_0,t_1]$.

To formulate the main result we introduce the following sets:

$$P(K;c)=\left\{f\in E:\exists m_{f,K}(t), L_{f,K}(t)\in L(I,[0,\infty)), \int_I \left[m_{f,K}(t)+L_{f,K}(t)\right]dt\le c\right\},$$

where $K\subset O$ is a compact set and $c>0$ is a fixed number independent of f;

$$B(h_0;\delta)=\{h\in[h_1,h_2]:|h-h_0|<\delta\},\ B(\sigma_0;\delta)=\{\sigma\in[\sigma_1,\sigma_2]:|\sigma-\sigma_0|<\delta\},$$

$$B(\tau_0;\delta)=\{\tau\in[\tau_1,\tau_2]:|\tau-\tau_0|<\delta\},\ B(x_{00};\delta)=\{x_0\in O:|x_0-x_{00}|<\delta\},$$

$$B(\varphi_0;\delta)=\{\varphi\in\Phi:\|\varphi-\varphi_0\|_1<\delta\},\ B(u_0;\delta)=\{u\in\Omega:\|u-u_0\|<\delta\},$$

$$B(f_0;K,c,\delta)=\{f\in P(K;c):\|f\|_K<\delta\},$$

where

$$\|f\|_K=\sup\left\{\left|\int_{s_1}^{s_2} f(t,x,y)dt\right|:(s_1,s_2,x,y)\in I^2\times K^2\right\},$$

$h_0\in[h_1,h_2]$, $\sigma_0\in[\sigma_1,\sigma_2]$, $\tau_0\in[\tau_1,\tau_2]$, $x_{00}\in O$ are the fixed points; $\varphi_0\in\Phi$, $u_0\in\Omega$ and $f_0\in E$ are the fixed functions, $\delta>0$ is a fixed number.

Theorem. Let $x_0(t)$ be a solution corresponding to $w_0=(h_0,\sigma_0,\tau_0,x_{00},\varphi_0(t),u_0(t),f_0)\in W$ and defined on $[\hat{\tau},t_1]$. Let $K_0\subset O$ be a compact set containing a certain neighborhood of the set $x_0([\hat{\tau},t_1])$. Then the following assertions hold:

2.1. there exists a number $\delta_0>0$ such that to each element

$$w=(h,\sigma,\tau,x_0,\varphi(t),u(t),f)\in B(w_0;K_0,c,\delta_0)=B(h_0;\delta_0)\times B(\sigma_0;\delta_0)\times B(\tau_0;\delta_0)\times B(x_{00};\delta_0)$$
$$\times B(\varphi_0;\delta_0)\times B(u_0;\delta_0)\times B(f_0;K_0,c,\delta_0)$$

there corresponds the solution $x(t;w)$ defined on the interval $[\hat{\tau},t_1]$ and satisfying the condition $x(t;w)\in K_0$;

2.2. for any arbitrary $\varepsilon>0$ there exists a number $\delta_1=\delta_1(\varepsilon)\in(0,\delta_0]$ such that the following inequality holds for any $w\in B(w_0;K_0,c,\delta_1)$:

$$\left|x(t;w)-x_0(t)\right| \le \varepsilon, \forall t \in I.$$

Remark. The theorem on the well-posedness for the quasi-linear neutral functional differential equation without perturbation of σ_0 and where $A\left(t,x\left(t\right),x\left(t-h\right),u\left(t\right)\right) \equiv A(t)$ is proved in [3].We note that if the right-hand side of the equation (2.1) is nonlinear in $\dot{x}(t-\sigma)$, then the problem (2.1)-(2.2) is ill-posed in general when a perturbation of $f_0(t,x,y)$ is small in the integral sense [3].

3 Conclusions and Future work

On the basis of the given Theorem can be proved the necessary conditions for optimality of delay parameters, initial vector, initial and control functions and also can be proved analytical relations between of solutions of the initial and perturbed equations. Future work will consider the case when the initial moment t_0 is non-fixed and a controlled quasi-linear neutral functional differential equation contains several variable delays.

4 Acknowledgments

This work was supported by Shota Rustaveli National Science Foundation of Georgia (SRNSFG), Grant No. YS-21-554.

References

[1] J. Hale, *Theory of functional differential equations.*Springer-Verlag New York, Heidelberg Berlin, 1977.

[2] V. Kolmanovski andA. Myshkis, *Introduction to the theory and applications of functional differential equations*. Kluwer Academic Publishers, 1999.

[3] T. Tadumadze, N. Gorgodze,Variation formulas of a solution and initial data optimization problems for quasi-linear neutral functional differential equations with discontinuous initial condition, Mem.Differential Equations Math.Phys.,**63** (2014), 1-77.

International Conference on Mathematical Analysis and Applications in Science and Engineering
ICMA^{2}SC'22
ISEP Porto-Portugal, June 27 - 29, 2022

A Fuzzy q-Symmetric Variational Problem via Granular Differentiability Approach

Tri Truong [1⋆] **Linh Nguyen**[2] **Baruch Schneider**[1]

[1] University of Ostrava, Department of Mathematics, Faculty of Science, 30. dubna 22, 701 03 Ostrava, Czech Republic
[2] University of Ostrava, Institute for Research and Applications of Fuzzy Modeling, CE IT4Innovations

[1⋆]tritruongvan@hotmail.com

Abstract: We investigate in this paper a fuzzy q-symmetric variational problem. Based on the relative distance measure fuzzy arithmetic (RDM-FA) and horizontal membership functions (HMFs), we first propose the new concepts of granular q-symmetric differentiability and integrability for fuzzy-valued functions. Then, fundamental foundations of q-symmetric calculus of variations based on HMFs are provided. With the help of HMFs and the granular q-symmetric differentiability, we derive the necessary optimality condition for the fuzzy q-symmetric variational problem. Finally, some numerical examples to illustrate the proposed approach are presented.

keywords: horizontal membership functions; granular differentiability; fuzzy variational problems; q-symmetric calculus of variations.

MSC2020: 03E72; 05A30; 49Jxx; 49Kxx.

1 Introduction

The calculus of variations, known as a field of optimization, works with the determinating of extrema or stationary values of functionals. It has various applications in many fields such as physics, engineering and applied mathematics. Extending the theory of classical variational calculus using the fuzzy set theory, founded by L. Zadeh, to deal with uncertainties has attracted increasing research interest. One of the earliest works proposed by Farhadinia (see [3]). In that work, by using the Buckley-Fuering derivative, he obtained the necessary optimality conditions for the fuzzy unconstrained and constrained variational problems. Since then there has been a great deal of interest in the study of variational problems and optimal control problems with the fuzzy environments. Notably, in [2], the authors studied the generalized fuzzy Euler-Lagrange equation and fuzzy isoperimetric problem with the help of fuzzy Caputo-type generalized Hukuhara fractional derivative. In [10], the authors considered the necessary optimality conditions for fuzzy variational problems, based on the generalized Hukuhara differentiability concept. Some further works relating to fuzzy variational problems and fuzzy differential equations being with generalized Hukuhara differentiability can be found in [11, 12]. Concerning approaches using generalized Hukuhara difference, although the major limitation of the Hukuhara and Seikkala derivatives, the diameter of the fuzzy-valued functions (FVFs)

must be assumed to be non-decreasing, is solved, this approach also leads to some shortcomings such as the existence of difference, the monotonicity of the vagueness, the multiplicity of fuzzy solutions and unnatural behavior in modeling phenomenon and so on. To overcome these drawbacks, in [6], Mazadarani proposed the new concept of differentiability motivated by HMFs (see [9]) to study fuzzy differential equations. By its convenience, there are various works such as the fuzzy Bang-Bang (FBB) control problem (see [7]), fuzzy variational problem and fuzzy optimal control (see [8]) that are established based on this tool.

Quantum calculus, especially q-symmetric quantum calculus, has various applications and plays an essential role in many fields of science, in particular, in quantum mechanics (see [4]). Quantum variational calculus allows us to study the calculus of variations for a class of non-differentiable functions by using difference operators such as q-difference operator, h-difference operator, q-symmetric difference operator, or Hahn's difference operator, in stead of classical derivatives. For works in quantum variational calculus and its applications, we refer to references [1, 5].

With above observations, we propose the new concepts of q-symmetric differentiability and integrability for FVFs by using Relative Distance Measure (RDM) variables. Fundamental foundation of q-symmetric calculus of variations based on HMFs are provided. With the help of HMFs and granular q-symmetric differentiability of FVFs, we obtain the necessary condition for the fuzzy variational problem which called fuzzy granular Euler-Lagrange equation.

2 Results and discussion

For our analysis, it is necessary to recall some theorical bases of horizontal fuzzy numbers which is called granular representation of fuzzy numbers and its operations are mentioned (see [6, 9]).

In Relative Distance Measure (RDM) interval arthmetic, an arbitrary interval $A = [\underline{a}, \overline{a}]$ is described by a set of numbers: $A = \{a \mid a = \underline{a} + (\overline{a} - \underline{a})\mu_a,\ \mu_a \in [0,1]\}$.

Definition 1 A fuzzy set (membership function) $u : [x, y] \subseteq \mathbb{R} \to [0, 1]$ is said to be a fuzzy number on $\mathbb{R}$ if it is normal, fuzzy convex, upper semicontinuous and compact supported. We denote by $\mathbb{R}_f$ the set of all fuzzy numbers on $\mathbb{R}$.

Let u be a fuzzy number. For $0 < \alpha \leq 1$, an α-level set of u is defined by $[u]^\alpha = \{s \in \mathbb{R} \mid u(s) \geq \alpha\}$ and $[u]^0 = \overline{\{s \in \mathbb{R} \mid u(s) > 0\}}$. The α-level set of u can be represented by $[u]^\alpha = [\underline{u}^\alpha, \overline{u}^\alpha]$, where $\underline{u}$ and $\overline{u}$ are lower and upper branches of u, respectively.

Definition 2 Let $u : [x, y] \subseteq \mathbb{R} \to [0, 1]$ be a fuzzy number and $[u]^\alpha = [\underline{u}^\alpha, \overline{u}^\alpha]$ be its α-level representation. The horizontal membership function $u^{gr} : [0, 1] \times [0, 1] \to [x, y]$, is defined by

$$u^{gr}(\alpha, \mu_u) = \underline{u}^\alpha + (\overline{u}^\alpha - \underline{u}^\alpha)\mu_u,$$

where $\alpha \in [0, 1]$ is called the membership degree of u and $\mu_u \in [0, 1]$ is called RDM variable. We denote the horizontal membership function of $u \in \mathbb{R}_f$ by $\mathcal{H}(u) = u^{gr}(\alpha, \mu_u)$. The α-level sets of the vertical membership function u is given by the following transformation

$$\mathcal{H}^{-1}(u^{gr}(\alpha, \mu_u)) = [u]^\alpha = [\inf_{\beta \geq \alpha} \min_{\mu_u} u^{gr}(\beta, \mu_u), \sup_{\beta \geq \alpha} \max_{\mu_u}(\beta, \mu_u)].$$

Definition 3 (Arithmetic Operations) Let $u, v \in \mathbb{R}_f$ and $\mathcal{H}(u)$ and $\mathcal{H}(v)$ be the horizontal membership functions of u and v, respectively. We denote by $\circledast$ one of basic operations on $\mathbb{R}_f$ including addition, subtraction, multiplication, and division. Then, $u \circledast v$ is a fuzzy number w satisfying

$$\mathcal{H}(w) = \mathcal{H}(u) * \mathcal{H}(v),$$

where the operation $*$ is understood the corresponding operations on $\mathbb{R}$. It is noticed that if $\circledast$ stands for the division operation, we need to assume $0 \notin \mathcal{H}(v)$. The difference between two fuzzy numbers in Definition 3 is called *granular difference* (*gr-difference*, for short). The *gr*-difference between two fuzzy numbers u and v is denoted by $u \ominus_{gr} v$.

Definition 4 (Ordering relation) Let $u, v \in \mathbb{R}_f$. Then, we say $u \leq v$ if and only if $\mathcal{H}(u) \leq \mathcal{H}(v)$, for all $\mu_u = \mu_v \in [0,1], \alpha \in [0,1]$.

2.1 q-symmetric calculus for fuzzy-valued functions

Let $q \in (0,1)$. In what follows, we denote by I^q the set $I^q = \{qx \mid x \in I\}$, where I is an interval of $\mathbb{R}$ containing 0. We note that $I^q \subseteq I$.

Definition 5 Let $q \in (0,1)$ and $F : I \to \mathbb{R}_f$ be a FVF. The FVF F is said to be *granular q-symmetric differentiable* at $t \in I^q$, if there exists a fuzzy number $\tilde{D}_q^{gr}[F](t) \in \mathbb{R}_f$ such that

$$\tilde{D}_q^{gr}[F](t) = \frac{F(q^{-1}t) \ominus_{gr} F(qt)}{t(q^{-1} - q)}, \; t \in I^q \backslash \{0\},$$

and $\tilde{D}_q^{gr}[F](0) = D^{gr}[F](0)$[1], provided F is granular differentiable at 0. Then, the fuzzy number $\tilde{D}_q^{gr}[F](t)$ is called the *granular q-symmetric derivative* of F at t.

Theorem 1 *Let $F : I \to \mathbb{R}_f$ be a FVF. Then, F is granular q-symmetric differentiable at $t_0 \in I^q$ if and only if its horizontal function $\mathcal{H}(F)$ is q-symmetric differentiable with respect to t at t_0. Moreover, we have $\mathcal{H}\left(\tilde{D}_q^{gr}[F](t_0)\right) = \frac{\tilde{\partial}_q F^{gr}(t_0, \alpha, \mu_F)}{\partial t}$.*

Definition 6 Let $a, b \in I$ and $a < b$. Let $F : I \to \mathbb{R}_f$ be a FVF and $F^{gr}(t, \alpha, \mu_F)$ be its horizontal membership function such that $F^{gr}(t, \alpha, \mu_F)$ is q-symmetric integrable on $[a,b]$. Let $\int_a^b F(t)\tilde{d}_q t$ denote the granular q-symmetric integral of F from a to b. Then, the FVF F is said to be *granular q-symmetric integrable* on $[a,b]$ if there exists a fuzzy number $u = \displaystyle\int_a^b F(t)\tilde{d}_q t$ such that $\mathcal{H}(u) = \int_a^b F^{gr}(t, \alpha, \mu_F)\tilde{d}_q t$.

2.2 Fuzzy q-symmetric variational Problem

In this section, we consider the necessary condition for fuzzy q-symmetric variational problem (**Fq-SVP**) defined by

$$\mathcal{J}(X) = \int_a^b L\left(s, X(qs), \tilde{D}_q^{gr} X(s)\right) \tilde{d}_q s \qquad \to \qquad \min$$

$$\text{subject to the constraints: } X(a) = \Lambda_1, \; X(b) = \Lambda_2,$$

where Λ_1, Λ_2 are fixed fuzzy numbers and the fuzzy curve $X(t)$ is granular q-symmetric differentiable with respect to $t \in [a,b]$. By using HMFs and the assumptions on the Lagrangian L, we establish the necessary optimality condition for (**Fq-SVP**) under fuzzy granular q-symmetric differentiability concept.

[1] $D^{gr}[F](0)$ is known as the granular derivative of F at 0 (see[6]).

3 Conclusions and Future work

In this paper, we studied the fuzzy q-symmetric variational problem under the granular differentiability approach. The main contributions are highlighted as follows: 1) Based on the horizontal membership functions of fuzzy numbers, we proposed the notions of granular q-symmetric derivative and integral for FVFs. Some fundamental characteristics of the proposed concepts are investigated; 2) We introduced granular fuzzy q-symmetric variational problem based on the granular q-symmetric differentiability and integrability of FVFs; 3) The granular Euler-Lagrange condition for the fuzzy q-symmetric variational problem is investigated. Some numerical examples are provided to illustrate the proposed methods.

Acknowledgments

The work of the first author and the third author have supported by the grant SGS03/PřF/2022.

References

[1] A. M.C. Brito da Cruz, N. Martins, The q-symmetric variational calculus, Computers & Mathematics with Applications, 64(7):2241–2250, 2012.

[2] O. S. Fard, M. Salehi, A survey on fuzzy fractional variational problems, Journal of Computational and Applied Mathematics, 271:71–82, 2014.

[3] B. Farhadinia, Necessary optimality conditions for fuzzy variational problems, Information Sciences, 181(7):1348–1357, 2011.

[4] A. Lavagno, G. Gervino, Quantum mechanics in q-deformed calculus, In Journal of Physics: Conference Series, volume 174, page 012071. IOP Publishing, 2009.

[5] A. B. Malinowska, D. F.M. Torres, The hahn quantum variational calculus, In Quantum Variational Calculus, pages 9–54. Springer, 2014.

[6] M. Mazandarani, N. Pariz, A. V. Kamyad, Granular differentiability of fuzzy-number-valued functions, IEEE Transactions on Fuzzy Systems, 26(1):310–323, 2017.

[7] M. Mazandarani, Y. Zhao, Fuzzy bang-bang control problem under granular differentiability, Journal of the Franklin Institute, 355(12):4931–4951, 2018.

[8] A. M. Mustafa, Z. Gong, M. Osman, The solution of fuzzy variational problem and fuzzy optimal control problem under granular differentiability concept, International Journal of Computer Mathematics, 98(8):1495–1520, 2021.

[9] A. Piegat, M. Landowski, Horizontal membership function and examples of its applications, International Journal of Fuzzy Systems, 17(1):22–30, 2015.

[10] J. Soolaki, O. S. Fard, A. H. Borzabadi, Generalized euler–lagrange equations for fuzzy variational problems, SeMA Journal, 73(2):131–148, 2016.

[11] J. Soolaki, O.S. Fard, A. H. Borzabadi, A necessary condition of pontryagin type for fuzzy control systems, Computational and Applied Mathematics, 37(2):1263–1278, 2018.

[12] T. Truong, L. Nguyen, B. Schneider, On the partial delta differentiability of fuzzy-valued functions via the generalized Hukuhara difference, Computational and Applied Mathematics, 40, 208 (2021)

International Conference on Mathematical Analysis and Applications in Science and Engineering
ICMA^{2}SC'22
ISEP Porto-Portugal, June 27 - 29, 2022

Probabilistic analysis of a general kinetic equation with uncertainty

J.-C. Cortés[1] **A. Navarro-Quiles**[2] **S.-M. Sferle**[1⋆]

[1] Instituto Universitario de Matemática Multidisciplinar, Universitat Politècnica de València, Spain
[2] Department of Statistics and Operational Research, Universitat de València, Spain

[1⋆]smsferle@doctor.upv.es

Abstract: Adsorption plays an important role in chemistry. There are many mathematical models that describe the interactions between adsorbents and adsorbates at the equilibrium. In this contribution, we will consider a randomization of the general kinetic model, by assuming that all its model parameters are continuous random variables with a given joint probability density function. Then, as the solution is a stochastic process, we will determine its first probability density function, which will allow us to have a complete probabilistic description of the model. Finally, some applications with real-world data are shown.

keywords: uncertainty; kinetic model; random variable; probability density function; random variable transformation technique.

MSC2020: 34-F05

1 Introduction

Adsorption is defined as the deposition or adhesion of molecular species such as atoms, ions or molecules on a surface. The adsorption method has important applications, for example it is broadly used in water and wastewater treatment processes [1].

There exist numerous mathematical models that describe the interactions between adsorbents and adsorbates at the equilibrium, as the Lagergren or Ho models for pseudo-first order (PFO) and pseudo-second order (PSO), [2, 3]. These models are defined by the following differential equations

$$\text{PFO:} \quad \frac{dq(t)}{dt} = k_1(q_e - q(t)), \tag{1}$$

$$\text{PSO:} \quad \frac{dq(t)}{dt} = k_2(q_e - q(t))^2, \tag{2}$$

where $q_e \geq 0$ is the adsorption capacity at equilibrium (mg/g), $q(t)$ the adsorption capacity at time t (mg/g) and $k_1 > 0$ (min^{-1}) and $k_2 > 0$ ($(\text{mg/g})^{-1}\ \text{min}^{-1}$) the adsorption rates.

The generalization of these models gives rise to the general kinetic model, which takes the following form

$$\frac{dq(t)}{dt} = k_n(q_e - q(t))^n, \tag{3}$$

with $n \geq 1$ being the order of the reaction. It is obtained experimentally, so it can also take fractional values. Notice that, from equation (3), PFO and PSO are directly derived by considering $n = 1$ and $n = 2$, respectively.

Kinetic models depend on several parameters, such as the amount adsorbed at equilibrium, q_e. Classically, the kinetic parameters are deduced by comparing the experimental data with the linearized equations of the model considered. Nevertheless, previous studies show that the incorrect application of the linear equation for the PFO and PSO kinetic models lead to erroneous values of the intrinsic parameters. Furthermore, since the parameters are calculated from experimental data and depend on molecular properties that are not completely known, they contain an intrinsic uncertainty. Therefore, it is more advisable to consider them as random variables rather than as deterministic constants. Consequently, this gives rise to the random differential equations, in particular to the following randomized general kinetic equation

$$\frac{dq(t,\omega)}{dt} = k_n(\omega)(q_e(\omega) - q(t,\omega))^{n(\omega)}, \tag{4}$$

whose randomized solution is

$$q(t,\omega) = q_e(\omega) - (q_e(\omega)^{1-n(\omega)} + k_n(\omega)(n(\omega)t - 1))^{\frac{1}{1-n(\omega)}}, \tag{5}$$

where $q_e(\omega), k_n(\omega)$ and $n(\omega)$ are assumed to be absolutely continuous random variables defined on a common complete probability space $(\Omega, F, \mathbb{P})$ with a known joint PDF $f_0(q_e, k_n, n)$. Notice that equation (5) is a stochastic process.

The objective is to obtain a complete probabilistic description of the solution stochastic process coming from the randomization of the deterministic counterpart. To do this, the first probability density function (1-PDF) must be calculated.

2 Results and discussion

To obtain the following semi-explicit expression of the 1-PDF of the solution stochastic process, we apply the Random Variable Transformation (RVT) technique [4]

$$f_1(q,t) = \int_0^\infty \int_1^\infty f_0\left(q_e, \frac{q_e^{1-n} - (q_e - q)^{1-n}}{t(1-n)}, n\right) \frac{1}{t(q_e - q)^n}\, dn dq_e. \tag{6}$$

The theoretical results are illustrated using the real-world data collected in Table 1.

t_i	0	0.089	0.138	0.247	0.494	0.750	0.997	1.995	2.992
q_i	0	15.064	25.335	37.661	46.819	50.157	52.468	56.234	57.518

Table 1: Adsorption capacity of methyl orange on bentonite, q_i, for different time instants t_i. Source [5].

Hereafter, we will present the results for the general model (4) for $n = 1, 2$. We will assume that model parameters are independent random variables, so we have estimated the following probability distributions for each model parameters

$$k_n(\omega) \sim \text{Unif}([a,b]), \quad 0 < a < b; \qquad q_e(\omega) \sim \text{N}_T(\mu,\sigma), \quad T = [0,\infty), \quad \mu, \sigma > 0.$$

Once, we have estimated the 1-PDF, $f_1(q,t)$, by its integration, it is straightforward to calculate the mean and 95% confidence intervals, which show that the uncertainty coming from our data is captured. The results are shown in Figure 1.

In Figure 2 we can see the 1-PDF for PFO and PSO models.

Comparing both models, we can conclude that the variability is lower in the PFO models, while the PSO model provides a better fit to these data.

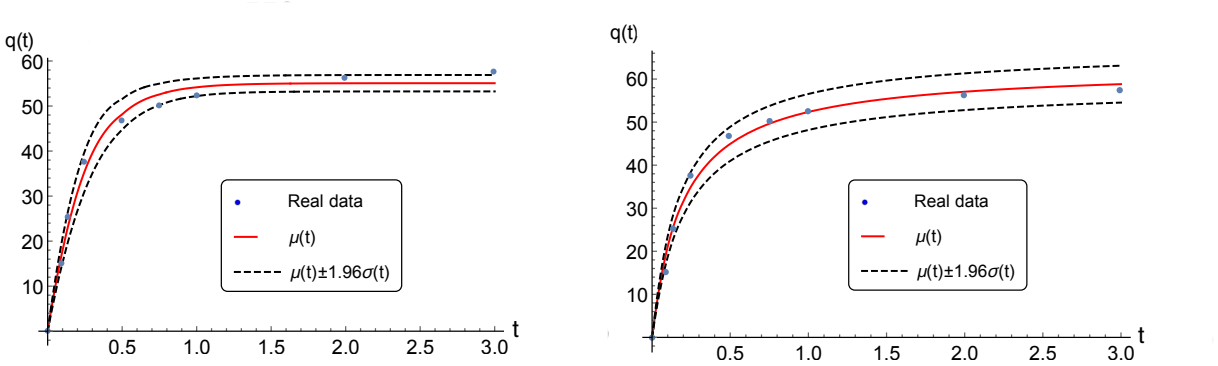

(a) PFO model (b) PSO model

Figure 1: Expectation (solid line) and 95% confidence intervals (dashed lines).

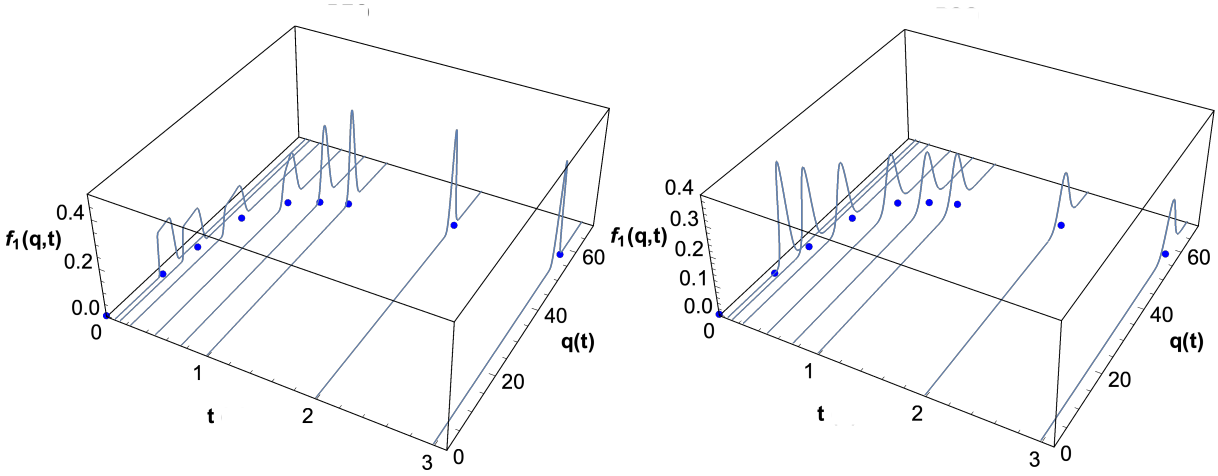

(a) PFO model (b) PSO model

Figure 2: 1-PDF visual representation of the solution stochastic process of the PFO and PSO random models.

3 Conclusions and Future work

We have studied, from a probabilistic point of view, a randomized general kinetic model from the 1-PDF of the solution stochastic process under very general assumptions, where we consider the parameters involved as dependent continuous random variables with arbitrary probability density functions.

Computing the probabilistic distribution of other quantities of interest, such as the time until a given adsorbed amount is reached, and using other techniques to estimate model parameters distributions from real data, such as Bayesian techniques, are some future work.

Acknowledgments

This work has been supported by the grant PID2020-115270GB-I00 funded by MCIN/AEI/10.13039/501100011033 and the grant AICO/2021/302 (Generalitat Valenciana).

References

[1] A. Reza, M. Ghaedi, A. Asfaram, S. Hajati, A. Mohammad, A. Bazrafshan, M. Reza, Modeling and optimization of simultaneous removal of ternary dyes onto copper sulfide nanoparticles loaded on activated carbon using second-derivative spectrophotometry, Journal of Taiwan Institute of Chemistry Engineering, **65** (2016), 212–224, https://doi.org/10.1016/j.jtice.2016.05.004.

[2] S. Lagergren, Zur theorie der sogenannten adsorption geloster stoffe, Kungliga Svenska Vetenskapsakademiens Handlingar, **24** (1898), 1–39.

[3] Y. S. Ho, G. McKay, Sorption of dye from aqueous solution by peat, Chemistry Engineering Journal, **70** (1998), 115–124, https://doi.org/ 10.1016/S1385-8947(98)00076-X.

[4] T. T. Soong, *Random Differential Equations in Science and Engineering*. New York: Academic Press, 1973.

[5] H. Moussout, H. Ahlafi, M. Aazza, H. Maghat, Critical of linear and nonlinear equations of pseudo-first order and pseudo-second order kinetic models, Karbala International Journal of Modern Science ElSevier, **4**(2) (2018), 244–254.

International Conference on Mathematical Analysis and Applications in Science and Engineering
ICMA^{2}SC'22
ISEP Porto-Portugal, June 27 - 29, 2022

Probability Density Evolution Simulation and its Applications in Random Differential Equations

V. J. Bevia[1⋆] **J.C. Cortés**[2] **R.J. Villanueva**[3]

[1,2,3] Instituto de Matemática Multidisciplinar, UPV, Spain

[1⋆] vibees@upv.es

Abstract: In this contribution, we are going to give a brief discussion about the latest developments in an alternative methodology for simulating the evolution of the probability density functions of solutions to random differential equations. We will show how the use of a specific theoretical approach, based on the Liouville equation, and the use of numerical methods belonging to areas, such as computational fluid dynamics, are used to obtain accurate and relatively cheap simulations, computationally speaking. We will showcase its versatility through a number of examples of real-world mathematical models.

keywords: Random Differential Equations; Liouville Equation; Uncertainty Quantification; Lagrangian methods.

MSC2020: 65-M75; 34-A34 ; 34-F05

1 Introduction

Montecarlo (MC) simulations (see [1, 2]) and generalized Polynomial Chaos expansions (gPCe, see [3]) are some of the most widely-known techniques used for uncertainty quantification of mathematical models given by ODEs or PDEs with random or stochastic terms, whose solutions are Stochastic Processes (SPs). However, MC simulations suffer from a very low convergence rate, and gPCe is meant to efficiently compute the solution moments, such as the mean and variance of the solution SP. The most desirable goal is to have an expression or approximate representation of the Probability Density Function (PDF) of the solution SP. One of the methods used to achieve this goal is the so-called Random Variable Transformation (RVT) method (see [4, 5]). However, this method has a significant drawback: it is only applicable when an explicit solution SP is known, which is generally not the case.

In this contribution, we are going to focus on a method based on the Liouville Equation (see [6]), also known as Continuity Equation in fluid dynamics or optimal transportation theory (see [7]). This method is relatively unknown in the setting of RDEs. The result can be stated as follows:

Theorem 1 *([6, Ch.6]). Let $\mathbf{X}(t)$, $t \geq t_0$ be the stochastic process verifying the following RDE in the mean square sense:*

$$\left\{ \begin{array}{rcl} \dfrac{\mathrm{d}\mathbf{X}(t)}{\mathrm{d}t} & = & \mathbf{g}(\mathbf{X}(t), t), \quad t > t_0, \\ \mathbf{X}(t_0) & = & \mathbf{X}_0 \in \mathrm{L}^2(\Omega, \mathbb{R}^n). \end{array} \right. \tag{1}$$

Then, the 1-PDF of the stochastic process $\mathbf{X}(t)$*, denoted by* f*, verifies the Liouville PDE:*

$$\partial_t f(\mathbf{x},t) + \nabla_{\mathbf{x}} \cdot [\mathbf{g}\, f](\mathbf{x},t) = 0, \tag{2}$$

being $\nabla_{\mathbf{x}}\cdot$ *the divergence operator with respect to variables* $(x_1,\ldots,x_n) = \mathbf{x}^{\mathsf{T}}$*. However, if* $\mathbf{g}(\cdot,t) \in \mathrm{C}^1(\mathcal{D})$ *and* $\nabla_{\mathbf{x}} \cdot \mathbf{g}(\cdot,t)$ *is Lipschitz continuous for all* $t \geq t_0$*, we may compute the product inside the divergence term in equation* (2)*, obtaining a more useful form of the Liouville equation:*

$$\partial_t f(\mathbf{x},t) + \mathbf{g}(\mathbf{x},t) \cdot \nabla_{\mathbf{x}} f(\mathbf{x},t) = -f(\mathbf{x},t)\, \mathrm{Div}_{\mathbf{x}} \mathbf{g}(\mathbf{x},t). \tag{3}$$

For the sake of simplicity, we only state the Liouville PDE theorem for the case of random initial conditions, although this result can easily be adapted to the case of random RDE coefficients.

This result allows the theoretical and numerical study of the probability distribution evolution of general dynamical systems defined by one or more RDEs. This is motivated by the possibility of studying the PDF evolution through its characteristic curves (see [8]). Particularly, if $\{\mathbf{X}(\cdot\,;\mathbf{x}_0)\}_{\mathbf{x}_0}$ is a family of characteristic curves for the PDE, whose solution we denote f, then it can be seen that

$$f(\mathbf{X}(t;\mathbf{x}_0),t) = f_0(\mathbf{x}_0) \exp\left(-\int_0^t \nabla_{\mathbf{x}} \cdot \mathbf{g}(\mathbf{X}(s;\mathbf{x}_0),s)\mathrm{d}s\right). \tag{4}$$

Now, this approach involves transforming the number of equations of the RDE system into "spatial" dimensions of the Liouville PDE. This fact limits the use of classical numerical methods, such as Finite Differences, Finite Volumes, or Finite Elements at dimensions higher than 3, which a 3-equation RDE system would form.

Therefore, we have resorted to the so-called Lagrangian methods, in which basically grid points are treated as particles that move according to characteristic curves of the PDE. The PDF values are updated at the curves instead of at the grid points. Also, a Wavelet compression-based Adaptive Mesh Refinement technique has been employed due to the large number of particles to be transported. Although this computational approach has its drawbacks, it has two overwhelming advantages for simulating the PDF of an RDE system: 1) It (almost) avoids the curse of dimensionality because the number of characteristic equations to be solved is directly proportional to the number of equations forming the RDE system. 2) It can be easily programmed in massively-parallel architectures, such as GPUs or several-core CPUs, greatly accelerating the simulation of the evolution of the PDF.

2 Results and discussion

In this section, we will show in detail an example from one of our latest works in the current setting of Liouville's Equation in RDE uncertainty quantification evolution. Also, we will mention some other works we have done in this setting for whoever is interested.

2.1 Random Duffing Model

The harmonically-forced Duffing equation is a classical mathematical model used in engineering when analyzing spring-damper vibration dynamics outside the "linear behavior" region of the spring (see [9, 10]). The model is given by the following nonlinear second-order differential equation:

$$\begin{cases} \frac{\mathrm{d}^2 X(t)}{\mathrm{d}t^2} + 2\xi \frac{\mathrm{d}X(t)}{\mathrm{d}t} + X(t) + \alpha X(t)^3 = A\cos(\nu\, t), \quad t > 0, \\ \\ X(0) = X_0,\ \dot{X}(0) = \dot{X}_0, \end{cases} \tag{5}$$

where the model parameters $\xi > 0$, $\alpha > 0$ and A, as well as the initial conditions X_0 and $\dot{X}_0$, are assumed to be second-order random variables, while $\nu = 3$ is the frequency of the external forcing and it is assumed deterministic. The corresponding Liouville PDE terms; that is, the flow function and its divergence are defined as follows:

$$\mathbf{g}(\mathbf{x}, t) = (x_2, -2\xi\, x_2 - x_1 - \alpha\, x_1^3 + A\, \cos(\nu\, t)), \quad \nabla_{\mathbf{x}} \cdot \mathbf{g}(\mathbf{x}, t) = -2\xi, \tag{6}$$

where $\mathbf{x} = (x_1, x_2)$. Figure 2 shows the final distribution as it has evolved through the Duffing equation, with the initial distribution at Figure 1. These figures show a preview of some of its interesting dynamics and the versatility of the Liouville approach to accurately simulate the PDF evolution.

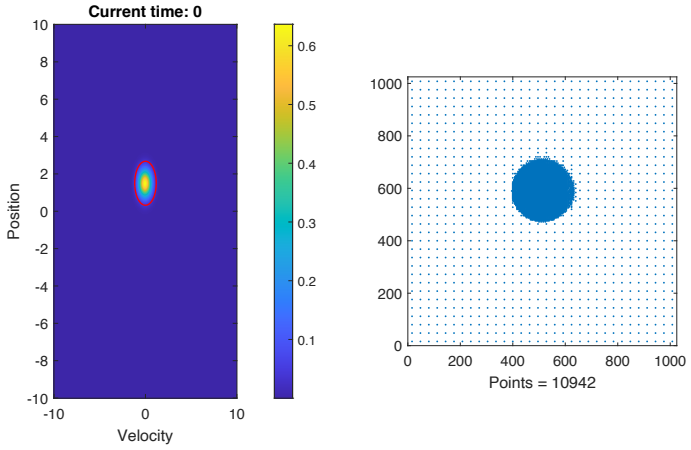

Figure 1: Left figure shows the joint PDF at time $t = 0$, with its 95% confidence region (red curve). The right figure shows the points selected by the AMR to be simulated.

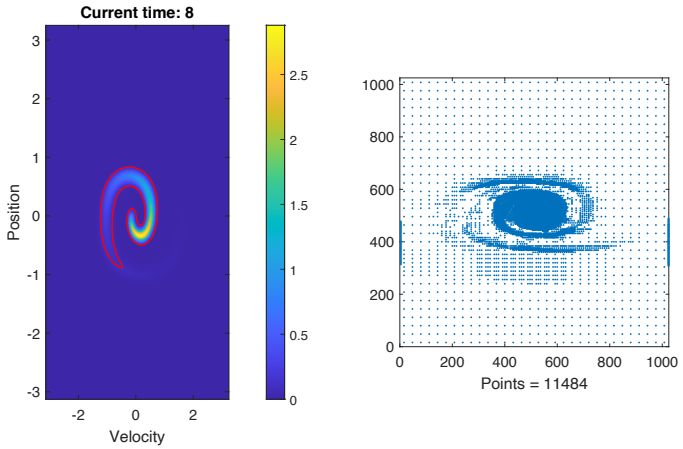

Figure 2: Left figure shows the joint PDF at time $t = 8$, with its 95% confidence region (red curve). The right figure shows the points selected by the AMR to be simulated.

3 Conclusions and future work

We have used the Liouville Equation to simulate the 1-Probability Density Function evolution of Stochastic Processes defined as solutions of Random Differential Equations both in the mean square and pathwise sense. We have shown that, by using specific numerical techniques such as Lagrangian methods and Adaptive Mesh Refinement, we can significantly increase the efficiency while maintaining the high precision of the simulations. We have shown the versatility of the Liouville approach with the used numerical techniques utilizing well-known models used in real-world mathematical modeling.

We are currently working on comparing the Montecarlo and Liouville approaches for random higher-dimensional problems (3D, 4D and 5D). Also, we are working to improve the efficiency and accuracy of the simulations via full-GPU implementation in low-level programming languages such as C-based CUDA. All this work has the primary goal of being useful in real-world scenarios with actual data, as we have shown in 1 and 2-D cases.

Acknowledgments

This work has been partially supported by the grant PID2020–115270GB–I00 funded by MCIN/AEI/10.13039/50110 0 011033 and the grant AICO/2021/302 (Generalitat Valenciana).

References

[1] Metropolis N, Ulam S. The Monte Carlo method. Journal of the American Statistical Association. 1949 Sep 1;44(247):335–341.

[2] Dunn W., Shultis J.K. Exploring Monte Carlo Methods. Elsevier, 2011.

[3] Xiu D, Karniadakis GE. The Wiener–Askey polynomial chaos for stochastic differential equations. SIAM journal on scientific computing. 2002;24(2):619-44.

[4] Dorini FA , Bobko N, Dorini LB, A note on the logistic equation subject to uncertainties in parameters. Computational and Applied Mathematics. 2018;37(2), 1496–1506.

[5] Falsone G, Laudani R. Exact response probability density functions of some uncertain structural systems. Archives of Mechanics. 2019;71(4-5), 315–336.

[6] Soong TT. Random Differential Equations in Science and Engineering. New York: Academic Press; 1973.

[7] Santambrogio, F. Optimal Transport for Applied Mathematicians: Calculus of Variations, PDEs, and Modeling. Birkhäuser: Springer International Publishing Switzerland, 2015.

[8] Evans, L.C. Partial Differential Equations. Providence, R.I.: American Mathematical Society, 2010.

[9] Duffing, G. (1918), Erzwungene Schwingungen bei veränderlicher Eigenfrequenz und ihre technische Bedeutung [Forced oscillations with variable natural frequency and their technical relevance] (in German), Heft 41/42, Braunschweig: Vieweg, vi+134 pp.

[10] Kovacic, I. and Brennan M.J. The Duffing Equation: Nonlinear Oscillators and their Behaviour. John Wiley & Sons. 2011.

International Conference on Mathematical Analysis and Applications in Science and Engineering
ICMA^{2}SC'22
ISEP Porto-Portugal, June 27 - 29, 2022

Oscillation criteria for second-order half-linear neutral functional differential equations

Irena Jadlovská[⋆]

Mathematical Institute, Slovak Academy of Sciences, Slovakia

[⋆]jadlovska@saske.sk

Abstract: Applying a recently developed method of iterated monotonicity properties of nonoscillatory solutions, we present new oscillation results for a class of second-order half-linear neutral functional differential equations. While in a non-neutral case, the obtained criterion is sharp, in the neutral case, our approach allows removing several disadvantages associated with the method based on a priori bound for the nonoscillatory solution. Several further research directions are discussed as well.

keywords: second-order differential equation; delayed argument; advanced argument; neutral term; sharp oscillation constant.

MSC2020: 49-XX; 34-XX; 92-XX.

1 Introduction

With regard to their practical importance, qualitative properties of second-order neutral differential equations have been studied extensively during the last decades. The aim of this work is to consider the oscillation problem for the second-order half-linear neutral functional differential equation

$$\left(r\left(z'\right)^{\alpha}\right)'(t)+q(t)x^{\alpha}(\sigma(t))=0, \quad t\geq t_0>0, \tag{1}$$

where $z(t)=x(t)+p(t)x(\tau(t))$ and

(H$_1$) $\alpha>0$ is a quotient of odd positive integers;

(H$_2$) $r(t)\in\mathcal{C}([t_0,\infty),(0,\infty))$ satisfies $R(t,t_0):=\int_{t_0}^{t} r^{-1/\alpha}(s)\mathrm{d}s\to\infty$ as $t\to\infty$;

(H$_3$) $\sigma(t)$, $\tau(t)\in\mathcal{C}([t_0,\infty),\mathbb{R})$, either $\sigma(t)\leq t$ or $\sigma(t)\geq t$, either $\tau(t)\leq t$ or $\tau(t)\geq t$, and $\lim_{t\to\infty}\sigma(t)=\lim_{t\to\infty}\tau(t)=\infty$;

(H$_4$) $q(t)\in\mathcal{C}([t_0,\infty),(0,\infty))$;

(H$_5$) $p(t)\in\mathcal{C}([t_0,\infty),[0,1))$ and there exists a constant $p_0\in[0,1)$ such that

$$\begin{aligned} &p_0\geq p(t) && \text{for } \tau(t)\leq t,\\ &p_0\geq p(t)\frac{R(\tau(t),t_0)}{R(t,t_0)} && \text{for } \tau(t)\geq t. \end{aligned} \tag{2}$$

For the reader's convenience, we define

$$\beta_* := \begin{cases} \dfrac{1}{\alpha} \liminf\limits_{t\to\infty} r^{1/\alpha}(t)q(t)R(t,t_0)R^{\alpha}(\sigma(t),t_0) & \text{for } \sigma(t)\le t, \\ \dfrac{1}{\alpha} \liminf\limits_{t\to\infty} r^{1/\alpha}(t)q(t)R^{\alpha+1}(t,t_0) & \text{for } \sigma(t)\ge t. \end{cases}$$

In addition, we put

$$\lambda_* := \begin{cases} \liminf\limits_{t\to\infty} \dfrac{R(t,t_0)}{R(\sigma(t),t_0)} & \text{for } \sigma(t)\le t, \\ \liminf\limits_{t\to\infty} \dfrac{R(\sigma(t),t_0)}{R(t,t_0)} & \text{for } \sigma(t)\ge t, \end{cases}$$

$$\delta_* := \liminf_{t\to\infty} \frac{R(t,t_0)}{R(\tau(t),t_0)} \quad \text{for } \tau(t)\le t,$$

$$\omega_* := \liminf_{t\to\infty} \frac{R(\tau(t),t_0)}{R(t,t_0)} \quad \text{for } \tau(t)\ge t.$$

Eq. (1) can be understood as a generalization of the half-linear differential equation (with $\sigma(t)=t$ and $p(t)=0$ in (1))

$$\left(r\left(x'\right)^{\alpha}\right)'(t) + q(t)x^{\alpha}(t) = 0 \tag{3}$$

widely investigated in the literature, see the excellent Došlý and Řehák monograph [1] for a compact summary of most results known up to 2005.

By using a method of iteratively improved monotonicity properties of nonoscillatory solutions (see [5] for a detailed description), we proposed recently a sharp extension of the classical (Hille-) Kneser oscillation criterion to the non-neutral case of (1)

$$\left(r\left(x'\right)^{\alpha}\right)'(t) + q(t)x^{\alpha}(\sigma(t)) = 0. \tag{4}$$

In particular, it has been shown that all solutions of (4) are oscillatory if

$$\beta_* > \begin{cases} 0 & \text{for } \lambda_* = \infty, \\ c(\alpha,\lambda_*) & \text{for } \lambda_* < \infty, \end{cases} \tag{5}$$

where

$$c(\alpha,\lambda_*) = \begin{cases} \max\left\{m(1-m)^{\alpha}\lambda_*^{-\alpha m} : 0<m<1\right\} & \text{for } \sigma(t)\le t, \\ \max\left\{m^{\alpha}(1-m)\lambda_*^{-\alpha m} : 0<m<1\right\} & \text{for } \sigma(t)\ge t, \end{cases}$$

for the delayed case $\sigma(t)\le t$, see [2, Theorem 2, Theorem 4] for $\alpha\ge 1$ and [3, Theorem 3] or [5, Corollary 2] for general α; and for the advanced case $\sigma(t)\ge t$, see [4, Theorem 1,Theorem 2]. Note that the oscillation constant $c(\alpha,\lambda_*)$ is best possible in the sense that the strict inequality in (5) cannot be replaced by a nonstrict one without affecting validity of the criterion. In the non-neutral case (3), condition (5) reduces to

$$\liminf_{t\to\infty} r^{1/\alpha}(t)R^{\alpha+1}(t)q(t) > \left(\frac{\alpha}{\alpha+1}\right)^{\alpha+1},$$

which is a famous Kneser-type oscillation criterion for (3), obtained as a direct consequence of the Sturmian comparison methods. The purpose of this work is to present an extension of (5) to a neutral equation (1).

2 Results and discussion

In this section, we present the main result of our work: oscillation criterion for (1). We essentially revise the commonly used investigation method based on establishing the lower bound of the ratio x/z, which makes possible to investigate (1) with help of (4). There have been two main disadvantages associated with this method: first, it gives usually sharp results only if $p(t) \to 0$ and moreover, it is not capable to detect potential dependence of the oscillation criteria on $\tau(t)$, see [5] for more details. Our technique allows to remove both the above mentioned disadvantages and to derive new results involving an unimprovable oscillation constant in a nonneutral case. The presented result, which extends [5, Theorem 2] with the advanced case $\sigma(t) \geq t$, is a consequence of the process of finding optimal values of a and b for a nonoscillatory solution x of (1) such that

$$az > r^{1/\alpha} z' R \quad \text{and} \quad bz < r^{1/\alpha} z' R,$$

which correspond to the monotonicities

$$\left(\frac{z}{R^a}\right)' < 0 \quad \text{and} \quad \left(\frac{z}{R^b}\right)' > 0.$$

Theorem 1 *If one of the conditions*

(C_1) $\beta_* > 0$ *and* $\lambda_* = \infty$*;*

(C_2) *either* $\tau(t) \leq t$ *and* $\delta_* = \infty$ *or* $\tau(t) \geq t$ *and* $\omega_* = \infty$*,*

(a) $\sigma(t) \leq t$*, and the equation*

$$\beta_* = m(1-m)^\alpha \lambda_*^{-\alpha m}$$

has no solution $m \in (0,1)$*, that is,*

$$\beta_* > \max\left\{m(1-m)^\alpha \lambda_*^{-\alpha m} : 0 < m < 1\right\};$$

(b) $\sigma(t) \geq t$*, and the equation*

$$\beta_* = m^\alpha (1-m) \lambda_*^{-\alpha m}$$

has no solution $m \in (0,1)$*, that is,*

$$\beta_* > \max\left\{m^\alpha (1-m) \lambda_*^{-\alpha m} : 0 < m < 1\right\};$$

(C_3) $\tau(t) \leq t$*,* $\delta_* < \infty$*,*

(a) $\sigma(t) \leq t$*, and the system*

$$\beta_* = \frac{m(1-m)^\alpha \lambda_*^{-\alpha m}}{(1 - p_0 \delta_*^{-k})^\alpha}$$
$$\beta_* = \frac{k^\alpha (1-k) \lambda_*^{-\alpha m}}{(1 - p_0 \delta_*^{-k})^\alpha}$$

has no solution $\{m \in (0,1), k \in (0,1)\}$*;*

(b) $\sigma(t) \geq t$*, and the equation*

$$\beta_* = \frac{m(1-m)^\alpha \lambda_*^{-\alpha m}}{(1 - p_0 \delta_*^{-m})^\alpha}$$

has no solution $m \in (0,1)$*, that is,*

$$\beta_* > \max\left\{\frac{m(1-m)^\alpha \lambda_*^{-\alpha m}}{(1 - p_0 \delta_*^{-m})^\alpha} : 0 < m < 1\right\};$$

(C_4) $\tau(t) \geq t$, $\omega_* < \infty$,

(a) $\sigma(t) \leq t$, *and the equation*

$$\beta_* = \frac{m(1-m)^\alpha \lambda_*^{-\alpha m}}{(1 - p_0 \omega_*^{-m})^\alpha}$$

has no solution $m \in (0,1)$, *that is,*

$$\beta_* > \max\left\{ \frac{m(1-m)^\alpha \lambda_*^{-\alpha m}}{(1 - p_0 \omega_*^{-m})^\alpha} : 0 < m < 1 \right\};$$

(b) $\sigma(t) \geq t$, *and the system*

$$\beta_* = \frac{m^\alpha (1-m) \lambda_*^{-\alpha m}}{(1 - p_0 \omega * ^{-k})^\alpha}$$

$$\beta_* = \frac{k(1-k)^\alpha \lambda_*^{-\alpha m}}{(1 - p_0 \omega_*^{-k})^\alpha}$$

has no solution $\{m \in (0,1), k \in (0,1)\}$*;*

is satisfied, then (1) *is oscillatory.*

3 Conclusions and Future work

The results based on the method of iteratively improved monotonicity properties open many fruitul problems for further research. It could be interesting to extend the method and establish corresponding results for neutral differential equations of the form (1) with either different ranges of $p(t)$ than those in (H_5), mainly $p(t) > 1$ or $-1 < p(t) \leq 0$; or with more general function $z(t)$, involving, e.g., mixed (delayed and advanced, or positive and negative) neutral terms.

It also remains open how to extend the approach presented in this work for neutral differential equations of higher-order ($n \geq 3$); half-linear delay differential equations of higher-order ($n \geq 3$); and/or corresponding classes of functional difference equations.

Acknowledgments

The work on this research has been supported by the Slovak Grant Agency VEGA no. 2/0127/20.

References

[1] O. Došlý, P. Řehák, *Half-linear differential equations*. Elsevier, 2005.

[2] I. Jadlovská, J. Džurina, *Kneser-type oscillation criteria for second-order half-linear delay differential equations*, Appl. Math. Comput. **380** (2020), 1–15.

[3] G. E. Chatzarakis, S. R. Grace, I. Jadlovská, *On the sharp oscillation criteria for half-linear second-order differential equations with several delay arguments*, Appl. Math. Comput. **397** (2021), 1–9.

[4] G. E. Chatzarakis, S. R. Grace, I. Jadlovská, *A sharp oscillation criterion for second-order half-linear advanced differential equations.*, Acta Mathematica Hungarica **163**(2) (2021), 552–562.

[5] I. Jadlovská, *New Criteria for Sharp Oscillation of Second-Order Neutral Delay Differential Equations*, Mathematics **9**(17) (2021), 1–23.

International Conference on Mathematical Analysis and Applications in Science and Engineering
ICMA^{2}SC'22
ISEP Porto-Portugal, June 27 - 29, 2022

SYMMETRIC FLOW MODELS OF AN IDEAL MICROPOLAR COMPRESSIBLE AND HEAT-CONDUCTING GAS

Ivan Dražić

University of Rijeka, Faculty of Engineering, Croatia

idrazic@riteh.hr

Abstract: The paper describes the flow model of an ideal heat-conducting and polytropic micropolar gas in three dimensions, but assuming two types of symmetry in the solution - spherical and cylindrical. The corresponding initial boundary value problems with homogeneous boundary conditions are analyzed and the existence of the solution, the solution properties and the possible methods for finding a numerical solution are commented.

keywords: micropolar fluid; spherical symmetry; cylindrical symmetry.

MSC2020: 76-XX; 35-XX; 65-XX.

1 Introduction

The micropolar continuum is a generalization of the classical model used in the mathematical analysis of materials, which takes into account the micro-scale behavior. In fact, the classical models usually consider only macro phenomena and neglect the influence of micro phenomena, which cannot give satisfactory results in areas with small geometries. Let us note that in addition to the standard hydrodynamic and thermodynamic variables (mass density (ρ), velocity ($\mathbf{v}$) and temperature (θ)), the microrotation vector ($\boldsymbol{\omega}$) is introduced to describe the microphenomena.

In recent years, the micropolar fluid model has found wide application in various fields of engineering. For example, the micropolar fluid model serves as a basic model for liquid crystals with rigid molecules, magnetic fluids, dust clouds, muddy fluids, some biological fluids, etc. For more information on the micropolar continuum, see the article [1] and references cited therein.

In this paper, we focus in particular on micropolar compressible gas assuming the ideal gas state equation and polytropy, and describe the flow model between thermally isolated and solid walls. This problem leads to an initial boundary value problem with homogeneous boundary conditions for velocity, microrotation and heat flux, as follows:

$$\partial_t \rho = -(\nabla \rho) \cdot \mathbf{v} - \rho \nabla \cdot \mathbf{v}, \tag{1}$$

$$\rho\, \partial_t \mathbf{v} = -\rho((\nabla \mathbf{v}) \cdot \mathbf{v}) - R\nabla\,(\rho\theta) + (\lambda + \mu - \mu_r)\nabla(\nabla \cdot \mathbf{v}) + (\mu + \mu_r)\Delta \mathbf{v} + 2\mu_r \nabla \times \boldsymbol{\omega}, \tag{2}$$

$$j_I \rho\, \partial_t \boldsymbol{\omega} = -j_I \rho((\nabla \boldsymbol{\omega}) \cdot \mathbf{v}) + 2\mu_r\,(\nabla \times \mathbf{v} - 2\boldsymbol{\omega}) + (c_0 + c_d - c_a)\nabla(\nabla \cdot \boldsymbol{\omega}) + (c_d + c_a)\Delta \boldsymbol{\omega}, \tag{3}$$

$$c_v\rho\,\partial_t\theta = -c_v\rho(\nabla\theta)\cdot\mathbf{v} + k_\theta\Delta\theta - R\rho\theta(\nabla\cdot\mathbf{v}) + \lambda(\nabla\cdot\mathbf{v})^2 +$$
$$\frac{\mu}{2}(\nabla\mathbf{v}+(\nabla\mathbf{v})^T):(\nabla\mathbf{v}+(\nabla\mathbf{v})^T) + 4\mu_r\left(\frac{1}{2}\nabla\times\mathbf{v}-\boldsymbol{\omega}\right)^2 + c_0(\nabla\cdot\boldsymbol{\omega})^2 + \tag{4}$$
$$(c_d+c_a)\nabla\boldsymbol{\omega}:\nabla\boldsymbol{\omega} + (c_d-c_a)\nabla\boldsymbol{\omega}:(\nabla\boldsymbol{\omega})^T,$$

$$\rho(\mathbf{x},0)=\rho_0(\mathbf{x}),\quad \mathbf{v}(\mathbf{x},0)=\mathbf{v}_0(\mathbf{x}),\quad \boldsymbol{\omega}(\mathbf{x},0)=\boldsymbol{\omega_0}(\mathbf{x}),\quad \theta(\mathbf{x},0)=\theta_0(\mathbf{x}), \tag{5}$$

$$\mathbf{v}|_{\partial\Omega}=\mathbf{0},\qquad \boldsymbol{\omega}|_{\partial\Omega}=\mathbf{0},\qquad \left.\frac{\partial\theta}{\partial\mathbf{n}}\right|_{\partial\Omega}=0, \tag{6}$$

defined on the domain $Q_T=\Omega\times]0,T[$, where $T>0$ is arbitrary and $\Omega\subset\mathbf{R}^3$.

For the full three-dimensional model in this case, a full mathematical analysis has not yet been performed, in particular, a full analysis of the existence and uniqueness of the solution. Therefore, three-dimensional models are often analyzed with certain simplifications, such as the spherical and cylindrical symmetry of the solutions analyzed here.

2 Results and discussion

In the mathematical analysis of compressible fluids it is convenient to use Lagrangian description. Let us emphasize that the convenience behind introducing the Lagrangian coordinates is to effectively eliminate the hyperbolic part of the system, given that the conservation law for mass becomes explicitly solvable once the velocity has been determined. At the same time, the other equations remains parabolic. Accordingly, all systems of partial differential equations are given below in the Lagrangian description.

In the case of spherical symmetry of the solution, where the flow between two concentric spheres is analyzed, the three-dimensional problem takes the following form:

$$\frac{\partial\rho}{\partial t} = -\frac{1}{L}\rho^2\frac{\partial}{\partial x}\left(r^2 v\right), \tag{7}$$

$$\frac{\partial v}{\partial t} = -\frac{R}{L}r^2\frac{\partial}{\partial x}(\rho\theta) + \frac{\lambda+2\mu}{L^2}r^2\frac{\partial}{\partial x}\left(\rho\frac{\partial}{\partial x}\left(r^2 v\right)\right), \tag{8}$$

$$\rho\frac{\partial\omega}{\partial t} = -\frac{4\mu_r}{j_I}\omega + \frac{c_0+2c_d}{j_I L^2}r^2\rho\frac{\partial}{\partial x}\left(\rho\frac{\partial}{\partial x}\left(r^2\omega\right)\right), \tag{9}$$

$$\rho\frac{\partial\theta}{\partial t} = \frac{k}{c_v L^2}\rho\frac{\partial}{\partial x}\left(r^4\rho\frac{\partial\theta}{\partial x}\right) - \frac{R}{c_v L}\rho^2\theta\frac{\partial}{\partial x}\left(r^2 v\right) + \frac{\lambda+2\mu}{c_v L^2}\left[\rho\frac{\partial}{\partial x}\left(r^2 v\right)\right]^2$$
$$-\frac{4\mu}{c_v L}\rho\frac{\partial}{\partial x}\left(r v^2\right) + \frac{c_0+2c_d}{c_v L^2}\left[\rho\frac{\partial}{\partial x}\left(r^2\omega\right)\right]^2 - \frac{4c_d}{c_v L}\rho\frac{\partial}{\partial x}\left(r\omega^2\right) + \frac{4\mu_r}{c_v}\omega^2, \tag{10}$$

$$\rho(x,0)=\rho_0(x),\quad v(x,0)=v_0(x),\quad \omega(x,0)=\omega_0(x),\quad \theta(x,0)=\theta_0(x), \tag{11}$$

$$v(0,t)=v(1,t)=0,\quad \omega(0,t)=\omega(1,t)=0,\quad \frac{\partial\theta}{\partial x}(0,t)=\frac{\partial\theta}{\partial x}(1,t)=0, \tag{12}$$

considered on the domain $Q_T=]0,1[\times]0,T[$.

The function $r(x,t)$ is defined by

$$r(x,t) = r_0(x) + \int_0^t v(x,\tau)d\tau,\ (x,t)\in Q_T \tag{13}$$

where

$$r_0(x) = \left(a^3 + 3L\int_0^x \frac{1}{\rho_0(y)}dy\right)^{\frac{1}{3}},\ x\in]0,1[\tag{14}$$

and $a > 0$ is a radius of smaller boundary sphere. For more information on this initial boundary problem, see [1].

In the case of cylindrical symmetry, where the problem is considered between two coaxial cylinders, we have

$$\rho(\mathbf{x},t) = \rho(r,t), \quad \theta(\mathbf{x},t) = \theta(r,t), \tag{15}$$

$$\mathbf{v}(\mathbf{x},t) = v^r(r,t)\mathbf{e}_1 + v^\varphi(r,t)\mathbf{e}_2 + v^z(r,t)\mathbf{e}_3, \tag{16}$$

$$\boldsymbol{\omega}(\mathbf{x},t) = \omega^r(r,t)\mathbf{e}_1 + \omega^\varphi(r,t)\mathbf{e}_2 + \omega^z(r,t)\mathbf{e}_3, \tag{17}$$

where

$$\mathbf{e}_1 = \frac{1}{r}(x_1, x_2, 0), \quad \mathbf{e}_2 = \frac{1}{r}(-x_2, x_1, 0), \quad \mathbf{e}_3 = (0,0,1), \tag{18}$$

and we observe the following problem:

$$\frac{\partial \rho}{\partial t} = -\rho^2 \frac{\partial}{\partial x}\left(r v^r\right), \tag{19}$$

$$\frac{\partial v^r}{\partial t} = -Rr\frac{\partial}{\partial x}(\rho\theta) + (\lambda+2\mu)r\frac{\partial}{\partial x}\left(\rho\frac{\partial}{\partial x}\left(rv^r\right)\right) + \frac{(v^\varphi)^2}{r}, \tag{20}$$

$$\frac{\partial v^\varphi}{\partial t} = (\mu+\mu_r)r\frac{\partial}{\partial x}\left(\rho\frac{\partial}{\partial x}\left(rv^\varphi\right)\right) - \frac{v^r v^\varphi}{r} - 2\mu_r r\frac{\partial \omega^z}{\partial x}, \tag{21}$$

$$\frac{\partial v^z}{\partial t} = (\mu+\mu_r)r\frac{\partial}{\partial x}\left(\rho\frac{\partial}{\partial x}\left(rv^z\right)\right) + (\mu+\mu_r)\frac{v^z}{\rho r^2} + 2\mu_r\frac{\partial}{\partial x}\left(r\omega^\varphi\right), \tag{22}$$

$$j_I\frac{\partial \omega^r}{\partial t} = (c_0+2c_d)r\frac{\partial}{\partial x}\left(\rho\frac{\partial}{\partial x}\left(r\omega^r\right)\right) + j_I\frac{\omega^\varphi v^\varphi}{r} - 4\mu_r\frac{\omega^r}{\rho}, \tag{23}$$

$$j_I\frac{\partial \omega^\varphi}{\partial t} = (c_d+c_a)r\frac{\partial}{\partial x}\left(\rho\frac{\partial}{\partial x}\left(r\omega^\varphi\right)\right) - j_I\frac{\omega^r v^\varphi}{r} - 2\mu_r r\frac{\partial v^z}{\partial x} - 4\mu_r\frac{\omega^\varphi}{\rho}, \tag{24}$$

$$j_I\frac{\partial \omega^z}{\partial t} = (c_d+c_a)r\frac{\partial}{\partial x}\left(\rho\frac{\partial}{\partial x}\left(r\omega^z\right)\right) + (c_d+c_a)\frac{\omega^z}{\rho r^2} + 2\mu_r\frac{\partial}{\partial x}\left(rv^\varphi\right) - 4\mu_r\frac{\omega^z}{\rho}, \tag{25}$$

$$\begin{aligned} c_v\frac{\partial\theta}{\partial t} = {} & k\frac{\partial}{\partial x}\left(r^2\rho\frac{\partial\theta}{\partial x}\right) + \rho\left[(\lambda+2\mu)\frac{\partial}{\partial x}\left(rv^r\right) - R\theta\right]\frac{\partial}{\partial x}\left(rv^r\right) - (\mu+\mu_r)\rho\left(\frac{\partial}{\partial x}\left(rv^\varphi\right)\right)^2 \\ & + (c_d+c_a)\rho\left(\frac{\partial}{\partial x}\left(r\omega^\varphi\right)\right)^2 + (c_0+2c_d)\rho\left(\frac{\partial}{\partial x}\left(r\omega^r\right)\right)^2 + (\mu+\mu_r)\rho r^2\left(\frac{\partial v^z}{\partial x}\right)^2 + \\ & (c_d+c_a)\rho r^2\left(\frac{\partial \omega^z}{\partial x}\right)^2 - 2c_d\frac{\partial}{\partial x}\left((\omega^r)^2 + (\omega^\varphi)^2\right) - 2\mu\frac{\partial}{\partial x}\left((v^r)^2 + (v^\varphi)^2\right) \\ & + 4\mu_r\frac{(\omega^r)^2}{\rho} + 4\mu_r\frac{(\omega^\varphi)^2}{\rho} + 4\mu_r\frac{(\omega^z)^2}{\rho} + 4\mu_r r\omega^\varphi\frac{\partial v^z}{\partial x} - 4\mu_r\omega^z\frac{\partial}{\partial x}\left(rv^\varphi\right), \end{aligned} \tag{26}$$

$$\rho(x,0) = \rho_0(x), \quad v^r(x,0) = v_0^r(x), \quad v^\varphi(x,0) = v_0^\varphi(x), \quad v^z(x,0) = v_0^z(x), \tag{27}$$

$$\theta(x,0) = \theta_0(x), \quad \omega^r(x,0) = \omega_0^r(x), \quad \omega^\varphi(x,0) = \omega_0^\varphi(x), \quad \omega^z(x,0) = \omega_0^z(x), \tag{28}$$

$$v^r(0,t) = v^r(L,t) = 0, \quad v^\varphi(0,t) = v^\varphi(L,t) = 0, \quad v^z(0,t) = v^z(L,t) = 0, \tag{29}$$

$$\omega^r(0,t) = \omega^r(L,t) = 0, \quad \omega^\varphi(0,t) = \omega^\varphi(L,t) = 0, \quad \omega^z(0,t) = \omega^z(L,t) = 0, \tag{30}$$

$$\frac{\partial\theta}{\partial x}(0,t) = \frac{\partial\theta}{\partial x}(L,t) = 0 \tag{31}$$

on the domain $Q_T =]0,L[\times]0,T[$, where

$$L = \int_a^b s\rho_0(s)ds, \qquad r(x,t) = r_0(x) + \int_0^t v^r(x,\tau)d\tau, \ (x,t) \in Q_T, \tag{32}$$

$$r_0(x) = \left(a^2 + 2 \int_0^x \frac{1}{\rho_0(y)}\, dy \right)^{\frac{1}{2}}, \tag{33}$$

and $a > 0$ is the radius of the smaller boundary cylinder. For more information on this initial boundary problem, see [2].

For both problems, the theorems of existence and uniqueness of the solution locally and globally in time are known, as are the stabilization properties. For additional conditions that must be valid for the proof of these properties to be implemented, we refer to [1, 2].

3 Conclusions and Future work

The described model of an ideal micropolar fluid in three dimensions has been studied only for the case of spherical and cylindrical symmetry of the solution, and the corresponding results are presented in this paper. In future research, efforts should certainly be made to solve the original problem and general domains, but also to extend the problem to the real micropolar fluid described in [3].

Special attention should certainly be given to the problem of finding a numerical solution to these problems. The article [1] describes two functional methods for finding an approximate solution. One is based on Faedo-Galerkin approximations and the other on the finite difference method, but this is certainly still an open area of research.

Acknowledgments

Ivan Dražić is supported by the Croatian Science Foundation under the project MultiFM (IP-2019-04-1140), as well as by the University of Rijeka, Croatia under the project uniri-prirod-18-118-1257 (Analysis of mathematical models of fluid mechanics and technical systems using data-driven algorithms for Koopman operator).

References

[1] Ivan Dražić, 3-D flow of a compressible viscous micropolar fluid model with spherical symmetry: A brief survey and recent progress, Reviews in Mathematical Physics, **30**(1) (2018), 1830001.

[2] Lan Huang, Ivan Dražić,, Exponential stability for the compressible micropolar fluid with cylinder symmetry in R^3, Journal of Mathematical Physics, **60**(2) (2019), 021507.

[3] Angela Bašić-Šiško, Ivan Dražić, Global solution to a one-dimensional model of viscous and heat-conducting micropolar real gas flow, Journal of Mathematical Analysis and Applications, **495**(1) (2021), 124690.

International Conference on Mathematical Analysis and Applications in Science and Engineering
ICMA^{2}SC'22
ISEP Porto-Portugal, June 27 - 29, 2022

F-TRANSFORM-BASED LAPLACE OPERATOR

Hana Zámečníková[1⋆] **Irina Perfilieva**[2]

[1] University of Ostrava, Czech republic
[2] IRAFM, University of Ostrava, Czech republic

[1⋆]hana.zamecnikova@osu.cz

Abstract: Simple and understandable representation is required in many research areas, but especially in mathematics. Therefore, we use existing possibilities of how to define Laplace operator and extend these by the possibility of representation of this operator by means of fuzzy transform. Fuzzy transform allows us to unify both - discrete and continuous - cases of definitions, which is one of the main advantages of this approach. Moreover, we show that this F-transform-based representation of the Laplace operator can be described in terms of well-known Laplace-Beltrami operator.

keywords: Laplace operator; fuzzy transform; fuzzy partition; proximity.

MSC2020: 49-XX; 34-XX; 92-XX.

1 Introduction

Laplace operator is an important notion appearing throughout many research areas. From our point of view, its main contribution is the fact it can provide interesting insight into function behavior. The easiest explanation is that it provides the average deviation from function values in the given neighborhood. We investigated this operator from a side of spaces with a fuzzy partition structure, trying to provide a simple representation, applicable to more general types of spaces in the end.

Motivated by various kinds of applications[1], *discrete Laplace operator* $\Delta_w : \mathbb{R}^X \to \mathbb{R}^X$ is commonly represented as follows

$$(\Delta_w f)(x) = -\sum_{y \sim x} w(x,y)(f(x) - f(y)), \tag{1}$$

where notation $y \sim x$ stands for all points y in the neighborhood of current point x, where the value of Laplacian is computed, and corresponding function $f : (X, w) \to \mathbb{R}$, where X is finite set of all possible argument values, so the sum in (1) is finite, and therefore well-defined. Relation $w : X \times X \to \mathbb{R}^0_+$ plays a role of weight, and is said to be reflexive and symmetric. Formula (1) is often introduced along with the concept of weighted graph, which provides the weights appearing in the formula.

However, in case of an unweighted graph with finite number of edges and vertices (therefore function f has only finite number of function values and can be written in a form of vector), this

[1] e.g. in image processing (or signal processing in general)

definition is identical to that of the so called *graph Laplacian* (*Laplacian matrix*). It is enough to identify $(\Delta_w f)(x)$ with the x^{th} entry of a resulting vector of a product $L \cdot f$, whereas matrix L is the difference of the degree matrix D and the adjacency matrix W of the graph, $L = D - W$.

Nevertheless, except the one special case of an unweighted graph, when these two representations coincides, this means we are in general unifying two different concepts, since each one of them operates on a completely different space. So how can we formally call both these terms by the same name? The answer can be found in an axiomatical point of view. Both of these are linear operators with specific properties[2], among which, vanishing on constant functions, symmetry, local support or positive-semidefiniteness can be mentioned. Therefore, if we claim that Laplace operator is an operator satisfying these properties [3], then we have an accurate representation. Then, based on the properties we can allege that (1), since it fulfills all the properties[3], can be considered to be the Laplace operator.

2 Laplace operator based on fuzzy transform

As mentioned, we would like to introduce the formula which represents the Laplace operator in the space with the fuzzy partition. So now, let us suppose that underlying space is endowed with the fuzzy partition, and let us reason about how to characterize the model of such a space.

2.1 Fuzzy partition

Since we assume not everybody is familiar with those concepts, let us briefly introduce few notions from fuzzy theory. As the most basic term appears *fuzzy set* which can be seen as generalization of classic set, and it is associated with its *membership function*, i.e. mapping $A : X \to [0, 1]$, where X is a non-empty set. Fuzzy sets $A_1, \ldots, A_n$, then establish a *fuzzy partition* of an interval $[a, b]$ with nodes $\{\mathbf{x}_i\}_{i=1}^n$ if for $k = 1, \ldots, n$ holds

1. $A_k(x_i) = 0$ if $x_i \notin (x_i - h, x_i + h)$, where h is a width of A_k support
2. $A_k(x_k) = 1$
3. covering property holds: $\sum_{k=1}^n A_k(x) > 0, \quad \forall x \in X \subseteq [a, b]$.

Fuzzy sets $A_1, \ldots, A_n$ are then called *basic functions*. For simplicity, from now on, let us assume basic functions to be triangular shaped.

2.2 Fuzzy transform

As we stated in the beginning, our goal is to represent discrete Laplace operator with fuzzy transfom, therefore, let us also mention this concept in short. *Discrete fuzzy transform* or *F-transform* is a result of weighted linear transformation with weights determined by basic functions.

Let $A_1, \ldots, A_n$ be a fuzzy partition of $[a, b]$ and a function f be defined on the set $X = \{x_1, \ldots, x_p\} \subseteq [a, b]$ that is sufficiently dense with respect to $A_1, \ldots, A_n$[4]. We say that the n-tuple of real numbers $F[f] = (F_1[f], \ldots, F_n[f])$ is a discrete F-transform [2] of f with respect to $A_1, \ldots, A_n$ if

$$F_k[f] = \frac{\sum_{j=1}^p f(x_j) A_k(x_j)}{\sum_{j=1}^p A_k(x_j)}. \tag{2}$$

[2] which we will not discuss in detail in this contribution, reader interested in this problematics can see e.g. [3]

[3] as shown in [3]

[4] there is an element $x_j \in X$ belonging to the support of A_k, formally $(\forall k)(\exists j) A_k(x_j) > 0$

2.3 Concept of the proximity space

Our analysis of the corresponding operator is happening in a space which is not necessarily equipped with a notion of distance. Therefore, we introduce so called *proximity space* (X, w), which represents a weaker environment than is e.g. metric space with a distance function.

The assumptions on so called *proximity measure* include non-negativity and symmetry of the underlying proximity function w. It is also possible to establish a connection of the proximity to the classic distance function [3].

2.4 Representation of the Laplace operator

The idea of including basic functions of the fuzzy partition is very natural, since it intuitively provides an information about how much does the given point belong to some set. In our case, describing in what degree does the point belong to a neighborhood of the point we are interested to know the value of Laplacian at. Here we claim the basic functions to be non-negative and symmetric functions, with a bounded support and range in $[0, 1]$, let $X \subseteq [a, b]$ be a finite set and the weights be defined as follows

$$w(x, y) = A_x(y) = A(x, y), \tag{3}$$

for every $x, y \in X$. In addition, each weight is multiplied by normalization coefficient. Then, based on equation (1), we can define discrete *Laplace operator* at every point by

$$\Delta f(x) = F_x[f] - f(x), \tag{4}$$

where symbol $F_x[f]$ stands for F-transform component computed at point x. It is worth mentioning that in our approach we do not distinguish between nodes and points (as it is usual when it comes to F-transform approach). This basically means, every point is considered to be a node of the fuzzy partition, therefore we have a component for each $x \in X$ and the latter equation is well-defined. When one observes the right-hand side of the equality, this is nothing more that a difference between an average value of the function f at point x and a function value at the same point. Therefore, this formula states the information about how the function differs from its average value (in some small neighborhood), which fully corresponds with the initial idea behind the definition of the Laplace operator. Moreover, since we also checked that all required axiomatical properties are fulfilled also in this case [3], we can justly claim expression (4) to be Laplace operator.

2.5 A note on convergence

It is necessary to mention that there also exists another operator, which is connected with the term Laplace operator - so called - Laplace-Beltrami operator, which is represented by a composition of two adjoint operators (divergence and gradient). So there occurs a natural question if the previously mentioned Laplace operators (graph Laplacian and discrete Laplace operator) can be described as special cases in terms of Laplace-Beltrami operator.

In the case of graph Laplacian, Belkin in his paper [1] has already adressed this question and proved that under certain specific conditions, graph Laplacian converges to the Laplace-Beltrami operator. Therefore, there immediately arises a question if this statement is valid also for F-transform-based Laplacian. And the answer is yes, and we reason on how it is possible to justify it in the following text.

So the main idea is to transform our representation to a form of a graph representation. Since F-transform is a linear operator, and in the discrete space every linear operator can be represented

in the form of matrix, we transform the Laplacian into a kind of matrix multiplication form. Considering F-transform, each element on (x, y)-position of the matrix of fuzzy transform F_x is defined as

$$F_x(x, y) = \frac{A_x(y)}{\sum_{y \sim x} A_x(y)} \tag{5}$$

and when the F-transform is applied to a function, the procedure corresponds to matrix multiplication

$$F_x[f] = F_x \cdot f = \sum_{y \sim x} F_x(x, y) f(y) \tag{6}$$

since f is know only in finite number of arguments when it comes to the discrete space. Finally, F-transform-based Laplacian is then a latter product minus the original function value vector, while the value in given point x corresponds to

$$\Delta f(x) = F_x[f] - f(x). \tag{7}$$

3 Conclusions and Future work

In spite of the fact there already exist quite a few definitions of so called Laplace operator, in this contribution, we introduced another one based on fuzzy transform. Its main advantage is that it allows us to unify the form of representation in both - discrete and continuous[5] - cases, since the structure of the formula remains the same. From the point of view of axiomatical definition, our representation has every right to be called Laplace operator because it satisfies all necessary properties one could expect in comparison to standard definitions. To this end, based on recent work of Belkin [1], we also investigated the convergence of our operator to the well-known Laplace-Beltrami operator. In our future research, we would like to investigate the convergence directly, without the need of transitioning F-transform to a form of matrix.

Acknowledgments

Authors would like to thank the reviewers for their valuable comments and thoughtful suggestions that helped to improve the quality of the contribution. The work of Irina Perfilieva was supported from ERDF/ESF by the project "Centre for the development of Artificial Inteligence Methods for the Automotive Industry of the region" No. CZ.02.1.01/0.0/0.0/17-049/0008414.

References

[1] Belkin, M., Niyogi, P., Towards a theoretical foundation for Laplacian-based manifold methods. Journal of Computer and System Sciences, **74**(8) (2008), 1289–1308.

[2] Perfiljeva, I., Fuzzy transforms: Theory and applications. Fuzzy sets and systems, **8** (2006), 993–1023.

[3] Zámečníková, H., Perfilieva, I., Discrete Laplace Operator in the Space with a Fuzzy Partition. In: Joint Proceedings of the 19th World Congress of the International Fuzzy Systems Association, The 12th Conference of the European Society for Fuzzy Logic and Technology (EUSFLAT) jointly with the AGOP, IJCRS, and FQAS conferences (IFSA-EUSFLAT), Atlantis Press 2021, pp. 147–152.

[5] it is not enough room to introduce the continuous version, but the main difference is that the sum in (1) is replaced by an integral

International Conference on Mathematical Analysis and Applications in Science and Engineering
ICMA^{2}SC'22
ISEP Porto-Portugal, June 27 - 29, 2022

Unproportional mosaicing

Vojtech Molek* Petr Hurtik Pavel Vlasanek David Adamczyk

Institute for Research and Applications of Fuzzy Modeling, University of Ostrava,
30. dubna 22, Ostrava, 701 03, Czech Republic

*vojtech.molek@osu.cz

Abstract: Data shift is gap between data distribution used for training and data distribution encountered in real-world. Data augmentations help narrow the gap by generating new data samples, increasing data variability, and data space coverage. We present new data augmentation: Unproportinal mosaicing. Our augmentation randomly splits an image into various-sized blocks and swap their content (pixels) while maintaining block sizes. Our method achieves a lower error rate when combined with the other state-of-the-art augmentations.

keywords: machine learning; image augmentation; augmentation consistency.

MSC2020: 68U05, 68T07, 68T45

1 Introduction

Deep neural networks (DNNs) excel in extracting features from data and, based on them, solving a wide range of problems. Considering image processing, the tasks of classification, segmentation, or object detection attracted the most attention of researchers. DNNs are data-driven, so the number of samples in the training dataset affects the performance of a trained model. To achieve good performance and generalization of the model, the data must have a high variability to cover as much of the data space as possible. Variability manifests as a different lighting condition, blur, perspective change, or geometric transformation in the case of image data. Quite often, variability is not explicitly captured in the data, leading to generalization failure, overfitting, and low accuracy. The difference between training and the distribution of real-world data is called a "data shift" [7].

The problem of data shift can be mitigated by data augmentation that produces new samples from existing ones [8]. It has been proven [4] that data augmentation also performs an implicit regularization that suppresses data shift more efficiently than explicit regularization, such as weight decay [3] or dropout [9].The construction of a proper data augmentation pipeline remains an open issue, resulting in the continuous development of new augmentation schemes. Existing augmentation techniques can be roughly divided into spatial and intensity groups. The spatial group includes translation, rotation, skewness, scaling, horizontal flipping, and cropping. The intensity group consists of histogram equalization, color jittering, blurring, or noise addition.

The described basic augmentations can be chained to create a complex augmentation pipeline, where the sequence can be ad-hoc or the result of a search algorithm. AutoAugment [1] searches for an optimal set of augmentation sub-policies and the augmentation magnitudes for a given

Figure 1: Demonstration of the proposed Unproportional mosaicing. Left: input image; Right: augmented output image.

dataset, using reinforcement learning. Its time complexity was improved by Fast AutoAugment [6] through a density matching search strategy. Tian et al. [10] took AutoAugment and implemented weight sharing known from Network Architecture Search. PBA [5] changes the augmentation search, and instead of looking for a fixed augmentation policy, it searches for the augmentation policy schedule, which is much less expensive. RandAugment [2] removed the AutoAugment search phase altogether. Instead, it chooses N augmentations of magnitude M from a set of possible augmentations.

Our contribution is a unique augmentation that combines resize, side length jittering, and blurring within a single image, making the augmentation strong and leading to better generalization.

2 Unproportional mosaicing

We suppose an image $F \subset \mathbb{R}^{w \times h}$. Furthermore, let $a(F, \theta)$ be an augmentation function of an image F according to the augmentation parameters θ. Standard spatial and intensity augmentations such as rotation, scaling, intensity change, etc., are applied over the whole image F with the same parameters. Such an augmentation creates new, augmentation consistent data samples (see Definition 1). The augmentations can be chained as $a(a(\dots F \dots, \theta_1), \theta_2)$, but the result will remain augmentation consistent.

Definition 1 *An image F is augmentation consistent with respect to intensity augmentation function a if for arbitrary $p_1, p_2 \in F$, $F(p_1) \leq F(p_2)$ holds $F'(p_1) \leq F'(p_2)$, where $F' = a(F, \theta)$ and consistent with respect to geometric augmentation function a if for arbitrary $R_1, R_2 \subseteq F$, $|R_1| \leq |R_2|$ holds $|a(R_1, \theta)| \leq |a(R_2, \theta)|$.*

When a model is trained, a set of augmentations is applied, usually with probability $p < 1$. A large enough batch of images ensures the stability of the training process by including all types of augmentations. The problem may arise when there are many augmentations involved, as a large batch requires large GPU memory. On the other hand, augmentation inconsistent images can reduce the need for larger batch size because the augmentations are not applied over the whole image but over its parts. Based on this fact, the primary motivation of our work is to create an augmentation inconsistent technique.

We propose combining aspect ratio, blurring, sharpening, shuffling, and resizing augmentations in a single image. Let $\mathbf{R} = \{R_1, ..., R_n\}, R_i \subset F$ be a set of rectangular areas such that $F = \bigcup_{\forall R \in \mathbf{R}} R$ and $\mathbf{T} = \{\theta_1, ..., \theta_n\}$ be a set of augmentation parameters such that $\theta_i \neq \theta_j$ holds for arbitrary $i \neq j$. The image processed by Unproportional augmentation is then defined as $\mathbf{R}' = \{a(R_1, \theta_1), ..., a(R_n, \theta_2)\}$ such that $|\mathbf{R}'| = |\mathbf{R}|$ is preserved. The problem is to define $\mathbf{T}$ to hold the equality. To solve it, we introduce the 'unproportional division'. The original grid-based division separates the input image into mutually exclusive blocks that have the same width and height. Our approach modifies this idea by extending block shapes from the same-sized blocks

to arbitrary-sized blocks. When the content from a rectangular area is placed into a different rectangular area, it is resized, causing suppressing/enhancing of high frequencies according to the used interpolation. Also, the ratio of side lengths is different, resulting in augmentation known as side length jittering. For visualization, see Figure 1. The proposed augmentation algorithm is shown in Algorithm 1.

Algorithm 1 Unproportional mosaicing augmentation pseudo code

Input: image F, image width w, image height h, aspect ratio G, number of rectangles N, number of steps J and probability P

if $P < P' \sim \mathcal{U}(0,1)$ **then**
  return F
end if
$\mathbf{B} \leftarrow \{\{0,0,w,h\}\}$
while $|\mathbf{B}| < N$ **do**
  random select rectangle $B \in \mathbf{B}$
  random select split $S \in \{\text{vertical, horizontal}\}$
  if S is horizontal **then**
    sample $T \sim \mathcal{U}(0, B_2 - B_0)$
    $B' \leftarrow \{B_0, B_1, T, B_3\}$
    $B'' \leftarrow \{T, B_1, B_2 - T, B_3)$
  else
    sample $T \sim \mathcal{U}(0, B_3 - B_1)$
    $B' \leftarrow \{B_0, B_1, B_2, T\}$
    $B'' \leftarrow \{B_0, T, B_2, B_3 - T\}$
  end if
  $\mathbf{B} \leftarrow \mathbf{B} \backslash B$
  $\mathbf{B} \leftarrow \mathbf{B} \cup B' \cup B''$
end while
Refine rectangles to get to the aspect ratio G, with J steps at most
Randomly swap image patches according to $\mathbf{B}$

To evaluate the performance, we trained three models: Wide-ResNet-40-2, Wide-ResNet-28-10, and Shake-Shake(26 2x32d). Wide-ResNets were trained in 200 epochs with a batch size of 128 using SGD optimizer with Nesterov momentum, learning rate 0.1, and cosine decay. Shake-Shake(26 2x32d) had the same parameters except for training epochs, 1800. For training, we have used the official Fast AutoAugmentation repository[1]. The results are shown in Table 1. For Fast AA, we report two scores: the first one is reported by the authors of Fast AA, and the second score is our rerun of Fast AA experiments using the said source code repository. The proposed augmentation leads to lower test error for all three tested neural networks.

Model	Fast AA	*Fast AA	Unproportional mosaicing
Wide-ResNet-40-2	3.7	3.72	**3.56**
Wide-ResNet-28-10	2.7	2.86	**2.46**
Shake-Shake(26 2×32d)	2.5	2.86	**2.77**

Table 1: Top-1 error rate on CIFAR10 test dataset; lower is better. Fast AA values are from [6] Table 3. *Fast AA are repeated experiments using authors repository. Unprop are our results, using unproportinal mosaicing on top of augmentations found by Fast AA.

[1] https://github.com/kakaobrain/fast-autoaugment

3 Summary

We have focused on data augmentation techniques in image processing to avoid data shift that leads to poor generalization of deep neural network models. We have introduced the notion of 'augmentation consistent image' and have discussed the disadvantages of such an image. To produce augmentation inconsistent images, we have designed a new augmentation technique called 'Unproportional mosaicing' that combines several basic augmentations. We have compared Unproportinal mosaicing with state-of-the-art augmentation algorithm, Fast AA, and showed that our proposed technique leads to lower error rate.

References

[1] Ekin D Cubuk, Barret Zoph, Dandelion Mane, Vijay Vasudevan, and Quoc V Le. Autoaugment: Learning augmentation strategies from data. In *Proceedings of the IEEE/CVF Conference on Computer Vision and Pattern Recognition*, pages 113–123, 2019.

[2] Ekin D Cubuk, Barret Zoph, Jonathon Shlens, and Quoc V Le. Randaugment: Practical automated data augmentation with a reduced search space. In *Proceedings of the IEEE/CVF Conference on Computer Vision and Pattern Recognition Workshops*, pages 702–703, 2020.

[3] Stephen Hanson and Lorien Pratt. Comparing biases for minimal network construction with back-propagation. *Advances in neural information processing systems*, 1:177–185, 1988.

[4] Alex Hernández-García and Peter König. Data augmentation instead of explicit regularization. *arXiv preprint arXiv:1806.03852*, 2018.

[5] Daniel Ho, Eric Liang, Xi Chen, Ion Stoica, and Pieter Abbeel. Population based augmentation: Efficient learning of augmentation policy schedules. In *International Conference on Machine Learning*, pages 2731–2741. PMLR, 2019.

[6] Sungbin Lim, Ildoo Kim, Taesup Kim, Chiheon Kim, and Sungwoong Kim. Fast autoaugment. *Advances in Neural Information Processing Systems*, 32:6665–6675, 2019.

[7] Joaquin Quiñonero-Candela, Masashi Sugiyama, Neil D Lawrence, and Anton Schwaighofer. *Dataset shift in machine learning*. Mit Press, 2009.

[8] Shashank Rajput, Zhili Feng, Zachary Charles, Po-Ling Loh, and Dimitris Papailiopoulos. Does data augmentation lead to positive margin? In *International Conference on Machine Learning*, pages 5321–5330. PMLR, 2019.

[9] Nitish Srivastava, Geoffrey Hinton, Alex Krizhevsky, Ilya Sutskever, and Ruslan Salakhutdinov. Dropout: a simple way to prevent neural networks from overfitting. *The journal of machine learning research*, 15(1):1929–1958, 2014.

[10] Keyu Tian, Chen Lin, Ming Sun, Luping Zhou, Junjie Yan, and Wanli Ouyang. Improving auto-augment via augmentation-wise weight sharing. *arXiv preprint arXiv:2009.14737*, 2020.

Prediction of dynamical systems driven by Lévy noise based on deep learning

Zi-Fei Lin[1,2*] Yan-Ming Liang[1] Jia-Li Zhao[1] Jiao-Rui Li[2] Tomasz Kapitaniak[3]

[1] School of Statistics, Xi'an University of Finance and Economics, Xi'an 710100, PR China

[2] Xi'an University of Finance and Economics, China (Xi'an) Institute for Silk Road Research, Xi'an 710100, PR China

[3] Division of Dynamics, Lodz University of Technology, Stefanowskiego 1/15, 90-924 Lodz, Poland

[1*] zifeilinxaufe@163.com

Abstract: In this paper, we study the prediction of dynamical systems driven by strong noise, which proves the wide applicability of deep learning in many fields. This is the first time that deep learning algorithms have been used to predict dynamic systems driven by strong noise. We not only study the effect of hyperparameters in deep learning on prediction, but also propose an improved model for prediction.The results show that deep learning can predict dynamic systems driven by strong noise, and the accuracy is guaranteed. Meanwhile, our proposed improved algorithm can improve the accuracy of prediction.

keywords: Reservior Computing; Rössler system; Lorenz system; noise ; Improve Reservoir Computing

1 Introduction

For the prediction analysis of nonlinear dynamic system, the control dynamics theory is usually used to construct the mathematical model of the system. The initial conditions of the numerical estimation system measured by the system state are used to predict the system. The accuracy of the traditional method will be affected by various factors, resulting in a poor prediction, and the result is not accurate enough. Recently, a non-traditional deep learning algorithm has been developed to judge the dynamic characteristics of nonlinear systems [1]. The algorithm is composed of reservoirs and recursive neural networks, which has the characteristics of fast and accurate computational speed, and is widely studied in various fields [2].

This paper proposes an improved reservoir computing algorithm for solving predictions of non-Gaussian noise-driven dynamic systems with strong noise intensity; and compares it with the original algorithm to investigate whether the improved reservoir calculation algorithm can improve the prediction efficiency in the case of strong noise-driven equations.Compared to traditional methods, our proposed algorithm improves efficiency with guaranteed accuracy, and it can be used as a general method for predicting dynamic systems, which has very broad utility in many areas of science and technology.

2 Results and discussion

In this paper, we choose Rössler system and Lorenz system which are driven by strong Lévy noise as examples to confirm the accuracy of RC algorithm[3-18] in the prediction of the system driven by strong Lévy noise.We make the noise intensities 0.1, 0.5, 1, and 1.25, respectively, and do so to determine whether the IRC algorithm can accurately predict dynamic systems driven by different noise intensities.

Through experiments, it was found that both algorithms predict the direction of the data very accurately and the prediction results are closer to the exact solution. The accuracy of the IRC algorithm is visually higher than that of the traditional RC algorithm, which profile confirms the superiority of the IRC algorithm in prediction.And we also calculated the evaluation metrics MAE and MSE, which also confirmed the superiority of the IRC algorithm over the traditional RC algorithm in terms of prediction.Two examples confirm that the IRC algorithm is more effective in handling systems driven by strong noise.

Meanwhile, we adjusted the spectral radius, the regularization parameter, and the number of neurons of the IRC algorithm.For the regularization parameters, we make them 0 and 0.01 to confirm whether the IRC algorithm can be overfitted and have inaccurate predictions.For the spectral radius,

we let it be 0 to confirm whether the prediction of the system is accurate when the reservoir is not memorable.For the number of neurons, we make it 30 and 3000 to confirm whether there is an effect on the prediction results when the number of neurons is too many and too few.After experiments, when the regularization parameter is 0, the prediction becomes inaccurate; it is 0.01, the prediction will be biased due to the occurrence of overfitting.When the spectral radius is 0, the prediction results appear inaccurate because the reservoir does not have memory. When the number of neurons is too small, although the prediction goes to the correct direction, the prediction accuracy is poor because too little information is learned, while when the number of neurons is too large, overfitting occurs, resulting in inaccurate prediction results and slow training speed.

3 Conclusions and Future work

Because some real-life data have high noise intensities, our use of the RC algorithm alone to predict chaotic systems is not sufficient to illustrate its advantages for prediction in dynamic systems. Therefore, in this paper, we add high-noise intensity non-Gaussian Lévy noise to the dynamic system to judge whether the deep learning algorithm can predict accurate. We proposed an improved reservoir calculation algorithm and confirmed that its prediction accuracy and efficiency are higher than the traditional RC algorithm. Meanwhile, we investigated the hyperparameters of the IRC algorithm and confirmed the important role played by the regularization parameter, spectral radius, and neurons in the prediction process. However, it is unclear if the accuracy of the prediction can be improved by the IRC algorithm when the dynamic system drove in low noise intensity, it can be used as a follow-up research direction. Our work proved that the IRC algorithm is effective to predict the transient of the dynamic system. It has very wide applicability in many fields.

References

[1] Manjunath, Gandhi, and Herbert Jaeger. "Echo state property linked to an input: Exploring a fundamental characteristic of recurrent neural networks." *Neural computation* 25.3 (2013): 671-696.

[2] Fan, Huawei, et al. "Long-term prediction of chaotic systems with machine learning." *Physical Review Research* 2.1 (2020): 012080.

[3] Khovanov, Igor A. "Stochastic approach for assessing the predictability of chaotic time series using reservoir computing." *Chaos: An Interdisciplinary Journal of Nonlinear Science* 31.8 (2021): 083105.

[4] Jaeger, Herbert, and Harald Haas. "Harnessing nonlinearity: Predicting chaotic systems and saving energy in wireless communication." *science* 304.5667 (2004): 78-80.

[5] Maass, Wolfgang, Thomas Natschläger, and Henry Markram. "Real-time computing without stable states: A new framework for neural computation based on perturbations." *Neural computation* 14.11 (2002): 2531-2560.

[6] Carroll, Thomas L. "Using reservoir computers to distinguish chaotic signals." *Physical Review E* 98.5 (2018): 052209.

[7] Vlachas, Pantelis R., et al. "Backpropagation algorithms and reservoir computing in recurrent neural networks for the forecasting of complex spatiotemporal dynamics." *Neural Networks* 126 (2020): 191-217.

[8] Nakai, Kengo, and Yoshitaka Saiki. "Machine-learning inference of fluid variables from data using reservoir computing." *Physical Review E* 98.2 (2018): 023111.

[9] Falahian, Razieh, et al. "Artificial neural network-based modeling of brain response to flicker light." *Nonlinear Dynamics* 81.4 (2015): 1951-1967.

[10] Follmann, Rosangela, and Epaminondas Rosa Jr. "Predicting slow and fast neuronal dynamics with machine learning." *Chaos: An Interdisciplinary Journal of Nonlinear Science* 29.11 (2019): 113119.

[11] Itoh, Yoshitaka, et al. "Reconstructing bifurcation diagrams only from time-series data generated by electronic circuits in discrete-time dynamical systems." *Chaos: An Interdisciplinary Journal of Nonlinear Science* 30.1 (2020): 013128.

[12] Zhang, Chun, et al. "Predicting phase and sensing phase coherence in chaotic systems with machine learning." *Chaos: An Interdisciplinary Journal of Nonlinear Science* 30.8 (2020): 083114.

[13] Jaeger, Herbert, and Harald Haas. "Harnessing nonlinearity: Predicting chaotic systems and saving energy in wireless communication." *science* 304.5667 (2004): 78-80.

[14] Pathak, Jaideep, et al. "Model-free prediction of large spatiotemporally chaotic systems from data: A reservoir computing approach." *Physical review letters* 120.2 (2018): 024102.

[15] Cui, Hongyan, Xiang Liu, and Lixiang Li. "The architecture of dynamic reservoir in the echo state network." *Chaos: An Interdisciplinary Journal of Nonlinear Science* 22.3 (2012): 033127.

[16] Lukoševičius, Mantas, and Herbert Jaeger. "Reservoir computing approaches to recurrent neural network training." *Computer Science Review* 3.3 (2009): 127-149.

[17] Maass, Wolfgang, Thomas Natschläger, and Henry Markram. "Real-time computing without stable states: A new framework for neural computation based on perturbations." *Neural computation* 14.11 (2002): 2531-2560.

[18] Pathak, Jaideep, et al. "Using machine learning to replicate chaotic attractors and calculate Lyapunov exponents from data." *Chaos: An Interdisciplinary Journal of Nonlinear Science* 27.12 (2017): 121102.

International Conference on Mathematical Analysis and Applications in Science and Engineering
ICMA^{2}SC'22
ISEP Porto-Portugal, June 27 - 29, 2022

Existence and approximation of solutions to a class of second-order functional differential equations

Rosana Rodríguez-López[1,2⋆]

[1] CITMAga, 15782 Santiago de Compostela, Spain.
[2] Departamento de Estatística, Análise Matemática e Optimización,
Facultade de Matemáticas, Universidade de Santiago de Compostela,
15782, Santiago de Compostela, Spain.

[1,2⋆]rosana.rodriguez.lopez@usc.es

Abstract: CONTRIBUTION IN MEMORY OF PROF. J.A. TENREIRO MACHADO, SUBMITTED TO SYMPOSIUM #9: DIFFERENCE & DIFFERENTIAL EQUATIONS WITH APPLICATIONS
This work is devoted to the development of the upper and lower solutions method and the monotone method for nonlinear second-order functional differential equations with piecewise constant arguments subject to boundary value conditions. Some of the results are connected with reference [1], a joint work with S. Buedo-Fernández, and D. Cao Labora.

keywords: boundary value problems; piecewise constant delay; iterative methods.

MSC2020: 34K07; 34K10; 34K12.

1 Introduction

Some references dealing with functional differential equations of second-order are, for instance, [10, 11, 14, 15, 16], where the functional dependence is given by the integer part function, and the right-hand term does not depend on x'. Concerning the development of upper and lower solutions method and the monotone iterative technique, we mention [4] for impulsive problems. In [6], the existence and multiplicity of periodic solutions for problems with no explicit dependence on x' is studied.

However, for the introduction in the model of a dependence on x' (a linear one), we refer to [5], some other works that consider problems without delay, or, more recently, [12], where Avery-Peterson fixed point theorem is applied to a thermostat model whose nonlinearity introduces the first-order derivative. On the other hand, in [9], it is analyzed the existence of periodic solutions for high-order functional differential equations including a linear dependence on the derivatives $x^{(i)}$, by applying coincidence degree theory.

More related with the specific contents of this contribution, the authors of [16] study the periodic boundary value problem for second-order functional differential equations of the type:

$$\begin{cases} -x''(t) = f(t, x(t), x([t])),\ t \in J = [0, T], \\ \qquad x(0) = x(T), \quad x'(0) = x'(T). \end{cases}$$

We also mention [3, 7], where some similar problems for first-order equations were analyzed.

Motivated by these works, in [8] a linear functional problem of the type

$$\begin{cases} x''(t) + ax'(t) + bx(t) + cx'([t]) + dx([t]) = \sigma(t),\ t \in J = [0,T], \\ x(0) = x(T), \\ x'(0) = x'(T) + \lambda \end{cases} \tag{1}$$

was studied through the analysis of the solutions to the family of impulsive linear boundary value problems

$$\begin{cases} x''(t) + ax'(t) + bx(t) + cx'([t]) + dx([t]) = 0,\ t \in \mathbb{R}, \\ x(0) = x(T), \\ x'(0^-) = x'(T^+), \\ x'(s^+) = x'(s^-) + 1, \end{cases} \tag{2}$$

for $s \in J$, a, b, c, d, $\lambda \in \mathbb{R}$, $T > 0$, and σ piecewise continuous. In this reference, it was proved that the solution to problem (1) can be calculated in terms of an integral expression whose kernel (Green's function) is provided by the solution of the family of problems (2) (see [13] for some other related results).

Another relevant tool is the study in [2], where the existence of constant sign solutions to (1) is studied in terms of relations between the values of the coefficients in the equation. These properties lead to comparison results, which are essential to develop iterative techniques for our problem of interest, whose right-hand side is influenced by x' and this term is also subject to a functional dependence.

2 Results and discussion

In this contribution, we study the existence and approximation of solutions to boundary value problems for second-order functional differential equations of the type:

$$\begin{cases} x''(t) = g(t, x(t), x'(t), x([t]), x'([t])),\ t \in J = [0,T], \\ x(0) = x(T), \\ x'(0) = x'(T) + \lambda, \end{cases} \tag{3}$$

where $\lambda \in \mathbb{R}$, and $g : J \times \mathbb{R}^4 \longrightarrow \mathbb{R}$ is continuous on $(J \setminus \{1, 2, \ldots, [T]\}) \times \mathbb{R}^4$ with finite limits

$$\lim_{t \to n^-} g(t,x,y,u,v), \quad g(n,x,y,u,v) = \lim_{t \to n^+} g(t,x,y,u,v), \qquad n \in \{1, 2, \ldots, [T]\}.$$

In particular, we adress the following issues:

a) Definition of relevant base spaces in relation with piecewise regular functions, and useful results on the expressions of the solutions for related linear problems [8, 2].

b) Presentation of comparison results for linear delay differential equations subject to boundary conditions, useful to compare two solutions and their derivatives.

c) Definition of the concepts of upper and lower solutions for (3), and deduction of the relation between solutions to comparable problems.

d) Study of the existence of solution to problem (3) in the functional interval determined by the upper and the lower solution through the application of fixed point results to a suitable integral operator, and comparison results. Besides, some estimates for the derivative of the solution are provided.

e) Development of the monotone iterative technique for problem (3), providing the existence of monotone sequences starting at the upper and lower solutions and converging uniformly to the respective maximal and minimal solutions to (3) in a certain region. Besides, estimates for the derivatives of the approximations of the solutions are given.

Acknowledgments

This research has been partially supported by grants PID2020-113275GB-I00 (AEI/FEDER, UE), and ED431C 2019/02 (GRC Xunta de Galicia).

References

[1] S. Buedo-Fernández, D. Cao Labora, R. Rodríguez-López, Boundary value problems for nonlinear second-order functional differential equations with piecewise constant arguments, submitted, 2022.

[2] S. Buedo-Fernández, D. Cao Labora, R. Rodríguez-López, S. Tersian, Analysis of the sign of the solution for certain second-order periodic boundary value problems with piecewise constant arguments, Mathematics **8** (2020), 1953; doi:10.3390/math8111953.

[3] A. Cabada, J.B. Ferreiro, J.J. Nieto, Green's function and comparison principles for first order periodic differential equations with piecewise constant arguments, J. Math. Anal. Appl. **291** (2004), 690–697.

[4] L. Chen, J. Sun, Boundary value problem of second order impulsive functional differential equations, J. Math. Anal. Appl. **323** (2006), 708–720.

[5] C. Corduneanu, Some classes of second order functional differential equations, Nonlinear Anal.: Theory, Methods & Appl. **71**(12) (2009), e865–e871.

[6] C. Guo, Z. Guo, Existence of multiple periodic solutions for a class of second-order delay differential equations, Nonlinear Analysis: Real World Applications **10**(5) (2009), 3285–3297.

[7] J.J. Nieto, A comparison result for a linear differential equation with piecewise constant delay, Glas. Mat. Ser. III **39**(59) (2004), 73–76.

[8] J.J. Nieto, R. Rodríguez-López, Green's function for second-order periodic boundary value problems with piecewise constant arguments, J. Math. Anal. Appl. **304** (2005), 33–57.

[9] L. Pan, Periodic solutions for higher order differential equations with deviating argument, J. Math. Anal. Appl. **343** (2008), 904–918.

[10] G. Seifert, Second order scalar functional differential equations with piecewise constant arguments, J. Difference Equ. Appl. **8** (2002), 427–445.

[11] G. Seifert, Second-order neutral delay-differential equations with piecewise constant time dependence, J. Math. Anal. Appl. **281** (2003), 1–9.

[12] C. Shen, H. Zhou, L. Yang, Existence of positive solutions of a nonlinear differential equation for a thermostat model, Mathematical Methods in the Applied Sciences **41**(16) (2018), 6145-6154.

[13] P. Yang, Y. Liu, W. Ge, Green's function for second order differential equations with piecewise constant arguments, Nonlinear Anal.: Theory, Methods & Appl. **64** (8) (2006), 1812–1830.

[14] R. Yuan, Pseudo-almost periodic solutions of second-order neutral delay differential equations with piecewise constant argument, Nonlinear Anal.: Theory, Methods & Appl. **41** (2000), 871–890.

[15] R. Yuan, On the second-order differential equation with piecewise constant argument and almost periodic coefficients, Nonlinear Anal.: Theory, Methods & Appl. **52** (2003), 1411–1440.

[16] F.Q. Zhang, Boundary value problems for second order differential equations with piecewise constant arguments, Ann. Differential Equations **9** (1993), 369–374.

International Conference on Mathematical Analysis and Applications in Science and Engineering
ICMA^{2}SC'22
ISEP Porto-Portugal, June 27 - 29, 2022

On the Stochastic Linear Quadratic Optimal Control Problem by Piecewise Constant Controls. The Infinite Horizon Time Case

Vasile Dragan[1,2] **Ioan-Lucian Popa**[3,4,⋆] **Samir Aberkane**[5,6]

[1] Institute of Mathematics "Simion Stoilow"
of the Romanian Academy, Bucharest, Romania
[2] Academy of the Romanian Scientists, Bucharest, Romania
[3] Department of Computing, Mathematics and Electronics,
"1 Decembrie 1918" University of Alba Iulia, Alba Iulia, 510009, Romania
[4] Faculty of Mathematics and Computer Science, Transilvania University of Brasov,
Iuliu Maniu Street 50, 500091 Brasov, Romania
[5] Université de Lorraine, CRAN, UMR 7039,
Campus Sciences, BP 70239, Vandoeuvre-les-Nancy Cedex, 54506, France
[6] CNRS, CRAN, UMR 7039, France

⋆lucian.popa@uab.ro

Abstract: This paper is devoted to the problem of indefinite stochastic linear quadratic (LQ) optimal control in an infinite horizon case. By restricting the set of admissible controls to the class of piecewise constant stochastic processes, we reformulated the above control problem under the setting of systems modelled by Itô differential equations controlled by impulses. We show that the solution of the indefinite stochastic LQ control problem is equivalent to the existence of a global stabilizing solution associated to a class of backward matrix linear differential equation with a Riccati type jumping operator.

keywords: stochastic linear quadratic optimal control; piecewise constant controls; infinite horizon; generalized Riccati equations.

MSC2020: 93E20; 49N10.

1 Introduction

One of the main differentiating characteristics of the stochastic linear quadratic control theory when compared to its deterministic counterpart appears when one allows the cost weighting matrices for the state and the control to be indefinite. Indeed, the fundamental finding of the pioneering work [1] is that a stochastic LQ problem with indefinite cost weighting matrices may still be well-posed. Beside the fact that the indefinite stochastic LQ theory is an interesting mathematical theoretic problem on its own, it has also a solid practical background. For example, one can cite the mean-variance portfolio selection problem [2, 3], pollution control problem [1] and so on. The finding of [1] has triggered extensive research since then on the indefinite stochastic LQ problem; see, for example, the follow-up works of [4, 5, 6, 7]. Recently, we have addressed in [8] the problem of indefinite stochastic LQ problem in the finite horizon case.

By following the *generalized Riccati equations* (GREs) setting introduced initially by [7], we succeeded to propose less conservative necessary and sufficient conditions for the solvability of the considered optimal control problem. The proposed solution path relies on the restriction of the class of admissible controls and the reformulation of the control problem under the setting of systems modelled by Itô differential equations with finite jumps (or impulsive stochastic systems). Linear impulsive systems are a class of hybrid systems in which the state propagates according to linear continuous-time dynamics except for a countable set of times at which the state can change instantaneously. Our aim in the present paper is to consider the infinite-horizon time counterpart of [8]. It is worth mentioning that the results developed in this article are far from being a trivial extension of the developments reported in [8]. This is mainly due to the stability considerations inherent to the infinite horizon case. The main mathematical object defined in order to resolve the considered optimal control problem is a class of backward matrix linear differential equation with a Riccati type jumping operator. By analogy with [7], such an object could be recalled as GREs with finite jumps. By adequately defining the notion of stabilizing solution for such a class of nonlinear equations with jumps, we succeeded to show that the solution of the indefinite stochastic LQ control problem in the infinite horizon case is equivalent to the existence of a global stabilizing solution associated with the considered GRE with finite jumps.

2 Results and discussion

2.1 The problem Setting.

We consider the controlled system having the state space representation described by

$$\begin{aligned} &dx(t) = (A_0(t)x(t) + B_0(t)u(t))dt + (A_1(t)x(t) + B_1(t)u(t))dw(t), \\ &x(t_0) = x_0, \end{aligned} \tag{1}$$

$t \geq t_0 \geq 0$, where $x(t) \in \mathbb{R}^n$ is the vector of the state parameters at the instance time t, while $u(t) \in \mathbb{R}^m$ are the vectors of control parameters. In (1), $\{w(t)\}_{t\geq 0}$ is a 1-dimensional standard Wiener process defined on a given probability space $(\Omega, \mathcal{F}, \mathcal{P})$. Beside the control system (1) we consider the performance criterion described by

$$J(t_0, x_0; u(\cdot)) = \mathbb{E}\left[\int_{t_0}^{\infty} (x_u^T(t)M(t)x_u(t) + u^T(t)R(t)u(t))dt\right] \tag{2}$$

where $x_u(\cdot) = x_u(\cdot, t_o, x_0)$ is the solution of the given initial value problem (IVP) (1). The class of the admissible controls, $\mathcal{U}_{ad}(t_0, x_0)$ considered in this work consists of all stochastic processes $\{u(t)\}_{t\geq t_0}$ of the form

$$u(t) = u_k, \;\; t_k \leq t < t_{k+1}, \;\; k \in \mathbb{Z}_+ = \{0, 1, 2, \ldots\} \tag{3}$$

where $0 \leq t_0 < t_1 < \ldots < t_k < t_{k+1} < \ldots$ is a partition of the interval $[t_0, \infty)$. In (3) $u_k : \Omega \to \mathbb{R}^m$ are random vectors with the properties u_k is measurable with respect to the $\sigma-$algebra $\mathcal{F}_{t_k}$;, $\sum\limits_{k=0}^{\infty} \mathbb{E}[|u_k|^2] < \infty$; and $\lim\limits_{t\to\infty} \mathbb{E}[|x_u(t; t_0, x_0)|^2] = 0$. Throughout this work, $\mathcal{F}_t \subset \mathcal{F}$ is the $\sigma-$algebra generated by the random variables $w(s)$, $0 \leq s \leq t$. As usual $\mathbb{E}[\cdot]$ stands for mathematical expectation. Regarding the matrix valued functions involved in (1) and (2) we make the assumption

H1) (a) $t \to (A_j(t), B_j(t)) : \mathbb{R}_+ \to \mathbb{R}^{n\times n} \times \mathbb{R}^{n\times m}$, $j = 0, 1$, $t \to (M(t), R(t)) : \mathbb{R}_+ \to \mathbb{R}^{n\times n} \times \mathbb{R}^{m\times m}$ are bounded and continuous matrix valued functions;
(b) $M(t) = M^T(t)$, $R(t) = R^T(t)$, for all $t \in \mathbb{R}_+$.

The optimal control problem on the unbounded interval $[t_0, \infty)$, that we want to solve, asks for finding a control $\tilde{u}(\cdot) \in \mathcal{U}_{ad}(t_0, x_0)$ which minimizes the cost functional (2) over the class of the admissible controls $\mathcal{U}_{ad}(t_0, x_0)$, i.e.

$$J(t_0, x_0; \tilde{u}(\cdot)) \leq J(t_0, x_0; u(\cdot)), \text{ for all } u(\cdot) \in \mathcal{U}_{ad}(t_0, x_0). \tag{4}$$

In order to obtain the control $\tilde{u}(\cdot)$ which satisfies the optimality condition (4) we reformulate this problem as an optimal control problem in which the controlled system is described by a system of Itô differential equations with jumps.

2.2 Main Results.

Substituting a control of type (3) in (1) and (2), respectively, we obtain

$$\begin{aligned} &dx(t) = (A_0(t)x(t) + B_0(t)u_k)dt + (A_1(t)x(t) + B_1(t)u_k)dw(t), \ \ t_k \leq t < t_{k+1}, \ \ k \in \mathbb{Z}_+ \\ &x(t_0) = x_0 \end{aligned} \tag{5}$$

and

$$J(t_0, x_0; u(\cdot)) = \mathbb{E}\left[\int_{t_0}^{\infty} x_u^T(t) M(t) x_u(t)\right] + \sum_{k=0}^{\infty} \mathbb{E}\left[u_k^T \int_{t_k}^{t_{k+1}} R(t)dt \; u_k\right]. \tag{6}$$

We set $v(t) = u_k$, $t_k \leq t < t_{k+1}$, $k \in \mathbb{Z}_+$. One sees that $t \to v(t) : [t_0, \infty) \to \mathbb{R}^m$ is derivable for all $t \neq t_k$, $k \in \mathbb{Z}_+$ and we have $\dot{v}(t) = 0$, $t_k < t < t_{k+1}$ and $v(t_k^+) \stackrel{\triangle}{=} \lim_{\substack{s \to 0 \\ s>0}} v(t_k + s) = u_k$, for all $k \in \mathbb{Z}_+$. Let $\xi(t) := (x^T(t) \ \ v^T(t))^T$. By direct calculations one can reformulate (5) as:

$$d\xi(t) = \mathcal{A}_0(t)\xi(t)dt + \mathcal{A}_1(t)\xi(t)dw(t), \ \ t_k < t \leq t_{k+1} \tag{7a}$$
$$\xi(t_k^+) = \mathcal{A}_d\xi(t_k) + \mathcal{B}_d u_k, \ \ k \in \mathbb{Z}_+. \tag{7b}$$
$$\xi(t_0) = \xi_0 = (x_0^T \ \ 0^T)^T \in \mathbb{R}^{n+m} \tag{7c}$$

where: $\mathcal{A}_j(t) = \begin{pmatrix} A_j(t) & B_j(t) \\ 0_{mn} & 0_{mm} \end{pmatrix}$, $j = 0, 1$, $\mathcal{A}_d = \begin{pmatrix} I_n & 0_{nm} \\ 0_{mn} & 0_{mm} \end{pmatrix}$ and $\mathcal{B}_d = \begin{pmatrix} 0_{nm} \\ I_m \end{pmatrix}$. Employing the coefficients of the controlled system (7) we define the following backward jump matrix linear differential equation (BJMLDE)

$$-\dot{Y}(t) = \mathcal{A}_0^T(t)Y(t) + Y(t)\mathcal{A}_0(t) + \mathcal{A}_1^T(t)Y(t)\mathcal{A}_1(t) + \mathcal{M}(t), \ \ t_k \leq t < t_{k+1} \tag{8a}$$
$$Y(t_k^-) = \mathcal{A}_d^T Y(t_k)\mathcal{A}_d - \mathcal{A}_d^T Y(t_k)\mathcal{B}_d(\mathcal{R}_k + \mathcal{B}_d^T Y(t_k)\mathcal{B}_d)^\dagger \mathcal{B}_d^T Y(t_k)\mathcal{A}_d, \ \ k \in \mathbb{Z}_+. \tag{8b}$$

where $\mathcal{M}(t) = \begin{pmatrix} M(t) & 0_{nm} \\ 0_{mn} & 0_{mm} \end{pmatrix}$ and $\mathcal{R}_k = \int_{t_k}^{t_{k+1}} R(t)dt$. Let $\begin{pmatrix} \tilde{Y}_{11}(t) & \tilde{Y}_{12}(t) \\ \tilde{Y}_{12}^T(t) & \tilde{Y}_{22}(t) \end{pmatrix}$ be the partition of the bounded and stabilizing solution $\tilde{Y}(t)$ of the BJMLDE (8). We define:

$$\tilde{F}_{1k} = -(\mathcal{R}_k + \tilde{Y}_{22}(t_k))^\dagger \tilde{Y}_{12}^T(t_k) + [I_m - (\mathcal{R}_k + \tilde{Y}_{22}(t_k))^\dagger (\mathcal{R}_k + \tilde{Y}_{22}(t_k))]\tilde{K}_{1k} \tag{9a}$$
$$\tilde{F}_{2k} = [I_m - (\mathcal{R}_k + \tilde{Y}_{22}(t_k))^\dagger (\mathcal{R}_k + \tilde{Y}_{22}(t_k))]\tilde{K}_{2k}. \tag{9b}$$

where $\tilde{K}_{1k} \in \mathbb{R}^{m \times n}$, $\tilde{K}_{2k} \in \mathbb{R}^{m \times m}$ adequately chosen such that $F_k(\tilde{Y}(t_k), \tilde{K}_k)$ is the optimal stabilizing feedback gain. The main result of this work is resumed by the following Theorem:

Theorem 1 *Assume*

(a) the assumption ***H1)*** *is fulfilled;*

(b) $\underline{h} \leq t_{k+1} - t_k \leq \bar{h}$ *for all* $k \in \mathbb{Z}_+$ *for some positive constants* $\underline{h}$ *and* $\bar{h}$*;*

(c) the BJMLDE with Riccati type jumping operator (8) has a bounded and stabilizing solution satisfying constraints of type:

$$\mathcal{R}_k + \tilde{Y}_{22}(t_k) \geq 0 \tag{10a}$$

$$[I_m - (\mathcal{R}_k + \tilde{Y}_{22}(t_k))^{\dagger}(\mathcal{R}_k + \tilde{Y}_{22}(t_k))]\tilde{Y}_{12}^T(t_k) = 0, \quad k \in \mathbb{Z}_+. \tag{10b}$$

We consider the piecewise constant control law

$$\tilde{u}(t) = \tilde{F}_{10}x_0, \quad t_0 \leq t < t_1 \tag{11a}$$

$$\tilde{u}(t) = \tilde{F}_{1k}x(t_k) + \tilde{F}_{2k}\tilde{u}(t_{k-1}), \; t_k \leq t < t_{k+1}, \; k \geq 1. \tag{11b}$$

Under the considered assumptions the control law (11) lies in $\mathcal{U}_{ad}(t_0, x_0)$ *and it is a solution of the optimal control problem (4). The minimal value of the cost functional (2) is* $J(t_0, x_0; \tilde{u}(\cdot)) = x_0^T\tilde{Y}_{11}(t_0^-)x_0$.

Acknowledgments

This research was funded by 1 Decembrie 1918 University of Alba Iulia through scientific research funds.

References

[1] S. Chen, X. Li, X. Y. Zhou, Stochastic linear quadratic regulators with indefinite control weight costs, SIAM J. Control Optim., **36** (1998), 1685–1702.

[2] E. B. Lim, X. Y. Zhou, Mean-variance portfolio selection with random parameters in a complete markets, Math. Oper. Res., **27** (2002), 101–120.

[3] X. Y. Zhou, D. Li, Continuous-time mean-variance portfolio selection: A stochastic LQ framework. Appl. Math. Optim., (2000), 19–33.

[4] S. Chen, J. Yong, Stochastic linear quadratic optimal control problems with random coefficients. Ann. Math. Ser. B, (2000), 323–338.

[5] S. Chen, J. Yong, Stochastic linear quadratic regulators with indefinite control weight costs.II. SIAM J. Control Optim., (2000), 1065–1081.

[6] Y. Hu, X. Y. Zhou, Indefinite stochastic Riccati equations. SIAM J. Control Optim., (2003), 123–137.

[7] M. Ait Rami, J. B. Moore, X. Y. Zhou, Indefinite Stochastic Linear Quadratic Control and Generalized Differential Riccati Equation. SIAM J. Control Optim., (2002), 1296–1311.

[8] Vasile Drăgan, Ivan G. Ivanov, On the stochastic linear quadratic control problem with piecewise constant admissible controls. Journal of the Franklin Institute, (2020), 1532–1559.

International Conference on Mathematical Analysis and Applications in Science and Engineering
ICMA^{2}SC'22
ISEP Porto-Portugal, June 27 - 29, 2022

A reaction-diffusion model of virus-immune system interaction: Lie symmetries

T.M. Garrido[1⋆] **A.P. Márquez**[1] **R. de la Rosa**[1]

[1] University of Cadiz, Spain

⋆tamara.garrido@uca.es

Abstract: The spread of a virus infection depends on many aspects of the virus-host interaction, such as, the virus multiplication, their transport and the immune response. It can be modeled by a reaction-diffusion system of equations with two arbitrary functions. This model considers the concentration of virus and immune cells, and neglects the delays in clonal expansion and apoptosis induction of the virus-specific T cells. In this work, the partial differential equation system is studied through the Lie symmetry analysis. Its Lie point symmetries are obtained in order to reduce the equations into ordinary differential equations.

keywords: reaction-diffusion system; virus-immune system; symmetries; reductions.

MSC2020: 22E70; 35B06.

1 Introduction

The ability of the immune system to restrain virus infections depends on many essential aspects of the virus-host interaction and the spatial transport. The use of reaction-diffusion systems for modeling infectious diseases makes it possible to take into account the spatial distribution of viruses and immune cells in various tissues and organs [1, 2].

The following reaction-diffusion system (RDS) models the virus-immune system interaction which neglects the delays in clonal expansion and apoptosis induction of the virus-specific T cells.

$$\begin{aligned} u_t &= d_1 u_{xx} + ku(1-u) - \sigma uv, \\ v_t &= d_2 v_{xx} + (c_0 + f(u)v)(1-v) - g(u)v. \end{aligned} \tag{1}$$

The first term in the right-hand side of first equation describes virus diffusion, the second term its production and the last term its elimination by the immune cells. Regarding right-hand side of the second equation, the first term describes random motion of immune cells, the second term gives the rate of the appearance of immune cells and the last term the rate of their death.

Here u, v are the normalized dimensionless concentrations of virus and immune cells respectively. Parameters d_1, d_2, k and σ are positive numbers, c_0 could be zero or a positive number, the functions $f(u)$ and $g(u)$ are positive and sufficiently smooth. Another reduced versions of the previous RDS model can be found in [3].

2 Lie point symmetries

In broad strokes, we have considered a one-parameter Lie group of point transformations acting on independent and dependent variables

$$\begin{aligned}\tilde{t} &= t + \varepsilon\tau(t,x,u,v) + \mathcal{O}(\varepsilon^2),\\ \tilde{x} &= x + \varepsilon\xi(t,x,u,v) + \mathcal{O}(\varepsilon^2),\\ \tilde{u} &= u + \varepsilon\eta^u(t,x,u,v) + \mathcal{O}(\varepsilon^2),\\ \tilde{v} &= v + \varepsilon\eta^v(t,x,u,v) + \mathcal{O}(\varepsilon^2),\end{aligned}$$

where ε is the group parameter and the associated vector field takes the following form

$$X = \tau(t,x,u,v)\partial_t + \xi(t,x,u,v)\partial_x + \eta^u(t,x,u,v)\partial_u + \eta^v(t,x,u,v)\partial_v.$$

The Lie group of transformations is admitted by the equation (1), and carry any solution of the equation into a one-parameter family of solutions of the equation, if the infinitesimal criterion for invariance of a partial differential equation is verified:

$$\begin{aligned}X^{(2)}\Big(-u_t + d_1u_{xx} + ku(1-u) - \sigma uv\Big) = 0,\\ X^{(2)}\Big(-v_t + d_2v_{xx} + (c_0 + f(u)v)(1-v) - g(u)v\Big) = 0,\end{aligned}$$

when the RDS holds, and where $X^{(2)}$ is the second order prolongation [4, 5]. Previous equations are known as the determining equations. It splits with respect to the differential consequences of u and v, and leads an overdetermined linear system of 51 equations for the infinitesimals together with the parameters d_1, d_2, k, σ, c_0 and the functions $f(u)$, $g(u)$.

Theorem 1 *The classification of all point symmetries admitted by the virus-immune system interaction model (1) is:*

(i) For d_1, d_2, k, σ non-zero parameters, c_0 an arbitrary parameters and $f(u)$, $g(u)$ arbitrary functions,

$$\begin{aligned}X_1 &= \partial_x,\\ X_2 &= \partial_t.\end{aligned}$$

(ii) For $d_1 = d_2$, $f(u) = \dfrac{k^2\sigma u^2 - k^2\sigma u - c_0\sigma^2}{k^2u^2 - 2k^2u + k^2}$ and
$g(u) = \dfrac{k^3u^3 - c_0k^2u^2 - 2k^3u^2 + k^2\sigma u^2 + 2c_0k^2u - 2c_0k\sigma u + k^3u - k^2\sigma u - c_0k^2 + 2c_0k\sigma - c_0\sigma^2}{k^2u^2 - 2k^2u + k^2}.$

Infinitesimal generators are X_1, X_2 and

$$X_3 = 2t\partial_t + x\partial_x + \frac{-2ku}{\sigma} - 2v + \frac{2k}{\sigma}\partial v.$$

3 Symmetry reductions

In order to determine solutions of the virus-immune system interaction model (1) that are not equivalent by the action of the group, we calculate the one-dimensional optimal system of subalgebras [6]:

i) For the case with arbitrary functions and parameters

$$\{\mathbf{X}_1 + \lambda \mathbf{X}_2\}.$$

ii) For the special case of the functions and parameters

$$\{\mathbf{X}_1 + \lambda \mathbf{X}_2, \mathbf{X}_3\}.$$

By using the optimal system, we calculate the similarity variables and solutions solving the characteristic system:

$$\frac{dt}{\tau} = \frac{dx}{\xi} = \frac{du}{\eta^u} = \frac{du}{\eta^v}$$

- For $\mathbf{X}_1 + \lambda \mathbf{X}_2$

$$\begin{array}{ll} \text{Similarity variables:} & z = x - \lambda t \\ \text{Similarity solutions:} & u(t,x) = U(z),\ v(t,x) = V(z). \end{array}$$

This allows us to reduce the partial differential equations (1) into a system of ordinary differential equations:

$$\begin{array}{l} kU^2 + \sigma uv - d_1 U'' - kU - \lambda U' = 0, \\ f(U)V^2 - \lambda V' - d_2 V'' - f(U)V + g(U)V + c_0 V - c_0 = 0. \end{array} \tag{2}$$

- For $\mathbf{X}_3$

$$\begin{array}{ll} \text{Similarity variables:} & z = \frac{x}{\sqrt{t}} \\ \text{Similarity solutions:} & u(t,x) = U(z),\ v(t,x) = \frac{1}{t}V(z) - \frac{k}{\sigma}(1 + U(z)). \end{array}$$

This allows us to reduce the partial differential equations (1) into a system of ordinary differential equations:

$$\begin{aligned} 2\sigma UV - zU' - 2d_1 U'' &= 0, \\ 4k^2\sigma UV + 2g(U)U^2Vk^2\sigma t + 2U^2Vc_0k^2\sigma t - 4g(U)UVk^2\sigma t - 4UVc_0k^2\sigma t & \\ +4c_0\sigma^2kUVt + 2c_0k\sigma^2t^2 + 2g(U)k^3t^2 - 2c_0\sigma^3V^2 - 2Vk^2\sigma + 2k^4U^4t^2 - 6k^4U^3t^2 & \\ +6k^4U^2t^2 - 2k^4Ut^2 - 4k^3U^3Vt\sigma + U'U^2k^3tz + 2U''U^2d_1k^3t + 8k^3U^2Vt\sigma & \\ -2k^2\sigma^2U^2Vt - 4c_0k^2U^2t^2\sigma - 2V''U^2d_1k^2\sigma - V'U^2k^2\sigma z - 2U'Uk^3tz - 4U''Ud_1k^3t & \\ -4k^3UVt\sigma + 2k^2\sigma^2UVt + 8c_0k^2Ut^2\sigma - 2c_0\sigma^2kUt^2 + 2g(U)Vk^2t\sigma & \\ +4V''Ud_1k^2\sigma + 2V'Uk^2\sigma z + 2c_0Vk^2t\sigma - 4c_0k\sigma^2Vt - 4c_0k^2t^2\sigma & \\ -2g(U)U^3k^3t^2 - 2U^3c_0k^3t^2 + 2k^3U^3t^2\sigma + 6g(U)U^2k^3t^2 + 2k^2\sigma^2U^2V^2 + 6U^2c_0k^3t^2 & \\ -4k^3U^2t^2\sigma - 6g(U)k^3Ut^2 - 2k^2\sigma^2UV^2 - 6c_0k^3Ut^2 + 2k^3Ut^2\sigma + k^3U'zt + 2d_1k^3U''t & \\ +2c_0\sigma^3Vt - 2d_1V''k^2\sigma - V'zk^2\sigma + 2c_0k^3t^2 - 2k^2\sigma U^2V &= 0. \end{aligned}$$

4 Conclusions and Future work

In the present work we have found new results for the reaction-diffusion system that models the virus-immune system interaction (1). The results are mainly related to symmetries, including optimal systems and symmetry reductions. Firstly, Lie point symmetries have been classified depending on functions $f(u)$ $g(u)$ and the parameters d_1, d_2, k, σ and c_0. Then, we have constructed the maximal Lie algebras, and the commutator and adjoint relations. By using these actions and the point symmetries generators, we have constructed the optimal systems of one-dimensional subalgebras for each maximal Lie algebra. Finally, we have obtained the symmetry reductions to reduce the governing system of PDEs to ODEs. As future work, we will study different solutions that can be obtained from the reduced equations.

References

[1] F. Graw, A.S. Perelson, Modeling Viral Spread, Annual Review of Virology **3**(1) (2016), 555–572.

[2] G.Bocharov, A. Meyerhans, N. Bessonov, S. Trofimchuk, V. Volpert, Spatiotemporal dynamics of virus infection spreading in tissues, PLoS One **11**(12) (2016).

[3] G.Bocharov, A. Meyerhans, N. Bessonov, S. Trofimchuk, V. Volpert, Interplay between reaction and diffusion processes in governing the dynamics of virus infections, Journal of Theoretical Biology **457** (2018), 221–236.

[4] G.W. Bluman, S.C. Anco, *Symmetry and Integration Methods for Differential Equations*. New York: Springer–Verlag, 2002.

[5] P.J. Olver, *Applications of Lie Groups to Differential Equations*. New York: Springer Science & Business Media, 2000.

[6] P.J. Olver, *Equivalence, invariants and symmetry*. Cambridge: Cambridge University Press, 1995.

International Conference on Mathematical Analysis and Applications in Science and Engineering
ICMA^{2}SC'22
ISEP Porto-Portugal, June 27 - 29, 2022

FROM UNEQUAL SIZE SAMPLE SUMS TO ESTIMATING THE STANDARD DEVIATION

Miguel CASQUILHO[1⋆] **Jorge BUESCU**[2]

[1]IST ("Instituto Superior Técnico"), University of Lisbon, Lisbon, Portugal
[2]FCUL ("Faculdade de Ciências"), University of Lisbon, Lisbon, Portugal

[1⋆]mcasquilho@tecnico.ulisboa.pt

Abstract: For Quality or related motives, in many industrial instances, the sums of unequal size samples are recorded, while the individual values are not. We undertake the computing of point estimation, with confidence intervals, of the standard deviation (and mean) of the individual items, considered Gaussian, from those sums alone. A common case of a sum is the weight of a load of bags on a truck, used as an illustration. For the parameters mean and standard deviation of the distribution, we derive: point estimates, leading to weighted statistics; and confidence intervals, for which we arrived at a plausible conjecture for the mean, and a proposal for the standard deviation. All the results can be effectively verified by computation on our web pages, namely, for industrial use.

keywords: Standard deviation; unequal size samples; sample sums; Web computing.

MSC2020: 62-08; 62F10; 62F25; 62P30; 65C05.

1 Introduction

We address the estimation of the parameters, μ and σ, of the assumed Gaussian distribution of the individual items, when only the sums of *unequal size* samples are recorded, as in common manufacturing processes. Our results, seemingly absent in the literature, are made accessible on our web site to any interested user, namely, a non-expert. The point estimations of μ and σ are performed analytically; and confidence intervals are calculated (i) analytically for μ through a plausible conjecture, and (ii) by simulation for σ, with a further theoretical step, open to investigation. With all the computing being verifiable on a web site, we make our methods and results available to "meet the need to improve the reuse of scholarly data" (Wilkinson et al. (2016) [8]), a goal immensely facilitated by the Internet.

In a factory (experience of the first author), the confirmation of the weight of a shipment (truck loaded with bags) is the last control step. The numbers of items (sample sizes) are mostly different, per each customer's order. Companies making numerous similar items control the quality of their production, through "statistical process control" (SPC). The mean and standard deviation of critical characteristics are monitored, as well as the compliance with specifications. The estimations herein also help confirm values previously calculated. Weighing sets of items is a daily operation in many industrial activities. The cardinality of the set may be fixed, such as a dozen, leading to equal size samples, but the more general case is that of unequal size samples.

Table 1: Number of bags and load weights with *unequal size* samples, for a certain period.

Truck, t	Number of bags, n_t	Load weight (kg), m_t	Average bag weight (kg), $\bar{x}_t = m_t/n_t$
1	5	125.05	**25.01**
2	11	274.67	**24.97**
3	26	650.52	**25.02**
4	58	1446.58	**24.94**

A literature search for *sample*, *size*, *sum*, *estimation* yields thousands of irrelevant references. A review of apparently related work provided useless information, such as the following sample. Dunnett (1980) [4] discusses the effect of unequal sizes on the error in comparisons, which is not the problem under consideration. Ramsey and Ramsey (2008) [6] compare procedures with unequal size samples. Montgomery (2013) [5] mentions variable size samples, but for control charts with "n_i not very different".

Our objective is to estimate μ and σ, especially the latter, from the sums of samples of known and (in general) unequal sizes, the individual items (weight of each bag) being assumed independent and identically distributed (i. i. d.) Gaussians. The computing is available in our web pages, with the default data used here. We follow the incitement from an editor in a Statistics journal (Colosimo, 2019 [3]) not only by sharing "data and code" (supplied by us if solicited), but also by providing execution on our web pages.

In the next Section: the point estimation of the parameters is derived for unequal size samples; confidence intervals for μ and σ are addressed, with a plausible conjecture for μ and a proposal for σ; and numerical results are shown. In the last Section, some conclusions are mentioned.

2 Results and discussion

The point estimation of μ and σ of the unequal size sample case is derived, equal size being a particular case (e.g., Walpole et al. (2012) [7]). The number of samples is denoted by T ("trucks"), $t = 1, \ldots, T$ is the number of the sample ("truck"). For each sample, t, its size is n_t (number of bags in truck), its sum is m_t, and the sample average is $\bar{x}_t = m_t/n_t$. The averages, which are not usual data, were calculated in an additional column in the example table (below). The realistic values of $\mu = 25$ kg and $\sigma = 0.2$ kg for the Gaussian are used throughout. To illustrate the estimation of μ and σ for unequal size samples, we include Table 1 with a set of prepared data from the said Gaussian. This might describe a certain period, say, one week, with 4 customers. For each truck in the 1.st column: the 2.nd is the number of bags; and the 3.rd, the net weight, with the 4.th, the calculated average weight.

For the point estimates, maximum likelihood was applied to the sample averages, $\bar{X}_t$, a statistic chosen from previous appraisal. The individual items being i. i. d. Gaussians with parameters μ and σ, it follows that the $\bar{X}_t$ are also Gaussian, with common mean μ (same) and standard deviation $\sigma/\sqrt{n_t}$. Thus, the likelihood is, with the usual application of logarithms,

$$\ln L\,(\mu,\ \sigma) = \sum_{t=1}^{T} \left\{ -\ln\left[(\sigma/\sqrt{n_t})\,\sqrt{2\pi} \right] - \frac{1}{2} \left(\frac{\bar{X}_t - \mu}{\sigma/\sqrt{n_t}} \right)^2 \right\}. \tag{1}$$

The estimators of μ and σ result from solving for the maxima of Equation (1), leading to the their maximum likelihood estimators

$$\hat{\mu} = \frac{\sum_{t=1}^{T} n_t \bar{x}_t}{\sum_{t=1}^{T} n_t} \tag{2}$$

$$\hat{\sigma}^2 = \frac{1}{T-1} \sum_{t=1}^{T} n_t \left(\bar{x}_t - \hat{\mu} \right)^2 . \tag{3}$$

For confidence intervals of μ and σ, a plausible conjecture for μ, which seems solid, and a proposal for σ are formulated, both requiring further study. A Monte Carlo simulation program provided

a pathway for these intervals. The conjecture ensued the search of either a "surrogate" equal size or even a function of the unequal sizes. The initial attempt was to constrain the surrogate size, n^*, to the interval $n_{\min} \leq n^* \leq n_{\max}$, to include the equal size case. The (conservative) *minimum* size, however, yielded no agreement with simulations (nor the *maximum*). A new perspective was the use of the arithmetic mean of the sample sizes,

$$n^* = \left\lfloor \frac{1}{T} \sum_{t=1}^{T} n_t \right\rceil = \lfloor \bar{n} \rceil \,. \tag{4}$$

Indeed, the simulated result reproduced the conjectured theoretical curve, a Student's-t with $n^* - 1$ degrees of freedom. Thus, the experimental (simulated) curve can be replaced by that Student's distribution, the influence from the nearest integer approximation being negligible.

As regards the confidence interval for σ, while simulation led to no "rule", progress was obtained as an incomplete proposal needing further work. As in the conjecture, we obtained full agreement between the simulated and a simple, theoretical curve, shown in Figure 2, which was found to be a chi-square with $T - 1$ degrees of freedom, and a scale factor b such that

$$f(x) = b\, \chi^2_{T-1}(b\, x). \tag{5}$$

The results above are now clarified through direct computing. The solution to this problem are programs written by us (Fortran 90, "gnuplot"), and the computing is open on the Internet, using HTML *forms* to pass the arguments to the programs, needing no software from the user. The computing system was IST's *cluster* (6 nodes, x86_64, Xeon®, CPU@2.0GHz, Debian 2021).

For the point estimates, results are shown for unequal size samples (data in Table 1), leading, through Equations (2) and (3), to values (at Casquilho (2020) [1]) that "reproduce" the base parameter ($\mu = 25$, $\sigma = 0.2$): $\hat{\mu} = 24.97$ kg, and $\hat{\sigma} = 0.20$ kg.

For the confidence intervals, the methodology found was based on Monte Carlo simulation, in view of the starting lack of a theoretical method. This led to the plausible and solid conjecture mentioned, allowing for effective, public web pages for ready computing.

Some specific problems were solved: the problem in Table 1 and two industrial dimension ones, corresponding to $T = 25$ and $T = 50$, respectively Case4, Case25 and Case50 in Casquilho (2020) [1] web page. A level of 95% for the confidence intervals is used, as well as a fixed random number generator. For Case4, the results are, in a compact notation, in Equation (6). For Case25 and Case50 the results are, respectively, in Equation (7).

$$24.928 < (\hat{\mu} = 24.968) < 25.007 \quad 0.05 < (\hat{\sigma} = 0.20) < 0.35 \,. \tag{6}$$

$$\begin{aligned} &24.924 < (\hat{\mu} = 24.928) < 24.931 \quad 0.20 < (\hat{\sigma} = 0.28) < 0.35 \\ &24.922 < (\hat{\mu} = 24.925) < 24.928 \quad 0.25 < (\hat{\sigma} = 0.31) < 0.37 \,. \end{aligned} \tag{7}$$

The conjecture for the confidence intervals for μ, and the proposal for σ are illustrated in Figure 1, showing (Casquilho (2021) [2]) the simulated, "stitching" curve and the regular theoretical Student's-t, with $n^* - 1$ degrees of freedom. It is based on a simulation with 0.125×10^6 trials, a "short" simulation so that the two curves may be distinguished. The proposal for the confidence intervals for σ is illustrated in Figure 2 (conditions of Figure 1), showing the simulated curve and the regular theoretical chi-square, with $T - 1$ degrees of freedom and a certain value of the scale factor, b, from the same short simulation (above), so that the two curves may be distinguished. The unsolved issue is the determination of b, disclosed through the simulation procedure.

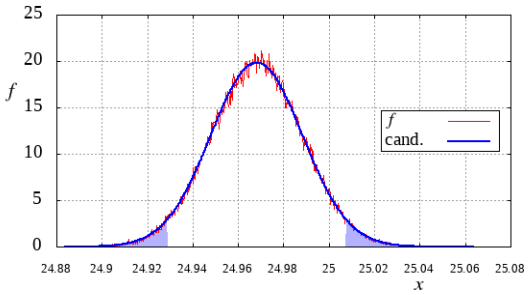

Figure 1: CI for μ: 'cand' the candidate curve, a Student's-t with $n^* - 1$ degrees of freedom.

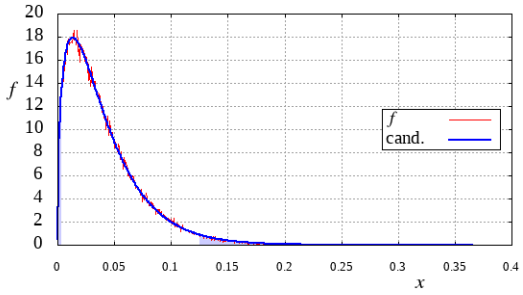

Figure 2: CI for σ: 'cand' the candidate curve, a chi-square with $T - 1$ degrees of freedom.

3 Conclusions and Future work

Starting from routinely recorded sums of unequal size samples, we provide methods to estimate μ and σ for the underlying Gaussian distribution. A non-specialist in Statistics, such as an engineer, can thus obtain those estimates and their confidence intervals. The point estimations for μ and σ are obtained from maximum likelihood. As to confidence intervals, a Monte Carlo procedure led to their determination and to a theoretical conjecture for μ and a proposal for σ. These methods solve the problem effectively.

Aiming to applicability, all the computing is available on our website, for these and other results, the Web being a computing tool we have since long suggested. Solutions and computational procedure are described there, permitting a practitioner to use them.

Acknowledgments

M. C. does research at CERENA, under FCT (Portuguese *Science and Technology Foundation*) Project UIDB/ECI/04028/2020. J. B. thanks CMAFCIO, FCT Project UID/MAT/04561/2020. CIIST, "Centro de Informática do IST" manages the computational system.

References

[1] M. Casquilho, Confidence intervals by simulation, `http://web.tecnico.ulisboa.pt/~mcasquilho/compute/qc/f-BagsSimulCI.php` (2020), accessed 10-Mar-2022.

[2] M. Casquilho, Estimates and confidence intervals for μ & σ, `http://web.tecnico.ulisboa.pt/~mcasquilho/compute/qc/f-BagsPECI.php` (2021), accessed 10-Mar-2022.

[3] B. M. Colosimo (Editor), Message from the Editor, *Journal of Quality Technology* **51:1** (2019), 1–2, or `http://web.tecnico.ulisboa.pt/~mcasquilho/compute/_quality/Colosimo2019.pdf`.

[4] D. W. Dunnett, Pairwise multiple comparisons in the homogeneous variance, unequal sample size case, *Journal of the American Statistical Association* **75** (1980) (372) 789–795.

[5] D. C. Montgomery, *Introduction to Statistical Quality Control*, 7.th ed. (2013), John Wiley & Sons., Inc., Hoboken, NY, USA.

[6] P. H. Ramsey and P. P. Ramsey, Power of pairwise comparisons in the equal variance and unequal sample size case, *British J. of Math. and Statistical Psy.* **61** (2008), 115–131.

[7] R. E. Walpole, R. H. Myers, S. L. Myers and K. Ye, *Probability & Statistics for Engineers & Scientists*, 9.th ed. (2012), Prentice-Hall, Boston, MA, USA.

[8] Mark D. Wilkinson et al., Comment: The FAIR Guiding Principles for scientific data management and stewardship, *Scientific Data* **3:160018** (2016).

International Conference on Mathematical Analysis and Applications in Science and Engineering
ICMA^{2}SC'22
ISEP Porto-Portugal, June 27 - 29, 2022

Efficient Algorithms for Joint Approximate Diagonalization of Multiple Matrices

Nela Bosner*

* Faculty of Science, Department of Mathematics, University of Zagreb, Croatia

*nela.bosner@math.hr

Abstract: Joint approximate diagonalization (JAD) of multiple matrices is a core problem in many applications, such as: blind source separation, parameter identification in exponential sum, canonical polyadic decomposition of a tensor used in chemometrics, telecommunications, psychometrics, data mining, machine learning, ... In this work we propose two numerical methods for computing JAD, based on constrained optimization on two different matrix manifolds, with emphasis on their numerical properties and efficiency. Following numerical analysis, we introduce modifications and parallel implementation of the proposed methods that increase their efficiency. Numerical experiments prove that these modifications speed-up execution time of the proposed methods by factor 3 – 4 per iteration, for large number of matrices.

keywords: joint approximate diagonalization; constrained optimization; conjugate gradient method; matrix manifolds.

MSC2020: 15A20; 58C05; 58C25; 47J25; 65J15; 65K10; 65Y05; 65Y20.

1 Introduction

Our goal is to efficiently solve the following problem: given a set of symmetric matrices $A^{(1)}$, $A^{(2)}$, ...,$A^{(m)} \in \mathbb{R}^{n\times n}$, find orthogonal or nonsingular $X \in \mathbb{R}^{n\times n}$ such that

$$A^{(p)} = X \cdot D^{(p)} \cdot X^T, \quad \text{for all } p = 1, \ldots, m,$$

where $D^{(p)}$ are either diagonal (exact diagonalization), or as diagonal as possible according to some criterion (approximate diagonalization) in case of noisy input data. The problem is divided into two variants:

(a) the solution X has to be orthogonal, and the problem is equivalent to finding spectral decompositions of the input matrices,

(b) X is only nonsingular, which is a more complex problem.

In practice, there are several approaches to solving this problem: Jacobi type methods, spectral decomposition of a random linear combination of matrices $A^{(p)}$, minimization of appropriate chosen function that measures diagonallity of $A^{(p)}$, and Riemannian optimization on appropriate chosen matrix manifold. Most of the methods converge slowly for large number of matrices m, and in some cases each iteration is numerically very expensive, or even require certain corrections

in order not to converge toward zero-matrix. Hence, we were focused on approach which needs no corrections, and which offers opportunity for efficient parallel implementation, especially for larger dimension n and large number of matrices m. This approach is based on Riemannian optimization by conjugate gradient method on

(a) Stiefel manifold (orthogonal group), when diagonalizing matrix X needs to be orthogonal,

(b) oblique manifold, otherwise,

since such optimization algorithms are adapted to utilize manifold geometry, and they guaranty that all intermediate result stay on the manifold. The conjugate gradient optimization method requires solution of 1-dimensional optimization problem in each iteration, has superlinear convergence, and is very simple for implementation and suitable for parallelization. This method has "cheaper" iterations than the other optimization methods commonly used in practice, such as Newton's method and trust region method, and until now it was not considered for optimization on the oblique manifold. The objective function on both manifolds is

$$F(X) = \frac{1}{2}\sum_{p=1}^{m} \|\mathrm{Off}(X^T A^{(p)} X)\|_F^2,$$

where for $B = [b_{ij}]$, $\mathrm{Off}(B) = B - \mathrm{Diag}(B)$, and $\mathrm{Diag}(B) = \mathrm{diag}(b_{11}, \ldots, b_{mm})$. Diagonalization or approximate diagonalization is represented by the minimization problem

$$\min_{X \in \mathcal{M}} F(X), \qquad \text{where } \mathcal{M} \text{ is appropriate manifold.}$$

2 Results and discussion

The Riemannian conjugate gradient optimization method requires concepts of tangent vector fields on the manifold, Riemannian metric, geodesic, parallel translation, gradient and Hessian on the manifold. These concepts are numerically quite simple for Stiefel and oblique manifolds. The first-order and second-order partial derivations of $F(X)$ are also easily obtained. The method requires the following terms, presented here for our objective function

$$F_X(X) = \left[\frac{\partial F}{\partial x_{rs}}(X)\right] = 2\sum_{p=1}^{m} A^{(p)} X \cdot \mathrm{Off}(X^T A^{(p)} X),$$

$$F_{XX}(X)(\Xi_1, \Xi_2) = \sum_{r,s=1}^{n}\sum_{u,v=1}^{n} \frac{\partial^2 F}{\partial x_{uv}\partial x_{rs}}(X)\xi_{rs}^{(1)}\xi_{uv}^{(2)} =$$

$$= 2\sum_{p=1}^{m}\left[\mathrm{tr}(\Xi_1^T A^{(p)}\Xi_2 \cdot \mathrm{Off}(X^T A^{(p)} X)) + \mathrm{tr}(X^T A^{(p)}\Xi_1 \cdot \mathrm{Off}(X^T A^{(p)}\Xi_2)) + \mathrm{tr}(\Xi_1^T A^{(p)} X \cdot \mathrm{Off}(X^T A^{(p)}\Xi_2))\right],$$

where Ξ_1 and Ξ_2 are tangent vectors. In the both expressions, terms involving multiplications with different matrices $A^{(p)}$ can be computed in parallel, which we exploited in our efficient implementation of the method. Moreover, since the products $A^{(p)}X$ and $B^{(p)} = X^T A^{(p)} X$ are used several times, they are computed once and stored. Besides that, we also optimize computation of the terms $\mathrm{tr}(A \cdot B)$ or $\mathrm{tr}(A^T \cdot B)$, where only diagonal element of the products are computed in parallel.

The 1-dimensional optimization problem solved in each iteration of conjugate gradient, concerns minimization of the objective function F on a geodesic $\Gamma(t)$, by solving equation $\frac{d}{dt}F(\Gamma(t)) = 0$.

(a) On Stiefel manifold, whose points are defined as elements of the set $\mathcal{S}_{n,n} = \{X \in \mathbb{R}^{n\times n} : X^T X = I\}$, geodesic $\Gamma(t)$ determined by $\Gamma(0) = X$, $\dot{\Gamma}(0) = \Xi$, and $\Theta = X^T\Xi$ is given by formula

$$\Gamma(t) = Xe^{\Theta t} \quad \text{and} \quad \frac{d}{dt}F(\Gamma(t)) = 2\sum_{p=1}^{m} \mathrm{tr}(\mathrm{Off}(C^{(p)})C^{(p)}\Theta), \text{ where } C^{(p)} = (e^{\Theta t})^T B^{(p)} e^{\Theta t}.$$

Computation of exponential function $e^{\Theta t}$ is implemented by "scaling and squaring" method, which is also suitable for parallelization, and it is optimized for evaluation with different parameter t.

(b) On oblique manifold, whose points are defined as elements of the set $\mathcal{O}_{n,n} = \{X \in \mathbb{R}^{n\times n} : \mathrm{Diag}(X^T X) = I\}$, geodesic $\Gamma(t)$ determined by $\Gamma(0) = X$, $\dot{\Gamma}(0) = \Xi = [\Xi_1, \ldots, \Xi_n]$, and $\Lambda_0 = \mathrm{diag}(\|\Xi_1\|_2, \ldots, \|\Xi_n\|_2)$ is given by formula

$$\Gamma(t) = X\cos(\Lambda_0 t) + \Xi\Lambda_0^{-1}\sin(\Lambda_0 t).$$

We showed that $\frac{d}{dt}F(\Gamma(t))$ can be transformed into the sum of 14 terms, where each of them is equal to trace of a certain diagonal matrix. All these terms are computed in parallel very efficiently.

Equation $\frac{d}{dt}F(\Gamma(t)) = 0$ for both variants is solved by bisection method, since we have explicit formulae for $\frac{d}{dt}F(\Gamma(t))$.

3 Conclusions and Future work

In our work, we proposed optimization algorithms for solving two variants of JAD problem, based on conjugate gradient method. Besides that, we developed efficient parallel implementations of the both variants. It should be mentioned, that orthogonal joint diagonalization is most easily solved by spectral decomposition of a random linear combination of matrices $A^{(p)}$, but in presence of noise this might not be the optimal solution. Our method on Stiefel manifold is best applied after spectral decomposition of a random linear combination, where it will give a better solution in a few iterations. Even in case when this spectral decomposition produce a solution which does not diagonalize all matrices $A^{(p)}$, our approach will complete the task. Numerical experiments confirmed that our modified implementations of the conjugate gradient method on two matrix manifolds are more efficient than the original versions. The modified algorithm on Stiefel manifold is 2-2.5 faster per iteration than the original version for dimensions $n = 1000, 2000$, and even 4 times faster for $n = 100$ and large number of matrices m (up to 1000). The speed-up factor per iteration for the modified algorithm on oblique manifold is between 2.6 and 3.3 for dimensions $n = 1000, 2000$, and between 1.2 and 2.1 for $n = 100$ and large number of matrices m. In future, we plan to consider different matrix manifolds and different objective functions with good numerical properties.

Acknowledgments

The author wants to thank Daniel Kressner for inspiration.

References

[1] P.-A. Absil, C. G. Baker, K. A. Gallivan, Trust-Region Methods on Riemannian Manifolds, Foundations of Computational Mathematics **7** (2007), 303–330.

[2] P. -. Absil and K. A. Gallivan, Joint Diagonalization on the Oblique Manifold for Independent Component Analysis, 2006 IEEE International Conference on Acoustics Speech and Signal Processing Proceedings, 2006, doi: 10.1109/ICASSP.2006.1661433.

[3] P.-A. Absil, R. Mahony, and R. Sepulchre, *Optimization Algorithms on Matrix Manifolds*. Princeton: Princeton University Press, 2008.

[4] A. Edelman, T. A. Arias, and S. T. Smith, The geometry of algorithms with orthogonality constraints, SIAM J. Matrix Anal. Appl. **20** (1998), 303–353.

[5] N. J. Higham, *Functions of matrices : theory and computation* , Philadelphia: SIAM, 2008.

International Conference on Mathematical Analysis and Applications in Science and Engineering
ICMA^{2}SC'22
ISEP Porto-Portugal, June 27 - 29, 2022

Numerical Treatments for Some Stochastic-Deterministic Chaotic Systems

N. H. Sweilam[1⋆] **S. M. AL−Mekhlafi**[2,3] **N. R. Alsenaideh**[4]

[1] Mathematics Department, Faculty of Science, Cairo University, Giza, Egypt
[2] Mathematics Department, Faculty of Education, Sana'a University, Yemen
[3]Department of Engineering Mathematics and Physics, Future University in Egypt
[4]Mathematics Department, Faculty of Science, Ain Shams University, Cairo, Egypt

[1⋆]nsweilam@sci.cu.edu.eg, [2,3]smdk100@gmail.com, [4]Wrd000000@hotmail.com

Abstract: Many real-life problems have processes that exhibit crossover behavior. Modeling processes based on crossover behaviors has proven to be a difficult task for mankind. In various instances, real-world difficulties have been observed as a result of the transition from Markovian to randomness processes, such as in epidemiology with the spread of infectious illnesses and even some chaos. To build the future state of the system and unpredictability, deterministic and stochastic approaches were developed independently. We aim at modeling behaviors of real-world exhibiting cross-over from deterministic to stochastic or vice versa. An example of new piecewise modeling is presented with illustrations of hybrid fractional derivatives chaos problems. Some important analyses including a piecewise existence and uniqueness are presented. We constructed new methods for solving these models. Numerical simulations are performed for different cases.

keywords: Stochastic-deterministic models, Piecewise numerical method; Hybrid fractional chaotic systems, Grünwald-Letnikov nonstandard finite difference method; Nonstandard Milstein method.

MSC2020: 26A33; 34C28; 60H10.

1 Introduction

1.1 Stochastic-Deterministic Models

- **The hyperchaotic finance model; Case 3:** We consider the piecewise hyperchaotic finance model [4], where the stochastic hyperchaotic finance model is defined in the first time region $(0, t_1]$ and the hybrid fractional order hyperchaotic finance model is defined in the second time region $(t_1, T]$:

$$\begin{cases} dX = & (Z + (Y - a)X + W)dt + \sigma_1 X dB_1(t), \\ dY = & (1 - bY - X^2)dt + \sigma_2 Y dB_2(t), \\ dZ = & (-X - cZ)dt + \sigma_3 Z dB_3(t), \qquad 0 < t \le t_1, \\ dW = & (-0.05XZ - \varrho W)dt + \sigma_4 W dB_4(t), \\ & W(0) = W_0, Z(0) = Z_0, Y(0) = Y_0, X(0) = X_0. \end{cases} \tag{1}$$

$$\begin{cases} {}_0^{CPC}D_t^{\alpha_1}X = & Z + (Y-a)X + W, \\ {}_0^{CPC}D_t^{\alpha_2}Y = & 1 - bY - X^2, \\ {}_0^{CPC}D_t^{\alpha_3}Z = & -X - cZ, \qquad t_1 < t \le T, \\ {}_0^{CPC}D_t^{\alpha_4}W = & -0.05XZ - \varrho W, \\ & W(t_1) = W_1, Z(t_1) = Z_1, Y(t_1) = Y_1, X(t_1) = X_1. \end{cases} \tag{2}$$

- **Bloch model with time delay; Case 3:** We consider the piecewise Bloch model with time delay [3], where the stochastic Bloch model is defined in the first time region $(0, t_1]$ and the hybrid fractional order Bloch model is defined in the second time region $(t_1, T]$:

$$\begin{cases} dX = & (\delta Y + aZ(t-\tau_c)\Big(Xsin(\Theta) - Ycos(\Theta)\Big) - bX)dt + \sigma_1 X dB_1(t), \\ dY = & (-\delta X - Z + aZ(t-\tau_c)\Big(Ysin(\Theta) + Xcos(\Theta)\Big) - bY)dt + \sigma_2 Y dB_2(t), \\ & 0 < t \le t_1, \\ dZ = & (Y - asin(\Theta)\Big(X^2 + Y^2\Big) - c\Big(Z-1\Big))dt + \sigma_3 Z dB_3(t), \\ & X(0) = X_0, Y(0) = Y_0, Z(0) = Z_0. \end{cases} \tag{3}$$

$$\begin{cases} {}_0^{CPC}D_t^{\alpha_1}X = & \delta Y + aZ(t-\tau_c)\Big(Xsin(\Theta) - Ycos(\Theta)\Big) - bX, \\ {}_0^{CPC}D_t^{\alpha_2}Y = & -\delta X - Z + aZ(t-\tau_c)\Big(Ysin(\Theta) + Xcos(\Theta)\Big) - bY, \\ & t_1 < t \le T, \\ {}_0^{CPC}D_t^{\alpha_3}Z = & Y - asin(\Theta)\Big(X^2 + Y^2\Big) - c\Big(Z-1\Big), \\ & Z(t_1) = Z_1, Y(t_1) = Y_1, X(t_1) = X_1. \end{cases} \tag{4}$$

2 Results and discussion

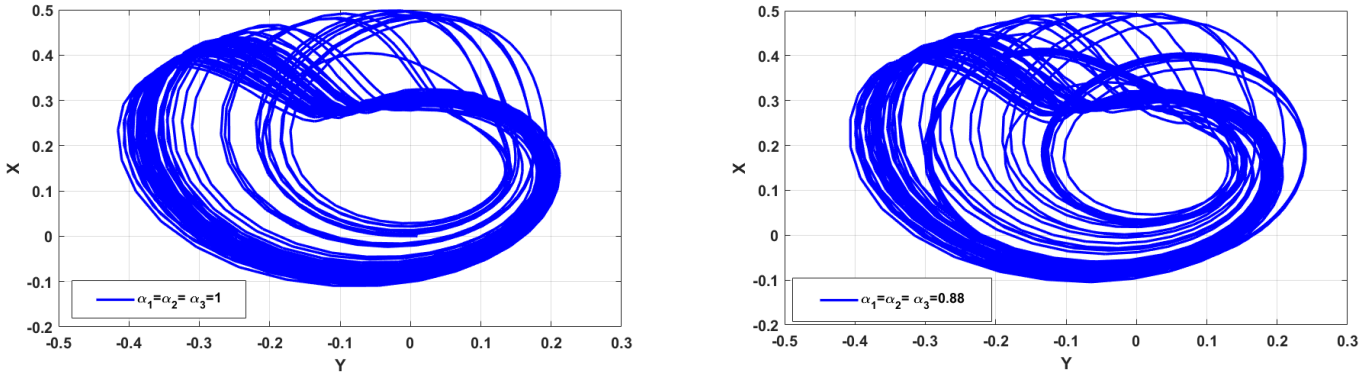

Figure 1: Numerical simulation for piecewise system (?? and ??), at $\sigma_1 = 0.03, \sigma_2 = 0.01, \sigma_3 = 0.005$, $t_1 = 1000$, $\tau_c = 0.001$.

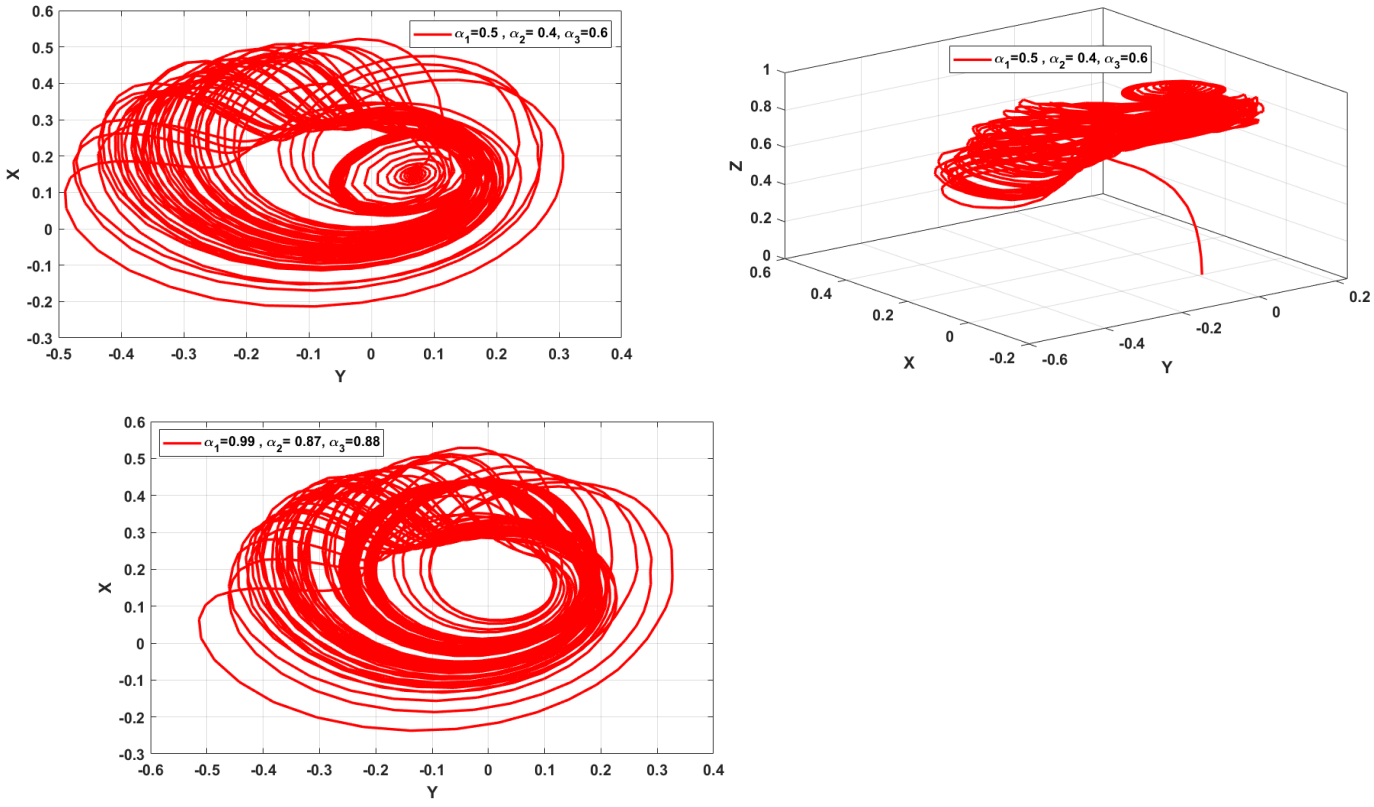

Figure 2: Numerical simulation for piecewise system (3 and 4), at different α and $\sigma_1 = 0.03, \sigma_2 = 0.01, \sigma_3 = 0.05$, $t_1 = 1000$, $\tau_c = 0.001$.

3 Conclusions and Future work

In this article, classes of nonlinear ordinary differential equations based on the concept of piecewise differentiation are given. Two chaotic models are considered; these models are the financial model and the Bloch model with time delay. The existence and uniqueness of the solutions for the proposed piecewise models are given. Numerical studies for the proposed piecewise models using CPC-GLNFDM are presented. The stability of the proposed method is studied. Numerical simulations for the proposed models explained the emergence of new behaviors. Simulated examples are presented alongside illustrative examples. The acquired results lead us to believe that this new approach is the way to model complicated real-world problems in the future.

Acknowledgments

We extend our sincere thanks and appreciation to the preparatory committee for the conference for giving us the opportunity to participate.

References

[1] I. Podlubny, Fractional differential equations, Academic Press, San Diego, Calif, USA, 198, (1999).

[2] A. Atangana, D. Baleanu, New fractional derivatives with non-local and non-singular kernel: theory and application to heat transfer model. Therm Sci, 20(2), 763-9, (2016).

[3] D. Baleanu, R. Magin, S. Bhalekar, and V. Daftardar-Gejji, Chaos in the fractional order nonlinear Bloch equation with Delay, Commun. *Chaos in Nonlinear Sci. Numer. Simul.*, 25(1-3) (2015) 41-49.

[4] A. Jajarmi, M. Hajipour, and D. Baleanu, New aspects of the adaptive synchronization and Hyperchaos suppression of a financial model, *Chaos, Solitons Fractals*, 99, (2017) 285?296.

[5] N. H. Sweilam , M. M. Abou Hasan, D. Baleanu, New studies for general fractional financial models of awareness and trial advertising decisions, *Chaos, Solitons and Fractals,* 104(2017), 772-784.

International Conference on Mathematical Analysis and Applications in Science and Engineering
ICMA^{2}SC'22
ISEP Porto-Portugal, June 27 - 29, 2022

Some 2-orthogonal polynomial eigenfunctions of differential operators

Teresa A. Mesquita[1⋆]

[1] Escola Superior de Tecnologia e Gestão, Instituto Politécnico de Viana do Castelo, Portugal, & Centro de Matemática da Universidade do Porto, Portugal

[1⋆] taugusta.mesquita@gmail.com

Abstract: The use of a general differential operator on the vectorial space of polynomial functions that does not increase the degree of polynomials [5] and its properties allowed the development of algebraic techniques for finding the corresponding polynomial eigenfunctions. We present further results of a recent symbolic approach [6] regarding differential relations of third order and a specific type of multiple orthogonal polynomials, namely the 2-orthogonal polynomial sequences. These polynomial sequences are described by the corresponding four-term recurrence relation, and its classical character is analysed.

keywords: d-orthogonal polynomials; differential operators; polynomial eigenfunctions.

MSC2020: 42C05 ; 33C45 ; 68W30 ; 33-04 ; 34L10 .

1 Introduction

The classical orthogonal polynomials are characterised as the polynomial eigenfunctions of the differential equation established by Bochner [1], that can be written in the form [2]:

$$a_2(x)y'' + a_1(x)y' + a_0(x)y + \lambda y = 0\,,$$

where $a_2(x)$, $a_1(x)$ $a_0(x)$ are polynomials of degrees at most 2,1, and 0, respectively, and $\lambda \neq 0$.

This second order differential relation can be rewritten in terms of the following differential operator [3, 5], defined on the vector space of polynomials with coefficients in $\mathbb{C}$, denoted by $\mathcal{P}$, where D is the standard derivative operator:

$$J = \sum_{n\geq 0} \frac{a_n(x)}{n!} D^n, \quad \deg a_n \leq n, \quad n \geq 0\,, \tag{1}$$

where

$$a_\nu(x) = \sum_{i=0}^{\nu} a_i^{[\nu]} x^i = a_0^{[\nu]} + a_1^{[\nu]} x + a_2^{[\nu]} x^2 + \cdots + a_\nu^{[\nu]} x^n\,.$$

With respect to the d-orthogonal polynomial sets, it is not yet established an analogous characterisation, though they are known to fulfil a recurrence relation of order $d+1$ [4]. In particular, for the case of 2-orthogonal polynomial sets, each sequence is uniquely defined by the three

numerical sequences $\{\beta_n\}_{n\geq 0}$, $\{\alpha_{n+1}\}_{n\geq 0}$ and $\{\gamma_{n+1}\}_{n\geq 0}$, called the recurrence coefficients, so that:

$$P_{n+3}(x) = (x-\beta_{n+2})P_{n+2}(x) - \alpha_{n+2}P_{n+1}(x) - \gamma_{n+1}P_n(x), \tag{2}$$
$$P_0(x) = 1,\ P_1(x) = x-\beta_0,\ P_2(x) = (x-\beta_1)P_1(x) - \alpha_1\,,\ \gamma_{n+1}\neq 0\,,\ n\geq 0. \tag{3}$$

Some families of d-orthogonal polynomials $\{P_n(x)\}_{n\geq 0}$ fulfil differential identities, in most cases with differential operators defined by coefficients depending on n. The operator J defined above has polynomial coefficients not depending on n, and also permits the definition of further operators $J^{(m)}$, as we see in (4), for any positive integer m, that often are raising operators.

Proposition 1 *[6] Given an operator J defined by* (1)*, and taking into account the definition of the operator $J^{(m)}$, $m\geq 0$:*

$$J^{(m)} = \sum_{n\geq 0} \frac{a_{n+m}(x)}{n!} D^n\,, \tag{4}$$

the following identities hold.

$$J^{(i)}\left(xp(x)\right) = J^{(i+1)}\left(p(x)\right) + xJ^{(i)}\left(p(x)\right)\,,\ i=0,1,2,\ldots. \tag{5}$$

Considering the problem of finding 2-orthogonal polynomial sets that fulfil the following differential identity

$$\left(a_0(x)I + a_1(x)D + \frac{a_2(x)}{2}D^2 + \frac{a_3(x)}{3!}D^3\right)\left(P_n(x)\right) = \lambda_n^{[0]}P_n(x)\,,\quad \lambda_n^{[0]}\neq 0\,, \tag{6}$$
$$\text{with}\ \ \lambda_n^{[0]} = a_0^{[0]} + \binom{n}{1}a_1^{[1]} + \binom{n}{2}a_2^{[2]} + \binom{n}{3}a_3^{[3]}\,,\ n\geq 0\,,$$

a symbolic approach based on the use of the content of Proposition 1, concluded that such polynomial sets $\{P_n\}_{n\geq 0}$ must fulfil an algebraic identity of the form $J^{(3)}\left(P_{n+2}(x)\right) = \sum_{i=n-4}^{n+5} \upsilon_{i,n}P_i(x)$. For given specific polynomial coefficients $a_\nu(x)$, $\nu = 0,1,2,3$, so that $\lambda_n^{[0]}\neq 0$, this latest identity yields a set of difference equations through which we find the recurrence coefficients of $\{P_n\}_{n\geq 0}$.

As an example of application of this method, we recall next a 2-orthogonal polynomial set constituted by polynomial eigenfunctions of the operator J defined below in (7).

Corollary 2 *[6] The 2-orthogonal polynomial sequence $\{P_n\}_{n\geq 0}$ fulfilling*

$$J\left(P_n(x)\right) = \lambda_n^{[0]}P_n(x)\,,\ n\geq 0\,,$$

where

$$J = a_0^{[0]}I + \frac{1}{24}xD + \frac{(x-1)^2}{3!}D^3\,, \tag{7}$$

is defined by the following recurrence coefficients

$$\beta_n = -12(n-1)n\,,\ n\geq 0\,, \tag{8}$$
$$\alpha_n = 12(n-1)n(2n-3)^2\,,\ n\geq 1\,, \tag{9}$$
$$\gamma_n = -4n(n+1)(2n-3)^2(2n-1)^2\,,\ n\geq 1. \tag{10}$$

2 Results and discussion

The method outlined in [6] has been applied into other third order differential operators. In some cases it has provided a negative response by assuring the nonexistence of such polynomial eigenfunctions, and in other cases it has given the full description of the solution, as we can illustrate with the next new result.

Proposition 3 *The 2-orthogonal polynomial sequence* $\{P_n\}_{n\geq 0}$ *fulfilling*

$$J\left(P_n(x)\right) = \lambda_n^{[0]} P_n(x)\,,\ n \geq 0\,,$$

where

$$J = a_0^{[0]} I + \frac{1}{24} xD + (x-1)D^2 + \frac{(x-1)^2}{3!} D^3\,, \tag{11}$$

is defined by the following recurrence coefficients

$$\beta_n = -12n(n+3)\,,\ n \geq 0\,, \tag{12}$$

$$\alpha_n = 12n(n+1)\left(4n(n+3)-15\right)\,,\ n \geq 1\,, \tag{13}$$

$$\gamma_n = -4n(n+1)\left(4n(n+3)-15\right)\left(4n(n+5)+1\right)\,,\ n \geq 1. \tag{14}$$

The previous result can be enlarged when we introduce parameters on the polynomial coefficients $a_1(x)$ and $a_2(x)$ of the operator J. Nevertheless, we must take into account the 2-orthogonal regularity conditions: $\gamma_n \neq 0$, for all positive integer n. In a similar way to the sequence of Corollary 2, the 2-orthogonal sequence described above fulfils Hahn's property and thus is Hahn classical.

3 Conclusions and Future work

The work developed so far facilitates the search for 2-orthogonal polynomial eigenfunctions of given differential operators defined by their polynomial coefficients $a_\nu(x)$. A new family has been described, though much more pairs of operators and polynomial sequences remain to catalogue in the study of 2-orthogonal polynomial solutions of differential identities.

Acknowledgments

The author T. A. Mesquita was partially supported by CMUP, which is financed by national funds through FCT-Fundação para a Ciência e a Tecnologia, I.P., under the project with reference UIDB/00144/2020.

References

[1] S. Bochner, *Über Sturm-Liouvillesche Polynomsysteme*, Math. Zeit. vol. 29 (1929), pp. 730-736.

[2] T. S. Chihara, *An Introduction to Orthogonal Polynomials*, Gordon and Breach, New York, 1978.

[3] P. Maroni, New results about orthogonality preserving maps, J. Korean Math. Soc. 42, No.2 (2005), 243-254.

[4] P. Maroni, *L'orthogonalité et les récurrences de polynômes d'ordre supérieur à deux* , Ann. Fac. Sci. Toulouse, Math. (5) 10, No. 1 (1989), 105-139.

[5] T. A. Mesquita and P. Maroni , *Around operators not increasing the degree of polynomials*, Integral Transforms Spec. Funct. 30, No.5 (2019), 383-399.

[6] T. A. Mesquita, *Symbolic Approach to 2-Orthogonal Polynomial Solutions of a Third Order Differential Equation*, Math.Comput.Sci.
DOI : 10.1007s11786-022-00525-8

International Conference on Mathematical Analysis and Applications in Science and Engineering
ICMA^{2}SC'22
ISEP Porto-Portugal, June 27 - 29, 2022

Poisson stability in Duffing equations

Akylbek Zhamanshin[1,2⋆] **Marat Akhmet**[1] **Madina Tleubergenova**[2]

[1] Middle East Technical University, Ankara, Turkey
[2] Aktobe Regional University, Aktobe, Kazakhstan

⋆akylbek78@mail.ru

Abstract: The standard Duffing equation is a second order differential equation with constant coefficients. When considering the original model with variable coefficients, wide application possibilities open up. The research considers Duffing equations with two-component Poisson stable coefficients and perturbations. The Poisson stable inputs and outputs of our research are functions, which are not only non-periodic, but are rather chaotic. The existence and uniqueness of the Poisson stable solutions have been proved. Numerical simulations of the solutions are provided.

keywords: Duffing equation; Poisson stable solution; asymptotic stability; numerical simulations.

MSC2020: 34A20; 34G05; 93D05.

1 Introduction

Classical Duffing equation is the second order differential equation with constant coefficients [1]. Considering the original model one can assume mechanical reasons for variable coefficients. For instance, not constant damping and driving force [2]. The second order differential equations, despite their small dimension produce strong difficulties for study [3], and are source for most modern complexity investigations. This is why, comprehensive modifications of the Duffing equation with subsequent new methods of investigation have to be in the focus of researchers.

In the present paper, we propose the model with Poisson stable coefficients and find conditions on the functions, such that the result-dynamics is Poisson stable. This version of the Duffing equation has not been considered in literature, at all. Another principal novelty of our research is *the method of included intervals* [4], which has been adapted for Poisson stable solutions in differential equations [5, 6].

The main subject of this article is the following equation,

$$x'' + p(t)x' + q(t)x + r(t)x^3 = F(t)\cos(\lambda t), \tag{1}$$

where $t, x \in \mathbb{R}$; λ is a real constant; $p(t)$, $q(t)$, $r(t)$ and $F(t)$ are continuous functions.

The next concept of recurrence is a fundamental for the present investigation.

Definition 1 *[7] A continuous and bounded function $\psi(t) : \mathbb{R} \to \mathbb{R}^n$ is called Poisson stable, if there exists a sequence t_k, which diverges to infinity such that the sequence $\psi(t + t_k)$ converges to $\psi(t)$ as $k \to \infty$ uniformly on bounded intervals of $\mathbb{R}$.*

The sequence t_k is said to be *the Poisson sequence* of the function $\psi(t)$. For fixed real constant $\omega > 0$, one can write that $t_k \equiv \tau_k(mod\ \omega)$, where $0 \leq \tau_k < \omega$, for all $k \geq 1$. The boundedness of the sequence τ_k implies that there exists a subsequence τ_{k_l}, which converges to a number τ_ω. That is, there exist a subsequence t_{k_l} of the Poisson sequence t_k and a number τ_ω such that $t_{k_l} \to \tau_\omega(mod\ \omega)$ as $l \to \infty$. In what follows, we shall call the number τ_ω as the *Poisson shift* for the Poisson sequence t_k with respect to the ω. It is not difficult to find that for the fixed positive ω the set of all Poisson shifts, T_ω, is not empty, and it can consist of several or even infinite number elements. The number $\kappa_\omega = inf\ T_\omega$, $0 \leq \kappa_\omega < \omega$, is said to be *the Poisson number* for the Poisson sequence t_k with respect to the number ω.

2 Results

This section presents the main result of our study. Let us denote $\omega = \frac{2\pi}{\lambda}$, and assume that the following conditions are satisfied.

(C1) The function $F(t)$ is Poisson stable. The coefficients are of two components such that $p(t) = p_0 + p_1(t)$, $q(t) = q_0 + q_1(t)$ and $r(t) = r_0 + r_1(t)$, where p_0, q_0 and r_0 are real constants, $p_1(t)$, $q_1(t)$, and $r_1(t)$ are Poisson stable functions;

(C2) there exists a Poisson sequence t_k common for functions $p_1(t)$, $q_1(t)$, $r_1(t)$, $F(t)$ and the Poisson number κ_ω is equal to zero;

(C3) $p_0 > 0, \quad p_0^2 - 4q_0 \leq 0.$

It can be easily shown that $p(t)$, $q(t)$, $r(t)$ and $F(t)$ are Poisson stable functions with the common Poisson sequence t_k. Condition (C3) implies that the eigenvalues of the matrix $A = \begin{pmatrix} 0 & 1 \\ -q_0 & -p_0 \end{pmatrix}$ have negative real parts and there exist numbers $K > 1$ and $\mu > 0$ such that $\|e^{At}\| \leq Ke^{-\mu t}$ for $t \geq 0$. We consider the equation (1) provided that a solution $x(t)$ and its derivative $x'(t)$ are bounded such that $\sup_{t\in\mathbb{R}} \mid x(t) \mid < H$, $\sup_{t\in\mathbb{R}} \mid x'(t) \mid < H$, where H is a fixed positive number. Let us introduce some notations

$$\sup_{t\in\mathbb{R}} \mid p_1(t) \mid = \alpha, \sup_{t\in\mathbb{R}} \mid q_1(t) \mid = \beta, \sup_{t\in\mathbb{R}} \mid r_0 + r_1(t) \mid = \gamma, \sup_{t\in\mathbb{R}} \mid F(t) \mid = \delta.$$

Throughout the paper, the following additional conditions are required.

(C4) $\frac{K}{\mu}(H(\alpha + \beta) + \gamma H^3 + \delta) < H;$

(C5) $\frac{K}{\mu}(\alpha + \beta + 3\gamma H^2) < 1.$

By using the method of included intervals, we have proved the next theorem.

Theorem 1 *The Duffing equation (1) admits a unique asymptotically stable Poisson stable solution provided that conditions (C1)-(C5) are satisfied.*

Example. Consider the following Duffing equation

$$x''(t) + (p_0 + p_1(t))x'(t) + (q_0 + q_1(t))x(t) + (r_0 + r_1(t))x^3(t) = F(t)\cos(2t), \qquad (2)$$

where the constants $p_0 = 5, q_0 = 3, r_0 = 0.002$. The functions $p_1(t) = -0.5\Theta(t)$, $q_1(t) = -\Theta^3(t)$, $r_1(t) = -0.4\Theta^2(t)$ and $F(t) = 1.5\Theta(t)$ are Poisson stable [6]. Conditions (C1)-(C5) are hold with $K = 2$, $\mu = 2.5$, $\lambda = 1$ (the period $\omega = \pi$), $H = 2$, $\alpha = 0.2$, $\beta = 0.064$, $\gamma = 0.064$ and $\delta = 0.6$. Since the elements of the Poisson sequence are multiples of 3π and the period is equal to π, the Poisson number is equal to zero. The trajectory of the Poisson stable solution is shown in Figure 1.

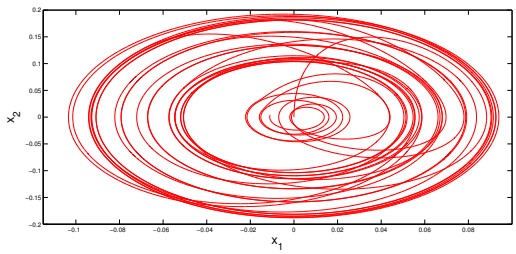

Figure 1: The trajectory of the Poisson stable solution, $x(t)$, of the equation (2).

Acknowledgments

A. Zhamanshin and M. Akhmet have been supported by 2247-A National Leading Researchers Program of TUBITAK, Turkey, N 120C138. M. Tleubergenova has been supported by the Science Committee of the Ministry of Education and Science of the Republic of Kazakhstan (grant No. AP09258737 and No. AP08856170).

References

[1] Duffing, G., *Erzwungene Schwingungen bei Veränderlicher Eigenfrequenz und ihre Technische Bedeutung (Forced oscillators with variable eigenfrequency and their technical meaning)* (in German), F. Vieweg Sohn, (1918), 41-42

[2] Estévez, P. G., Kuru, Ş., Negro, J., Nieto, L.M., *Solutions of a Class of Duffing Oscillators with Variable Coefficients*, International Journal of Theoretical Physics, **50** (2011), 2046-2056

[3] Holmes, P., Whitley, D., *On the attracting set for Duffing's equation*, Physica D, 7 (1983) 111-123

[4] M. Akhmet, M. Tleubergenova, A. Zhamanshin, Quasilinear differential equations with strongly unpredictable solutions, Carpathian Journal of Mathematics, **36** (2020), 341-349

[5] M. Akhmet, Domain Structured Dynamics: unpredictability, chaos, randomness, fractals, differential equations and neural networks, IOP Publishing, 2021.

[6] M. Akhmet, M. Tleubergenova, A. Zhamanshin, Modulo periodic Poisson stable solutions of quasilinear differential equations, Entropy, **23**(11) (2021) 1535.

[7] Sell, G. R., *Topological dynamics and ordinary differential equations*, Van Nostrand Reinhold Company, London, 1971

International Conference on Mathematical Analysis and Applications in Science and Engineering
ICMA^{2}SC'22
ISEP Porto-Portugal, June 27 - 29, 2022

Cosine and sine functions on Time Scales

Aldo Pereira[1⋆] **Jaqueline G. Mesquita**[2] **Rodrigo Ponce**[3]

[1] Universidad de La Serena, Chile
[2] Universidade de Brasília, Brasil
[3] Universidad de Talca, Chile

[1⋆]aldo.pereira@userena.cl

Abstract: Cosine and sine families, defined on Banach spaces, are a useful tool in the study of many types of abstract evolution equations. In this talk, inspired by [2], we introduce a definition of cosine and sine functions on time scales [1] that encompasses the continuous and discrete cases, allowing to include as domain the sets of real and integer numbers. Also, we investigate the relationship between the abstract cosine function and its generator.

keywords: dynamic equation on time scales; cosine function; sine function; abstract Cauchy problem.

MSC2020: 47D06; 34G10; 34K30; 34N05

1 Introduction

We investigate the abstract second–order Cauchy problem

$$u^{\Delta\Delta}(t) = Au(t),\ t \in \mathbb{T}_0^+, \qquad u(0) = x, \qquad u^{\Delta}(0) = y, \tag{1}$$

where $x, y \in X$, and A is a closed linear operator in a Banach space X. This formulation satisfies all the properties for the operator solutions in the already known cases $\mathbb{T} = \mathbb{R}$ and $\mathbb{T} = \mathbb{Z}$. With this formulation, we proceed to develop a solution of the problem (1), defining the solution operators. The use of Laplace Transform will be necessary, to include the case $\mathbb{T} = \mathbb{R}$, and must to be valid for all types of time scales.

Definition 1 A classical solution of (1) is a function $u \in \mathcal{C}^2_{rd}(\mathbb{T}_0^+, X)$ such that $u(t) \in D(A)$ for every $t \in \mathbb{T}_0^+$ and satisfies the problem (1).

Definition 2 A mild solution of (1) is a function $u \in \mathcal{C}_{rd}(\mathbb{T}_0^+, X)$ which satisfies

$$\int_0^t \int_0^s u(r)\,\Delta r\,\Delta s = \int_0^t (t - \sigma(s))u(s)\,\Delta s \in D(A)$$

and for all $t \in \mathbb{T}_0^+$,

$$u(t) = x + ty + A\int_0^t (t - \sigma(s))u(s)\,\Delta s.$$

2 Results and discussion

The first result brings an important property of a mild solution of (1).

Theorem 1 *Let $u \in \mathbb{C}_{rd}(\mathbb{T}_0^+, X)$, $\omega \in D\{u\}$. Assume $\lambda \in \mathbb{C}$ is such that*

$$\lim_{t\to\infty} e_{\ominus\lambda}(t,0) = 0, \qquad \lim_{t\to\infty} u(t)e_{\ominus\lambda}(t,0) = 0, \qquad \lim_{t\to\infty} e_{\ominus\lambda}(t,0)\int_0^t u(s)\,\Delta s = 0, \tag{2}$$

and $Re_\mu(\lambda)(t) > Re_\mu(\omega)(t)$ for all $t \in \mathbb{T}_0^+$. Then, u is a mild solution of (1) if, and only if, $\widehat{u}(\lambda) \in D(A)$ and $\lambda x + y = (\lambda^2 - A)\widehat{u}(\lambda)$, for all λ which satisfies (2).

This property allows to define the operator solutions for the problem (1).

Definition 3 A strongly rd-continuous function $C : \mathbb{T}_0^+ \to \mathcal{L}(X)$ is called a *cosine function with generator A* if the following conditions are satisfied: $C(0) = I$ and there exists $\omega \in \mathbb{R}$ such that $(\omega, \infty)_{\mathbb{T}} \subset \rho(A)$, $\lambda^2 \in D\{C\}$, and for all $x \in X$,

$$\widehat{C}(\lambda)x = \int_0^\infty e^\sigma_{\ominus\lambda}(t,0)C(t)x\,\Delta t = \lambda(\lambda^2 - A)^{-1}x, \qquad Re_\mu(\lambda^2)(t) > \omega, t \in \mathbb{T}_0^+. \tag{3}$$

Definition 4 A strongly rd-continuous function $S : \mathbb{T}_0^+ \to \mathcal{L}(X)$ is called a *sine function with generator A* if the following conditions are satisfied: $C(0) = I$ and there exists $\omega \in \mathbb{R}$ such that $(\omega, \infty)_{\mathbb{T}} \subset \rho(A)$, $\lambda^2 \in D\{C\}$, and for all $x \in X$,

$$\widehat{S}(\lambda)x = \int_0^\infty e^\sigma_{\ominus\lambda}(t,0)S(t)x\,\Delta t = (\lambda^2 - A)^{-1}x, \qquad Re_\mu(\lambda^2)(t) > \omega, t \in \mathbb{T}_0^+. \tag{4}$$

Our definitions of abstract sine and cosine functions on time scales are directly related with the existence of mild solutions to problem (1).

Theorem 2 *Let $A \in L(X)$. Then, the problem (1) has a unique mild solution.*

This result allows us to write an explicit formula for the solution of our second order problem (1). Such equality, with the property for cosine function defined in formula (3), and the respective formula for sine function given in formula (4), yield

$$u(t) = C(t)x + S(t)y$$

as the unique solution of equation (1).

References

[1] M. Bohner, A. Peterson, Dynamic Equations on Time Scales: An Introduction with Applications, Birkhäuser, Boston, 2001.

[2] H.R. Henríquez, C. Lizama, J.G. Mesquita: Semigroups on time scales and applications to abstract Cauchy problems, Top. Meth. in Nonlinear Analysis **56** (2020), no. 1, 83–115.

International Conference on Mathematical Analysis and Applications in Science and Engineering
ICMA^{2}SC'22
ISEP Porto-Portugal, June 27 - 29, 2022

ON SOME RECENT RESULTS FROM THE THEORY THE MHD EQUATIONS

Jiří Neustupa[1⋆]

[1] Czech Academy of Sciences, Institute of Mathematics, Žitná 25, 115 67 Prague 1, Czech Republic

[1⋆]neustupa@math.cas.cz

Abstract: We explain some new regularity criteria for weak solutions to the MHD equations. The criteria impose a posteriori conditions on the negative part of an associated pressure or on the positive part of the so called Bernoulli pressure.

keywords: MHD equations; pressure; regularity.

MSC2020: 35B65; 35Q30; 35Q35; 76W05; 76D05.

1 Introduction

We deal with the system of the *magneto-hydro-dynamic equations* (shortly *MHD equations*)

$$\partial_t \mathbf{u} + \mathbf{u}\cdot\nabla\mathbf{u} - \mathbf{curl}\,\mathbf{b}\times\mathbf{b} \;=\; -\nabla p + \frac{1}{\mathcal{R}_f}\,\Delta\mathbf{u}, \tag{1}$$

$$\partial_t \mathbf{b} - \mathbf{curl}(\mathbf{u}\times\mathbf{b}) \;=\; \frac{1}{\mathcal{R}_m}\,\Delta\mathbf{b}, \tag{2}$$

$$\mathrm{div}\,\mathbf{u} \;=\; \mathrm{div}\,\mathbf{b} \;=\; 0 \tag{3}$$

in a domain $\Omega \subset \mathbb{R}^3$ in the time interval $(0,T)$ (where $0 < T \le \infty$). These equations describe the motion of a viscous incompressible electrically conductive fluid in the absence of an external specific body force and an external magnetic induction. The system (1)–(3) represents the equations in the so called dimensionless form. The unknowns are the velocity $\mathbf{u} \equiv (u_1, u_2, u_3)$ of the fluid, the magnetic field $\mathbf{b} \equiv (b_1, b_2, b_3)$ and the pressure p. The positive parameters $\mathcal{R}_f$ and $\mathcal{R}_m$ represent the *fluid Reynolds number* and the *magnetic Reynolds number.*

We consider the so called Navier–type boundary conditions

$$\text{a)}\quad \mathbf{u}\cdot\mathbf{n} = \mathbf{b}\cdot\mathbf{n} = 0, \qquad \text{b)}\quad \mathbf{curl}\,\mathbf{u}\times\mathbf{n} = \mathbf{curl}\,\mathbf{b}\times\mathbf{n} = \mathbf{0} \qquad \text{on } \partial\Omega\times(0,T) \tag{4}$$

for both the velocity $\mathbf{u}$ and the magnetic field $\mathbf{b}$ (where $\mathbf{n}$ denotes the outer normal vector field on $\partial\Omega$) and the initial conditions

$$\mathbf{u}\big|_{t=0} = \mathbf{u}_0, \qquad \mathbf{b}\big|_{t=0} = \mathbf{b}_0 \qquad \text{in } \Omega, \tag{5}$$

where both $\mathbf{u}_0$ and $\mathbf{b}_0$ are supposed to be divergence–free. (Naturally, the conditions (4) make sense if $\Omega \neq \mathbb{R}^3$.)

The equations (1) and (2) are often written in the modified form

$$\partial_t \mathbf{u} + \mathbf{u}\cdot\nabla\mathbf{u} - \mathbf{b}\cdot\nabla\mathbf{b} \;=\; -\nabla\big(p + \tfrac{1}{2}|\mathbf{b}|^2\big) + \frac{1}{\mathcal{R}_f}\,\Delta\mathbf{u}, \tag{1}$$

$$\partial_t \mathbf{b} + \mathbf{u}\cdot\nabla\mathbf{b} - \mathbf{b}\cdot\nabla\mathbf{u} \;=\; \frac{1}{\mathcal{R}_m}\,\Delta\mathbf{b}. \tag{2}$$

Note that if $\mathbf{b}_0 = \mathbf{0}$ then one can consider $\mathbf{b} = \mathbf{0}$ and the system (1)–(3) reduces just to the well known Navier–Stokes equations.

We assume that Ω is either the whole space $\mathbb{R}^3$ or a bounded domain in $\mathbb{R}^3$ with the boundary of the class $C^{2+(\iota)}$ for some $\iota > 0$.

By analogy with the theory of the Navier–Stokes equations, if $\mathbf{u}_0$ and $\mathbf{b}_0$ lie in the space $\mathbf{L}^2_\sigma(\Omega)$ (which is the closure of the linear space of all infinitely differentiable divergence–free vector functions in Ω, with a compact support in Ω, in $\mathbf{L}^2(\Omega)$) then the IBVP (1)–(5) has the so called suitable weak solution, which is a pair of functions $\mathbf{u}, \mathbf{b}$ in $L^\infty(0,T;\, \mathbf{L}^2_\sigma(\Omega)) \cap L^\infty(0,T;\, \mathbf{W}^{1,2}(\Omega))$, completed by an associated pressure $p \in L^{5/3}(Q_T)$, such that these functions satisfy in an appropriate sense the equations (1), (2), the boundary conditions (4), the initial conditions (5) and in addition to that, also the so called localized energy inequality. (See, e.g., [4], [5] for the definitions and further details.)

A space–time point $(\mathbf{x}, t) \in Q_T$ is said to be a *regular point* of the solution $(\mathbf{u}, \mathbf{b}, p)$ if there exists a neighborhood $U(\mathbf{x}, t) \subset Q_T$ of this point such that both $\mathbf{u}$ and $\mathbf{b}$ are essentially bounded in $U(\mathbf{x}, t)$. Other points in Q_T are called *singular points*.

It follows from [3] that $\mathbf{u}, \mathbf{b}$ are Hölder–continuous in some neighborhood of each regular point.

It is shown in [4] that if $\Omega = \mathbb{R}^3$ then p is essentially bounded in some space–time neighborhood of each regular point of $(\mathbf{u}, \mathbf{b}, p)$, and if Ω is a smooth bounded domain in $\mathbb{R}^3$ then ∇p is essentially bounded in some neighborhood of any regular point.

Using this fact and the information that the 1D Hausdorff measure of the set of singular points is zero (see [1]), one can show that p can be modified by an additive function $\zeta = \zeta(t) \in L^{5/3}(0,T)$, so that $p + \zeta$ is an associted pressure with a weak solution $(\mathbf{u}, \mathbf{b})$, too, and $p + \zeta$ is is essentially bounded in some space–time neighborhood of each regular point of the solution $(\mathbf{u}, \mathbf{b}, p + \zeta)$. Denote by $\mathscr{P}$ the class of associated pressures with the same property. We further assume that p has already been modified so that $p \in \mathscr{P}$.

Suppose that Φ is the so called Young function. It means that Φ can be expressed in the form $\Phi(s) = \int_0^s \varphi(\sigma)\ \mathrm{d}\sigma$ for $s \geq 0$, where φ has the following properties: $\varphi(0) = 0$, $\varphi(\sigma) > 0$ for $\sigma > 0$, φ is right-continuous and non-decreasing on $[0, \infty)$ and $\lim_{\sigma\to\infty}\ \varphi(\sigma) = \infty$. It follows directly from the definition that the Young function has a series of further properties, see e.g. [6, Lemma 4.2.2]. If D is a domain in $\mathbb{R}^3$ then the Orlicz space $L^\Phi(D)$ is the space of all measurable functions f on D with the finite norm defined by

$$\|f\|_{L^\Phi(D)} \;:=\; \inf\{\lambda > 0;\ \int_D \Phi\Big(\frac{|f(\mathbf{x})|}{\lambda}\Big)\ \mathrm{d}\mathbf{x} \leq 1\}. \tag{6}$$

Formula (6) represents the so called Luxemburg norm in $L^\Phi(D)$, see [6].

In this paper, we consider a Young function Φ that has these additional properties:

(i) $s^{-3/2}\,\Phi(s)$ is monotone increasing on $[0, \infty)$ and and tends to infinity as $s \to \infty$,

(ii) $\Phi(s)^{-2/3} \in L^1((1, \infty))$.

One can prove that the next theorem holds (see [5], [2]).

Theorem 1 *Suppose that*

α) Ω be either the whole space $\mathbb{R}^3$ or a bounded domain in $\mathbb{R}^3$ with the boundary of the class $C^{2+\alpha}$ for some $\alpha > 0$,

β) the Young function Φ satisfies the conditions (i) and (ii),

γ) $(\mathbf{u}, \mathbf{b}, p)$ is a suitable weak solution of the MHD equations (1)–(3) in $\Omega \times (0, T)$ with the Navier–type boundary conditions (5) (in the case $\Omega \neq \mathbb{R}^3$),

δ) Ω' is a sub-domain of Ω and $0 \leq T_1 < T_2 \leq T$.

Then the vector fields $\mathbf{u}$ and $\mathbf{b}$ are Hölder continuous in $\Omega' \times (T_1, T_2)$ if at least one of the following conditions holds;

1) $p_- \in L^\infty(T_1, T_2;\, L^\Phi(\Omega'))$,

2) $\mathcal{B}_+ \in L^\infty(T_1, T_2;\, L^\Phi(\Omega'))$, where $\mathcal{B} := p + \frac{1}{2}|\mathbf{u}|^2 + \frac{1}{2}|\mathbf{b}|^2$.

Here, p_- denotes negative part of p, $\mathcal{B} := p + \frac{1}{2}|\mathbf{u}|^2 + \frac{1}{2}|\mathbf{b}|^2$ and $\mathcal{B}_+$ denotes the positive part of $\mathcal{B}$.

Acknowledgments

The author has been supported by the Grant Agency of the Czech Republic, No. 22-08633J and the Academy of Sciences of the Czech Republic (RVO 67985840).

References

[1] H. J. Choe, M. Yang, Hausdorff measure of the singular set in the incompressible magnetohydrodynamic equations, Comm. Math. Phys. **336**(1) (2015), 171–198.

[2] H. J. Choe, J. Neustupa, M. Yang, Improved regularity criteria for the MHD equations in terms of pressure using an Orlicz norm, Applied Mathematical Letters, online https://doi.org/10.1016/j.aml.2022.108121.

[3] A. Mahalov, B. Nicolaenko, T. Shilkin, $L_{3,\infty}$ solutions to the MHD equations, J. of Math. Sci. **143**(2) (2007), 2911–2923.

[4] J. Neustupa, M. Yang: On the role of the pressure in the theory of MHD Equations, Nonlinear Analysis: Real World Appl. **60** (2021), Article No. 103283, 23 pp.

[5] J. Neustupa, M. Yang, New regularity criteria for weak solutions to the MHD equations in terms of an associated pressure, J. Math. Fluid Mech. **23** (2021), Article no. 73, 24 pp., online https://doi.org/10.1007/s00021-021-00597-9.

[6] L. Pick, A. Kufner, O. John, S. Fučík, *Function Spaces I. De Gruyter Series in Nonlinear Analysis and Applications 14*. De Gruyter, Berlin–Boston 2013.

International Conference on Mathematical Analysis and Applications in Science and Engineering
ICMA^{2}SC'22
ISEP Porto-Portugal, June 27 - 29, 2022

EXISTENCE RESULTS FOR NONLINEAR BOUNDARY VALUE PROBLEMS WITH A GENERALIZED LAPLACIAN

Mirosława Zima

University of Rzeszów, Poland

mzima@ur.edu.pl

Abstract: We discuss existence of solutions to differential equations of the form

$$(\varphi(u'))' = f(t, u, u'),$$

where f is continuous and φ is a homeomorphism, subject to nonlinear boundary conditions. Our methods of proofs are based on the extension of Mawhin's continuation theorem for quasi–linear operators.

keywords: nonlinear boundary conditions; homeomorphism; quasi–linear operators.

MSC2020: 34B15; 47N20; 34B10.

1 Introduction

We discuss existence results for the boundary value problem consisting of the differential equation

$$(\varphi(u'))' = f(t, u, u'), \tag{1}$$

where f is continuous and φ is a homeomorphism, and the nonlinear boundary conditions

$$g(u(0), G(u')) = 0, \quad h(u'(1), H(u)) = 0, \tag{2}$$

where g, h are continuous functions and G, H are continuous functionals. Our methods of proofs make use of the extension of Mawhin's continuation theorem for quasi–linear operators due to Ge and Ren [1]. The talk is based on a joint work with Katarzyna Szymańska–Dębowska.

2 Results and discussion

Our main existence result is the following theorem.

Theorem 1 *Let the following assumptions be satisfied:*

(A1) $f : [0, 1] \times \mathbb{R}^2 \to \mathbb{R}$ *is continuous;*

(A2) $\varphi : \mathbb{R} \to \mathbb{R}$ *is a homeomorphism such that* $\varphi(0) = 0$ *and* $\varphi(\pm\infty) = \pm\infty$*;*

(A3) $g, h : \mathbb{R}^2 \to \mathbb{R}$ *are continuous;*

(A4) $G, H : (C([0,1], \mathbb{R})) \to \mathbb{R}$ *are continuous functionals taking bounded sets into bounded sets;*

(A5) there exist M_1,$M_2 \in \mathbb{R}$, $M_1 \le 0 \le M_2$ *and* $\beta \in \{-1, 1\}$ *such that for all* $y \in \mathbb{R}$ *we have*

$$\beta\, h(M_1, y) \le 0, \quad \beta\, h(M_2, y) \ge 0;$$

(A6) there exist m_1, $m_2 \in \mathbb{R}$, $m_1 < m_2$ *and* $\alpha \in \{-1, 1\}$ *such that for all* $y \in \mathbb{R}$ *the following conditions are satisfied*

$$\alpha\, g(m_1, y) < 0, \quad \alpha\, g(m_2, y) > 0.$$

(A7) for each $t \in [0,1]$ *and* $x \in [m_1 + M_1, m_2 + M_2]$ *we have*

$$f(t, x, M_1) \le 0, \quad f(t, x, M_2) \ge 0.$$

Then problem (1)–(2) *has a solution* u *satisfying*

$$m_1 + M_1 \le u(t) \le m_2 + M_2, \quad M_1 \le u'(t) \le M_2, \quad t \in [0,1].$$

3 Conclusions and Future work

Similar results can be obtained for the boundary value problem with (2) replaced by

$$g(u'(0), G(u)) = 0, \quad h(u(1), H(u')) = 0.$$

Let us mention that Theorem 1 extends the results from [2] to the problem involving a generalized p-Laplacian and the functionals G and H.

References

[1] W. Ge, J. Ren, An extension of Mawhin's continuation theorem and its application to boundary value problems with a p-laplacian, Nonlinear Anal. **58** (2004), 477–488.

[2] I. Rachůnková, Topological degree methods in BVPs with nonlinear conditions, Ann. Math. Sil. **10** (1996), 103–110.

International Conference on Mathematical Analysis and Applications in Science and Engineering
ICMA^{2}SC'22

ISEP Porto-Portugal, June 27 - 29, 2022

Exact solvability conditions for the model with a discrete memory effect

Natalia Dilna

Institute of Mathematics, Slovak Academy of Sciences,
Štefánikova 49, 814 73 Bratislava, Slovakia

dilna@mat.savba.sk

Abstract: The exact conditions sufficient for the unique solvability of the initial value problem for the model with a discrete memory effect described by the system of linear fractional functional differential equations are established. The unique solution is presented by the Neumann's series.

keywords: fractional order functional differential equations; unique solvability; Caputo derivative; initial value problem; model with a discrete memory effect

MSC2020: 34A08; 34K37; 47H07; 74D05.

1 Introduction

Let us consider fractional functional differential equation (FFDE) for model with a discrete memory effect

$$D_a^{\frac{1}{2}} u(t) = \sum_{i=1}^{t_i \le t} F_i(t) u(t_i) + r(t), \quad t \in [a,b], \tag{1}$$

where $D_a^{\frac{1}{2}}$ is the Caputo fractional derivative of order $\frac{1}{2}$, $a < t_1 < t_2 < \cdots < t_m < b$ are given, $r : [a,b] \to \mathbb{R}^n$ is integrable function and $F_i \in C([a,b], GL_n(\mathbb{R}))$, $i = 0, 1, \ldots, m$, are defined by

$$F_i(t) := \begin{pmatrix} f_{11}^i(t) & f_{12}^i(t) & \ldots & f_{1n}^i(t) \\ f_{21}^i(t) & f_{22}^i(t) & \ldots & f_{2n}^i(t) \\ \vdots & \vdots & \ddots & \vdots \\ f_{n1}^i(t) & f_{n2}^i(t) & \ldots & f_{nn}^i(t) \end{pmatrix}, \quad \text{and set} \quad \varsigma := \begin{pmatrix} \sigma_1 & 0 & \ldots & 0 \\ 0 & \sigma_2 & \ldots & 0 \\ \vdots & \vdots & \ddots & \vdots \\ 0 & 0 & \ldots & \sigma_n \end{pmatrix},$$

$\{\sigma_1, \sigma_2, \ldots, \sigma_n\} \subset \{-1, 1\}$. If $u = (u_i)_{i=1}^n \in \mathbb{R}^n$, then $|u|_\infty = \max_{1 \le i \le n} |u_i|$ and $C([a,b], \mathbb{R}^n)$ is the Banach space of continuous functions $[a,b] \to \mathbb{R}^n$ with the norm $C([a,b], \mathbb{R}^n) \ni u \to \max_{s \in [a,b]} |u(s)|_\infty = \max_{t \in [a,b]} \operatorname{ess\,sup} |u(t)|$.

The main goal of our investigations is to establish the exact conditions sufficient for the unique solvability of the initial value problem

$$u(a) = c, \tag{2}$$

for systems of linear FFDE (1) presented by isotone, in a sense, operator (see Definition 3). For this aim, we use Theorem 2 from [1]. The mentioned theorem was established using the method of test elements studied for the estimation of the spectral radius of a linear operator based on knowledge of the value of the operator on a single, suitably chosen, element of the space. The unique solution of the problem (1), (2) is presented in view of the Neumann's series.

Definition 1 *By a solution of the linear boundary-value problem* (1) *and* (2), *we understand continuous vector function* ($u \in C([a,b],\mathbb{R}^n)$) *possessing property* (2) *and satisfying relation* (1) *for almost all* t *from the interval* $[a,b]$.

Definition 2 *For a function* $u \in [a,b]$ *the Caputo derivative of fractional order* q *is defined by*

$$D_a^q u(t) = \frac{1}{\Gamma(1-q)}\Big(\frac{d}{dt}\Big)\int_a^t (t-s)^{-q}\big(u(s)-u(a)\big)ds, \quad 0<q<1, \quad \Gamma(q) := \int_0^\infty t^{q-1}e^{-t}dt.$$

Definition 3 *For a certain given* $\{\sigma_1,\sigma_2,\dots,\sigma_n\} \subset \{-1,1\}$ *an operator*

$$C([a,b],\mathbb{R}^n) \ni u \mapsto (lu)(t) := \sum_{i=1}^{t_i\le t} F_i(t)u(t_i) \tag{3}$$

is a $\vec{\sigma}$*-positive operator if the fact that, for all* $t \in [a,b]$, *the relation*

$$\varsigma u(t) \ge 0, \tag{4}$$

is true implies that $\varsigma \sum_{i=1}^{t_i\le t} F_i(t)u(t_i) \ge 0$, *for almost every* t *from* $[a,b]$.

Let us fix arbitrary $y_0 \in C([a,b],\mathbb{R}^n)$ and introduce the sequence of functions

$$y_k(t) := \frac{1}{\Gamma(\frac12)}\int_a^t \frac{1}{(t-s)^{\frac12}}\sum_{i=1}^m F_i(s)\chi_i(s)y_{k-1}(t_i)ds. \tag{5}$$

with properties

$$\sigma_k y_k(t) > 0, \quad t \in (a,b], \quad y_k(a) = 0, \tag{6}$$

where $\chi_i(t)$ is the characteristic function of the interval $[t_i,b]$: $\chi_i(t) = 1$, if $t \in [t_i,b]$ and $\chi_i(t) = 0$, if $t \notin [t_i,b]$. The following inclusion is then satisfied obviously: $\{y_k \ge 0\} \subset C([a,b],\mathbb{R}^n)$.

2 Results and discussion

Let us put $y_0(t) = \xi(t-a)$, $\xi \in \mathbb{R}^n$.

Theorem 1 *Assume that*

$$\varsigma F_i(t)\varsigma \ge 0 \quad \textit{for almost all} \quad t \in [a,b], \quad 1 \le i \le n \tag{7}$$

is fulfilled. Suppose that there exist a number $\alpha > 1$. *Additionally, there are fulfilled the succeeding differential inequalities*

$$\varsigma\Big(\frac{4\xi\Big(t-a\Big)^{\frac32}}{3\Gamma(\frac12)} - \alpha\sum_{i=1}^{t_i\le t} F_i(t)\,\xi(t_i-a)\Big) \ge 0 \tag{8}$$

for a certain $m \ge 0$, *all* $\nu = 1,2,\dots,n$, *and almost all* $t \in [a,b]$.

Then the nonhomogeneous non-local boundary-value problem (2) *for FFDE* (1) *has a unique solution* $u(\cdot)$ *for arbitrary* $c \in \mathbb{R}^n$ *and integrable function* $r : [a,b] \to \mathbb{R}^n$, *and this solution is representable in the form* $u(t) = \sum_{k=0}^n r^{[k]}(t)$, $t \in [a,b]$, *where*

$$r^{[k]}(t) = \frac{1}{\Gamma(\frac12)}\sum_{i=1}^m \int_a^t (t-s)^{-\frac12}F_i(s)\chi_i(s)r^{[k-1]}(t_i)ds,$$

$$r^{[0]}(t) = c + \frac{1}{\Gamma(\frac12)}\int_a^t (t-s)^{\frac12}r(s)ds.$$

If, furthermore, for all $\nu = 1, 2, \ldots, n$ *and* $t \in [a, b]$*, the inequalities*

$$\sigma_\nu\Big(c_\nu + \frac{1}{\Gamma(\frac{1}{2})}\int_a^t (t-s)^{-\frac{1}{2}} r_\nu(s)ds\Big) \geq 0 \tag{9}$$

are true, then the components $(u_\nu)_{\nu=1}^n$ *of the unique solution* $u(\cdot)$ *of the initial value problem* (2) *for FFDE* (1) *satisfy the conditions* (4)*. The corresponding homogeneous initial value problem has only a trivial solution.*

To prove Theorem 1 we use

Theorem 2 (Theorem 2 [1]) *Assume that the linear operator* $l = (l_k)_{k=1}^n$ *is* $\vec{\sigma}$*-positive. Suppose that there exist a number* $\alpha > 1$*, a function* $y_0 \in C([a, b], \mathbb{R}^n)$*, and a certain integer* $k \geq 0$ *such that the components of the function* $(y_{k,\nu})_{\nu=1}^n$ *of the respective function* y_k *are continuous and satisfy conditions* (6)*. Additionally, there are fulfilled the succeeding differential inequalities*

$$\sigma_\nu\Big(D_a^q y_{k,\nu}(t) - \alpha(l_\nu y_{k+m})(t)\Big) \geq 0 \tag{10}$$

for a certain $m \geq 0$*, all* $\nu = 1, 2, \ldots, n$*, and almost all* $t \in [a, b]$*.*

Then the nonhomogeneous non-local boundary-value problem (2) *for FFDE*

$$D_a^q u(t) = (lu)(t) + r(t), \quad t \in [a, b], \quad 0 < q < 1, \tag{11}$$

has a unique solution $u(\cdot)$ *for arbitrary* $c \in \mathbb{R}^n$ *and* $r : [a, b] \to \mathbb{R}^n$*, and this solution is representable in the form*

$u(t) = r_c(t) + \frac{1}{\Gamma(q)}\int_a^t (t-s)^{q-1}(lr_c)(s)ds + \frac{1}{\Gamma(q)}\int_a^t (t-\cdot)^{q-1} l\Big(\frac{1}{\Gamma(q)}\int_a^{\cdot}(t-s)^{q-1}(lr_c)(\xi)d\xi\Big)(s)ds + \ldots,$
where the functional series converges uniformly on $[a, b]$ *and* $r_c(t) := c + \frac{1}{\Gamma(q)}\int_a^t (t-s)^{q-1} r(s)ds$*.*

If, furthermore, for all $\nu = 1, 2, \ldots, n$ *and* $t \in [a, b]$*, the inequalities* (9) *are true, then the components* $(u_\nu)_{\nu=1}^n$ *satisfy the conditions* (4)*. The corresponding homogeneous initial value problem has only a trivial solution.*

Obviously, condition (7) is condition on $\vec{\sigma}$-positivity of the operator l from (11) defined by (3). Since (8) is a particular case of the differential inequality (10) for $k = 0$, $m = 0$, $y_0(t) = \xi(t-a)$, $\xi \in \mathbb{R}^n$, then the assertion of Theorem 1 is an immediate consequence of Theorem 2.

3 Conclusions and Future work

Summarizing, we apply derived abstract results from [1] to the model with discrete memory (1), (2). Here are established exact conditions sufficient for the unique solvability of the initial-value problem for the system of linear fractional functional differential equations determined by isotone operators. A possible future work would be to study several coupled FFDEs with different fractional derivatives. We also intend to extend the method of this paper to such kinds of systems.

Acknowledgments

This research was supported in part by the Slovak Grant Agency VEGA-SAV, Grants No. 2/0127/20.

References

[1] N. Dilna, M. Fečkan, Exact solvability conditions for the con-local initial value problem for systems of linear fractional functional differential equations, Mathematics **10** (2022) 1759. https://doi.org/10.3390/math10101759

International Conference on Mathematical Analysis and Applications in Science and Engineering
ICMA^{2}SC'22

ISEP Porto-Portugal, June 27 - 29, 2022

Some regularity results for solutions to the Navier-Stokes equations

Petr Kučera[1⋆]

[1] Czech Technical University in Prague, Czech Republic

[1⋆]petr.kucera@cvut.cz

Abstract: We present some criteria of regularity of the Navier-Stokes equations. In the first part we present results on robustness of the Navier-Stokes equations, in the second part we deal with the conditional regularity of the weak solutions to the Navier- Stokes equations. We present one optimal regularity criterion for bounded domains with Navier's, Navier-type and Dirichlet boundary conditions.

keywords: Navier-Stokes equations; Regularity criteria; Flow of energy.

MSC2020: 35Q30, 75D05.

1 Introduction

Let $\Omega = \mathbb{R}^3$ or Ω be a simply connected three-dimensional bounded domain with the boundary $\partial\Omega$ of the Hölder class $C^{2+\beta}$ for some $\beta > 0$. Suppose that $0 < T < \infty$ and put $Q_T = \Omega \times (0, T)$. We study the initial–boundary value Navier–Stokes problem

$$\partial_t \boldsymbol{u} - \nu\,\Delta \boldsymbol{u} + (\boldsymbol{u}\cdot\nabla)\boldsymbol{u} + \nabla\mathcal{P} \;=\; \mathbf{0} \qquad \text{in } Q_T, \tag{1}$$

$$\operatorname{div} \boldsymbol{u} \;=\; 0 \qquad \text{in } Q_T, \tag{2}$$

$$\boldsymbol{u}(0) \;=\; \boldsymbol{u}_0 \qquad \text{in } \Omega. \tag{3}$$

We denote by $\boldsymbol{u}$ the velocity, $\mathcal{P}$ is the pressure and $\boldsymbol{u}_0$ denotes the initial condition. For simplicity, we suppose the kinematic viscosity ν to be equal to 1. We add Navier's boundary conditions

$$\boldsymbol{u}\cdot\boldsymbol{n} = 0, \quad [((\nabla\boldsymbol{u}) + (\nabla\boldsymbol{u})^T)\boldsymbol{n}]_\tau + \gamma\boldsymbol{u} = \mathbf{0} \quad \text{on } \partial\Omega \times (0,T), \tag{4}$$

where $\gamma > 0$ denotes the friction coefficient between the fluid and the fixed wall and $\boldsymbol{n}$ is the outer normal vector on $\partial\Omega$, or Navier-type boundary conditions

$$\boldsymbol{u}\cdot\boldsymbol{n} = 0, \quad \boldsymbol{\omega}\times\boldsymbol{n} = \mathbf{0} \quad \text{on } \partial\Omega \times (0,T), \tag{5}$$

where $\boldsymbol{\omega} = \nabla\times\boldsymbol{u}$, or Dirichlet boundary conditions

$$\boldsymbol{u} = 0 \quad \text{on } \partial\Omega \times (0,T). \tag{6}$$

Now we define weak and strong solutions of the problem (1)–(4). Weak and strong solutions of problems (1)–(3) and (5) and (1)–(3)and (6) are defined in a similar way.

Definition 1 We say that $\boldsymbol{u} \in L^\infty(0,T;\, \mathbf{L}^2_\sigma(\Omega)) \cap L^2(0,T;\, \boldsymbol{W}^{1,2}_\sigma(\Omega))$ a *weak solution* of the problem (1)–(4) with initial velocity $\boldsymbol{u}_0 \in \mathbf{L}^2_\sigma(\Omega)$ if

$$\int_0^T \int_\Omega \left[-\boldsymbol{u}\cdot\partial_t\boldsymbol{\phi} + \left((\nabla\boldsymbol{u}) + (\nabla\boldsymbol{u})^T\right)\nabla\boldsymbol{\phi} + (\boldsymbol{u}\cdot\nabla)\boldsymbol{u}\cdot\boldsymbol{\phi}\right] \mathrm{d}\boldsymbol{x}\,\mathrm{d}t + \nu \int_0^T \int_{\partial\Omega} \gamma\, \boldsymbol{u}\,\boldsymbol{\phi}\,\mathrm{d}\boldsymbol{x}\,\mathrm{d}t$$
$$- \int_\Omega \boldsymbol{u}_0\cdot\boldsymbol{\phi}(0)\,\mathrm{d}\boldsymbol{x} = 0$$

for all $\boldsymbol{\phi} \in C^\infty([0,T];\, \boldsymbol{W}^{1,2}_\sigma(\Omega))$ such that $\boldsymbol{\phi}(T) = \mathbf{0}$.

Definition 2 Let $\boldsymbol{u}$ be a weak solution of the system (1)–(4). Suppose that the inequality

$$\left\|\boldsymbol{u}(t)\right\|_2^2 + \int_0^t \left\|\nabla\boldsymbol{u}(\xi) + (\nabla\boldsymbol{u})^T(\xi)\right\|_2^2 \mathrm{d}\xi + 2\gamma \int_0^t \left\|\boldsymbol{u}(\xi)\right\|_{2,\partial\Omega}^2 \mathrm{d}\xi \le \left\|\boldsymbol{u}(s)\right\|^2$$

holds for every $t \in (0,T)$ and for almost every $s \in (0,t)$. Then we say that $\boldsymbol{u}$ satisfies the strong energy inequality.

Definition 3 Let $\boldsymbol{u}$ be a weak solution of the system (1)–(4). We say that $\boldsymbol{u}$ is regular if there exist real numbers p, r such that $3 < r < \infty$, $2 < p < \infty$, $2/p + 3/r = 1$ and

$$\boldsymbol{u} \in L^p_{loc}((0,T];\, \mathbf{L}^r(\Omega)).$$

2 Presented results

Theorem 1 summarizes the results published in [2] and [3]. These results relate to the robustness of the solution of the regular Navier-Stokes equations.

Theorem 1 *Let $\boldsymbol{u}$ be a regular solution of (1)–(4) of (1–(3) and (5) on the time interval $(0,T)$ (where $0 < T \le \infty$). Then to every $\epsilon > 0$, there exists $\delta > 0$ such that if $\boldsymbol{v}_0 \in \boldsymbol{W}^{1,2}_\sigma(\Omega)$ satisfies*

$$\|\boldsymbol{v}_0 - \boldsymbol{u}(0)\|_3 \;<\; \delta \tag{7}$$

then there exists a unique regular solution $\boldsymbol{v}$ with the initial velocity $\boldsymbol{v}_0$, on the same time interval $(0,T)$. The solution $\boldsymbol{v}$ satisfies the estimate

$$\|\boldsymbol{v}(t) - \boldsymbol{u}(t)\|_3 \;<\; \epsilon \tag{8}$$

for all $t \in (0,T)$.

Theorem 1 can also be interpreted as a theorem on the continuous dependence of a strong solution on the initial condition. The perturbed strong solution $\boldsymbol{v}$ exists on the same time interval $(0,T)$, where the "basic" solution $\boldsymbol{u}$ exists. In the case $T = \infty$, inequality (8) yields that any strong solution $\boldsymbol{u}$ on the time interval $(0,\infty)$ is stable in the L^3–norm.

Theorems 2 and 3 present results published in [1]. These results deal with the conditional regularity of the weak solutions to the Navier-Stokes equations.

Theorem 2 *Let $\lambda \ge 1$ and $\boldsymbol{u}$ be a weak solution of either the problem (1)–(4) or the problem (1), (2), (3) and (5). Let $\boldsymbol{u}$ satisfy the strong energy inequality and be equipped with the initial condition $\boldsymbol{u}_0 \in \mathbf{L}^3_\sigma(\Omega)$. If*

$$\boldsymbol{u}\cdot\nabla|\boldsymbol{u}|^\lambda \in L^p(0,T;\, L^r(\Omega)),\ \text{where } \frac{2}{p} + \frac{3}{r} = \lambda + 2,\ r \in \Big(\frac{3}{\lambda+2}, \infty\Big],$$

then $\boldsymbol{u}$ is regular on $(0,T]$.

Theorem 3 *Let $\lambda \in [1,2]$ and $\boldsymbol{u}$ be a weak solution of the problem (1)–(3) and (6). Let $\boldsymbol{u}$ satisfy the energy inequality and be equipped with the initial condition $\boldsymbol{u}_0 \in \mathbf{L}^3_\sigma(\Omega)$. If*

$$\boldsymbol{u} \cdot \nabla |\boldsymbol{u}|^\lambda \in L^p(0,T;\, L^r(\Omega)), \ \text{where } \frac{2}{p} + \frac{3}{r} = \lambda + 2, \ r \in \Big(\frac{3}{\lambda+2}, \frac{3}{\lambda+1}\Big],$$

then $\boldsymbol{u}$ is regular on $(0,T]$.

Let velocity $\boldsymbol{w}$ and pressure $\mathcal{Q}$ solve the equations (1) and (2) in $\mathbb{R}^3 \times (0,T)$. Then the rescaled functions $\boldsymbol{w}_\mu$, $\mathcal{Q}_\mu$, $\mu > 0$, defined as $\boldsymbol{w}_\mu(x,t) = \mu \boldsymbol{w}(\mu x, \mu^2 t)$ and $\mathcal{Q}_\mu(x,t) = \mu^2 \mathcal{Q}(\mu x, \mu^2 t)$ solve (1) and (2) in $\mathbb{R}^3 \times (0, T/\mu^2)$. The spaces $L^p(0,T;\mathbf{L}^r(\Omega))$ with $2/p + 3/r = 1$ are called critical since their norms are invariant with regard to the presented scaling, i.e., $\|\boldsymbol{w}\|_{L^p(0,T;\mathbf{L}^r(R^3))} = \|\boldsymbol{w}_\mu\|_{L^p(0,T/\mu^2;\mathbf{L}^r(R^3))}$. One can verify that $\|\boldsymbol{w}\cdot\nabla|\boldsymbol{w}|^\lambda\|_{L^p(0,T;\mathbf{L}^r(R^3))} = \|\boldsymbol{w}_\mu \cdot \nabla |\boldsymbol{w}_\mu|^\lambda\|_{L^p(0,T/\mu^2;\mathbf{L}^r(R^3))}$ provided $\frac{2}{p} + \frac{3}{r} = \lambda + 2, \ r \in \Big(\frac{3}{\lambda+2}, \frac{3}{\lambda+1}\Big]$. In this sense criterion presented in Theorems 2 and 3 is optimal.

For $\lambda = 1$ $\boldsymbol{u}\cdot\nabla|\boldsymbol{u}|$ corresponds with flow of velocity magnitude and for $\lambda = 2$ $\boldsymbol{u}\cdot\nabla|\boldsymbol{u}|$ corresponds with flow of energy.

Acknowledgments

The author was supported by the European Regional Development Fund, project No. CZ.02.1.01/0.0/0.0/16_019/0000778.

References

[1] Zhengguang Guo, Petr Kučera, Zdenek Skalak, Regularity criteria for the Navier-Stokes equations in terms of the velocity direction and the flow of energy, Mathematical Methods in the Applied Sciences, **45**(9) (2022), 5321–5340.

[2] Petr Kučera, Jiří Neustupa, On L-3-stability of strong solutions of the Navier-Stokes equations with the Navier-type boundary conditions, Journal of Mathematical Analysis and Applications, **405** 2 (2013), 731-737.

[3] Petr Kučera, Jiří Neustupa, On robustness of a strong solution to the Navier-Stokes equations with Navier's boundary conditions in the L-3-norm, Nonlinearity, **30** 4 (2017), 1564-1583.

International Conference on Mathematical Analysis and Applications in Science and Engineering
ICMA^{2}SC'22
ISEP Porto-Portugal, June 27 - 29, 2022

Analysis of a stochastic differential equation with nonlocal discrete diffusion modeling life tables

José Valero[1⋆] **Tomás Caraballo**[2] **Francisco Morillas**[3]

[1] University Miguel Hernández de Elche, Spain
[2] Universidad de Sevilla, Spain
[3] Universidad de Valencia, Spain

[1⋆]jvalero@umh.es, [2]caraball@us.es, [3]Francisco.Morillas@uv.es

Abstract: In this work, we study an stochastic system of differential equations with nonlocal discrete diffusion. For two type of noises we study the existence of either positive or probability solutions. Finally, we perform numerical simulations and discuss the application of the results to life tables for mortality in Spain.

keywords: stochastic equations; ordinary differential equations; nonlocal problems; discrete diffusion; life tables.

MSC2020: 34A12; 34C60; 34D05; 34D20; 34D23; 60J65; 62P05; 65C99.

1 Introduction

Diffusion processes can be sometimes modeled by nonlocal operators, which take into account the influence of the value of the variable in the whole domain (or in part of them) and not only in the current point. We consider the following stochastic system of differential equations:

$$\begin{aligned} \frac{d}{dt}u_i(t) &= \sum_{r\in D} j_{i-r}u_r(t) - u_i(t) + \sum_{r\in\mathbb{Z}\setminus D} j_{i-r}g_r(t) + b\sigma_i(u_i(t))\frac{dw_i}{dt},\ i\in D,\ t>0, \\ u_i(0) &= u_i^0,\ i\in D, \end{aligned} \tag{1}$$

where $w_i(t)$ are independent Brownian motions and $b>0$ is the intensity of the white noise. We will assume the following assumptions on the kernel $\{j_i\}$ and the functions $\{g_i(\cdot)\}$:

$(H1)$ $j_i \geq 0$ for all $i\in\mathbb{Z}$.

$(H2)$ $\sum_{i\in\mathbb{Z}} j_i = 1$.

$(H3)$ $g\in C([0,+\infty), l_2^\infty)$,
where $l_2^\infty = \{(u_i)_{i\in\mathbb{Z}\setminus D} : \sup_{i\in\mathbb{Z}\setminus D}|u_i|\}$.

We will consider two specific type of noises. Namely: 1) $\sigma_i(v) = v$ (linear case); 2) $\sigma_i(v) = v(1-v)$. The choice of the noise in the second case is motivated by the fact that we are interested in studying variables like the probability of death, which take values in the interval $[0,1]$.

We present some theoretical results concerning the properties of solutions of the stochastic system. First, we prove in the linear case the existence of a unique positive solution whenever the initial datum is positive. Second, we establish in the second case that if the initial condition takes values in the interval $(0,1)$, then the solution remains in this interval for any future time.

Also, we perform numerical simulations of solutions and analyse the efficiency of model (1) for prediction of mortality using data from Spain.

2 Properties of solutions

In this section, under certain conditions on the functions of the problem, we will establish first that for any positive initial condition there exists a unique globally defined solution which is almost sure positive. Then we will prove that if the initial condition lies in the interval $(0,1)$, then the solution remains there for all positive times. This is important for the application to life tables.

First, we will consider a standard linear noise, that is, we study the system

$$\begin{aligned} \frac{d}{dt}u_i(t) &= \sum_{r\in D} j_{i-r}u_r(t) - u_i(t) + \sum_{r\in\mathbb{Z}\setminus D} j_{i-r}g_r(t) + bu_i(t)\frac{dw_i}{dt},\ i\in D,\ t>0, \\ u_i(0) &= u_i^0,\ i\in D. \end{aligned} \tag{2}$$

Denote $\mathbb{R}^m_+ = \{v\in\mathbb{R}^m : v_j > 0 \text{ for all } j\}$. We prove first the existence of global positive solutions.

Lemma 1 *Assume that $g_r(t)\geq 0$ for all r and t. Then for any $u^0\in\mathbb{R}^m_+$ there exists a unique globally defined solution $u(\cdot)$ such that $u(t)\in\mathbb{R}^m_+$ almost sure for $t\geq 0$.*

Corollary 2 *Let $u^0, v^0\in\mathbb{R}^m$ be two initial conditions satisfying $u_i^0 > v_i^0$ for any $i\in D$. Also, $g^u, g^v\in C([0,+\infty), l_2^\infty)$ are such that $g_i^u(t)\geq g_i^v(t)$ for all $i\in D$ and $t\geq 0$. Then, $u_i(t) > v_i(t)$, for all $i\in D$ and $t\geq 0$, where $u(\cdot)$, $v(\cdot)$ are the unique solutions to problem (2) corresponding to $\{u^0, g^u\}$ and $\{v^0, g^v\}$, respectively.*

Second, we are going to consider the system

$$\begin{aligned} \frac{d}{dt}u_i(t) &= \sum_{r\in D} j_{i-r}u_r(t) - u_i(t) + \sum_{r\in\mathbb{Z}\setminus D} j_{i-r}g_r(t) + bu_i(t)(1-u_i(t))\frac{dw_i}{dt}, \\ u_i(0) &= u_i^0, \end{aligned} \tag{3}$$

where $i\in D$, $t>0$.

We are interesting in proving that if the components of the initial condition lie within the interval $(0,1)$ and the functions $g_r(t)$ take values in $[0,1]$, then the components of the solution $u(t)$ also lie in $(0,1)$ for any $t\geq 0$ a.s. This is important for applying the results to life tables, as in such situation the variable is a probability.

Lemma 3 *Assume that $g_r(t)\in[0,1]$ for all r and t. Then for any $u^0\in\mathbb{R}^m$ such that $u_i^0\in(0,1)$, for any $i\in D$, the unique solution $u(\cdot)$ to (3) satisfies almost sure that $u_i(t)\in(0,1)$ for all $i\in D$ and $t\geq 0$.*

3 Application to life tables

The mortality table is the most widely used tool for studying the survival of a population. This instrument is based on the so-called biometric functions. In this work we will focus on the probability of death, denoted by q_x^t.

We solve numerically system (1) by using the Euler-Maruyama method. In the resolution of this system, the mortality data for the year 2010 from the National Institute of Statistics (of Spain) are used as initial values. Also, the mortality values for 2019 are used as a reference for the suitability of the estimates.

In relation to the values of the parameters that are used for the resolution of the stochastic system, we observe first that ages are taken from 0 to 100 (thus, $m_1 = 0$, $m_2 = 100$). The function g is defined to be piecewise constant, with $g_i = 0.41$, for $i > 100$, and $g_i = 0.001802$, for $i < 0$; the choice of the value 0.41 is the one proposed in [1, 2] as the convergence value of the limit mortality. The value 0.001802 is obtained applying static kernel graduation to the initial series of values. The time step is one year, which is subdivided into 50 sub-periods for the intermediate calculations. A Gaussian kernel with bandwidth equal to 1 is used.

Figure 1 shows (in logarithmic scale) the observed mortality values for the years 2010 and 2019, together with 50 trajectories obtained in the numerical resolution of the system. It can be seen that all of them contain the three parts in which the mortality curve is traditionally subdivided: adaptation to the environment, social or accident hump, and natural longevity. Therefore we can say that the system preserves the qualitative properties of the mortality curve and, in this sense, is adequate.

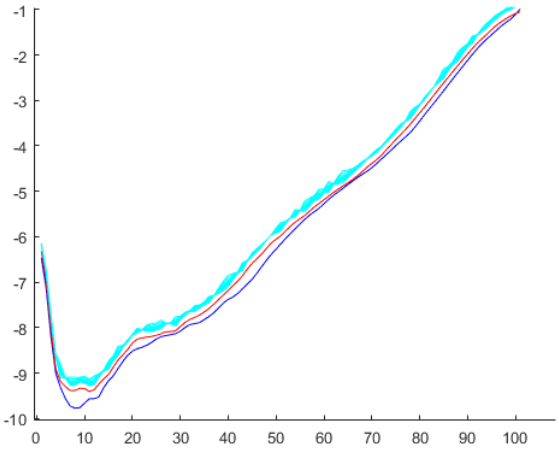

Figure 1: Ensemble of estimates of mortality

Although the proposed model is adequate from the qualitative point of view, it is evident that the estimated mortality rates are not between the initial values $\{q_x^{2010}\}$ and the observed limit values $\{q_x^{2019}\}$. This is due to the fact that the model does not take into account the improvements in mortality, which, as it was already mentioned, is the essential nature of dynamic mortality models. It is easy to obtain an initial correction of the estimates using the average annual improvement rate, $\overline{IR}$, which is calculated as the arithmetic mean of the improvement rates by age:

$$IR_x = \frac{q_x^t}{q_x^{t+1}}.$$

We have obtained that $\overline{IR} = 0.03$. Figure 2 shows the new graphic after this correction. Now, the set of corrected predictions lies between the observed values in 2010 and 2019.

Figure 2 shows how a simple correction provides reasonable estimates in magnitude for a short period of time. However, it can be seen that these estimates are not equally adequate for all ages. This is due to the fact that the improvement in mortality does not affect all ages in the same way and, therefore, it is necessary to introduce appropriate correction rates for each age, for example incorporating the history of mortality through delay terms as has benn carried out, in the deterministic system, in the previous work [3]. In this sense, the study of the stochastic model with delay would be an improvement of the current work.

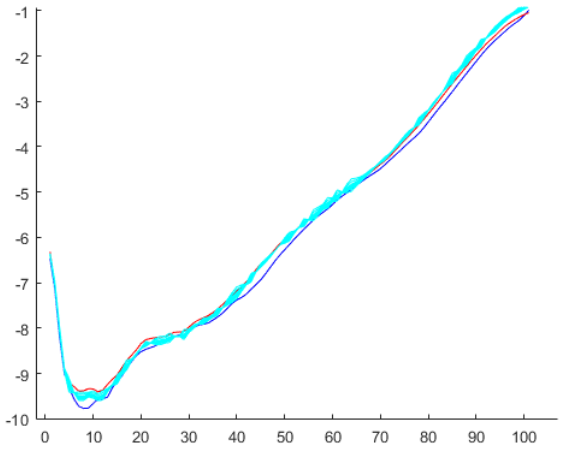

Figure 2: Ensemble of estimates of mortality

Acknowledgments

This work has been partially supported by the projects PGC2018-096540-B-I00 (Spanish Ministry of Science, Innovation and Universities), PID2019-108654GB-I00 (Spanish Ministry of Science and Innovation), P18-FR-4509 (Junta de Andalucía) and by the Generalitat Valenciana, project PROMETEO/2021/063.

References

[1] Barbi E., Lagona F., Marsili M., Vaupel J.W., Kenneth W.W., The plateau of human mortality: demography of longevity pioneers, Science, **360** (2018), 1459-1461.

[2] Dolgin E., Longevity data hint at no natural limit on lifespan, Nature, **559** (2018), 14-15.

[3] Morillas F., Valero J., On a retarded nonlocal ordinary differential system with discrete diffusion modeling life tables, Mathematics, **9** (2021), 220.

International Conference on Mathematical Analysis and Applications in Science and Engineering
ICMA^{2}SC'22
ISEP Porto-Portugal, June 27 - 29, 2022

Point symmetries and conservation laws of the generalized Krichever-Novikov equations in 2+1 dimensions

S.C. Anco **J. Hornick*** **T. Wolf**

Department of Mathematics and Statistics
Brock University, St Catharines Canada

*jh10en@brocku.ca

Abstract: The generalized Krichever-Novikov equation in two dimensions is studied. This equation arises in the study of integrable systems. A classification of Lie point symmetries and conservation laws is presented. The equation has a variational formulation. It is determined which point symmetries are variational. Each variational symmetry yields a conservation law multiplier, the corresponding conservation laws are deduced.

keywords: Krichever-Novikov equation; symmetries; conservation laws.

MSC2020: 49-XX; 34-XX; 92-XX.

1 Introduction

Generalized Krichever-Novikov equation (gKN)

$$u_t - u_{xxx} + \frac{3}{2}\frac{u_{xx}^2}{u_x} - \frac{f(u)}{u_x} = 0$$

- For $f(u)$ an arbitrary quartic polynomial, it is integrable (infinite number of higher order local symmetries and conserved densities)
- No master symmetry was known until work in [2]; it was obtained from finding a conservation law in which t, x appear explicitly
- 2D generalization of the equation is known:

$$\Big(\frac{u_t - u_{xxx}}{u_x} + \frac{\frac{3}{2}(u_{xx}^2 - \sigma u_y^2) + f(u)}{u_x^2}\Big)_x + \sigma\Big(\frac{u_y}{u_x}\Big)_y = 0, \quad \sigma = const.$$

- integrable equation (Lax pair)

2 Variational formulation

The 2D gKN equation is the extremal of a functional given by a Lagrangian:

$$L = \frac{1}{2}\frac{u_t}{u_x} - \frac{1}{2}\frac{u_{xx}^2 + \sigma u_y^2}{u_x^2} + \frac{1}{3}\frac{f(u)}{u_x^2} \quad \text{modulo total divergence}$$

Extremal is obtained from the Euler operator:

$$E_u(L) = \frac{1}{u_x}\left(\left(\frac{u_t - u_{xxx}}{u_x} + \frac{\frac{3}{2}(u_{xx}^2 - \sigma u_y^2) + f(u)}{u_x^2}\right)_x + \sigma\left(\frac{u_y}{u_x}\right)_y\right)$$

3 Noether's Theorem

For arbitrary $f(u)$: point symmetries are the span of

$$\mathrm{X}_1 = \partial_t, \quad \mathrm{X}_2 = F(t)\partial_x, \quad \mathrm{X}_3 = \frac{1}{2}\sigma F'(t) y \partial_x + F(t)\partial_y$$

where $F(t)$ is an arbitrary function.

For specific $f(u)$: point symmetries consist of

$$\begin{aligned}
&a) \quad f(u) = C\exp(-4au), \quad \mathrm{X}_{4\mathrm{a}} = 3at\partial t + ax\partial x + 2ay\partial y + 2\partial u\\
&b) \quad f(u) = C(u+b)^{2-4a}, \quad \mathrm{X}_{4\mathrm{b}} = 3at\partial t + ax\partial x + 2ay\partial y + (u+b)\partial u\\
&c) \quad f(u) = C(u+b)^4\exp(4a/(u+b)),\\
&\qquad \mathrm{X}_{4\mathrm{c}} = 3at\partial t + ax\partial x + 2ay\partial y + (u+b)^2\partial u\\
&d) \quad f(u) = C(u+b+c)^{2+2a/c}(u+b-c)^{2-2a/c},\\
&\qquad \mathrm{X}_{4\mathrm{d}} = 3at\partial t + ax\partial x + 2ay\partial y + ((u+b)^2 - c^2)\partial u\\
&e) \quad f(u) = C((u+b)^2 + c^2)^2\exp\left((-4a/c)\arctan((u+b)/c)\right),\\
&\qquad \mathrm{X}_{4\mathrm{e}} = 3at\partial t + ax\partial x + 2ay\partial y + ((u+b)^2 + c^2)\partial u\\
&f) \quad f(u) = C(u+b)^4,\\
&\qquad \mathrm{X}_{4\mathrm{f}} = 3t\partial t + x\partial x + 2y\partial y - 2(u+b)\partial u, \quad \mathrm{X}_{5\mathrm{f}} = (u+b)^2\partial u
\end{aligned}$$

where a, b, c, C are arbitrary non-zero constants.

The variational point symmetries of the 2D gKN equation are given by:

$$\begin{aligned}
&\mathrm{X}_1 = \partial_t,\\
&\mathrm{X}_2 = F(t)\partial_x,\\
&\mathrm{X}_3|_{\sigma^2=1} = \pm\tfrac{1}{2}yF'(t)\partial_x + F(t)\partial_y,\\
&\mathrm{X}_{4b}|_{a=0} = (u+b)\partial_u,\\
&\mathrm{X}_{4c}|_{a=0} = \mathrm{X}_{5f} = (u+b)^2\partial u,\\
&\mathrm{X}_{4d}|_{a=0} = \mathrm{X}_{4e}|_{a=0} = ((x+b)^2 + c^2)\partial_u.
\end{aligned}$$

4 Conservation Laws

Conserved densities arising from variational point symmetries:

$$\begin{aligned} T_1 &= \big(\tfrac{1}{2}(u_{xx}^2 + \sigma u_y^2) - \tfrac{1}{3}f(u)\big)/u_x^2, \\ T_2 &= 0, \\ T_3 &= F(t)u_y/u_x, \\ T_{4\mathrm{b}} &= \tfrac{1}{2}(u+b)/u_x, \\ T_{4\mathrm{c}} &= \tfrac{1}{2}(u+b)^2/u_x, \\ T_{4\mathrm{d}} &= \big((u+b)^2 - c^2\big)/u_x. \end{aligned}$$

For future work, the goal is to search for nonlocal conservation laws involving t,x explicitly.

References

[1] G.W. Bluman, A.F. Cheviakov, S.C. Anco. Applications of Symmetry Methods to Partial Differential Equations, Springer.

[2] S.C. Anco, E. Avdonina, A. Gainetdunova, L. Galiakberova, NH. Ibragimov, T. Wolf, Symmetries and conservation laws of the generalized Krichever-Novikov equation, J. Phys. A: Math. and Theor. 49 (2016), 105201

International Conference on Mathematical Analysis and Applications in Science and Engineering
ICMA^{2}SC'22
ISEP Porto-Portugal, June 27 - 29, 2022

Exact solitary wave solutions for a coupled gKdV-NLS system

S.C. Anco[1] **J. Hornick**[1] **R. Zhao**[2] **T. Wolf**[1]

[1]Department of Mathematics and Statistics
Brock University, St Catharines Canada
[2]Department of Mathematics
Queen's University, Kingston Canada

Abstract: Exact solitary wave solutions are derived for a coupled gKdV-NLS system with a nonlinearity power p in the convective term. The solutions describe bright and dark solitary waves on a background and are obtained for $p = 1, 2, 3, 4$. Cases $p > 1$ have not been studied previously in the literature.

keywords: KdV; NLS; coupled system; solitary wave; exact solution

MSC2020: 35Qxx

1 Introduction

The phenomena of energy transport in an anharmonic crystal material [1, 2] can be modelled by a coupled gKdV-NLS system

$$u_t + \alpha u^p u_x + \beta u_{xxx} = \gamma(|\psi|^2)_x \tag{1}$$

$$i\psi_t + \kappa\psi_{xx} = \sigma u\psi \tag{2}$$

in which $u(x,t)$ is real-valued and $\psi(x,t)$ is complex-valued. In this system, $p > 0$ is nonlinearity power, and $\alpha, \beta, \gamma, \kappa, \sigma$ are real non-zero constants.

There is a strong interest in studying exact solutions which describe frequency-modulated solitary waves

$$u = U(\xi), \quad \psi = e^{i\omega t}\Psi(\xi), \quad \xi = x - ct \tag{3}$$

where c is the wave speed, and ω is the modulation frequency. For the KdV case $p = 1$, some solutions have been found in Ref. [1], while for the mKdV case $p = 2$, no exact solutions were found [2]. Nothing has been done for higher nonlinearities $p \geq 3$.

In the present work, we derive exact solutions for $p = 1, 2, 3, 4$, starting from the travelling wave ODE system satisfied by U and Ψ. The method is new:
(i) obtain first integrals by use of multi-reduction symmetry theory [3];
(ii) apply a hodograph transformation which leads to triangular (decoupled) system;
(iii) introduce an ansatz for polynomial solutions of the base ODE;
(iv) characterize conditions under which solutions yield solitary waves;
(v) solve an algebraic system for the coefficients in the ansatz under those conditions.

The resulting solitary waves exhibit a wide range of features: bright and dark peaks; single peaked and multi-peaked; zero and non-zero backgrounds.

We will use the dimensionless form of the system (1)–(2):

$$u_t + s_1 u^p u_x + u_{xxx} + s_2(|\psi|^2)_x = 0 \tag{4}$$
$$i\psi_t + \psi_{xx} + ku\psi = 0 \tag{5}$$

where

$$s_1 = \begin{cases} 1, & p = \text{ odd} \\ \pm 1, & p = \text{ even} \end{cases}, \quad s_2 = \begin{cases} \pm 1, & p = \text{ odd} \\ 1, & p = \text{ even} \end{cases} \tag{6}$$

and $k \neq 0$ is an arbitrary constant.

Substitution of the invariant form (3) into the coupled equations (4) and (5) yields an ODE system for $U(\xi)$ and $\Psi(\xi)$:

$$U''' + (s_1 U^p - c)U' + s_2(|\Psi|^2)' = 0 \tag{7a}$$
$$\Psi'' - ic\Psi' + (kU - w)\Psi = 0 \tag{7b}$$

It will be useful to consider the polar form of this system, which arises from expressing Ψ in amplitude-phase form

$$\Psi = A\exp(i\Phi) \tag{8}$$

The polar variables $A(\xi)$ and $\Phi(\xi)$, along with $U(\xi)$, satisfy the coupled ODEs

$$U''' + (s_1 U^p - c)U' + 2s_2 AA' = 0 \tag{9a}$$
$$A'' + (kU + c\Phi' - \Phi'^2 - w)A = 0 \tag{9b}$$
$$A\Phi'' + (2\Phi' - c)A' = 0 \tag{9c}$$

This system for $U(\xi)$, $A(\xi)$, $\Phi(\xi)$ consists of one third-order ODE (9a) and two second-order ODEs (9b) and (9c). Therefore, the general solution would require a total of seven integrations. As noted in the work [1, 2], inspection of the ODEs suggest that only a few explicit integrations are possible.

The steps (i) to (v) in our new method will now be carried out. Symmetry multi-reduction yields four conservation laws for the gKdV–NLS system (4)–(5), each of which is inherited as a first integral by the ODE system. Three of the four first integrals are functionally independent, and hence the ODE system is reduced to one second-order ODE and two first-order ODEs

$$U'' = cU - s_1\tfrac{1}{p+1}U^{p+1} - s_2A^2 + C_1 \tag{10}$$
$$\begin{aligned}\tfrac{1}{2}kU'^2 + s_2A'^2 = {} & kC_1U + \tfrac{1}{2}kcU^2 - s_1\tfrac{1}{(p+2)(p+1)}kU^{p+2} - s_2kUA^2 \\ & - s_2(\tfrac{1}{4}c^2 + \omega)A^2 - s_2{C_2}^2A^{-2} - C_3\end{aligned} \tag{11}$$
$$\Phi' = \tfrac{1}{2}c + C_2A^{-2} \tag{12}$$

where C_1, C_2, C_3 are free constants. Next, this reduced system can be decoupled into a triangular form, without any assumptions, by applying the hodograph transformation

$$A = F(U) \tag{13}$$

This yields

$$U'' = cU - s_1\tfrac{1}{p+1}U^{p+1} - s_2F(U)^2 + C_1 \tag{14}$$
$$U'^2 = \frac{(kC_1U + \frac{1}{2}kcU^2 - s_1\frac{1}{(p+2)(p+1)}kU^{p+2} - s_2((\frac{1}{4}c^2 + \omega) + kU)F(U)^2 - C_3)F(U)^2 - s_2{C_2}^2}{F(U)^2(\frac{1}{2}k + s_2F'(U)^2)} \tag{15}$$
$$\Phi' = \tfrac{1}{2}c + C_2F(U)^{-2} \tag{16}$$

The second-order ODE (14) now has the form of a nonlinear oscillator equation. It possesses the first integral

$$U'^2 = -s_2 2G(U) - s_1 \tfrac{2}{(p+1)(p+2)} U^{p+2} + cU^2 + 2C_1 U + 2C_4, \quad G(U) = \int F(U)^2 \, dU \tag{17}$$

where C_4 is an arbitrary constant. Equating equations (17) and (14), and replacing

$$F(U)^2 = G'(U), \quad F'(U) = 2G''(U)/F(U), \tag{18}$$

yields

$$\begin{aligned} &\tfrac{1}{2}(s_2 G(U) + s_1 \tfrac{1}{(p+1)(p+2)} U^{p+2} - \tfrac{1}{2} cU^2 - C_1 U - \tilde{C}_4) G''(U)^2 \\ &= (kU + \tfrac{1}{4}c^2 + \omega) G'(U)^2 - (kG(U) - s_2(\tilde{C}_3 + k\tilde{C}_4)) G'(U) + {C_2}^2 \end{aligned} \tag{19}$$

This is a second-order ODE for $G(U)$. Hence, the following result has been obtained.

Theorem 1.1 *Any solution of the second-order ODE* (19) *for* $G(U)$ *yields a solution of the ODE system* (10)–(12) *by quadratures: First, integrate ODE* (17)*, which is separable, to get* $U(\xi)$*. Second, substitute* $U(\xi)$ *into transformations* (18) *and* (13) *to get* $A(\xi)$*. Last, substitute* $A(\xi)$ *into ODE* (12) *and integrate to get* $\Phi(\xi)$*. The resulting expressions* $(U(\xi), A(\xi), \Phi(\xi))$ *give a frequency-modulated travelling wave* (3)*.*

An effective ansatz for solving the ODE (19) is to take $G(U)$ as a polynomial in U, whose degree is determined by balancing powers in the ODE (19). This leads to the expression

$$G(U) = -s_1 s_2 \tfrac{1}{(p+1)(p+2)} U^{p+2} + g_3 U^3 + g_2 U^2 + g_1 U + g_0 \tag{20}$$

where g_0, g_1, g_2, g_3 are constant parameters which can be determined from the ODE (19).

Solutions exist for $p = 1, 2, 3, 4$ and take the form

$$U(\xi) = b + s_3 h \operatorname{sech}^2\big(\sqrt{gh/2}\,\xi\big) \tag{21}$$

$$A(\xi) = \sqrt{g_1 + 2g_2 U(\xi) + 3g_3 U(\xi)^2 - s_1 s_2 \tfrac{1}{p+1} U(\xi)^{p+1}} \tag{22}$$

$$\Phi(\xi) = \frac{c}{2}\xi + C_1 \int_0^\xi \frac{d\xi}{A(\xi)^2} + \phi \tag{23}$$

where $s_3 = s_2 \operatorname{sgn}(g_3) = \pm 1$, $g = |g_3|$, $h = \frac{1}{2}\sqrt{d}/g$, $b = -\frac{1}{3}(s_3 h + (g_2 - s_2 \frac{1}{2} c)/g_3)$, $d = (c - s_2 2g_2)^2 + 12 g_3 (s_2 C_1 - g_1) > 0$. The wave profile U is similar to a KdV soliton, while the profile for A can have several different shapes depending on p and the solution parameters (k, c, ω, b, h) and the signs s_3, s_2, s_1. These parameters obey a set of equations and inequalities, which differ for each case of p. In each of the four cases, there is an allowed range for b and h.

Hence, large multi-parameter families of solitary waves are obtained.

References

[1] L.A. Cisneros-Ake, J.F. Solano Pelaez, Bright and dark solitons in the unidirectional long wave limit for the energy transfer on anharmonic crystal lattices, Physica D 346 (2017), 20–27.

[2] L.A. Cisneros-Ake, H. Parra Prado, D.J. Lopez Villatoro, R. Carretero-Gonzalez, Multi-hump bright solitons in a Schrodinger–mKdV system, Physics Letters A 382 (2018), 837–845.

[3] S.C. Anco and M.L. Gandarias, Symmetry multi-reduction method for partial differential equations with conservation laws, Commun. Nonlin. Sci. Numer. Simul. 91 (2020), 105349.

International Conference on Mathematical Analysis and Applications in Science and Engineering
ICMA^{2}SC'22
ISEP Porto-Portugal, June 27 - 29, 2022

About the structure of attractors for a nonlocal Chafee-Infante problem

Rubén Caballero Toro[1⋆] **Alexandre Carvalho**[2] **Pedro Marín-Rubio**[3] **José Valero** [1]

[1] Universidad Miguel Hernández, Spain
[2] Universidade de São Paulo, Brazil
[3] Universidad de Sevilla, Spain

[1⋆]ruben.caballero@umh.es,[2]andcarva@icmc.usp.br, [3]pmr@us.es, [1]jvalero@umh.es

Abstract: In this work, we study the structure of the global attractor for the multivalued semiflow generated by a nonlocal reaction-diffusion equation in which we cannot guarantee uniqueness of the Cauchy problem. In particular, we analyse the existence and properties of stationary points studying their stability. Therefore, we characterize the attractor in terms of the stationary points and their connections.

keywords: reaction-diffusion equations; nonlocal equations; global attractors; multivalued dynamical systems; structure of the attractor; stability

MSC2020: 35B40; 35B41; 35B51; 35K55; 35K57.

1 Introduction

If we consider the non-local equation

$$\frac{\partial u}{\partial t} - a(\|u\|^2_{H^1_0})\frac{\partial^2 u}{\partial x^2} = \lambda f(u) \tag{1}$$

with Dirichlet boundary conditions, then it is possible to define a suitable Lypaunov functional. In [1] it is shown that regular and strong solutions generate (possibly) multivalued semiflows having a global attractor which is described by the unstable set of the stationary points. In the case where the function f is odd and equation (1) generates a continuous semigroup the existence of fixed points of the type given in the Chafee-Infante problem was established in [2]. Moreover, if a is non-decreasing, then they coincide with the ones in the Chafee-Infante problem.

2 Setting of the problem

Previous results are extended for a more general function f: strictly concave if $u > 0$ and strictly convex if $u < 0$. Also, we will impose: $f \in C(\mathbb{R})$, $f(0) = 0$, $f'(0) = 1$, growth and dissipation conditions: for $p \geq 2$, $C_i > 0$, $i = 1, .., 4$, we have $|f(u)| \leq C_1 + C_2|u|^{p-1}$ and

$$f(u)u \leq C_3 - C_4|u|^p, \text{ if } p > 2, \quad \limsup_{u\to\pm\infty} \frac{f(u)}{u} \leq 0, \text{ if } p = 2.$$

It is worth mentioning that we focus on the particular situation where the domain is one-dimensional and the function f is of the type of the standard Chafee-Infante problem, for which the dynamics inside the attractor has been completely understood [3].

3 New results

Our goal is to describe the structure of the attractor as accurately as possible. For this aim, the first question tackled is about existence of solution.

Theorem 1 *Assume the existence of constants* $\beta, \gamma > 0$ *such that*

$$f(u)\, u \leq \gamma + \beta u^2 \text{ for all } u \in \mathbb{R}.$$

Then, for any $u_0 \in H_0^1(\Omega)$ *problem (1) has at least one strong solution.*

Using the property of upper semicontinuity, existence and characterization of the attractor is obtained. By this way, we focus on equilibria and we have the same dynamic than in the classical Chafee-Infante equation.

Theorem 2 *If* $\lambda \leq a(0)\, \pi^2 (k+1)^2$ *and* a *is non-decreasing, then there are exactly* $2k+1$ *fixed points:* $0,\ u^{\pm}_{1,d_1^*}, ..., u^{\pm}_{k,d_k^*}$. *Also, the only unstable fixed points are* 0 *and* $u^{\pm}_{k,d_k^*}$, $k \geq 2$.

Finally, in view of the lap number concept, we obtain that the only allowed connexion between equilibra are from those who have more zeros towards those with less. By this way, the global attractor $\mathcal{A}$ consists of the set of stationary points (which has $2n+1$ elements) and the bounded complete trajectories that connect them (the heteroclinic connections).

Acknowledgements

The author is a fellow of Programa FPU del Ministerio de Educación Cultura y Deporte, reference FPU15/03080.

References

[1] Caballero, R.; Marín-Rubio, P.; Valero, J. Existence and characterization of attractors for a nonlocal reaction-diffusion equation with an energy functional. *J. Dynamics Differential Equations* 2022, 34, 443-480.

[2] Carvalho, A.N.; Li, Y.; Luna, T.L.M.; Moreira, E. A non-autonomous bifurcation problem for a non-local scalar one-dimensional parabolic equation. *Commun. Pure Appl. Anal.* 2020, 19, 5181-5196.

[3] Henry, D. Some infinite-dimensional Morse-Smale systems defined by parabolic partial differential equations. *J. Differential Equations 1985*, 59, 165-205.

International Conference on Mathematical Analysis and Applications in Science and Engineering
ICMA^{2}SC'22

ISEP Porto-Portugal, June 27 - 29, 2022

THE CONDITIONAL REGULARITY OF THE WEAK SOLUTIONS TO THE NAVIER-STOKES EQUATIONS

Zdenek Skalak[1⋆]

[1] Czech Technical University, Prague, Thákurova 7, 166 29 Prague 6, Czech Republic

[1⋆]zdenek.skalak@cvut.cz

Abstract: We discuss several new regularity criteria for the weak solutions to the Navier-Stokes equations based on the rate of change of some fundamental physical quantities, like the velocity or pressure, along the streamlines. We compare these criteria with some results from the literature.

keywords: Navier-Stokes equations; optimal regularity criteria; velocity magnitude; pressure; kinetic energy.

MSC2020: 35Q30; 76D05.

1 Introduction and Presentation of Results

We consider the Navier-Stokes equations for the viscous incompressible fluid in the entire three-dimensional space, i.e.

$$\frac{\partial u}{\partial t} - \Delta u + u \cdot \nabla u + \nabla \pi = 0 \quad \text{in } \mathbb{R}^3 \times (0, \infty), \tag{1}$$

$$\nabla \cdot u = 0 \quad \text{in } \mathbb{R}^3 \times (0, \infty), \tag{2}$$

$$u|_{t=0} = u_0, \tag{3}$$

where $u = u(x,t) = (u_1(x,t), u_2(x,t), u_3(x,t))$ and $\pi = \pi(x,t)$ denote the velocity of the fluid and its pressure respectively. $u_0 = u_0(x)$ is the initial velocity.

If $u_0 \in L^2_\sigma$ (solenoidal functions from L^2) the problem (1) - (3) possesses at least one global weak solution $u \in L^\infty_{\text{loc}}([0,\infty); L^2_\sigma) \cap L^2_{\text{loc}}(0,\infty; W^{1,2})$ satisfying the energy inequality

$$||u(t)||_2^2 + 2\int_0^t ||\nabla u(\tau)||_2^2 \, d\tau \leq ||u_0||_2^2$$

for every $t \geq 0$. If moreover $u_0 \in L^2_\sigma \cap W^{1,2}$ then these solutions are regular on a time interval $(0, \delta)$, $\delta > 0$, which means that $\nabla u \in L^\infty_{\text{loc}}(0, \delta; L^2)$. As is well known the regularity of u on every interval $(0, T)$, $T > 0$, is an outstanding open problem (see [6] for the definitions and further details). Nevertheless, the regularity of u can be achieved by endowing it with some reasonable additional conditions. Mention here specifically a simple version of the following classical regularity result usually referred to as the Prodi-Serrin conditions: a weak solution u equipped with the initial condition $u_0 \in L^2_\sigma \cap W^{1,2}$ and satisfying the energy inequality is regular on $(0, T)$, $T > 0$, if $u \in L^p_{\text{loc}}(0, T; L^r)$, where $2/p + 3/r = 1$ and $r \in [3, \infty]$.

It is well known that if u and p solve the system (1) - (3) then the same is true for the rescaled functions u_η, p_η, $\eta > 0$, defined as

$$u_\eta(x,t) = \eta u(\eta x, \eta^2 t), \quad p_\eta(x,t) = \eta^2 p(\eta x, \eta^2 t).$$

The spaces $L^p(0,T;L^r)$, where $2/p + 3/r = 1$ are called critical since their norms are invariant with regard to the presented scaling, i.e. $||u||_{L^p(0,T;L^r)} = ||u_\eta||_{L^p(0,T/\eta^2;L^r)}$ for every $\eta > 0$. In this sense the Prodi-Serrin conditions are optimal.

We will now present several new optimal regularity criteria in terms of the rate of change of some fundamental physical quantities along the streamlines and compare these criteria with some famous criteria from the literature. In the following we denote $\hat{a} = a/|a|$ for any vector a.

Let us start with the criterion based on $\hat{u} \cdot \nabla |u|^\lambda$, $\lambda \in [1, \infty)$. As is discussed below, for $\lambda = 1$ and $\lambda = 2$ this quantity has a clear physical interpretation.

Theorem 1 *Let u be a weak solution of (1)–(3) satisfying the energy inequality and equipped with the initial condition $u_0 \in L^2_\sigma \cap W^{1,2}$. Suppose that $\lambda \in [1, \infty)$ and*

$$\hat{u} \cdot \nabla |u|^\lambda \in L^p_{loc}(0, \infty; L^r),$$

where $2/p + 3/r = 1 + \lambda$ and $r \in (\max(1, 3/(1+\lambda)), \infty)$. Then u is regular on $(0,T)$ for every $T > 0$.

If $\lambda = 1$ then Theorem 1 shows that controlling the rate of change of the velocity magnitude along the streamlines provides the regularity of the solution. Since obviously

$$\Big|\hat{u} \cdot \nabla |u|\Big| \leq |\nabla |u||,$$

it specially means that if $\nabla |u| \in L^p_{\text{loc}}(0, \infty; L^r)$ with $2/p + 3/r = 2$ and $r \in (3/2, \infty)$, then u is regular on $(0,T)$ for every $T > 0$. We can compare this result with a result by Vasseur who proved in [7] that the regularity is obtained if one is able to control the rate of change of the velocity direction. More precisely, he proved that if div $\hat{u} \in L^p_{\text{loc}}(0, \infty; L^r)$, where $2/p + 3/r = 1/2$ and $r \in [6, \infty]$, then u is regular on every $(0,T)$. So the above criterion for $\lambda = 1$ and the Vasseur's criterion are complementary: if one controls either the rate of change of the velocity direction or the rate of change of the velocity magnitude, the blow-up of the solution is excluded.

It is known (see [4]) that if $\partial_3 u \in L^p_{\text{loc}}(0, \infty; L^r)$, where $2/p + 3/r = 2$ and $r \in (3/2, 6]$, then u is regular on $(0,T)$ for every $T > 0$. The extension of this result to $r \in (6, \infty)$ is still an open problem. One can formulate a similar problem in terms of $\partial_3 |u|$: prove the regularity of u on every $(0,T)$ under the assumption that $\partial_3 |u| \in L^p_{\text{loc}}(0, \infty; L^r)$, where $2/p + 3/r = 2$ and $r \in (3/2, \infty)$. Since

$$|\partial_3 |u|| \leq \Big|\frac{\partial u}{\partial x_3}\Big|,$$

it is clear that the problem in terms of $\partial_3 |u|$ is stronger than the problem in terms of $\partial_3 u$. It is interesting to compare the problem in terms of $\partial_3 |u|$ with the above result for $\lambda = 1$. While in the first case we differentiate the velocity magnitude in a fixed direction and the problem has not yet been solved, in the second case $|u|$ is differentiated in the variable direction of the velocity and we have got an optimal criterion for every $r \in (3/2, \infty)$.

If $\lambda = 2$ then Theorem 1 shows that controlling the rate of change of the energy along the streamlines provides the regularity of the solution.

Theorem 2 *Let u be a weak solution of (1)–(3) satisfying the energy inequality and equipped with the initial condition $u_0 \in L^2_\sigma \cap W^{1,2}$. Then u is regular on $(0,T)$ for every $T > 0$ if*

$$\Psi \equiv ((\hat{u} \cdot \nabla)u) \cdot \hat{u} \in L^p_{loc}(0, \infty; L^r), \text{ where } \frac{2}{p} + \frac{3}{r} = 2 \text{ and } r \in \Big(\frac{3}{2}, \infty\Big). \tag{4}$$

While the vector $(\hat{u} \cdot \nabla)u$ is a derivative of the velocity in the direction of the velocity, Ψ from (4) is the projection of this vector into the velocity direction. The velocity is generally dependent on the space and time variables. If we replace the variable direction of the velocity by the fixed direction $(0, 0, 1)$, we get instead of Ψ only one item of the velocity gradient $\partial_3 u_3$. While the critical condition (4) yields the regularity, the regularity results in terms of $\partial_3 u_3$ are not even optimal (see e.g. [1], [2], [5] and [9]).

Theorem 3 *Let u be a weak solution of (1)–(3) satisfying the energy inequality and equipped with the initial condition $u_0 \in L^2_\sigma \cap W^{1,2}$. Let $\mathcal{P}$ be the associated pressure. Then u is regular on $(0, T)$ for every $T > 0$ if*

$$\nabla \mathcal{P} \cdot \hat{u} \in L^p_{loc}(0, \infty; L^q), \text{ where } \frac{2}{p} + \frac{3}{q} = 3 \text{ and } q \in (1, \infty). \tag{5}$$

Thus, controlling the derivative of the pressure along the streamlines yields the regularity. If we replace the direction $\hat{u}$ with the fixed direction $(0, 0, 1)$, i.e. if we differentiate the pressure not along the streamlines but in the fixed direction $(0, 0, 1)$ we obtain the criterion in terms of $\partial_3 \mathcal{P}$. Regarding this criterion, the best result reached so far is non-optimal and has been published in [8]. It says that u is regular if $\partial_3 \mathcal{P} \in L^p(0, T; L^q)$, where $2/p + 3/q = 2 + 1/q$ and $q \in (1, \infty)$.

Acknowledgments

The author was supported by the European Regional Development Fund,

project No. CZ.02.1.01/0.0/0.0/16_019/0000778.

References

[1] C. Cao, E.S. Titi, Global regularity criterion for the 3D Navier-Stokes equations involving one entry of the velocity gradient tensor, Arch. Rational Mech. Anal. **202** (2011), 919–932.

[2] D. Fang, C. Qian, The regularity criterion for 3D Navier-Stokes equations involving one velocity gradient component, Nonlinear Analysis **78** (2013), 86–103.

[3] Z. Guo, P. Kucera, Z. Skalak, The application of anisotropic Troisi inequalities to the conditional regularity for the Navier-Stokes equations, Nonlinearity **31** (2018), 3707–3725.

[4] H. Chen, D. Fang, T. Zhang, Remark on the regularity criteria for Navier-Stokes equations in terms of one direcional derivative of the velocity, arXiv:2007.10888v1 [math.AP] 21 Jul 2020.

[5] Z. Skalak, A regularity criterion for the Navier-Stokes equations via one diagonal entry of the velocity gradient, Comm. Math. Sci. **19** (2021), 1101–1112.

[6] H. Sohr, *The Navier-Stokes Equations, An Elementary Functional Analytic Approach*. Birkhäuser Verlag, Basel, Boston, Berlin 2001.

[7] A. Vasseur, Regularity criterion for 3D Navier-Stokes equations in terms of the direction of the velocity, Appl. Math. **54** (2009), 47–52.

[8] Z. Zhang, Navier-Stokes equations with regularity in one directional derivative of the pressure, Math.Meth.Appl.Sci. **38** (2015), 4019–4023.

[9] Y. Zhou, M. Pokorný, On the regularity of the solutions of the Navier-Stokes equations via one velocity component, Nonlinearity **23** (2010), 1097–1107.

International Conference on Mathematical Analysis and Applications in Science and Engineering
ICMA^{2}SC'22
ISEP Porto-Portugal, June 27 - 29, 2022

Precise Laplace approximation for mixed rough differential equation

Yong Xu[1⋆] **Xiaoyu Yang** [1] **Bin Pei**[1]

[1] Northwestern Polytechnical University, Xi'an, 710072, China

[1⋆]hsux3@nwpu.edu.cn

Abstract: This work focuses on the Laplace approximation for the rough differential equation (RDE) driven by mixed rough path (B^H, W) with $H \in (1/3, 1/2)$ as $\varepsilon \to 0$. Firstly, based on geometric rough path lifted from mixed fractional Brownian motion (fBm), the Schilder-type large deviation principle (LDP) for the law of the first level path of the solution to the RDE is given. Due to the particularity of mixed rough path, the main difficulty in carrying out the Laplace approximation is to prove the Hilbert-Schmidt property for the Hessian matrix of the Itô map restricted on the Cameron-Martin space of the mixed fBm. To this end, we imbed the Cameron-Martin space into a larger Hilbert space, then the Hessian is computable. Subsequently, the probability representation for the Hessian is shown. Finally, the Laplace approximation is constructed, which asserts the more precise asymptotics in the exponential scale.

keywords: Large deviation principle; Laplace approximation; Mixed rough path; fractional Brownian motion.
MSC2020: 60F10; 60G22; 60H10.

1 Introduction

In this paper, we consider the rough differential equation (RDE) driven by mixed rough paths as follows,

$$dY_t^\varepsilon = \left[\sigma\left(Y_t^\varepsilon\right)|\hat{\sigma}\left(Y_t^\varepsilon\right)\right]\varepsilon d(B^H, W)_t + \beta\left(\varepsilon, Y_t^\varepsilon\right)dt, \quad Y_0^\varepsilon = 0, \tag{1}$$

where $\varepsilon > 0$ is a small parameter. And $[\sigma|\hat{\sigma}]$ denotes the block matrix with $\sigma \in C_b^\infty\left(\mathbb{R}^n, \mathrm{Mat}(n, d_1)\right)$ and $\hat{\sigma} \in C_b^\infty\left(\mathbb{R}^n, \mathrm{Mat}(n, d_2)\right)$, and $\beta \in C_b^\infty\left([0,1] \times \mathbb{R}^n, \mathbb{R}^n\right)$ with C_b^∞ being the set of bounded smooth functions with bounded derivatives. $(B^H, W)_t \in G\Omega_p(\mathbb{R}^{d_1+d_2})$, where $G\Omega_p(\mathbb{R}^{d_1+d_2})$ is the geometric rough path space, represents the mixed geometric rough path, which will be introduced in Section 2. Let $\left(\Omega, \mathcal{F}, \{\mathcal{F}_t\}_{t\geq 0}, \mathbb{P}\right)$ be a completely probability space, $(b_t^H)_{t\geq 0}$ is $\mathbb{R}^{d_1}$-valued fractional Brownian motion (fBm) with Hurst index $H \in (1/3, 1/2)$, $(w_t)_{t\geq 0}$ is $\mathbb{R}^{d_2}$-valued Brownian motion (Bm). For each time t, we denote by $\mathcal{F}_t$ the σ-field generated by the random variables $\{(b_s^H, w_s), 0 \leq s \leq t\}$ and all $\mathbb{P}$-null sets. The expectation with respect to $\mathbb{P}$ is denoted by $\mathbb{E}$.

Let $Y^\varepsilon = \hat{\Phi}_\varepsilon(\varepsilon(B^H, W), \lambda) : G\Omega_p\left(\mathbb{R}^{d_1+d_2+1}\right) \mapsto G\Omega_p\left(\mathbb{R}^n\right)$ denote the Itô map corresponding to (1) with $\lambda_t = t$. The purpose of this paper is to prove the Laplace approximation for $Y^{\varepsilon,1}$ under natural assumptions, the first level path of the solution map,

$$J(\varepsilon) := \mathbb{E}\left[\exp\left(-\frac{F\left(Y_t^{\varepsilon,1}\right)}{\varepsilon^2}\right)\right], \tag{2}$$

where F is a suitable real-valued bounded continuous function. See Section 2 for precise assumptions.

To investigate the precise Laplace asymptotics for the first level path of Y_t^ε, firstly, we prove that the mixed fBm can be lifted to the mixed geometric rough path. Then, we give the Schilder-type LDP for the laws of the first level path of the solution to the above RDE (1), which provides the asymptotics of $J(\varepsilon)$ with $\varepsilon \to 0$ on logarithmic scale. Furthermore, it proceeds to show the Laplace approximation, providing more precise asymptotics in the exponential scale. Due to the particularty of mixed rough path, the main difficulty in carrying out the Laplace asymptotics is to analyze Hilbert-Schmidt property for the Hessian matrix of the Itô map restricted on the Cameron-Martin space. To this end, we imbed the Cameron-Martin space into a larger Hilbert space. We prove the Hilbert-Schmidt property with an orthonormal basis in this Hilbert space. Then, the probability representation for the Hessian is analyzed. Finally, the precise Laplace asymptotics for RDE driven by mixed rough path is constructed.

2 Results and discussion

Denote $C_0^{p-\mathrm{var}}(\mathbb{R}^n)$ the space of continuous paths in $\mathbb{R}^n$ with p-variation ($2 < p < 3$) starting at 0. Let $Y^\varepsilon = \hat{\Phi}_\varepsilon(\varepsilon(B^H, W), \lambda) : G\Omega_p\left(\mathbb{R}^{d_1+d_2+1}\right) \mapsto G\Omega_p\left(\mathbb{R}^n\right)$ denote the Itô map corresponding to (1) with $\lambda_t = t$. Denote the $Y^{\varepsilon,1}$ is the first level path of the solution map. Consider the solution map $\hat{\Phi}_\varepsilon(\varepsilon(B^H, W) + (\gamma, \eta), \lambda)$,

$$d\tilde{Y}_t^\varepsilon = \left[\sigma\left(\tilde{Y}_t^\varepsilon\right)|\hat{\sigma}\left(\tilde{Y}_t^\varepsilon\right)\right](\varepsilon d(B^H, W)_t + (\gamma_t, \eta_t)^{\mathrm{T}}) + \beta\left(\varepsilon, \tilde{Y}_t^\varepsilon\right)dt, \quad \tilde{Y}_0^\varepsilon = 0. \tag{3}$$

Denote $\phi^{(\varepsilon)} = \tilde{Y}^{\varepsilon,1}$ the first level path of the solution map. Now $\hat{\Phi}_0((\gamma, \eta), \lambda)$ is the solution map lying above $\phi^0 = \Psi(\gamma, \eta) \in C_0^{q-\mathrm{var}}\left(\mathbb{R}^n\right)$ with $1 < q < 2$, satisfying that

$$d\phi_t^0 = \left[\sigma\left(\phi_t^0\right)|\hat{\sigma}\left(\phi_t^0\right)\right]d(\gamma_t, \eta_t)^{\mathrm{T}} + \beta\left(0, \phi_t^0\right)dt, \quad \phi_0^0 = 0. \tag{4}$$

We assume

A1. The function F is real-valued bounded continuous on $C_0^{p'-\mathrm{var}}(\mathbb{R}^n)$ with $p' > 1/H$.

A2. The function $F_\Lambda := F \circ \Phi + ||(\cdot, \cdot)||_{\mathcal{H}}^2/2$ attains its minimum at a unique point $(\gamma, \eta)^{\mathrm{T}} \in \mathcal{H}$, with $\Phi(\gamma, \eta) = \phi^0$.

A3. The function F is $m+3$ times Fréchet differentiable on a neighborhood $U(\phi^0)$ with $\phi^0 \in C_0^{p'-\mathrm{var}}(\mathbb{R}^n)$. Furthermore, there exist positive constants $M_1, M_2, \cdots$ such that

$$\left|\nabla^j F(\eta)\langle z, \ldots, z\rangle\right| \le M_j \|z\|_{p'-\mathrm{var}}^j \quad (j = 1, \ldots, m+3),$$

hold for any $\eta \in U(\phi^0)$ and $z \in C_0^{p'-\mathrm{var}}(\mathbb{R}^n)$.

A4. The bounded self-adjoint operator A on $\mathcal{H}$, which is related to the Hessian matrix $\nabla^2(F \circ \Psi)(\gamma, \eta)\big|_{\mathcal{H}\times\mathcal{H}}$, is strictly larger than $-Id_{\mathcal{H}}$.

Then, here follows our main result.

Theorem 2.1 *Under Assumptions* (A1)-(A4)*, we have the following asymptotic expansion with* $\varepsilon \to 0$*. There exist constants* $c, \alpha_0, \alpha_1, \cdots$ *s.t.*

$$\mathbb{E}\left[\exp\left(-F\left(Y^{\varepsilon,1}\right)/\varepsilon^2\right)\right] = \exp\left(-F_\Lambda(\gamma, \eta)/\varepsilon^2\right)(-c/\varepsilon) \cdot \left(\alpha_0 + \alpha_1\varepsilon + \cdots + \alpha_m\varepsilon^m + O\left(\varepsilon^{m+1}\right)\right), \tag{5}$$

for any $m \ge 0$.

3 Conclusions and Future work

In this work, we lift the mixed fBm to the mixed geometric rough path. Based on the LDP, the precise Laplace asymptotics for RDE driven by mixed rough path is constructed. Delays are ubiquitous in many fields, and it has received attention in a long time. As a result, it is worthy to studying the precise Laplace asymptotics for rough functional differential equations driven by rough paths in the future.

Acknowledgments

This work was partly supported by the NSF of China (Grant 12072264), the Shaanxi Provincial Key R&D Program (Grants 2020KW-013, 2019TD-010).

International Conference on Mathematical Analysis and Applications in Science and Engineering
ICMA^{2}SC'22

ISEP Porto-Portugal, June 27 - 29, 2022

VIRTUAL OPERATORS GENERATED BY OPERATOR FAMILIES

Vladimir Vasilyev

Belgorod State National Research University, Russia

vbv57@inbox.ru

Abstract: We consider special classes of linear bounded operators in Banach spaces and suggest certain operator variant of symbolic calculus. It permits to describe Fredholm properties of elliptic pseudo-differential operator on manifolds with non-smooth boundaries.

keywords: local operator; Fredholmness; index.

MSC2020: 35S15; 47A05; 58J05.

1 Introduction

We consider some abstract so called local operators acting in some functional spaces. Such operators and corresponding equations plays important role in the theory of pseudo-differential operators and equations. There are a few approaches to the theory of pseudo-differential operators and equations on non-smooth manifolds and manifolds with non-smooth boundarues, but it seems the suggested abstract variant is very close to this theory. Some first steps were done in the author's papers [1,2], and here we present this abstract variant and give some applications.

2 Results and discussion

2.1 General concept

Let M be a compact m-dimensional manifold with a boundary ∂M, and $A(x)$ be a certain operator-function defined on M. Let $M_k, k = 0, 1, ..., m-1$, be smooth k-dimensional sub-manifolds on ∂M so that by definition $M_{m-1} \equiv \partial M, M_0$ consists of isolated points on ∂M. Further, we introduce a set of operator classes $\mathfrak{T}_k, k = 0, 1, ..., m$, so that for $x \in M_k$, $A(x) : H_k^{(1)} \to H_k^{(2)}$ is a linear bounded operator, where $H_k^{(j)}, k = 0, 1, ..., m, j = 1, 2$, are some Banach spaces.

We say that sub-manifold M_k is a singular k-sub-manifold if $\forall x \in M_k$ we have $A(x) \in \mathfrak{T}_k$. Additionally, we will assume that if $x \in M_r \cap M_{k-1} \neq \emptyset$ then $A(x) \in \mathfrak{T}_{k-1}$.

Theorem 1. *If the family $A(x)$ consists of local Fredholm operators and this family is continuous on each component $\overline{M_k \setminus \cup_{i=0}^{k-1} M_i}, k = 0, 1, ..., m$, then it generates a unique Fredholm operator A acting in the spaces $\sum_{k=0}^{m} \oplus H_k^{(1)} \to \sum_{k=0}^{m} \oplus H_k^{(2)}$.*

2.2 Pseudo-differential operators

We consider a certain integro-differential operator A on m-dimensional compact manifold M with a boundary. This operators is defined by the function $A(x,\xi),(x,\xi) \in \mathbf{R}^{2m}$. We will suppose that the symbol has the order $\alpha \in \mathbf{R}$, i.e.

$$c_1(1+|\xi|)^\alpha \le |A(x,\xi)| \le c_2(1+|\xi|)^\alpha,$$

for all admissible x,ξ with universal positive constants c_1, c_2.

We consider such a compact manifold M with a boundary that there are some smooth compact sub-manifolds M_k of dimension $0 \le k \le m-1$ on the boundary ∂M of manifold M which are singularities of a boundary. These singularities are described by a local representative of operator A in a point $x_0 \in M$ on the map $U \ni x_0$ in the following way

$$(A_{x_0}u)(x) = \int\limits_{D_{x_0}} \int\limits_{\mathbf{R}^m} e^{i\xi\cdot(x-y)} A(\varphi(x_0),\xi)u(y)d\xi dy, \quad x \in D_{x_0},$$

where $\varphi : U \to D_{x_0}$ is a diffeomorphism, and the canonical domain D_{x_0} has a distinct form depending on a placement of the point x_0 on manifold M. We consider following canonical domains D_{x_0}: $\mathbf{R}^m, \mathbf{R}^m_+ = \{x \in \mathbf{R}^m : x = (x', x_m), x_m > 0\}, W^k = \mathbf{R}^k \times C^{m-k}$, where C^{m-k} is a convex cone in $\mathbf{R}^{m-k}$. For instance, if we consider a cube Q in 3-dimensional space then we have 4 canonical domains: $\mathbf{R}^3$ for inner points, $\mathbf{R}^3_+ = \{x \in \mathbf{R}^3 : x = (x_1,x_2,x_3), x_3 > 0\}$ for six 2-faces, $\mathbf{R} \times C^2 = \{x \in \mathbf{R}^3 : x = (x_1,x_2,x_3), x_>0, x_3 > 0\}$ for twelve 1-dimensional edges, and $C^3 = \{x \in \mathbf{R}^3 : x = (x_1,x_2,x_3), x_1 > 0, x_2 > 0, x_3 > 0\}$ for eight vertices.

Such an operator A will be considered in Sobolev–Slobodetskii spaces $H^s(M)$, and local variants of such spaces will be spaces $H^s(D_{x_0})$.

Definition 1. *The symbol of an operator A is called the operator-function $A(x) : M \to \{A_x\}_{x\in M}$ which is defined by local representatives of the operator A.*

Under some additional assumptions on smoothness properties of the function $A(x,\xi)$ one has the following

Theorem 2. *The operator A has a Fredholm property iff its symbol is composed by Fredholm operators.*

Definition 2. *An operator A is called an elliptic operator if its symbol is composed by invertible operators.*

Corollary 1. Elliptic operator is a Fredholm operator.

Theorem 3. *If the classical elliptic symbol $A(x,\xi)$ admits k-wave factorization with respect to the cones C^{m-k} with indices $æ_k(x), k = 0,1,\cdots,m-2$ satisfying the condition*

$$|æ_k(x) - s| < 1/2, \quad \forall x \in M_k, \quad k = 0,1,\cdots,m-1,$$

then the operator $A : H^s(M) \to H^{s-\alpha}(M)$ has a Fredholm property.

3 Conclusions and Future work

We have described a new approach to constructing the theory of pseudo-differential equations and related boundary value problems. This approach is based on general principles for special local operators.

In our opinion such considerations will be useful for discrete situations in which pseudo-differential operators are defined in functional spaces of discrete variable. Some first considerations in this direction were done, for example, in *Math. Model. Anal.*, 2018, **23**, 492–506. Moreover, discrete situation is more accessible, since it permits to apply computer calculations. We hope to develop these studies in this direction including a comparison between discrete and continuous cases.

Acknowledgments

This work was supported by the State contract of the Russian Ministry of Science and Education (contract No 1.7311.2017/8.9).

References

[1] V.B. Vasilyev, Elliptic operators and their symbols, Demonstr. Math. **52**(1) (2019), 361–369.

[2] V.B. Vasilyev, Operator symbols. II. ArXiv: Math.FA/1911.08099, pp. 1–13.

International Conference on Mathematical Analysis and Applications in Science and Engineering
ICMA^{2}SC'22
ISEP Porto-Portugal, June 27 - 29, 2022

A five dimensional model with two distributed time delays

L. Harding[1] **E. Kasilik**[2⋆] **M. Neamţu**[3⋆] **Loredana F. Vesa**[24⋆]

[1] University of East Anglia, School of Economics, Norwich Research Park, United Kingdom
[2] Dept. of Mathematics and Computer Science, West University of Timişoara, Romania
[3] Dept. of Economics and Economic Modelling, West University of Timişoara, Romania
[4] Dept. of Mathematics, Politehnica University of Timişoara, Romania
⋆ Institute for Advanced Environmental Research, West University of Timişoara, Romania

[24⋆]loredana.vesa@e-uvt.ro

Abstract: The purpose of this paper is to build and analyse a model of labour market slack considering unemployment along with employment in which the number of hours is limited to a level below that preferred by employees, which thus become 'underemployed'. The distributed time are considered into the policy respons. We observe jobs separation and matching, but also moves in and out of underemployment, as well as allowing for migration to an open economy with delayed policy intervention. We analyse the stability behaviour of the resulting equilibrium for our dynamic system, including models with Dirac and weak kernels. The numerical simulations support the theoretical results.

keywords: unemployment model; stability analysis; time delays

MSC2020: 49-XX; 34-XX; 92-XX.

1 Introduction

With the focus on understanding the dynamics of unemployment, in a previous mathematical model (investigated in [8]), using some concepts from [5, 3], the following variables were considered: number of unemployed, employed, and new vacancies; a time delay has been incorporated into the rate of change for the creation of new vacancies.

Furthermore, Misra et al. [6] demonstrated the link between the improvement of workers' capabilities and the reduction of unemployment by utilizing skill development programs. The impact of training programs has also been investigated in [1]. Moreover, Harding and Neamţu [2] considered migration as a contributing factor when defining unemployment policies, including distributed time delay. In [7, 4], the optimal control analysis has been completed.

In [3] we investigated the interaction between the number of unemployed people, immigrants, temporary employees, regularly employed people, and the number of available vacancies in the setting up of delay differential equations. The distributed time delay has been included to reflect the rate of change in available vacancies' dependence on past regular employment levels. The global asymptotic stability findings are presented both for the employment free equilibrium and the positive equilibrium.

The present paper proposes a five-dimensional mathematical model for studying unemployment, based on the past history of the state variables.

We reconsider the possibility of 'time limited jobs' or underemployment, as an intermediary status in the labour market - between regular employment and unemployment. Our system allows for both job creation, as well as policy intervention to limit unemployment, but also the possibility that migrants are taking some of the regular positions.

The potential impact of our findings is related to upcoming biological and economical mathematical models connected to population dynamics.

The most important benefit could be related to the strategic policy makers of our society. Our system allows for both job creation, as well as policy intervention to limit unemployment, but also the possibility that migrants are taking some of the regular positions.

2 Results and discussion

In this paper, our aim was to test the significance of taking underemployment and migration into account when formulating policy to address unemployment. Consequently, the proposed model is described by a nonlinear differential system with distributed time delays as follows:

$$\begin{cases} \dot{U}(t) = a_1 - a_2U(t)V(t) + a_3R(t) - a_4U(t) + a_5T(t) - b_1\int_0^\infty h_1(s)U(t-s)ds \\ \dot{M}(t) = m_1 - m_2M(t)V(t) - b_2M(t) \\ \dot{T}(t) = a_4U(t) - a_5T(t) - c_1T(t)V(t) - b_3T(t) \\ \dot{R}(t) = a_2U(t)V(t) + m_2M(t)V(t) + c_1T(t)V(t) - a_3R(t) - b_4R(t) \\ \dot{V}(t) = b_4\int_0^\infty h_2(s)R(t-s)ds - b_5V(t) \end{cases} \tag{1}$$

We take into account the following variables: the number of unemployed persons U, the number of immigrants M, the number of those underemployed or persons working limited hours T, the number of regularly employed persons R, and the number of available vacancies V. All the parameter are positive real numbers. The integral terms appearing in system (1) represent distributed time delays with the kernel functions h_1 and h_2 which are probability density functions.

The positivity and boundedness of solutions are provided and the local asymptotic stability findings are presented both for the employment free equilibrium and the positive equilibrium according to distributed time delays.

In the absence of delays the equilibrium point is locally asymptotically stable, if the system parameters satisfies certain conditions. In addition in the absence of the delay in the first equation of system (1) the positive equilibrium point is globally asymptotically stable if the rate of firing from regular employment is zero [3].

In the presence of two distributed time delays in system (1), if the basic reproduction number R_0, which has the role of a threshold parameter that prognosticate whether the unemployment, immigration and underemployed problems will increase or decrease, is less than 1 then the employment free equilibrium point is locally asymptotically stable under some conditions, otherwise is unstable, for any choice of the delay kernels. In the case of Dirac kernels, it is proved that there is a Hopf bifurcation and as a result, the stable equilibrium becomes unstable as the delay crosses some critical values. Moreover, for the positive equilibrium point of the system (1), the Hopf bifurcation curves are found numerically and the stability region is plotted in the parameter plane of the two average time delays.

We thus observed the evolution of unemployment, underemployment, regular employment, migration, market jobs and government supported vacancies with a delayed policy intervention.

3 Conclusions and Future work

The paper introduced a five-dimensional mathematical model that facilitates the understanding of new ways for studying the labour market while observing the levels of unemployment, migration, fixed term contractors, full time employment and the number of available vacancies. Two distributed time delays have been considered.

Where both kernels are weak Gamma kernels, under some conditions of parameters, the equilibrium point is locally asymptotically stable.

As a future work we develop the mathematical model proposed by introducing control and we study the model in the framework of stability theory and bifurcations.

References

[1] Raneah Al-Maalwi, Sarah Al-Sheikh, HA Ashi, and Sharefa Asiri. Mathematical modeling and parameter estimation of unemployment with the impact of training programs. *Mathematics and Computers in Simulation*, 182:705–720, 2021.

[2] L. Harding and M. Neamţu. A dynamic model of unemployment with migration and delayed policy intervention. *Computational Economics*, 51(3):427–462, 2018.

[3] Eva Kaslik, Mihaela Neamţu, and Loredana Flavia Vesa. Global stability analysis of an unemployment model with distributed delay. *Mathematics and Computers in Simulation*, 185:535–546, 2021.

[4] U.K. Mallick and Md.H.A. Biswas. Optimal analysis of unemployment model taking policies to control. *Advanced Modeling and Optimization*, 20(1):303–312, 2018.

[5] A.K. Misra and Arvind K. Singh. A delay mathematical model for the control of unemployment. *Differential Equations and Dynamical Systems*, 21(3):291–307, 2013.

[6] A.K. Misra, Arvind K. Singh, and Pushkar Kumar Singh. Modeling the role of skill development to control unemployment. *Differential Equations and Dynamical Systems*, pages 1–13, 2017.

[7] S.B. Munoli, S.R. Gani, and S.R. Gani. A mathematical approach to employment policies: An optimal control analysis. *International Journal of Statistics and Systems*, 12(3):549–565, 2017.

[8] C.V. Nikolopoulos and D.E. Tzanetis. A model for housing allocation of a homeless population due to a natural disaster. *Nonlinear Analysis: Real World Applications*, 4(4):561–579, 2003.

International Conference on Mathematical Analysis and Applications in Science and Engineering
ICMA^{2}SC'22
ISEP Porto-Portugal, June 27 - 29, 2022

Increasing the applicability of Chebyshev-Secant-type methods

Nisha Yadav[1⋆] **Sukhjit Singh**[1] **M.A. Hernández-Verón**[2] **Eulalia Martínez**[3]

[1] Department of Mathematics,
Dr B. R. Ambedkar National Institute of Technology, Jalandhar, India.
[2] Dept. of Mathematics and Computation,
University of La Rioja. Logroño, Spain.
[3] Instituto Universitario de Matemática Multidisciplinar,
Universitat Politècnica de València. València, Spain.

[1⋆]nisha.ma.21@nitj.ac.in,[1]kundalss@nitj.ac.in,
[2]mahernan@unirioja.es,[3]eumarti@mat.upv.es

Abstract: In this study, we introduce a new semilocal convergence result for derivative free improved Chebyshev-Secant-type methods (ICSTM) under weaker conditions using auxiliary points. The existence and uniqueness theorem is established for the solution using recurrence relations. The domain of parameters is also presented for both differentiable and non-differentiable cases. Finally, a nonlinear integral equation of mixed Hammerstein type arising in electro-magnetic fluid dynamics, dynamic models of chemical reactors, and vehicular traffic theory is considered to check the applicability of our work. It can be easily observed that improved convergence domains are obtained as compared to earlier studies [4].

keywords: Chebyshev-Secant-type method; Semilocal Convergence; Recurrence Relations; Domain of parameters; Nonlinear Integral Equations.

MSC2020: 45G10; 47H99; 65J15.

1 Introduction

Many real life problems occuring in various fields of Science and Engineering can be expressed in the form

$$\mathcal{H}(\vartheta) = 0, \tag{1}$$

where $\mathcal{H} : \mathcal{D} \subseteq Y \to Z$ is nonlinear operator which is defined on a non-empty open convex domain $\mathcal{D}$ of a Banach space Y to Z. Sometimes we are not able to obtain a closed form solution to (1), so we use iterative approaches to solve these equations. The most commonly used iterative methods for approximating the solution is the Newton's method [1] and it is defined by

$$\vartheta_0 \in \mathcal{D}, \qquad \vartheta_{i+1} = \vartheta_i - [\mathcal{H}^{'}(\vartheta_i)]^{-1}\mathcal{H}(\vartheta_i), \quad i \geq 0. \tag{2}$$

This method has good accessibility, quadratic convergence and minimal operational cost.

To obtain derivative-free techniques, it is general to approximate derivatives by divided differences (see [2, 3]). In [4], the improved Chebyshev-Secant-type methods (ICSTM) for non-differentiable operator are established and given by

$$\begin{aligned} \vartheta_{i+1} &= \vartheta_i - A_i^{-1}\mathcal{H}(\vartheta_i), \quad A_i = [\vartheta_i, \nu_i; \mathcal{H}], \\ \omega_i &= \vartheta i + a(\vartheta_{i+1} - \vartheta_i), \\ \nu_{i+1} &= \vartheta_i - A_i^{-1}(b\mathcal{H}(\vartheta_i) + c\mathcal{H}(\omega_i)), \quad i \geq 0, \end{aligned} \tag{3}$$

where $\vartheta_0, \nu_0 \in \mathcal{D}$ are two initial points, a, b and c are non-negative real parameters and $[\nu, \omega; \mathcal{H}] \in L(Y, Z)$ is a bounded linear first-order divided difference. The semilocal convergence, domain of parameters and dynamics of ICSTM (3) are established in [4] and convergence analysis is discussed by using recurrence relations on first-order divided differences with weaker continuity conditions.

In this work, we analyze the semilocal convergence of the method (3) by using conditions on the initial approximation and auxiliary points. Recurrence relations are established using auxiliary points under more generalized conditions [5] for non-differentiable operators. Further, we discuss the domain of parameters for both differentiable and non-differentiable operators.

2 Semilocal convergence analysis

In this section, we establish the semilocal convergence analysis of ICSTM (3) under the following (S) conditions:

(S1) There exist $\vartheta_0, \nu_0, \tilde{\vartheta} \in \mathcal{D}$, $\mu > 0$, $\theta > 0$, such that $\|\vartheta_0 - \tilde{\vartheta}\| = \mu$, $\|\vartheta_0 - \nu_0\| = \theta$, $[\tilde{\vartheta}, \vartheta_0; \mathcal{H}]^{-1} \in L(Z, Y)$ and $\|[\vartheta_0.\nu_0; \mathcal{H}]^{-1}\mathcal{H}(\vartheta_0)\| \leq \eta$.

(S2) $\|[\tilde{\vartheta}, \vartheta_0; \mathcal{H}]^{-1}([\nu, \omega; \mathcal{H}] - [y, z; \mathcal{H}])\| \leq \rho(\|\nu - y\|, \|\omega - z\|)$ holds for all $\nu, \omega, y, z \in \mathcal{D}$ with $\nu \neq \omega$ and $y \neq z$, where $\rho : \mathbb{R}_+ \times \mathbb{R}_+ \to \mathbb{R}_+$ is a non-decreasing continuous function in both arguments.

(S2') $\|[\tilde{\vartheta}, \vartheta_0; \mathcal{H}]^{-1}([\nu, \omega; \mathcal{H}] - [\tilde{\vartheta}, \vartheta_0; \mathcal{H}])\| \leq \rho_0(\|\nu - \tilde{\vartheta}\|, \|\omega - \vartheta_0\|)$ holds for all $\nu, \omega \in \mathcal{D}$ with $\nu \neq \omega$, where $\rho_0 : \mathbb{R}_+ \times \mathbb{R}_+ \to \mathbb{R}_+$ is a non-decreasing continuous function in both arguments.

(S3) $(1 - b) = c(1 - a)$ with $a \in (0, 1]$.

(S4) The equation

$$(\chi_0(\kappa) + 1 - \chi(\kappa))\eta - (1 - \chi(\kappa))\kappa = 0 \tag{4}$$

where $\chi_0(\kappa) = \dfrac{\mathcal{M}}{1 - \rho_0(\mu + \kappa, \kappa)}$, $\chi(\kappa) = \dfrac{\mathcal{N}}{1 - \rho_0(\mu + \kappa, \kappa)}$,
$\mathcal{M} = \max\left(\dfrac{ac\rho(\eta, \theta)}{1 - \rho_0(\mu, \theta)}, \rho(\eta, \theta), a\rho(\eta, \theta)\right)$ and $\mathcal{N} = \max(ac\rho(\eta, \eta), \rho(\eta, \eta))$, has atleast one positive root and let r be the smallest root.

(S5) $B(\vartheta_0, r) \subseteq \mathcal{D}$ and $\chi_0(r) + \chi(r) < 1$.

Under the above conditions, we can prove the following recurrence relations for $q \geq 2$ and existence-uniqueness theorem for the solution of (1) :

(i_q) $\|\vartheta_{q+1} - \vartheta_q\| \leq \chi(r)\|\vartheta_q - \vartheta_{q-1}\| \leq \chi(r)^{q-1}\|\vartheta_2 - \vartheta_1\| \leq \chi(r)^{q-1}\chi_0(r)\|\vartheta_1 - \vartheta_0\| < \eta$,

(ii_q) $\|\vartheta_{q+1}-\vartheta_0\| \leq \|\vartheta_{q+1}-\vartheta_q\| + \|\vartheta_q-\vartheta_{q-1}\| + \ldots + \|\vartheta_1-\vartheta_0\|$
$\leq (\chi(r)^{q-1} + ... + \chi(r) + 1)\|\vartheta_2-\vartheta_1\| + \|\vartheta_1-\vartheta_0\|$
$< \dfrac{1}{1-\chi(r)}\|\vartheta_2-\vartheta_1\| + \|\vartheta_1-\vartheta_0\| < \left(1+\dfrac{\chi_0(r)}{1-\chi(r)}\right)\eta = r,$

(iii_q) $\|\nu_{q+1}-\vartheta_{q+1}\| \leq \chi(r)\|\vartheta_{q+1}-\vartheta_q\|,$

(iv_q) $\vartheta_{q+1}, \nu_{q+1} \in B(\vartheta_0, r).$

Theorem 1 *Assume that the conditions* (S) *are satisfied. Then, the sequences* $\{\vartheta_i\}$, $\{\nu_i\}$ *and* $\{\omega_i\}$ *generated by the method* (3) *are well defined, remains in* $B(\vartheta_0, r)$ *for each* $i = 0, 1, 2, ...$ *and converges to a unique solution* $\vartheta^* \in \overline{B(\vartheta_0, r)}$ *of* (1).

3 Conclusions

The semilocal convergence analysis of Chebyshev-Secant-type methods is presented for solving nonlinear equations in Banach spaces. The sufficient convergence conditions involving auxiliary points are weaker than in previous studies. Further, the convergence domains are established for the solution. We have also discussed the domain of parameters for both differentiable and non-differentiable cases. Numerical examples involving nonlinear mixed Hammerstein-type integral problems are worked out and obtained the larger convergence domains as compared to earlier studies [4].

Acknowledgments

This research was partially supported by the project Ministerio de Economía y Competitividad under grant PGC2018-095896-B-C21-C22 and EEQ/2018/000720 under DST-SERB and Ministry of Human Resource Development, New Delhi, India.

References

[1] J. A. Ezquerro and M. A. Hernández-Verón, Mild differentiability conditions for Newton's method in Banach spaces, Springer Nature, 2020.

[2] I. K. Argyros, J. A. Ezquerro, J. M. Gutiérrez, M. A. Hernández-Verón, and S. Hilout, On the semilocal convergence of efficient Chebyshev–Secant-type methods, Journal of Computational and Applied Mathematics, **235**(10) (2011), 3195–3206.

[3] I. K. Argyros and H. Ren, On the semilocal convergence of derivative free methods for solving nonlinear equations, Journal of Numerical Analysis and Approximation Theory, **41**(1) (2012), 3–17.

[4] A. Kumar, D. K. Gupta, E. Martínez, and J. L. Hueso, Convergence and dynamics of improved Chebyshev-Secant-type methods for non differentiable operators, Numerical Algorithms, **86**(3) (2021), 1051–1070.

[5] I. K. Argyros, M. A. Hernández-Verón, and M. J. Rubio, Convergence of Steffensen's method for non-differentiable operators, Numerical Algorithms, **75**(1) (2017), 229–244.

International Conference on Mathematical Analysis and Applications in Science and Engineering
ICMA^{2}SC'22

ISEP **Porto-Portugal, June 27 - 29, 2022**

SECOND ORDER SEMILINEAR INCLUSIONS WITHOUT COMPACTNESS

Martina Pavlačková[1] **VALENTINA TADDEI**[2⋆]

[1] Moravian College of Olomouc, Czech Republic
[2] University of Modena and Reggio Emilia, Italy

[2⋆]valentina.taddei@unimore.it

Abstract: The existence of a mild solution to the Cauchy problem for semilinear second-order differential inclusion in a Banach space is investigated in the case when the nonlinear term also depends on the first derivative.

keywords: second-order Cauchy problem; Banach spaces; fundamental system; approximation solvability method; mild solution.

MSC2020: 34A60; 34G25.

The talk deals with the Cauchy problem for a second-order differential inclusion in a Banach space of the form

$$\left.\begin{array}{c} \ddot{x}(t) \in A(t)x(t) + F(t, x(t), x'(t)), \\ x(0) = x_0,\ \dot{x}(0) = \overline{x}_0. \end{array}\right\} \tag{1}$$

in a reflexive Banach space E admitting a Schauder basis. The inclusion is semilinear, since $\{A(t)\}_{t\geq 0}$ is a family of closed and linear operators, whose domain $D(A(t)) = D(A)$ for every $t \geq 0$ is dense in E, that generates a fundamental system $\{S(t,s)\}_{t,s\geq 0}$.

We first consider an impulsive boundary value problem associated to (1), namely

$$\left.\begin{array}{l} \Delta x(t_k) = I_k(x(t_k),\, x'(t_k)),\ k = 1, 2, \ldots, m, \\ \Delta \dot{x}(t_k) = \overline{I}_k(x(t_k),\, x'(t_k)),\ k = 1, 2, \ldots, m, \end{array}\right\} \tag{2}$$

(see [1]), with I_k, $\overline{I}_k \in C(E \times E,\, E)$, for all $k = 1, 2, \ldots, m$, then the existence of a solution

$$x : [0, +\infty) \to E \tag{3}$$

in a non compact interval (see [2]).

The solution is understood in a mild sense, i.e. as solution we mean a continuously differentiable x such that, for all t,

$$x(t) = -\frac{\partial}{\partial s} S(t,s)\Big|_{s=0} x_0 + S(t,0)\overline{x}_0 + \int_0^t S(t,s) f(s)\, ds,$$

where f is an integrable selection of $F(\cdot, x(\cdot), x'(\cdot))$.

The proofs of our results are based on the usage of a fixed point theorem for multivalued mappings. The use of the fixed point theorem in an infinite dimensional Banach space requires

strong compactness conditions, which are usually guaranteed by assuming the compactness of the fundamental system generated by the linear term or some conditions based on the measure of noncompactness of the nonlinear term. To overcome this problem, the approximation solvability method is applied, which consists of introducing a sequence of approximating problems with values in finite-dimensional spaces, combined with the usage of the weak topology, which allows avoiding any requirement of compactness. A limiting argument then leads to a solution to the original problem. The existence of a mild solution for the Cauchy impulsive problem as well as the existence of a mild solution in the non compact interval are obtained by a step-by-step reduction to problems without impulses in compact intervals. We are able to consider the case of a nonlinear term depending also on the first derivative and with a linear growth condition.

The talk concludes with an application of the obtained results to the generalized telegraph equation with a Balakrishnan–Taylor-type damping term.

References

[1] Martina Pavlačková, Valentina Taddei, Mild solutions of second-order semilinear impulsive differential inclusions in Banach spaces, Mathematics, **10** (4) (2022), art. no. 672, 1–25.

[2] Martina Pavlačková, Valentina Taddei, Bounded mild solutions of abstract second-order semilinear inclusions in a non-compact interval, preprint.

International Conference on Mathematical Analysis and Applications in Science and Engineering
ICMA^{2}SC'22

ISEP Porto-Portugal, June 27 - 29, 2022

A coupled finite-volume solver for numerical simulation of log-conformation tensor based viscoelastic flows

C. Fernandes[1]

[1] LASI - Associate Laboratory of Intelligent Systems,
IPC - Institute for Polymers and Composites,
Polymer Engineering Department,
School of Engineering of the University of Minho,
Campus de Azurém, 4800-058 Guimarães, Portugal.

[1⋆]cbpf@dep.uminho.pt

Abstract: In this work, a block coupled algorithm for the solution of transient, laminar, incompressible, non-isothermal, viscoelastic flow problems based on the log-conformation tensor approach is presented. The inter-equation coupling of the incompressible Cauchy momentum equations, log-conformation tensor constitutive equations and energy equation is obtained by deriving a pressure equation in a procedure based on the Schur complement. The divergence of the log-conformation tensor term in the momentum equations is implicitly discretized in this work. In addition, the velocity field is considered implicitly in the log-conformation tensor constitutive equations by expanding the advection term, rotation terms and the rate of deformation terms with a second order Taylor series expansion. Finally, the advection and diffusion terms in the energy equation are also discretized implicitly. All the equations, comprising the continuity, momentum, log-conformation tensor constitutive model and energy, are block-coupled into a single system of equations. The validation of the newly-developed algorithm was performed for the viscoelastic matrix-based Oldroyd-B fluid flow in a two-dimensional axisymmetric 4:1 planar sudden contraction geometry.

keywords: Viscoelasticity, Log-conformation tensor, Non-isothermal effects, Fully-implicit coupled solver, OpenFOAM.

MSC2020: 74D05; 74D10; 76A05; 76A10.

STABILITY AND FLIP BIFURCATION OF A THREE DIMENSIONAL EXPONENTIAL SYSTEM OF DIFFERENCE EQUATIONS

C. Mylona[1*], G. Papaschinopoulos[2], C. J. Schinas[3*]

[1] Democritus University of Thrace, Greece

[2] Democritus University of Thrace, Greece

[3] Democritus University of Thrace, Greece

[3*] cschinas@ee.duth.gr

Abstract: The stability of the zero equilibrium and the occurrence of flip bifurcation for a three-dimensional systems of exponential difference equations is investigated in this research. Moreover, the stability of this system is studied in the special case when one of the eigenvalues is equal to -1 and the remaining eigenvalues have absolute value less than 1, using center manifold theory.

keywords: Difference equations, stability, flip bifurcation, center manifold, dynamical systems, discrete dynamics.

MSC2020: 39A28, 39A30.

References

[1] L. Berg, S. Stevic, J. Diblik, B. Iricanin, Z. Smarda, On some systems of difference equations, Appl. Math. Comput. 2011, **218**, 1713-1718.

[2] S. Elaydi, *Discrete Chaos*, Second Edition, Chapman \& Hall/CRC, Boca Raton, London, New York, 2008.

[3] D. Tilman, D. Wedin, O. Marichev, , Oscillations and chaos in the dynamics of a perennial grass, Nature 1991, **353**, 653-655.

International Conference on Mathematical Analysis and Applications in Science and Engineering
ICMA^{2}SC'22
ISEP Porto-Portugal, June 27 - 29, 2022

High order schemes for a subdiffusion problem

Carla Jesus[1], Ercília Sousa [1⋆]

[1] CMUC, Department of Mathematics, University of Coimbra

ecs@mat.uc.pt

Abstract: We consider an equation that captures a subdiffusive behaviour that can appear for instance in biological models. This equation involves a time Riemann-Liouville fractional derivative on the right hand side of the differential equation and the diffusive coefficient can depend on space and time. Subdiffusion processes appear most of the times described by a differential equation with a Caputo fractional derivative on the left hand side of the equation. However, many times this is only a correct model if the diffusive coefficient does not depend on time [1, 3]. To obtain an high order numerical method for the subdiffusion problem with a diffusion coefficient that depends on space and time, a numerical method is derived using an approach based on fractional splines [2]. The main purpose of this work is to apply the fractional splines to approximate the fractional integral and hence explain how to solve the subdiffusion problem using this approach. It is discussed how the order of convergence of the numerical method depends on the regularity of the solution, the degree of the spline and the order of the fractional derivative.

keywords: Fractional differential equations, finite differences, subdiffusion problems

MSC2010: 65M06; 65M12; 65M15; 35R11.

Acknowledgments

This work was partially supported by the Centre for Mathematics of the University of Coimbra – UID/MAT/00324/2019, funded by the Portuguese Government through FCT/MEC and co-funded by the European Regional Development Fund through the Partnership Agreement PT2020. C. Jesus was also supported by FCT, through scholarship PD/BD/142955/2018, under POCH funds, co-financed by the European Social Fund and Portuguese National Funds from MEC.

References

[1] E. Heinsalu, M. Patriarca, I. Goychuk, P. Hänggi, Use and abuse of a fractional Fokker-Planck dynamics for time-dependent driving, Phys. Rev. Lett. **99** (2007), 120602.

[2] C. Jesus, E. Sousa, Numerical method with fractional splines for a subdiffusion problem, BIT Numer. Math. **60** (2020), 1075–1111.

[3] M. Magdziarz, J. Gajda, T. Zorawik, Comment on fractional Fokker-Planck equation with space and time dependent drift and diffusion, J. Stat. Phys. **154** (2014), 1242–1250.

International Conference on Mathematical Analysis and Applications in Science and Engineering
ICMA^{2}SC'22
ISEP Porto-Portugal, June 27 - 29, 2022

Weak Pontryagin's Maximum Principle for Optimal Control Problems Involving a General Analytic Kernel

Faïçal Ndaïrou[1⋆] **Delfim F. M. Torres**[1]

[1] University of Aveiro, Portugal

[1⋆]faical@ua.pt

Abstract: This talk emphasizes on proving a duality relation and an integration by parts formula for fractional operators with a general analytical kernel. Based on these basic results, we are able to prove a new Grønwall's inequality and continuity and differentiability of solutions of control differential equations. This allow us to obtain a weak version of Pontryagin's maximum principle. Moreover, our approach also allow us to consider mixed problems with both integer and fractional order operators and derive necessary optimality conditions for isoperimetric variational problems and other problems of the calculus of variations.

keywords: fractional operators with general analytical kernels; optimal control problems; Pontryagin extremals; calculus of variations; isoperimetric problems.

MSC2020: 26A33; 49K15.

Acknowledgments

This research was funded by the Portuguese Foundation for Science and Technology (FCT) through CIDMA, grant number UIDB/04106/2020. The first author was supported by FCT through the PhD fellowship PD/BD/150273/2019.

References

[1] Fernandez, A.; Özarslan, M.A.; Baleanu, D. On fractional calculus with general analytic kernels. Appl. Math. Comput. 2019, 354, 248–265.

[2] Ndaïrou, F.; Torres, D.F.M. Weak Pontryagin's Maximum Principle for Optimal Control Problems Involving a General Analytic Kernel. arXiv 2021, arXiv:2109.02136.

International Conference on Mathematical Analysis and Applications in Science and Engineering
ICMA^{2}SC'22
ISEP Porto-Portugal, June 27 - 29, 2022

Differential equations with state-dependent delays and their solution manifolds

Hans-Otto Walther[1⋆]

[1] Justus–Liebig–Universität Gießen, Germany

[1⋆] chojk.walther@t-online.de

Abstract: The lecture begins with some basic theory for differential equations with state-dependent delays [2, 1]. A toy example is the scalar equation

$$x'(t) = g(x(t), x(t-r)), \quad r = d(x(t)),$$

with functions $g : \mathbb{R}^2 \to \mathbb{R}$ and $d : \mathbb{R} \to [0, h]$. Systems of such equations are in general not covered by the familiar theory for *Retarded Functional Differential Equations* where delays are constant. This is due to a specific lack of smoothness caused by variable delay, and it is only on associated *solution manifolds* in the Banach space of continuously differentiable maps $[-h, 0] \to \mathbb{R}^n$ that initial values uniquely determine solutions which are differentiable with respect to the initial data - as required for linearization, local invariant manifolds, Poincaré return maps, and more from dynamical systems theory. The second part of the lecture deals with the nature of solution manifolds. For a large class of differential systems with state-dependent delays it can be shown that the associated solution manifolds are not very complicated [3, 4, 5].

keywords: Delay differential equation; state-dependent delay; solution manifold; almost graph.

MSC2020: 34-K-05; 34-K-43; 58-B-99.

References

[1] F. Hartung,T. Krisztin, T., H.O. Walther, H.O., and J. Wu, Functional differential equations with state-dependent delay: Theory and applications. In: *HANDBOOK OF DIFFERENTIAL EQUATIONS, Ordinary Differential Equations*, vol. 3, pp. 435–545, Canada, A., Drabek., P. and A. Fonda eds., Amsterdam: Elsevier, 2006.

[2] H.O. Walther, The solution manifold and C^1-smoothness for differential equations with state dependent delay, J. Dif. Eqs. **195** (2003), 46–65.

[3] H.O. Walther, Solution manifolds which are almost graphs, J. Dif. Eqs. **293** (2021), 226–248.

[4] H.O. Walther, A finite atlas for solution manifolds of differential systems with discrete state-dependent delays, Dif. Int. Eqs. **35** (2022), 241–276.

[5] H.O. Walther, On solution manifolds of differential systems with discrete state-dependent delays, Discrete Cont. Dyn. Systs. Series S, accepted.

International Conference on Mathematical Analysis and Applications in Science and Engineering
ICMA^{2}SC'22
ISEP Porto-Portugal, June 27 - 29, 2022

The effect of the same damping parameter presence in a system of linear and nonlinear oscillators

Maaita J.O.[1,2⋆] **Laskaridis L.**[1] **Prousalis D.**[1] **Volos Ch.**[1]

[1] Aristotle University of Thessaloniki, Greece
[2] International Hellenic University, Greece
[3] Max-Planck-Institute for the Physics of Complex Systems.

⋆jmaay@physics.auth.gr

Abstract: We present how the addition of the same damping parameter of the nonlinear oscillator to the linear oscillator affects the system's dynamical behavior.

keywords: Nonlinear oscillations; chaotic behavior; Electronic circuits.

MSC2020: 34-xx; 37-xx.

In this work, we study a system of a cubic nonlinear oscillator coupled to a linear oscillator. The question is: What is the effect, to the system's dynamics, of adding the same damping parameter of the nonlinear oscillator in the linear oscillator ?

A nonlinear electronic circuit can emulate such a system. So, our work is essential for its theoretical results and its possible practical use and applications.

Firstly, we study the dynamics of the coupled oscillators where the linear oscillator is undamped

Then we study the dynamics of the coupled oscillators with the damped linear oscillator and compare the two systems.

Finally, we present an electronic circuit emulation of the system with the damped linear oscillator and discuss its dynamical behavior.

Acknowledgments

Results presented in this work have been produced using the AUTH Compute Infrastructure and Resources.

References

[1] Nayfeh A.H, Mook D.T, *Nonlinear Oscillations*, Wiley, 1995.

[2] Guckenheimer J., Holmes P.J.: *Nonlinear Oscillations, Dynamical Systems, and Bifurcations of Vector Fields*, Springer- Verlag New York, 1983.

International Conference on Mathematical Analysis and Applications in Science and Engineering
ICMA^{2}SC'22
ISEP Porto-Portugal, June 27 - 29, 2022

Prediction capabilities of data-driven operator based algorithms on some classes of differential equations

Nelida Črnjarić - Žic[1⋆] **Senka Maćešić**[2]

[1] University of Rijeka, Faculty of Engineering, Croatia
[2] University of Rijeka, Croatia

[1⋆]nelida@riteh.hr

Abstract: Nowadays, the possibilities of predicting the behavior of different dynamical systems are in the focus of the research in many scientific disciplines. In this paper we consider the dynamical systems generated by chosen nonlinear and non-autonomous ordinary differential equations. These dynamical systems are approximated by using the Koopman operator based data-driven algorithms applied on the observable functions evaluated at some finite set of the system states. The learned model is then used as a prediction tool to envisage the values of the observable functions in the future system states. The aim of this work is to test and analyze the prediction capabilities of such data-driven algorithms on simple examples in order to make a foundation for understanding their behavior in the prediction task in more complex systems, even in those for which the associated differential equations modeling the system are not known.

keywords: differential equations; Koopman operator, data-driven algorithms, DMD algorithm, prediction.

MSC2020: 34A34; 37M10; 37M99; 47B33.

1 Introduction

Our starting assumption is that observed data is generated by an ordinary differential equation system of the form

$$\frac{d}{dt}\mathbf{x}(t) = \mathbf{F}(\mathbf{x}(t)).$$

The associated dynamical system is defined with a flow map $\mathbf{S}^t$ describing the evolution of the state space in time. In this work we use the technique based on the *Koopman operator*, whose action defined on the space of observable functions is given by $\mathcal{K}^t f(\mathbf{x}) = f(\mathbf{S}^t(\mathbf{x}))$. The Koopman operator theory gives the connection between the underlying dynamical system and the spectral properties of the associated Koopman operator. The numerical algorithms that extract the spectral structure of the finite dimensional approximation of the Koopman operator, such as the dynamic mode decomposition (DMD) [4] are crucial for obtaining Koopman mode decomposition (KMD) [1]. The KMD is here used for the reconstruction and prediction of the dynamical system.

Let us suppose that the values of the system observables $\mathbf{f}_i \in \mathbf{R}^N$ are acquired at the equidistant time moments t_i, $i = 1, 2, ...$ and that the data up to the actual time moment t_{p-1} were known, while the data at the next time moment t_p is still unknown. For an active window of size w,

starting at t_b and ending at t_{p-1}, we lift the observables into the higher dimensional space $\mathbf{R}^l$, $l = N \cdot n_H$, and arrange them as columns of a $l \times (m_H + 1)$ (block) Hankel matrix:

$$\mathbf{H} = \begin{pmatrix} \mathbf{f}_b & \mathbf{f}_{b+1} & \cdots & \mathbf{f}_{b+m_H-1} & \mathbf{f}_{b+m_H} \\ \mathbf{f}_{b+1} & \mathbf{f}_{b+2} & \cdots & \mathbf{f}_{b+m_H} & \mathbf{f}_{b+m_H+1} \\ \vdots & \vdots & \ddots & \vdots & \vdots \\ \mathbf{f}_{b+n_H-1} & \mathbf{f}_{b+n_H} & \cdots & \mathbf{f}_{b+n_H+m_H-2} & \mathbf{f}_{b+n_H+m_H-1} \end{pmatrix} = \begin{pmatrix} \mathbf{h}_0 & \mathbf{h}_1 & \ldots & \mathbf{h}_{m_H} \end{pmatrix}. \quad (1)$$

Our prediction tool will be KMD related with a Hankel matrix of the acquired observable values. We apply to it enhanced DMD algorithm [4], which provides us with a set of Ritz values and vectors $(\mu_j, \mathbf{v}_j), j = 1, 2, ..., r$. We can determine the coefficients α_j such that $\mathbf{h}_k = \mathbf{K}^k \mathbf{h}_0 = \sum_{j=1}^{m_H} \mu_j^k \alpha_j \mathbf{v}_j + \delta_{k,m_H} \hat{\mathbf{r}}_{m_H}$, $k = 0, \ldots, m_H$, where $\mathbf{K}$ denotes the approximation of the projection of the Koopman operator to the subspace spanned by first m_H columns of matrix $\mathbf{H}$, δ_{k,m_H} is the Kronecker delta symbol, and $\hat{\mathbf{r}}_{m_H}$ is the residual of the orthogonal projection of $\mathbf{h}_{m_H}$ onto the span of the first m_H columns of matrix $\mathbf{H}$. The approximate decomposition of the snapshots $\mathbf{f}_k$ is given by active KMD

$$\tilde{\mathbf{f}}_k = \sum_{j=1}^{r} \widehat{\mathbf{v}}_j \alpha_j \mu_j^{k-(b+n_H-1)}. \quad (2)$$

For $k = b + n_H, ..., p - 1$, (2) is a *reconstruction* of the acquired data, while for $k = p, p + 1, \ldots, p+\tau$, (2) is an *extrapolation* of the active KMD, and it gives us *predictions* for future data snapshots. The important tool for measuring the quality of Ritz pairs as approximating pair of the Koopman eigenvalues and eigenvectors are residuals $\eta_i = \|\mathbf{K}\mathbf{v}_i - \mu_i \mathbf{v}_i\|$ obtained from the enhanced DMD algorithm [4]. By using only Ritz pairs with small residuals the reduced KMD could be used as a prediction tool and in that case we say that the reduced KMD is used.

2 Results and discussion

2.1 Lorenz system.

The first test case that we consider is the Lorenz dynamical systems, modeled by

$$\dot{\mathbf{x}} = \begin{pmatrix} \dot{x} \\ \dot{y} \\ \dot{z} \end{pmatrix} = \begin{pmatrix} \sigma(y - x) \\ x(\rho - z) - y \\ xy - \beta z \end{pmatrix}. \quad (3)$$

We use (3) to test the prediction potential of the KMD. It is well known that the model exhibits the chaotic behavior for some initial conditions - we take here $\sigma = 10$, $\beta = 8/3$, and $\rho = 28$. The long term exponential divergence of nearby trajectories leads to unpredictability of this system. However, we can consider the prediction capabilities of the algorithm for shorter prediction times. We have generated data using numerical simulation (ODE solver) of (3) with the time step $\Delta t = 0.01s$. For computing the KMD, the scalar observable $\mathbf{f} = x$ and active windows of size $w = 400$ and 300×100 Hankel matrices are used. By sliding the active windows along the computational domain we get prediction at different times. The dynamics is predicted for 250 time steps. One can observe that, while inside one of the butterfly wings, the system behaves in a predictable manner. After a switch between two wings happens, the columns of the Hankel matrix do not lie in Koopman invariant subspace and the Ritz pairs obtained from the algorithm are not good approximations of Koopman eigenvalues and eigenvectors. In the right columns of the first raw of Figure 1, the real and imaginary parts of the eigenvalues extracted from the sliding active windows are presented. For each active window, the Ritz pairs with the residual below $\eta_r = 0.01$ are selected. We conclude that on the part of the domain where switching between butterfly wings arise, there exist no Ritz pairs with small residuals. On the other

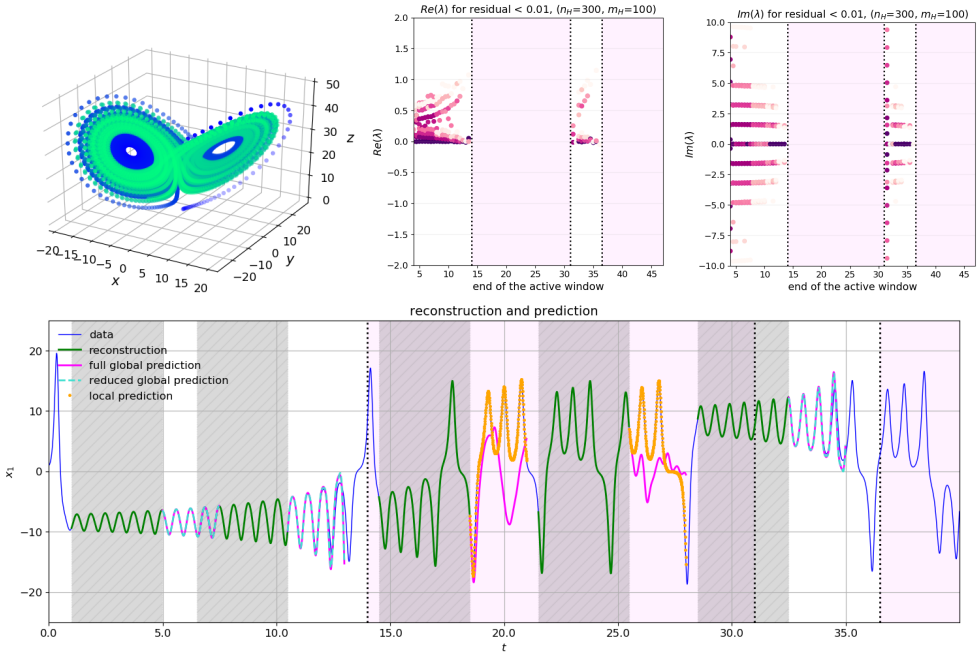

Figure 1: Prediction of the Lorenz system.

hand, on the part of the domain where this is not the case, there are enough Ritz pairs with small residuals that approximate and predict the dynamics of the system quite well. In this way the state space can be actually split into domains over which prediction is possible and those on which this is not the case. The orange curve in Figure 1 uses local algorithm with shorter prediction times of few steps, which could be an appropriate choice when the global prediction does not work. Furthermore, the reduced prediction is obtained by KMD with a reduced number of modes that uses only the Ritz pairs with small residuals. One can observe that the reconstruction and prediction capabilities are comparable with those using the full KMD.

2.2 Nonautonomous differential equations system.

Oscillator with the driven amplitude. The considered dynamical system is nonautonomous and given with

$$\begin{pmatrix} \dot{x}_1 \\ \dot{x}_2 \end{pmatrix} = \begin{pmatrix} (\sigma_0 + A_d \cos(\omega_d t) + B_d \sin(\omega_d t))x_1 + \omega_0 x_2 \\ -\omega_0 x_1 + (\sigma_0 + A_d \cos(\omega_d t) + B_d \sin(\omega_d t))x_2 \end{pmatrix}. \tag{4}$$

By rewriting it in the skew product formulation

$$\begin{pmatrix} \dot{p}_1 \\ \dot{p}_2 \end{pmatrix} = \begin{pmatrix} \omega_d p_2 \\ -\omega_d p_1 \end{pmatrix}, \quad \begin{pmatrix} \dot{x}_1 \\ \dot{x}_2 \end{pmatrix} = \begin{pmatrix} -\omega_0 x_1 + (\sigma_0 + p_1)x_2 \\ (\sigma_0 + p_1)x_1 + \omega_0 x_2 \end{pmatrix} \tag{5}$$

it generates the skew product flow of the form $\mathbf{S}_s(t,(p,\mathbf{x})) = (\theta^t(p), \mathbf{S}^{t,p}(\mathbf{x}))$. It can be considered as autonomous flow on a larger space $P \times X$, thus we can associate with it the Koopman operator. By taking long enough trajectories of the Hankel matrix, we hope that we capture the dynamics on the attractor and that the columns are in Koopman invariant subspace. As proved in [1], in that case, the Hankel DMD will converge to the true eigenvalues and eigenfunctions of the Koopman operator. In that case the KMD will have good prediction capabilities. This is nicely visible in Figure 2 where one can observe that very accurate prediction is obtained, even with the reduced KMD with relatively small number of terms. On the other hand, if in this nonautonomous case just small time windows are taken into account, the algorithm fails with an error which does not depend on Δt. The details and analysis of the intrinsic error that arise when data driven algorithms are applied in nonautonomous setting can be found in [2].

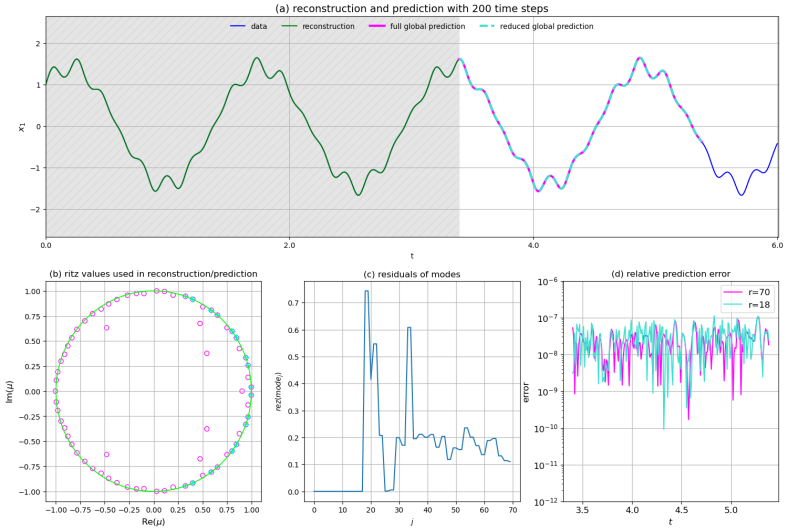

Figure 2: Oscillator with the driven amplitude. Active window of size $w = 340$, prediction $\tau = 300$ (a) solution and prediction; (b) Ritz values; (c) residuals; (d) relative prediction error.

3 Conclusions and Future work

In this work, the prediction capabilities of a model that is determined using DMD style data-driven algorithm on some chosen dynamical systems are analyzed. The model uses KMD which is composed of spectral elements of the Koopman operator and is based on some theoretical properties of the Koopman operator. In the first example, the classical autonomous system was observed and situations in which the applied algorithm has good or bad prediction properties were analyzed. Using the residual for detecting the Ritz pairs that could approximate well the Koopman eigenvectors and eigenvalues, we conclude that it can be used as a good estimator of the prediction capabilities of the built KMD model. Although the used data-driven algorithm was developed primarily for autonomous systems, there are possibilities to apply it successfully in non-autonomous framework also, as is shown in the second example. In the further work, the possibility of prediction with the used approach will be considered on more complex systems, especially those that have a stochastic component involved.

Acknowledgments

This work was supported by the University of Rijeka, Croatia under the project uniri-prirod-18-118-1257.

References

[1] Arbabi, H. and Mezić, I., Ergodic theory, Dynamic Mode Decomposition and Computation of Spectral Properties of the Koopman operator, SIAM J. Appl. Dyn. Syst., 16(4) (2017)

[2] Maćešić, S., Črnjarić-Žic, N., Mezić, I., Koopman operator family spectrum for nonautonomous systems, SIAM J. Appl. Dyn. Sys., 17(4) (2018)

[3] Tu, J. H., Rowley, C. W., Luchtenburg, D. M., Brunton, S. L., Kutz, J. N., On dynamic mode decomposition: theory and applications, J. Comp. Dyn., 2(1) (2014)

[4] Drmač, Z., Mezić, I., Mohr, R., Data driven modal decompositions: analysis and enhancements, SIAM J. Sci. Comput., 40(4) (2018)

International Conference on Mathematical Analysis and Applications in Science and Engineering
ICMA^{2}SC'22
ISEP Porto-Portugal, June 27 - 29, 2022

OSCILLATION CRITERIA FOR SECOND ORDER NEUTRAL DELAY DIFFERENTIAL EQUATIONS

Sandra Pinelas

Academia Militar, Portugal

sandra.pinelas@gmail.com

Abstract: This work deals with the oscillatory behavior of solutions of second order quasilinear neutral delay differential equation where it is introduced some new sufficient conditions for the oscillation. The oscillation results depend on only one condition improving some known results.

keywords: Quasilinear; Neutral differential equation; Second order; Oscillation.

MSC2020: 34C10; 34K11.

International Conference on Mathematical Analysis and Applications in Science and Engineering
ICMA^{2}SC'22
ISEP Porto-Portugal, June 27 - 29, 2022

STABILITY FOR TIME SCALE DYNAMICS

Sergey Kryzhevich[1⋆]

[1] Gdańsk University of Technology, Poland

[1⋆]serkryzh@pg.edu.pl

Abstract: Structural stability and shadowing are studied for time scale systems.

keywords: time scales; structural stability; hyperbolicity.

MSC2020: 34-XX; 37-XX; 39-XX.

We consider a dynamic system on a time scale $x^\Delta = f(t,x)$, $x \in \mathbb{R}^n$, $t \in \mathbb{T}$. Theory of such dynamics is well-developed, see [1] and references therein. This is an effective approach to study non-uniform numerical methods or systems with strong nonlinearities.

We say that the considered system is *structurally stable* if all solutions are unique and for any $\varepsilon > 0$ there exists a $\delta > 0$ such that for any $g(t,x) : |g(t,x)| < \delta$, $|g'_x(t,x)| < \delta$ and any $t_0 \in \mathbb{T}$ there is a homeomorphism h of the space $\mathbb{R}^n$ such that $|\varphi_f(t,x_0) - \varphi_{f+g}(t,h(x_0))| < \varepsilon$ for any $x_0 \in \mathbb{R}^n$, $t \in \mathbb{T}$. Here $\varphi_f(t,x_0)$ and $\varphi_{f+g}(x_0)$ are solutions of systems $x^\Delta = f(t,x)$ and $x^\Delta = f(t,x) + g(t,x)$ with initial conditions $x(t_0) = x_0$.

For systems of ordinary differential equations, conditions for global structural stability were obtained in [1] (see references therein). It was proved that a system is structurally stable if its linearizations are uniformly hyperbolic on families of segments. We formulate and prove an analog of this statement for time scale systems as well as sufficient conditions for shadowing.

In our proofs, we need to use specific approaches of time scale systems theory [2]. Remarkably, the classical results for structural stability of autonomous ODEs (C.Robinson, 75) are, in general, non-applicable for systems on time scales, even for the autonomous ones.

References

[1] Kryzhevich S. G., Pliss V. A., Structural stability of nonautonomous systems, Diff. equations 2003. **39**(10), 1395–1403.

[2] Bohner M., Martynyuk A. A., Elements of stability theory of A. M. Liapunov for dynamic equations on time scales. Nonlinear Dyn. Syst. Theory 2007. **7**(3), 225–251.

Exponential Lag Synchronization of Cohen-Grossberg Neural Networks with Discrete and Distributed Delays on Time Scales

Vipin Kumar[1⋆] **Jan Heiland**[1] **Peter Benner**[1]

[1]Max-Planck Institute for Dynamics of Complex Technical Systems,
Sandtorstraße 1, 39106 Magdeburg, Germany.

[1⋆]vkumar@mpi-magdeburg.mpg.de

Abstract: We modeled a new class of Cohen-Grossberg Neural Networks with mixed delays on an arbitrary time domain by using the time scales theory. We establish the exponential lag synchronization results by applying the feedback controller. We mainly use the unified matrix-measure theory and Halanay inequality to establish these results. In the last, we provide some simulated examples to show the effectiveness of the obtained analytical results.

keywords: Synchronization; Neural Networks; Time Scales.

MSC2020: 34K24; 92B20; 34N05.

References

[1] M. Bohner and A. Peterson. Dynamic Equations on Time Scales. Birkhauser, Boston, MA, 2001.

[2] M. Bohner and A. Peterson. Advances in Dynamic Equations on Time Scales. Birkhauser, Boston, MA, 2003.

[3] Q. Xiao and Z. Zeng. Lagrange stability for T-S fuzzy memristive neural networks with time-varying delays on time scales. IEEE Trans. Fuzzy Syst., 26(3):1091-1103, 2018.

[4] Q. Xiao and T. Huang. Stability of delayed inertial neural networks on time scales: A unified matrix-measure approach. Neural Networks, 130:33-38, 2020.

International Conference on Mathematical Analysis and Applications in Science and Engineering
ICMA^{2}SC'22
ISEP Porto-Portugal, June 27 - 29, 2022

Partial Control and Beyond: Forcing Escapes and Controlling Chaotic Transients with the Safety Function

Miguel A. F. Sanjuán

Nonlinear Dynamics, Chaos and Complex Systems Group,

Universidad Rey Juan Carlos, Tulipán s/n, 28933 Móstoles, Madrid, Spain

miguel.sanjuan@urjc.es

Abstract: A new control algorithm based on the partial control method has been developed. The general situation we are considering is an orbit starting in a certain phase space region Q having a chaotic transient behavior affected by noise, so that the orbit will definitely escape from Q in an unpredictable number of iterations. Thus, the goal of the algorithm is to control in a predictable manner when to escape. While partial control has been used as a way to avoid escapes, here we want to adapt it to force the escape in a controlled manner. We have introduced new tools such as escape functions and escape sets that once computed makes the control of the orbit straightforward. The partial control method aims to avoid the escape of orbits from a phase space region Q where the transient chaotic dynamics takes place. The technique is based on finding a special subset of Q called the safe set. The chaotic orbit can be sustained in the safe set with a minimum amount of control. We have developed a control strategy to gradually lead any chaotic orbit in Q to the safe set by using the safety function. With the technique proposed here, the safe set can be converted into a global attractor of Q. This is joint work with Gaspar Alfaro and Rubén Capeáns, URJC, Spain.

keywords: partial control; chaotic transients; safety function

References

[1] Juan Sabuco, Miguel A. F. Sanjuán and James A. Yorke. Dynamics of Partial Control. Chaos 22, 047507, (2012).
[2] Ruben Capeáns, Juan Sabuco, and Miguel A.F. Sanjuán. A new approach of the partial control method in chaotic systems. Nonlinear Dynamics 98, 873--887 (2019)
[3] Gaspar Alfaro, Rubén Capeáns, and Miguel A. F. Sanjuan. Forcing the escape: Partial control of escaping orbits from a transient chaotic region. Nonlinear Dynamics 104, 1603–1612 (2021)
[4] Rubén Capeáns and Miguel A. F. Sanjuán. Beyond partial control: Controlling chaotic transients with the safety function. Nonlinear Dynamics 107, 2903–2910 (2022)

International Conference on Mathematical Analysis and Applications in Science and Engineering
ICMA^{2}SC'22
ISEP Porto-Portugal, June 27 - 29, 2022

Unpredictable solutions of quasilinear differential equations with generelized piecewise constant arguments

Zakhira Nugayeva[1,2⋆] **Marat Akhmet**[3] **Duygu Aruğaslan Çinçin**[4]
Madina Tleubergenova[1,2]

[1] K. Zhubanov Aktobe Regional University, Aktobe, Kazakhstan
[2] Institute of Information and Computational Technologies Almaty, Kazakhstan
[3] Middle East Technical University, Ankara, Turkey
[4] Süleyman Demirel University, Isparta, Turkey

⋆zahira2009.85@mail.ru

Abstract: An unpredictable solution is investigated for a quasilinear differential equation with generalized piecewise constant argument. Sufficient conditions are provided for the existence, uniqueness and exponential stability of the unpredictable solution. The results are illustrated by example and simulations.

keywords: Poisson stability; unpredictable solution; Poincare chaos; generalized piecewise constant argument; exponential stability.

MSC2020: 34A20; 34G05; 93D05.

1 Introduction and preliminaries

Periodic, quasi-periodic and almost periodic oscillations originated in the theory of celestial dynamics and had been speeded to all areas of applied mathematics. More complex behaviors are recurrent and Poisson stable motions. Poisson stable oscillations play important role in theory of differential equations [1]. In [2, 3], we have developed a recurrence in functional spaces to a more refined level, and the Poisson stable functions are assigned with the unpredictability property. Moreover, we utilize the new method, *the method of included intervals* [4, 6, 7, 8, 9], to verify the Poisson stability of solutions of differential equations and oscillations of neural networks. The proof of the unpredictability simultaneously verifies the Poincare chaos of the Bebutov dynamics in the functional space with the topology of uniform convergence on compact sets of the real axis. It opens new prospects for control and synchronization of chaos in differential equations. This time, we proceed the initial steps of constructing the basics of the theory and prove the existence of the unpredictable solution for a special type of hybrid systems, differential equations with generalized piecewise constant arguments [10, 11]. We have joined the chaos concept with the most flexible and convenient differential equations for applications.

Fix two real valued sequences $\theta_i,\ \xi_i,\ i \in \mathbb{Z}$, such that $\theta_i < \theta_{i+1},\ \theta_i \leq \xi_i \leq \theta_{i+1}$ for all $i \in \mathbb{Z},\ |\theta_i| \to \infty$ as $|i| \to \infty$.

We consider the following quasilinear system with generalized piecewise constant argument of mixed type

$$x'(t) = Ax(t) + f(x(t)) + g(x(\gamma(t))) + h(t), \tag{1}$$

where $t \in \mathbb{R}$, $x \in \mathbb{R}^m$ for a fixed $m \in \mathbb{N}$, $A \in \mathbb{R}^{m\times m}$ is a constant matrix and $\gamma(t) = \xi_i$ if $\theta_i \le t < \theta_{i+1}$, $i \in \mathbb{Z}$. Throughout this paper, we assume that the functions $f, g : D \to \mathbb{R}^m$ are continuous on a bounded domain $D = \{x \in \mathbb{R}^m : \|x\| < H\}$, where H is a positive constant. $h : \mathbb{R} \to \mathbb{R}^m$ is a uniformly continuous and bounded function. Moreover, it is assumed that all eigenvalues of the matrix A have negative real parts and $\|A\| = \overline{\lambda}$. In this case, it can be concluded that there exist real numbers $\sigma \ge 1$ and $\lambda > 0$ such that $\|e^{At}\| \le \sigma e^{-\lambda t}$ for all $t \ge 0$.

Definition 1 *[3] A uniformly continuous and bounded function $v : \mathbb{R} \to \mathbb{R}^m$ is unpredictable if there exist positive numbers ϵ_0, δ and sequences t_n, u_n both of which diverge to infinity such that $v(t + t_n) \to v(t)$ as $n \to \infty$ uniformly on compact subsets of $\mathbb{R}$ and $\|v(t + t_n) - v(t)\| \ge \epsilon_0$ for each $t \in [u_n - \delta, u_n + \delta]$ and $n \in \mathbb{N}$.*

In the present paper the following conditions are required for the system (1):

(C1) functions f and g satisfy a Lipschitz condition with constants L_f, L_g : $\|f(u_1) - f(u_2)\| \le L_f\|u_1 - u_2\|$ and $\|g(u_1) - g(u_2)\| \le L_g\|u_1 - u_2\|$ for all $u_1, u_2 \in D$;

(C2) $\exists\ m_f > 0$, $m_g > 0$ such that $\sup\limits_{\|x\|<H} \|f(x)\| \le m_f$ and $\sup\limits_{\|x\|<H} \|g(x)\| \le m_g$;

(C3) $\exists\ m_h > 0$ such that $\sup\limits_{t\in\mathbb{R}} \|h(t)\| \le m_h$;

(C4) $\dfrac{\sigma}{\lambda}(m_f + m_g + m_h) < H$;

(C5) $\dfrac{\sigma}{\lambda}(L_f + L_g) < 1$;

(C6) $\exists\ \theta > 0$ such that $\theta_{i+1} - \theta_i \le \theta$ for all $i \in \mathbb{Z}$;

(C7) $-\lambda + \sigma(L_f + \big(1 - \theta[(\overline{\lambda} + L_f)(1 + L_g\theta)e^{(\overline{\lambda}+L_f)\theta} + L_g]\big)^{-1} L_g) < 0$;

(C8) $\theta[(\overline{\lambda} + L_f)(1 + L_g\theta)e^{(\overline{\lambda}+L_f)\theta} + L_g] < 1$;

(C9) $\exists\ \{\eta_n\}$ with $\eta_n \to \infty$ as $n \to \infty$ such that $\theta_{i-\eta_n} + t_n - \theta_i \to 0$ and $\xi_{i-\eta_n} + t_n - \xi_i \to 0$ as $n \to \infty$ on each finite interval of integers, where t_n is the sequence defined in Definition 1.

2 Main results

Let $\mathcal{P}$ be defined as the space of vector-functions $\phi : \mathbb{R} \to \mathbb{R}^m$, $\phi = (\phi_1, \phi_2, ..., \phi_m)$ with unpredictable functions such that $\|\phi\|_1 < H$.

A function $x(t)$ which is bounded on the whole real axis is a solution of system (1) if and only if it satisfies the following integral equation

$$x(t) = \int_{-\infty}^{t} e^{A(t-s)} \left[f(x(s)) + g(x(\gamma(s))) + h(s)\right] ds.$$

Define an operator Π on $\mathcal{P}$ as follows

$$\Pi\phi(t) = \int_{-\infty}^{t} e^{A(t-s)} \left[f(\phi(s)) + g(\phi(\gamma(s))) + h(s) \right] ds.$$

The following assertions are needed for the proof of the main result of the paper.

Lemma 1 *The operator* Π *is invariant in* $\mathcal{P}$.

Lemma 2 *The operator* Π *is contractive on the space* $\mathcal{P}$.

The following theorem is proved by the method of included intervals.

Theorem 3 *Assume that the conditions (C1)-(C9) are fulfilled. If the function* h *is unpredictable, then the system (1) has a unique exponentially stable unpredictable solution.*

Example. Consider the following quasilinear system with the generalized piecewise constant argument of mixed type

$$\begin{aligned} x'(t) = &\begin{pmatrix} 0.1 & -0.6 & 0 \\ 0.1 & -0.4 & 0 \\ 0 & 0 & -0.3 \end{pmatrix} \begin{pmatrix} x_1(t) \\ x_2(t) \\ x_3(t) \end{pmatrix} + \begin{pmatrix} 0.01 \tanh(\frac{x_1(t)}{25}) \\ 0.01 \tanh(\frac{x_2(t)}{25}) \\ 0.01 \tanh(\frac{x_3(t)}{25}) \end{pmatrix} \\ &+ \begin{pmatrix} 0.01 \tanh(\frac{x_1(\gamma(t))}{20}) \\ 0.01 \tanh(\frac{x_2(\gamma(t))}{20}) \\ 0.01 \tanh(\frac{x_3(\gamma(t))}{20}) \end{pmatrix} + \begin{pmatrix} -4\Theta^3(t) + 0.02 \\ 0.5\Theta(t) - 0.03 \\ 3\Theta^3(t) + 0.01 \end{pmatrix}, \end{aligned} \tag{2}$$

where $\Theta(t)$ - is the unpredictable function, which was defined in the paper [5]. Moreover, the functions $h_1(t) = -4\Theta^3(t) + 0.02,\ h_2(t) = 0.5\Theta(t) - 0.03,\ h_3(t) = 3\Theta^3(t) + 0.01$ are unpredictable in accordance with Lemmas 1.4 and 1.5 given in [4]. The argument function $\gamma(t) = \xi_k$ is defined by the sequences $\theta_k = \frac{3}{4}k$, $\xi_k = \frac{\theta_k + \theta_{k+1}}{2} + \varphi_k = \frac{3(2k+1)}{8} + \varphi_k,\ k \in \mathbb{Z}$.

The conditions (C1)-(C9) are valid for the system (2) with $\lambda = 0.1, \bar{\lambda} = 0.7$, $L_f = 0.0004, L_g = 0.0005$, $m_f = m_g = 0.01$, and moreover $m_h = 0.19$, $\sigma = 20$, $H = 38$. Thus, by the Theorem 3, system (2) has a unique exponentially stable unpredictable solution $x(t)$.

To imagine the behavior of the unpredictable oscillation $x(t)$, we consider the simulation of another solution $\psi(t)$, with initial values $\psi_1(0) = -1.1951, \psi_2(0) = -0.2828, \psi_3(0) = 0.1587$. We consider the graph of the function $\psi(t)$, which approaches to the unpredictable solution $x(t)$ of the system (2), as time increases. The coordinates of the function $\psi(t)$, which exponentially converges to the unpredictable solution $x(t)$, are shown in Figure 1. The solution of system (2) is continuous function with discontinuous derivatives, and it continuously differentiable within intervals $[\theta_k, \theta_{k+1}), k \in \mathbb{Z}$.

Acknowledgments

Z. Nugayeva and M. Tleubergenova are supported by the Science Committee of the Ministry of Education and Science of the Republic of Kazakhstan (Grants No. AP09258737 and No. AP08856170). M. Akhmet is supported by 2247-A National Leading Researchers Program of TUBITAK, Turkey, N 120C138.

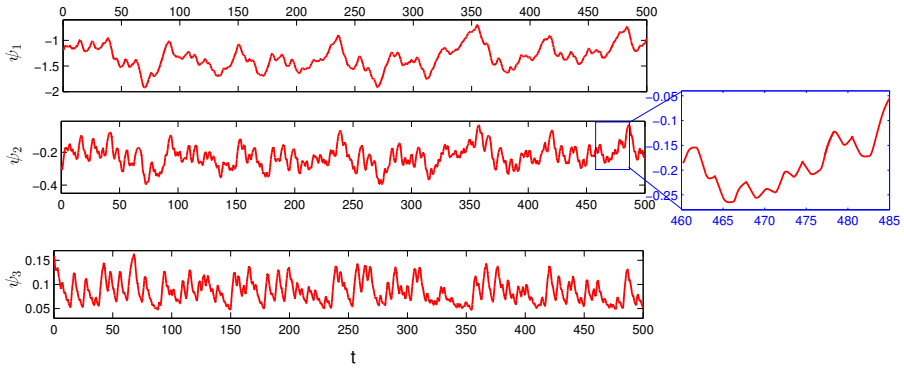

Figure 1: The coordinates of the function $\psi(t)$, which exponentially converge to the coordinates of the unpredictable solution $x(t)$.

References

[1] G.R. Sell, Topological dynamics and ordinary differential equations, Van Nostrand Reinhold Company, London, 1971.

[2] M.U. Akhmet, Fen, M.O., Unpredictable points and chaos. *Commun. Nonlinear Sci. Numer. Simulat.* **40**, (2016), 1-5.

[3] Akhmet, M.U., M.O. Fen, Poincare chaos and unpredictable functions, *Commun. Nonlinear Sci. Numer. Simulat.* **48**, (2017), 85-94.

[4] M. Akhmet, M.O. Fen, M. Tleubergenova, A. Zhamanshin, Unpredictable solutions of linear differential and discrete equations, *Turk. J. Math.* **43**, (2019), 2377-2389.

[5] M. Akhmet, R. Seilova, M. Tleubergenova, A. Zhamanshin, Shunting inhibitory cellular neural networks with strongly unpredictable oscillations, *Commun. Nonlinear Sci. Numer. Simulat.* **89**, (2020), 05287.

[6] M. Akhmet, D. Aruğaslan Çinçin, M. Tleubergenova, Z. Nugayeva, Unpredictable oscillations for Hopfield-type neural networks with delayed and advanced arguments, *Mathematics* **9**, (2021), 571.

[7] M. Akhmet, M. Tleubergenova, A. Zhamanshin, Quasilinear differential equations with strongly unpredictable solutions, *Carpathian J. Math.* **36**, (2020), 341-349.

[8] M.U. Akhmet, M.O. Fen, E.M. Alejaily, Dynamics with Chaos and Fractals, Springer, Cham, Switzerland, 2020.

[9] M. Akhmet, Domain Structured Dynamics: unpredictability, chaos, randomness, fractals, differential equations and neural networks, IOP Publishing, 2021.

[10] M.U. Akhmet, Integral manifolds of differential equations with piecewise constant argument of generalized type, *Nonlinear Analysis* **66** (2007), 367-383.

[11] M. Akhmet, Nonlinear Hybrid Continuous/Discrete-Time Models, Atlantis Press, Paris, 2011.

International Conference on Mathematical Analysis and Applications in Science and Engineering
ICMA^{2}SC'22
ISEP Porto-Portugal, June 27 - 29, 2022

MATHEMATICAL MODELLING AND ANALYSIS OF NON-NEWTONIAN NANOFLUID FLOWS OVER STRETCHING SHEETS

G. Bognár

University of Miskolc, Hungary

v.bognar.gabriella@iuni-miskolc.hu

Abstract: A mathematical model describing the flow and heat transfer characteristics of non-Newtonian fluids in a porous and linearly stretching sheet is investigated in a magnetic field. The mass transport of a water-based nanofluid is investigated in the presence of first-order slip. Similarity transformations are used to reduce the system of nonlinear partial differential equations to a nonlinear ordinary differential equation. The flow characteristics are analytically investigated from the solution of the boundary value problem on a half line. The exact solution of the momentum nonlinear ordinary differential equation is given for different scenarios of the fluid flow. The influence of the parameters of the porous medium, the magnetic field and the slip on the velocity field is analysed.

keywords: Nanofluid; MHD flow; stretching surface; stretching/shrinking; transpiration velocity; similarity method; exact solution.

MSC2020: 35C06; 76M55; 76W05.

1 Introduction

In some materials, e.g. pigment-softening pastes, non-Newtonian rheological properties have been observed at shear. Thixotropy, dilatancy and a markedly elastic solid response to suddenly applied stresses were observed and explained by flocculation of particles. A similar result was described by Casson [1] for pigment-oil suspensions of the ink type. Originally developed to characterize printing inks, the structure-based model, the Casson model, is widely used to characterize a number of food dispersions.

The term "nanofluid" is applied to a liquid containing a suspension of nano sized solid particles (nanoparticles). The addition of nanoparticles to the base fluid can cause a significant change in the characteristic properties of the base fluid. For this reason, they have also appeared in several industrial and medical applications.

Steady-state laminar MHD boundary layer flow problems driven by moving boundaries have been extensively studied. Pavlov [3] studied boundary layer flow in an electrically conducting fluid under the action of a plate when the magnetic field is transverse. Chakrabarti and Gupta [4] extended the work of Crane [2] by including the effect of the transverse magnetic field on the MHD flow over a stretching plate.

In the present work, we study the flow of Casson nanofluid over a stretching sheet under first-order slip in the presence of a magnetic field.

2 Problem formulation

In this paper we study the fluid flow over a stretching sheet and investigate the flow characteristics in a magnetic field under a first-order slip condition. We seek exact solutions to the boundary layer equation obtained from the Navier-Stokes equations using simplifications according to boundary layer theory. The problem considered here is the steady boundary layer flow of a non-Newtonian, Casson type nanofluid due to a moving flat surface in an otherwise quiescent fluid medium. Let us consider a laminar, steady boundary layer flow of an electrically conducting and incompressible Casson nanofluid that passes through a stretched perforated sheet. The laminar boundary layer flow is generated by a plate stretching in the x direction, where the stretching surface is moving at a speed of $U(x) = \pm U_w x/L$, $U_w > 0$ with shrinking (negative sign) or stretching (positive sign) velocity.

The sheet is placed in the plane $y = 0$, the fluid is in the half space $y > 0$. The fluid flow is considered in a constant vertical magnetic field $\mathbf{H}_0 = (0, H_0)$. Let the velocity vector of the fluid flow is denoted with $(u(x, y), v(x, y))$. The surface is assumed in general to be permeable and a lateral suction/injection with a constant suction rate of $(0, -V_0)$ is applied. The flow of otherwise quiescent fluid is only caused by the movement of the sheet. A constant suction rate of $(0, -V)$ is applied, $V > 0$ is the suction, while $V < 0$ is the fluid injection at $y = 0$.

The governing equations for zero pressure gradient laminar boundary layer flow of a Casson nanofluid are as follows

$$\frac{\partial u}{\partial x} + \frac{\partial v}{\partial y} = 0, \tag{1}$$

$$u\frac{\partial u}{\partial x} + v\frac{\partial u}{\partial y} = \nu_{nf}\Big(1 + \frac{1}{\gamma}\Big)\frac{\partial^2 u}{\partial y^2} - \frac{\sigma H_0^2}{\rho}u, \tag{2}$$

where ρ_{nf} is the fluid density, $\nu_{nf} = \mu_{nf}/\rho_{nf}$ is the kinematic viscosity, and σ is the electrical conductivity of the fluid. The parameter γ is the Casson parameter. The density of the nanofluid will be calculated according to [6]

$$\rho_{nf} = (1 - \phi)\rho_b + \phi\rho_p, \tag{3}$$

where ρ_b denotes the density of the base fluid and ρ_p the density of nanoparticles, and ϕ is the volume fraction. For the determination of the viscosity of the nanofluid we refer to [5]. The boundary conditions for the present Casson model are given below

$$u(x, 0) = U_w\frac{x}{L}d + \Big(1 + \frac{1}{\gamma}\Big)\, A\frac{\partial u}{\partial y}(x, 0), \tag{4}$$

$$v(x, 0) = -V, \ \lim_{y\to\infty} u(x, y) = 0. \tag{5}$$

The constant $A > 0$ is the first-order slip coefficients.

We introduce the stream function as ψ be then $(u, v) = (\frac{\partial\psi}{\partial y}, -\frac{\partial\psi}{\partial x})$; moreover, variable η and dimensionless stream function $f(\eta)$ in the following forms:

$$\eta = \sqrt{Re}\frac{y}{L}, \quad \psi = \nu_{nf}\sqrt{Re}\frac{x}{L}f(\eta). \tag{6}$$

Using (6), the fluid velocity components are given by

$$u = U(x)f'(\eta), \ v = -\frac{V}{V_p}f(\eta), \tag{7}$$

where the Reynolds number and the dimensionless suction/injection parameter are defined as

$$Re = \frac{U_w L}{\nu_{nf}}, \ \ V_p = \frac{VL}{\nu_{nf}\sqrt{Re}}. \tag{8}$$

.

Substituting (6)-(7) in (1)-(2) and in (4)-(5), we obtain the following nonlinear third order boundary value problem

$$\left(1+\frac{1}{\gamma}\right)f''' + ff'' - f'^2 - Mf' = 0, \tag{9}$$

$$f(0) = V_p; \quad f'(0) = d + cf''(0) = 0; \quad \lim_{\eta\to\infty} f'(\eta) = 0, \tag{10}$$

where $0 \leq \eta < \infty$, $c = (1+1/\gamma)A\sqrt{Re}/L \geq 0$ and the magnetic parameter defined by

$$M = \frac{\sigma L^2 H_0^2}{\rho_{nf}\nu_{nf}Re}. \tag{11}$$

We introduce $d = \pm(1+m)$, where positive and negative signs correspond to the stretching and shrinking sheet cases, respectively, and m is the dimensionless mass transfer induced slip parameter such that $mV_p \leq 0$. The exact solution to (9)-(10) can be searched in the form

$$f(\eta) = V_p + \frac{d}{\alpha(1+c\alpha)}(1-e^{-\alpha\eta}), \tag{12}$$

where α is a positive root of the polynomial of degree three equation

$$a_3\alpha^3 + a_2\alpha^2 + a_1\alpha + a_0 = 0, \tag{13}$$

with $a_3 = -(c+\frac{c}{\gamma})$, $a_2 = cV_p - 1 - \frac{1}{\gamma}$, $a_1 = V_p + Mc$, $a_0 = M + d$.

3 Results and discussion

The solutions to boundary value problem (9)-(10) will be discussed in some special cases. The Crane solution [2] belongs to the problem of Newtonian fluid flow in non-magnetic field, when there is no suction or injection and no slip, i.e.,

$$\frac{1}{\gamma} = 0, \quad M = 0, \quad c = 0, \quad V_p = 0 \tag{14}$$

the solution has the form

$$f(\eta) = 1 - e^{-\alpha\eta}. \tag{15}$$

Pavlov [3] investigated the Crane's problem with magnetic field, i.e.,

$$\frac{1}{\gamma} = 0, \quad M \neq 0, \quad c = 0, \quad V_p = 0, \tag{16}$$

the solution has the form

$$f(\eta) = \frac{1}{\alpha}(1-e^{-\alpha\eta}), \quad \alpha = \sqrt{1+M}. \tag{17}$$

Bhattacharya et al. [7] gave the exact solution for Casson fluid in magnetic field with suction/injection,

$$\frac{1}{\gamma} \neq 0, \quad M \neq 0, \quad c = 0, \quad V_p \neq 0 \tag{18}$$

in the form

$$f(\eta) = V_p + \frac{1}{\alpha}(1-e^{-\alpha\eta}), \tag{19}$$

where $\alpha = \frac{V_p+\sqrt{V_p^2+4(1+1/c)(1+M)}}{2(1+1/c)}$ for shrinking and $\alpha = -\frac{V_p+\sqrt{V_p^2-4(1+1/c)(1+M)}}{2(1+1/c)}$ for stretching sheet.

Our aim is to investigate the solution to (9)-(10) when

$$\frac{1}{\gamma} \neq 0, \quad M \neq 0, \quad c \neq 0, \quad V_p \neq 0. \tag{20}$$

The impact of various dimensionless parameters are analyzed for the flow structures. Both the shrinking sheet case (d=+(1+m)) and stretching sheet case (d=-(1+m) are considered. The dependence on the Casson effect and the magnetic parameter are analyzed numerically.

4 Future work

The energy equation can be added to the governing equations. Then the similarity transformations can be applied to reduce the nonlinear partial differential equations system to a nonlinear coupled ordinary differential equation system. The heat transfer characteristics will be studied with two types of boundary conditions, namely with prescribed surface temperature and heat flux. Knowing the exact solution to the momentum nonlinear ordinary differential equation, the temperature equation will be solved. The parameter dependency will be analyzed for the temperature field.

Acknowledgments

This work was supported by project no. 129257 implemented with the support provided to the corresponding author from the National Research, Development and Innovation Fund of Hungary, financed under the K18 funding scheme.

References

[1] Casson N. A flow equation for pigment-oil suspensions of printing ink type. In: Mill, C.C., Ed., Rheology of Disperse Systems, Pergamon Press, Oxford (1959) 84–102.

[2] Crane LJ. Flow past a stretching plate. Z Angew Math Phys (ZAMP). **388**(21) (1970), 645–647.

[3] Pavlov KB. Magnetohydrodynamic flow of an incompressible viscous fluid caused by deformation of a plane surface. Magnitnaya Gidrodinamika. **4** (1974), 146–147.

[4] Chakrabarti A, Gupta AS. Hydromagnetic flow and heat transfer over a stretching sheet. Q Appl Math. **37** (1979), 73–78.

[5] Klazly M, Bognar G. A novel empirical equation for the effective viscosity of nanofluids based on theoretical and empirical results International Communications in Heat and Mass Transfer **135** (2022), Paper: 106054.

[6] Klazly M, Bognar G. CFD Study for the Flow Behaviour of Nanofluid Flow over Flat Plate International Journal of Mechanics **14**(1) (2020), 49–57.

[7] Bhattacharyya K, Hayat T, Alsaedi A. Exact solution for boundary layer flow of Casson fluid over a permeable stretching/shrinking sheet. Z Angew Math Mech. **94**(6) (2014), 522–528.

International Conference on Mathematical Analysis and Applications in Science and Engineering
ICMA^{2}SC'22
ISEP Porto-Portugal, June 27 - 29, 2022

Multi-class Semantic Segmentation for Prostate Cancer Radiotherapy Treatment Optimization

Bruno Mendes[1,2⋆] **Inês Domingues**[3,1] **João Santos**[1,4]

[1] Centro de Investigação do Instituto Português de Oncologia do Porto (CI-IPOP), Portugal
[2] Faculdade de Engenharia da Universidade do Porto (FEUP), Portugal
[3] Politécnico de Coimbra, ISEC, DEIS, Portugal
[4] Instituto de Ciências Biomédicas Abel Salazar (ICBAS), Portugal

[1⋆]brunomendes81@gmail.com

Abstract: External Beam Radiotherapy (EBRT) is suggested as a curative option for localised and locally advanced disease and as a palliative option for the metastatic low-volume disease. Current planning systems provide ATLAS based segmentation methods, and although initial contours are fast, the manual adjustment required is very time-consuming and shown to be longer than manual. Deep learning methods have proven to be highly effective, precise and fast, improving treatment outcomes. This work is an attempt at a segmentation framework for EBRT prostate patients. As a crucial step in treatment effectiveness, it is imperative to be precise. Medical experts use their knowledge and expertise to perform these manual segmentations. Their perception of the positions of the organs is sometimes anatomically holistic. So, what if our U-Net needed to perceive the position of all organs to improve segmentation results? With this in mind, we attempted a multi-class semantic segmentation for prostate cancer radiotherapy treatment planning optimization. The results suggest that the awareness of the prostate and bladder improves the segmentation results for the rectum.

keywords: U-Net; Prostate Cancer; Multi-class; Semantic Segmentation; Radiotherapy.

MSC2020:

1 Introduction

The first described Prostate Cancer (PCa) case goes back to 1853, when John Adams, a surgeon at the London Hospital, followed a histological examination for cirrhosis of the prostate gland. He reported the condition as an orphan disease. In 2020, it was the second most frequent malignancy, with 1.414.259 new cases and responsible for 7.3% of all cancer deaths in men [6]. The prostate gland is part of the male reproductive system and about the size of a walnut. It is located in the pelvis surrounding the prostatic urethra and below the bladder [5]. Silently asymptomatic in an early stage, has been traditionally diagnosed by Digital Rectal Examination (DRE) and Prostate Specific Antigen (PSA), usually originating from the peripheral zone of the prostate, adjacent to the rectum.

Current guidelines suggest EBRT as a curative option for localised and locally advanced disease and as a palliative option for metastatic low-volume disease [3]. In the EBRT workflow, volumes

are drawn manually by highly trained medical experts on top of a Computed Tomography (CT) scan, a time consuming and error-prone task. EBRT systems do offer some automated contouring solutions. Most of them are ATLAS based. In a recent study, Zabel et al. [7] compared the impact of deep learning and ATLAS based segmentation methods with the traditional manual segmentation of the bladder and rectum. Couto, Domingues, and Santos [2] evaluated four algorithms to segment the bladder in PCa patients: k-means and several classifiers, a U-Net, active contours and graph-based methods. A U-Net followed by morphological operations to select the connected region gave the best results. Recently, Almeida et al. [1] presented a framework to perform a 3D segmentation of the prostate, bladder and rectum using CT images. The proposed architecture introduced an active contour method and an attention gate to a traditional U-Net, improving the segmentation outcomes of deep learning.

In this work, we intend to explore and evaluate the use of a U-Net for a multi-class semantic segmentation framework to automate and speed the segmentation task in EBRT planning workflow. With the rectum presenting itself as a very challenging organ to segment, this approach tries to mimic the anatomical visualization of medical experts, a holistic segmentation. The presence of the prostate and bladder in a multi-class model seems to improve dramatically the ability to contour the rectum.

2 Results and discussion

This work is retrospective research that used treatment plans available at Instituto Português de Oncologia do Porto Francisco Gentil (IPO-PORTO). All patients had undergone a CT scan as part of the EBRT treatment. To train the models, we used an Intel Xeon Platinum 8253 CPU@2.20GHz, with 187 Gb of RAM and an Nvidia Quadro RTX 6000/8000 (24Gb/48Gb GDDR6). The image dataset has CT images from 71 patients. All studies ranged from 2019 to 2021 with curative intent, and patients were between 51 and 89 years old. Images were acquired in a 16 slice CT scanner from General Electric, GE Optima 580 available at the IPO-PORTO for EBRT, with 2.5 mm slice thickness, 120 Kvp and automatic tube current modulation. All images were anonymized and had the approval of use from the ethics committee. Segmentations were performed manually by medical experts in the available EBRT planning system and converted to an Nearly raw raster data (Nrrd) volume together with the corresponding Label map for prostate, bladder and rectum structures.

A custom dataset holding the images in cache for training was designed. A 2D U-Net was created and trained from scratch, with the ability to output a multi-class segmentation. The implementation is almost identical to the one proposed by Ronneberger, Fischer, and Brox [4] with slight modifications. We added a padding of 1 in the double convolution blocks in both encoder and decoder arm, avoiding the cropping in the skip connections as both sizes will match, as long as the input size is a multiple of 8. Single class models for the prostate, bladder and rectum were built and also a multi-class model containing all three organs. Class weights for the CrossEntropyLoss function were also computed to address class balancement.

To evaluate the quality of the segmentations the Dice Similarity Coefficient (DSC) and the Jaccard Index (JI) were computed and a ReduceLROnPlateau scheduler, which monitors the improvement of the DSC and adjusts the learning rate accordingly. Besides, images were center-cropped, assuring the segmentation was completely visible thus reducing the amount of background. The train/validation split was 80/20, assuring that images from the same patient only appear either on training or validation. The settings for the runs and the obtained results are shown in Table 1. Figure 1 shows the segmentations for the single class models and Figure 2 for the multi-class model.

Table 1: Settings and results. Mean values and standard deviations are shown for the 100 runs.

	Prostate	Bladder	Rectum	Multi-class
# Train	881	1462	2410	2739
# Val.	215	380	636	719
# Epochs	100	100	100	100
# Batch size	10	10	10	10
# Workers	10	10	10	10
Optimizer	Adam	Adam	Adam	Adam
Learning Rate	1×10^{-3}	1×10^{-3}	1×10^{-3}	1×10^{-3}
Image size	128x128	256x256	256x256	256x256
Time (min)	22	68	98	117
Acc	0.96 ± 0.04	0.98 ± 0.02	0.02 ± 0.10	0.97 ± 0.04
DSC	0.73 ± 0.08	0.90 ± 0.05	0.02 ± 0.01	0.71 ± 0.10
JI	0.77 ± 0.00	0.91 ± 0.00	0.01 ± 0.00	0.67 ± 0.00
Train Loss	0.06 ± 0.07	0.04 ± 0.02	0.69 ± 0.03	0.06 ± 0.14
Val. Loss	0.48 ± 0.21	0.03 ± 0.04	0.60 ± 0.05	0.22 ± 0.09

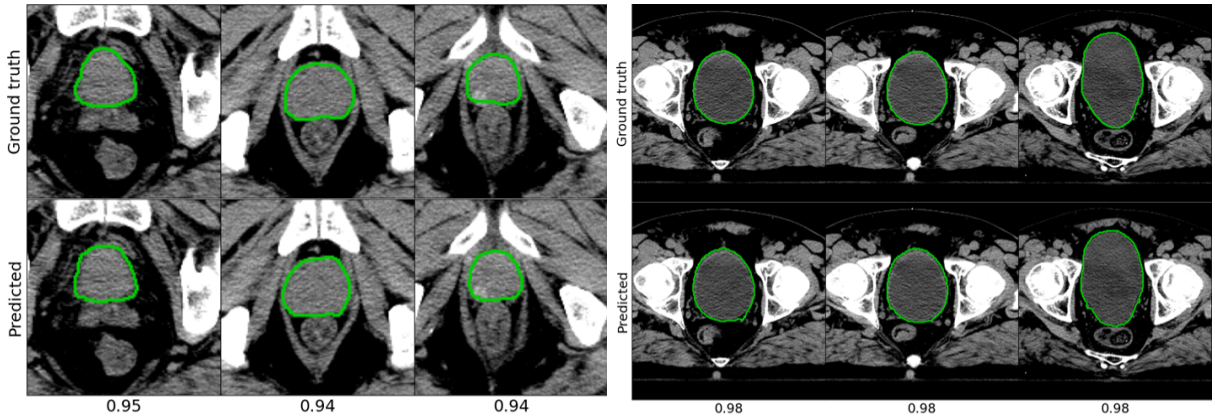

(a) Prostate model. (b) Bladder model.

Figure 1: Top 3 DSC for the prostate and bladder model.

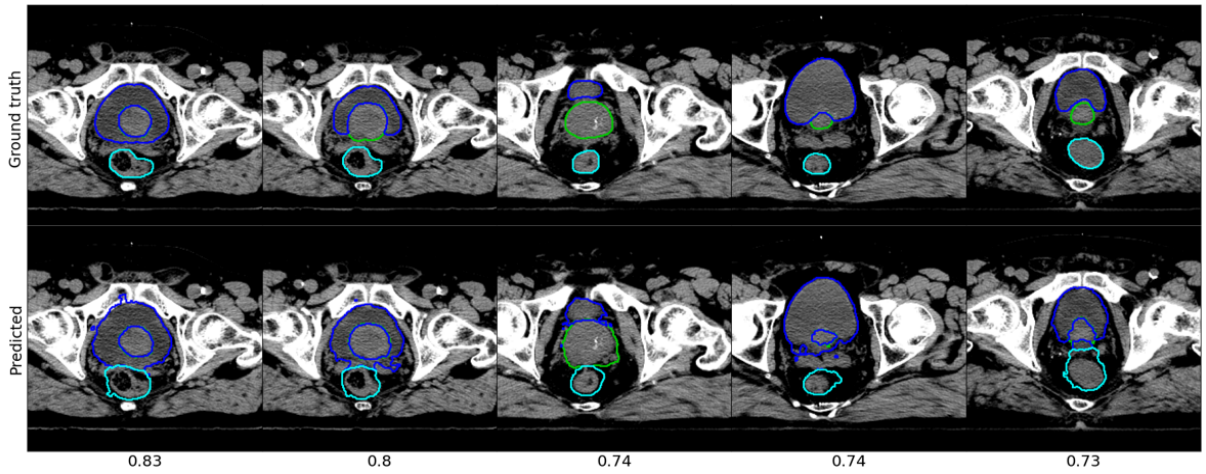

Figure 2: Top 5 DSC for multi-class model. Bladder in dark blue; prostate in green; rectum in light blue.

The prostate is a relatively small organ, at least when compared to the bladder. The number of slices in the volume that contain the prostate structure is much less than the other organs. The bladder can also be filled with urine, which is often the case in EBRT patients. The rectum is a small organ when in an axial view but very extensive in volume. Therefore, the number of selected images for training was higher than for other organs. Still the single-class model

could not predict precisely the rectum in any image (obtained segmentations are omitted for simplicity). The high heterogeneity of the Hounsfield Unit (HU) values found in the rectum may present a challenge. In a multi-class scenario, images with at least one segmentation were considered. Although the obtained mean DSC and JI were lower than the ones obtained for single class models, the predicted segmentations included the rectum.

3 Conclusions and Future work

For Prostate cancer, the main segmentation challenges may arise from the wide diversity in patients HU from the CT, even for the same organ. A young prostate does not have the same attenuation coefficient as an older prostate. The same for other organs. Besides, the bladder may be filled with urine and the rectum with gas. A previously treated organ, either with surgery or radiotherapy, also has a different attenuation coefficient than an untreated one. This diversity may provide challenges to overcome, searching for an accurate segmentation framework.

When performing manual segmentation, medical experts rely on Magnetic Ressonance Imaging (MRI) images, to increase soft-tissue contrast. Besides, their expertise and anatomical knowledge allows them to draw a contour based on a 3D mental representation of the volume. For some 2D images, it may seem impossible to segment any structure, at least for an untrained eye. Our visual perception is sometimes improved by the awareness of other structures.

In this work, the results suggest that training a model using a multi-class strategy, seems to improve the segmentation results for a previously challenging organ such as the rectum. Although our multi-class model is not yet capable of quantifying the segmentations separately for each class, the predictions for the rectum have improved dramatically. Still, some improvements need to be done. A custom function is required to compute segmentation accuracy separately for each class. Also, the dataset is small and unbalanced but data collection is an ongoing process and data augmentation techniques will also be explored.

References

[1] Gonçalo Almeida et al. "Segmentation of male pelvic organs on computed tomography with a deep neural network fine-tuned by a level-set method". In: *Computers in biology and medicine* 140 (2022), p. 105107.

[2] Ana Couto, Inês Domingues, and João Santos. "Comparison of bladder segmentation techniques in CT scans". In: *Portuguese Conference on Pattern Recognition (RecPad)* (2021).

[3] C Parker et al. "Prostate cancer: ESMO Clinical Practice Guidelines for diagnosis, treatment and follow-up". In: *Annals of Oncology* 31.9 (2020), pp. 1119–1134.

[4] Olaf Ronneberger, Philipp Fischer, and Thomas Brox. "U-net: Convolutional networks for biomedical image segmentation". In: *International Conference on Medical image computing and computer-assisted intervention*. Springer. 2015, pp. 234–241.

[5] Omesh Singh and Srinivasa Rao Bolla. "Anatomy, Abdomen and Pelvis, Prostate". In: *StatPearls [Internet]* (2019). URL: `https://www.ncbi.nlm.nih.gov/books/NBK540987/` (visited on 01/16/2021).

[6] Hyuna Sung et al. "Global Cancer Statistics 2020: GLOBOCAN Estimates of Incidence and Mortality Worldwide for 36 Cancers in 185 Countries". In: *CA: a cancer journal for clinicians* (2021).

[7] W Jeffrey Zabel et al. "Clinical evaluation of deep learning and atlas-based auto-contouring of bladder and rectum for prostate radiation therapy". In: *Practical Radiation Oncology* 11.1 (2021), e80–e89.

International Conference on Mathematical Analysis and Applications in Science and Engineering
ICMA²SC'22
ISEP Porto-Portugal, June 27 - 29, 2022

FRACTAL BROWNIAN MOTION VS GLOBAL ASSESSMENT OF COP EXCURSION DURING IMPULSE PHASE ON STANDARD MVJ

Carlos Rodrigues[1*] **Miguel Correia**[2] **João Abrantes**[3]
Benedetti Rodrigues[4] **Jurandir Nadal**[5]

[1] INESC TEC, Portugal
[2] FEUP, Portugal
[3] ULHT, Portugal
[4] UFPE, Brazil
[5] UFRJ, Brazil

[1*]carlos.b.rodrigues@inesctec.pt

Abstract: This study confronts fractal Brownian motion assessment for structure analysis with global analysis as complementary tools to address the center of pressure (CoP) excursion during impulse phase on standard maximum vertical jump (MVJ) expanding CoP analysis from static to dynamic natural human activities such as MVJ and corresponding lower limb muscle stretch-shortening cycle (SSC). This way, feet CoP contact control was assessed during impulse phase with long and short SSC in terms of dynamic stabilometry and differences were detected at short and long-term regime on structural analysis pointing to distinct stochastic process at each MVJ type, in line with global analysis at short, middle, and long-time range and detected behavior on unconstrained standing studies.

keywords: fractal Brownian motion; COP excursion; countermovement

MSC2020: 60J60; 60J65; 28A80.

1 Introduction

Gait presents from phylogenetic and ontogenetic perspectives, as a determinant advantage for human being [1]. On human phylogenetic evolution to biped gait our visual perspective has shifted from the ground to the horizon, increasing our distance to the floor and modifying the orientation of the field of vision, thus increasing our vision scope and the number of visual *stimuli* contributing to development of the brain. It released our hands from support at the ground contact, making them available for manipulating objects and developing tools, potentiating learning and brain development.

Human biped gait contributed also to the development of the brain through the greater complexity of stability control in relation to quadruped gait, increasing our progression velocity and improving our chances of survival whether escaping predators and enhance our hunting chances. On ontogenetic evolution we covered a similar path at different time scale from crawling to walking, running, and jumping [2], with such advantage on posture, dexterity, and performance that only when we lose these capacities, we truly become aware of their importance. Thus, gait as a contact control task requires precise control of the ground reaction force acting at the feet center of pressure (CoP), since it is responsible along with gravity force acting at the center of mass (CoM) by the acceleration of the whole-body CoM [3].
The central nervous system (CNS) is responsible for muscles active control under the feedback of the proprioceptive system, for the actuation of musculoskeletal system towards human movement [4]. Despite isolated isometric, concentric, and eccentric muscle action gathered larger research attention, natural human action corresponds to muscle stretch-shortening cycle (SSC), with muscle stretch preceding muscle contraction for efficient submaximal and powerful maximal activity [5]. Although muscle SSC can be observed at gait and running its higher expression and accessibility is performed on standard maximum vertical (MVJ), with long SSC on countermovement jump (CMJ) and short SSC on drop jump (DJ) for comparison with squat jump (SJ) without SSC [6].
According to the importance of CoP excursion during feet ground contact, its influence has been assessed on orthostatic equilibrium, gait, running and standard MVJ [7], with an open issue on advantage of fractal Brownian motion vs global assessment of CoP excursion to capture CoP underlying control on different MVJ impulse.

2 Results and discussion

Results from fractal Brownian motion analysis of CoP excursion presented during impulse phase at each MVJ type, two distinct behaviors for the short- and long-term regime regarding the average square distances $<\Delta R^2>$ for increasing Δt time steps as well as for the corresponding log-log plots, leading to different diffusion coefficient D and Hurst index scale exponent H, critical time t_c and $<\Delta R^2_c>$ average square distance threshold between the two regimes [7]. Thus, DJ presented lower t_c than SJ and CMJ, with CMJ presenting higher $<\Delta R^2_c>$ than SJ and DJ ($p<0.05$). SJ and CMJ presented lower short- and long-term diffusion coefficients D_s and D_l than DJ pointing to higher stochastic activity and postural instability on DJ in relation to SJ, CMJ, with higher D_s than D_l on SJ and CMJ thus pointing to short-term open loop control higher stochastic activity than at long-term closed loop control and the opposite at DJ. Short-term Hurst index exponent H_s presented higher mean value at SJ than CMJ ($p<0.05$) and DJ ($p\geq0.05$) with higher mean at CMJ than DJ ($p\geq0.05$). H_s presented mean value higher than 0.5 on SJ ($p<0.05$), CMJ and DJ ($p\geq0.05$) pointing on short-term regime to stochastic process positively correlated and persistent behavior maintaining movement direction. Regarding long-term Hurst index exponent H_l presented higher mean value at DJ than CMJ ($p<0.05$) and SJ ($p\geq0.05$), with CMJ higher mean value than SJ ($p\geq0.05$). Furthermore, H_l presented at DJ mean value higher than 0.5 pointing at long-term regime to stochastic process positively correlated and persistent behavior maintaining movement direction whereas SJ and CMJ presented lower mean H_l than 0.5 pointing to stochastic process negatively correlated with anti-persistent behavior and tendency for future inversion of past tendency.
Regarding global analysis of CoP excursion, focusing on accumulated square distance ΣR^2 of CoP during impulse, three different phases were detected at short, middle, and long-time range for each MVJ type [8]. Thus, SJ presents slow ΣR^2 increase before

- 350ms, with larger ΣR^2 growth between -350ms and -150ms and growth increase from -150ms to take-off. As regards to CMJ a steady growth is dominant from -800ms to take-off. Finally, DJ presented initial sharp growth of ΣR^2 from - 200ms and -150ms followed by reduced growth from -150 ms and -10 ms with new sharp growth from -10ms to take-off.

3 Conclusions and Future work

Fractal Brownian motion assessment and global analysis presented as complementary tools to address CoP excursion during impulse phase on standard MVJ. Whereas fractal Brownian motion assessment allowed detection of structural analysis with two distinct behaviors for short- and long-term regime at different MVJ, global analysis conducted to distinct time phases detection during the impulse on SJ, CMJ and DJ. Presented structural and global analysis constitute an expansion of static stabilometry analysis to dynamic stabilometric assessment during impulse phase on different MVJ involving long and short lower limb muscle SSC for comparison with no SSC. Future work may include the application of different structural analysis and new global variable assessment of CoP excursion on dynamic stabilometry during impulse phase on standard MVJ and corresponding muscle SSC.

References

[1] W.E.H. Harcourt-Smith, *The origins of bipedal locomotion*. W. Harcourt-Smith (Ed.). Handbook of Paleoanthropology (2nd Ed., Chap. 5, pp 1483 – 1518). Berlin Heidelberg: Springer-Verlag, 2007.

[2] K. E. Adolph, S. R. Robinson, *The road to walking: What learning to walk tells us about development*. P.D. Zelazo (Ed.). Oxford library of psychology. The Oxford handbook of developmental psychology (Vol. 1): Body and mind (pp 403 – 443). Oxford: University Press, 2013.

[3] V.I. Schenau, V. Soest, On the biomechanical basis of dexterity. M.L. Latash and M.T. Turvey (eds.). Dexterity and its development. New Jersey: Lawrence Erlbaun Associates, Inc., Publishers, 1996.

[4] D.A. Winter, *Biomechanics and motor control of human movement*, 4th ed. Hoboken, NJ: John Wiley & Sons, 2009.

[5] J. Hamill, K.M. Knutzen, *Biomechanical basis of human movement*. Philadelphia, PA: Lippincott Williams & Wilkins, 1995.

[6] P.V. Komi, *Strength and Power in Sport*, 2nd ed. Oxford, UK: Blackwell Science, 1992.

[7] C. Rodrigues, M. Correia, J. Abrantes, M. Rodrigues, J. Nadal (2021). Fractal Brownian motion assessment of the center of pressure excursion during impulse phase on standard vertical jump. IEEE Engineering in Medicine and Biology Society. Annual International Conference, 2021, 4808–4811.

[8] C. Rodrigues, M.V. Correia, J.M.C.S. Abrantes, M. Silva, M. Benedetti, J. Nadal (2015). Estabilometria do centro de pressão durante a fase de impulsão em diferentes contra-movimentos verticais. Book of abstracts 6th Portuguese Congress on Biomechanics, 2015, 217–218.

International Conference on Mathematical Analysis and Applications in Science and Engineering
ICMA^{2}SC'22
ISEP Porto-Portugal, June 27 - July 1, 2022

Building a script that emulates VeriSoft® in the Gamma Analysis of Complex Radiotherapy Treatments

Leyla Ebrahimpour[1⋆] **Inês Domingues**[2] **Sofia Isabel Silva**[1]
Diana Pimparel[1] **Joana Lencart**[1] **Bruno Mendes**[1] **Filipe Dias**[1]
João Santos[1,3]

[1] Centro de Investigação do Instituto Português de Oncologia do Porto (CI-IPOP), Física Médica, Radiobiologia e Protecção Radiológica, Porto, Portugal
[2] Politécnico de Coimbra, ISEC, DEIS, Portugal
[3] Instituto de Ciências Biomédicas Abel Salazar (ICBAS), Porto, Portugal

⋆L.ebrahimpour@gmail.com

Abstract: For a Radiotherapy treatment plan (TP) to be delivered to the cancer patients more accurately, patient-specific quality assurance (PSQA) should be performed before the treatment. During this process, the quality of the TPs is evaluated using the Gamma Passing Rate (GPR) metric which is calculated by Verisoft® software. We have developed an in-house script that can evaluate the TP before delivery to the patient. We discuss the method that is used in Verisoft® to calculate GPR and we compare the results. To the best of our knowledge, this is the first script that has been developed to emulate Verisoft®. Such in-house software allows the analysis of several patient measurements at once and can be integrated into larger software tools, to streamline the PSQA process in radiotherapy.

keywords: Radiotherapy; Quality Assurance; Gamma Passing Rate.

1 Introduction

When planning a Radiotherapy treatment, it is necessary to determine the radiation dose that reaches the patient. The treatment plan (TP) needs to go through a quality control process which is called patient-specific quality assurance (PSQA) process to evaluate if the dose is either excessive or insufficient. Gamma index [1] is the most commonly used metric to evaluate the dose distribution. It compares point by point, the computed dose with the one delivered by the linear accelerator (LINAC).

In this work, an in-house software was developed to evaluate the detector measurement points by using the gamma index. Our results are validated by comparison with the commercial software, VeriSoft®[1].

[1] https://www.ptwdosimetry.com/en/products/verisoft/

2 Methodology

The dose distribution of the samples in this work was measured with OCTAVIUS II[2] which receives the dose in the PSQA process before it is delivered to the patient. It consists of a 2D matrix of ionization chambers, displayed isotropically. In the process of PSQA, the measured dose at the evaluating points of the 2D matrix with the resolution of 10 mm is compared to the dose at the reference points with the resolution of 1 mm. The goal of this project was to write a script that evaluates the detector measurement points based on Depuydt et al. paper [2] and calculates the gamma index [1] and the dose difference for each approved point. The script evaluates the points in three levels and the output of the script determines the Gamma Passing Rate (GPR) which is an indicator to approve or not the measurement output of the LINAC. The gamma index [1] which compares the reference dose distribution ($D_r(r_r)$) to the evaluating dose distribution ($D_c(r_c)$) at an evaluating point with the position of r_c is calculated by:

$$\Gamma_r(r_c, D_c) = \sqrt{\left(\frac{\Delta r^2}{\Delta d_M^2}\right) + \left(\frac{\Delta D^2}{\Delta D_M^2}\right)} \tag{1}$$

where $\Delta r = |r_r - r_c|$ demonstrates the distance between the reference and the evaluating point and $\Delta D = D_c(r_c) - D_r(r_r)$ is the dose difference between the evaluating point at r_c and the reference point at r_r. Δd_M and ΔD_M stand for the acceptance criteria for the distance-to-agreement (DTA) and for the dose difference (in percentage with respect to the dose at the evaluating point) respectively [2]. In order to evaluate a plan, first, the acceptance criteria are set by the user. Then the gamma index is calculated for each evaluating point. If the evaluating point does not fulfil the $\Gamma_r(r_c, D_c) \leq 1$ criterion, it must be evaluated through the second and/or the third level. The percentage of the total number of evaluating points that can pass one of the three levels is reported as GPR $(\Delta D_M)\%/(\Delta d_M)$mm. Figure 1 shows a simple diagram of how an evaluating point may pass or fail while passing through three levels of evaluation process.

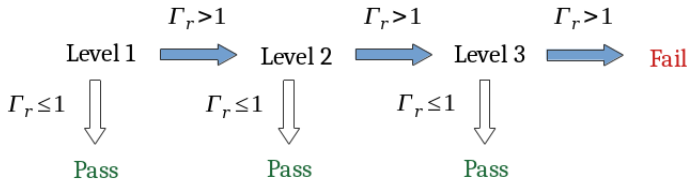

Figure 1: Graphic illustrating the evaluation process of each evaluating point on the 2D dose distribution matrix.

3 Results and discussion

A group of volumetric modulated arc therapy (VMAT) TPs from 12 patients was selected to evaluate the in-house script. Each of the plans has 2 arc fields. The 12 patients come from different treatment site groups and LINACs: Head and Neck (patients 1 to 3) and Mediastinum (patients 4 to 6) plans, treated in a Varian®[3] Trilogy LINAC; and Lung (patients 7 to 9) and Prostate (pelvis) plans (patients 10 to 12), treated in a Varian Novalis LINAC. A subgroup of 5 plans were used to fine-tune the details of the script.

In Table 1 the preliminary results for a test group of patients 1 to 5 (In-house script-V1 column) have been compared to VeriSoft®'s output in terms of the number of evaluated points and the values of GPR 3%/3mm. The difference between the number of evaluated points in some cases made us suspicious about the way VeriSoft® selects the points. VeriSoft® claims that the

[2]https://www.ptwdosimetry.com/en/products/octavius-ii/
[3]https://www.varian.com/

analysis is based on Depuydt et al. Paper [2]. There the number of evaluated points is defined as the number of points above or equal to a threshold. The threshold is defined as 10% of the maximum calculated dose which was used in the script. Upon reading the VeriSoft® document in more detail, it was found that VeriSoft® does not use the maximum calculated dose. To get a threshold, it considers the down-sampled maximum which is a sample of the calculated values only in positions where there are measured dose values. Our in-house script was thus changed based on this hypothesis and in Table 1 it is clear that the difference between the number of evaluated points decreased with respect to the results of the first version. There is an absolute difference of 0.5 % between GPR 3%/3mm of the script and the VeriSoft® in the worst case which is very satisfactory.

Table 1: Comparison of the number of evaluated (EV) points and GPR 3%/3mm by Verisoft® with the outputs of the first version (V1) and second version (V2) of the in-house script.

		No. of EV points (GPR 3%/3mm (%))		
Patient No.	Arc	In-house script-V1	In-house script-V2	VeriSoft®
1	RA1	281 (98.9)	287 (97.9)	288 (97.9)
	RA2	283 (98.2)	291 (97.9)	284 (98.2)
2	RA1	391 (99.7)	396 (99.8)	395 (99.7)
	RA2	375 (99.2)	384 (98.7)	385 (98.4)
3	RA1	427 (98.6)	427 (98.4)	427 (98.6)
	RA2	420 (99.0)	421 (99.0)	420 (98.8)
4	RA1	434 (98.4)	435 (97.0)	436 (97.0)
	RA2	422 (99.3)	422 (99.0)	423 (99.3)
5	RA1	188 (100.0)	203 (99.0)	197 (99.5)
	RA2	164 (100.0)	169 (100.0)	167 (100.0)

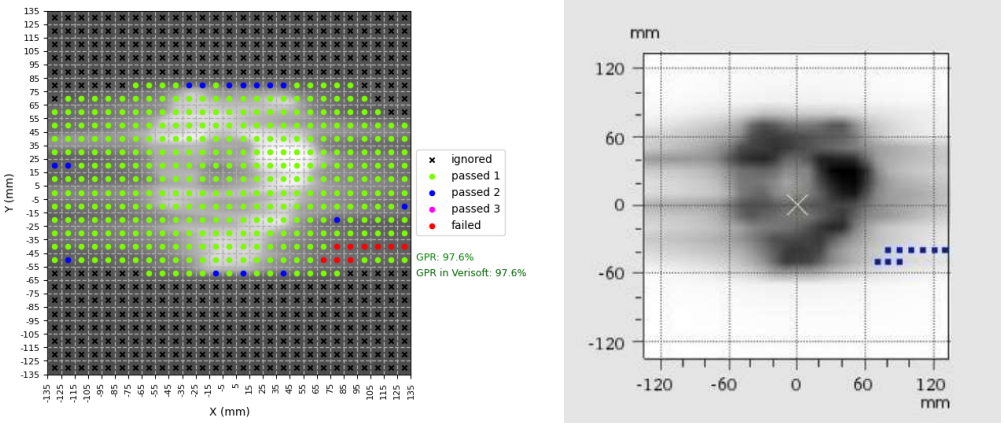

(a) (b)

Figure 2: Comparison of the outputs of the (a) script and (b) VeriSoft® in terms of the dose distribution and the status of the evaluating points in the Octavius II 2D matrix. The red dots in plot (a) correspond to the blue dots in plot (b) which represent the failed points.

We also noticed that there are two tables in the VeriSoft® for the calculated doses. The "Measurement Resolution" and the "High Resolution" tables. While the high-resolution table shows the calculated dose values with 1 mm resolution, we expected that the measurement resolution table contains the calculated dose values in the positions of the evaluating points (with 10 mm resolution). However, we found out that the values of the calculated dose in the positions of the evaluating points are different in the two tables. This could be one of the reasons for the difference between the number of evaluated points in Verisoft® and in our results. Yet the question remains. What are the values in the table of "Measurement Resolution"? As it is mentioned in the VeriSoft®'s Manual, the table contains "calculated mean values under the virtual chamber areas". It seems that the mean of calculated doses within an area around each evaluating point

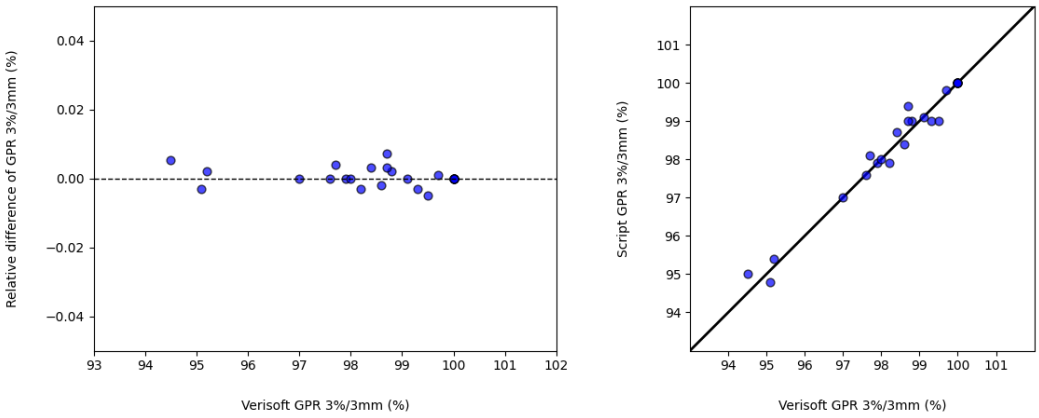

(a) (b)

Figure 3: Comparison of the outputs of the script and VeriSoft® software in terms of the (a) relative difference and (b) the absolute value of GPR 3%/3mm.

is calculated and inserted in the "Measurement Resolution" table. As a final attempt, we used the maximum of the "Measurement Resolution" table in VeriSoft® to calculate the threshold. This was done for all 24 samples (12 patients and 2 arcs for each patient). Although the number of evaluated points changed for 7 of the samples, the GPR 3%/3mm did not change at all with respect to the results of the second version of the script in Table 1. We were thus confident that we can use the maximum of the calculated values in positions of the evaluating points to calculate the threshold. Another thing that should be highlighted is the DTA criterium in level 3 of the evaluation process. There are no references which give us more details about level 3. The DTA that we used for level 3 was primarily 4 mm but then changed to 3.5 mm because GPR 3%/3mm was higher than Verisof's output in some cases and it was because there were points that were passing through level 3 while they must not. The output of the script in terms of the dose distribution over the Octavius II® 2D matrix and the failed points has been compared to the output of VeriSoft® in Figure 2 for one of the patients. The dose distribution and the failed points are perfectly matched however the latter may differ occasionally by one or two points for other patients. Figure 3 represents a comparison between the outputs of the script and the VeriSoft® by representing (a) the relative difference and (b) the absolute value of GPR 3%/3mm. These results indicate the good agreement of the outputs.

4 Conclusions and Future work

In this work, an in-house program was developed to calculate the GPR of complex radiotherapy treatments based on the methodology in Depuydt et al. paper [2]. Our results show a very good agreement with the output of VeriSoft® which is widely used to evaluate the detector measurement points in the process of Quality Assurance (QA) in radiotherapy. In the future, the script is used in a sequence of analyses of the radiotherapy treatment data which intends to improve and streamline the PSQA process through artificial intelligence methods.

References

[1] Low DA, Harms WB, Mutic S, Purdy JA. A technique for the quantitative evaluation of dose distributions. Med Phys. 1998 May;25(5):656-61. doi: 10.1118/1.598248. PMID: 9608475.

[2] Depuydt T, Van Esch A, Huyskens DP. A quantitative evaluation of IMRT dose distributions: refinement and clinical assessment of the gamma evaluation. Radiother Oncol. 2002 Mar;62(3):309-19. doi: 10.1016/s0167-8140(01)00497-2. PMID: 12175562.

International Conference on **M**athematical **A**nalysis and **A**pplications in **S**cience and **E**ngineering
ICMA^{2}SC'22

ISEP **Porto-Portugal, June 27 - July 1, 2022**

Calculating and employing Complexity Indexes to compare and improve the quality of the VMAT plan delivery in Radiotherapy Treatments

Leyla Ebrahimpour[1⋆] **Sofia Isabel Silva**[1] **Diana Pimparel**[1]
Joana Lencart[1] **Bruno Mendes**[1] **Filipe Dias**[1] **Inês Domingues**[2]
João Santos[1,3]

[1] Centro de Investigação do Instituto Português de Oncologia do Porto (CI-IPOP), Física Médica, Radiobiologia e Protecção Radiológica, Porto, Portugal
[2] Politécnico de Coimbra, ISEC, DEIS, Portugal
[3] Instituto de Ciências Biomédicas Abel Salazar (ICBAS), Porto, Portugal

⋆L.ebrahimpour@gmail.com

Abstract: The process of patient-specific quality assurance (PSQA) is performed before radiotherapy treatment of the cancer patient to assure that the patient receives the appropriate dose. One way to streamline this process and assess the deliverability or quality of treatment plans (TPs) before the PSQA measurement is to use Complexity Indexes (CIs). In this work, we have developed in-house scripts to calculate a selective sample of CIs on a sample of prostate patients with various complexities. We compare the strength of the selected CIs to distinguish the TPs in terms of fractionation, and its impact on complexity, which leads us to select more promising CIs to evaluate the quality of TPs in the future through being employed in artificial intelligence methods.

keywords: Complexity Index; VMAT; Radiotherapy; Quality Assurance

1 Introduction

In order to perform a volumetric modulated arc therapy (VMAT), the safety and deliverability of each radiotherapy treatment plan (TP) must be examined by medical physicists in the process of patient-specific quality assurance (PSQA), to verify whether the dose delivered by the linear accelerator (LINAC) corresponds to the calculated dose to be delivered to the patient. The therapeutic photon beam comes out of a part of the LINAC called gantry, which can be rotated around the patient and is shaped by a multileaf collimator (MLC). The MLC has 2 banks of 60 leaves each, which move independently to colimate the beam. In VMAT treatments, the movements of MLC, the gantry speed (GS) and acceleration and the dose rate (DR) variations are subject to errors that can affect the dose delivered to the patient [5]. The Gamma Passing (approval) Rate (GPR) so far has been the standard parameter to determine if the plan can be delivered to the patient, despite being known to miss relevant positional errors of the MLC leaves [5]. There are significant studies [1, 2, 3, 4] about the possible metrics, called Complexity Indexes (CIs) that may help to assess the plan deliverability and to streamline the PSQA process. Modulation complexity score applied to VMAT ($MCSv$) [1] and four Modulation Indexes (MIs): MI_s, MI_a, MI_t [3], and MI_c [4], can be considered as CIs which have shown moderate to good correlations to GPR [4, 6]. These CIs are focused on the variations of mechanical parameters

under the assumption that an increase in mechanical parameter modulation will increase the uncertainty in delivery [3]. While $MCSv$ only takes the MLC positions into account [1], the MLC speed, MLC acceleration and dose rate variations are taken into account on the calculation of the MIs [3]. Additionally, MI_c considers dose calculation uncertainty which is usually affected by small or irregular fields [4] and can be quantified using a thinning algorithm. In this work, we developed in-house scripts to calculate $MCSv$ and four MIs. The purpose is to implement the best known CIs at a Radiotherapy department, to study, compare and improve the deliverability of VMAT treatments, and, prospectively, optimize the use of material and human resources.

2 Data and Methodology

Table 1 shows a summary of a sample of 71 prostate patients (in a total of 136 treatment arcs/beams) consisting of 5 types of fractionations which was used for the computation of the selected CIs in this work. These were treated mainly on a Varian®[1] Novalis LINAC, except the SBRT treatments, programmed for a Varian® Truebeam LINAC.

Table 1: Summary of the Prostate sample used for CIs computation in this work.

Fractionation	Treatment site	Dose (Gy)	Daily dose frac (Gy)
Moderate Hypofractionated	PR[a]	60.00	3
SIB[b]	PR/PL[c]	70.20	2.7
Conventional fractionation	PL; PR+VS;[d] PR; PR	45;15;20;18	1.8;2.143;2;2
Special Cases	PR+VS;PR+VS;PR	55;15;55	2.5;2.5;2.75
SBRT[e]	PR	36.25	7.25

[a] Prostate; [b] Simultaneous Integrated Boost; [c] Pelvis; [d] Vesicle; [e] Stereotactic Body Radiotherapy

The scripts to calculate the selected CIs were programmed in Python 3.9.9. $MCSv$ was calculated using the relation A4 in Masi et al. 2013 [1] (hereafter Masi13):

$$MCS_{arc} = \sum_{i=1}^{I-1} \left[\frac{(AAV_{cpi} + AAV_{cpi+1})}{2} \times \left(\frac{(LSV_{cpi} + LSV_{cpi+1})}{2}\right) \times \left(\frac{MU_{CPi,i+1}}{MU_{arc}}\right) \right] \quad (1)$$

where, $MU_{CPi,i+1}$ is the delivered dose in MU between i^{th} and $(i+1)^{th}$ control point. Control points (CPs) are equally-spaced discretization points in the angular space swept by the gantry around the patient. LSV (leaf sequence variability) takes the differences in position between adjacent MLC leaves at each CP into account and is calculated by relation A2 in Masi13. AAV (aperture area variability) considers the area defined by the apertures of opposing leaves at each CP and is calculated based on the relation A3 in Masi13. The calculation of MIs were done based on the relations in Park et al. 2014 [3] (hereafter Park14) and Park et al. 2015 [4] (hereafter Park15). Here we suffice to write the relations for the calculation of MI_c:

$$MI_c = \sum_{n=1}^{120} Individual\ MI_{c,n} \quad (2)$$

where, $Individual\ MI_{c,n} = \int_0^k z_c(f)df$ is the individual $MI_{c,n}$ of n^{th} MLC leaf with k = 0.2, 0.5, 1 and 2 in this study. $z_c(f)$ is calculated as follows.

$$z_c(f) = \left(\frac{1}{N_{cp}-2}\right) \sum_{i=1}^{N_{cp}} \left\{ N_i \begin{pmatrix} f; MLC\ speed_i > f\sigma_{MLC\ speed} \\ or MLC\ accel_i > \alpha f \sigma_{MLC\ accel} \end{pmatrix} W_{GA,i+1} W_{MU,i+1} W_{AI,i} \right\} \quad (3)$$

The values of f which varies between 0.01 and 2 with a step of 0.01 has been defined by Webb [7]. N_{cp} is the total number of CPs for a given VMAT plan, $MLC\ speed_i$ and $MLC\ accel_i$ indicate the speed and the acceleration of the MLC between the i_{th} and $(i+1)^{th}$ or $(i+2)^{th}$ CP respectively. $\sigma_{MLC\ speed}$ and $\sigma_{MLC\ accel}$ are the standard deviations of the MLC speed and the MLC acceleration respectively, α is a weighting factor for the acceleration which is calculated based on the time between the i^{th} and the $(i+2)^{th}$ CP. $W_{GA,i+1}$, $W_{MU,i+1}$ and $W_{AI,i}$ indicate

[1] https://www.varian.com/

the gantry acceleration, the dose rate variation, and the field aperture irregularity (AI) weighting factors which are calculated by the relations (12) and (13) in Park14 and relation (2) in Park15 respectively. In order to calculate $W_{AI,i}$, a thinning algorithm of image processing techniques was developed to enable us taking the size and irregularity of field apertures at each CP into account. $N_i(f;)$ is a conditional counting for the i_{th} CP which is 1 if the conditions are met otherwise it becomes 0. If there is no modulation in GS, DR or AI, the weighting factors become 1 and the values of MIs will be the same if one calculates MI_a, MI_t, or MI_c. In the calculation of MI_s and MI_a there is no weighting factor and MI_t only misses $W_{AI,i}$ with respect to MI_c.

3 Results and discussion

Table 2 shows the mean value of the selected CIs utilizing 40 treatment arcs from prostate and prostate plus vesicle TPs with 2.034° angular distance between CPs from our conventional sample which is compared to a group of 40 plans with a majority of prostate and prostate plus vesicle TPs in Masi13 and to a group of 20 prostate TPs in Park14 and Park15.

Table 2: Comparison of the values of selected CIs with Masi13, Park14 and Park15.

Reference	k	MI_s	MI_a	MI_t	MI_c	$MCSv$
This work	0.5	15.01±2.21	18.04±2.61	22.42±5.48	24.01±4.41	0.25±0.05
	1.0	24.50±3.95	29.38±4.55	37.39±7.18	39.07±7.56	
Park14	0.5	10.01±0.95	14.98±1.49	15.28±1.46	-	0.59±0.07
	1.0	11.63±1.37	22.67±2.30	23.11±2.26	-	
Park15	0.5	-	-	16.3±3.8	19.3±4.8	0.57±0.11
	1.0	-	-	-	29.4±8.0	
Masi13	-	-	-	-	-	0.307

For $MCSv$, our result seems to be more consistent with the result in the original source (Masi13). There is also a good agreement between our results and the results in Park14 and Park15 for the values of MI_s (k=0.2), MI_a (k=0.2, 0.5, 1.0), MI_t (k=0.2, 0.5), and MI_c however, it is not possible to make an exact comparison because the samples used in each of the studies are not selected based on the same criteria. They include single institution dataset (in Masi13) and multi-institution dataset (in Park14 and Park15), and from different LINACS, which may affect the complexity of the plans. The values of MIs are increasing as k increases which is expected based on the relation of individual $MI_{c,n}$. In addition, when more uncertainties are taken into account the value of the modulation index increases for the same k. MI_c always show the highest value for the same k with respect to the rest of MIs. Figure 1 represents the

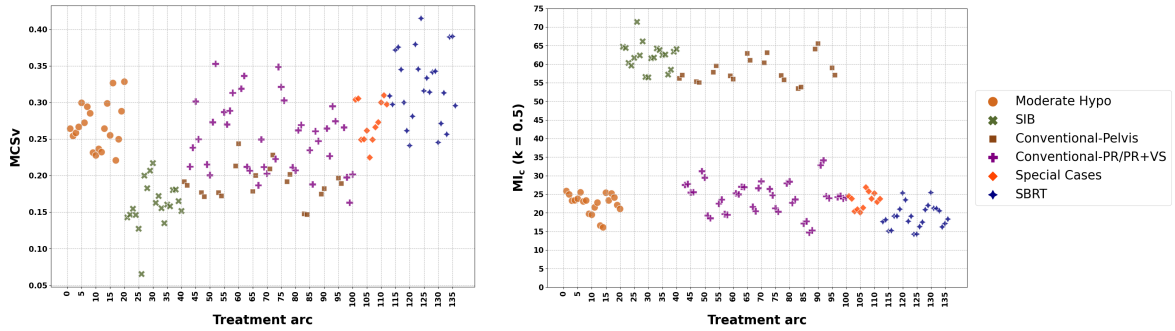

(a) (b)

Figure 1: Comparison of the values of (a) $MCSv$ and (b) MI_c (k = 0.5) for different fractionations of the sample summarized in Table 1. We only show the results of the calculation of MI_c because MIs result in the same output in terms of the distinction between different fractionations.

complexity values of our patient sample using $MCSv$ and MI_c (k=0.5). $MCSv$ varies between 0 and 1. The more complex the plan means the closer the $MCSv$ value to 0. Comparing the plots in Figures 1 clearly confirms the strengths of MI_c on the distinction of the plans based on their complexity comparing to $MCSv$. Figure 1(b), indicates that Pelvis TPs can be clearly distinct from prostate and prostate plus vesicle TPs in the conventional sample. For

the whole patient sample, weak correlations were obtained between $MCSv$ and GPR using the Spearman′s correlation coefficient ($r_s = 0.134$, $p - value = 0.202$) and between MIs and GPR ($r_s = -0.297$, $p - value = 0.004$). Considering only the high dose per fraction (7.25 Gy) SBRT TPs in Truebeam LINAC, the mean values of MI_t and MI_c are shown in Table 3, while the correlations between the selected CIs and GPR $3\%/3mm$ are displayed on the graphs of Figure 2. The dose (MU/Gy) was also found a well-correlated parameter with MIs for SBRT TPs. The best correlation between MIs and GPR $3\%/3mm$ occurs using MI_c (k = 2.0) with

Table 3: The mean values of $MCSv$, MI_t and MI_c for SBRT treatment plans.

k	0.2	0.5	1.0	2.0
MI_t	8.00±1.25	17.54±2.99	29.11±5.37	42.95±8.17
MI_c	8.06±2.08	18.27±4.83	30.33±8.26	44.76±12.29
$MCSv$		0.32±0.05		

$r_s = -0.565$ and $p - value = 0.004$. The correlation between dose (MU/Gy) and MI_c (k = 2.0) (Figure 2(b)) yields $r_s = -0.568$ and $p - value = 0.004$. These results demonstrate that MI_c and dose (MU/Gy) could be used as metrics to predict the probability of the plan's failure before PSQA process for SBRT plans in the future. Figure 2(c) shows the very good correlation between dose (MU/Gy) and GPR $3\%/3mm$ with $r_s = -0.659$ and $p - value = 0.000$.

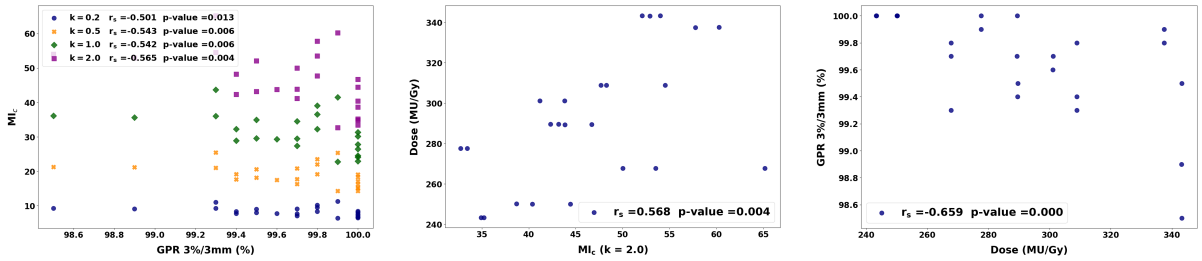

(a) (b) (c)

Figure 2: Correlation between (a) GPR $3\%/3mm$, (b) dose (MU/Gy) and MI_c; and between (c) dose (MU/Gy) and GPR $3\%/3mm$ for SBRT treatment plans.

4 Conclusions and Future work

Our results confirm that the in-house scripts to calculate $MCSv$, MI_s, MI_a, MI_t, and MI_c based on the instructions in Masi13, Park14, and Park15 can be used to score the complexities of TPs in Radiotherapy. The results demonstrate that $MCSv$ does not seem to be a promising metric to score the complexity of the TPs precisely. However, MI_t and MI_c may help to analyze and to distinguish the TPs in terms of complexity. Besides, using MI_t and MI_c for analyzing the prostate conventional sample leads us to the conclusion that pelvis plans have higher complexities than prostate and prostate plus vesicle plans. The good correlation of MI_c with PSQA results together with the support of the good correlation of the dose (MU/Gy) with PSQA outcome for SBRT prostate TPs, indicate that MI_c and dose (MU/Gy) could be used as metrics to predict the failure probability of the SBRT plans before PSQA process in the future. As future work, they can also be thought of as metrics to be used during the optimization process in VMAT planning and in the artificial intelligence methods applied to improve the quality of TPs and streamline the PSQA process.

References

[1] L Masi et al. 2013; doi: 10.1118/1.4810969.
[2] V Hernandez et al. 2018; doi: 10.1016/j.phro.2018.02.002.
[3] SY Park et al. 2014; doi: 10.1088/0031-9155/59/23/7315.
[4] SY Park et al. 2015; doi: 10.1088/0031-9155/60/18/7101.
[5] G Heilemann et al. 2013; doi: 10.1118/1.4789580.
[6] S Chiavassa et al. 2019; doi: 10.1259/bjr.20190270.
[7] S Webb et al. 2003; Biol. 48 2051.

International Conference on Mathematical Analysis and Applications in Science and Engineering
ICMA^{2}SC'22
ISEP Porto-Portugal, June 27 - 29, 2022

Using a Logit Approach to Determine the Occurrence of Barotrauma Under Hyperbaric Oxygen Therapy: a Case Study

M. Filomena Teodoro[1,2⋆] **Sofia S. Teles**[1]

[1] CINAV, Portuguese Naval Academy, Portuguese Navy,
Base Naval de Lisboa, Alfeite, 2810-001 Almada, Portugal
[2] CEMAT - Center for Computational and Stochastic Mathematics,
Instituto Superior Técnico, Lisbon University,
Avenida Rovisco Pais, n. 1, 1048-001 Lisboa, Portugal

[1⋆]mteodoro64@gmail.com

Abstract: The purpose of this work was to determine the incidence and severity of the barotrauma and to identify the possibility of middle ear barotrauma in a large number of patients undergoing regular hyperbaric oxygen therapy. To explore and clarify this issue in terms of incident, seriousness and recurrence, age, gender, clinical signs, specific history of chronic rhinitis and symptoms of nasal obstruction during the occurrence were registered. A first approach can be found in [6, 7, 8] where the authors perform a descriptive statistical analysis and apply some elementary and intermediate statistical techniques such as variance analysis[5]. Here a Logit model is built allowing to relate the occurrence of barotrauma with the clinical profile of patients. We could conclude that Hyperbaric Oxigen Therapy is a safe terapy.

keywords: barotrauma; hyperbaric oxigen therapy; logit.

MSC2020: 62-XX; 92-XX.

1 Introduction

Hyperbaric Oxygen Therapy (HBOT) is a treatment in which 100% oxygen is given in a room under pressure above sea level, providing an increase of perfusion of 0_2 in the tissues reducing inflammation and hypoxia of cells, which helps to treat ischemia and infection [1, 3]. The complications are not yet well known. Making an effort to better understand one of the complications due the HBOT, the barotrauma of the medium ear, was collected medical information about the patients than undergo to HBOT treatment and analyzed the gravity degree of the barotrauma and if it was in one or two ears, in the case of occurrence. Also, has continuation of the work presented in [6, 7, 8] was developed a LOGIT model [2, 4, 5, 9] so we could relate the barotrauma occurrence with the medical profile of the patients.

2 Results and discussion

Were evaluated the clinical details of 1732 patients who were submitted to HBOT between 2012 and 2016 at the Portuguese Naval Center for Underwater and Hyperbaric Oxigen Therapy. The incidence of BTOM was 8.3%. Between the patients that suffered barotrauma, 62% were an unilateral case, 34% on the right ear; 28% on the left ear; 21% on both ears. Significant association with barotrauma occurrence were gender, diagnosis of osteorradionecrosis of the mandible and personal history of allergic rhinitis.

3 Conclusions

The aim of this work was to determine the incidence and severity, and obtain eventual risk factors for barotrauma of the middle in the patients submitted to HBOT. Female gender, diagnosis of osteorradionecrosis of the mandible and personal history of allergic rhinitis were identified as risk factors. Taking into consideration the data set, it was concluded that OTHB is an efficient and safe therapeutic. Correct teaching of active equalization maneuvers and careful monitoring during the first sessions can greatly reduce the incidence of barotrauma. In the present case study, there was an incidence of BTOM of 8.3%, being, in the great majority, of low gravity. The risk of recurrence should be taken into account, and some patients should therefore take prophylactic medication for the remaining duration of treatment.

Acknowledgments

This work was supported by Portuguese funds through the *Center for Computational and Stochastic Mathematics* (CEMAT), *The Portuguese Foundation for Science and Technology* (FCT), University of Lisbon, Portugal, project `UID/Multi/04621/2019`, and *Center of Naval Research* (CINAV), Naval Academy, Portuguese Navy, Portugal.

References

[1] C. Acott, A Brief History of Diving and Decompression Illess, SPUMS Journal, **29**(2) (1999), 98–109.

[2] D. Hosmer, S. Lemeshow and R. X. Sturdivant, *Applied Logistic Regression, 3rd edition.* New York: John Wiley, 2013.

[3] D. Mathieu (ed.), *Handbook on hyperbaric medicine.* Dordrecht: Springer Netherlands, 2006.

[4] J.A. Nelder and R.W.M. Wedderburn, Linear Models, Journal of the Royal Statistical Society. Series A **35** (1972), 370–384.

[5] A.C. Tamhane and D.D. Dunlop, : *Statistics and Data Analysis: from Elementary to Intermediate.* New Jersey: Prentice Hall, 2000.

[6] S. Teles, *O Barotraumatismo do Ouvido Médio em Doentes a Fazer Oxigenoterapia Hiperbárica.* Master Thesis, Medical Faculty, Lisbon University, 2017.

[7] M. Filomena Teodoro, Sofia Teles, Marta C. Marques, Francisco G. Guerreiro, Barotraumatism Occurrence and Hyperbaric Oxygen Therapy, a Preliminary Analysis. In: Simos, T. et al. (eds) Numerical Analysis and Applied Mathematics. AIP Conference Proceedings **1978**, AIP, Melville, New York (2018), 460007. `https://doi.org/10.1063/1.5044069`

[8] M. Filomena Teodoro, Sofia Teles, Marta C. Marques, Francisco G. Guerreiro, Relating Hyperbaric Oxygen Therapy and Barotraumatism Occurrence: A Linear Model Approach. In: O. Gervasi et al. Computational Science and Its Applications. ICCSA 2018. Lecture Notes in Computer Science, **10961**. Springer, Cham (2018). https://doi.org/10.1007/978-3-319-95165-2_34

[9] M. Antónia Turkman, and Giovanni Silva, *Modelos Lineares Generalizados da teoria a prática.* Lisboa: Sociedade Portuguesa de Estatística, 2000.

International Conference on Mathematical Analysis and Applications in Science and Engineering
ICMA^{2}SC'22
ISEP Porto-Portugal, June 27 - 29, 2022

Attitute and Practice of Embarked Staff About Zika Virus

M. Filomena Teodoro[1,2⋆] **João Faria**[1] **Rosa Teodósio**[3,4]

[1] CINAV, Portuguese Naval Academy, Portuguese Navy,
Base Naval de Lisboa, Alfeite, 2810-001 Almada, Portugal
[2] CEMAT - Center for Computational and Stochastic Mathematics,
Instituto Superior Técnico, Lisbon University,
Avenida Rovisco Pais, n. 1, 1048-001 Lisboa, Portugal
[3] IHMT - Institute of Hygiene and Tropical Medicine
[4] UNL - Universidade Nova de Lisboa,
Rua da Junqueira 100, 1349-008 Lisbon, Portugal

[1⋆]mteodoro64@gmail.com

Abstract: The purpose of this study was to investigate the knowledge, attitude and practices (KAP) to prevent the spread of Zika virus (Zika) between the boarded staff in navy ships. This work is the continuation of [3, 4] where it was applied a factor analysis. A statistical analysis by generalized least squares was the chosen approach to analyze the implemented questionnaire about the Zikv disease. Were considered two groups of participants. One of groups consisted with people that already had navigated in endemic areas of ZIKV, the other group had the staff who would go navigate in endemic areas. There were evidenced uneven responses between specific questions about ZIKV and between groups. The results obtained are consistent with similar studies [7].

keywords: KAP; questionnaire; GLM; Zika virus

MSC2020: 62-XX; 92-XX.

1 Introduction

The Zika Virus was firstly identified at 1947 in a rhesus monkey in Uganda. From sixties to eighties very few cases were detected and their majority were benign. Due the enlargement of urban centers, the increment and facility of airflow between countries and the existence of asymptomatic travelers, the dissemination of Zika, had a huge increase [11, 10], also there was a great increment of asymptomatic carriers [2, 1]. Our case study consider military staff embarked on Portuguese Navy ships. Knowing that military staff can be exposed to ZIKV during their journeys in sea, prevention of disease and promotion of the health of the staff is an important issue. To plann intervention strategies, through health education actions, it is needed to evaluate the literacy about zika virus, also their attitude and practice. With such objective was implemented a questionnaire in [3], similar to [7]. A statistical approach was applied in [4, 8]. Detailing, it was applied a factorial analysis, some factors associated with kap were identified. Such factors were considered in the present work as variables in a generalized linear models approach[5, 6, 9].

2 Results and conclusions

Summarizing the data, several groups of individuals were preliminary considered, 148 individuals answered to a questionnaire about Zika. The first step organizes the data and get some simple measures by descriptive statistic techniques and performs some intermediate level techniques, e.g, proportion tests, independence tests, etc. All groups present a minimum and maximum age of 25 and 56 years, with a mean age of 35. All groups have identical distribution of ages(can hapen small differences when certain ship garrison has some staff absent.

The groups were composed of 80% men and 20% women. The distribution per gender is statistically different ($p-value = 0.025$). We can confirm that nobody answered correctly (or wrongly) all seven questions that composed the initial questionnaire. Respectively, we have 10.9%of staff that answered correctly to one question. Three correct answers was the most frequent result. The maximum of number of correct answers was 6 with a percentage of 6%. We can infer the the boarded still has a low level of literacy about Zika .

Acknowledgments

This work was supported by Portuguese funds through the *Center for Computational and Stochastic Mathematics* (CEMAT), *The Portuguese Foundation for Science and Technology* (FCT), University of Lisbon, Portugal, project `UID/Multi/04621/2019`, and *Center of Naval Research* (CINAV), Naval Academy, Portuguese Navy, Portugal.

References

[1] Cao-Lormeau and et al., Guillain Barré Syndrome outbreak associated with Zika virus infection in French Polynesia: a case control study, The Lancet **387**(10027) (2016), 1531–1539.

[2] European Centre for Disease Prevention and Control (ECDPC), Rapid risk assessment. Zika virus disease epidemic, Potential association with microcephaly and Guillain Barreé syndrome. 6th update, 20/05/ 2016. Stockholm.

[3] J. Faria, *Conhecimentos, atitudes e práticas de prevenção sobre Zika da população embarcada em navios da Marinha Portuguesa*. Master Thesis. Lisboa, Instituto de Higiene e Medicina Tropical, Universidade Nova de Lisboa, 2019.

[4] J. Faria, R. Teodósio and M.F. Teodoro, Knowledge of the Boarded Population About Zika Virus. In: O. Gervasi et al. Computational Science and Its Applications-ICCSA 2019. Lecture Notes in Computer Science, **11621**. Cham: Springer (2019), 97–110. `https://doi.org/10.1007/978-3-030-24302-9$_$8`

[5] D. Hosmer, S. Lemeshow and R. X. Sturdivant, *Applied Logistic Regression, 3rd edition*. New York: John Wiley, 2013.

[6] J.A. Nelder and R.W.M. Wedderburn, Linear Models, Journal of the Royal Statistical Society. Series A **35** (1972), 370–384.

[7] C. Rosalino, and et al., Conhecimentos, atitudes e práticas sobre Zika de viajantes visitando o Rio de Janeiro, Brasil, durante os Jogos Olímpicos e Paraolímpicos de 2016: Inquérito no Aeroporto Internacional António Carlos Jobim, Rio de Janeiro, 2016.

[8] A.C. Tamhane and D.D. Dunlop, *Statistics and Data Analysis: from Elementary to Intermediate.* New Jersey: Prentice Hall, 2000.

[9] M. Antónia Turkman, and Giovanni Silva, *Modelos Lineares Generalizados da teoria a prática.* Lisboa: Sociedade Portuguesa de Estatística, 2000.

[10] L. Waldell and J. Greig,Scoping Review of the Zika Virus Literature, PLoS ONE **11**(5) (2016), e0156376.

[11] Camila Zanluca, and et al. First report of autochthonous transmission of Zika virus in Brazil. Rio de Janeiro: Mem Inst Oswaldo Cruz, 110(4), 569-572 (2015)

International Conference on Mathematical Analysis and Applications in Science and Engineering
ICMA^{2}SC'22
ISEP Porto-Portugal, June 27 - 29, 2022

Response models in experimental studies of fresh properties of cement pastes: Part I – typical approach through changes one-variable-at-a-time

Lino Maia[1,2*]

[1] CONSTRUCT-LABEST, Faculty of Engineering (FEUP), University of Porto, Rua Dr. Roberto Frias, 4200-465 Porto, Portugal.

[2] Faculty of Exact Sciences and Engineering, University of Madeira, Campus da Penteada, 9020-105 Funchal, Portugal.

[1*]linomaia@fe.up.pt

Abstract: The experimental plan affects the fresh properties cement-based materials. This document regards to Part I of a major work wherein workability of cement-based pastes is evaluated. Here, several cement-based paste compositions incorporating distinct constituent materials were tested and their effect on the measured. The overall work is composed by two parts. Here, in Part I, basic and typical run of experiments wherein only one input parameter is studied at once were applied. The results of Part I shown that basic run of experiments is easy and quick of develop and leads to results of easy analyses, however advanced and scientific analyses are difficult.

keywords: Approach; Cement paste; Response Models; Trial-error.

MSC2020: 49-XX; 34-XX; 92-XX.

1 Introduction

The road to produce concrete can be understood as very easy as well as demanding high-tech and scientific knowledge. On the one hand, it is just mixing gravel, sand, cement, water and eventually admixtures and additions in a trial-error method and 'a concrete' is produced. However, on the other hand when specific and unusual properties are required and no fail is accepted, high-tech and scientific kwon-how is crucial to achieve and define responsibilities.
As a part of a major research work on the fresh properties of cement-based pastes wherein different experimental approaches were used, the present paper reports the findings of the Part I of the research wherein the experimental program was carried out performing changes in the input variables within the traditional approach 'one-variable-at-a-time'. Other results of the overall research work can be found in the Part II wherein the experimental program was carried out through a statistical approach, i.e. applying a central composite design of experiments. Thus, the major goals of this paper (Part I) are (i) to characterize the primary effects of the different constituent materials of cement pastes on the fresh properties and parallelly (ii) to analyze and ponder about the type of research methodology applied, namely advantages and disadvantages of the traditional approach of changing one-variable-at-a-time when compared to an experimental program planed based on a central composite design. Therefore, in this paper 92 mix compositions are done while in the Part II only 15 mix compositions were executed. The overall research was carried out in cement-based pastes with the mini-cone [1] and the Marsh funnel [2] tests being performed to evaluate fresh properties. Being aware that results from Part I and Part II do not compare between themselves, rather they complement the overall characterization, the used approaches are evaluated and compared.

2 Results and discussion

In this experimental program it was also evaluated the loss of workability with the time. Two superplasticizers were tested in order to detect differences. Figure 1 shows graphically the loss of deformability of the two superplasticizer from immediately after mixing to 60 minutes after starting mixing. Similarly, Figure 2 shows the increase of viscosity.

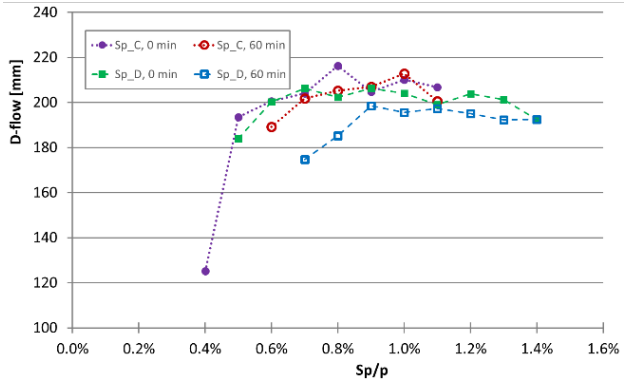

Figure 1 – Effect of two superplasticizers on the flow ability of mixes immediately after mixing and 60 minutes after start mixing

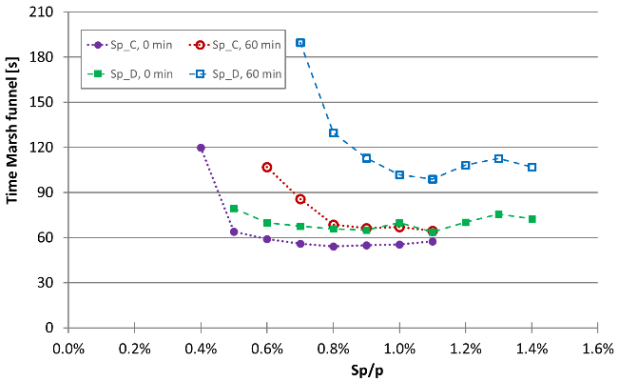

Figure 2 – Effect of two superplasticizers on the viscosity immediately after mixing and 60 minutes after start mixing evaluated through time of the Marsh funnel

Results of the flow ability immediately after mixing of mixes composition are reported Table 1 as well as the corresponding coefficients of the linear regressions and the R^2.

Table 1 – Linear regressions of the flow ability of mixes with different limestone filler content and different types of cement.

#	Mix	D1a	D1b	D2a	D2b	D-flow	Linear regression
1	100%C,0%F-1	90	90	91	91	90.5	
2	100%C,0%F-2	95	95	100	101	97.8	
3	100%C,0%F-3	109	110	112	114	111.3	a= 0.006961
4	100%C,0%F-4	123	123	129	130	126.3	b= 0.770234
5	100%C,0%F-5	139	139	140	141	139.8	R2= 0.978597
6	100%C,0%F-6	143	143	145	146	144.3	
7	100%C,0%F-7	151	151	153	153	152.0	
8	70%C,30%F-1	93	94	99	99	96.3	
9	70%C,30%F-2	105	105	111	112	108.3	
10	70%C,30%F-3	119	119	129	129	124.0	a= 0.008278
11	70%C,30%F-4	125	126	130	131	128.0	b= 0.510641
12	70%C,30%F-5	135	135	135	135	135.0	R2= 0.967530
13	70%C,30%F-6	144	142	147	147	145.0	
14	70%C,30%F-7	152	152	146	146	149.0	
15	85%C,15%F-1	92	93	93	93	92.8	
16	85%C,15%F-2	102	102	105	105	103.5	
17	85%C,15%F-3	119	119	116	116	117.5	a= 0.007501
18	85%C,15%F-4	129	129	123	123	126.0	b= 0.660015
19	85%C,15%F-5	141	141	141	141	141.0	R2= 0.953415
20	85%C,15%F-6	127	128	145	145	136.3	
21	85%C,15%F-7	155	155	150	151	152.8	
22	55%C,45%F-1	78	79	77	78	78.0	
23	55%C,45%F-2	89	89	88	87	88.3	
24	55%C,45%F-3	94	94	98	98	96.0	
25	55%C,45%F-4	120	121	115	114	117.5	a= 0.006733
26	55%C,45%F-5	133	132	116	116	124.3	b= 0.636062
27	55%C,45%F-6	123	123	132	132	127.5	R2= 0.980954
28	55%C,45%F-7	144	144	150	151	147.3	
29	55%C,45%F-8	144	145	162	162	153.3	
30	55%C,45%F-9	155	150	166	168	159.8	
31	0%C,100%F-1	105	106	105	105	105.3	
32	0%C,100%F-2	115	115	123	125	119.5	
33	0%C,100%F-3	125	125	133	134	129.3	a= 0.007514
34	0%C,100%F-4	145	145	145	146	145.3	b= 0.329800
35	0%C,100%F-5	141	142	148	149	145.0	R2= 0.919727
36	0%C,100%F-6	144	144	148	148	146.0	
37	0%C,100%F-7	154	155	165	165	159.8	
38	100%C+, 0%F-1	93	92	-	-	92.5	
39	100%C+, 0%F-2	102	102	-	-	102.0	a= 0.008734
40	100%C+, 0%F-3	114	113	-	-	113.5	b= 0.954350
41	100%C+, 0%F-4	141	139	-	-	140.0	R2= 0.963781
42	100%C+, 0%F-5	158	160	-	-	159.0	
43	80%C, 20%C+, 0%F-1	97	98	-	-	97.5	
44	80%C, 20%C+, 0%F-2	114	114	-	-	114.0	a= 0.008849
45	80%C, 20%C+, 0%F-3	133	135	-	-	134.0	b= 0.683382
46	80%C, 20%C+, 0%F-4	156	156	-	-	156.0	R2= 0.977411
47	80%C, 20%C+, 0%F-5	161	163	-	-	162.0	

3 Conclusions and Future work

In this paper the typical approach wherein the input parameters were changed within the approach one-variable-at-a-time to characterize their effect on the fresh state of cement-based pastes – the results found are in agreement with the literature [4-9]. A vision of the advantages and disadvantages of the approach one-variable-at-a-time to apply response models when compared with the one applied in the Part II is portrayed below.

- Advantages

- Basic studies allow understanding the primary effects of the input parameter on the responses. It is easier to test different materials and check their main effects.
- Simple experimental plans: with a few mixtures some tends are recognized.
- Experimental plans may be adapted during the plan.
- Trail-error experiments may be enough to check some doubts.
- Appropriate to detect primary linear regressions.
- Advanced expertise in statistics is not mandatory.
- Interesting for rudimentary analysis.

- Disadvantages

- Studies are usually conducted under small and basic sets to be easier to interpretate and analyze and consequently do not allow applying advanced response models being typically reported through linear regressions with the R^2.
- Studies are not extensive, therefore data is not published because their scientific interpretation lacks support.
- When several parameters need to be studied, the experimental program increased drastically and the interpretation of results and the comparison between parameters are difficult.
- No advanced response models are obtained to identify secondary and cross effects.
- As the results lack of a scientific approach frequently they are not deeply studied – here, in this paper, that happened with the SRA study.

Acknowledgments

This work is financially supported by: Base Funding – UIDB/04708/2020 of the CONSTRUCT – Instituto de I&D em Estruturas e Construções - funded by national funds through the FCT/MCTES (PIDDAC). This work is funded by national funds through FCT – Fundação para a Ciência e a Tecnologia, I.P., under the Scientific Employment Stimulus – Institutional Call – CEECINST/00049/2018.

References

[1] Kantro, D. L. Influence of water-reducing admixtures on properties of cement paste - a miniature slump test. Cem. Concr. Aggregates 2, 95–102 (1980).

[2] EN 445:2008 - Grout for prestressing tendons - Test methods.

[3] Nunes, S., Oliveira, P. M., Coutinho, J. S. & Figueiras, J. Interaction diagrams to assess SCC mortars for different cement types. Constr. Build. Mater. 23, 1401–1412 (2009).

[4] Yahia, A., Tanimura, M. & Shimoyama, Y. Rheological properties of highly flowable mortar containing limestone filler-effect of powder content and W/C ratio. Cem. Concr. Res. 35, 532–539 (2005).

[5] Petit, J. Y. & Wirquin, E. Effect of limestone filler content and superplasticizer dosage on rheological parameters of highly flowable mortar under light pressure conditions. Cem. Concr. Res. 40, 235–241 (2010).

[6] Juvas, K., Kappi, A., Salo, K. & Nordenswan, E. The Effects of Cement Variations on Concrete Workability. Nord. Concr. Res. 26, 39–46 (2001).

International Conference on Mathematical Analysis and Applications in Science and Engineering ICMA²SC'22

ISEP **Porto-Portugal, June 27 - 29, 2022**

Response models in experimental studies of fresh properties of cement pastes: Part II – statistical approach based in a central composite design

Lino Maia[1,2*]

[1] CONSTRUCT-LABEST, Faculty of Engineering (FEUP), University of Porto, Rua Dr. Roberto Frias, 4200-465 Porto, Portugal.

[2] Faculty of Exact Sciences and Engineering, University of Madeira, Campus da Penteada, 9020-105 Funchal, Portugal.

[1*]linomaia@fe.up.pt

Abstract: In this work Part II, the fresh properties of cement-based pastes were evaluated through the mini-slump test and the time in Marsh funnel. Several cement-based paste compositions were studied with run of experiments being developed based in a central composite design in order to allow to carry out scientific analyzes and to apply response models. The approach allows changes in multiple input parameters at once. The results shown the ability of this type of approach to detect cross effects, to predict results and to allow composition optimization. The approach used in this Part II is faced with basic and simple approaches wherein only one input parameters is changed at once.

keywords: Approach; Central Composite Design; Response Models.

MSC2020: 49-XX; 34-XX; 92-XX.

1 Introduction

Understanding fresh properties of cement-based materials is one of the key factors for correctly choosing the constituent materials and their mix proportions. That is especially important for specific applications wherein the fresh properties play a major role. Many researches [1-5] have being published on the topic with the overall conclusion being that the as constituent materials are different a characterization is required.

As a part of a major research work to characterize fresh properties of cement-based pastes wherein different experimental approaches were used, the present paper reports the findings of the Part II of the research wherein the design of experiments was developed through a central composite design. Thus, the major goals of this work Part II are (i) to characterize the primary and cross effects due to the constituent materials of cement-based pastes on the fresh properties and parallelly (ii) to analyze and ponder about the type of research methodology applied, namely advantages and disadvantages when compared to typical approaches. Therefore, in this paper only 15 mix compositions are performed for this specific purpose which compared with the 92 mix compositions done in the Part I. The overall research was carried out in cement-based pastes with the mini-cone [6] and the Marsh funnel [7] tests being performed to evaluate fresh properties. Note that DOE of Part I and Part II are for distinct studies. Therefore, they do not compare between themselves. They complement each other for the overall research characterization and are here analyzed to evaluated and compared approaches.

2 Results and discussion

Two powders were used: (i) commercial cement CEM I 42.5R and (ii) limestone filler. A third-generation superplasticizer and distilled water was used in all mixes. Mix compositions were defined by changing the following input parameters: water-to-cement ratio (w/c); superplasticizer-to-powder ratio (Sp/p); water-to-powder ratio (w/p). All mix compositions were prepared in a single batch which was prepared for 1.40 L. Fifteen mixtures were planned based in central composite design with three variables (A, B and C) corresponding to the three-input parameter (w/c, Sp/p, w/p), respectively. The central composition (i.e. the mix with the coded values A=w/c=0, B=Sp/p=0, C=w/p=0) was define with the actual values w/c=0.2886, Sp/p=0.80%, w/p=0.5333. The maximum changes of the input parameters in regarding to the central composition were 6.3%, 25.0% and 10.0% for w/c, Sp/p and w/p, respectively. Table 1 reports the data corresponding to each mix composition of the DOE.

Table 1 – Mix compositions of the central composite design and the corresponding test results.

std	w/c	Sp/p	w/p	cem	Filler	Sp	water	D0	t0	D60	t60
1	-1	-1	-1	1690.3	1046.7	19.159	461.15	19.95	82.50	19.18	140.12
2	1	-1	-1	1587.9	1136.0	19.067	461.21	20.28	80.06	19.18	138.69
3	-1	1	-1	1690.3	1046.7	24.634	457.87	20.25	78.50	19.35	107.75
4	1	1	-1	1587.9	1136.0	24.515	457.94	19.93	76.09	19.45	100.03
5	-1	-1	1	1804.4	861.3	18.660	493.35	18.13	67.50	18.43	112.72
6	1	-1	1	1695.0	956.5	18.561	493.41	19.63	63.03	19.68	90.44
7	-1	1	1	1804.4	861.3	23.991	490.15	21.35	61.56	21.25	87.28
8	1	1	1	1695.0	956.5	23.864	490.23	21.90	59.34	20.78	75.78
9	-1.6818	0	0	1806.6	901.6	21.666	475.88	19.98	68.46	20.20	109.87
10	1.6818	0	0	1594.1	1086.8	21.447	476.01	21.18	57.82	20.43	85.78
11	0	-1.6818	0	1693.7	1000.0	16.162	479.18	19.53	78.34	16.85	215.80
12	0	1.6818	0	1693.7	1000.0	26.937	472.71	20.35	67.37	19.93	86.56
13	0	0	-1.6818	1579.3	1188.9	22.145	442.55	18.80	87.97	18.43	144.03
14	0	0	1.6818	1800.5	823.8	20.994	507.09	21.93	53.03	21.88	74.34
15	0	0	0	1693.7	1000.0	21.550	475.95	20.30	70.97	20.00	105.25

The testing results of Table 1 – wherein the D0 and t0 are the flow diameter and the Marsh funnel time, respectively, immediately mixing and the D60 and t60 are the flow diameter and the Marsh funnel time, respectively, 60 minutes after mixing – were then analyzed in term of analysis to detect correlations between all the variables (either input or response). Those correlations might be expressed in a correlation matrix – Figure 1. This allowed a primary perception of the effect the input variable in the response variables.

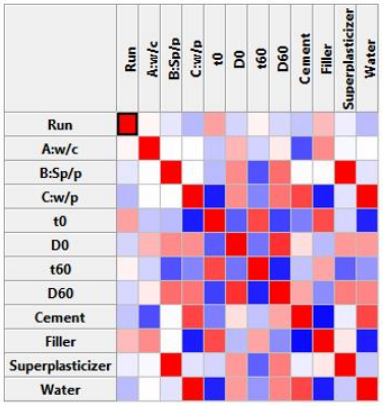

	Run	A:w/c	B:Sp/p	C:w/p	t0	D0	t60	D60	Cement	Filler	Superplasticizer	Water
Run	1,000	0,030	-0,090	-0,269	0,364	-0,161	0,041	-0,152	-0,223	0,260	-0,061	-0,263
A:w/c		1,000			-0,216	0,283	-0,167	0,072				
B:Sp/p			1,000		-0,260	0,452	-0,677	0,570				
C:w/p				1,000	-0,892	0,436	-0,475	0,535				
t0					1,000	-0,631	0,716	-0,746	-0,501	0,703	-0,159	-0,863
D0						1,000	-0,542	0,803	0,118	-0,261	0,393	0,389
t60							1,000	-0,870	-0,231	0,350	-0,620	-0,404
D60								1,000	0,339	-0,445	0,507	0,472

Figure 1 – Correlation matrix of the variables.

After that, assisted by the software Design-Expert 13 Annual Network (Serial Number: 0964-0841-3719-3394) the statistical procedure ANOVA was applied to the Reduced Quadratic Model fitting for the D0, t0, D60 and t60. The regression models were found significant after several analyses as the ones presented in the Figure 2 for the t0. With the response models obtained, analyses of the results were carried out to understand the influence of each input variable in the response variable (Figure 3). Especial attention was paid on cross effects.

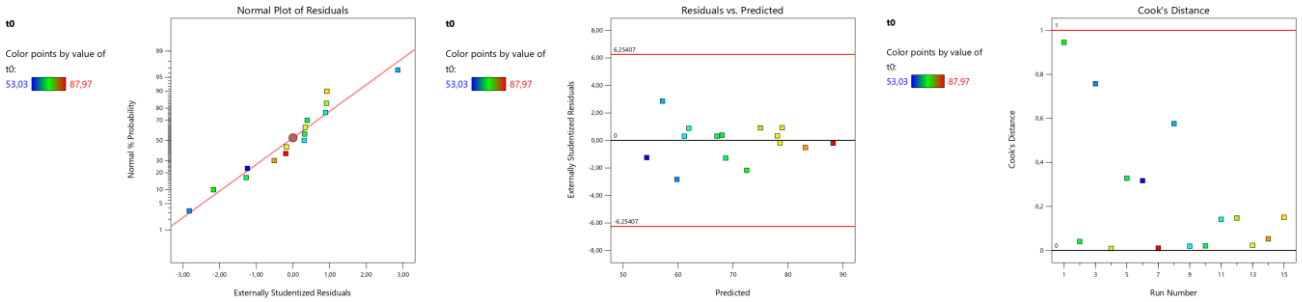

Figure 2 – Analysis of the quadratic model applied: left) normal plot of residuals, center) the Externally Studentized Residuals distribution vs. predicted, and right) the Cook's Distance.

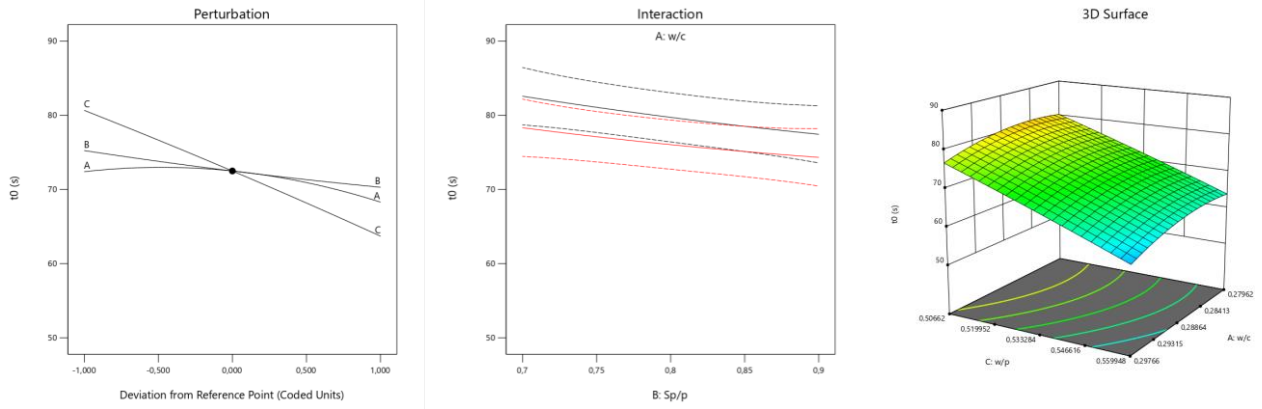

Figure 3 – Plotted results: left) Primary effect of the input parameters, center) Interaction effect of the w/c and S/p, and right) 3D model visualization.

3 Conclusions and Future work

In this paper a central composite design of experiments wherein the input parameters were changed all at once to characterize their effect on the fresh state of cement-based pastes. A vision of the advantages and disadvantages of the approach based in factorial design to apply response models when compared with the one applied in the Part II is portrayed below.

- Advantages

- It allows complex studies with many factors' interactions with a reduced number of experiments.
- As DOE is well-defined, it allows determining response models for more scientifically understand effects.
- Besides the primary effects, models can also detect the crossed effects of two factor interaction and quadratic effects (or even higher terms).
- Software assists the user and provides statistical analysis and several graphs.
- It is easy to predict results for other mix compositions.
- It allows to find out optimized compositions.

- Disadvantages

- The range of the mix compositions (input parameters) is reduced and well-defined with the response models being suitable only nearby that range.
- Previous trial-error testes are normally necessary to define the range of the input parameter to defined DOE.
- DOE has be complete, i.e. does not allow basic studies.
- It is functional only when a software is available.
- Models must be careful interpretated and effects and tends may not be easily understood.
- If advanced models are not necessary or understood, results from DOE are difficult to interpretate.

Acknowledgments

This work is financially supported by: Base Funding – UIDB/04708/2020 of the CONSTRUCT – Instituto de I&D em Estruturas e Construções - funded by national funds through the FCT/MCTES (PIDDAC). This work is funded by national funds through FCT – Fundação para a Ciência e a Tecnologia, I.P., under the Scientific Employment Stimulus – Institutional Call – CEECINST/00049/2018.

References

[1] I. Galobardes, R. P. Salvador, S. H. P. Cavalaro, A. Figueiredo, and C. I. Goodier, "Adaptation of the standard EN 196-1 for mortar with accelerator," Constr. Build. Mater., vol. 127, pp. 125–136, 2016, doi: 10.1016/j.conbuildmat.2016.09.147.

[2] B. Yogitha, M. Karthikeyan, and M. G. Muni Reddy, "Progress of sugarcane bagasse ash applications in production of Eco-Friendly concrete - Review," Mater. Today Proc., vol. 33, pp. 695–699, 2020, doi: https://doi.org/10.1016/j.matpr.2020.05.814.

[3] R. Gettu, R. G. Pillai, M. Santhanam, and B.S. Dhanya, "Ways of Improving the Sustainability of Concrete Technology Through the Effective Use of Admixtures," Indian Inst. Technol. Madras, Chennai, no. April, p. 21, 2018.

[4] Douglas C. Montgomery, Introduction to Statistical Quality Control, 7.ed. John Wiley and Sons Inc., 2013.

[5] A. M. Matos, S. Nunes, C. Costa, and J. L. Barroso-Aguiar, "Spent equilibrium catalyst as internal curing agent in UHPFRC," Cem. Concr. Compos., vol. 104, 2019, doi: 10.1016/j.cemconcomp.2019.103362.

[6] Kantro, D. L. Influence of water-reducing admixtures on properties of cement paste - a miniature slump test. Cem. Concr. Aggregates 2, 95–102 (1980).

[7] EN 445:2008 - Grout for prestressing tendons - Test methods.

International Conference on Mathematical Analysis and Applications in Science and Engineering
ICMA^{2}SC'22
ISEP Porto-Portugal, June 27 - 29, 2022

Inspection in the ceramics and glass industry

João Mendes[1,2] **N.M. Fonseca Ferreira**[1,3] **Victor Daniel Neto Dos Santos**[1]

[1] Coimbra Polytechnic - ISEC, Coimbra, Portugal

[2] CTCV, Coimbra, Portugal

[3] GECAD - Knowledge Research Group on Intelligent Engineering and Computing for Advanced Innovation and Development of the Engineering Institute of Porto (ISEP), Polytechnic Institute of Porto (IPP), Porto, Portugal

Abstract: This paper presents an autonomous inspection method in the task of automatic location and evaluation of defects on the surface of ceramic pieces. The paper presents an explanation/presentation of the automation process that re-quires automation, robotic systems, artificial intelligence, communication networks, among others, creating more autonomous processes and less de-pendent on labor, the inclusion of automation has a fundamental role that uses a set of techniques aimed at making automatic the realization of tasks.

keywords: Ceramics, Automation, Robotics, Artificial vision

MSC2020: 49-XX; 34-XX; 92-XX.

1 Introduction

Industrial automation consists of recreating several processes, replacing human labor with various equipment, ensuring gains in quantity and quality of production while offering more competitive prices to consumers. This evolution is largely linked to the recent advance of microelectronics, which has invaded the productive sectors despite

offering great progress in production, replacing people's work with robotic systems, providing enormous productivity gains by integrating different tasks between management and production. [1]
The Ceramics industry in Portugal has an incredibly significant number of companies, being the largest European exporter of ceramic dishes for domes-tic use. Nevertheless, this type of industry employs many people. Considering the dimensions mentioned, it is imperative to monetize and improve various processes, to ensure increasingly optimized and efficient solutions. Much of the research and development in this area of knowledge has been carried out at the CTCV. [2]
The CTCV was founded in 1987, is composed of a multidisciplinary team, with great experience accumulated over the years, and with excellent specialized training. It offers a set of integrated solutions that go through specialized consulting, auditing, professional training, measurement, testing, and solutions in Ceramics. He has worked on more than 30 I&D projects in the last 10 years, involving about 100 national and international partners. [2]
Recently, in the new buildings located in the iParque, it gave rise to new re-search projects, one of them in the Area of Robotics and Automation. Through the development in this area came the opportunity to create a partnership with the ISEC, allowing the support of the acquisition of essential knowledge in this technological area, and in the future promotion of I&D projects. [3]

2 Results and discussion

In the ceramics industry, despite technological advances, the process of quality control, for the most part, is carried out through human visual inspection. For this type of control, people with a high degree of experience in the presence of defects are used, such is their specificity and variety. With the automation of other processes and the increase of productivity and competitive-ness of companies, the process of quality control requires speed and reliability. The reduction of human resources with specific training, and with the in-crease in productivity of companies, the biological wear and tear of the hu-man body is one of the main factors that reduce quality control. Automation is not only for repetitive and easy-to-execute processes, but also able to make previously programmed decisions, or even create systems that develop intelligence. Having said that, a fully autonomous process has been developed for the inspection of ceramic defect-in-control parts. [4]
This prototype is composed of a robotic mechanical system, which allows to manipulate the objects of ceramics to inspect. It adds an acquisition and pre-processing module (image acquisition system) suitable for the geometries of ceramic surfaces, as well as a computer vision and artificial intelligence software/algorithm module, which allows the development of a set of visible defects in diffuse lighting. At the same time, it entails a three-dimensional processing of information for the development of geometry defects, and these elements are automatically controlled, using automation thus dividing into different systems.
The System of Control is composed for an automaton that can control all devices and a HMI designed, to provide human interaction.
The transport system consists of three carpets, one of inlet and two output, where a selection and separation of parts with and without defect will be carried out.
The Manipulation system consists of a robotic cell, with a maximum range of 1045mm, and the robot is positioned in the center of the prototype. This robot will have integrated a griped, composed of 3 tools powered by com-pressed air, where each is responsible for placing, removing, and turning, respectively.

It is below mirrored in Figure 1, the structure of the robotized cell - in a) -, and in b) the manipulation system mentioned above in detail.

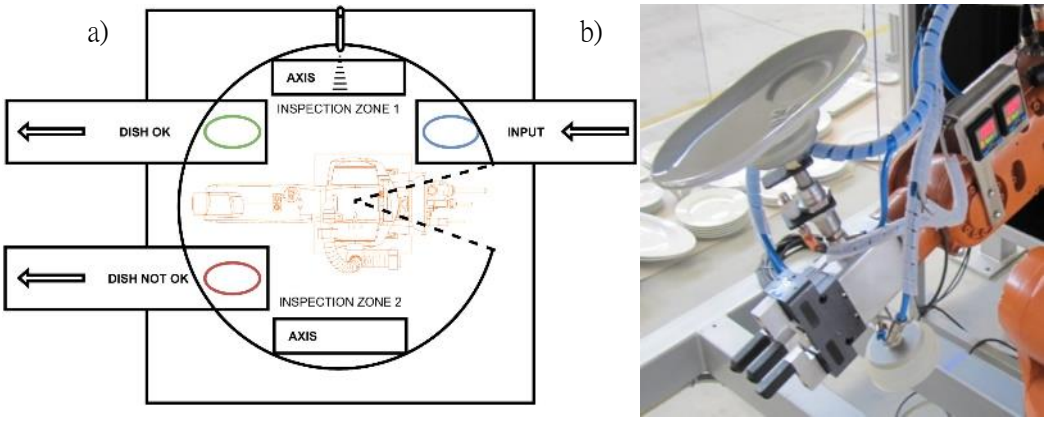

Figure 1 - a) Cell structure b) Manipulation system

The System of acquisition shown below in Figure 2, contains a camera, laser, and lighting, which is positioned above the plate. The plate is positioned on a support, coupled to a linear axis, which is acquired by performing a linear movement below the chamber.
2D vision and 3D vision are indispensable for capturing the necessary im-ages, responsible for the design of brightness and color defects, and geometry defects, respectively.

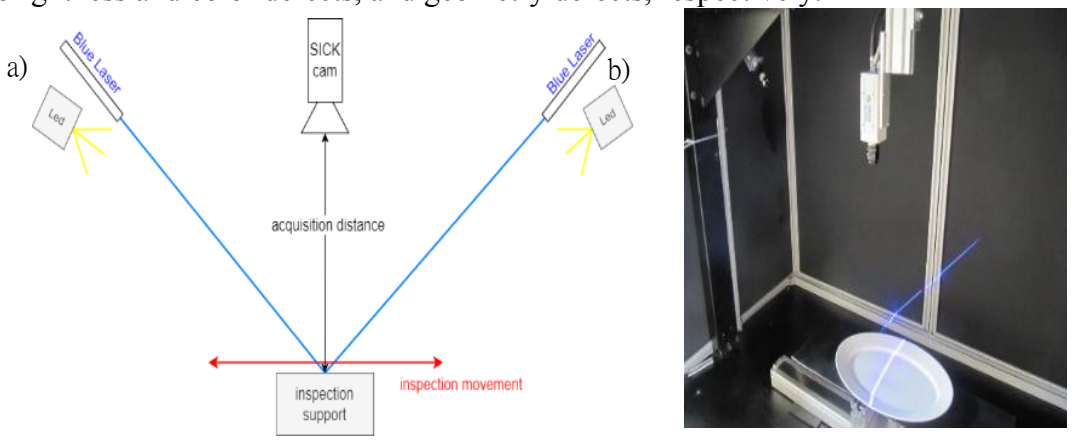

Figure 2 - Acquisition system: a) projected, b) realized

The prototype developed at an early stage works as follows: the ceramic pieces are routed to the entrance mat, which has in its terminus a sensor that has the function of sending a signal to the automaton. Therefore, the robot – which is in a resting position – waits for information that the object (dish) is positioned at the entrance. Then a 2D camera captures an image of the dish in that same position. With this two information, the robot can process and collect the dish, using the tool number 1.
After detaining the dish, the robot starts its defect-checking functionality through a free inspection system, which contains 2 tools. To perform the inspection of a dish, it is placed on a platform that is moved through a linear motor. This movement is performed through an instruction divided into 3 phases, only two of them illuminated by 1 laser, contrary to the movement of the platform, acquiring the necessary images. After the 3 phases, the process is repeated, distinguishing itself from the previous sequence because at this moment, the robot mobilizes the dish (turns it), exposing the opposite face of the dish to the vision system. Subsequently, a new acquisition movement is carried out, where after the inspection process of the dish and the robot has the number 2 tools available, shifts the plate to its output respective carpet. That said, a project was elaborated with many instructions coupled to several PLC programming languages, to connect the systems built with the control system.

3 Conclusions and Future work

It is thus concluded that the automation of ceramic inspection processes is a safe and practical step for the modernization of the ceramic industry, since without this automation, ceramic companies are dependent on an increasingly small set of workers specialized in the inspection of ceramics.
However, the identification of ceramic defects is a challenge for artificial vision, because the environment in the ceramic industry may not be conducive to having a lot of dust, which prevent the realization of the process, re-quiring the maintenance of the prototype with more frequency
Comparing this system with existing ones has a great advantage over the other inspection systems because as the manipulation is carried out by a robotic arm it will not be difficult to adapt to new types of inspections, besides for parts that take a long time to be analyze this system can have several inspection systems or even develop inspection system with specific environments for different types of dishes, which gives a large diverse number of ap-plications and flexibility.
In a future project, the implementation of artificial intelligence in the identification of new defects is an added value in this sector, as it is thus possible to implement this inspection method with a virtually zero error rate, increasing reliability and corresponding with the requirements of industry 4.0.

Acknowledgments

This prototype was only possible with the partnership of CTCV and ISEC, and with the supply of material from the company Aleluia Cerâmicas, S.A.

References

[1] A. Sioma, "Automated control of surface defects on ceramic tiles using 3D image analysis.," Materials, p. 13(5), 2020.

[2] A. M. Luísa Pinto, "A história de uma caneca feita por robots," Público, 12/12/2020.

[3] P. a. N. F. Magalhaes, "Inspection Application in an Industrial Environment with Collaborative Robots," Automation 3, pp. 3(2):258-268.

[4] CTCV, "CTCV QUEM SOMOS," [Online]. Available: https://www.ctcv.pt/quemsomos.html. [Acedido em 05 05 2022].

International Conference on Mathematical Analysis and Applications in Science and Engineering
ICMA^{2}SC'22
ISEP Porto-Portugal, June 27 - 29, 2022

Vision Systems Applied in the Ceramic Industry

André Daniel Martins Santos[1,2] **N.M. Fonseca**[1,3]

[1] Coimbra Polytechnic - ISEC, Coimbra, Portugal
[2] CTCV, Coimbra, Portugal
[3] GECAD - Knowledge Research Group on Intelligent Engineering and Computing for Advanced Innovation and Development of the Engineering Institute of Porto (ISEP), Polytechnic Institute of Porto (IPP), Porto, Portugal

Abstract: This article aims to study the application of computer vision in the field of Ceramics, as well as the technologies used. It intends to make known the basic concepts of vision systems, as well as present different ways of identifying positions of objects of the ceramic industry, presenting the advantages and disadvantages as well as highlighting the advances in this area.

keywords: Computer vision, human vision, ceramics

MSC2020: 49-XX; 34-XX; 92-XX.

1 Introduction

In Portugal the number of companies in the fields of Ceramics is quite significant, also is the largest European exporter of ceramic dishes, in addition this type of industry employs a high number of people [1]. Since it is an area under investigation there is a need to monetize and improve various processes to find more optimized and efficient solutions, many of these research and developments have been made in the CTCV [2] technology center of ceramic and glass. This center was founded in 1987, composed by a multidisciplinary team with great experience accumulated over the years, offers a set of integrated solutions that go through specialized consulting, professional training, and

solutions in the fields of Ceramics. The new building located in the iParque, gave rise to new projects and research, on Robotics and Automation (Figure 1).

Figure 1 - Identification of Defects and Pick and Place of Ceramic Parts

When we pretend to do complex analysis, with higher quality, we must replicate the industrial line with the use of several "sensors" that are in constant communication [3]. One of these sensors, which we will address more significantly, is what relates to vision system.

2 Results and discussion

The "Mako" chamber is a camera with monochrome lens and a resolution of 2K. The choice of camera was made considering the quality / price. In relation to communication, this was performed through the Ubuntu system (Linux) using the ethernet network, which allowed programming in OpenCV, since is an open system. The development of the program was done through one of these examples that allows the camera to visualize the frames it captures images in a fast way, to give the effect of a live video allowing changes to be made and check their influences on the image.
A program has been created to save a removed image in the camera. This program wants to save the image, which is later imported into another program. To perform its analysis was used the function cv2.imwrite which allows the save of the frame in a jpeg image (Figure 2).

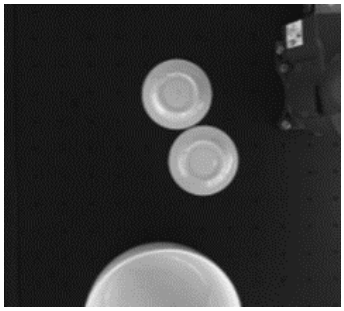

Figure 1 - Saved Image

After obtaining the image, the next step is to treat it, in a first phase it is necessary to convert it to shades of gray making the dish more visible, then you will detect the dishes and its centers, so that this information is sent to a robotic arm a posteriori. Attention should be paid to other variables, such as real coordinates. Through this image it is possible to easily remove the coordinates of the pixels, but to remove the coordinates of the world in relation to the robot a cartesian axis with several points was created, to make comparations between them and discover a constant measure that allows the calculation of the actual values. The following equation was created where DP is

Distance from dish in pixels and DR is Distance from dish in real values. The values 50 is the measure between the holes and the 135 is the same measure but in pixels.

$$\frac{50 \times DP}{135} = DR$$

Equation 1 - Calculation of Real Plate Coordinates

Figure 2 - Setup Camera Reality/Simulator

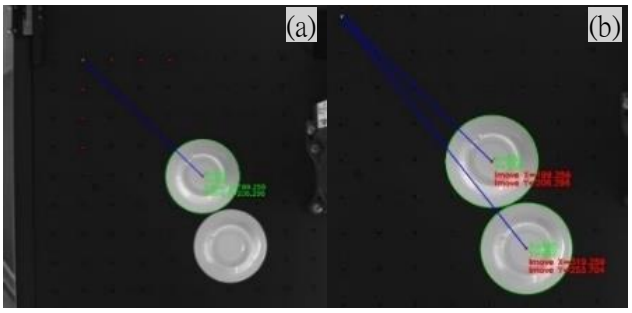

Figure 3 - Cartesian Image(a)/Detect Centers(b)

To represent the points, the cv2.circle function was used, adding the constant values so that all had the same distance between them and measured with a ruler the actual value (Figure 4 (a)). Considering the values obtained in the experiment presented, the calculation of the actual coordinate with the center of the dish was calculated and identified with a red dot, next to this point the coordinates are presented in the image and in the real world.

In the end, the program gets this image (Figure 4 (b)), highlighting the coordinates that the robot will use, these distances represent the distance that the robot must make to catch the dish, being necessary to have a reference point to make the difference between two points and discover the space between them.

The final state of the program has the steps that are present in the flowchart. You start by loading the camera The next step, after re-moving the image, will be to convert it to shades of gray, making the dish even more visible. After this begins to detect centers, if you do not detect any will not open any image with the detect if you detect will calculate the center of the dish and use this value to reach the distance in coordinates of the robot so that the dish is picked up. Then a human instruction is needed to place the calculated coordenates before going to the next dish.

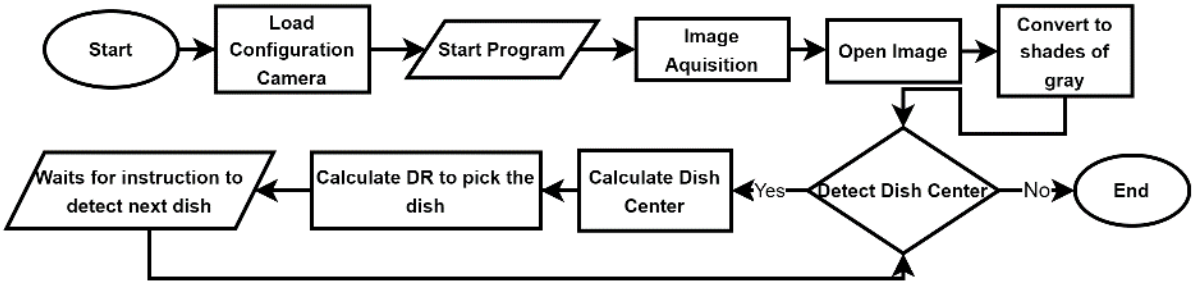

Lighting represents an important condition for a good processing of an image and may influence in a positive or negative way. Good lighting makes it possible to do better and more easily highlight regions of interest present in the image, so more efficient processing is possible, however it can also have disadvantages, such as reflections. The type of light that was used is directional used to characterize a direction and illuminate the objects present in that area [4].

3 Conclusions and Future work

The results of this experiment were quite positive and promising for the future, since the error of position of the robot to grab the dish is greatly reduced. However, it is not yet fully optimized, because it uses several programs and it is still a slow system at level of seconds, but for static pick and place, not demanding, it turns out to work very well. Despite detecting the dish, it is only possible in 2D, because if it were higher, it could not detect it so well and the robot would not have the perception that it had to climb to grab it. So, although this program works it turns out to have some limitations.

Considering the results obtained in this project the results were quite positive and undoubtedly are an added value for various applications It should al-so be noted that the vision is a more valuable for the ceramics industry, particularly for the perception of defects in the dishes or the advantage it gives robots to identify the best position to grasp.

References

[1] L. M. M. Martins, "Inspeção Visual Automática em Problemas Industriais," Dissertação para obtenção do Grau de Mestre em Engenharia Mecânica, pp. 1-85, Novembro 2013.

[2] CTCV, "CTCV QUEM SOMOS," [Online]. Available: https://www.ctcv.pt/quemsomos.html. [Acedido em 05 05 2022].

[3] D. T. FABRE, "Desenvolvimento de um sistema de visão para inspeção automatizada de peças da indústria cerâmica," pp. 1-88, 2019.

[4] A. M. Luísa Pinto, "A história de uma caneca feita por robots," Público, 12/12/2020.

International Conference on Mathematical Analysis and Applications in Science and Engineering
ICMA^{2}SC'22
ISEP Porto-Portugal, June 27 - 29, 2022

Development of grippers in the ceramic industry

Rogério Abel Almeida Torres[1,2] **N.M. Fonseca Ferreira**[1,3]
[1] Coimbra Polytechnic - ISEC, Coimbra, Portugal
[2] CTCV, Coimbra, Portugal
[3] GECAD - Knowledge Research Group on Intelligent Engineering and Computing for Advanced Innovation and Development of the Engineering Institute of Porto (ISEP), Polytechnic Institute of Porto (IPP), Porto, Portugal
[1*] rogerioliro@hotmail.com, [2*] nunomig@isec.pt

Abstract: Robotics encompasses the study and development of many areas, one of which is the area of manipulation. This area allows a robotic arm to orient and grab desired objects through actuators, which can be vacuum, fingers, among others. Usually, each gripper is designed to grab a particular group of objects or even a single object's profile. Some objects, such as ceramic pieces that are fragile and have a smooth surface, require special attention to the force and the grip method exerted on them. For this end, there are grippers equipped with load sensors capable of evaluating the measured values and acting by them.

keywords: Gripper, Industrial Manipulation, Robotics, Ceramic Industry

MSC2020: 49-XX; 34-XX; 92-XX.

1 Introduction

In the area of industry, there is an increasing adhering to the use of industrial manipulators in the execution of dangerous tasks. Industrial manipulators are robots

commonly used to grab and handle heavy loads, allowing operators to move objects quickly, conveniently, and safely, reducing the effort required by them and the number of work accidents in the industrial sector. (Benotsmane, Dudás, & Kovács, 2021)
A robotic gripper is the subsystem of the industrial robot responsible for ensuring the correct handling of the workpiece. The term gripper can also be applied in cases where it grabs the parts through suction or electromagnetism. (Zhang, Xie, Zhou, Wang, & Zhang, 2020)

2 Mechanical gripper and sensorial feedback

A mechanical gripper is a final actuator that uses fingers triggered by a mechanism to grab an object. The use of replaceable fingers allows its exchange due to wear and interchangeability. (Hu, Wan, & Harada, 2019).
The surface of ceramics is not conducive to be handled through impact-type grippers since this material easily slips. However, if its fingers are specially designed in accordance with the profile of the workpiece, it is possible to apply them in the ceramic industry. The next images show the differences between a standard gripper and a special profile gripper printed with resin handling a cup of coffee.

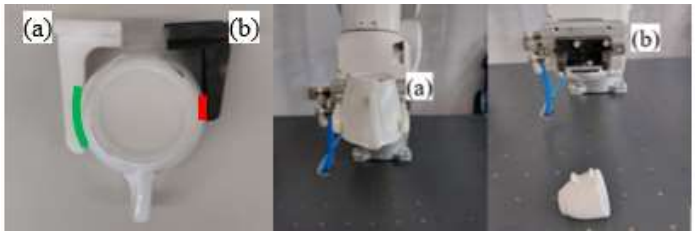

Figure 1 - Custom gripper (a) and standard gripper (b)

As seen in Figure 1, the custom tweezers (a) display a bigger contact area (green) between the cup and the tweezers compared to the contact area (red) of the standard tweezers (b). A test was mate with the cup orientation reversed to demonstrate the stability of the tweezers. In the test with the customized tweezers (a), the gripper showed no difficulties in manipulating the cup, while in the test with the standard tweezers (b), the cup slipped and damaged when performed the same exercise. To prevent the damage of the ceramic material when being manipulated, an impact-type gripper prototype was created with a force sensor. The FX293X force sensor does not convert the force measured directly to an SI (international system of units), so a calibration with known masses was realized to obtain the following equation, where "y" is the mass converted to kilograms (kg), "x" the value obtained from the sensor, and "TARA" the value of TARA.

(a) $$y = {}^{13.7172}/_{1000} * (x - TARA)\ [kg]$$

The gripper was then programmed and powered by the Arduino NANO to open and close its fingers with the impulse of a button that activates the Tower Pro Sg90 Servo Motor. This servo motor can only exert a maximum force around 0.5 kg, so a threshold was created at 0.44 kg to represent the maximum force that the gripper can exert on the object. (see Figure 2)

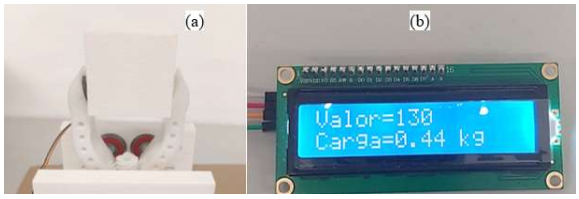

Figure 2 - Gripper holding a box (a) and its value of force (b)

3 Vacuum gripper

It uses one or more suction cups to hold parts with flat surfaces. The vacuum created between the suction cup and the surface of the workpiece creates enough suction force to lift the piece. Between all grippers, this is the one that consumes less energy, but is subject to more accidents due to misaligned suction cups and other leaks that do not ensure an airtight seal. (Gabriel, Fahning, & Meiners, 2020) A vacuum gripper with a rotary engine was created to execute coffee plate glazing with a Yaskawa robot. (see Figure 3)

Figure 3 - Vacuum suction cup with rotary engine

4 Multiple end actuator gripper

This gripper uses two or more clamping devices to handle objects. Reduces cycle time per part up to half by holding multiple workpieces at the same time. These grippers can also have different shapes to hold distinct pieces that pass through the same working path. (Sriskandarajah & Shetty, 2018) In ceramic production it is common to exist in the same treatment line a set of varied pieces of ceramics, implying the use of distinct grippers. Given the added value of the ceramic piece being low, the time lost in a robotic gripper exchange presents time losses that are reflected in high monetary losses. Therefore, the most common solution is the use of several actuators per gripper. (See Figure 4)

Figure 4 - Multiple end Gripper, two suction cups (blue) and one mechanical gripper (green)

5 Conclusion

Although it is a simple task for humans, there are multiple obstacles to the manipulation robot handle various objects. The shape, material, or size of objects can be not conducive to handling with conventional grippers, being often necessary to develop a gripper with special profiles. The use of vacuum grippers is the simplest solution to handle ceramic objects but not applicable to all environments, such as lifting heavy workpieces like toilets. Therefore, the best solution today is the use of multiple end actuators in the same robotic gripper. This way, it is cheaper, and it saves a lot of time in the overall process.

References

[1] Ali, H., Hoi, L. H., & Seng, T. C. (2011). Design and Development of Smart Gripper with Vision Sensor for Industrial Applications.

[2] Benotsmane, R., Dudás, L., & Kovács, G. (2021). Survey on New Trends of Robotic Tools in the Automotive Industry. Vehicle and Automotive

Engineering 3.

[3] Gabriel, F., Fahning, M., & Meiners, J. (2020). Modeling of vacuum grippers for the design of energy efficient vacuum-based handling processes. In Prod. Eng. Res. Devel. 14 (pp. 545–554).

[4] Garcia-Muiña, F., González-Sánchez, R., Ferrari, A., & Settembre-Blundo, D. (2018). The Paradigms of Industry 4.0 and Circular Economy as Enabling Drivers for the Competitiveness of Businesses and Territories: The Case of an Italian Ceramic Tiles Manufacturing Company.

[5] Hogreve, S., Prigge, M., Köbisch, K. O., & Tracht, K. (2020). Encapsulation of sensory gripper fingers with silicone rubber. In Procedia CIRP (pp. 439-444).

International Conference on Mathematical Analysis and Applications in Science and Engineering
ICMA²SC'22
ISEP Porto-Portugal, June 27 - 29, 2022

Comparison of response models from full, fractionated and small central composite design of experiments in cement-based mortars

Nara Cangussu[1,2*] **Ana Mafalda Matos**[1] **Lino Maia**[1]

[1] CONSTRUCT, Faculty of Engineering, University of Porto, Rua Dr. Roberto Frias, 4200-465 Porto, Portugal
[2] Center of Exact and Technological Sciences, Civil Engineering Course, State University of Montes Claros (UNIMONTES), Campus Prof. Darcy Ribeiro, Montes Claros, Brazil.
[3] Faculty of Exact Sciences and Engineering, University of Madeira, Campus da Penteada, 9020-105 Funchal, Portugal.

*up202010605@g.uporto.pt

Abstract:

Experimenters often do not have adequate time, resources or budget to carry out large number of experiments. DOE based in factorial designs are a powerful tool for designing and optimizing advanced cement-based materials, such as high performance self-compacting mortars, where many constituents raw-materials are employed (binder phase, granular materials, and admixtures) and several engineering as aesthetics requirements. The objective of this work was to compare response models from full, fractional, and small Central Composite Design of experiments applied to mortars properties.

keywords: cement-based composite; Central Composite Design; design of experiments; response model; six sigma.

MSC2010: 26A##; 34A##; 93B##.

1 Introduction

Design Of Experiments (DOE) is a systematic approach to understanding how process and product parameters affect response variables such as processability, physical properties, or product performance and uses statistical methodology to analyze data and predict product property performance under all possible conditions within limits selected for the experimental design [1]. However, the number of interactions between factors required for factor planning increases dramatically with the number of factors. Consequently, they also increase the chances that the interactions will not significantly affect the response. For this reason, fractional planning is proposed instead of full planning [2]. Because the size of an experiment increases rapidly with increasing number of levels and factors, there is a need to reduce the number of treatments in order to save time and reduce the cost of experimentation [3]. Factorial designs can be a powerful tool for designing and optimizing composite materials, where many constituent raw materials are employed (binder phase, granular materials and admixture(s)). Then, the objective of this work was compare the response models obtained from a full, a fractionated and a small central composite design to described, predict high performance self-compacting mortar properties.

2 Central composite design

The dataset available in Maia (2021) [4] regarded to a design of experiments carried out in mortars with commercial materials through a central composite design with five independent variables (key factors): (i) Vw/Vc - water to cement volume ratio; (ii) Sp/p – superplasticizer to powder mass ratio; (iii) Vw/Vp - water to powder volume ratio; (iv) Vs/Vm - sand to mortar volume ratio; (v) Vfs/Vs - fine sand to total sand volume ratio. The dataset corresponding to a full central composite design (2^5 augmented by 10 axial runs plus 8 central runs) [4], was analyzed previously by the authors. For this current study, the full factorial plan (2^5) was reduced to two half fractions (2^{5-1} augmented by 10 axial runs plus 6 central runs). In addition, a small plan (11 mixtures, augmented by 10 axial runs plus 5 central runs), was analyzed. Four dependent variables, i.e., response variables, were considered: (i) slump-flow diameter (D-flow); (ii) the time in the V-funnel (T-funnel); (iii) flexural strength, at 24 hours, determined by the three-point loading method (F,24h); (iv) compressive strength at 24 hours (Rc,24h) [4].

3 Response models

The statistical procedure will consist namely in:

a) Full quadratic Model fitting (ANOVA);

b) Model adequacy checking and diagnosis (plot analysis, Kolmogorov–Smirnov, Shapiro-Wilk, Durbin-Watson, Cook's distances);

c) Evaluation of significant individual and interaction effects.

Design-Expert software was used to assist in: analyses the results for each response variable by examining summary plots of the data, fitting a model using regression analysis and ANOVA, validating the model by examining the residuals for trends and outliers, leverage points, autocorrelation and violation of statistical assumptions, in general, and interpreting the model graphically. A detailed description of this procedure can be found in a previous publication by the authors [5], [6], [7] and/or in specialized bibliography [2], [8]. The central composite design adopted allows for the estimation of a full quadratic model as presented in Eq. 1.

$$y = \beta_0 + \sum_{i=1}^{k} \beta_i x_i + \sum_{i=1}^{k} \beta_{ii} x_i^2 + \sum_{i<j} \sum \beta_{ij} x_i x_j + \varepsilon \qquad \text{Eq. 1}$$

where y represents the response variable; xi correspond to the design variables considered; the letter β is used for model parameters (β0 is the independent term, βi represents the linear effect of x, βii represents the quadratic effect of xi and βij represents the linear-by-linear interaction between xi and xj); and ε is the fitting error. The model parameters (β0, βi, βij) can be estimated by means

of a multilinear regression analysis. In the course of the analysis, it may happen that some of the terms in Eq. (1) may not be significant. The regression of Dflow is presented in Table 1 only for response variable Dflow due to length limitations

The models generated with reduced values for D-flow and T-funnel, initially, resulted in a significant Lack of Fit. This fact led to the withdrawal some values. In case of fractional plans (A and B) for the D-flow, in order to reach the non-significant Lack of Fit, fewer points were excluded. However, the small model did not respond well to treatment, and they were excluded as initially proposed for the full plan. For the T-funnel Small plan, just applying the inverse transform, as recommended for full plan, adjusted the model and obtained Lack of Fit not significant. In the case of the Fractional A, 2 values were excluded based on the linearity of the normal plot of the residuals. In the case of the Fractional A, no was excluded, but the lack of was significant if no transform of variable is applied. The F,24h and Rc,24h considered all values and resulted in a not significant Lack of Fit for all types of plans. The **Error! Reference source not found.** shows the fitted models for D-flow for full, fractionated and small central composite design (an example for comparison among plans), and the respective linear correlation factors (R^2). For a direct comparison, Fractionated B is shown with no transform of variable (i.e. with significant lack of fit).

Table 1 – Fitted models for D-flow for full, fractionated and small central composite design (design variables in coded values).

	FULL	**Fractionated A**	**Fractionated B**	**Small**
Model Terms	**D-flow (mm)**	**D-flow (mm)**	**D-flow (mm)**	**D-flow (mm)**
Independent	343.75	338.36	337.66	343.90
Vw/Vc	8.92	4.50	7.45	6.22
Sp/p	4.58	*NS*	*NS*	*5.69*
Vw/Vp	**19.42**	**16.28**	**17.60**	**18.69**
Vs/Vm	**-34.92**	**-37.37**	**-35.83**	**-34.70**
Vfs/Vs	-1.42	*NS*	*NS*	*NS*
(Vw/Vc) x (Vw/Vp)	-5.36	*NS*	*-5.87*	*NS*
(Vw/Vc) x (Sp/p)	-2.89	*NS*	*NS*	*NS*
(Vw/Vc) x (Vs/Vm)	*NS*	4.51	4.56	*5.16*
(Vw/Vp) x (Vs/Vm)	3.11	*NS*	*NS*	*NS*
(Vw/Vp) x (Vfs/Vs)	2.98	*NS*	*NS*	*NS*
(Sp/p) x (Vfs/Vs)	1.89	*NS*	*NS*	*NS*
(Vs/Vm) x (Vfs/Vs)	*NS*	*NS*	*NS*	*NS*
$(Vw/Vc)^2$	**-20.67**	*NS*	*NS*	***-19.79***
$(Vw/Vp)^2$	*NS*	*NS*	*NS*	*NS*
$(Vs/Vm)^2$	*NS*	***-13.86***	***-14.35***	*NS*
$(Vfs/Vs)^2$	*NS*	*NS*	*NS*	*NS*
Error term (ε)				
R^2	0.9858	0.9830	0.9759	0.9885
Adj-R^2	0.9802	0.9793	0.9696	0.9808

NS: non-significant term. The three most significant parameters are typed **bold** and the most significant term is also underlined.

4 Conclusions

DOE permit examine factors simultaneously in one experiment, in order to obtain a sound knowledge of physical and chemical mechanisms concerned. The generated models for Fractional and Small plans allowed to find answers with values close to the results of the samples obtained with Full plan. All models found high linear correlation R^2. It possible to estimate a relatively large number of main effects using a small number of experimental units.

Acknowledgments

This work is funded by: Base Funding – UIDB/04708/2020 of the CONSTRUCT – Instituto de I&D em Estruturas e Construções - funded by national funds through the FCT/ MCTES (PIDDAC); by the national funds through FCT, Fundação para a Ciência e a Tecnologia, I.P., under the Scientific Employment Stimulus (Institutional Call, CEECINST/00049/2018); and the national funds through FCT, Fundação para a Ciência e a Tecnologia, I.P., under individual Scientific Employment Stimulus 2021.01765.CEECIND.

References

[1] J. R. Wagner, E. M. Mount, and H. F. Giles, "Design of Experiments," in Extrusion, William Andrew Publishing, 2014, pp. 291–308.
[2] B. de B. Neto, I. S. Scarminio, and R. E. Bruns, Como Fazer Experimentos, 4.ed. Porto Alegre: Artmed Editora SA, 2010.
[3] T. U. Eindhoven, Designs with a small number of runs for factorial experiments, no. 1993. 2022.
[4] L. Maia, "Experimental dataset from a central composite design to develop mortars with self-compacting properties and high early age strength," Data Br., vol. 39, p. 107563, 2021, doi: 10.1016/j.dib.2021.107563.
[5] A. M. Matos, L. Maia, S. Nunes, and P. Milheiro-Oliveira, "Design of self-compacting high-performance concrete: Study of mortar phase," Constr. Build. Mater., vol. 167, pp. 617–630, Apr. 2018, doi: 10.1016/j.conbuildmat.2018.02.053.
[6] S. Nunes, "Performance-based design of self-compacting concrete (SCC): a contribution to enchance SCC mixtures robustness," Faculty of Enginnering of University of Porto, 2008.
[7] A. M. Matos, S. Nunes, C. Costa, and J. L. Barroso-Aguiar, "Spent equilibrium catalyst as internal curing agent in UHPFRC," Cem. Concr. Compos., vol. 104, 2019, doi: 10.1016/j.cemconcomp.2019.103362.
[8] Douglas C. Montgomery, Introduction to Statistical Quality Control, 7.ed. John Wiley and Sons Inc., 2013.

International Conference on Mathematical Analysis and Applications in Science and Engineering
ICMA²SC'22
ISEP Porto-Portugal, June 27 - 29, 2022

Numerical modeling and optimization of self-compacting mortars: central composite design approach with

Nara Cangussu[1,2*] **Ana Mafalda Matos**[1] **Lino Maia**[1,3]

[1] CONSTRUCT, Faculty of Engineering, University of Porto, Porto, Portugal

[2] Center of Exact and Technological Sciences, Civil Engineering Course, State University of Montes Claros (UNIMONTES), Campus Prof. Darcy Ribeiro, Montes Claros, Brazil.

[3] Faculty of Exact Sciences and Engineering, University of Madeira, Campus da Penteada, 9020-105 Funchal, Portugal.

*up202010605@g.uporto.pt

Abstract:

The current work developed Statistical models to reach high-performance self-compacting cement-based mortars for structural purposes. A central composite design approach was employed to describe mortar fresh and hardened properties (mechanical strength) in function of key mortar mixture design parameters. The fitted models allow to model and predict flowability and viscosity properties and find a range where self-compacting behavior existed. Sand to mortar volume ratio exhibited the main effect on flowability and viscosity, with a positive effect, which is explained by decreases in paste volume. As expected, the water to cement volume ratio had the highest effect on both flexure and mechanical strength of mortars.

keywords: Design of experiments; response model;

MSC2010: 26A##; 34A##; 93B##.

1 Introduction

The design of cement-based materials can be complex since they must meet several current requirements. Even though the selection of the material should try to improve robustness, making the mixture more tolerant to raw material variability, for economic reasons, it depends much on local availability so there is no fixed rule for the amount/type of aggregates, cement, additions and admixtures [1]. Thus, a decisive factor for the design of advanced cementitious materials, such as SCC, is the clear understanding of the effect of each constituent raw material and their interactions on final product properties [2]. Besides, the design and optimization of such mixtures need intensive laboratory testing, particularly if new and unconventional supplementary cementitious materials or aggregates are incorporated [3]. Therefore, a more scientific and multi-scale approach to mix-design is needed, in which key mixture design variables can explain the composite properties. DOE allows to mathematically model the influence of mixture parameters on relevant composite properties and their interactions [4], to allow an appropriate adjustment for individual constringent, as raw materials or "in situ" conditions, and come up with an optimal mixture for specifically defined requirements, including cost and sustainability indicators, in a reduced time [5], [6], [7], [8]. In the current work statistical analysis of data, model fitting, validation and optimization from data available in the literature at [9] concerning a full central composite design employed to optimize high-performance self-compacting cement-based mortars were performed. The objective of the central composite design (CCD) developed was to fit a model to mathematically describe the fresh (flowability and viscosity) and hardened (flexural and compressive strength) state properties of high-performance self-compacting cement-based mortars.

2 Central composite design

Maia (2021) (Maia 2021) performed a wide experimental programme in high performance self-compacting mortars, by means of a full CCD 2^5. In total, 64 mortar mix compositions were done that corresponded to a full factorial design 2^5 augmented by 10 axial runs plus 8 central runs, resulting in a CCD with 50 mortar trial mix composition. The CCD complied five independent variables (factors): (i) Vw / Vc - water to cement volume ratio; (ii) Sp/p – superplasticizer to powder mass ratio; (iii) Vw/Vp - water to powder volume ratio; (iv) Vs/Vm - sand to mortar volume ratio; (v) Vfs/Vs - fine sand to total sand volume ratio. The effect of each key factor was evaluated at five levels $-\alpha$, -1, 0, +1, $+\alpha$, as shown in Table 1. In order to make the design rotatable, the value of α was taken equal to $n_F^{1/4}$, where n_F is the number of points in the factorial part of the design. In the current study, this corresponds to taking an equal to 2.3784. Four dependent variables, i.e., response variables, were considered: (i) slump-flow diameter (D-flow); (ii) the time in the V-funnel (T-funnel); (iii) flexural strength, at 24 hours, determined by the three-point loading method (F,24h); (iv) uniaxial compressive strength at 24 hours (Rc,24h) (Maia 2021).

Table 1 - Correspondence between coded values and actual values of design variables.

Design Variables	-2.3784	-1	0	+1	+2.3784
X_1: Vw/Vc	0.682	0.805	0.895	0.894	1.108
X_2: Sp/p	0.019	0.022	0.024	0.025	0.029
X_3: Vw/Vp	0.434	0.513	0.570	0.627	0.706
X_4: Vs/Vm	0.366	0.432	0.480	0.528	0.594
X_5: Vfs/Vs	0.043	0.250	0.400	0.550	0.757

3 Response models

The statistical procedure to obtain regression models to describe the response variables in terms of design variables consisted in: (i) Fitting a second-order polynomial model using regression analysis and ANOVA including the removal of non-significant terms in the model (p-value >0.05) and using backward method to eliminate non-significant terms in the regression model;

(ii) Model adequacy checking and diagnosis (plot analysis, Kolmogorov–Smirnov, Shapiro-Wilk, Durbin-Watson, Cook's distances); (iii) Evaluation of significant individual and interaction effects, among other computations; (iv) Mixtures optimization using desirability function. Design-Expert software was used to assist in: analyses the results for each response variable by examining summary plots of the data, fitting a model using regression analysis and ANOVA, validating the model by examining the residuals for trends and outliers, leverage points, autocorrelation and violation of statistical assumptions, in general, and interpreting the model graphically. The central composite design adopted allows for the estimation of a full quadratic model as presented in Equation Eq. 1.

$$y = \beta_0 + \sum_{i=1}^{k} \beta_i x_i + \sum_{i=1}^{k} \beta_{ii} x_i^2 + \sum_{i<j} \sum \beta_{ij} x_i x_j + \varepsilon \qquad \text{Eq. 1}$$

where y represents the response variable; xi correspond to the design variables considered; the letter β is used for model parameters (β0 is the independent term, βi represents the linear effect of x, βii represents the quadratic effect of xi and βij represents the linear-by-linear interaction between xi and xj); and ε is the fitting error. The model parameters (β0, βi, βij) can be estimated by means of a multilinear regression analysis. In the course of the analysis, it may happen that some of the terms in Eq. (1) may not be significant. The final equations in terms of coded factors are presented in Table 2. A variable transformation of the form 1/y was used in order to stabilize the Tfunnel response variance and improve the resulting model, which is in accordance with previous studies [6], [10]. From the coded equation can be identified the relative impact of the factors by comparing the factor coefficients. Higher values indicate higher influence of the design variable in the response. For each model, the three most significant parameters are typed bold and the most significant term is also underlined. A positive coefficient means that the response (or transformed response) variable will increase if the given mixture parameter increases and vice-versa.

Table 2 – Fitted models (design variables in coded values).

Model Terms	**D-flow (mm)**	**1/T-funnel (s)**	**F,24h**	**Rc,24h**
Independent	343.75	0.0688	11.43	60.65
Vw/Vc	8.92	**0.0115**	**-0.4053**	**-6.17**
Sp/p	4.58	0.0050	*NS*	*NS*
Vw/Vp	**19.42**	**0.0245**	**-0.2610**	**-1.19**
Vs/Vm	**-34.92**	**-0.0302**	0.2608	0.2655
Vfs/Vs	-1.42	-0.0016	*NS*	**-1.33**
(Vw/Vc) x (Vw/Vp)	-5.36	*NS*	*NS*	*NS*
(Vw/Vc) x (Sp/p)	-2.89	-0.0020	*NS*	*NS*
(Vw/Vc) x (Vs/Vm)	*NS*	-0.0037	*NS*	*NS*
(Vw/Vp) x (Vs/Vm)	3.11	-0.0061	0.1826	*NS*
(Vw/Vp) x (Vfs/Vs)	2.98	*NS*	*NS*	*NS*
(Sp/p) x (Vfs/Vs)	1.89	*NS*	*NS*	*NS*
(Vs/Vm) x (Vfs/Vs)	*NS*	*NS*	*NS*	-0.4934
$(Vw/Vc)^2$	**-20.67**	-0.0017	*NS*	0.5639
$(Vw/Vp)^2$	*NS*	0.0011	*NS*	0.5486
$(Vs/Vm)^2$	*NS*	*NS*	**-0.2834**	*NS*
$(Vfs/Vs)^2$	*NS*	-0.0014	*NS*	*NS*
Error term (ε)				
R^2	0.9858	0.9922	0.6619	0.9588
Adj-R^2	0.9802	0.9897	0.6216	0.9519

NS: non-significant term. The three most significant parameters are typed **bold** and the most significant term is also underlined.

From regression models presented in Table 1, it can be perceived that Vs/Vm exhibited the strongest effect, a negative effect, on the fresh state properties, i.e., Dflow and T-funnel. This can be explained by the reduction on paste content. The factor Vw/Vp impacted fresh state properties

as expected, but with a positive effect. This as expected, since a high water content increase the flowability. Vw/Vc was by far the main factor determining the mechanical strength, both flexure and compression.In addition, Vs/Vm was also significant, but in this case a negative effect was observed. A significant quadratic term on Vs/Vm was also found Signiant for Flexure strength. Sp/p exhibited the lowest influence on high performance self-compacting mortar properties. This can be explained by the short range of variation of Sp/p in the experimental plan, which was determined by the strong dispersion action of the superplasticizer used (Viscocrete 3008).

4 Conclusions

- Quadratic models were found to be adequate to describe the mortar properties – slump-flow diameter, V-funnel time, flexure and compressive strength – over the experimental region;
- Vs/Vm was the main effect on the slump-flow diameter and V-funnel. An increase of Vs/Vm reduces the slump-flow diameter and t-funnel;
- Vw/Vc was found to be the most influencing variable flexure and compressive strength. An increase of Vw/Vc reduces the flexure and compressive strength;
- Sp/p exhibited the lowest influence on high performance self-compacting mortar properties, which might be explained by the limited range dosages employes in the current work;
- Numerical optimization allowed further improvement of the mortar properties in the fresh state and in terms of mechanical bahaviour;
- DOE definitively is a power tool to better understand, optimize and design the mortar phase when very demanding performance requirements exists.
- The compressive strength model (Rc,24h), among the four obtained, was the one that best translated the results found.

Acknowledgments

This work is funded by: Base Funding – UIDB/04708/2020 of the CONSTRUCT – Instituto de I&D em Estruturas e Construções - funded by national funds through the FCT/ MCTES (PIDDAC); by the national funds through FCT, Fundação para a Ciência e a Tecnologia, I.P., under the Scientific Employment Stimulus (Institutional Call, CEECINST/00049/2018); and the national funds through FCT, Fundação para a Ciência e a Tecnologia, I.P., under individual Scientific Employment Stimulus 2021.01765.CEECIND.

References

[1] I. Galobardes, R. P. Salvador, S. H. P. Cavalaro, A. Figueiredo, and C. I. Goodier, “Adaptation of the standard EN 196-1 for mortar with accelerator,” Constr. Build. Mater., vol. 127, pp. 125–136, 2016, doi: 10.1016/j.conbuildmat.2016.09.147.

[2] B. Yogitha, M. Karthikeyan, and M. G. Muni Reddy, "Progress of sugarcane bagasse ash applications in production of Eco-Friendly concrete - Review," Mater. Today Proc., vol. 33, pp. 695–699, 2020, doi: https://doi.org/10.1016/j.matpr.2020.05.814.

[3] R. Gettu, R. G. Pillai, M. Santhanam, and B.S. Dhanya, "Ways of Improving the Sustainability of Concrete Technology Through the Effective Use of Admixtures," Indian Inst. Technol. Madras, Chennai, no. April, p. 21, 2018.

[4] Douglas C. Montgomery, Introduction to Statistical Quality Control, 7.ed. John Wiley and Sons Inc., 2013.

[5] A. M. Matos, S. Nunes, C. Costa, and J. L. Barroso-Aguiar, "Spent equilibrium catalyst as internal curing agent in UHPFRC," Cem. Concr. Compos., vol. 104, 2019, doi: 10.1016/j.cemconcomp.2019.103362.

[6] A. M. Matos, L. Maia, S. Nunes, and P. Milheiro-Oliveira, “Design of self-compacting high-performance concrete: Study of mortar phase,” Constr. Build. Mater., vol. 167, pp. 617–630, 2018, doi: 10.1016/j.conbuildmat.2018.02.053.

[7] S. Nunes, A. M. Matos, T. Duarte, H. Figueiras, and J. Sousa-Coutinho, “Mixture design of self-compacting glass mortar,” Cem. Concr. Compos., vol. 43, pp. 1–11, 2013, doi: 10.1016/j.cemconcomp.2013.05.009.

[8] S. Nunes, "Performance-based design of self-compacting concrete (SCC): a contribution to enchance SCC mixtures robustness," Faculty of Enginnering of University of Porto, 2008.

[9] L. Maia, "Experimental dataset from a central composite design to develop mortars with self-compacting properties and high early age strength," Data Br., vol. 39, p. 107563, 2021, doi: 10.1016/j.dib.2021.107563.

[10] S. Nunes, A.M. Matos, T. Duarte, H. Figueiras, J. Sousa-Coutinho Mixture design of self-compacting glass mortar Cem. Concr. Compos., 43 (2013), pp. 1-11,

International Conference on Mathematical Analysis and Applications in Science and Engineering
ICMA^{2}SC'22
ISEP Porto-Portugal, June 27 - 29, 2022

Numerical methods for nonlocal and nonlinear parabolic equations with applications in hydrology and climatology

Łukasz Płociniczak[1⋆]

[1] Faculty of Pure and Applied Mathematics, Wroclaw University of Science and Technology, Poland

[1⋆]lukasz.plociniczak@pwr.edu.pl

Abstract: We present some of our results concerning numerical discretizations of nonlinear and fractional in time parabolic equations. Along with a collection of various methods and statements about their convergence and stability, we stress their motivation and real-world applications.

keywords: subdiffusion; Caputo derivative; nonlinearity; nonsmooth data; time-dependent coefficient.

MSC2020: 35K55; 65M60; 35R11.

1 Introduction

Many natural and industrial phenomena exhibit nonlocal behaviour in temporal or spatial dimension. The former is responsible for processes for which its whole history influences the present state. The latter, on the other hand, indicates that faraway regions of the domain may have some impact on local points. This is useful in describing media of high heterogeneity.

Partial differential equations that are nonlocal involve one or several integral operators that encode this behaviour. For example, Riemann-Liouville or Caputo derivatives are used in temporal direction, while fractional Laplacian or its relatives describe spatial nonlocality. When it comes to numerical methods the discretization of these requires more care than their classical versions. Moreover, it is usually much more expensive, both on CPU and the memory, to conduct simulations involving nonlocal equations.

In this talk we will present several approaches to discretize nonlocal and nonlinear parabolic equations with various real-world applications such as hydrology and climatology. These include: transformation into a pure integral equation for the time-fractional porous medium equation and Galerkin spectral methods for a general parabolic equation with temporal nonlocality. We will prove stability and convergence of these methods illustrating all the theoretical results with numerical simulations implemented in Julia programming language with parallelization. The talk is based on [2, 3, 1, 4, 5].

Acknowledgments

The author has been supported by the National Science Centre, Poland (NCN) under the grant Sonata Bis with a number NCN 2020/38/E/ST1/00153.

References

[1] Hanna Okrasińska-Płociniczak and Łukasz Płociniczak. Second order scheme for self-similar solutions of a time-fractional porous medium equation on the half-line, Applied Mathematics and Computation **424C** (2022), 127033.

[2] Łukasz Płociniczak, Numerical method for the time-fractional porous medium equation, SIAM Journal on Numerical Analysis **57**(2) (2019), 638–656.

[3] Łukasz Płociniczak, Linear Galerkin-Legendre spectral scheme for a degenerate nonlinear and nonlocal parabolic equation arising in climatology, arXiv preprint **2106.05140** (2021).

[4] Łukasz Płociniczak, A linear Galerkin numerical method for a quasilinear subdiffusion equation, arXiv preprint: **2107.10057** (2022).

[5] Łukasz Płociniczak, Error of the Galerkin scheme for a semilinear subdiffusion equation with time-dependent coefficients and nonsmooth data, arXiv preprint **2202.13728** (2022).

Transport models and internal transport barriers by stochastic solutions

R. Vilela Mendes
CMAFcIO, Faculdade de Ciências,
Universidade de Lisboa
rvilela.mendes@gmail.com

Abstract:

The technique of stochastic solutions is applied to linear and nonlinear partial differential equations.

A stochastic solution is a stochastic process that, for arbitrary initial conditions, generates the solution. In addition to providing a very convenient formulation for linear problems, this technique has also allowed to obtain new exact solutions for many nonlinear problems.

In the particular case of one-dimensional plasma transport equations, the technique is applied to the characterization and control of internal transport barriers.

It is also explained how new exact solutions may be obtained for nonlinear diffusion equations, using diffusion and branching processes.

keywords: Stochastic solutions; internal transport barriers

References

[1] Y. LeJan and A. S. Sznitman; *Stochastic cascades and 3-dimensional Navier-Stokes equations*, Prob. Theory and Relat. Fields 109 (1997) 343-366.

[2] E. C. Waymire; *Probability & incompressible Navier-Stokes equations: An overview of some recent developments*, Prob. Surveys 2 (2005) 1-32.

[3] R. Vilela Mendes and F. Cipriano; *A stochastic representation for the Poisson-Vlasov equation,* Comm. Nonlinear Sci. and Num. Simul. 13 (2008) 221-226 and 1736.

[4] E. Floriani, R. Lima and R. Vilela Mendes; *Poisson-Vlasov : Stochastic representation and numerical codes,* Eur. Phys. J. D 46 (2008) 295-302 and 407.

[5] R. Vilela Mendes, *Poisson-Vlasov in a strong magnetic .eld: A stochastic solution approach",* J. Math. Phys. 51 (2010) 043101.

[6] E. Floriani and R. Vilela Mendes; *A stochastic approach to the solution of magnetohydrodynamics equations*, J. Comp. Phys. 242 (2013) 777-789.

International Conference on Mathematical Analysis and Applications in Science and Engineering
ICMA^{2}SC'22
ISEP Porto-Portugal, June 27 - 29, 2022

Study of species' migration in biological population under symmetry analysis

Sumanta Shagolshem[1] **B. Bira**[1] **D. Zeidan**[2⋆]

[1] Department of Mathematics
SRM Institute of Science and Technology, Kattankulathur, Chennai, India
[2] School of Basic Science and Humanities
German Jordanian University, Amman, Jordan

[2⋆]dia.zeidan@gju.edu.jo

Abstract: In this present study, Lie symmetry analysis is employed to the two dimensional normal biological population model (NBPM). This technique represents a substantial advancement over the other techniques in this field to obtain some exact solutions. Systematically, we present the procedure to obtain the similarity solutions and the corresponding reduced ordinary differential equation (ODE) using Lie point symmetries. Further, by exploiting the symmetry properties, we obtain some exact solutions for the model which is new to the literature.

keywords: Lie point symmetry, biological population model, similarity solution, exact solution

MSC2020: 76M60; 35G20; 35B08

1 Introduction

Over the decades, the development of mathematical models help in describing a wide range of physical phenomena in natural sciences and engineering efficiently. Biological experts believe that dispersion or emigration plays an important part in the regulation of a species' population. The mathematical modeling of such phenomenon is very important in the study of the population density and mathematical strategies for controlling the emigration of species' population [1, 2, 3]. On the other hand, Lie group analysis [4, 5, 6] is one of the powerful and convenient tools to handle such problems. The technique's fundamental premise is that for any subgroup of the group symmetry, one can reduce the original partial differential equation(PDE) to an equation with fewer independent variables which make us easy to solve it.

The authors in [7] study Chaplygin gas equations and obtain some exact solutions whereas, the authors in [8] obtained some new exact solutions for compressible isentropic Navier-Stokes equation using the same technique. Sil and Raja Sekhar [9] also construct some exact solutions for an integrable soliton equation using nonlocal symmetry. The main aim of this paper is to solve the nonlinear 2^{nd}-order normal biological population model which is in the form:

$$\frac{\partial \varrho}{\partial t} = \frac{\partial^2 \varrho^2}{\partial x^2} + \frac{\partial^2 \varrho^2}{\partial y^2} + \mathcal{F}(\varrho), \qquad t \geq 0, \qquad x, y \in \mathbb{R}$$

where ϱ and $\mathcal{F}$ represents the population density and the population supply due to births and deaths respectively. In our present problem, considering the Malthusian Law [10], we take $\mathcal{F}(\varrho) = c\varrho$ where c is a constant to obtain the following equation:

$$\frac{\partial \varrho}{\partial t} - 2\Big(\frac{\partial \varrho}{\partial x}\Big)^2 - 2\varrho\frac{\partial^2 \varrho^2}{\partial x^2} - 2\Big(\frac{\partial \varrho}{\partial y}\Big)^2 - 2\varrho\frac{\partial^2 \varrho^2}{\partial y^2} + c\varrho = 0, \quad t \geq 0, \quad x, y \in \mathbb{R}. \tag{1}$$

2 Symmetry group of transformation

Let us consider a one-parameter Lie group of transformation for (1) as

$$\begin{aligned} x^* &= x + \epsilon\theta_1(x, y, t, \varrho) + O(\epsilon^2), \quad y^* = y + \epsilon\theta_2(x, y, t, \varrho) + O(\epsilon^2), \\ t^* &= t + \epsilon\theta_3(x, y, t, \varrho) + O(\epsilon^2), \quad \varrho^* = \varrho + \epsilon\phi(x, y, t, \varrho) + O(\epsilon^2), \end{aligned} \tag{2}$$

with ϵ as a parameter and $\theta_1,\ \theta_2,\ \theta_3$ and ϕ are the infinitesimals which are to be determined. Using Maple package, we obtain the infinitesimals transformation for (1) in the following form:

$$\theta_1 \ = \ a_2y + a_3x + a_5, \ \ \theta_2 = -a_2x + a_3y + a_6, \ \ \theta_3 = a_1e^{-ct} + a_4, \ \ \phi = \varrho(a_1ce^{-ct} + 2a_3),$$

where $a_i (i = 1 \cdots 6)$ are the arbitrary parameters and the associated six generators are given below:

$$\begin{aligned} Y_1 &= \frac{\partial}{\partial t}, \quad Y_2 = \frac{\partial}{\partial x}, \quad Y_3 = \frac{\partial}{\partial y}, \quad Y_4 = y\frac{\partial}{\partial x} - x\frac{\partial}{\partial y}, \\ Y_5 &= x\frac{\partial}{\partial x} + y\frac{\partial}{\partial y} + 2\varrho\frac{\partial}{\partial \varrho}, \quad Y_6 = \frac{1}{e^{ct}}\frac{\partial}{\partial t} + \frac{c\varrho}{e^{ct}}\frac{\partial}{\partial \varrho}. \end{aligned} \tag{3}$$

Based on the above generators, we proceed the following sections.

3 Reduction of independent variables

In this section, first we reduce the given PDE (1) to a PDE with two independent variables by introducing similarity variables associated with the following characteristic equations:

$$\frac{dx}{a_2y + a_3x + a_5} = \frac{dy}{-a_2x + a_3y + a_6} = \frac{dt}{a_1e^{-ct} + a_4} = \frac{d\varrho}{\varrho(a_1ce^{-ct} + 2a_3)}, \tag{4}$$

and successively, we reduced the PDE with two variables to an ODE and construct the particular exact solutions in the following subsections:

3.1 When $a_1 = a_2 = 0$

For this case, one can obtained the following similarity variables:

$$\xi = (a_3x + a_5)e^{-\frac{a_3}{a_4}t}, \quad \zeta = (a_3y + a_6)e^{-\frac{a_3}{a_4}t}, \quad \varrho = P(\xi, \zeta)e^{\frac{2a_3}{a_4}t}. \tag{5}$$

Using (5) in (1), we obtained the reduced PDE:

$$P\Big(\frac{2a_3}{a_4} - c\Big) - \frac{a_3}{a_4}\Big(\xi P_\xi + \zeta P_\zeta\Big) - 2a_3^2\Big(P_\xi^2 + PP_{\xi\xi} + P_\zeta^2 + PP_{\zeta\zeta}\Big) = 0. \tag{6}$$

Further, the infinitesimals transformation for are obtained as:

$$f_1 = -b_1\zeta + b_2\xi, \quad f_2 = b_1\xi + b_2\zeta, \quad h_1 = 2b_2P. \tag{7}$$

We write the characteristic equation for (7) as below and study the solutions in the following cases:

$$\frac{d\xi}{b_1\zeta + b_2\xi} = \frac{d\zeta}{-b_1\xi + b_2\zeta} = \frac{dP}{2b_2P}. \tag{8}$$

Case-I: $b_1 = 0$

Under this case, we solve (8) and obtained the following similarity variables:

$$\eta(\xi,\zeta) = \frac{\xi}{\zeta}, \qquad P = \zeta^2\mathbb{P}(\eta),$$

and substituting in (6) yields the following ODE:

$$\mathbb{P}'' + \frac{\mathbb{P}'^2}{\mathbb{P}} - \frac{6\eta}{1+\eta^2}\mathbb{P}' + \frac{1}{1+\eta^2}\Big(6\mathbb{P} + \frac{c}{2a_3^2}\Big) = 0. \tag{9}$$

The equation (9) is solved for $\mathbb{P} = -\dfrac{c}{12a_3^2}$ and obtain the solution of (1) as follow:

$$\varrho(x,y,t) = -\frac{c}{12a_3^2}(a_3y + a_6)^2$$

Case-II: $b_2 = 0$

For this case, the reduced ODE obtained using the similarity variables $\eta(\xi,\zeta) = \frac{1}{2}(\xi^2+\zeta^2),\ P = \mathbb{P}(\eta)$ is given as:

$$\mathbb{P}'' + \frac{\mathbb{P}'^2}{\mathbb{P}} + \frac{\mathbb{P}'}{2\eta\mathbb{P}}\Big(2\mathbb{P} + \frac{\eta}{a_3a_4}\Big) + \frac{1}{2\eta}\Big(\frac{c}{2a_3^2} - \frac{1}{a_3a_4}\Big) = 0.$$

Solving the above equation for $c = \dfrac{4a_3}{a_4}$, one can find the solution of the governing equation (1):

$$\varrho(x,y,t) = -\frac{1}{4a_3a_4}\Big[(a_3x + a_5)^2 + (a_3y + a_6)^2\Big].$$

3.2 When $a_2 = a_3 = a_4 = 0$

For this case, the characteristic equations is:

$$\frac{dx}{a_5} = \frac{dy}{a_6} = \frac{dt}{a_1e^{-ct}} = \frac{d\varrho}{ca_1e^{-ct}\varrho},$$

and the similarity variables are:

$$\xi = \frac{a_1x}{a_5} + \frac{e^{ct}}{c}, \quad \zeta = \frac{a_1y}{a_6} + \frac{e^{ct}}{c}, \quad \varrho = P(\xi,\zeta)e^{ct}. \tag{10}$$

Using (10) to the governing equation (1), one can obtain the reduced PDE as:

$$P_\xi + P_\zeta - 2\Big(\frac{a_1}{a_5}\Big)^2\Big(P_\xi^2 + PP_{\xi\xi}\Big) - 2\Big(\frac{a_1}{a_6}\Big)^2\Big(P_\zeta^2 + PP_{\zeta\zeta}\Big) = 0, \tag{11}$$

Applying symmetry analysis to (11), one can obtain the exact solution for (1) as:

$$\varrho(x,y,t) = e^{ct}\Big[\frac{1}{2}\Big(\frac{a_5}{a_1}\Big)^2\Big(\frac{a_1x}{a_5} + \frac{e^{ct}}{c}\Big) + b_7\Big]. \tag{12}$$

4 Conclusions and Future work

Lie group analysis is implemented to find similarity and special exact solutions to PDE that characterise the two-dimensional biological populations. The symmetry generators are used to create similarity variables, which leads to a simplified equations with fewer independent variables, and eventually to an ODE. Finally, we construct some exact solution for the governing PDE. It can be extended to finding optimal algebra and constructing conservation laws which help in finding nonlocal symmetry.

Acknowledgments Authors would like to acknowledge the support provided by SRM Institute of Science and Technology, India, and the German Jordanian University, Amman, Jordan.

References

[1] F. Shakeri, M. Dehghan, Numerical solution of a biological population model using He's variational iteration method, Computers & Mathematics with Applications, **54** (2007), 1197–1209.

[2] A. Arafa, S. Rida, H. Mohamed, Homotopy analysis method for solving biological population model, Communications in Theoretical Physics, **56**(5) (2011), 797.

[3] V.K. Srivastava, S. Kumar, M.K. Awasthi, B.K. Singh, Two-dimensional time fractional-order biological population model and its analytical solution, Egyptian journal of basic and applied sciences, **1**(1) (2014), 71–76.

[4] G.W. Bluman, S. Kumei, *Symmetries and differential equation*. New York: Springer, 1989.

[5] L.V. Ovsiannikov, *Group Analysis of Differential Equations*. Elsevier Inc, Academic Press, 1982.

[6] P.J. Olver, *Applications of Lie Groups to Differential Equations*. New York: Springer-Verlag, 1993.

[7] P. Satapathy, T. Raja Sekhar, Nonlocal symmetries classifications and exact solution of Chaplygin gas equations, Journal of Mathematical Physics, **59**(8) (2018), 081512.

[8] R. Jiwari, V. Kumar, S. Singh, Lie group analysis, exact solutions and conservation laws to compressible isentropic Navier–Stokes equation, Engineering with Computers (2020), 1–10.

[9] S. Sil, T. Raja Sekhar, D. Zeidan, Nonlocal conservation laws, nonlocal symmetries and exact solutions of an integrable soliton equation, Chaos, Solitons & Fractals, **139** (2020), 110010.

[10] M.E. Gurtin, R.C. MacCamy, On the diffusion of biological populations, Mathematical biosciences, **33** (1977), 35–49.

International Conference on Mathematical Analysis and Applications in Science and Engineering
ICMA^{2}SC'22
ISEP Porto-Portugal, June 27 - 29, 2022

Symmetry Analysis and Power Series Solution for Cancer Tumor Model

S. Gimnitz Simon[1] **B. Bira**[2] **D. Zeidan**[3]$\star$

[1] Department of Mathematics
SRM Institute of Science and Technology, Kattankulathur, India
[2] Department of Mathematics
SRM Institute of Science and Technology, Kattankulathur, India
[3] School of Basic Sciences and Humanities, German Jordanian University, Amman, Jordan

[3]$\star$dia.zeidan@gju.edu.jo

Abstract: In this paper, we consider a time-fractional cancer tumor model where the killing rate is space-dependent. Applying Lie symmetry analysis, we obtain the infinitesimal transformations. Under the invariance condition the given fractional partial differential equation(FPDE) is reduced to fractional ordinary differential equations(FODE). Finally, we derive the power series solution for the governing equation.

keywords: Time-fractional cancer tumor model; Lie symmetry analysis; power series solution

MSC2020: 34K37; 76M60; 35C10

1 Introduction

Fractional differential equations plays significant role in the better understanding of engineering, science, medical science, space science etc. (see, [1, 2, 3]). Particularly, in the field of medical science, the cancer cell's growth rate may differ from patient to patient and hence needs to be identified and treated as soon as possible, to prevent the accidental death. Many researchers are working tirelessly for the better understanding of the problem through mathematical model [4, 5]. In real life incidents, this physical process won't happen in a linear way and hence can be represented by non-linear FPDE. Whereas, for the given FPDE, we don't have luxury to construct the exact solutions explicitly. Many engineers and research scientists used different numerical and analytical techniques to solve it exactly and numerically (see, [6, 7]). For example, the authors in [8], used homotopy analysis method to solve the given non-linear FPDEs numerically, whereas, the variational iteration method is used by the authors in [9].

On the other hand, symmetry analysis is one of the efficient technique to handle such problems (For more details, see, [10, 11]). The authors, obtained the exact solution for time-fractional variant Boussinesq-Burgers equation using Lie group analysis in [12]. For the application of this technique, to solve FDEs, we refer [13]. The study of FDEs under invariance condition the author is referred to [14].

2 Symmetry analysis

In the present study, we consider time-fractional cancer tumor model[5] as:

$$\frac{\partial^\alpha u(x,t)}{\partial t^\alpha} = \frac{\partial^2 u(x,t)}{\partial x^2} - \frac{2}{x^2}u(x,t), \tag{1}$$

where $u(x,t)$ is the concentration of cancer tumor cells and α is the fractional order i.e $0 < \alpha < 1$. Let us consider the one parameter Lie group of transformations:

$$\begin{aligned} x^* &= x + \epsilon\xi(x,t,u) + O(\epsilon^2), \\ t^* &= t + \epsilon\tau(x,t,u) + O(\epsilon^2), \\ u^* &= u + \epsilon\phi(x,t,u) + O(\epsilon^2), \end{aligned}$$

where ϵ is the group parameter and $\xi,\ \tau$, and ϕ are the infinitesimals which are to be determined. From the straight forward calculation we obtain the following infinitesimals transformations for (1) as:

$$\begin{aligned} \xi(x,t,u) &= 2\alpha a_3 x + a_5 \\ \tau(x,t,u) &= a_2 + 4\ t a_3 \\ \phi(x,t,u) &= G_5(x,t) + 3\alpha u a_3 - 2u a_3 + u a_1 \end{aligned}$$

where $a_1,\ a_2$ and a_3 are the arbitrary constants and the associated infinitesimal generators are,

$$\begin{aligned} X_1 &= 2\alpha x\frac{\partial}{\partial x} + 3\alpha u\frac{\partial}{\partial u} - 2u\frac{\partial}{\partial u} + 4t\frac{\partial}{\partial t}, \\ X_2 &= u\frac{\partial}{\partial u}, \qquad X_3 = \frac{\partial}{\partial t}, \qquad X_4 = \frac{\partial}{\partial x}. \end{aligned}$$

3 Symmetry reduction and power series solution

In this section, we consider the generator X_1 and write the corresponding characteristic equation as below:

$$\frac{dx}{2\alpha x} = \frac{dt}{4t} = \frac{du}{(3\alpha - 2)u}. \tag{2}$$

Solving (2), yields the similarity variables:

$$\xi = x\ t^{\frac{-\alpha}{2}}, \qquad u = t^{\frac{3\alpha-2}{4}}U(\xi). \tag{3}$$

Using the above similarity variables, we reduce the FPDEs to a non-linear FODE via the following theorem.

Theorem 1. *The usage of (3) in (1), gives rise to the following non-linear FODE*

$$\Big[\frac{-\alpha+2}{4} - \frac{\alpha}{2}\xi\frac{\partial}{\partial\xi}\Big]\Big(K^{\frac{3\alpha+2}{4},1-\alpha}_{\frac{2}{\alpha}}U\Big)(\xi) - U_{\xi\xi} + \frac{2}{\xi^2}U(\xi) = 0. \tag{4}$$

Proof.

$$\begin{aligned} \frac{\partial^\alpha u(x,t)}{\partial t^\alpha} &= \frac{1}{\Gamma(1-\alpha)}\frac{\partial}{\partial t}\int_0^t \frac{u}{(t-s)^\alpha}ds, \\ &= \frac{1}{\Gamma(1-\alpha)}\frac{\partial}{\partial t}\int_0^t \frac{s^{\frac{3\alpha-2}{4}}U(xs^{\frac{-\alpha}{2}})}{s^\alpha(\frac{t}{s}-1)^\alpha}ds \end{aligned}$$

Substituiting $\frac{t}{s} = z$, we get

$$\frac{\partial^\alpha u(x,t)}{\partial t^\alpha} = \frac{1}{\Gamma(1-\alpha)}\frac{\partial}{\partial t}\int_1^\infty \frac{t^{\frac{-\alpha+2}{4}}U(\xi)z^{\frac{\alpha}{2}}}{z^{\frac{-\alpha+6}{4}}(z-1)^\alpha}dz = t^{\frac{-\alpha-2}{4}}\Big[\frac{-\alpha+2}{4} - \frac{\alpha}{2}\xi\frac{\partial}{\partial\xi}\Big](K_{\frac{2}{\alpha}}^{\frac{3\alpha+2}{4},1-\alpha}U\Big)(\xi),$$

where the Erdelyi-Kober operator is given as $K_\beta^{\tau,\alpha}(\xi) = \frac{1}{\Gamma(\alpha)}\int_1^\infty \frac{z^{-(\tau+\alpha)}}{(z-1)^{1-\alpha}}U(\xi z^{\frac{1}{\beta}})dz$. Using the above in (1) we get (4), hence the theorem.

Further, in order to construct the power series solution of (1), we replace the Erdelyi-Kober operator in (4) using the following formula [17]:

$$I_c^{(a,b)}U(\xi) = \sum_{s=0}^\infty \lambda_s U^{(s)}(\xi)\frac{\xi^s}{s!}, \quad \text{where} \quad \lambda_s = \sum_{j=0}^s \binom{s}{j}(-1)^{s-j}\frac{\Gamma(a+\frac{j}{c}+1)}{\Gamma(a+b+\frac{j}{c}+1)}. \tag{5}$$

Usage of (5) in (4) yields

$$\left(K_1 + \frac{2}{\xi^2}\right)U - K_2\xi U' - U'' = 0, \tag{6}$$

where

$$K_1 = \frac{\Gamma\left(\frac{3\alpha+2}{4}+1\right)}{\Gamma\left(1+\frac{2-\alpha}{4}\right)} \quad \text{and} \quad K_2 = \frac{\left(1+\frac{\alpha}{2}\right)\Gamma\left(\frac{3\alpha+2}{4}+1\right)}{\Gamma\left(2+\frac{2-\alpha}{4}\right)}.$$

Now we consider the power series in the form $U(\xi) = \sum_{n=0}^\infty a_n\xi^n$, and putting in (6) and simplifying we get the solution of (6) as:

$$U(\xi) = a_0 + a_1\xi + \frac{K_1a_0}{2}\xi^2 + \sum_{n=3}^\infty \frac{a_{n-2}(K_1-K_2)}{(n-1)(n)}\xi^n,$$

$$\text{where} \quad a_n = \begin{cases} a_n, & n = 0,1 \\ \frac{K_1a_0}{2}, & n = 2 \\ \frac{(K_1-K_2)a_{n-2}}{n(n-1)}, & n \geq 3 \end{cases}$$

and subsequently the solution of the given FPDE can be written as:

$$u(x,t) = t^{\frac{3\alpha-2}{4}}\Big[a_0 + a_1x\,t^{\frac{-\alpha}{2}} + \frac{K_1a_0}{2}\Big(x\,t^{\frac{-\alpha}{2}}\Big)^2 + \sum_{n=3}^\infty \frac{a_n(K_1-K_2)}{(n-1)(n)}\Big(x\,t^{\frac{-\alpha}{2}}\Big)^n\Big].$$

4 Conclusions and Future work

In this article, we investigate the time-fractional cancer tumor model through Lie symmetry analysis. First, we obtained the symmetry group of transformation which leaves the governing equation invariant. Then, we reduce the given FPDE to FODE using the similarity variables. Finally, we construct a solution for the given model using a power series, which can provide useful information towards the better understanding of the physical model. Further, we plan to extend this work upto the convergence analysis of the series solutions, construction of optimal algebras, and study the behaviour of solution graphically for different values of α.

Acknowledgments The authors gratefully acknowledge the support of SRM Institute of Science and Technology, India, and the German Jordanian University, Amman, Jordan.

References

[1] A.A. Kilbas, H.M. Srivastava, J.J. Trujillo, *Theory and Applications of Fractional Differential Equations*. Amsterdam : Elsevier,**204**, 2006.

[2] R. Hilfer ed., *Applications of fractional calculus in physics*. World scientific, 2000.

[3] M. Rahimy, Applications of fractional differential equations, Appl. Math. Sci,**4**(50)(2010), 2453-2461.

[4] P.K. Burgess, P.M. Kulesa, J.D. Murray, E.C. Alvord Jr, The interaction of growth rates and diffusion coefficients in a three-dimensional mathematical model of gliomas, J. Neuropathol. Exp. Neurol.,**56**(6)(1997), 704-713.

[5] O.S Iyiola, F.D Zaman, A fractional diffusion equation model for cancer tumor, AIP Advances,**4**(10)(2014), 107121.

[6] H. Mandal, B. Bira, D. Zeidan, Optimal algebra and power series solution of fractional Black-Scholes pricing model, Soft Comput.,**25**(8)(2021), 6075-6082.

[7] J. Jiang, Y Feng, S. Li, Exact solutions to the fractional differential equations with mixed partial derivatives, Axioms,**7**(1)(2018), 10.

[8] M. Dehghan, J. Manafian, A. Saadatmandi, Solving nonlinear fractional partial differential equations using the homotopy analysis method, Numerical Methods for Partial Differential Equations: An International Journal,**26**(2)(2010), 448-479.

[9] M. Inc, The approximate and exact solutions of the space-and time-fractional Burgers equations with initial conditions by variational iteration method. J. Math. Anal. Appl.,**345**(1)(2008), 476-484.

[10] G.W. Bluman, S. Kumei, *Symmetries and Differential Equations*. New York : Springer-Verlag, 1989.

[11] P.J. Olver, *Applications of Lie Groups to Differential Equations*. New York : Springer, 1993.

[12] B. Bira, H. Mandal, D. Zeidan, Exact solution of the time fractional variant Boussinesq-Burgers equations, Applications of Mathematics,**(66)**(3)(2021), 437-449.

[13] E. Yasar, Y. Yildirim, C.M. Khalique, Lie symmetry analysis, conservation laws and exact solutions of the seventh-order time fractional Sawada-Kotera-Ito equation, Results Phys,**(6)**(2016), 322-328.

[14] E. Buckwar, Y. Luchko, Invariance of a partial differential equation of fractional order under the Lie group of scaling transformations, J. Math. Anal. Appl.,**227**(1)(1998), 81-97.

[15] Z Cen, J Huang, A Xu, A Le, Numerical approximation of a time fractional Black-Scholes equation, Comput. Appl. Math**75**(2018), 2874-2887.

[16] O.S. Iyiola, A numerical study of ito equation and sawada-kotera equation both of time-fractional type, Adv. Math.: Sci. J. (discontin.)**2**(2)(2013), 71-79.

[17] L. Plociniczak, Approximation of the Erdelyi-Kober operator with application to the time-fractional Porous medium equation, SIAM J Appl Math,**74**(4)(2014), 1219-1237.

THE EFFECT OF BOUSSINESQ COUPLE STRESS FLUID FLOW WITH MASS TRANSPIRATION THROUGH A POROUS STRETCHING SHEET

K. N. Sneha[1] **U. S. Mahabaleshwar**[2] **Dia Zeidan**[3*]

[1] Department of Mathematics, Shivagangotri, Davangere University, Davangere, India
[2] Department of Mathematics, Shivagangotri, Davangere University, Davangere, India
[3] 3School of Basic Sciences and Humanities, German Jordanian University, Amman, Jordan
[3*] dia.zeidan@gju.edu.jo

Abstract: The current paper aims at conferring exact solutions for steady two dimensional flows of a couple stress fluids in a porous medium. The flow is occurred due to linear stretching sheet. The non-linear partial differential equations governing the incompressible steady flow of a couple stress fluids are converted to highly non-linear ordinary differential equations utilizing the similarity transformations. It is noticed that the fluids help in the reduction of drag forces and also act as a cooling agent. The required solutions are obtained analytically by graphical representation. The solution depends on the analytical values of inverse Darcy number and couple stress parameter. The results have possible technological applications in fluid-based systems involving stretching/shrinking surface. The present work of the Couple Stress fluid flow with mass transpiration due to a stretching/shrinking surface is deliberated in the velocity profiles.

Keywords: Couple stress fluid; porous medium; stretching sheet

MSC2020: 76A05; 76D05; 76S99

1 Introduction

Non-Newtonian fluid flow has numerous uses in industries and modern technology, and the study of non-Newtonian fluid flow has attracted the interest of researchers due to its numerous applications in physiology, technology, and industry. Non-Newtonian fluids are those in which there is no linear relationship between the stress and the strain rate. Most polymer solutions, cosmetics, paints, pastes, food items, agricultural and dairy wastes, and other non-Newtonian fluids are classified as such. Siddappa [1] studied the flow of non–Newtonian fluid through a

stretching plate, and when this flow is evaluated over a stretching sheet, it is relevant to numerous industrial applications such as plastic sheet extrusion, glass & sheet cooling methods, dynamics of bio-fluid & several manufacturing related applications [2]. Sakiadis [3-4] was the first to study on viscous flow due to a continuous moving sheet, and he also worked on the boundary layer on a flat surface. Crane [5] expanded on his research for stretching sheets. He pointed out that in the polymer business, a stretching plate is occasionally required. Stokes [6] proposed the essential concept of pair stress. Mekeimer [7] investigated the problem of peristaltic transport of a couple stress fluid in a uniform and non-uniform channel in the latter research dealing with the couple stress model. Maitra [8] investigated the flow of a pair stress boundary layer past a stretched sheet. Joseph developed the basic equations of a layer of fluid heated from below in a porous media in a work [9]. Mahabaleshwar [10] researched the couple stress fluid caused by perforated sheets undergoing linear stretching [11]. The primary goal of this study is to find an analytical solution for two-dimensional steady Couple stress fluid flow over a porous media is investigated in this work. Furthermore, the velocity profiles are examined using a variety of graphs in order to illustrate their physical implications and to introduce the comparison of the consequences of the physical limitations imposed on the velocity profiles and streamlines.

2 Mathematical formulation and solution

The important expressions for conservation of mass and linear momentum with couple stress parameter and porous media term are given by:

$$\frac{\partial u}{\partial x}+\frac{\partial v}{\partial y}=0, \tag{1}$$

$$u\frac{\partial u}{\partial x}+\mathrm{v}\frac{\partial u}{\partial y}=\nu\frac{\partial^2 u}{\partial y^2}-\frac{\eta_0}{\rho}\frac{\partial^4 u}{\partial y^4}-\frac{\nu}{K}u, \tag{2}$$

The velocity at the stretching sheet is linear in x and the boundary conditions related to the flow problem are

$$\begin{aligned} &u=\lambda a x,\ \mathrm{v}=0,\ \text{at}\ \ y=0,\\ &u=0, \qquad\qquad \text{as}\ y\to\infty. \end{aligned} \tag{3}$$

The following similarity will be introduced. The Blasius conversion for velocity is as follows:

$$u=cxf_{\eta}(\eta),\ \mathrm{v}=-\sqrt{c\nu}\,f(\eta),\ \eta=y\sqrt{\frac{c}{\nu}}. \tag{4}$$

Eqs. (2) are transformed into ODE using the similarity transformation Eqs. (4).

$$C f_{\eta\eta\eta\eta\eta}-f_{\eta\eta\eta}+f f_{\eta\eta}-\left(f_{\eta}\right)^2+Da^{-1}f_{\eta}=0. \tag{5}$$

$C=\dfrac{c\eta_0}{\nu^2\rho}$ is couple stress fluid parameter, $Da^{-1}=\dfrac{\nu}{cK\rho_f}$ is the inverse Darcy number ,

The enforced velocity constraints are as follows:

$$\begin{aligned} &f(0)=V_C, \quad f_{\eta}(0)=d, \quad \text{at}\quad \eta=0,\\ &f_{\eta}(\infty)\to 0, \qquad\qquad \text{as}\quad \eta\to\infty. \end{aligned} \tag{6}$$

Eq. (6) regulating boundary conditions has an exact analytical solution.

$$f(\eta)=d\left(\frac{1-\exp(-\beta\eta)}{\beta}\right), \tag{7}$$

Where β determined from the solution of biquadratic

$$C\beta^4-\beta^2+\left(1+Da^{-1}\right)=0, \tag{8}$$

Eq. (8) is biquadratic and can have four solutions, which it follows that:

$$\beta = \sqrt{\frac{1 \pm \sqrt{1 - 4C\left(1 + Da^{-1}\right)}}{2C}}. \tag{9}$$

3 Results and discussion

The current discussion examines the couple stress fluid flow through a porous medium. The variations of velocity components along the sheet that is, transverse velocity components are represented in Fig.1. Thus, Fig.1 illustrates the impact $f(\eta)$ via η for various values of Da^{-1}. When rises the value of inverse Darcy number then boundary layer thickness decreases. Fig. 2 The effect of $f_\eta(\eta)$ via η for is varying Da^{-1}. Here it is examined that the axial velocity increases with the increase of inverse Da^{-1}. Fig. 3a-b. The 2-Dimensional representation of *u* and *v* the velocity component along *X*-direction and *Y*-direction for constant values of all parameters included.Figs.4a-b for various combinations of parameters, the flow patterns are rather altered for mass transpiration. Here streamline approaches in the stretching/shrinking cases for the different parameters as shown in the figures.

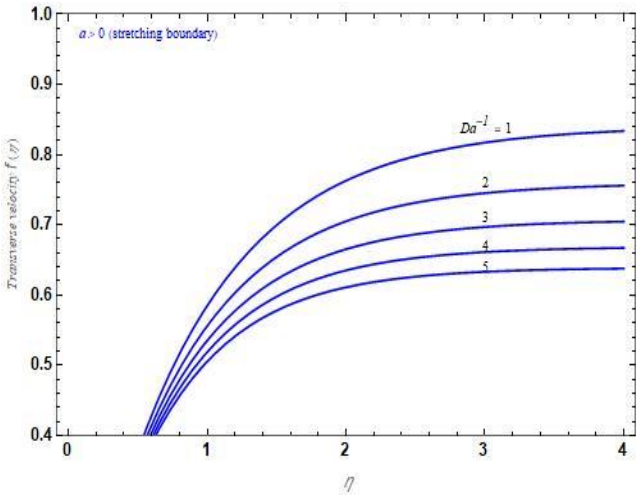

Fig.1: The effect of $f(\eta)$ via η is varying Da^{-1}.

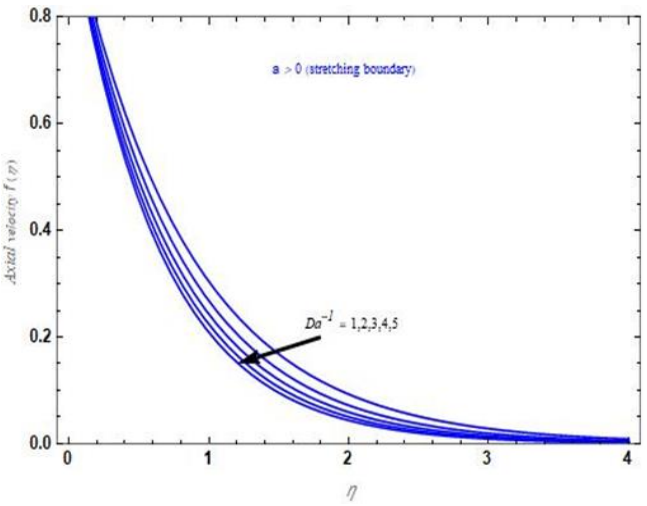

Fig.3-4: The effect of $f_\eta(\eta)$ via η for varying Da^{-1}

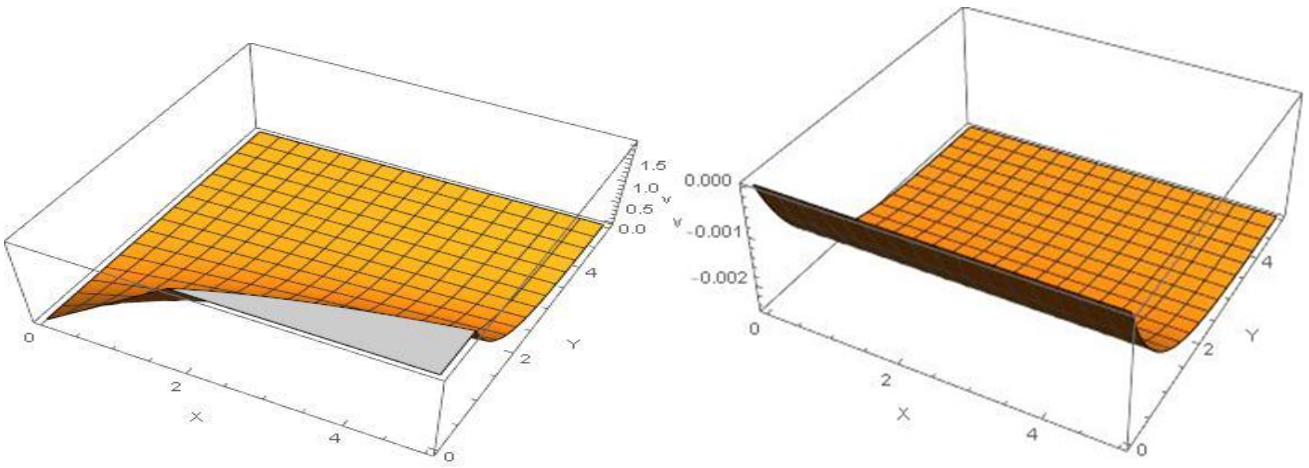

Fig.3a-b: 3-D of velocity profile along *x, y*-direction for the stretching sheet for various parameters.

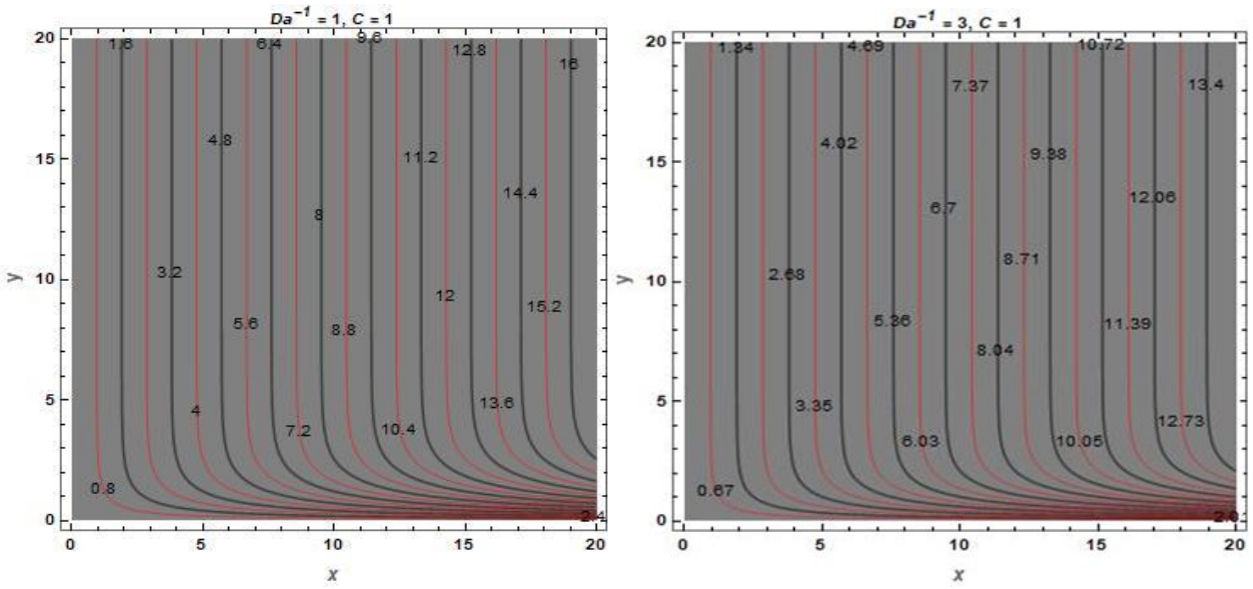

(a) (b)

Fig.7: The contour plots of the stream function for (a) stretching sheet (b) shrinking sheet

4 Conclusions

An exact analytical solution has been obtained for the transverse velocity and axial velocity during cooling of a stretching/shrinking boundary. Streamlines are distorted when couple stress is present. The axial/transverse velocity profile is found to decrease with the strengthening of the inverse Darcy number. Future studies will include the addition of nanofluids as well as the addition of an energy equation and concentration. There are well-known solutions to several standardized differential equations of second order with variable coefficients, such as Legendre's equation and Kummer's equation. If the differential equation we're looking at doesn't fit into one of these categories, we'll have to convert it to one of them; otherwise, we'll have to find another way to solve it.

Acknowledgments

The support provided by the German Jordanian University, Amman, Jordan, and Davangere University, Davangere, India, is greatly appreciated and acknowledgement.

References

[1] B. Siddappa, M.S. Abel, *Non-Newtonian flow past a stretching plate*, ZAMP, 1985.

[2] E.G Fisher, Extrusion of Plastics, *third ed-Nenes-Butterworld*, London, 1976.

[3] Sakiadis, *Boundary layer behavior on continuous solid surfaces: I Boundary layer equations for 2-D axis symmetric flow*, AJCHEJ, 1961.

[4] Sakiadis, Boundary *layer behavior on continuous solid surfaces: II. The boundary layer on a flat surface,* AIChEJ, 1961.

[5] L.J. Crane. *Flow past a stretching plate*, J. Appl. Math. Phys. (ZAMP), 21, 645–647, 1970.

[6] V.K. Stokes. *Couple stress fluids*, phys. Fluids, 1966.

[7] Mekeimer, *Peristaltic transport of a couple stress fluid in uniform and non-uniform channels*. Bio rheology, 2002.

[8] S. N. Maitra, *Couple stress boundary layer flow past a stretching sheet revisited*, Current Science, 74, 1038–1039, 1998.

[9] D.D. Joseph, *Stability of Fluid Motions Vol I*. II (Belin Springer –Verlag), 1976.

[10] U.S. Mahabaleshwar, I. E. Sarris, A. A. Hill, G. Lorenzini and I. Pop. *An MHD couple stress fluid due to a perforated sheet undergoing linear stretching with heat transfer*, Int. J. Heat and Mass Transfer., 105, 157–167, 2017.

[11] U.S. Mahabaleshwar, K. R. Nagaraju, P. N. Vinay Kumar, D. Baleanu and G. Lorenzini. *An exact analytical solution of the unsteady magnetohydrodynamics nonlinear dynamics of laminar boundary layer due to an impulsively linear stretching sheet*, Contin. Mech. Thermodyn., 29, 559–567, 2017.

AN EXACT ANALYTICAL SOLUTION OF A MASS TRANSPIRATION DUE TO STRETCHING/SHRINKING SHEET WITH SLIP PARAMETER

R. Mahesh [1] **K. N. Sneha**[2] **U. S. Mahabaleshwar** [3] **Dia Zeidan**[4*]

[1] Department of Mathematics, Shivagangotri, Davangere University, Davangere, India
[2] Department of Mathematics, Shivagangotri, Davangere University, Davangere, India
[3] Department of Mathematics, Shivagangotri, Davangere University, Davangere, India
[4] School of Basic Sciences and Humanities, German Jordanian University, Amman, Jordan
[4*] dia.zeidan@gju.edu.jo

Abstract: The present article examines the steady Magnetohydrodynamics movement over a stretching/shrinking sheet in the presence of mass transpiration. In this study, mass transpiration is used to analyse the behaviour of flow towards a Newtonian fluid over a stretching/shrinking surface. The implicit limited component approach is used to solve the system of PDE with an associated boundary layer. These equations, as well as the relevant boundary conditions, are solved analytically. The associated results are described via graphical representation. The flow patterns depend on four non-dimensional parameters mass transpiration, Chandrasekhar's number and inclined angle. The findings might have technical applications in fluid-based systems that include stretching/shrinking materials. The work has several technical and technological applications, including MHD power generators, polymer manufacturing, filament spinning.

Keywords: Magnetohydrodynamics; mass transpiration; stretching/shrinking surface

MSC2020: 76W05; 76S05; 76D03

1 Introduction

The investigation of mass transpiration in magnetohydrodynamics (MHD) flow across a stretching/shrinking flat sheet has a wide range of essential applications in the polymer processing

sector. It is employed in the creation of artificial film, glass fiber, as well as in the production of food, crystal growth. Magnetohydrodynamic flow plays a vital role in the field of medicines in cancer tumor therapy by generating hypothermia and minimizing bleeding in severe injuries. By Researchers are frequently attracted to investigate the problem of flow through a stretching plate. Crane [1] initially investigated the characteristics of the stretched plate's boundary layer in the presence of viscous flow and an ambient fluid medium. Many scholars perform study on stretching sheet problems as a result of Crane's dilemma. Extrusion procedures in the metal and plastic industries really heavily on the movement caused by a moving boundary [2, 4]. Sakiadis [5-6] pioneered this field by studying boundary layer flow on a constantly extending surface with a constant speed. Tsou [7] used experiments to confirm his findings. Other scholars generalized the surface boundary criteria as a result of these studies [8–10]. A novel solution branch was discovered for both impermeable and permeable stretching sheets [11], indicating that numerous stretching surface solutions are conceivable under certain conditions. The results are accurate NS equation solutions. The exact solution of the whole governing Navier–Stokes equations for the problem is given in a closed-form equation.

2 Mathematical model and solution

Consider the steady laminar boundary layer MHD flow of a stretching/shrinking sheet at $y = 0,$ the flow being confined in $y > 0$.

$$\frac{\partial u}{\partial x}+\frac{\partial u}{\partial y}=0, \tag{1}$$

$$u\frac{\partial u}{\partial x}+v\frac{\partial u}{\partial y}=\nu\frac{\partial u}{\partial y}-\frac{\sigma B_0^2}{\rho}u, \tag{2}$$

Subjected to the boundary conditions

$$u=dcx+A\frac{\partial u}{\partial y}, \quad v=v_w, \text{ at } y=0, u=0, \text{ as } y\to\infty. \tag{3}$$

The following are the reduced equations obtained using the similarity transformation

$$u=cxf_\eta(\eta), \quad v=-\sqrt{(c\nu)}\,f(\eta), \quad \eta=\sqrt{\frac{c}{\nu y}}. \tag{4}$$

The governing equations are reduced in the form

$$f_{\eta\eta\eta}+ff_{\eta\eta}-f_\eta^2-Qf_\eta=0. \tag{5}$$

The B. Cs are (3) becomes

$$f(0)=V_c, f_\eta(0)=\lambda+A\left(\sqrt{\frac{c}{\nu}}\right)f_{\eta\eta}(0) \text{ at } y=0, \quad f_\eta(\eta)\to 0 \text{ as y}\to\infty. \tag{6}$$

With the help of new boundary condition,

$$f(\eta)=V_c+\frac{d\left[1-exp(-\beta\eta)\right]}{\beta(1+\lambda\beta)}. \tag{7}$$

Where the β value is determined from the solution of the equation is,

$$\lambda\beta^3+\beta^2+(V_c-Q)\lambda\beta+(V_c-d-Q)=0. \tag{8}$$

3 Results and discussion

The current work investigates the steady magnetohydrodynamic flow over a stretching/shrinking sheet in the presence of mass transpiration. The behavior of flow approaching a Newtonian fluid. Using similarity variables, the controlling non-linear PDEs are turned into ODEs the outcome can be determined using graphical representations. The graph is plotted as transverse velocity $f(\eta)$ against η for various values of parameterV_c. Keeping parameters as *d=1, λ=1* and *Q=1* as constant in Fig.1. It is

observed that the transverse velocity increases with increasing of mass transpiration V_c. Fig.2 axial velocity profile for various positive values of magnetic parameter, keeping parameters as $V_c = 1$, $d = 1$, $\lambda = 1$ constant. It is observed that the axial velocity increases with increasing magnetic parameter Q. Fig.3 gives the three dimensional representation of the velocity along X and Y directions respectively. Fig. 4 a-b gives the graphical representation of stream function.

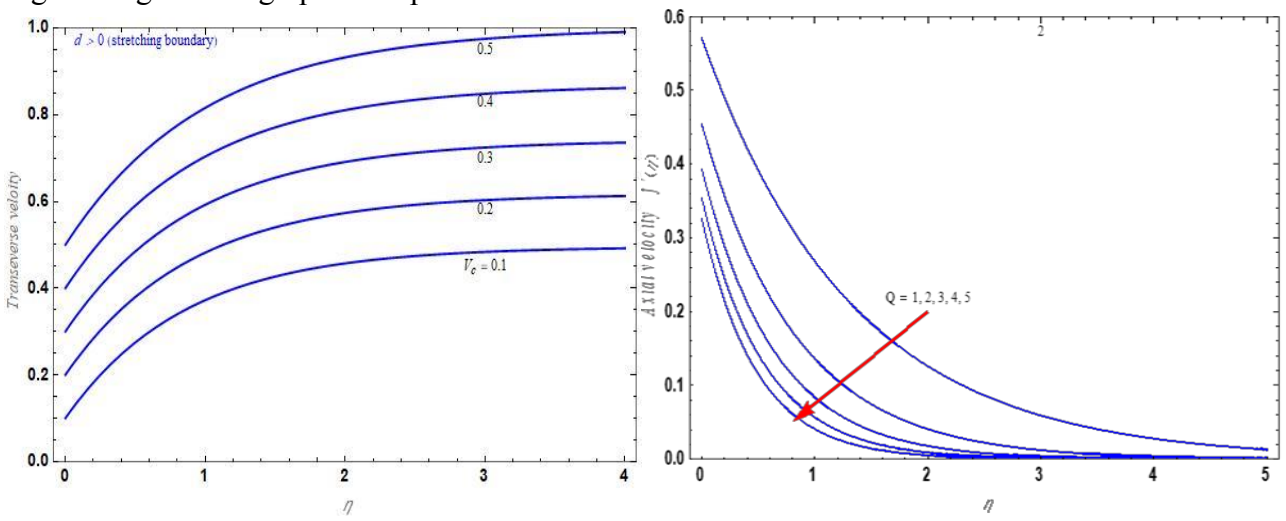

(a) (b)

Fig.1: Influence of $f(\eta)$ versus η for varying V_c. **Fig.2:** Effect of $f_\eta(\eta)$ verses η for varying Q.

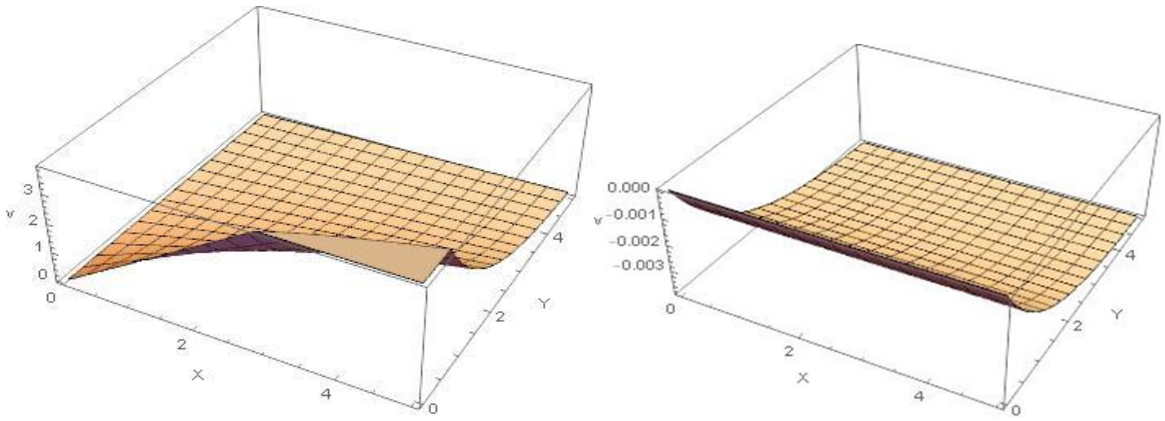

Fig.3: 3-D of velocity profile along *x, y*-direction for various parameters $V_c = 1, Q = 1, d = 1, \lambda = 1$.

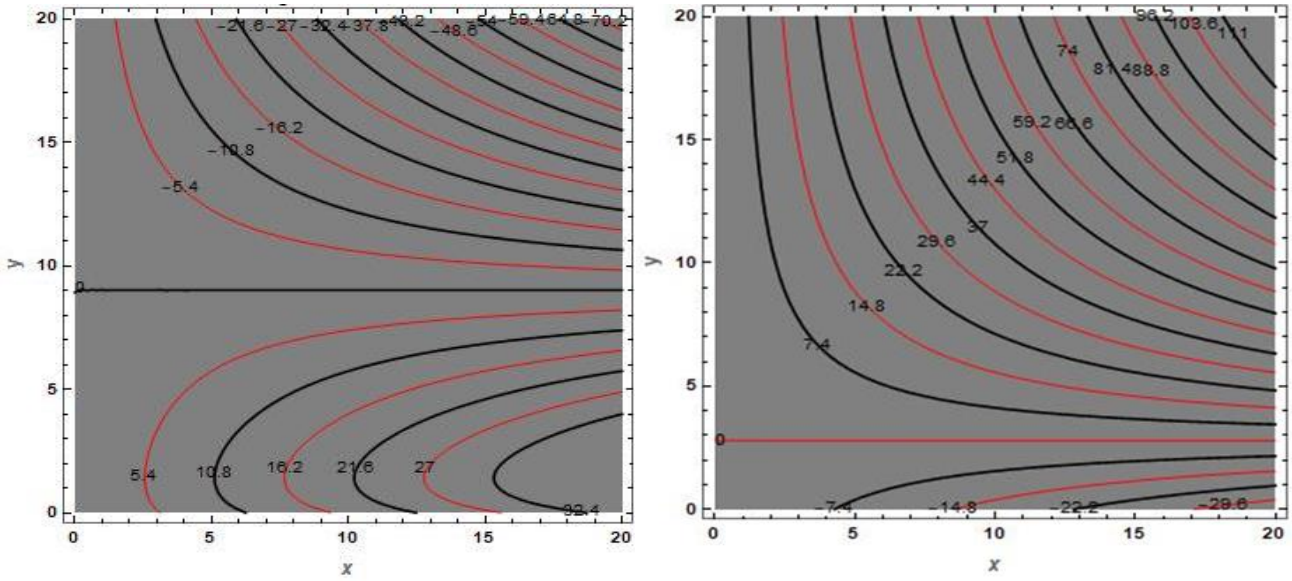

(a) (b)

Fig. 4: The contour plots of the stream function for (a) stretching boundary (b) shrinking boundary.

4 Conclusions and Future work

An exact analytical solution has been obtained for the transverse velocity and axial velocity during cooling of a stretching/shrinking boundary. Axial and transverse velocity increases as the magnetic parameters is also increases. The streamlines approaches in the stretching/shrinking cases for the different parameters. Future work will be extended through the adding some nanofluids and also extended with energy equation, concentration. Many standardized differential equations of second order with variable coefficients, such as Kummer's equation have well-known solutions. If the differential equation under examination does not follow any of these categories, we must seek another method of solution.

Acknowledgments

The authors would like to acknowledge the support provided by Davangere University, Davangere, India, and the German Jordanian University, Amman, Jordan.

References

[1] Crane LJ. Flow past a stretching plate. Z Angew Math Phys 21(4) (1970), 645.

[2] Altan T, Oh S, Gegel H. Metal forming fundamentals and applications. Metals Park, OH: American Society of Metals; (1979).

[3] Fisher EG. Extrusion of plastics. New York: Wiley; (1976).

[4] Tadmor Z, Klein I. Engineering principles of plasticating extrusion. Polymer science and engineering series. New York: Van Nostrand Reinhold; (1970).

[5] Sakiadis BC. Boundary-layer behavior on continuous solid surface: I. Boundary-layer equations for two-dimensional and axisymmetric flow. J AIChe (1961);7:26–8.

[6] Sakiadis BC. Boundary-layer behavior on continuous solid surface: II. Boundary-layer equations for two-dimensional and axisymmetric flow. J AIChe 1961; 7:221–5.

[7] Tsou FK, Sparrow EM, Goldstain RJ. Flow and heat transfer in the boundary-layer on a continuous moving surface. Int J Heat Mass Transfer 1967; 10:219–35.

[8] Banks WHH. Similarity solutions of the boundary-layer equations for a stretching wall. J Mech Theor Appl 1983; 2:375–92.

[9] Dutta BK, Roy P, Gupta AS. Temperature field in flow over a stretching sheet with uniform heat flux. Int Commun Heat Mass Trans 1985; 12:89–94.

[10] Chen CK, Char MI. Heat transfer of a continuous stretching surface with suction and blowing. J Math Anal Appl 1988; 135:568–80.

[11] Liao SJ. A new branch of solutions of boundary-layer flows over a stretching flat plate. Int J Heat Mass Transfer 2005; 49(12):2529–39.

International Conference on Mathematical Analysis and Applications in Science and Engineering
ICMA^{2}SC'22
ISEP Porto-Portugal, June 27 - 29, 2022

ONLINE EDUCATION OF FUTURE MATHEMATICS TEACHERS IN A VIRTUAL REALITY ENVIRONMENT

Angelika Schmid[1*] **Lilla Korenova**[2]

[1] Faculty of Education, University of Ostrava, Czech Republic

[2] Faculty of Education, University of Ostrava, Czech Republic

[1*] angelika.schmid@osu.cz

Abstract: With the coming of the Covid-19 pandemic, day-to-day has education moved to online space. Schools and universities were looking for suitable platforms for online teaching. At the Faculty of Education of the University of Ostrava, within the courses Geometry for the 1st and 2nd year of future mathematics teachers, we used the commonly available online platforms LMS MOODLE and MS TEAMS. The aim of the project "Improving the quality of education and strengthening students' motivation to learn by deploying a 3D virtual university campus based on virtual and augmented reality technologies in the teaching process", which began before the pandemic, was to develop a virtual reality for students of the Faculty of Education of the University of Ostrava and the University Technical University of Ostrava. This virtual reality platform was primarily designed to increase student motivation. The situation has allowed us to involve this new online tool in the teaching process. This gave us the opportunity to better test its use in online teaching. In this environment, we have implemented ready-made videos and GeoGebra software applets, as well as online meetings, in virtual classrooms. In this paper, we present experience with teaching using these online technologies. We have also applied the constructionist form of teaching in the environment of virtual reality. As part of the action research, we used a qualitative methodology to examine students' motivation, their digital literacy, and teamwork in a virtual environment. We also investigated the influence of GeoGebra applets in the virtual reality environment on the development of algorithmic thinking and spatial imagination of students' courses Geometry. We will point out the advantages and disadvantages of such teaching, not only the opinions of teachers, but also the views of students, and based on our experience, we will suggest recommendations for the future.

keywords: GeoGebra; Virtual Reality; online learning; training future teachers

MSC2020: 97-02; 97B50; 97G40; 97C70.

1 Introduction

With the coming of the Covid-19 pandemic, when online learning has become essential, the selection of suitable platforms for online teaching was important. Finding appropriate ways to teach mathematics and geometry was even more challenging in this context. Within the courses Geometry for future mathematics teachers at primary schools, at the Faculty of Education of the University of Ostrava we have used before Covid-19 in non-online teaching dynamic software GeoGebra and the commonly available online platforms LMS MOODLE for access to teaching electronic materials. When COVID-19 came, we also started using MS TEAMS for online teaching.

The following year we also started using new tool by online teaching. It was a virtual reality environment, which was developed as part of the project "Improving the quality of education and strengthening students' motivation to learn by deploying a 3D virtual university campus based on virtual and augmented reality technologies in the teaching process", which began before the pandemic. This virtual reality platform was primarily designed to increase motivation of students of the Faculty of Education of the University of Ostrava and the Technical University of Ostrava. This situation gave us the opportunity to include this virtual reality as a new online tool in the teaching process and to test its use in online teaching.

We have taken measure benefits of this new online tool with a pilot survey. As part of the action research, we used a qualitative methodology to examine students' motivation, their digital literacy, and teamwork in a virtual environment. We also investigated the influence of GeoGebra applets in the virtual reality environment on the development of algorithmic thinking and spatial imagination of students' courses Geometry. We were observing whether the virtual reality environment helps them with GeoGebra to study geometry. We have researched by teaching the motivation of students and their involvement in the teaching process. In this environment, we have implemented ready-made videos and GeoGebra software applets and observed how it influences on their motivation. In virtual reality were virtual classrooms for online meetings for communication and discussion. We could watch improvement of teamwork's.

We have also taught online with MS TEAMS to helps explained solving of exercises using GeoGebra software. By homework's student had to solve exercises and this solving to send to the teacher using one type of online format. At beginning they used classical methods of drawing and sent photos of their solving. With the time more of them used GeoGebra, they discover benefits of virtual drawing. Some of them made own GeoGebra applets and also teaching videos with explaining their solutions.

2 Results and discussion

Research results and their interpretation - during the direct and indirect research we recorded, we used a digital virtual environment, namely the use of GeoGebra software and the Virtual Reality software "Virtulog". When monitoring the students' activities in the Geometry course, we noticed an increased interest of students in a more detailed explanation of the procedure for solving geometric problems, in the visualization and mathematical understanding of construction problems using the GeoGebra software. We noted positive motivation and the so-called "AHA" effect. For some students, this type of teaching also supported creativity in the form of creating videos with the presentation of task solutions.

We can state that, in addition to the increase in external and internal motivation, there was also an increase in students' understanding of geometric connections and this supported their algorithmic thinking. Based on our observations, we recommend using a combination of Virtual Reality and GeoGebra software in the future.

3 Conclusions and Future work

The result of our survey was the identification of benefits and disadvantages. Positives are that students were more motivated and interested of a new virtual space, also because of novelty phenomenon. For most students using GeoGebra brought better understood of geometry, although 2-3 students leaned towards classical methods. Including GeoGebra into virtual reality gave some aha-effects. By online teaching with virtual reality, we and

also our students created materials that will be usable in the next years for next students. For us was this new challenge that also improved our competence for future teaching and started improving teaching competence of our students.

As negative we have to mention some technical problems. Using virtual reality application by teaching had increased technical requirements. This kind of teaching it is not useful by slowly internet connection. For the virtual environment teaching it is necessary to better set the technical parameters. The problem was when only online teaching was possible. During testing we share one test in LMS MOODLE for theoretical knowledge and we replaced the final test for uploading a video explaining the solution procedure - some students drew, some used GeoGebra - it was more difficult and harder.

Online teaching in virtual reality environment has a lot of positives as a motivation but there is space for improvement.

Acknowledgments

This research was supported by project SGS07/PDF/2022 "Mobile technologies and interactive whiteboard in pre-primary and primary education"

References

[1] Z. Berger-Haladová, A. Ferko, Towards Augmented Reality Educational Authoring. In E. Smyrnova-Trybulska (Ed.) E- Learning and STEM Education. „ELearning", 11, Katowice-Cieszyn: Studio Noa for University of Silesia, (2019), 587-608.

[2] R. Bohdal, Devices for Virtual and Augmented Reality. In: Augmented Reality in Educational Settings, Brill Sense, (2019), 410-444.

[3] H. Kaufmann, D. Schmalstieg, M. Wagner, Construct3D: a virtual reality application for mathematics and geometry education. In Education and information technologies, (2000), 263-276.

[4] L Korenova, What to use for mathematics in high school: PC, tablet or graphing calculator?, International Journal for Technology in Mathematics Education, 22(2) (2015).

[5] L. Korenova, M. Kis, Zs. Lavicza, P. Ostradicky, T. Prodromou, New directions in nationwide technology integration into mathematics teaching: the Geomatech Project, DIVAI (2018).

[6] L. Korenova, J. Hvorecky, Applying QR Codes in Facilitating Mathematics and Informatics Education, (2018).

[7] L. Korenova, K. Kostolanyova, P. Ostradicky, Analysis of dependences between utilization of mobile technologies in math education and students' technical backgrounds. ICERI 2019: conference proceedings. Valencia: IATED, (2019), 11283-11289.

[8] L. Korenova, R. Krpec, J. Guncaga, Zs. Lavicza,. Enhancing students' mathematics learning skills with GeoGebra Apps. ICERI 2019: conference proceedings. Valencia : IATED, (2019), 10762-10769.

[9] A. Kukulska-Hulme, J. Traxler, Mobile teaching and learning, in: Mobile Learning. Routledge, (2007), 41-60.

[10] OECD, Education at a Glance 2018: OECD Indicators, OECD Publishing, Paris, (2015), https://doi.org/10.1787/eag-2018-en.

[11] M. Václavík, et al. Particular Analysis of Normality of Data in Applied Quantitative Research. In: 2nd Computational Methods in Systems and Software 2018: Computational and Statistical Methods in Intelligent Systems, Advances in Intelligent Systems and Computing (vol. 859) 2018-09-12 Szczecin, Poland. Cham: Springer, (2019), 353-365, ISBN 978-3-030-00210-7.

[12] J. Hvorecký, L. Koreňová, "Learning Critical Thinking without Teacher's Presence." Proceedings of 12th International Scientific Conference on Distance Learning in Applied

Informatics, (2018), 293-302.

International Conference on Mathematical Analysis and Applications in Science and Engineering
ICMA^{2}SC'22
ISEP Porto-Portugal, June 27 - 29, 2022

An approach to signal filtering with mathematical transfer functions using Fourier series

Fernando Carvalho[1⋆] **Pedro Reis**[1] **Vítor Cardoso**[1] **Sandra Aires**[1,2]
Ana Costa[1] **António Sousa**[1,2] **Pedro Guedes**[1,3]

[1] Instituto Superior de Engenharia do Porto, P.Porto, Porto, Portugal
[2] LEMA, ISEP, Porto, Portugal
[3] INESC-TEC, Porto, Portugal

[1⋆]fjc@isep.ipp.pt

Abstract: Filters are well-known devices frequently included in electrical systems. Their modeling can also be an interesting domain to introduce mathematical skills to engineering students. In this work it is presented a comparative study between three low-pass filters: Ideal, 2nd order Butterworth and RLC filters. The whole work was implemented having this intended comparison in mind. The three filters were developed and applied in parallel - the same cut-off frequency was set for these low-pass filters; also, both a Butterworth filter and a RLC circuit filter were tuned to have the same quality factor and precisely the same transfer function. A set of discontinuous periodical signals was used to study the behavior of the three filters. For each signal from this set, the corresponding representation given by a partial sum of the Fourier series is considered as the input signal, from which the filter output signal is obtained. These outputs were obtained by multiplying the input signal complex Fourier coefficients by the complex transfer function values of each filter, corresponding to each harmonic frequency. All the calculations were performed with Python programming language together with a dedicated library that was developed by the authors of this work. This library, based on sympy, numpy and matplotlib, was developed for teaching support in Mathematics Laboratory courses. Main results of this work are the filtering effects on signals' spectral and temporal representation. Figures included in this manuscript show a small sample of results obtained for the square wave input signal. The full article will present an expanded set of results obtained for other input signals. It will contain a results discussion based on the comparison of the different filtered signals' spectra, together with the comparison of energy losses calculated based on RMS values and the time-delays caused by the different kinds of filters. This analysis will be carried out for each input signal. From the teaching view, the main advantage of this work is the insight about the filtering processes that it offers to engineering students.

keywords: Fourier analysis; low-pass filter; Butterworth filter; signal filtering; Python.

MSC2010: 26A##; 34A##; 93B##.

1 Introduction

In this work it is presented a comparative study between three low-pass filters: Ideal, Butterworth and RLC circuit. For this purpose, each signal to be filtered was represented by a Fourier series partial sum at a predefined order [1–3].

Ideal filtering is the simplest form to filter a signal; mathematically consists in truncating the Fourier series representation using a predefined cut-off frequency [4], and adding the same time delay to all the harmonics. For the same cut-off frequency, a Butterworth filter transfer function was parametrized to work as a 2nd order low-pass filter with a unitary gain at the null frequency [4, 5]. Then, the complex transfer function of a low-pass filter based on the RLC circuit represented in the Figure 1 was calculated using the equation (1) that models the circuit [4–6].

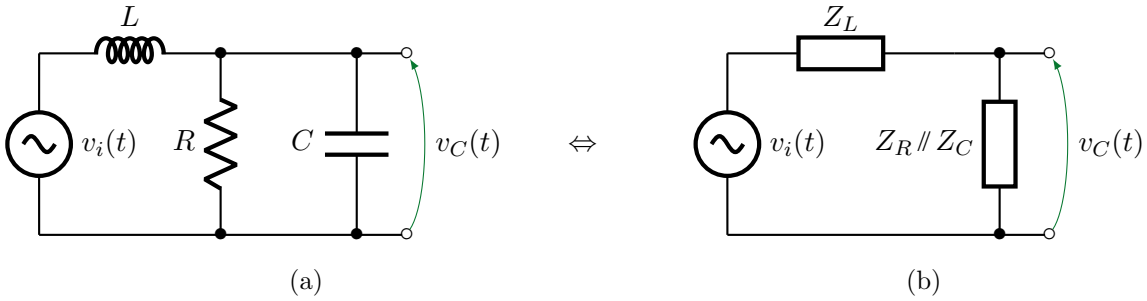

Figure 1: (a) 2nd order RLC filter; (b) equivalent voltage divider circuit based on impedances.

$$H(j\omega) = \frac{Z_R /\!\!/ Z_C}{Z_L + Z_R /\!\!/ Z_C} \tag{1}$$

The RLC filter was tuned to give the same response as the Butterworth filter. This was achieved by imposing the same cut-off frequency and the quality factor for both filters and having in consideration the existing mathematical relations between these two parameters and the values of R, L and C (detailed in the full paper).

2 Results and discussion

In the full paper they will be demonstrated the effects of the referred filters on a set of signals represented by their correspondent Fourier series (partial sum). It will be concluded that the filtering effects produced by RLC filter coincide with the Butterworth ones. In fact, the RLC filter is the physical implementation of the Butterworth filter model. And this fact can be understood in the Figure 2, where the unilateral and continuous module and phase spectra of the used filters transfer functions are represented.

The Figure 3 shows the spectra (composed by 20 harmonics and the average value) obtained from the representation of a square wave in Fourier series, $v_i(t)$, and the correspondent filtered signals, $v_{ideal}(t)$ using the Ideal, $v_B(t)$ the Butterworth and $v_C(t)$ the RLC filters, where $v_B(t) = v_C(t)$. In this example, the filters were tuned with a cut-off frequency equal to the 10th harmonic frequency.

The results depicted in the Figure 4 are obtained from the signals (spectra in Figure 3) and shows the temporal representation of the original signal $v_o(t)$ with: $v_i(t)$ representation in (a); the signal filtered by an ideal filter (b); the signal filtered by a Butterworth or a RLC filter (c).

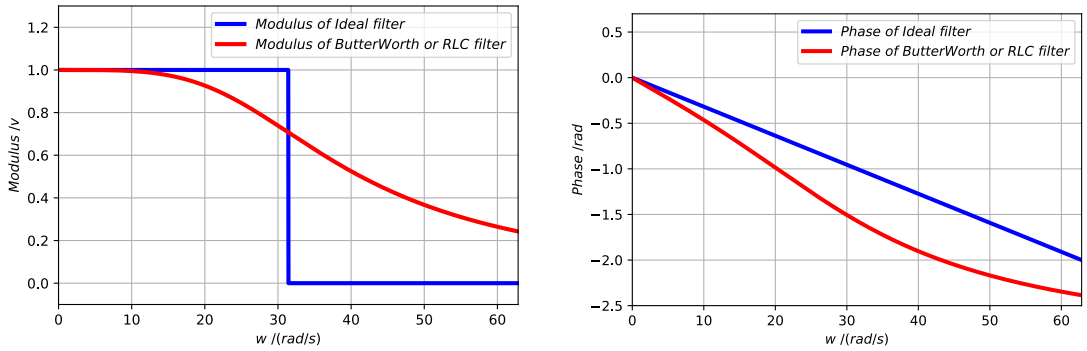

(a) (b)

Figure 2: Transfer functions of the Ideal, Butterworth or RLC low-pass filters: (a) Modulus; (b) Phases.

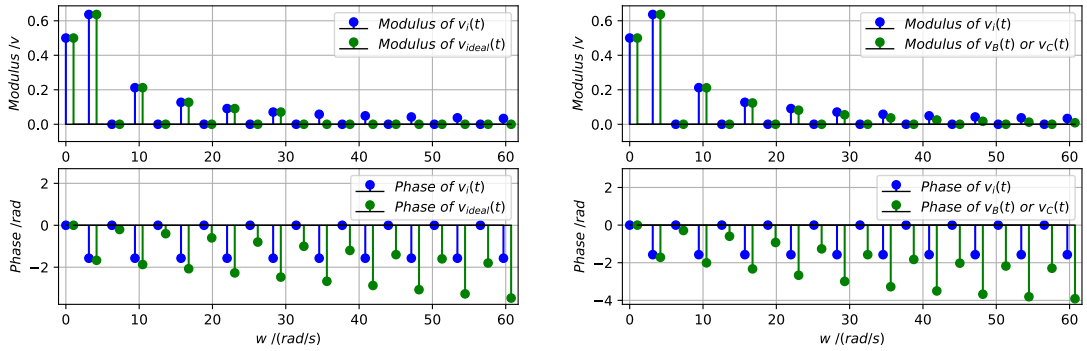

(a) (b)

Figure 3: Spectrum of a square wave, $v_o(t)$, composed of 20 harmonics and the correspondent average value: (a) Fourier Series partial sum, $v_i(t)$, and the filtered signal using the ideal filter, $v_{ideal}(t)$; (b) $v_i(t)$ and the filtered signal using the Butterworth, $v_B(t)$, or RLC filter, $v_C(t)$.

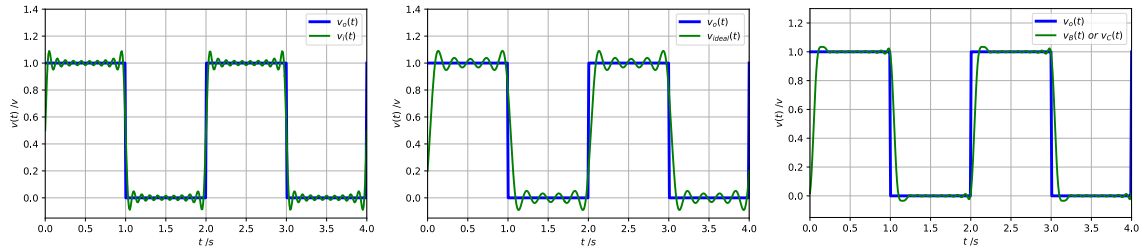

(a) (b) (c)

Figure 4: Temporal representation of square wave $v_o(t)$ with: (a) Fourier Series partial sum of 20th order, $v_i(t)$; (b) $v_{ideal}(t)$, for ideal filtering; (c) $v_B(t)$, for Butterworth or $v_C(t)$ for RLC filtering.

3 Conclusions and Future work

In this work they were studied several filters from the teaching view. Its main advantage is the insight about the filtering processes that it allows to the engineering students, reducing the difficulties that the learning of this concept typically represents. This work also shows that the RLC filter is the physical implementation of the Butterworth filter model.

References

[1] William Bolton, *Fourier series*, Longman, 1995.

[2] Erwin Kreyszig, *Advanced engineering mathematics*, John Wiley & Sons, 1999.

[3] Murray Spiegel, *Análise de Fourier*, McGraw do Brasil, 1976.

[4] Harry Lam, *Analog and digital filters: Design and realization*. Prentice Hall, 1979.

[5] Stephen Butterworth, *On the Theory of Filter Amplifiers in Wireless Engineer*, vol. 7, 1930, pp. 536-541.

[6] Arthur Williams and Fred Taylor, *Electronic Filter Design Handbook*, McGraw-Hill, 4th ed., 2006.

International Conference on Mathematical Analysis and Applications in Science and Engineering
ICMA^{2}SC'22
ISEP Porto-Portugal, June 27 - July 1, 2022

Numerical approach to signal filtering with ODEs - classical programming and the Xcos didactic tool

Pedro Reis[1⋆] **Fernando Carvalho**[1] **Vítor Cardoso**[1] **Sandra Aires**[1,2]
Ana Costa[1] **António Sousa**[1,2] **Pedro Guedes**[1,3]

[1] Instituto Superior de Engenharia do Porto, P.Porto, Porto, Portugal
[2] LEMA, ISEP, Porto, Portugal
[3] INESC-TEC, Porto, Portugal

[1⋆]mps@isep.ipp.pt

Abstract: Ordinary differential equations, ODEs, and ODEs systems are very useful mathematical representation models to simulate and analyse dynamical phenomena. The RLC electrical circuit that works as a second order low-pass filter, is a usual example of the kind of application whose behaviour can be modelled and simulated, using a ODEs system. In this work a ODEs system with constant coefficients is studied. The Kirchhoff rules are applied to the referred circuit getting a first order ODEs system, which is numerically solved using the SCILAB, a clone of MATLAB, development platform, by considering two different approaches. The forward Euler method is the simplest numerical integrative procedure and is initially applied; then the visual simulation with pictographic programming based on the XCOS block diagram tool is performed using the predefined objects. The Fourier coefficients of several signals, such as a square wave, are determined. Then the Fourier series, truncated at a given order (partial sum) - see figure 3a - is used as input signal to be filtered by the RLC circuit modelled by the ODEs system (1). The filtered signal, shown in Figure 3b, results of the Euler numerical resolution of this system of differential equations. After that, the same result of the Figure 3b is obtained by using the second approach, which considers the ODEs system implementation pictogram in Figure 2. Thus, two entirely numerical approaches were applied along this work. It was possible yet to observe the complete response of the system, verifying the transient and steady state components associated to the solution. The Xcos is an informatics application that allows creating system models by connecting graphic blocks and revealed to be a very useful didactic tool that makes the implementation of complex numerical simulations accessible to students who have almost no programming skills - this is a very advantage in relation to the first approach.

keywords: differential equation systems; Fourier analysis; signal filtering; forward Euler method; Xcos.

MSC2010: 26A##; 34A##; 93B##.

1 Introduction

Ordinary differential equations [1–3], ODEs, and systems of ODEs, are very useful mathematical representation models to simulate and analyse dynamical phenomena. The process of a physical signal filtering is the operation that performs some changes on original signal in order to get the most relevant information. Low-pass filter are frequently used with the aim of eliminating high frequency harmonics that are susceptible to represent noise.

The RLC electrical circuit shown in Figure 1, that works as a second order low-pass filter, is a usual example application system whose behaviour can be modelled and simulated using a ODEs system [5]. The RLC filter can be tuned in order to exhibit the same behaviour as the Butterworth filter [4].

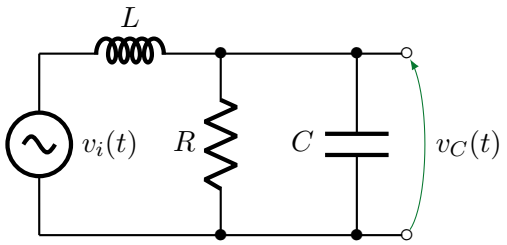

$$\Leftrightarrow \quad \begin{cases} \dfrac{d}{dt}\Big(i_L(t)\Big) = \dfrac{v_i(t) - v_C(t)}{L} \\ \dfrac{d}{dt}\Big(v_C\,(t)\Big) = \dfrac{i_L(t)}{C} - \dfrac{v_C(t)}{RC} \end{cases} \tag{1}$$

Figure 1: 2nd order RLC filter.

Any particular solution of the ODEs system in (1) is the sum of the transient and steady state components [5]. Given the short duration of the transient state its presence and behaviour can only be noticed in the initial instants of the simulations.

2 Results and discussion

The pictogram of Figure 2, shows the way the ODEs system was implemented in the Xcos didactic tool [6].

Figure 3 shows an example of results obtained for a square wave input signal, $v_o(t)$, of a square wave and its representation, $v_i(t)$. While in Figure 3a it can be seen the original signal, $v_o(t)$, together with its representation by a 20th order Fourier series partial sum, $v_i(t)$, Figure 3b, shows the square wave, $v_o(t)$, together with the results of $v_i(t)$ signal filtering, $v_C(t)$. The filers were tuned with a cut-off frequency equals to the 10th harmonic frequency. Note that the filtering results obtained by using the forward Euler numeric integrative procedure are exactly the same as those obtained from the Xcos simulation.

3 Conclusions and Future work

In this work two entirely numerical approaches were applied to solve the same filtering problem. Thus, comparing the obtained solutions, both composed by the sum of transient and steady state components of the filtered signal, it was possible to observe the same complete response of the system.

The Xcos revealed to be a very useful didactic tool that makes the implementation of complex numerical simulations accessible to students who have almost no programming skills. This was the reason why the students in laboratory mathematics classes preferred the second approach.

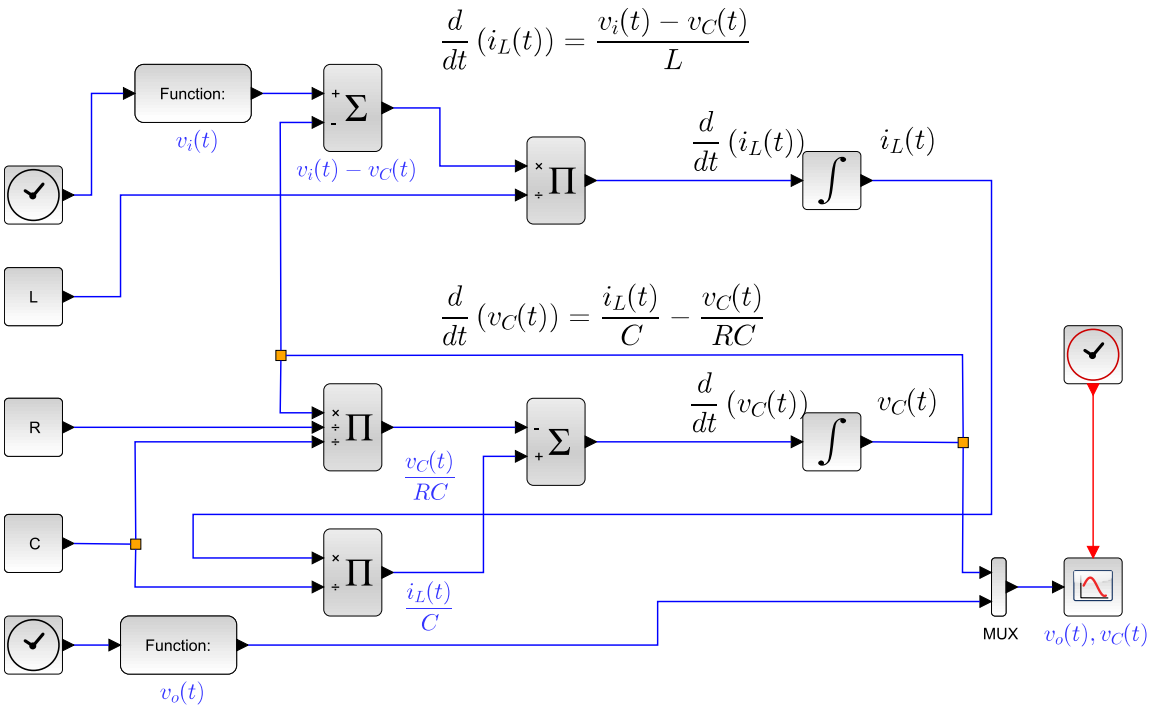

Figure 2: ODEs system implementation pictogram of 2nd order RLC filter.

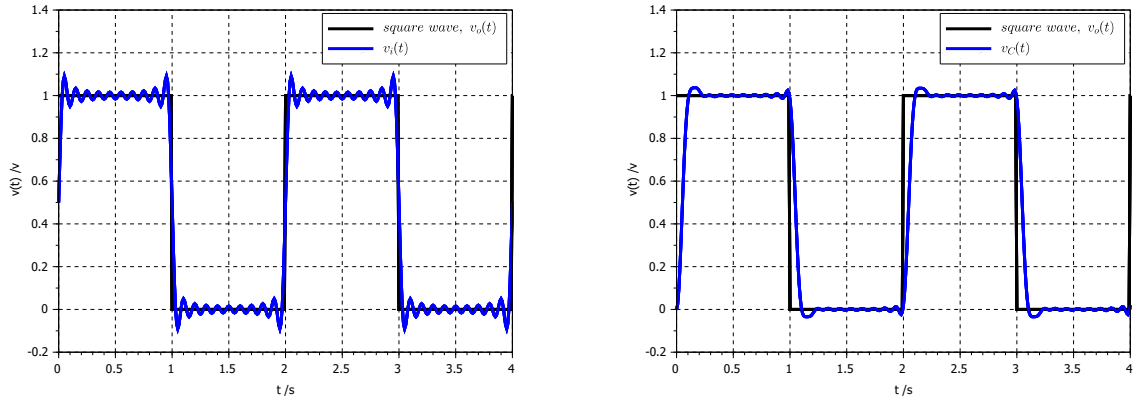

(a) (b)

Figure 3: Example of results: (a) a square wave signal, $v_o(t)$, and its representation by a 20th order Fourier series partial sum, $v_i(t)$; (b) a square wave signal, $v_o(t)$, and the filtered signal of $v_i(t)$ obtained by using the forward Euler numerical integrative procedure or obtained from the Xcos simulation, $v_C(t)$.

References

[1] Erwin Kreyszig, Advanced engineering mathematics, John Wiley & Sons, 1999.

[2] Murray Spiegel, Análise de Fourier, McGraw do Brasil, 1976.

[3] Stanley J. Farlow, An introduction to differential equations and their applications, McGraw-Hill, 1994.

[4] Stephen Butterworth, On the Theory of Filter Amplifiers in Wireless Engineer, vol. 7, 1930, pp. 536-541.

[5] Ana M. Castro, Ana J. Viamonte and António Sousa, Cálculo II, Publindustria, 2016.

[6] Xcos, https://www.scilab.org/software/xcos. Last access at 03/01/2020.

International Conference on Mathematical Analysis and Applications in Science and Engineering
ICMA^{2}SC'22
ISEP Porto-Portugal, June 27 - 29, 2022

Teaching Differential Equations for Understanding

Svitlana Rogovchenko[1] **Yuriy Rogovchenko**[1⋆]

[1] University of Agder, Norway

[1⋆]yuriyr@uia.no

Abstract: Mastery of differential equations is important for future scientists, economists, engineers because of the frequent use of differential equations for modelling of different real-life phenomena. Recent empirical research reports difficulties which students experience with the comprehension of the definition of a differential equation and its solutions. In this paper, we discuss how the students' experience in learning these important notions and their conceptual understanding can be improved by solving non-routine problems on Existence and Uniqueness Theorems.

keywords: differential equations; Existence and Uniqueness Theorems; conceptual understanding.

MSC2020: 97C70; 97D70.

1 Introduction

Differential equations (DEs) are often employed for modelling of a wide range of real-life phenomena in natural and social sciences, engineering, economics. Not surprisingly, courses in DEs are taught at most universities. However, educational research on learning and teaching DEs is scarce, there are "fewer than two dozen empirical studies published in top journals" which does not match well "the centrality of differential equations (DEs) in the undergraduate curriculum, as well as the move away from a "cookbook" course to one that emphasizes modelling, qualitative, graphical and numerical methods of analysis"[6, p. 555]. Therefore, "we need to explore the variety of ways in which content, instruction, and technology can be profitably coordinated to promote student learning"[5, p. 84].

Although "the teaching of 'practical' mathematics is becoming much more focused on the process of modelling of engineering systems - this results in a decrease in the teaching of calculation techniques, but it does not mean that all manual work with mathematics can be replaced: there is a need to find the right balance"[4, p. 9]. Furthermore, due to a rapidly growing use of digital technology in engineering education, "there are significant dangers in losing the teaching of pen-and-paper mathematical techniques to 'button pressing"' [4, p. 10].

Recent empirical research actively explored students' understanding of the concepts of a DE and its solutions [1, 3, 5, 7, 10, 12] revealing many difficulties. Regretfully, many students wrongly believe that the success in DEs courses can be achieved by learning only solution routines. For instance, Arslan reported that "students were successful in algebraic solutions of DEs, but not in conceptualizing DEs and the solution of DEs concepts ... algebraic solutions of DEs can be

found even without a deep understanding and conceptualization of DEs, which is why students do not feel any need to understand DEs and related concepts" [1, p. 887]. Many students concentrate their attention on learning specific solution techniques but "often fail to relate them to other concepts or ideas" [3, p. 76]. Arslan [1] pointed out students' difficulties with the fundamental concepts including a DE itself, the general and particular solutions. Students tend to consider the general solution "as if it consisted of a unique solution" [1, p. 880], they usually "failed to report general solutions" [3, p. 74], and "made little or no attempt to place the solution in context, be it a solution to an equation or a DE" [7, p. 48]. In summary, "research has pointed to the various challenges that students face with this concept" [6, p. 555].

2 Results and discussion

Very recently, the authors [10] analysed five different tasks used in the literature to test students' conceptual understanding of the general and particular solutions to DEs. Regretfully, only one problem was designed to engage students into inquiry and contribute eventually to their conceptual understanding of DEs. We argued that the correct formation of the concept in Vygotsky's sense, as a scientific concept, is achieved only through the rigorous explanation of all relevant definitions and theoretical results. This explanation should necessarily include Existence and Uniqueness Theorems (EUTs) which connect all important notions meaningfully complementing the definition of a solution to a DE. We believe that conceptual understanding of DEs can be fostered by the use of inquiry-based pedagogy [5] and non-routine problems [8, 10, 12]. First successful steps in this direction were already made by the authors in the cited papers. The research question we address in this paper is: *How does the work on non-routine problems facilitate engineering students' conceptual understanding of DEs and solutions to DEs?*

To begin with, we analyse the problems on the EUTs that do not require the use of computer in the course textbook [2]. It turns out that they belong to one of the following four categories: (1) determine (without solving the problem) an interval in which the solution of the given initial value problem is certain to exist â six problems; (2) state where in the ty-plane the hypotheses of the theorem are satisfied â six problems; (3) solve the given initial value problem and determine how the interval in which the solution exists depends on the initial value y_0 â four problems; (4) explain why the existence of two solutions of the given problem does not contradict the uniqueness part of the theorem â one problem.

Given that the nature of all but one problems on EUTs in the course textbook is procedural, the problems in our assignment were designed to engage students in a deeper reflection about EUTs and related notions. Our teaching experiment was organised in the final part of a DEs course for senior mechatronics students in their fourth year of studies. We employed the inquiry by design technique (Richards, 1991) where lecturers âdesign tasks and projects that stimulate to ask questions, pose problems, and set goalsâ and students âmust learn to inquire systematicallyâ and âmust actively construct their own knowledgeâ [9, p. 38]. Students worked for three weeks on an assessed assignment â a set of non-routine problems on the topic of EUTs designed by the authors with the focus on the development of conceptual understanding rather than procedural skills. The data collected include students written work (all three scripts), answers to pre- and post- questionnaires, audio recordings of the small group discussions, and the recording of the class presentation of solutions. The audio records were transcribed, and the data were analysed after the course work was completed and the letter grades were assigned. We analyse students' work and discuss their feedback on the assignment.

Acknowledgments

The authors gratefully acknowledge a small research award from MatRIC, The Centre for Research, Innovation and Coordination of Mathematics Teaching, project number 170803.

References

[1] Arslan, S. Do students really understand what an ordinary differential equation is? International Journal of Mathematical Education in Science and Technology, **41** (2010), 873-888.

[2] Boyce, W.E., & DiPrima, R.C., *Elementary Differential Equations and Boundary Value Problems*, 10th ed., Chennai: John Wiley & Sons, Inc., 2013.

[3] Camacho-Machín, M., Perdomo-Díaz, J., Santos-Trigo, M., An exploration of students' conceptual knowledge built in a first ordinary differential equations course (Part II). The Teaching of Mathematics, **15**(2) (2012), 63-84.

[4] Kent, P., Noss, R., *Mathematics in the University Education of Engineers*. The Ove Arup Foundation, 2000.

[5] Rasmussen, C.L., New directions in differential equations: A framework for interpreting students' understandings and difficulties. The Journal of Mathematical Behavior, **20**(1) (2001), 55-87.

[6] Rasmussen C., Wawro M., Post-calculus research in undergraduate mathematics education. In J. Cai (ed) Compendium for research in mathematics education, Reston, VA: National Council of Teachers of Mathematics, 2017, 551- 581.

[7] Raychaudhuri, D. (2014). Adaptation and extension of the framework of reducing abstraction in the case of differential equations, International Journal of Mathematical Education in Science and Technology, **45**(1) (2014), 35-57.

[8] Rezvanifard, F., Radmehr, F., Rogovchenko, Yu. Advancing engineering students' conceptual understanding through puzzle-based learning: a case study with exact differential equations, Teaching Mathematics and its Applications: An International Journal of the IMA, (2022), hrac005.

[9] Richards, J., Mathematical discussions. In von Glasersfeld (ed.), *Radical Constructivism in Mathematics Education*, Kluwer Academic Publishers, 1991, 13-51.

[10] Rogovchenko, S., Rogovchenko, Yu., Conceptual understanding of solutions to differential equations: How do assessment tasks promote it? In J. Hodgen, E. Geraniou & G. Bolondi (Eds.). Proceedings of the 12th Congress of European Research in Mathematics Education (CERME12). ERME (in press).

[11] Rogovchenko, S., Treffert-Thomas, S., Rogovchenko, Yu., The use of nonstandard problems in an Ordinary Differential Equations course for engineering students reveals commognitive conflicts. Proceedings of the Annual Conference on Research in Undergraduate Mathematics Education (RUME), 2020, 1141-1145.

[12] Treffert-Thomas, S., Rogovchenko, S., Rogovchenko, Yu., The use of nonstandard problems in an ODE course for engineering students. Proceedings of the International Groups for the Psychology of Mathematics Education, 4 (2018), 283 â 290.

International Conference on Mathematical Analysis and Applications in Science and Engineering
ICMA^{2}SC'22
ISEP Porto-Portugal, June 27 - 29, 2022

Modelling an electrical circuit using a system of differential equations

Ana C. Meira Castro[1,3⋆] **António Varejão Sousa**[1,2] **Ana Júlia Viamonte**[1,2]

[1] Instituto Superior de Engenharia do Porto, P.Porto, Porto, Portugal
[2] LEMA, ISEP, Porto, Portugal
[3] CERENA, Porto, Portugal

⋆amc@isep.ipp.pt

Abstract: The study of relevant phenomena and processes in several areas such as engineering sciences, social sciences, etc. often uses mathematical modelling. Typically, the model involves, in its formulation, one or more interrelated quantities and their variations. In cases where there is a relationship between an independent variable, a dependent variable and its derivatives, the relationship is expressed in the form of an equation known as a differential equation or a system of differential equations.
In this paper, a classroom activity is presented. Students are faced with an electrical circuit that they have to model, using their knowledge in the field of physics and electromechanics, combined with their knowledge in mathematics, in particular with regard to differential equations. Then, they are asked to find the electric current in series RLC electric circuit for a sinusoidal voltage source by considering the exact solution and the approximate solution, based on complex impedance analysis. In the end, they are asked to compare the two results obtained and formulate conclusions.
This activity will allow students to acquire sensitivity to recognize the specificities related to the two different approaches to solve a problem modelled with differential equations. In particular, it will allow students to become aware of the possible effects that the transient and steady state components of the solution may have on the series RLC circuit for a sinusoidal voltage source.

keywords: modelling; differential equations; series RLC circuit; sinusoidal voltage source.

MSC2010: 26A##; 34A##; 93B##.

1 Introduction

Problem solving and the study of relevant phenomena and processes in the areas of engineering sciences, social sciences, etc. often uses mathematical modelling. The model often involves one or more interrelated quantities and their variations in its formulation. In cases where there is a relationship between an independent variable, a dependent variable and its derivatives, the relationship is expressed in the form of an equation known as ordinary differential equation (ODE) or a system of ODEs.

In the manuscript, a classroom activity is presented in which students are confronted with a series Resistor-Inductor-Capacitor (RLC) electric circuit (Fig. 1) for a sinusoidal voltage source. It is intended that students model the problem and solve it in two different ways taught in distinct

course units and comment on the results obtained. To achieve the goal, students are asked to model the circuit based on Kirchhoff's laws.

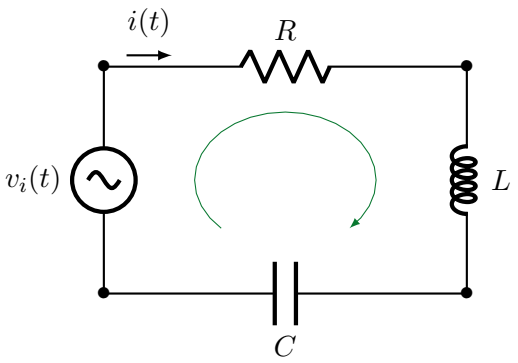

Kirchhoff's Current Law (KCL)
In a node, the sum of the incoming electric currents is equal to the sum of the outgoing currents.

Kirchhoff's Voltage Law (KVL)
In a closed network, the sum of the voltage drops in the components is equal to the algebraic sum of the voltage sources.

Figure 1: Series RLC electric circuit and the Kirchoff's Laws applied to electric circuits; L represents an inductor, R the resistor and C the capacitor; $v(t)$ is the voltage source.

Although the both approaches allow to calculate the electric current of an electric circuit, they produce different solutions:

1. real solution obtained by solving the differential equation that translates the time domain model;
2. complex solution obtained by using a formulation based on complex impedance analysis from frequency domain model.

Students are then asked to compare the two solutions, by using their graphical representation and to point out conclusions, highlighting the behaviour of both the transient and steady state components of the electric current.

2 Model formulation

2.1 Time domain model

From the application of KVL one obtains $v_L(t) + v_R(t) + v_C(t) = v(t)$. The term $v(t)$ is the source voltage, the voltage drops across the inductor is given by $v_L = L\,\frac{di}{dt}$, the voltage drops across the resistor is $v_R = R\,i(t)$ and the voltage drops across the capacitor is $v_C = \frac{1}{C}\,q(t)$. L, R and C coefficients are the inductance, the resistance and the capacitance values. In this way, it is possible to model the RLC circuit through a differential equation that can be formulated in terms of electric charge $q(t)$ and electric current $i(t)$, in order to time t, as shown in Eq. (1).

$$L\,\frac{di}{dt} + R\,i + \frac{1}{C}\,q = v\,(t) \tag{1}$$

Due to the inherent difficulty in solving this equation that would require knowledge in solving systems of differential equations or the Laplace transform, here, we opted to convert this equation in a 2nd order ODE; to do so, it should be noted that the definition of electric current is given by Eq. (2).

$$i\,(t) = \frac{dq}{dt} \tag{2}$$

Thus, the problem can be formulated by the Eq. (3), in order to $q(t)$, which is classified as a 2nd order linear ODE with constant coefficients and its resolutions is covered in the mathematics curriculum of engineering courses.

$$L\,\frac{d^2q}{dt^2} + R\,\frac{dq}{dt} + \frac{1}{C}\,q = v\,(t) \tag{3}$$

By solving Eq. (3), the electric charge is obtained, which allows to calculate the electric current from the circuit. The general solution for Eq. (3) is the sum of two terms, $q(t) = q_s(t) + q_t(t)$, called steady state and transient components. An relevant analysis is performed for sinusoidal voltage sources with $v(t) = A\cos(\omega t + \phi)$, where A, ω and ϕ are the amplitude, frequency and phase of the signal. In this situation, applying Eq. (2) to the two components of the electric charge, give the two components of the electric current and are shown in Eq. (4).

$$\begin{cases} i_s(t) = \frac{AR}{R^2+\left(L\omega-\frac{1}{C\omega}\right)^2}\cos(\omega t+\phi) + \frac{A\left(L\omega-\frac{1}{C\omega}\right)}{R^2+\left(L\omega-\frac{1}{C\omega}\right)^2}\sin(\omega t+\phi) \\ i_t(t) = C_1 e^{-\frac{1}{2}\left(\frac{R}{L}-\sqrt{\frac{CR^2-4L}{L^2C}}\right)t} + C_2 e^{-\frac{1}{2}\left(\frac{R}{L}+\sqrt{\frac{CR^2-4L}{L^2C}}\right)t} \end{cases} \tag{4}$$

2.2 Frequency domain model

The RLC circuit analysis is also a study theme in other curricular units where electric circuit analysis is a fundamental topic. The typical approach in these subjects, also performed following Kirchoff's laws, assumes that the voltage source is sinusoidal and the voltage drops are governed by the complex impedance of each component. Assuming this approach, the voltage drops in the components of a circuit is generically defined by $\widetilde{V} = \widetilde{Z}\widetilde{I}$ where $\widetilde{V}$ and $\widetilde{I}$ are the complex voltage source and complex current. The complex impedance for each component are $\widetilde{Z}_L = j\omega L$ for the inductor, $\widetilde{Z}_R = R$ for the resistor and $\widetilde{Z}_C = \frac{1}{j\omega C}$ for the capacitor; here, j is the imaginary unit. The application of KVL results in the Eq. (5).

$$j\omega L\ \widetilde{I} + R\ \widetilde{I} + \frac{1}{j\omega C}\ \widetilde{I} = \widetilde{V} \tag{5}$$

The complex voltage source is $\widetilde{V} = A\,e^{j(\omega t+\phi)}$. Thus, the current solution of the Eq. (5) is given by the Eq. (6)

$$\widetilde{I} = \frac{A\,e^{j(\omega t+\phi)}}{j\omega L + R + \frac{1}{j\omega C}} \tag{6}$$

The time magnitude is the real part of the corresponding complex magnitude. Thus, as $v(t) = \Re\left(\widetilde{V}\right)$ and $i(t) = \Re(\widetilde{I})$, one obtains the solution for $i(t)$, as indicated by Eq. (7).

$$i(t) = \frac{AR}{R^2+\left(L\omega-\frac{1}{C\omega}\right)^2}\cos(\omega t+\phi) + \frac{A\left(L\omega-\frac{1}{C\omega}\right)}{R^2+\left(L\omega-\frac{1}{C\omega}\right)^2}\sin(\omega t+\phi) \tag{7}$$

Comparing this solution with $i_s(t)$ from Eq. (4) in 2.1 section, one concludes that they are the same, but $i_t(t)$ is missed.

2.3 Initial value problem

To implement the model, the following conditions were proposed to the circuit: the components have the following values - $R = 2\,\Omega$, $L = 2\,\mathrm{H}$, $C = \frac{2}{37}\,\mathrm{F}$, $v(t) = 2\cos(6t)\,\mathrm{V}$; $q(0) = \frac{4}{37}\,C$ and $i(0) = 0$,A are assumed for initial conditions. Students are now faced with an initial value problem (IVP) that they will have to solve by adopting the two proposed methodologies. The first approach allowed the exact solution, to be obtained by solving the ODE for the charge, $q(t)$, which by derivation resulted in the electric current, $i(t)$.

$$i(t) = \left[-\frac{5232}{12025}\sin(3t) + \frac{576}{12025}\cos(3t)\right]e^{-\frac{1}{2}\,t} + \frac{2568}{12025}\sin(6t) + \frac{576}{12025}\cos(6t) \tag{8}$$

The second approach, based on complex impedance analysis, and solving the eq. 5 in order to $\widetilde{I}$, will only allow to determine a component of $i(t)$ identified as steady state component.

$$i_s(t) = \frac{2568}{12025}\sin(6t) + \frac{576}{12025}\cos(6t) \tag{9}$$

3 Results and discussion

In the first approach, we are allowed to obtain the transient $i_t(t)$ and steady state $i_s(t)$ components of the electric current $i(t)$; in the second approach, only the steady state component is calculated. To compare the two solutions, students are invited to proceed of their graphical representations, which are suggestive of the behavior of each component versus the exact solution. Then they should discuss, comment, and draw some conclusions about these different approaches. The plots depicted in Fig. 2 show the results in the first initial moments.

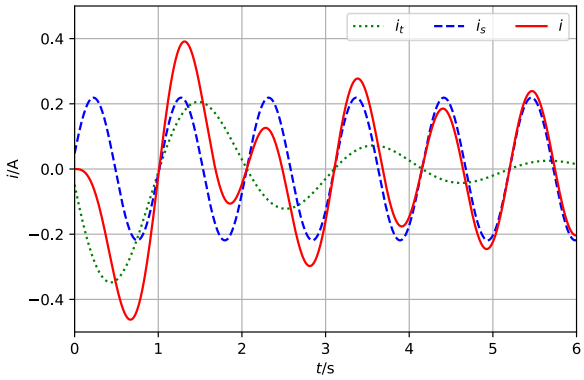

Transient component $i_t(t)$ and steady state component $i_s(t)$ of electric current $i(t)$

$$i_t(t) = \left[-\frac{5232}{12025}\sin(3t) + \frac{576}{12025}\cos(3t)\right] e^{-\frac{1}{2}\ t}$$

$$i_s(t) = \frac{2568}{12025}\sin(6t) + \frac{576}{12025}\cos(6t)$$

$$i(t) = i_t(t) + i_s(t)$$

Figure 2: Electric current graph for the proposed series RLC circuit and with the transient and steady state components.

This approach allows for the establishment of discussion points, regarding the advantages and disadvantages of the two methodologies. It is also intended that students become aware of the existence of a transient component that, despite fading in time, can assume high values in the initial instants and be a source of problems in the circuit operation.

4 Conclusions and Future work

The analysis of the algebraic results obtained and their graphs, allowed the students to acquire sensitivity to recognize the specificities associated with the two approaches in solving the same problem, i.e. either modelled with differential equations or using simpler alternative approaches. In particular, it allowed them to become aware of the possible effects that transient and steady-state components can have on a series RLC electrical circuit for a sinusoidal voltage source.

This activity was enhanced by the use of computer algebra system tools, initially with the wxMaxima, then MATLAB and its Symbolic Math Toolbox, and lately with Python and Sympy library.

References

[1] Ana C. Meira Castro, Ana Júlia Viamonte, António Varejão Sousa; Cálculo II - Conceitos, Exercícios e Aplica cões; Publindústria, 2nd edition, 2016, ISBN 978-989-723-172-8.

[2] Kreyszig, E., Advanced Engendering Mathematics, 10th edition, Willey, 2011, ISBN 978-0-470-45836-5.

International Conference on Mathematical Analysis and Applications in Science and Engineering
ICMA^{2}SC'22
ISEP Porto-Portugal, June 27 - 29, 2022

Mann's iteration scheme for Fredholm integral equation

BARACHE Bahia1[1⋆] **SOUFIT Massinissa**[2] **HOCINE Safia**[3]

[1] University of Bejaia, Algeria Laboratory of LMA
[2] University of Bejaia, Algeria
[3] University of Bejaia, Algeria

[1⋆] bahia.barache@univ.bejaia.dz

Abstract: This work deals with the Mann's stochastic iteration under functional random errors. At first, we establish an exponential inequality of Brenstien-Frechet that enable us to prove the almost complete convergence to the fixed point. Then we study the rate of convergence of this algorithm. Finally, we build a confidence set for the fixed point.

keywords: Fixed point iteration; Fredholm integral equation; Rate of convergence.

MSC2020: 47j26; 45B05; 41A25.

1 Introduction

Many mathematical problems arising from various domains are modeling by Fredholm integral equations. This one can be writing like a fixed point equation $A(u) = u$ with a solution u_{ex} and A is an operator from a Banach space E to E. Finding the exact solution using analytic methods, in general, is difficult or impossible. Therefore, we use numerical methods to calculate the approximate solution. The most powerful method are iterative ones. Fixed point theory provides conditions under which operator defined in which space have existence and uniqueness of a solution.
Mathematically, a fixed point problem for Fredholm integral equation is presented under the following form

$$\lambda \int_a^b K(x,t)u(t)dt + f(x) = u(x); \tag{1}$$

where $[a,b] \subset \mathbb{R}$, $t \in [a,b]$, $x \in [a,b]$ and $\lambda \in \mathbb{R}$. Let A an operator defined on a Banach space $\mathbb{E} = C([a,b] \subset \mathbb{R}, \mathbb{R})$ by

$$A(u(x)) = \lambda \int_a^b K(x,t)u(t)dt + f(x); \tag{2}$$

such that $K : [a,b] \times [a,b] \to \mathbb{R}$ is a continues map then

$$\exists M \in \mathbb{R}, \forall (x,t) \in [a,b] \times [a,b] : |K(x,t)| < M.$$

The operator A is a $c-$contraction from $\mathbb{E}$ to $\mathbb{E}$ if

$$|\lambda| < \frac{1}{M(b-a)}.$$

then the classical result in fixed point theory is Banach fixed-point theorem; it ensures the existence and uniqueness of a fixed point of a contraction self-map in a metric space. It gives us a constructive numerical method (Picard's iteration scheme)[3] to approximate the fixed point. After that, in 1953, Mann[4] introduced new method for an other map where Picard's iteration scheme fails to converge. Later, many modified algorithm were introduced by considering the stochastic part.
In this work we use the Mann's iterative algorithm with errors as described in [4]. This algorithm considered the committed errors at each evaluation of the approximated fixed point u_n. These errors are supposed to be functionals random variables.
In this paper, we establish Briestein-Frechet inequality which allow us to prove the almost complete convergence of the used algorithm to the fixed point. Then to cheek the feasibility and validity of our theoretical results, we consider numerical example.

2 Results and discussion

2.1 Preliminaries

Let $(\Omega, \mathbb{F}, P)$ be a probability space and $\mathbb{E} = C([a,b] \subset \mathbb{R}, \mathbb{R})$ a real Banach space. Let $(\mathbb{E}, \mathfrak{B})$ be a measurable space, where $\mathfrak{B}$ denotes the σ-algebra of all Borel subsets generated by all open subsets in $\mathbb{E}$, and A a contraction mapping defined in 2. Under this conditions the problem 1 admits just one fixed point. In general, the exact solution is impossible to find using analytic methods. Then The approximative are useful in this cases.
We use the following stochastic Mann's algorithm

$$u_{n+1} = (1-a_n)u_n + a_n A(u_n) + b_n \varepsilon_n \tag{3}$$

satisfying

$$\sum_{n=1}^{\infty} a_n = \infty \quad \text{and} \quad \sum_{n=1}^{\infty} b_n < \infty$$

with $\varepsilon_n : (\Omega, \mathbb{F}, P) \to \mathbb{E}$ is a functional random variable denoting noise. Moreover, assume that the sequence $(\varepsilon_n)_n$ is zero mean and $\sup \mathbb{E}(\varepsilon_n) < \infty$.
Without loss of generality, we take

$$a_n = \frac{a}{n} \quad \text{and} \quad b_n = \frac{a}{n^2}, \quad a \in \mathbb{R}_+^*$$

Then the algorithm 3 can be writhen as follow

$$u_{n+1} = (1-\frac{a}{n})u_n + \frac{a}{n}[A(u_n) + \frac{1}{n}\varepsilon_n] \tag{4}$$

2.2 Assumptions

We now introduce some classical hypothesis that will be useful tools for us to get results.

- (H_1) The fixed point u_{ex} satisfies

$$\exists N > 0, ||u_1 - u_{ex}|| < N.$$

- (H_2) The constant λ is such that

$$|\lambda| < \frac{1}{M(b-a)} \Rightarrow 0 < c = |\lambda| M(b-a) < 1 \Rightarrow (\forall u, v \in \mathbb{E} : ||A(u) - A(v)|| < c||u - v||).$$

- (H_3) Constant a and c are such that

$$a(1-c) < 1$$

Remark 1 *The assumption (H_1) is classical, the existence of u_{ex} and the arbitrary choice of x_1 allow us to assume such supposition. To assume the existence and uniqueness of a fixed point for the problem 1 according to Banach's theorem of fixed point we must introduce the assumption (H_2). The assumption (H_3) will be useful for specifying the rate of almost complete convergence of the stochastic Mann's iteration algorithm.*

Theorem 1 *Under the assumption of theorem* (3) *in[1], the algorithm 4 converges almost completely to the fixed-point u_{ex} of A.*

Theorem 2 *under assumption (H_3), we get*

$$u_{n+1} - u_{ex} = O\sqrt{\frac{\ln n}{n^{a(1-c)-\rho}}}.$$

3 Conclusions and Future work

These inequalities alow us a possibility to build a confidence field to the unique fixed point of our problem. For new research directions we suggested to do the same work with functionals mixing random errors.

References

[1] B. Barache, I. Arab, A. Dahmani, Exponontial Inequalities for Mann's Iterative Scheme with Functional Random Errors, Sequential Analysis,

37 (2018), 18–30.

[2] W.R. Mann, Mean Value Methods in Iteraton, Proceedings of American Mathematical Society, **4** (1953), 506–510.

[3] R.P. Agrawa, D. O'Regon, D.R. Sahu, *fixed point Theory for Lipschitzian-type Mapping and Applications*. Springer: 2009.

[4] V. Berinde, *Iteration Approximation of fixed points*. Springer: Lecteurs Notes in Mathematics, 2007.

International Conference on Mathematical Analysis and Applications in Science and Engineering
ICMA^{2}SC'22
ISEP Porto-Portugal, June 27 - 29, 2022

Perturbation analysis of Probabilistic Boolean networks with gene perturbations

Massinissa SOUFIT[1] **Baya TAKHEDMIT**[2⋆] **Karim ABBAS**[3]

[1] Research Unit LaMOS , University of Bejaia, Algeria
[2] Research Unit LaMOS , University of Bejaia, Algeria
[3] Research Unit LaMOS , University of Bejaia, Algeria

[2⋆]baya.takhedmit@univ-bejaia.dz

Abstract: In this work,we introduce a new bound to analysis a stochastic boolean network with perturbation, by using power series expansions. More specifically, we have considered the analysis of a SBNP with three genes.

keywords: Power series expansions; Stochastic boolean network; Markov chains.

MSC2020: 30E; 37N; 65C.

1 Introduction

Stochastic boolean network with perturbation (SBNP) have received much attention in modeling genetic regulatory networks. A SBNP can be regarded as a Markov chain process and is characterised by a transition probability matrix.
In this work, we propose a new bound based on the special structure of a transition probability matrix of PBNs with gene perturbation to compute its stationary distribution. Various numerical examples are presented to show the performance of the used approach.

2 Results and discussion

Let us consider a Markov chain X on the denombrable state space $S = \{1, 2, ...\}$, P denote the transition kernel of a Markov chain in S having unique stationary distribution π. Indeed, P must be a stochastic matrix; that is, $p_{ij} \geq 0$, and $\sum_{j\geq 0} p_{ij} = 1$, for all $i \geq 0$.
Consider a PBNs with gene perturbation [3]. This network is modeled by a homogeneous Markov chain with discrete time of transition probability matrix $\widetilde{A}$ (the nominal matrix) defined by [2]:
$\widetilde{A} = (1-p)^n A + \widetilde{P}_n$
Let $\widetilde{P}_n$ be the $2^n \times 2^n$ perturbation matrix of a PBN with n genes, then we have for n=1,2,...

$$\widetilde{P}_n = Q_n - (1-p)^n I_{2^n} = \underbrace{Q_1 \otimes Q_1 \otimes ... \otimes Q_1}_{n\ terms} - (1-p)^n I_{2^n}, \tag{1}$$

where

$$Q_1 = \begin{pmatrix} 1-p & p \\ p & 1-p \end{pmatrix}.$$

Suppose this Markov chain is ergodic with a unique stationary distribution π. Note the fundamental matrix associated with this chain by [4]:

$$Z = (I - \widetilde{A} + \Pi)^{-1}. \tag{2}$$

We note the matrix of transition probabilities of the perturbed model which is of the same structure as the original model, by: $\bar{A} = (1-p)^n A + \bar{P}_n$, where

$$\bar{P}_n = \underbrace{I_2 \otimes I_2 \otimes ... \otimes I_2}_{r \ terms} \otimes Q_1 \otimes Q_1 \otimes ... \otimes Q_1 - (1-p)^n I_{2^n}, \qquad n > r.$$

Similarly, we assume that the Markov chain describing the state of the perturbed model is ergodic with a unique stationary distribution $\bar{\pi}$.

Let X a Markov chain, which verifies the $\widetilde{X}$ be a Markov chain having a transition kernel Q such that $E = ||P - Q||$. For any matrix norm it holds with the above notation that:
If

$$||E|| < \frac{1 - ||T||}{1 + ||\pi||}$$

then

$$||\tilde{\pi} - \pi|| < ||E||.||Z|| \left[\frac{1 - ||T||}{1 - ||T|| - ||E||(1 + ||\pi||)} \right].$$

Where T is the taboo kernel as also called residual matrix in the literature[1].
We analyze the effect of the perturbation (change in value) of the probability p on the stationary distribution π.
The graphical representation of the new bound made on the computation of the stationary distributions is given in the following figure.

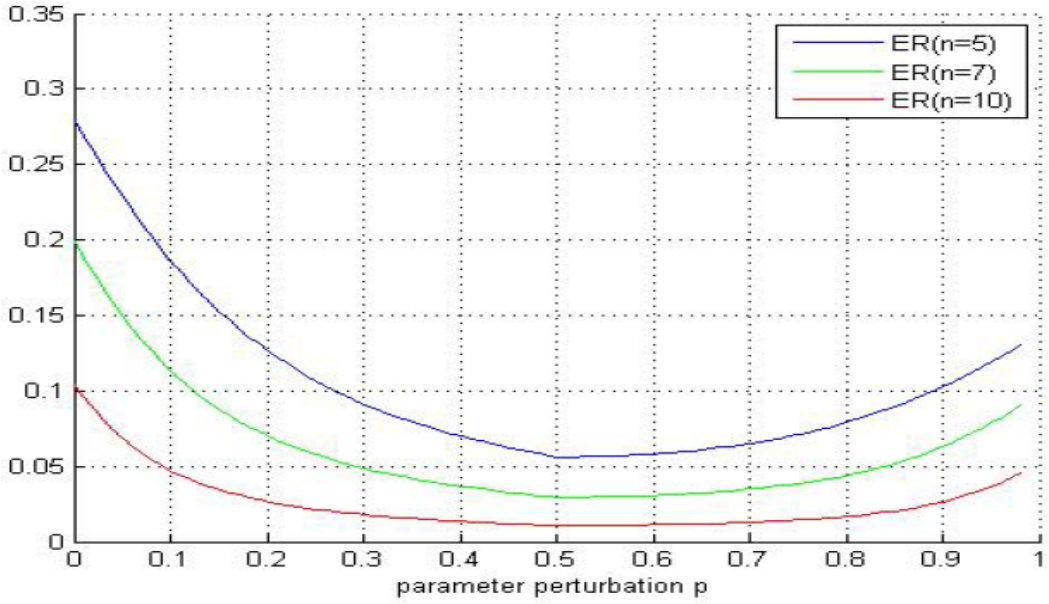

Figure 1: The effect of perturbation of the probability p on the stationary distribution π

3 Conclusions and Future work

In this work, we have been able to illustrate numerically the effect of changing the values of the probability of perturbation $'p'$ on the calculation of the stationary distribution of a stochastic Boolean network with perturbation of different genes.
Analyzing of more complex networks in the presence of parametric uncertainties will also be the topic of ongoing research.

References

[1] K. Abbas, J. Berkhout and B. Heidergott, *Markov Chains: Models, Algorithms and Applications*. International Series on Operations Research and Management Science, Springer, New York, (2006).

[2] W. Xu, W. Ching, S. Zhang, W. Li, X. Chen (2011) *A matrix perturbation method for computing the steady-state probability distributions of probabilistic Boolean networks with gene perturbations*. J.Comput. Appl. Math. 235 2242–2251.

[3] I. Shmulevich, E.R. Dougherty, W.Zhang (2002) *Gene perturbation and intervention in probabilistic boolean networks*, 1320–1324.

[4] J.L. Barlow, (2000) *Stable computation with the fundamental matrix of a Markov chain*. SIAM J. Matrix Anal. Appl. 22: 230–241.

International Conference on Mathematical Analysis and Applications in Science and Engineering
ICMA^{2}SC'22
ISEP Porto-Portugal, June 27 - 29, 2022

The influence of indirect effects in the dynamics of a three-dimensional population model

Renato Colucci[1] **Érika Diz-Pita**[2⋆] **M. Victoria Otero-Espinar**[2]

[1] Universitá Politecnica delle Marche, Ancona, Italy
[2] Universidade de Santiago de Compostela - CITMAga, Spain

[1⋆] erikadiz.pita@usc.es

Abstract: We consider a population model in dimension three, with two prey and one predator, and we include in the system a term representing the indirect effects of predation. This effects are important as showed by several experiments with different species. We study the stability of this new proposed system and other theoretical related topics as the existence of Hopf bifurcation and the problem of persistence. We also illustrate the results with numerical simulations.

keywords: predator-prey system; indirect effects; stability; limit cycle.

MSC2020: 34C05; 37C07; 34C23; 34C60.

1 Introduction

Population dynamics is a widely studied topic in Biomathematics, but in light of the real experiments carried out by biologists, systems that model the interaction between populations can be constantly improved. In our case, we consider the system proposed by Sharma and Samanta in [3], it is:

$$\begin{aligned} \dot{x} &= rx\left(1-\frac{x}{k}\right)-\frac{cxz}{a+\alpha\eta y+x}, \\ \dot{y} &= y(\beta-\delta z), \\ \dot{z} &= \frac{bxz}{a+\alpha\eta y+x}+\gamma yz-mz, \end{aligned} \tag{1}$$

where the variables represent, respectively, the population densities of the two prey species and the predator species. In this model, a Holling type II functional response is considered for the interaction between the first prey and the predator, and the handling time of predator for the second prey is also taken into account. For the interaction between the second prey and the predator a Holling type I functional response is considered. It is also assumed an exponential growth for the second prey and, as a consequence, there is a huge availability of individuals of this species and no searching time.

Due to this availability of the second prey, it seems reasonable to suppose that the predator prefers to predate the second prey, and the first one take advantages of it. This situation can be modeled by adding the term $-Lyz$ in the second equation and the term Lyz in the first one.

This term represents the indirect effect of predation and the parameter $L > 0$ measures the intensity of indirect effects. With this modification, and maintaining the other characteristics of the initial model, we propose the system

$$\begin{aligned} \dot{x} &= rx\left(1-\frac{x}{k}\right) - \frac{cxz}{a+\alpha\eta y+x} + Lyz, \\ \dot{y} &= y(\beta-\delta z) - Lyz, \\ \dot{z} &= \frac{bxz}{a+\alpha\eta y+x} + \gamma yz - mz, \end{aligned} \tag{2}$$

with all the parameters positive. The study of this system has been initiated in [2].

The importance of indirect effects in ecosystems with a predator species and prey species has been analyzed for biologists in the last years. It has been concluded, for example, that preys may change their normal activity just by the presence of predators. Actually, many kinds of indirect effects have been described in the literature. Another example is the case of predator Daphnia with two groups of Phytoplankton, in which the predator prefers to predate the prey group with a smaller size, and the other prey group takes advantages of it. This model has been studied in [1] and has motivated our work.

2 Results

As a first approach to the dynamics of the system, we study the dynamics on the invariant planes, reducing the dimension of the system. In the invariant plane $z = 0$ the dynamics is simple, with only two singular point which are hyperbolic: a saddle and an unstable node.

On the other hand, the dynamics on the invariant plane $y = 0$ is more complex, and apart from the two singular points that always exist, there is another one which is not over the axis and appears for the parameters satisfying the condition $kb > m(k + a)$. For this singular point we have proved that it undergoes a supercritical Hopf bifurcation at $m_0 = b(k - a)/(a + k)$. Also we have proved that for $m < m_0$, the system has a unique and stable limit cycle bifurcating from the singular point. We ilustrate the result with numerical simulation, for example, for the case with $m = 0.18 > m_0$ in Figure 1 and for the case with $m = 0.05 < m_0$ in Figure 2.

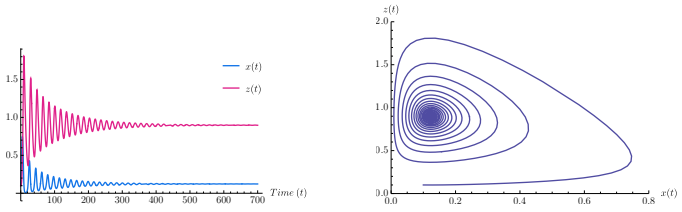

Figure 1: Numerical results for $m = 0.18 > m_0$.

For this restricted system we have also studied the existence of periodic orbits in a more general way, and not only attending to those that appear by a Hopf bifurcation. We have proved that the system does not have periodic orbits in the set $\{(x, z) \in \mathbb{R}^2 : x, z \geq 0\}$ if condition

$$r\left(1-\frac{a}{k}\right) + \frac{bk - m(k+a)}{k} < 0,$$

holds.

Then, going back to the system in dimension three, we obtain and study the stability of the singular points in the boundary. These singular points are $(0, 0, 0)$, $(k, 0, 0)$ and, if $kb > m(a+k)$ also the point

$$\left(ma/(b-m), 0, \frac{r}{c}\left(\frac{ba}{b-m}\right)\left(1-\frac{ma}{k(b-m)}\right)\right).$$

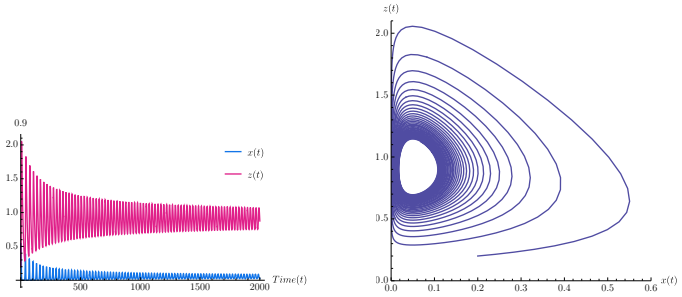

Figure 2: Numerical results for $m = 0.05 < m_0$, where a stable limit cycle attracts nearby solutions

We have proved that the two first singular points in the boundary are saddles, and we have given a classification of when the third singular point is unstable and when it is asymptotically stable.

We have also studied the existence of positive singular points and we have given a necessary and sufficient condition for the existence of at least one of those singular points. This condition is not included due to their extension, but we have also obtained a simpler sufficient condition for system (2) to have at least one positive equilibrium, which is:

$$kbr\frac{\delta + L}{\beta} < 4cm.$$

In the cases in which there exists a positive singular point, we have given sufficient and necessary conditions for the asymptotic stability, which are $s_1, s_2, s_3 > 0$ and $s_1 s_2 - s_3 > 0$, with f_{ij} for $i = 1, 2, 3$ and $j = x, y, z$ the components of the Jacobian matrix and

$$s_1 = -Trace(J(E^*)),\ s_2 = \begin{vmatrix} f_{1x} & f_{1y} \\ 0 & 0 \end{vmatrix} + \begin{vmatrix} f_{1x} & f_{1z} \\ f_{3x} & 0 \end{vmatrix} + \begin{vmatrix} 0 & -y^*(\delta + L) \\ f_{3y} & 0 \end{vmatrix},\ s_3 = -Det(J(E^*)).$$

We have also proved some results that guarantee a sort of weak persistence of the three species by studying the weakly $\rho-$repelling property of the invariant sets. We say that set $M \subset \mathbb{R}^3_+$ is weakly $\rho-$repelling if there is no solution $x(t)$ of the system starting at x_0, with $\rho(x_0) > 0$, such that $x(t) \to M$ as $t \to +\infty$.

Assuming the condition

$$r\left(1 - \frac{a}{k}\right) + \frac{bk - m(k + a)}{k} < 0,$$

then the invariant sets of the boundary $\partial\mathbb{R}^3_+$ are weakly $\rho-$repelling if

$$bk < k(a + m) \text{ or if } bk > k(a + m) \text{ and } \beta > \frac{ab(bk - m(a + k))r(L + \delta)}{ck(b - m)^2}.$$

Also under the same condition the invariant sets $\{E_0, E_1, E_2\}$ of $\partial\mathbb{R}^3_+$ are acyclic.

Finally we are interested in perform a general bifurcation analysis but, due to the complexity of the system, which has a high number of parameters, it does not seem feasible.

We have made a numerical study of this bifurcation. As an example, if we set the values

$$a = b = c = \alpha = \eta = r = 1, \quad k = \beta = 1/2, \quad \delta = 4/10, \quad \gamma = L = 1/10,$$

we obtain the bifurcation value $m_H = 0.2617$. As m passes trough this value $m = m_H$, a limit cycle appears by Hopf bifurcation of the positive singular point. In Figure 3(a) we include the solutions for the value $m = m_H$, which converge to a the periodic solution. We then include the

solutions in two other cases studied by numerical simulations: the case with $m = 2/10 < m_H$ in Figure 3(b) and the case with $m = 4/10 > m_H$ in Figure 3(c).

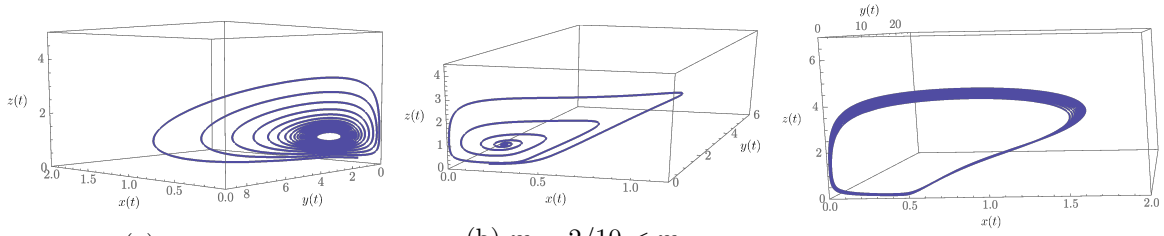

(a) $m = m_H$ (b) $m = 2/10 < m_H$ (c) $m = 4/10 > m_H$

Figure 3: Numerical solutions for different values of the bifurcation parameter m.

3 Conclusions and future work

We have proposed a model which represents the dynamics of an ecosystem with a predator species and two prey species and which is a modification of the system proposed in [3]. We have supposed that the predator prefers to predate the more available prey population and the other one take advantages of it. This is a particular case of indirect effects of predation, which have been pointed out in the literature as an important factor in the evolution of coexisting species.

Then, appart from continue with the study of this system, obtaining more results related, for example, with the Hopf bifurcation and the existence of limit cycles, we would like to study the influence of the inclusion of indirect effects in some other known models.

Acknowledgments

The first author has been partially supported by G.N.A.M.P.A – INdAM (Italy) and MIUR (Italy). The second and third authors are partially supported by the Ministerio de Ciencia e Innovación, Agencia Estatal de Investigación (Spain), grant PID2020-115155GB-I00 and the Consellería de Educación, Universidade e Formación Profesional (Xunta de Galicia), grant ED431C 2019/10 with FEDER funds. The first author is also supported by the Ministerio de Educación, Cultura y Deporte of Spain, contract FPU17/02125.

References

[1] Colucci, R. Coexistence in a one-predator, two-prey system with indirect effects. Journal of Applied Mathematics, **2013** (2013), 625391.

[2] Colucci, R., Diz-Pita, É., Otero-Espinar, M. V. Dynamics of a Two Prey and One Predator System with Indirect Effect, Mathematics, **9** (2021), 436.

[3] Sharma, S., Samanta, G.P. Dynamical Behaviour of a Two Prey and One Predator System. Differential Equations and Dynamical Systems, **22** (2014), 125–145.

Geometric Properties of Analytic Functions Defined by (p,q) Derivative Operator Involving Poisson Distribution

S.Santhiya[1] **K.Thilagavathi**[2⋆]

[1] School of Advanced Science
Vellore Institute of Technology, Vellore-632014, Tamilnadu, India.
[2⋆] School of Advanced Science
Vellore Institute of Technology, Vellore-632014, Tamilnadu, India.

[1]ssanthiya105@gmail.com
[2⋆]kthilagavathi@vit.ac.in

Abstract: The purpose of the present paper is to find the necessary and sufficient condition for the function to be in the subclass of $C(d, \delta, \mu, \beta)$ of analytic functions involving poisson distribution defined by (p, q) derivative operator. Further, we find distortion bounds, covering theorem, radius of starlikeness and convexity for functions belonging to this class are obtained and motivated by results on (p, q) derivative operator [see[1, 2, 3, 4, 5]].

keywords: Univalent functions; Starlike functions; Convex functions; Poisson distribution; (p, q) Derivative operator; Hadamard product.

MSC2020: 30C45; 30C55.

References

[1] R. Chakrabarti and R. Jagannathan,"A (p, q)-oscillator realization of two-parameter quantum algebras", *J. Phys. A* ,24(13) (1991), L711-L718.

[2] V.Gupta, "(p, q)-Baskakov-Kantorovich operators," *Appl. Math. Inf. Sci.* ,10(4), 1551-1556 (2016).

[3] Muhammet Kamali , Sezgin Akbulut,"On a subclass of certain convex functions with negative coefficients",*Applied Mathematics and Computation*,145 (2003) 341-350.

[4] C.MilovanoviÂ´, GV, Gupta, V, Malik, N ," (p, q)-beta functions and applications in approximation ,"*Bol. Soc. Mat. Mexicana*,(2016). arXiv:1602.06307v2 [math.CA].

[5] M. Mursaleen, K. J. Ansari and A. Khan,"Some approximation results by (p, q)-analogue of Bernstein-Stancu operators",*Appl. Math. Comput.* ,264 (2015), 392-402.

International Conference on Mathematical Analysis and Applications in Science and Engineering
ICMA^{2}SC'22
ISEP Porto-Portugal, June 27 - 29, 2022

Third Hankel Determinant Problem for Bounded Turning Functions, Starlike and Convex Functions Involving Pascal Distribution Series

S.Santhiya[1] **K.Thilagavathi**[2⋆]

[1] School of Advanced Science
Vellore Institute of Technology, Vellore-632014, Tamilnadu, India.
[2⋆] School of Advanced Science
Vellore Institute of Technology, Vellore-632014, Tamilnadu, India.

[1]ssanthiya105@gmail.com
[2⋆]kthilagavathi@vit.ac.in

Abstract: In this article, we focus is on the Hankel determinant for the subclasses of bounded turning functions, starlike and convex functions involving the Pascal distribution series. Also we obtained the functional $|d_2d_3 - d_4|$which gives the sharp upper bounds for each of these classes and we investigate a method of classical analysis planned by libera and zlotkiewicz[1, 2].

keywords: Univalent functions; Starlike functions; Convex functions; Bounded Turing Functions.

MSC2020: 30C45; 30C55.

References

[1] R. J.Libera, and E. J.Zlotkiewicz,*Early coefficient of the inverse of a regular convex function*,Proc. Amer. Math. Soc. 85 (2) (1982), 225-230.

[2] R. J.Libera, and E. J.Zlotkiewicz,*Coefficient bounds for the inverse of a function with derivative in P*, Proc. Amer. Math. Soc. 87 (2) (1983), 251-257.

The influence of the tail of claims distribution on the stability bounds of the univariate classical risk model

Safia HOCINE[1⋆] **Djamil AÏSSANI**[2] **Aicha BARECHE**[3]

[1,2,3] Research Unit LaMOS, Faculty of Exact Sciences
[1,2,3]University of Bejaia, 06000 Bejaia, Algeria.

[1⋆] safia.hocine@univ-bejaia.dz

Abstract: Ruin theory for the univariate risk models has been discussed extensively in the literature. Many results are summarized in the book written by Asmussen and Albrecher (2010) [2]. In this work, we consider the problem of stability of the univariate classical risk model, in particular at the stability bounds of the univariate classical risk model established by Kalashnikov (2000) [3] using two approaches. The first one is based on the strong stability method developed for general Markov chains [1, 5]. The second approach is based on the regenerative processes theory [4]. Based on numerical and graphical results, a comparative study between the stability bounds on the ruin probability obtained using both approaches and considering a Weibull claim amounts distribution is carried out to show the influence of the tail of claims distribution on these stability bounds.

keywords: Heavy-tailed distribution; Markov Chain; Regenerative Processes; Risk Models; Ruin Probability; Strong Stability.

MSC2020: 62G32; 60G07; 91B05; 91G70; 47A55; 47A58.

References

[1] D. Aïssani and N. V. Kartashov, Ergodicity and Stability of Markov chains with respect to operator topology in the space of transition kernels, Doklady Akademii Nauk Ukrainskoi S.S.R., series A, Vol. 11 (1983),3-5.

[2] S. Asmussen and H. Albrecher, *Ruin probabilities.*, World Scientific, Second Ed., New Jersey, 2010.

[3] V. Kalashnikov, The Stability concept for stochastic risk models, Laboratory of Actuariat Mathematics, Univarsity of Copenhagen, Working Paper Nr 166, (2000).

[4] V. Kalashnikov, *Topics on Regenerative Processes.*, CRC Press, (1994).

[5] N. V. Kartashov, Strong Stable Markov Chains, VSP, Utrecht, (1996).

Authors Index

NAME	PAGE
A. Castelo	317
A. Qadi El Idrissi	281
Анар Assanova	273
Aicha Bareche	573
Akhil Srivastav	13, 19, 21
Akylbek Zhamanshin	109, 393
Alain Mehauté	193
Alberto Pinto	249, 251, 253, 255
Aldo Pereira	397
Alessandro Borri	47
Alexandre Afonso	317
Alexandre Carvalho	425
Alina Gavrilut	193
Almudena del Pilar Márquez	105, 373
Álvaro Martínez-Rubio	425
Ana C. Meira Castro	569
Ana Costa	557, 561
Ana Júlia Viamonte	569
Ana Mafalda Matos	525, 529
Ana Navarro Quiles	269, 337
Ana Niño-López	43, 49, 93
Anabela Silva	175
Andjelka N. Hedrih	111
André Santos	517
Andrea De Gaetano	47
Angela Bašić-Šiško	277
Angelika Schmid	537
António Sousa	557, 561, 569
Arran Fernandez	143, 159
Arvet Pedas	225, 229, 233
Asli Larbi	265
Aurelian Cernea	171
Aurelio A. de Los Reyes	25
Aziz Khan	115
Bahia Barache	573
Baruch Schneider	333
Baya Takhedmit	577
Bin Pei	213
Blas M. Vinagre	147
Bob Kooi	13, 21
Bruno Mendes	489, 493
Bruno Valdemar Guerrero Borges	23
Candace M. Kent	1
Carla Jesus	135
Carlo Delfin S. Estadilla	25

Carlos A. Braumann 27
Carlos Alberto Valentim 53
Carlos Andreu-Vilarroig 57, 61
Carlos M. Vinagre 147
Carlos Rodrigues 489
Catalina Tobón 101
Célio Fernandes 449
Chaima Bouzouina 143
Changpin Li 139
Christos Schinas 451
Christos Volos 459
Chrysoula Mylona 451
Clara Burgos Simón 179
Cristiana J. Silva 131
Cristina Muresan 119
Cristina Perez Diukina 57
Damián Knopoff 5
Daniel Cao Labora 183
David Adamczyk 357
David M. Chan 1
Delfim F. M. Torres 455
Dia Zeidan 281, 537, 541, 545, 549
Diana Pimparel 489, 493
Diego Mauricio Murillo Gómez 189
Dimitrios Prousalis 459
Djamil AÏssani 589
Dmitriii Tayurskii 193
Duygu Aruğaslan Çinçin 473
Elena López Navarro 285
Elena Recio 105
Elvin Moore 47
Elvio Accinelli 249
Emanuel Guariglia 187
Enyu Fan 139
Ercília Sousa 453
Eric Goncalves da Silva 281
Érika Diz-Pita 581
Eulalia Martínez 443
Eva Kaslik 439
Eva-H. Dulf 123
Evgeniya Korobko 297
Faïçal Ndaïrou 455
Felix Sadyrbaev 81
Fernando Carvalho 557, 561
Fernando Saldaña 19
Filipe Dias 489, 493
Francesco Giannino 201

Francisco Morillas 413
G. Bognár 477
Gabriel Bengochea 155
Gani Stamov 127
Garyfalos Papaschinopoulos 451
Gerardo Toraldo 201
Givanni Falsone 269
Gonçalo Jacinto 27
Hana Zámečníková 353
Hanna Britt Soots 225
Hans-Otto Walther 457
Haruka Tomobe 261
Hidekazu Yoshioka 261
Hugo Gómez 65
Inês Domingues 481, 489, 493
Inés Tejado 147
Ioan-Lucian Popa 369
Irena Jadlovska 345
Irina Pefilieva 217
Isabel S. Jesus 135
Isabela Birs 119
Ivan Dražić 349
Ivanka Stamova 127
Iyad Suwan 237
Jamal Odysseas Maaita 459
James Hornick 417, 421
Jan Awrejcewicz 73
Jan Heiland 469
Janusz Gajda 161
Jasmina Bogdanovic-Jovanovic 111
Jaume Llibre 77
Javier López-de-la-Cruz 85
Jia-Li Zhao 361
Jiaohui Xu 209
Jingshu Wu 139
Jiri Neustupa 399
Joana Lencart 489, 493
João Abrantes 485
João Faria 501
João Mendes 513
João P. Almeida 251
João Santos 481, 489, 493
Jochen Merker 9
Jorge Buescu 377
Jorge Marques 203, 289
José Antonio Rabi 53
José Augusto Ferreira 65

José Luis Díaz Palencia 93, 293
José Martins 253
José Valero 413, 425
José Vicente Romero Bauset 285
Josef Diblik 297
Josef Rebenda 31, 35
Juan A. Aledo 61
Juan Alzate-Marulanda 101
Juan Carlos Cortés López 179, 285
Juan Carlos Orengo 61
Juan Ugarte 97, 101, 189
Juan-Carlos Cortés 57, 61
Juliana Bertoco 317
Jurandir Nadal 485
K Thilagavathi 585, 587
Kaido Lätt 197, 225
Kamal Shah 115, 237
Karim Abbas 577
Katica (Stevanović) Hedrih 111
Kjetil Holm 31, 35
Kunihiko Hamagami 261
Larysa Dzyubak 73
Laura Villafuerte Altúzar 179
Lavinia Birdac 69
Lazaros Laskaridis 459
Levente Kovacs 123
Leyla Ebrahimpour 489, 493
Liliana Harding 439
Lilla Korenova 553
Linh Nguyen 333
Lino Maia 505, 509, 525, 529
Loredana Flavia Vesa 439
Loredana-Camelia Culda 257
Lucian Mocan 123
Luís Castro 175, 309
Luís Ferrás 301, 305, 317
Luis Pinto 65
Łukasz Płociniczak 533
M Filomena Teodoro 497, 501
M. Manuela Rodrigues 163, 167
M. Victoria Otero-Espinar 77, 581
Madina Tleubergenova 109, 393, 473
Magda Rebelo 301, 305, 317
Maira Aguiar 3, 5, 13, 17, 19, 21, 23
Manar A. Alqudah 115
Manoj Kumar 117
Manuel Ortigueira 155

Marat Akhmet 109, 393, 473
Marcelo Ebert 289
Marco Aurélio Benedetti Rodrigues 485
Margus Lillemäe 229
María Dolores Roselló Ferragud 285
Maria Luísa Morgado 301, 305, 317
María Luz Gandarias 89, 105
María Rosa 43, 49, 89
Martina Pavlackovà 447
Massinissa Souffit 573
Mehmet Ali Özarslan 239
Miguel A. F. Sanjuán 471
Miguel Angel Hernández Verón 443
Miguel Casquilho 377
Miguel Correia 485
Mihaela Neamtu 39, 257, 439
Mikk Vikerpuur 229, 233
Milton Ferreira 163, 167, 245
Miroslawa Zima 403
Motoh Tsujimura 261
Nara Cangussu 525, 529
Natalia Dilna 405
Nela Bosner 381
Nelida Črnjarić-Žic 461
Nelson Faustino 203
Nelson Vieira 163, 167, 245
Nico Stollenwerk 3, 5, 13, 19, 21
Nicole Cusimano 5
Nisha Yadav 443
Noosheza Rani 159
Nuno Ferreira 513, 517, 521
Oana Brandibur 151
Oleksandr Dzyubak 73
Patrícia A. Filipe 27
Pavel Vlasanek 357
Pedro Guedes 557, 561
Pedro Marín-Rubio 425
Pedro Reis 557, 561
Peter Benner 469
Petr Hurtik 469
Petr Kučera 409
Philippe Riot 193
R. Vilela-Mendes 535
Rafael de La Rosa 373
Rafael Jacinto Villanueva Micó 179
Raluca Muresan 69
Ramiro S. Barbosa 135

Renato Colucci 581
Renato Soeiro 255
Richard Zhao 421
Rita Guerra 309
Rogério Torres 521
Rosa Teodósio 501
Rosalía Leiva 317
Rosana Rodríguez-López 313, 365
Rossella Laudani 269
Roxana Matei 39
Rubén Caballero Toro 425
Ruifang Wang 213
S Santhiya 585, 587
Safia Hocine 573, 589
Salvador Chulián 43, 49, 89
Samir Aberkane 369
Sandra Aires 557, 561
Sandra Pinelas 463
Sandugash Mynbayeva 325
Sebastian Escobar-Pajoy 97
Senka Maćešić 461
Sergey Kryzhevich 467
Sergio Adriani David 53
Shaoying Zeng 139
Shekhar Singh Negi 207
Simona Panunzi 47
Sofia S. Teles 497
Sofia Silva 489, 493
Sorina Madalina Sferle 337
Stephen Anco 417, 421
Steven Giraldo-Mora 101
Sukhjit Singh 443
Suzan Cival Buranay 241
Svitlana Rogovchenko 565
Swar Ramo 31, 35
Syed Abbas 117
Tamara María Garrido Letrán 373
Tea Shavadze 329
Teresa A. Mesquita 389
Thabet Abdeljawad 115, 237
Thi Minh Tam Pham 217
Thomas Wolf 417, 421
Tomás Caraballo 179, 209, 413
Trayan Stamov 127
Tri Truong 333
Urve Kangro 221
Valentina Taddei 447

Vanessa Steindorf 13, 19, 21
Vasile Dragan 369
Vicenc Torra 207
Vicente Bevia 341
Victor Santos 513
Vipin Kumar 469
Vítor Cardoso 557, 561
Vizda Anam 17
Vladimir Vasilyev 435
Vojtěch Molek 357
Xiaoyu Yang 431
Yan-Ming Liang 361
Yong Xu 213, 431
Yuriy Rogovchenko 31, 35, 565
Zahra Alijani 221
Zakhira Nugayeva 473
Zdenek Skalak 427
Zi-Fei Lin 361
Zubair Ahmad 201